AD-A277 520

AGARD-R-796

AGARD-R-796

②

AGARD

ADVISORY GROUP FOR AEROSPACE RESEARCH & DEVELOPMENT

7 RUE ANCELLE 92200 NEUILLY SUR SEINE FRANCE

This document has been approved
for public release and sale; its
distribution is unlimited.

DTIC
ELECTE
MAR 3 1 1994
S F D

AGARD REPORT 796

Characterisation of Fibre Reinforced Titanium Matrix Composites

(La Caractérisation des Matériaux Composites à Matrice de Titane Renforcés par Fibres)

*Papers presented at the 77th Meeting of the AGARD Structures and Materials Panel,
held in Bordeaux, France, 27th—28th September 1993.*

94-09717

NORTH ATLANTIC TREATY ORGANIZATION

Published February 1994

Distribution and Availability on Back Cover

DISCLAIMER NOTICE

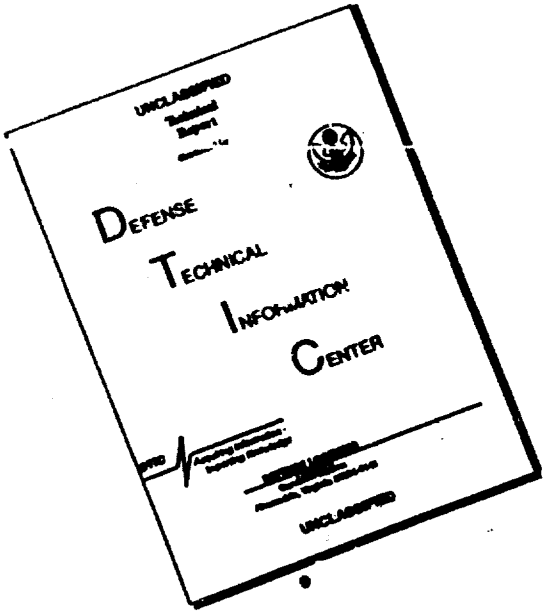

UNCLASSIFIED

DEFENSE TECHNICAL INFORMATION CENTER

UNCLASSIFIED

THIS DOCUMENT IS BEST QUALITY AVAILABLE. THE COPY FURNISHED TO DTIC CONTAINED A SIGNIFICANT NUMBER OF PAGES WHICH DO NOT REPRODUCE LEGIBLY.

AGARD

ADVISORY GROUP FOR AEROSPACE RESEARCH & DEVELOPMENT
7 RUE ANCELLE 92200 NEUILLY SUR SEINE FRANCE

AGARD REPORT 796

Characterisation of Fibre Reinforced Titanium Matrix Composites

(La Caractérisation
des Matériaux Composites à
Matrice de Titane Renforcés par Fibres)

Papers presented at the 77th Meeting of the AGARD Structures and Materials Panel, held in Bordeaux, France, 27th—28th September 1993.

North Atlantic Treaty Organization
Organisation du Traité de l'Atlantique Nord

The Mission of AGARD

According to its Charter, the mission of AGARD is to bring together the leading personalities of the NATO nations in the fields of science and technology relating to aerospace for the following purposes:

— Recommending effective ways for the member nations to use their research and development capabilities for the common benefit of the NATO community;

— Providing scientific and technical advice and assistance to the Military Committee in the field of aerospace research and development (with particular regard to its military application);

— Continuously stimulating advances in the aerospace sciences relevant to strengthening the common defence posture;

— Improving the co-operation among member nations in aerospace research and development;

— Exchange of scientific and technical information;

— Providing assistance to member nations for the purpose of increasing their scientific and technical potential;

— Rendering scientific and technical assistance, as requested, to other NATO bodies and to member nations in connection with research and development problems in the aerospace field

The highest authority within AGARD is the National Delegates Board consisting of officially appointed senior representatives from each member nation. The mission of AGARD is carried out through the Panels which are composed of experts appointed by the National Delegates, the Consultant and Exchange Programme and the Aerospace Applications Studies Programme. The results of AGARD work are reported to the member nations and the NATO Authorities through the AGARD series of publications of which this is one.

Participation in AGARD activities is by invitation only and is normally limited to citizens of the NATO nations.

The content of this publication has been reproduced
directly from material supplied by AGARD or the authors.

Published February 1994

Copyright © AGARD 1994
All Rights Reserved

ISBN 92-835-0735-5

Printed by Specialised Printing Services Limited
40 Chigwell Lane, Loughton, Essex IG10 3TZ

Preface

The combination of stiffness, strength and high temperature resistance provided by fibre reinforced titanium matrix composites offers major benefits for aircraft engine and airframe applications, where these materials could be used to reduce weight or improve performance. In this regard, they are important to AGARD for the increased mission capability they offer for future aircraft systems and they are of particular interest to the Structures and Materials Panel, which is in a position to address some of the technical issues that may otherwise delay serious consideration of the materials by potential users.

At its 77th Meeting in the fall of 1993, the Structures and Materials Panel held a workshop on the subject of characterisation of titanium composites. This is a major aspect of these materials that must be addressed if they are to become accepted for use, and the workshop was intended to provide a forum for the exchange of information in this important area. Characterisation in this case refers to the understanding of the behaviour of the composites as it relates to the ability to predict their performance in real-life applications. It covers various topics that include mechanical test techniques, NDE methods, life prediction models and other factors that will affect the level of confidence with which these relatively new materials will be accepted for application. These are all issues where a coordinated approach to testing and a mutual agreement regarding data interpretation would enhance the possibility of their use by the AGARD community.

In a sense, with metal matrix composites in general, and titanium matrix composites in particular, we are following the same course that has been taken by the polymer matrix composites community in the past in bringing composite materials from research to application. Polymer matrix composites are now widely used in aerospace but the path to this acceptance was not straightforward, involving a long time period and a very large financial investment — an investment applying not only to the development and scale-up phases but also to the characterisation and component demonstration activities.

With titanium composites, we are presently at a stage where matrix alloys, reinforcing fibres and composite consolidation processes are available for the fabrication of structural components. Several countries are involved in the development of manufacturing processes for titanium composites, and in some cases facilities already exist for the production of large-scale products suitable for use on airframes or in engines. At this point, their future acceptance will depend on several other factors. Apart from cost — a significant issue in its own right, but one that must be addressed in other ways — these include the establishment of suitable test methods for determining properties, the understanding of the relationship of these properties to component behaviour, and the development of methods for assessing product integrity from a design confidence point of view.

Accordingly, through presentations and discussion, the workshop addressed the questions of what the designer needs to know about the behaviour of titanium composites, what measurements and test methods are available and in use, what materials modelling techniques are applicable, how do modelling predictions relate to component behaviour, and what further tests and analysis procedures need to be developed. We hope that the publishing of the workshop papers will act as a catalyst for further work on these unique materials, eventually leading to their wider acceptance in aerospace applications.

Dr T.M.F. Ronald
Sub-Committee Chairman

Accesion For
NTIS CRA&I ✓
DTIC TAB
Unannounced
Justification
By
Distribution /
Availability Codes
Dist | Avail and / or Special
A-1

Préface

Les qualités combinées de rigidité, de résistance mécanique et thermique présentées par les matériaux composites à matrice de titane renforcée par fibres de carbone offrent des avantages importants pour les applications cellule et moteur, où l'emploi de ces matériaux autoriserait à la fois une diminution de masse et des performances améliorées.

A cet égard ces applications sont importantes pour l'AGARD, car elles permettent d'augmenter les capacités opérationnelles des futurs systèmes aériens et, en même temps, elles représentent un intérêt particulier pour le Panel des Structures et Matériaux, qui est parfaitement en mesure d'examiner certaines questions techniques dont la solution lèvera les obstacles et devrait permettre une meilleure prise en compte de ces matériaux par des utilisateurs potentiels.

Lors de sa 77ème Session en automne 1993, le Panel AGARD des Structures et Matériaux a organisé un atelier sur la caractérisation des matériaux composites à base de titane. Il s'agit d'un aspect très important qui doit être étudié pour permettre l'adoption de ces matériaux. L'atelier devait servir de forum pour un échange d'informations sur ce sujet important. Dans ce cas, la caractérisation se réfère à l'analyse du comportement des matériaux composites, et, plus précisément, à la capacité de prévoir leurs performances dans des applications réelles. Il traitait de différents sujets, y compris les techniques des essais mécaniques, les méthodes d'évaluation non destructives NDE, les modèles de prévision des cycles de vie et d'autres facteurs qui influenceront le climat de confiance nécessaire à l'acceptation de ces matériaux relativement nouveaux pour des applications industrielles. Autant de questions où une approche coordonnée vis à vis des essais, alliée à un accord mutuel sur l'analyse des données servirait à promouvoir leur adoption par la communauté AGARD.

D'une certaine façon, en ce qui concerne les matériaux composites à matrice métallique en général et les composites à matrice de titane en particulier, nous suivons la même voie que celle qui a été adoptée dans le passé par la communauté des matériaux composites à matrice de polymères: faire passer les matériaux composites du domaine de la recherche à celui des applications. Aujourd'hui, l'utilisation des composites à matrices de polymères est très répandue dans le domaine aérospatial, mais le chemin qui a mené à cette adoption n'a pas été sans détours, car il a entraîné des délais très longs et un investissement financier considérable — un investissement qui s'applique non seulement aux phases de développement et de mise à l'échelle, mais aussi aux activités de caractérisation et de démonstration des composants.

Dans le cas des matériaux composites à matrice de titane, nous sommes actuellement au point où les matrices métalliques, les matrices à fibres renforcées et des procédés de consolidation des matériaux composites sont disponibles pour la fabrication de composants structuraux. A l'heure actuelle, certains pays développent des procédés de fabrication de matériaux composites au titane, et dans certains cas, où des installations existent déjà pour la production en série de composants aéronautiques de cellule ou de moteur. Aujourd'hui, leur adoption future dépend d'un certain nombre d'autres facteurs. La question du coût mise à part — bien qu'elle ait sa propre importance et qu'il faudrait peut-être aborder d'une autre façon — ces facteurs concernent l'établissement de méthodes d'essais convenables pour la détermination des caractéristiques, l'analyse du rapport entre ces caractéristiques et le comportement des composants, ainsi que l'élaboration de méthodes pour l'évaluation de l'intégrité du produit du point de vue du niveau de confiance structural.

Ainsi, par le biais de présentations et de discussions, l'atelier a pu aborder les questions suivantes: que doit savoir le concepteur sur le comportement des matériaux composites? Quelles sont les méthodes d'essais et de contrôle qui sont employées? Quelles sont les techniques de modélisation de matériaux applicables? Quel est le rapport entre les prévisions issues de la modélisation et le comportement des composants? Et quelles sont les procédures d'essais et d'analyses qui restent à développer.

Nous espérons que la publication des communications présentées à l'atelier servira de catalyseur pour de futurs travaux sur ces matériaux singuliers, amenant ainsi une plus large adoption pour des applications aérospatiales.

Dr T.M.F. Ronald
Président du sous-comité

Structures and Materials Panel

Chairman: Mr Roger Labourdette
Directeur Scientifique des Structures
ONERA
29 ave de la Division Leclerc
92322 Châtillon Cedex
France

Deputy Chairman: Dipl.Ing. O. Sensburg
Deutsche Aerospace Structures
Militärflugzeuge LME 202
Postfach 80 11 60
8000 Munich 80
Germany

SUB-COMMITTEE

Chairman: Dr T.M.F. Ronald
Head, Materials Technology
Aeronautical Systems Center
ASD/NAF, Bldg 52
2475 K St, 3, Wright-Patterson AFB
OH 45433-7644
United States

Members

E. Campo	IT	L. Minges	US
H.J.G. Carvalhinhos	PO	G. Oddone	IT
D. Chaumette	FR	D.B. Paul	US
P. Costa	FR	B.F. Peters	CA
M. Doruk	TU	R. Potter	UK
C.R. Gostelow	UK	A. Rodriguez	SP
J.P. Immarigeon	CA	M. Scolaris	IT
W.C. Kessler	US	A. Starke	US
M.J. Kilshaw	UK	J. Waldman	US
P. Marchese	IT		

PANEL EXECUTIVE

Dr Jose M. Carballal, Spain

Mail from Europe:
AGARD—OTAN
Attn: SMP Executive
7, rue Ancelle
92200 Neuilly-sur-Seine
France

Mail from US and Canada:
AGARD—NATO
Attn: SMP Executive
Unit 21551
APO AE 09777

Tel: 33(1)47 38 57 90 & 57 92
Telex: 610176 (France)
Telefax: 33 (1) 47 38 57 99

Contents

Page

Preface iii

Préface iv

Structures and Materials Panel v

Reference

Technical Evaluation Report T
by J.G.R. Hansen

SESSION I – BACKGROUND – DESIGN REQUIREMENTS AND APPLICATIONS

Possibilities and Pitfalls in Aerospace Applications of Titanium Matrix Composites 1
by J.M. Larsen, S.M. Russ and J.W. Jones

Applications of Titanium Matrix Composite to Large Airframe Structure 2
by T.M. Wilson

SCS-6^{TM} Fiber Reinforced Titanium 3
by J. Henshaw

Paper 4 withdrawn

Processing of Titanium Matrix Composites 5
by E.A. Feest and J. Cook

Composites Based on Titanium with the External and Internal Reinforcement 6
by A.I. Khorev

SESSION II – CHARACTERISATION AND TESTING

Manufacture and Properties of Sigma Fibre Reinforced Titanium 7
by J.G. Robertson

Properties of TMC Processed by Fibre Coating and HIPing 8
by H.J. Dudek and R. Leucht

Fibre-Matrix Interface Properties in Ti-Matrix Composites: Chemical Compatibility and Micromechanical Behaviour 9
by A. Vassel, R. Mévrel, J.P. Favre and J.F. Stohr

Oxidation Behavior of Potential Titanium Aluminide Matrix Materials 10
by J. Cook, E.U. Lee, W.E. Frazier, T.-H.T. Mickle and J. Waldman

Paper 11 withdrawn

Methodologies for Thermal and Mechanical Testing of TMC Materials 12
by G.A. Hartman and D.J. Buchanan

Ultrasonic Nondestructive Characterization Methods for the Development and Life Prediction of Titanium Matrix Composites 13
by P. Karpur, D.A. Stubbs, T.E. Matikas, M.P. Blodgett and S. Krishnamurthy

Reference

SESSION III — LIFE PREDICTION

Metal Matrix Composites — Analysis of Simple Specimens and Model Components under Creep and Fatigue Loading 14
by G.F. Harrison, B. Morgan, P.H. Tranter and M.R. Winstone

Residual Strength and Life Prediction Techniques for Ti MMC 15
by J.A. Harter, D. Harmon and R. Post

Process/Composite Concurrent Tailoring of SiC/Ti Composites 16
by C.C. Chamis and D.A. Saravanos
(not presented at the Workshop)

Micromechanical Modeling of Damage Growth in Titanium Based Metal-Matrix Composites 17
by J.A. Sherwood and H.M. Quimby

Crack Growth under Cyclic Loading in Fibre Reinforced Titanium Metal Matrix Composites 18
by P. Bowen

Prediction of Thermal and Mechanical Stress-Strain Responses of TMC's Subjected to Complex TMF Histories 19
by W.S. Johnson and M. Mirdamadi

SESSION IV — DESIGN NEEDS

Pre-standardisation Work on Fatigue and Fracture Testing of Titanium Matrix Composites 20
by J.H. Tweed, J. Cook, N.L. Hancox, R.J. Lee and R.F. Preston

ASTM and VAMAS Activities in Titanium Matrix Composites Test Methods Development 21
by W.S. Johnson, D.M. Harmon, P.A. Bartolotta and S.M. Russ

Développement de Méthodes d'Essais Mécaniques pour CMM à Base Titane (Traction-Fatigue Oligocyclique) 22
par B. Dambrine et M. Hartley

Modelling and Testing Fibre Reinforced Titanium for Design Purposes 23
by L.N. McCartney

TECHNICAL EVALUATION REPORT

James G. R. Hansen
Engineering Technology Division
Oak Ridge National Laboratory
Oak Ridge, Tennessee 37831 USA

1. SUMMARY

This paper presents a technical evaluation of the Workshop on "Characterisation of Fibre Reinforced Titanium Matrix Composites" held at the 77th meeting of the AGARD Structures and Materials Panel on September 27-28 in Bordeaux, France.

2. INTRODUCTION

Fibre reinforced titanium matrix composites (TMC) offer major benefits for aircraft engine and airframe applications, where the combination of stiffness, strength and high temperature resistance provided by these materials can be used to reduce weight and improve performance. While their development has matured to the point that they are available in various product forms, their widespread acceptance will depend on several factors, the primary one being cost. Other factors include establishment of suitable test methods for determining properties, understanding the relationship of these properties to composite behavior and development of methods for assessing product integrity from a design confidence point of view. These issues involve a strong emphasis on life prediction methodology. The goal of this AGARD workshop was to provide a forum for discussions and information exchange in the areas of test requirements and techniques that might help the eventual acceptance of TMC in aerospace applications. It addressed the questions of what the designer needs to know about the behavior of TMC, what measurement and test methods are available and in use, how results are related to materials modeling and component behavior, and what test and analysis techniques need to be developed.

3. CONTENT OF PRESENTATIONS

3.1 Materials, Processing, Manufacturing and Applications

Data on numerous TMC material systems was presented during the workshop. Primary TMC coated reinforcing fibres discussed were SCS-6 and SCS-9 produced by Textron Specialty Materials and SM1140+ and SM1240 produced by British Petroleum Metal Composites Limited. TMC matrices included titanium (Ti-15-3, Ti-6-4 and TIMETAL®21S) and titanium aluminide (α_2 and high niobium content α_2).

Numerous processing methods were presented. The primary method to produce airframe [illegible] for the U.S. National Aero-Space Plane (NASP) has been the HIPing of foil-fibre-foil materials (Paper 2). In order to maintain fibre spacing, crossweave has been incorporated. McDonnell Douglas Corporation demonstrated both detailed processing steps and details of tooling and stacking sequences used to fabricate NASP parts. Details of the NASP TMC Factory installed at Textron for production of NASP airframe parts as large as 4 ft by 8 ft panels were presented (Paper 3). British Petroleum presented their method of producing large TMC sheets (Paper 7). The method maintains excellent fibre spacing and alignment by filament winding fibres and then including titanium matrix powder in the polymer binder. Fibre layers and titanium foil layers are then alternated. The fibres are constrained by the powder during HIPing so they do not migrate.

Engine materials must be produced with extreme care. When fabricating discs, essentially no fibres wound in the hoop direction may touch one another. One method to attain this level of quality is to coat individual fibres with titanium matrix material and then use the composite wires to shape a part which is subsequently HIPed. This method is applicable to titanium aluminide matrices, which are difficult to process to foil. Deposition rates reported via physical vapour deposition include 60 μm/hr by DLR for magnetron sputtering and 90 μm/hr by AEA Harwell for their Sputter Ion Plate process (Papers 5 & 8). In addition DRA Farnborough is developing a high rate process using electron beam evaporation and vapour deposition. Materials produced from composite wires exhibit uniform fibre spacing, even at a volume fraction of 57%!

TMCs are an enabling technology for hypersonic airframes and future generation turbine engines. The high specific stiffness, specific strength and environmental resistance at high temperature attainable with TMCs are necessary if the NASP airframe is to have the required low mass fraction. Airframe laminates must support biaxial loading, so they tend to be balanced and in many cases are quasi-isotropic.

The consensus opinion was that the primary near term application of TMCs is in advanced turbine engines. TMCs provide the flexibility to design a new class of compact engines with dramatically increased thrust to weight ratios. Spinning parts require greatest strength in the hoop direction, so unidirectional laminates are possible with fibres wound circumferentially, utilizing the tremendously high unidirectional properties of TMCs. Engine discs now using materials at 550°C (titanium alloys) and 650°C (superalloys) can be replaced with 650°C (titanium alloy matrix composite) and 800°C (titanium aluminide composite) capable material. Estimated improvements include a 60% weight reduction in the combustor and a 130°C gas temperature increase. Compressor rotors can be designed to eliminate the heavy bore section required today for discs, reducing volume and allowing the compressor to be significantly reduced in size.

3.2 Characterisation and Testing

Reactivity studies quantified interaction between fibre and matrix. An interesting result: a high niobium content

Technical Evaluation Report on Structures and Materials Panel Meeting on 'Characterisation of Fibre Reinforced Titanium Matrix Composites', September 1993.

titanium aluminide (Ti-14Al-19Nb) TMC sustained an order of magnitude longer hold time at temperature before the fibre coating was consumed (Paper 9). The result was linked to the decrease of reactivity and diffusion when the aluminum content of the alloy is increased.

A fundamental issue in material development is understanding the link between macromechanical and micromechanical behavior. Shear stresses from fragmentation and push-out tests were compared computationally to increase micromechanical understanding (Paper 9). This knowledge demonstrates significant potential for optimising interface behavior and for predicting macromechanical behavior, i.e. strength, thermal fatigue and bridged crack growth.

An outstanding review was presented summarizing trends in mechanical property data developed since 1990 in support of the NASP program (Paper 1). Data was plotted in several interesting formats. TMC properties (specific strength, specific modulus, failure strain, specific rupture stress, specific fatigue stress range and fatigue crack growth rate) for a number of materials and laminates were plotted versus temperature and compared versus high temperature capability monolithic metals. It was noted that at high temperatures monolithic metals compare favorably with all but unidirectional TMC laminates. TMC and monolithic metal mechanical properties were also plotted versus percent [0] plies, illustrating excellent properties of unidirectional laminates. Balanced laminates are less effective. Strength of quasi-isotropic TMC was shown to be inferior to monolithic metals over the temperature range from room temperature to 800°C.

NASP data was from airframe materials which need not maintain the same degree of precise manufacturing as engine materials. Model TMC engine material, adhering to stringent fibre spacing requirements, demonstrates excellent transverse properties. Unidirectional TMC produced by British Petroleum with a Ti-6-4 matrix attained a transverse failure strain of 1% - 3% (and a longitudinal fibre strain of .98%), depending on fibre volume fraction (Paper 7). Properties were attributed to excellent fibre spacing.

Nondestructive evaluation (NDE) methods were presented for micro-property evaluation and global NDE (Paper 13). During TMC development, micro-property evaluation demonstrated on single fibre model systems was shown to be useful in assessing consolidation, matrix microstructure, fibre fragmentation, and interface oxidation damage. A global NDE method utilized ultrasound to correlate NDE data with tensile and fatigue properties. A damage parameter was developed for use in screening TMC for initial manufacturing flaws and for quantifying in-service damage. This research is in its initial stages of development, but shows great promise.

The philosophy behind a test machine designed specifically for testing low ductility TMCs and CMCs was presented (Paper 12). Since test material is expensive, the test machine was designed to accommodate minimum size test specimens (100mm long). Grip alignment is maintained to high tolerance throughout loading. Grips need no tabs if dogbone specimens are used at room temperature to maintain failure away from the stress concentration of the grips. Specimens are straight sided for elevated temperature testing. The machine incorporates a horizontal load axis to minimize convective cooling and extensometry forces on the specimen. Wright Laboratory has had excellent results testing TMC with this test machine in complicated load scenarios, including low cycle fatigue with compression, thermomechanical fatigue and thermomechanical crack growth. Because European specimens have failed in grips during fatigue testing, researchers have conducted finite element studies and used laser moire interferometry to predict stress concentrations at tabs (Papers 20 & 22). Explanations for these undesirable failures include the facts that a) composites made with the relatively small diameter SM1240 fibre are thinner, thus making misalignment more important, and b) the composite tested was of high quality without defects, so the stress concentration at the grips was more likely to initiate failure.

An ASTM Subcommittee D30.07 round robin in TMC tensile and isothermal fatigue testing at room and elevated temperature has been conducted by six U.S. laboratories (Paper 21). For static tests there was no statistical lab-to-lab variability reported and no statistical difference between data from dogbone and straight specimens. However, there was lab-to-lab statistical variability in fatigue tests, which is currently being examined.

3.3 Life Prediction

Two presentations pointed out the need for improvements in fatigue response of TMCs. Considering the high tensile strength of TMC, the increase in fatigue life of the composite over unreinforced titanium is disappointing (Paper 8). At low stress and a large number of cycles, performance is just equal to that of unreinforced matrix material. In addition, after a few cycles at a fairly low stress level at 650°C, the elastic modulus of a quasi-isotropic laminate drops by 25% (Paper 1).

There was disagreement as to whether sustained load tests should be termed creep. Nonetheless, during sustained load at elevated temperature, matrix stress relaxes and load is shed to the fibres. If the fibres become overloaded, they fail and subsequently the composite fails (Paper 14). In this situation extensive damage is evident throughout the test specimen, not just localized to the material near the fracture surface.

Understanding crack growth in TMCs is the first step in developing lifing procedures based on damage tolerance. An extensive study of crack growth at room temperature indicates that it may be possible to develop crack arrest maps to predict behavior of dominant cracks that form in TMCs (Paper 18). Failure of fibres is controlled primarily by the level of K_{max} applied after fibres have been breached by a matrix crack, and the extent of fibre failure determines composite integrity. It is interesting to note that TIMETAL®21S has a higher K_{max} than other titanium alloys tested. Room temperature crack growth has been measured on large (406 mm x 63.5 mm) center cracked coupons (Paper 15). The work is intended to determine whether results from testing small coupons scale directly to larger coupons representative of airframe structure. If scale effects are to be deciphered, this work must be closely coordinated with persons testing material coupons.

3.4 Design Needs

A presentation discussing TMC modeling required for design was helpful in putting modeling efforts presented at the meeting in perspective (Paper 23). TMC modeling is made difficult by complicated behavior including the presence of thermal residual stresses, plastic flow and viscoplastic behavior, anisotropic yielding, nonlinear stress strain behavior, a difference in tensile and compressive behavior, and the influence of temperature on properties. The importance of proper material modeling during structural design was demonstrated by failure of a large TMC Wing Torque Box at design limit load and room temperature (Paper 2). A factor contributing to the premature failure was the lack of finite element models to account for the difference in static, nonlinear tensile and compressive behavior of TMC.

Both microscopic and macroscopic models are needed for design and behavior understanding. A micromechanical model was presented which utilized a complex unified constitutive theory with many internal state variables (and material constants) to model the viscoplastic behavior of unit cells incorporating fibre and matrix elements (Paper 17). The model is able to represent strain rate effects. Macroscopic models will be the primary tool for analyzing TMC structural designs. The VISCOPLY code incorporates the simple vanishing fibre diameter micromechanics model in a macromechanics laminate code (Paper 19). The viscoplastic model utilized in VISCOPLY captures monolithic and composite response with just two parameters at each temperature. Fibre matrix interface failure is modeled by reducing the fibre modulus in the micromechanics model by a factor of ten. Excellent correlation was achieved between predicted composite stress strain plots and experimental data for a thermomechanical fatigue loading representative of a generic hypersonic flight profile. In addition, constituent fibre and matrix response is predicted. Designers should find the VISCOPLY code to be a very useful analytical tool without excess complexity.

It was previously discussed that laminate mechanical properties vary linearly with the percent of [0] plies (Paper 1). In addition that presentation pointed out that designers of TMC structures must account for TMC weaknesses, such as low transverse strength and relatively low fatigue strength (as compared to the high tensile strength). Hoop wound engine discs take advantage of the superb TMC unidirectional properties. Airframes utilize more balanced laminates to resist biaxial loads. In addition airframes are stiffness critical and must primarily resist buckling (the NASP fuselage demonstration article had a maximum stress of only 16 ksi at design limit load). A judicious selection of laminates is critical to effective airframe design.

Design methods are ultimately evaluated based on their performance in predicting the response of test articles. Both airframe and engine TMC articles have been tested. Large airframe articles fabricated primarily by McDonnell Douglas for the NASP program were fabricated and tested under mechanical and thermal loads in an oxidizing environment (Paper 2). Articles performed well, resisting buckling, the predominant failure mode for stiffness critical fuselage structure. A prototype disc fabricated by Rolls Royce has been tested to overspeed failure (Paper 14). The burst speed of 26,700 rpm attained is 7% higher than predicted from average room temperature tensile test data. These successful test programs lead us to the conclusion that application of TMC could be very near if cost can be reduced.

3.5 Additional Note

AGARD welcomed first time participation by Russia (Paper 6) at a Structures and Materials Panel workshop. The presentation highlighted material properties of Russian TMC made by the foil-fibre-foil technique at the All-Russian Institute of Aviation Materials.

4. CONCLUSIONS

1. Engine application of TMC will probably precede airframe application. Application of TMCs is of strategic importance to engine manufacturers, because of the increased performance and fuel economy achievable through TMC application. International economic competition will drive their use. A promising application is in engine discs, however, it is possible that the first engine application will be for low temperature, stiffness critical parts, exploiting the high modulus of TMC.
2. Cost will determine how soon TMCs will be utilized in aerospace applications. Automated material processing is needed to drive the cost down, and no processes with sufficient automation are available today. Engine parts are relatively small as compared to airframe parts, improving prospects for their automated processing. A number of promising approaches are currently being pursued to produce discs with high material quality (no touching fibres and reproducible properties). The goal of a proposed ARPA project is to reduce material costs for engine components to $500 lb, only achievable with a highly automated process.
3. Inadequate material reproducibility has been a significant problem for organizations evaluating TMC and for efforts at establishing material allowables. It was encouraging that many presentations emphasized methods to process high quality material with reproducible properties.
4. There is no international consensus on test methods for TMC. Success of attaining specimen failure in the gage section for tensile and fatigue testing has been mixed. Solutions for avoiding specimen failure in the grips include high accuracy grip alignment and use of test specimen tabs.
5. TMC test method round robins are extremely valuable for assessing reproducibility of test methods between laboratories. TMC is so expensive that data must be assembled from many organizations to properly characterise material behavior. Additionally, modelers must be confident of basing their models on reliable data.
6. Considerably more work needs to be accomplished to understand TMC damage mechanisms and their evolution under sustained load at high temperature, a topic of prime importance for engine applications. Issues include the difference between data taken with hot and cold grips.
7. NDE of TMCs is in initial development, but early activities show great promise. It is efficient and synergistic to develop NDE methods at the same time that material is being characterised and mechanical property data is being generated.
8. Damage tolerant design methods are necessary for long life engine structures. Safe life is inappropriate. Bridged crack growth must be understood and

modeled, possibly by utilizing the stress intensity factor range due to bridging, ΔK_{br}. Novel designs offer potential to utilize benign, nonpropagating, bridged cracks.

9. Designers must radically alter their designs and modify their methods to successfully incorporate TMC.

5. RECOMMENDATIONS

1. This AGARD workshop should be repeated about four years hence. At that time it might be desirable to combine TMCs and ceramic matrix composites into one meeting on advanced high temperature composites.
2. AGARD members should continue to meet in appropriate forums to discuss test standards and conduct test method round robins. Since AGARD countries are already participating in VAMAS Technical Work Area 15 on Metal Matrix Composites, which plans to include a round robin on TMC, there is no need to conduct a separate AGARD TMC round robin. Contact Steve Johnson at NASA Langley Research Center or Neil McCartney at the National Physical Laboratory for VAMAS details.

Possibilities and Pitfalls in Aerospace Applications of Titanium Matrix Composites

James M. Larsen[1], **Stephan M. Russ**[1], **and J. Wayne Jones**[2]

[1] Materials Directorate, Wright Laboratory
WL/MLLN Bldg 655, 2230 Tenth Street, Suite 1
Wright-Patterson Air Force Base, OH 45433-7817, USA

[2] The University of Michigan
Department of Materials Science and Engineering
Ann Arbor, MI 48109-2136, USA

1. SUMMARY

High-temperature, light-weight materials represent enabling technology in the continued evolution of high-performance aerospace vehicles and propulsion systems being pursued by the U.S. Air Force. In this regard, titanium matrix composites (TMC's) appear to offer unique advantages in terms of a variety of weight-specific properties at high temperatures. However, a key requirement for eventual structural use of these materials is a balance of mechanical properties that can be suitably exploited by aircraft and engine designers without compromising reliability. An overview of the current capability of titanium matrix composites is presented, with an effort to assess the balance of properties offered by this class of materials. Emphasis is given to life-limiting cyclic and monotonic properties and the roles of high-temperature, time-dependent deformation and environmental effects. An attempt is made to assess the limitations of currently available titanium matrix composites with respect to application needs and to suggest avenues for improvements in key properties.

2. INTRODUCTION

Titanium matrix composites [1,2,3], continuously reinforced with silicon carbide (SiC) fibers, are being seriously considered as enabling structural materials in advanced aerospace applications such as high performance turbine engines [4,5] and hypervelocity vehicles [6]. Recognizing that the structural limits of more conventional aerospace materials have largely been reached, aircraft and engine designers have turned to TMC's as a potential avenue to significantly increase performance-to-weight capability. In comparison to currently available aerospace titanium and nickel-base alloys, on a density corrected basis, titanium matrix composites appear to offer important advantages in terms of specific strength and stiffness. Moreover, by selective construction of the composite, it appears possible to improve temperature-dependent properties and resistance to crack growth. The utility of this material system, however, may be dictated by its applicability to the variety of product forms needed by the aerospace industry: for example, nominally unidirectional composite rings and rods to be used in engines and laminated plates and beams needed for aircraft structures. Ultimately, the viability of TMC's will be measured in terms of the balance between specific structural needs and application requirements versus cost and reliability issues.

Within the U.S. Air Force, the Integrated High Performance Turbine Engine Technology (IHPTET) initiative is the primary force driving the introduction of TMC's in turbine engine components. This initiative, which is funded cooperatively by the U.S. Air Force, Army, Navy, National Aeronautics and Space Administration (NASA), and Advanced Research Projects Agency (ARPA), involves research and development by seven major aerospace companies and a variety of Government research organizations. The objective of the program is to double turbine engine propulsion capability through an integrated approach in which advanced materials enable innovative structural designs and improved aerothermodynamics to achieve higher thrust-to-weight ratios and lower specific fuel consumption. Although the major payoff comes from rotating components such as structural rings, a variety of rotating and static components are being considered, including turbine engine blades, vanes, stators, actuators, struts, and nozzles. Most of these applications permit the use of unidirectional composite construction.

Another force behind the development of TMC's is generic hypersonic vehicle technology. Technically defined as achieving speeds of Mach 5 and greater, hypervelocity flight requires new high-temperature materials with improved weight-specific properties. In addition to structural beams, a hypervelocity vehicle will require large areas of structurally-stiffened, composite panels that will experience biaxial loading. In these applications composite laminates of various architectures are anticipated.

Ultimately, the use of TMC's in structural applications will depend on a number of factors that include: life-cycle cost, producibility, a range of mechanical properties, and reliability and maintainability in service. To qualify a new material for use in a critical structural component, a comprehensive testing and

Presented at an AGARD Meeting on 'Characterisation of Fibre Reinforced Titanium Matrix Composites', September 1993.

analysis program must be conducted, and this can only be justified if the payoff for using the material is substantial. TMC's, for example, must demonstrate mechanical properties that exceed, at least in key areas, the capability of less-costly monolithic materials. Coupled with this requirement are the needs for high reliability in extended use and the ability to predict component life accurately.

The objectives of this paper are to examine the state of development of titanium alloy matrix composites and explore the prospects for application of this class of materials for a variety of high temperature aerospace structural applications. The approach will involve comparing and contrasting, on a density corrected basis, first- and second-generation TMC's with more traditional aerospace alloys: monolithic titanium and nickel-base alloys. Emphasis will be placed on considering the balance of properties needed for long-term structural use under realistic combinations of cyclic and sustained load in a high-temperature oxidizing environment. An attempt will be made to relate material properties and the underlying microstructural mechanisms that control useful life and to outline possible avenues for future improvements of this class of materials.

3. MATERIALS

The information to be presented comes from a variety of sources. In each case, a primary consideration was the availability of an extensive range of mechanical property data that could be used in a broad-based comparison of material capability. Results on the first-generation titanium aluminide composite, SCS-6/Ti-24Al-11Nb, are from a U.S. Air Force contract with Allison Gas Turbine Division of General Motors, reported by Gambone [7,8], as well as from efforts by the authors and our colleagues on identical material produced under the contract. Data on the second-generation TMC, SCS-6/TIMETAL®21S, are from recent work of the authors and our Air Force colleagues. The capability of the composite materials, and their monolithic matrix alloys, will be compared with a variety of monolithic materials: the nickel-base superalloy IN100 [9,10], which is used in turbine disks, the high temperature titanium alloy Ti-1100 [11,12,13], and a relatively new titanium aluminide alloy [14]. All the property comparisons are for tests conducted in air. The data are presented on a density-corrected basis because of the anticipated use of the material in turbine engine and aircraft applications, where benefits in weight-specific properties are crucial.

3.1 SCS-6 Fiber

Both of the composites to be discussed contained the silicon carbide fiber SCS-6, manufactured by Textron Specialty Materials Division. The fiber, which is produced by chemical vapor deposition on a carbon monofilament core, is β-phase SiC having a radially columnar grain structure and a double-pass, carbon-rich outer coating, which is added to control reactions with titanium alloy matrices and to prevent fiber damage during normal handling. The fiber has a nominal diameter of 142 μm. The room temperature elastic modulus of the fiber was approximately 385 GPa, and the measured tensile strength of the fiber was 4200 MPa at room temperature and 3620 MPa at 650°C [7].

3.2 SCS-6/Ti-24Al-11Nb

The SCS-6/Ti-24Al-11Nb composite panels, which were nominally 150 mm by 150 mm and 8 plies in thickness, were fabricated at Textron Materials and Manufacturing Technology Center by hot isostatic pressing alternating layers of woven fiber mat and matrix foil. Composite architectures of $[0]_8$, $[0/90]_{2S}$, $[0/\pm45/90]_S$ (quasi-isotropic) were produced, and micrographs of the $[0]_8$ material are presented in Fig. 1. The material contained a nominal fiber volume fraction of 0.35, and the equiaxed microstructure of the matrix alloy (Ti-24Al-11Nb, atomic percent) contained approximately 90 percent continuous α_2 phase (ordered $D0_{19}$ structure) surrounding small islands of disordered β phase [15]. At the fiber-matrix interface, a thin reaction zone is present, and within 5 to 10 μm of the fiber, the composite matrix is single-phase α_2. The development of the microstructure was dictated by the HIP consolidation, which was performed below the β transus, followed by a slow cool to room temperature. General discussion of foil-fiber-foil composite fabrication may be found in [16,17].

3.3 SCS-6/TIMETAL®21S

Metastable beta titanium alloys have received attention as matrix materials for continuous fiber composites, because they overcome the problems of low ambient-temperature ductility and processing difficulties inherent to titanium aluminides such as Ti-24Al-11Nb. (See [18] for a review of the physical metallurgy of metastable beta alloys.) However, a considerable tradeoff in elevated temperature mechanical properties and, to a lesser extent, oxidation resistance is required for the substitution of beta alloys for aluminides in TMC's. A new metastable beta alloy developed by TIMET, designated as TIMETAL®21S (Ti-15Mo-2.7Nb-3Al-0.2Si, weight percent), offers superior oxidation resistance to the Ti-15V-3Cr-3Al-3Sn metastable beta alloy that has been used previously for TMC's, while maintaining the strip formability required for composite fabrication. Oxidation of TIMETAL®21S at 815°C has been reported to be only 3-4 times greater (by weigh gain) than representative alpha-two and gamma titanium aluminides, and is attributed to the presence of Mo as the primary beta phase stabilizer. The retention of room temperature ductility, characteristic of beta alloys, facilitates the fabrication of composites by the foil-fiber-foil method. A representative cross section of a $[0]_4$ composite is shown in Fig. 2. The volume fraction of the $[0]_4$, $[0/90]_S$, and $[0/\pm45/90]_S$ laminates tested was nominally 0.35, although variations in actual volume fraction in this material of ±0.03 existed on a panel-to-panel basis.

Substantial strengthening in this alloy can be produced by solution heat treatment and subsequent aging to form a fine distribution of alpha in a beta matrix. The elevated temperature strength of TIMETAL®21S is considerably better than other metastable beta alloys but certainly not equivalent to the aluminides at the highest anticipated use temperature of 815°C. The standard as-heat-treated microstructure for SCS-6/TIMETAL®21S composites is shown in Fig. 2. Here the SiC fiber, the two fiber coating layers, and the reaction zone resulting from consolidation are visible. The small reaction zone indicates good matrix fiber compatibility, as has been borne out by numerous thermal exposure studies. In this example, aging was carried out for 8 hours at 620°C to produce a fine, uniform intragranular distribution of acicular alpha precipitates in a beta matrix. Aging at this temperature has been shown to preclude the formation of omega phase during thermal exposures at lower temperatures. The alpha precipitate morphology shown in Fig. 2 is stable for extended times at the aging temperature or at lower temperatures. However, exposure to higher temperatures and the influence of oxygen pickup can result in considerable changes in the as-heat-treated microstructure, as is detailed in a later section.

4. MECHANICAL PROPERTIES

The discussion to follow attempts to present an objective comparison of a range of mechanical properties available from the "best" well-characterized material in each of the various classes of advanced aerospace materials. In the monolithic α_2 class, the recently developed Ti-24Al-17Nb-1Mo was identified as having the "best" balance of mechanical properties. However, Ti-24Al-11Nb was also included in some cases where Ti-24Al-17Nb-1Mo data were unavailable. For convenience the following discussion will use the term α_2 alloy to refer collectively to Ti-24Al-17Nb-1Mo and Ti-24Al-11Nb. The terms *α_2 composite* and *β composite* will be used to represent SCS-6/Ti-24Al-11Nb and SCS-6/TIMETAL®21S, respectively.

Since titanium matrix composites are expected to serve as potential replacements for existing aerospace alloys, state-of-the-art high temperature materials were selected as a basis for comparison. The high-temperature turbine engine disk alloy selected was IN100 (PWA specification 1074), an isothermally forged, nickel-base, powder metallurgy alloy produced by Pratt & Whitney Aircraft and used in turbine disks in the F100 engine [9,19]. The other primary material of comparison was the high-temperature titanium alloy Ti-1100 produced by TIMET, Inc. [11-13]. The data from the monolithic materials are represented by mean trend lines; no attempt has been made to use statistical design allowable lower-bound data, since equivalent data were not available for the composites. In all cases the data are presented on a density-corrected (weight-specific) basis using the densities listed in Table 1.

4.1 Tensile Behavior

Figure 3 presents data of density-corrected (specific) ultimate strength of four SCS-6/Ti-24Al-11Nb composite laminates and the fiberless matrix alloy. The data are mildly temperature dependent and illustrate the range of properties offered by various composite architectures of this materials system. The $[0]_4$ composite exhibits a strength approximately three times the strength of the fiberless matrix alloy, although the strength of this material in the $[90]_4$ orientation is approximately half the value of the matrix alone. The laminates exhibit strengths that are roughly proportional to the [0] fiber content. The strength of the matrix alloy and the various laminates decreases only slightly with temperature. A similar plot of SCS-6/TIMETAL®21S laminates is shown in Fig. 4. Here, the trends in laminate strength are similar to those for Ti-24Al-11Nb composite, but the effect of the much higher strength of the TIMETAL®21S matrix alloy at low temperatures is evident. As shown, the matrix alloy is significantly stronger than the $[0/\pm45/90]_S$ composite at room temperature, but the strengths of the two materials cross at 500°C, and the composite has superior strength at the higher temperatures. For purposes of comparison, the data of Figs. 3 and 4 are presented collectively in Fig. 5. Although the TIMETAL®21S composite laminates are significantly stronger at room temperature than all of the equivalent Ti-24Al-11Nb laminates, the significant reduction in strength of the TIMETAL®21S matrix at elevated temperature results in approximately equal strengths for SCS-6/Ti-24Al-11Nb and SCS-6/TIMETAL®21S composites above 650°C. Strengths of the matrix alloys cross at 600°C.

Material	Density (Mg/m^3)	Calculated Density: SCS-6/Matrix $(V_f = 0.35)$
SCS-6 fiber	3.045	
Ti-24Al-11Nb	4.67	4.101
TIMETAL®21S	4.931	4.271
Ti-1100	4.516	
Ti-24Al-17Nb-1Mo	4.93	
IN100	7.868	
Ti-6Al-2Sn-4Zr-2Mo	4.544	

Table 1 – Fiber, alloy, and composite densities used in calculating weight-specific properties.

Because the SCS-6/TIMETAL®21S laminates have superior strengths to equivalent SCS-6/Ti-24Al-11Nb material, and for clarity of presentation, the following two figures omit the latter material. Figure 6 presents data of specific strength of the SCS-6/TIMETAL®21S laminates compared with the yield strengths of the various monolithic aerospace alloys. The yield strengths of most of the laminates were undefined, since these specimens failed before achieving 0.2 percent plastic strain. On this basis the three monolithic alloys fall in a narrow band well below the $[0]_4$ composite, while the $[0/90]_S$ material exceeds the strength of the monolithic alloys at temperatures less than approximately 650°C. The quasi-isotropic material exhibits strengths comparable to the monolithic alloys up to approximately 500°C.

A similar plot of specific ultimate strength of all the materials is presented in Fig. 7. On this basis, Ti-24Al-17Al-1Mo and IN100 display similar behavior, with specific strength approaching the $[0/90]_S$ laminate up to about 500°C. The quasi-isotropic material strength is inferior to all three monolithic materials over the full range of temperature. Of all materials, the unidirectional composite continues to exhibit by far the highest and lowest strength in the $[0]_4$ and $[90]_4$ orientations, respectively.

As shown in the preceding figures, the ultimate strengths of both SCS-6/Ti-24Al-11Nb and SCS-6/TIMETAL®21S are strongly dependent on laminate architecture. This effect is more easily visualized by plotting the strength against a geometric parameter, such as the volume fraction of [0] fibers in the laminate, as illustrated in Figs. 8a and 8b for the β and α_2 composites, respectively, for a variety of temperatures. With the possible exception of the quasi-isotropic laminate, the ultimate strengths are proportional to the volume fraction of [0] fibers. The low strength of the [90] material reflects the very weak fiber/matrix bond that exists in these composites, combined with the effect of matrix strength. Considering the values of the data for the $[0/\pm45/90]_S$ laminates, it appears that the contribution of the [±45] plies is only slightly greater than for [90] plies, and the benefit of the [±45] plies appears to be reduced as temperature increases.

Figure 9 presents data of tensile ductility measured as percent elongation for the composites and the various monolithic materials. All of the laminates exhibit failure strains that are much less than the more conventional materials, although Ti-24Al-17Nb-1Mo approaches the composite ductility at low and high temperature. It should be noted, however, that the plotted failure strain represents total strain at failure for the composites and plastic elongation for the monolithic materials. The low strains at failure for the composites containing [0] plies are dictated by the behavior of the SiC fiber, which fails at a total strain of approximately one percent.

Figure 10 illustrates measurements of specific Young's modulus for the various materials, and only the [0] composites exhibit outstanding behavior. The specific stiffness of the cross-ply and $[90]_8$ laminates is slightly higher than that of conventional materials. These data are somewhat misleading, however, because the measurements were from initial loading of tension tests. During initial loading, separation of the fiber/matrix interface occurs in the off-axis plies, and thereafter a drop in modulus is often observed in laminates containing off-axis fibers. For example, as shown in Fig. 11, in fatigue at 650°C SCS-6/TIMETAL®21S $[0/\pm45/90]_S$ laminates undergo a drop in modulus of approximately 25 percent during the first few cycles of fatigue.

4.2 Stress Rupture

To provide a measure of long-term, high-temperature capability of the various materials, the Larson-Miller parameter was used to correlate stress-rupture lives for a range of test conditions. The density-corrected Larson-Miller plot, shown in Fig. 12a, presents data from both composite systems and the comparison materials. The $[0]_8$ and $[90]_8$ SCS-6/Ti-24Al-11Nb composite orientations exhibit the best and the worst capability of this material, respectively, and the associated $[0/90]_S$ and $[0/\pm45/90]_S$ laminates data fall in the intermediate range. The available data [20] indicate that the SCS-6/TIMETAL®21S composite significantly outperforms the α_2 composite in all but the [90] orientation. The IN100, Ti-24Al-17Nb-1Mo, and Ti-1100 monolithic alloys are obviously competitive with the SCS-6/Ti-24Al-11Nb cross-ply laminates, but the TIMETAL®21S composite has significantly more attractive properties. For clarity, Fig. 12b re-plots these results, omitting the SCS-6/Ti-24Al-11Nb data. The β composite laminates exhibit good creep resistance, particularly considering the extremely limited creep capability of the monolithic β matrix alloy.

As shown in Fig. 13, the creep capability of the various laminates is proportional to the volume fraction of [0] plies. The [0] plies are primarily responsible for the measured creep resistance, while the [90] and [±45] plies contribute very little to creep resistance. The creep rupture capability of the [90] oriented specimens is controlled by the creep resistance of the matrix alloy, which is substantially better for Ti-24Al-11Nb than TIMETAL®21S. It is speculated that the difference in slope between the two composite systems is due to the presence of a Mo crossweave that was used in weaving the fiber mat in the Ti-24Al-11Nb composite. As will be discussed, this crossweave oxidized readily, leading to early cracking and penetration of the atmosphere to the fiber-matrix interface region and resulting degradation of the fibers.

4.3 Fatigue

Assessing the fatigue capabilities of a variety of materials is an involved process, considering the wide range of potential usage and test conditions. For comparison purposes, data are presented for tests performed at 650°C and stress and strain ratios of near 0. Fig. 14 compares density-corrected trends from available data for the β composite, the α_2 composite, IN100, and Ti-24Al-11Nb monolithic materials. Monolithic Ti-24Al-11Nb was used for this comparison as opposed to Ti-24Al-17Nb-1Mo or Ti-25Al-10Nb-3V-1Mo because of a lack of data in the literature on the latter alloys at the necessary temperatures and stress ratios. The trend for the Ti-24Al-11Nb plate material was taken from two sets of data, one at a strain ratio of 0 and 0.17 Hz and the other at a stress ratio of 0.05 and 30 Hz, generated under a contract performed by Pratt and Whitney Aircraft [21]. The IN100 curve was supplied to the authors by Pratt and Whitney Aircraft and is an estimate based on low cycle fatigue at other temperatures and yield stress data [22]. The SCS-6/Ti-24Al-11Nb $[0]_8$ curve was generated using a frequency effect model proposed by Nicholas and Russ for this composite system [23]. The model predicts cycles-to-failure as a function of applied stress and was developed using data at frequencies ranging from 0.0028 to 30 Hz. The curve in Fig. 14 represents the predicted values for a frequency of 1 Hz. The SCS-6/TIMETAL®21S curves describe data generated by the authors, and all tests were performed at a stress ratio of 0.1 and 1 Hz. The trends indicate that the two [0] composites have very similar S-N behavior at 650°C and show significant improvement over the monolithic Ti-24Al-11Nb. The unidirectional composites do not show the same advantage over IN100; when comparing lives for a specific stress range of 110 MPa/(Mg/m^3) the fatigue lives of all three materials are within a factor of 2. However, the composites may be superior for higher stresses with lifetimes below 10^5 cycles, where IN100 data were not available. The $[0/90]_S$ and $[0/\pm45/90]_S$ SCS-6/TIMETAL®21S laminates demonstrate performances worse than the monolithic materials and the unidirectional composites over the entire range of lives compared.

Looking at the reduction in specific fatigue strength as a function of the [0] fiber volume fraction in the SCS-6/TIMETAL®21S composite, Fig. 15, with the exception of the $[0/90]_S$ lay-up, a relatively linear relationship is evident. For this comparison, values of specific stress range were taken at 10^4 and 10^5 cycles from the curves representing the laminates' S-N behavior. Data on a [0/90/0] lay-up have also been included for completeness. Multiple small cracks initiating at [90] fibers have been observed under comparable test conditions by Russ and Hanson for a $[0/90]_{2S}$ lay-up [24] and may provide the explanation for the relatively low fatigue lives of this laminate.

4.4 Fatigue Crack Growth

Material comparisons on the basis of fatigue crack propagation are also particularly complex. In addition to effects of temperature, stress ratio, and frequency, crack growth rates in TMC's depend acutely on the degree of crack bridging by unbroken fibers, which is dependent on specimen geometry and stress level. For illustrative purposes, however, some example data for tests of [0] material in the two composite materials are presented in Fig. 16, along with data from some of the monolithic comparison materials. The SCS-6/Ti-24Al-11Nb [25,26] and SCS-6/TIMETAL®21S [27] composite data represent crack growth in specimens containing a center hole tested at a range of stress levels at 650°C, R=0.1, and the indicated frequencies. Significant, although incomplete, crack bridging occurred in both composite materials, giving rise to excellent crack growth resistance. Although not shown, data from $[0/90]_S$ and $[0/\pm45/90]_S$ SCS-6/TIMETAL®21S tests indicate much more rapid crack growth rates, consistent with the volume fraction of [0] fibers in each laminate.

5. MICROSTRUCTURAL STABILITY AND DAMAGE MECHANISMS

Some of the shortcomings evident in the data of both SCS-6/Ti-24Al-11Nb and SCS-6/TIMETAL®21S are associated with microstructural and mechanistic issues that are now reasonably well understood, as discussed below. Eliminating, or minimizing, these effects in future titanium matrix composite materials provides approaches to improvement of overall material performance.

5.1 SCS-6/Ti-24Al-11Nb

Crossweave Effects

Much of the SCS-6/Ti-24Al-11Nb composite fabricated to date has incorporated molybdenum crossweave wire to maintain fiber spacing during fabrication. Superior room temperature tensile properties of composites consolidated with this crossweave was the basis for its choice; however, in-depth characterization of mechanical properties in a number of studies has revealed the detrimental nature of the Mo crossweave [23,28,29]. Not only does Mo form brittle intermetallic reaction products with Ti-24Al-11Nb [30], it also forms MoO_3 which is volatile above 700°C [31]. When present on exposed composite surfaces in air at high temperatures, these crossweave wires oxidize and provide a direct path for environmental attack of the fibers. This attack is manifested by the presence of molybdenum on many fracture surfaces of specimens tested at elevated temperature in air under tension, creep, and thermal and thermomechanical fatigue. Figure 17 presents an example of composite damage due to oxidation of the Mo crossweave [3].

Ideally, if a crossweave is to be utilized, it should be manufactured from the same alloy as the matrix. However, progress in the processing of ribbon and thin gage wire must be made before identical alloys for both matrix and crossweave can be incorporated into intermetallic matrix composites. The use of alternative crossweave materials [32], in spite of their improved performance over molybdenum, are generally considered interim solutions, and a transition to composite processing techniques that avoid the use of crossweave materials altogether is an option currently being considered.

Thermal Fatigue/Environmental Effects

Thermal fatigue of TMC's results in significant variations in constituent residual stress states [33] due to the large difference in coefficient of thermal expansion (CTE) between the matrix and the fiber ($CTE_{matrix} \approx 2 * CTE_{fiber}$). SCS-6/Ti-24Al-11Nb has been shown to be particularly vulnerable to damage by thermal fatigue [34,35,36,37], due to the low tolerance of the matrix alloy to interstitial oxygen, which leads to oxide notch formation and crack growth [38]. It has been shown that thermal cycling $[0]_4$ SCS-6/Ti-24Al-11Nb between 150 and 815°C in air results in almost a total loss in residual strength after only 500 cycles, while no effect on strength was observed when the material was cycled in an inert environment [3]. Although elimination of the atmosphere alleviated the environmental problem, initial attempts to use a surface coating to achieve the same protection were unsuccessful due to early cracking of the coating, which lead to a rate of loss in residual strength equivalent to the uncoated material [3].

5.2 SCS-6/TIMETAL®21S

As described earlier, metastable beta alloys such as TIMETAL®21S have received considerable attention as matrices for TMC's, in part, because they offer substantial improvements in ambient-temperature ductility, albeit at a substantial loss in elevated temperature strength when compared to titanium aluminides, such as Ti-24Al-11Nb. At the higher intended service temperatures, however, microstructure evolution, surface and interface oxidation, and matrix oxygen enrichment create a situation where matrix and composite mechanical properties are strongly dependent on thermal history.

Figure 18 shows the interior and near-surface microstructures of a $[0]_4$ SCS-6/TIMETAL®21S composite subjected to isothermal exposure in air at 815°C for 500 ks (139 hours). In the specimen interior, where oxygen enrichment is minimized, the development of a coarse distribution of blocky alpha is observed, as shown in Fig. 18a. The near-surface matrix microstructure for this exposure is shown in Fig. 18b. Air exposure has led to the development of a substantial oxide scale and to the stabilization of a high volume fraction of acicular alpha. Although, considerably coarser than the alpha in the as-heat-treated microstructure, the alpha morphology resulting from oxygen stabilization is considerably finer than that observed farther from the specimen surface.

Paris and Bania [39] have shown that considerable strengthening can result from oxygen levels above 0.25 w% in TIMETAL®21S. This strengthening is accompanied by a substantial loss in room temperature ductility. This is illustrated dramatically in Figure 19 which shows the room temperature tensile fracture surface of an as-heat-treated $[0]_4$ SCS-6/TIMETAL®21S sample, Fig. 19a, and a sample which had been thermally cycled for 500 cycles between 150 and 815°C, Fig. 19b. In the as-heat treated sample, matrix failure is by microvoid coalescence, and the fracture is completely ductile. In the thermally cycled sample, however, the outer matrix region fails in a macroscopically brittle manner, illustrating the damaging influence of oxygen embrittlement during the relatively modest time at the higher temperatures during thermally cycling.

Under service conditions where significant oxygen contamination can be anticipated, it is clear that the as-heat-treated properties in alloys such as TIMETAL®21S cannot be used to model or predict damage accumulation processes over an extended service lifetime. For example, Revelos et al [38] have demonstrated that the damage accumulation processes in thermal fatigue of composites with a TIMETAL®21S matrix are essentially the same as those observed in similar composites with Ti-24Al-11Nb as the matrix. Thermal fatigue in continuous fiber composites is essentially an out-of-phase thermomechanical fatigue condition where matrix damage predominates. Based on starting microstructures it would be expected that the more ductile TIMETAL®21S matrix would be substantially less prone to thermal fatigue degradation than Ti-24Al-11Nb. The susceptibility of TIMETAL®21S to thermal fatigue, and by inference to thermomechanical fatigue, can be attributed to embrittlement of the near-surface regions by oxygen and to the development of oxide notching as a major damage mechanism. These damage accumulation processes are shown in Fig. 20 where a longitudinal section reveals the penetration of an oxide-filled crack which has progressed from the surface to the first fiber layer, resulting in severe fiber interface degradation by oxidation. Thus oxide scale formation and subsequent cracking, coupled with near-surface matrix embrittlement promote relatively rapid damage accumulation during thermal fatigue and, in effect, render the potential improvements from a more ductile (as-heat-treated) matrix ineffective.

6. DISCUSSION

The range of mechanical properties possible from titanium matrix composite laminates represent an important, exploitable asset of this class of materials, but tailoring these materials to suit specific application needs must be accomplished with full knowledge of the long-term ramifications of the selected approach. Significant property enhancements are very often achieved by sacrificing other properties, and material and structural designers must be ever vigilant to avoid solving one problem by creating another.

At present the extremely limited availability of fibers compatible with the aggressive processing steps required in fabrication of titanium alloy composites severely restricts options for design and development of improved materials in this class. Thus, most of the recent efforts to develop improved TMC's have focused on the matrix alloy. In this regard, comparison of the first- and second-generation materials employing the same fiber (SCS-6) but having titanium matrices (Ti-24Al-11Nb and TIMETAL®21S) with dramatically different properties provides insight into the potential improvements in TMC's through matrix alloy selection.

As shown in Figs. 3-5, a significant improvement in composite strength at low temperatures was achieved by substituting TIMETAL®21S for Ti-24Al-11Nb, but no advantage was exhibited at the higher temperatures. Each of the materials in the [0] orientation was of substantially greater strength than the conventional monolithic alloys, but the corresponding [90] strength severely limits the possible applications of such a unidirectional composite. Achieving more balanced in-plane strength by constructing laminates containing off-axis plies significantly reduces the maximum strength – in some cases to values less than those possible from existing monolithic materials, particularly on the basis of specific ultimate strength. Obviously, tailoring the laminate to fit the specific structural need is essential.

The limited ductility available from these composites (Fig. 9) represents a significant challenge to structural designers who have traditionally had the luxury of using much more forgiving materials. Although ductility is not typically a design limiting property, ductility sufficient to accommodate structural assembly is necessary, and the ability to redistribute concentrated loads is important.

As shown in Fig. 10, laminates containing off-axis plies do not exhibit the outstanding stiffness available from [0] composites, and an appreciable drop in stiffness of the cross-ply laminates occurs during fatigue (Fig. 11). Both of these factors place an additional premium on laminate tailoring.

Composite creep also represents a significant design challenge. Although [0] plies significantly resist creep strains, [90] and [±45] off-axis plies pose little resistance to creep. This fact, combined with [0]-ply matrix stress relaxation due to creep, tends to quickly increase [0] fiber stress in cross-ply laminates. As shown, the SCS-6/TIMETAL®21S cross-ply laminates demonstrate relatively good creep capability. As discussed below, however, interpretation of the significance of these composite data is complicated.

A key concern involved in applying coupon creep data to prediction of behavior of a structural component relates to load transfer between the fiber and the matrix. It is well known that transfer of interfacial shear stress in both SCS-6/Ti-24Al-11Nb and SCS-6/TIMETAL®21S composites occurs primarily due to the compressive residual stress which clamps the matrix around the fiber at low temperatures. At elevated temperatures this residual stress approaches zero, due to the differential thermal expansion between the matrix and the fiber. In conventional test specimens, mechanical grips are used to apply loads to the ends of the specimen. Under these circumstances [0] fibers are artificially loaded at their ends, significantly enhancing load transfer. In structural applications, no such compressive force will be applied, and load transfer must occur naturally. This is particularly acute at the points of introduction of loads into the structure. In structural rings, which are essentially continuous unidirectional composites, loading is largely circumferential. However, most other geometrical configurations require loading either by bonded joints or pin loading. Under these circumstances fiber/matrix load transfer and matrix creep behavior become crucial, suggesting that the poor creep capability of β titanium alloys such as TIMETAL®21S may be a severe detriment.

The fatigue data of Fig. 14 are somewhat alarming. The SCS-6/TIMETAL®21S $[0/90]_S$ and $[0/\pm45/90]_S$ laminate data fall well below the capability of monolithic IN100 and Ti-24Al-11Nb. Although the [0] data for both the α_2 and β composites appear approximately equivalent to the IN100 data, it should be noted that, while the specific tensile strengths of the two composites were approximately equal at 650°C, their [0] strength was approximately double that of the IN100. Obviously this strength advantage was not retained in these fatigue tests. Based on the equivalence of the [0] data for the two composites, there appears to be no appreciable effect of alloy matrix on [0] fatigue performance under these 650°C test conditions, indicating a dominant role for the fiber. This has been demonstrated through analytical modeling for TMF lives [40,41] for both SCS-6/Ti-24Al-11Nb and SCS-6/TIMETAL®21S. Although not available, the associated data for fatigue in the [90] orientation can be expected to be very low.

The presence of [0] fibers in the composites offers significant advantages in terms of improved resistance to fatigue crack propagation. As noted earlier, the beneficial effect of crack bridging tends to scale with the volume fraction of [0] fibers.

Thermal fatigue, combined with environmental effects, poses an unusual problem due to the cyclic residual stresses in the composite matrix, which are not present in unconstrained monolithic materials subjected to thermal cycling. As noted earlier, titanium composites of both matrices undergo significant damage under thermal fatigue, and the mechanisms of damage are essentially the same for both materials. A protective coating may provide a solution to this problem *if* the integrity of the coating can be maintained throughout the composite's service life.

7. CONCLUDING REMARKS

A key issue in the comparison of TMC properties with the monolithic materials is the performance of the various laminates. Although [0] data for the various mechanical properties were often outstanding, properties of the [90] orientation of the same material were typically extremely low, and the laminate behavior was roughly described by a rule mixtures of the lamina. In many instances the $[0/\pm45/90]_S$, and to a lesser extent the $[0/90]_S$ laminates exhibited mechanical properties that were approximately equal to, or less than, properties available from the monolithic materials. Many of the deficiencies in the mechanical behavior of [90] and cross-ply laminates appear to be the result of the very weak fiber/matrix interface under transverse stress, which severely restricts the load carrying capability of the off-axis plies. Recognizing that the issues of material cost and reliability in extended service must still be addressed, it appears that use of laminates of either of the TMC's examined must proceed with great care. It is essential that the laminates be tailored to the specific application, with full recognition of the specific design needs. For example, composite ring components in turbine engines must be designed such that the radial stresses do not exceed the [90] properties of the unidirectional composite, if this material is to be used. In panel configurations, it is crucial that the laminate be tailored to fit the actual stress state, in order to utilize the attractive properties that TMC's potentially offer.

It should be remembered that SCS-6/Ti-24Al-11Nb represents a first-generation titanium aluminide composite, and although SCS-6/TIMETAL®21S shows significant advances, further improvements in TMC properties through design of the composite as a system (fiber, matrix, and interface) appear likely. Future materials offer important potential improvements in terms of environmental resistance, as well as matrix strength and creep resistance at high temperatures and ductility at low temperatures. Presently, the development of high temperature titanium matrix composites using an integrated approach are targeting improvement in matrix alloys to circumvent the environmental and ductility limitations of first-generation alloys. Titanium alloys that contain the orthorhombic Ti_2AlNb phase exhibit significantly higher room-temperature ductility, toughness, and specific strength than Ti-24Al-11Nb [42,43]. Smith et al [44,45] chose this class of alloys (specifically, Ti-22Al-23Nb) as an improved matrix material based upon knowledge of the limitations of existing matrix alloys. Moreover, efforts are underway to improve transverse creep and tensile properties by developing fiber coatings to improve fiber/matrix bonding without sacrificing the fracture toughening benefits that exist under [0] loading. More research in this area is, however, required. Another potential avenue for improvement in properties, particularly for cross-ply laminates, is to increase the fiber volume fraction (V_f). Not only does increasing V_f have the potential to improve the various mechanical properties, but it also results in a reduction of composite density. However, careful selection and processing of the matrix material, combined with innovative consolidation methods, will probably be required to achieve a meaningful increase in fiber volume fraction.

From the point of view of composite usage and reliability in critical structural applications, it is clear that design philosophies must be developed for using materials that have very limited ductility. In addition, methods for nondestructive evaluation of initial and service-induced damage must be developed and demonstrated, and much work is needed to develop mature approaches for life prediction of these materials in the complex thermomechanical environment in which they are required to operate.

Ultimately, the widespread use of titanium matrix composites will depend on a combination of factors that include life-cycle cost, fabricability, consistent material properties that significantly exceed capabilities of current materials, and reliability in long-term service. Although a number of important advancements are in progress, much work remains, and unprecedented cooperation among the materials-development and mechanical-design communities will be required to attain the full potential of these novel materials.

8. ACKNOWLEDGMENTS

This overview was compiled by the authors, two of which (J. M. Larsen and S. M. Russ) are members of the Materials Behavior Branch, Materials Directorate, Wright Laboratory, Wright-Patterson Air Force Base, OH and were funded by the Air Force Office of Scientific Research under project 2302P101. J. W. Jones, a Materials Directorate visiting scientist on sabbatical leave from the University of Michigan, was supported under a contract with Systran Corporation of Dayton, Ohio. We would like to acknowledge the helpful efforts of E. J. Dolley and A. L. Hutson who aided in collection, analysis, and presentation of the data.

9. REFERENCES

1. J. M. Larsen, K. A. Williams, S. J. Balsone, and M. A. Stucke, *High Temperature Aluminides and Intermetallics*, S. H. Whang, C. T. Liu, D. P. Pope, J. O. Stiegler, Eds. (The Minerals, Metals & Mater. Soc., Warrendale, PA, 1990) pp. 521-556.
2. R. A. MacKay, P. K. Brindley, and F. H. Froes, *JOM*, pp. 23-29, May, 1991.
3. J. M Larsen, W. C. Revelos, and M. L. Gambone, "An Overview of Potential Titanium Aluminide Matrix Composites in Aerospace Applications," *Intermetallic Matrix Composites II*, D. B. Miracle, D. L. Anton, and J. A. Graves, Eds., MRS Proceedings, Vol. 273, Materials Research Society, Pittsburgh, PA, 1992, pp. 3-16.
4. Wright Laboratory (WL/POT), "Integrated High Performance Turbine Engine Technology Initiative," Wright-Patterson AFB, OH, 1991.
5. S. W. Kandebo, *Aviation Week & Space Technology*, February 24, 1991.
6. T. M. F. Ronald, *Advanced Materials & Processes*, 29-37, 1989.
7. M. L. Gambone, "Fatigue and Fracture of Titanium Aluminides, Vol. I," U.S. Air Force report WRDC-TR-89-4145.I, Wright-Patterson Air Force Base, OH, 1989.
8. M. L. Gambone, "Fatigue and Fracture of Titanium Aluminides, Vol. II," U.S. Air Force report WRDC-TR-89-4145.II, Wright-Patterson Air Force Base, OH, 1989.
9. J. M. Larsen, B. J. Schwartz, and C. G. Annis, Jr., "Cumulative Damage Fracture Mechanics Under Engine Spectra," Air Force Materials Laboratory Report AFML-TR-79-4159, Wright-Patterson Air Force Base, OH, 1979.
10. B. A. Cowles, private communication, Pratt & Whitney Aircraft, West Palm Beach, FL, 1989.
11. P. J. Bania, "An Advanced Alloy for Elevated Temperatures," *J. of Metals*, 1988, pp. 20-22.
12. P. J. Bania, "Ti-1100: A New Elevated Temperature Titanium Alloy," *Space Age Metals Technology*, SAMPE, 1988, pp. 286-297.
13. P. J. Bania, "Ti-1100: A New High Temperature Titanium Alloy," *Proc. Sixth World Conference on Titanium*, Cannes, France, 1988, P. Lacombe, R. Tricot, and G. Beranger, Eds., (Societe Francaise de Metallurgie, Les Editions de Physique, Les Ulis, France, 1989).
14. M. J. Blackburn and M. P. Smith, "Development of Improved Toughness Alloys Based on Titanium Aluminides," U.S. Air Force report WRDC-TR-89-4045, Wright-Patterson Air Force Base, OH, 1989.
15. P. R. Smith, C. G. Rhodes, and W. C. Revelos, in *Interfaces in Metal-Ceramic Composites*, R. Y. Lin, et. al., eds., TMS Warrendale, PA, 1990, pp. 35-58.
16. S. L. Semiatin, R. L. Goetz, and W. R. Kerr, "Consolidation of Continuous Fiber Intermetallic Matrix Composites," *Intermetallic Matrix Composites II*, D. B. Miracle, D. L. Anton, and J. A. Graves, Eds., MRS Proceedings, Vol. 273, Materials Research Society, Pittsburgh, PA, 1992, pp. 351-364.

17. C. C. Bampton and J. A. Graves, "Process Modeling for Titanium Aluminide Matrix Composites," *Intermetallic Matrix Composites II*, D. B. Miracle, D. L. Anton, and J. A. Graves, Eds., MRS Proceedings, Vol. 273, Materials Research Society, Pittsburgh, PA, 1992, pp. 366-376.
18. F. H. Froes and H. B. Bomberger, "The Beta Titanium Alloys," *J. of Metals*, 37(1985)28-37.
19. B. A. Cowles, Private Communication, Pratt and Whitney Aircraft, West Palm Beach, FL, 1989.
20. M. Khobaib, University of Dayton Research Institute, Dayton, OH, USA, 1993.
21. D. P. DeLuca, B. A. Cowles, F. K. Haake, and K. P. Holland, "Fatigue and Fracture of Titanium Aluminides," U.S. Air Force Report WRDC-TR-89-4136, Wright-Patterson Air Force Base, OH, February 1990, p. 284.
22. J. Fisher, Pratt and Whitney Aircraft, West Palm Beach, FL, private communication, August 1993.
23. T. Nicholas and S. M. Russ, "Elevated Temperature Fatigue Behavior of SCS-6/Ti-24Al-11Nb," *Journal of Materials Science and Engineering*, A153, 1992, pp. 514-519.
24. S. M. Russ and D. G. Hanson, "Fatigue and Thermomechanical Fatigue of a SiC/Titanium $[0/90]_{2S}$ Composite," *Fatigue '93, Vol. II*, J. P. Bailon and J. I. Dickson, Eds., Chameleon Press, London, U.K., 1993, pp. 969-974.
25. J. R. Jira and J. M. Larsen, "Crack Bridging Behavior in Unidirectional SCS-6/Ti-24Al-11Nb Composite," in *FATIGUE 93, Vol. 2*, J.-P. Bailon and I. J. Dickson, Eds., Engineering Materials Advisory Services, Ltd., *U. K., 1993, pp. 1085-1090.*
26. R. John, J. R. Jira, J. M. Larsen, and N. E. Ashbaugh, "Analysis of Bridged Fatigue Cracks in Unidirectional SCS-6/Ti-24Al-11Nb Composite," in *FATIGUE 93, Vol. 2*, J.-P. Bailon and I. J. Dickson, Eds., Engineering Materials Advisory Services, Ltd., U. K., 1993, pp. 1091-1096.
27. J. M. Larsen, J. R. Jira, R. John, and N. E. Ashbaugh, "Crack Bridging Effects in Notch Fatigue of SCS-6/β21S Composite," presented at the 1993 TMS Annual Meeting, Denver, CO, Feb. 1993.
28. M. Khobaib, in Proceeding of the American Society for Composites, edited by S. S. Sternstein (Technomic Publishing, Lancaster, PA 1991) pp. 638-647.
29. B. R. Kortyna and N. E. Ashbaugh, U.S. Air Force report WL-TR-91-4020, P. R. Smith, S. J. Balsone, and T. Nicholas, Eds., Wright-Patterson Air Force Base, OH, February 1991, pp. 467-483.
30. G. Das, presented at the 1991 TMS Annual Meeting, New Orleans, LA, 1991 (unpublished).
31. M. G. Fontana and N. D. Green, *Corrosion Engineering*, McGraw Hill, New York, 1978, p. 179.
32. M. Mrazek, S. M. Russ, and J. M. Larsen, presented at the 1990 American Institute for Aeronautics and Astronautics Mini-Symposium, Dayton, OH, June 1990 (unpublished).
33. D. Coker, N. E. Ashbaugh, and T. Nicholas, "Analysis of Thermomechanical Cyclic Behavior of Unidirectional Metal Matrix Composites," *Thermomechanical Fatigue Behavior of Materials, ASTM STP 1186*, H. Sehitoglu, Ed., 1993, pp. 50-69.
34. S. M. Russ, "Thermal Fatigue of Ti-24Al-11Nb/SCS-6" in *Metallurgical Transactions A*, 1990, vol. 21A, pp. 1595-1602.
35. W. C. Revelos and I. Roman, "Laminate Thickness and Orientation Effects on an SCS-6/Ti-24Al-11Nb Composites Under Thermal Fatigue," *Intermetallic Matrix Composites II*, D. B. Miracle, D. L. Anton, and J. A. Graves, Eds., MRS Proceedings, Vol. 273, Materials Research Society, Pittsburgh, PA, 1992, pp. 53-58.
36. W. C. Revelos and P. R. Smith, *Metall. Trans. A*, 23, 587 (1992).
37. P. K. Brindley, R. A. MacKay, and P A. Bartolotta in *Titanium Aluminide Composites*, P. R. Smith, S. J. Balsone and T. Nicholas, Eds., WL-TR-91-4020, Wright-Patterson AFB, OH, 1991, pp. 484-496.
38. W. C. Revelos, J. W. Jones, E. Dolley, submitted to Metallurgical Transactions, 1993.
39. W. M. Parris and P. J. Bania, "Oxygen Effects on the mechanical Properties of TIMETAL®21S", submitted for publication.
40. S. M. Russ, T. Nicholas, M. Bates, and S. Mall, "Thermomechanical Fatigue of SCS-6/Ti-24Al-11Nb Metal Matrix Composite," *Failure Mechanisms in High Temperature Composite Materials*, AD-Vol. 22/AMD-Vol. 122, G. K. Haritos, G. Newaz and S. Mall, Eds., American Society of Mechanical Engineers, New York, 1991, pp. 37-43.
41. S. Mall, D. G. Hanson, T. Nicholas, and S. M. Russ, "Thermomechanical Fatigue Behavior of a Cross-Ply SCS-6/β21-S Metal Matrix Composite," *Constitutive Behavior of High Temperature Composites*, MD-Vol. 41, B. S. Majumdar, G. M. Newaz and S. Mall, Eds., American Society of Mechanical engineers, New York, 1992, pp. 91-106.
42. S. Ashley, *Mechanical Engineering*, 49-52 (Dec. 1991).
43. R. G. Rowe, *Advanced Materials & Processes*, 33-35 (Mar 1992).
44. P. R. Smith, J. A. Graves, and C. G. Rhodes, "Evaluation of a SCS-6/Ti-22Al-23Nb Orthorhombic Composite," *Intermetallic Matrix Composites II*, D. B. Miracle, D. L. Anton, and J. A. Graves, Eds., MRS Proceedings, Vol. 273, Materials Research Society, Pittsburgh, PA, 1992, pp. 43-52
45. J. A. Graves, P. R. Smith, and C. G. Rhodes, "Evaluation of a Ti-22Al-23Nb Orthorhombic Alloy for Use as the Matrix in a High Temperature Ti-Based Composite," *Intermetallic Matrix Composites II*, D. B. Miracle, D. L. Anton, and J. A. Graves, Eds., MRS Proceedings, Vol. 273, Materials Research Society, Pittsburgh, PA, 1992, pp. 31-42.

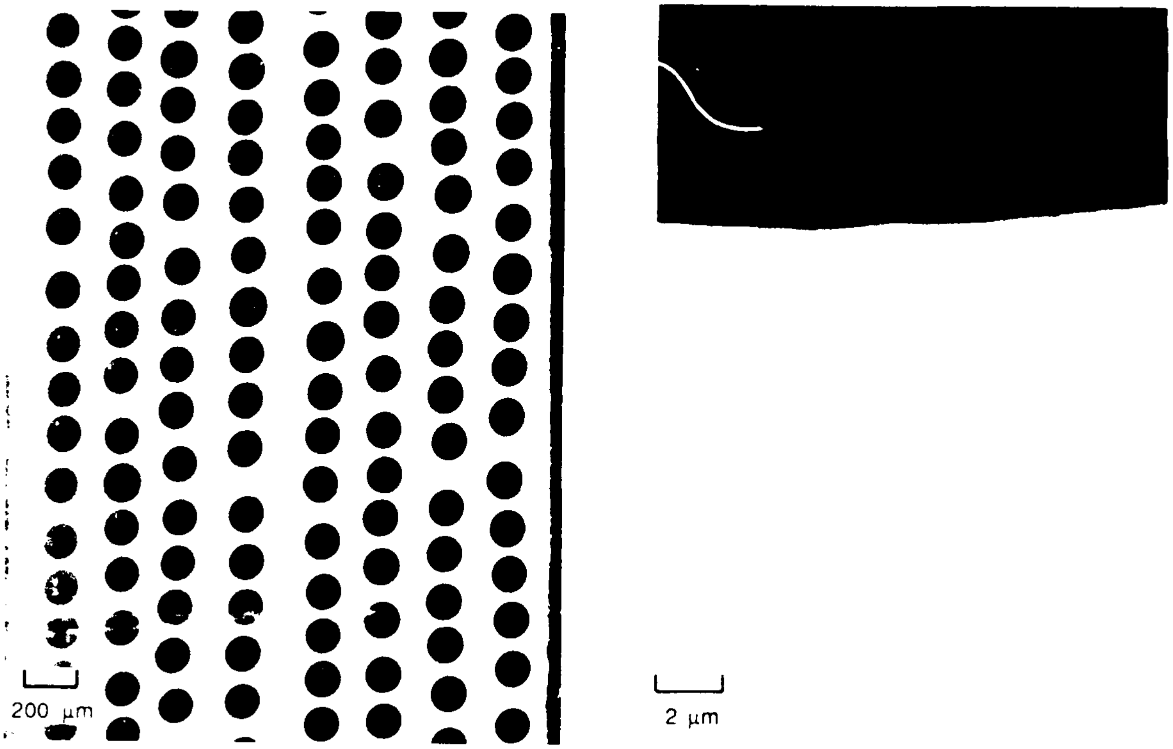

Fig. 1. Micrographs of $[0]_8$ SCS-6/Ti-24Al-11Nb

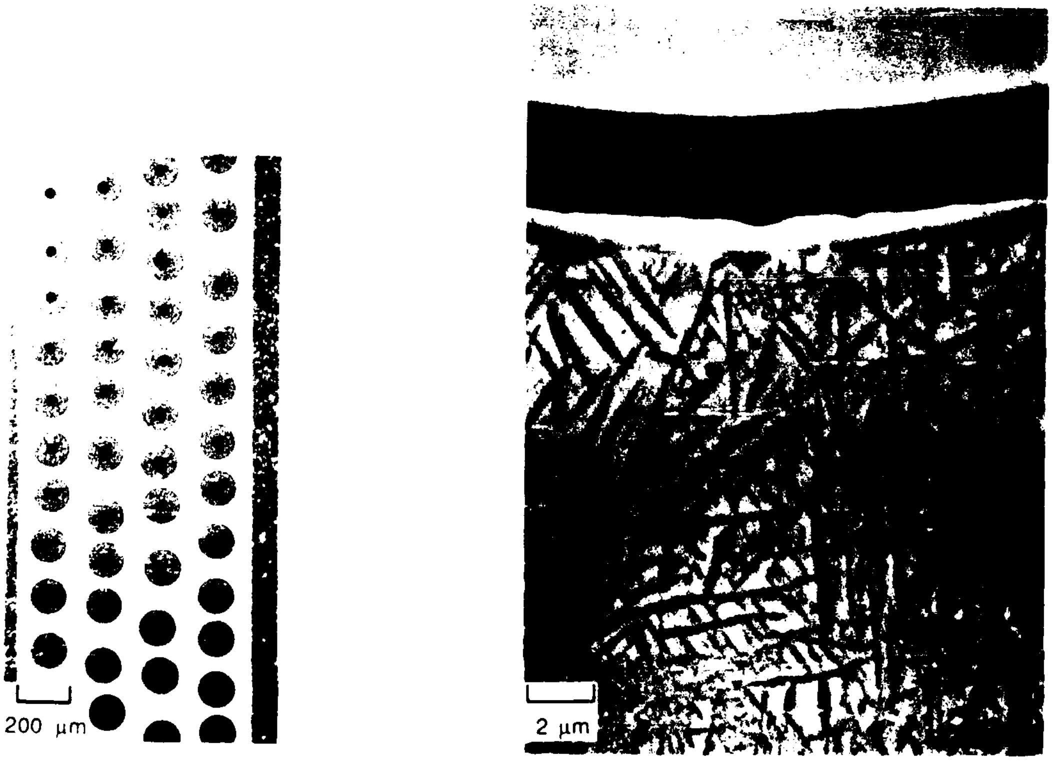

Fig. 2. Micrographs of $[0]_4$ SCS-6/TIMETAL®21S

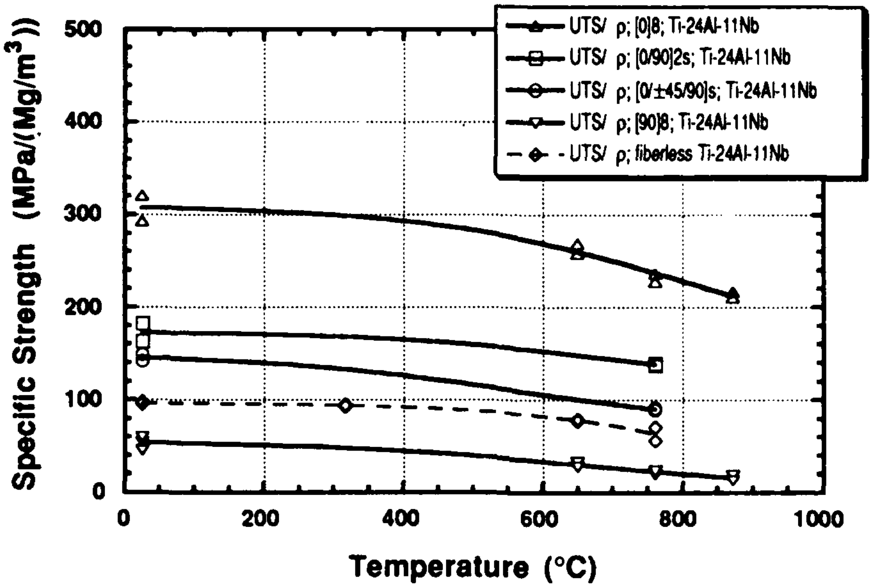

Fig. 3. Density-corrected ultimate strengths of SCS-6/Ti-24Al-11Nb laminates and fiberless Ti-24Al-11Nb.

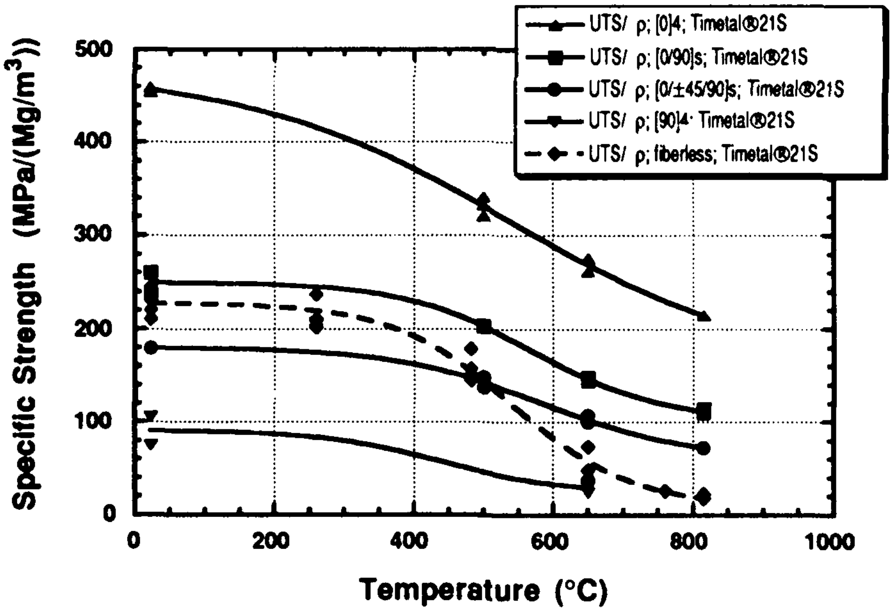

Fig. 4. Density-corrected ultimate strengths of SCS-6/TIMETAL®21S laminates and fiberless TIMETAL®21S.

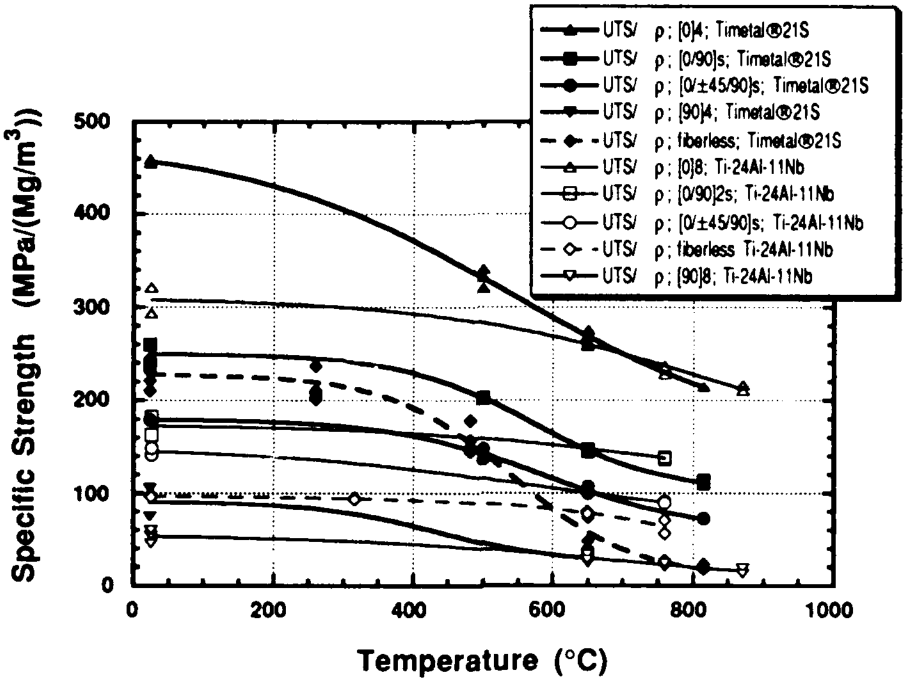

Fig. 5. Density-corrected ultimate strengths of SCS-6/Ti-24Al-11Nb and SCS-6/TIMETAL®21S laminates and the fiberless matrix alloys.

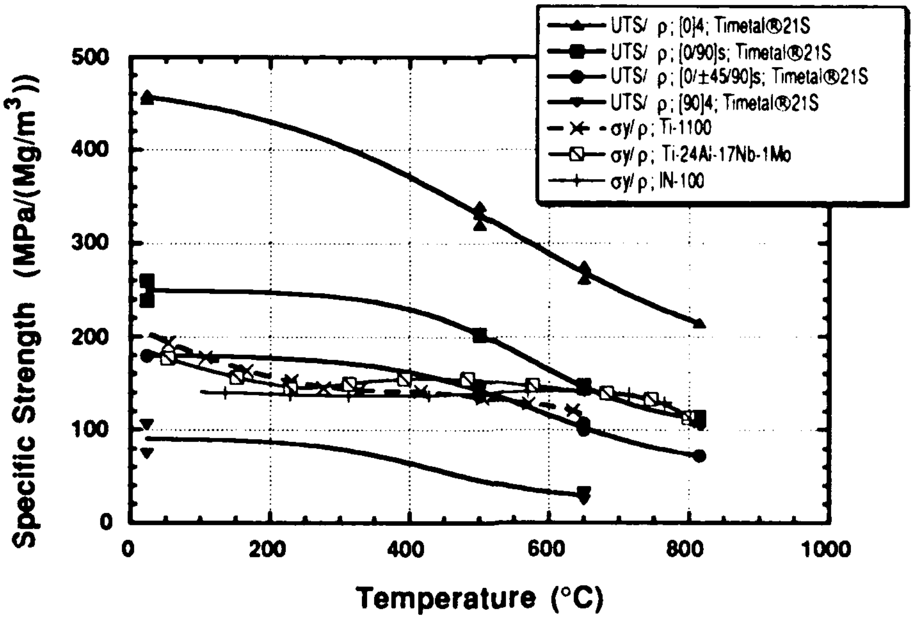

Fig. 6. Density-corrected ultimate strengths of SCS-6/TIMETAL®21S laminates compared with the yield strengths of more conventional aerospace materials.

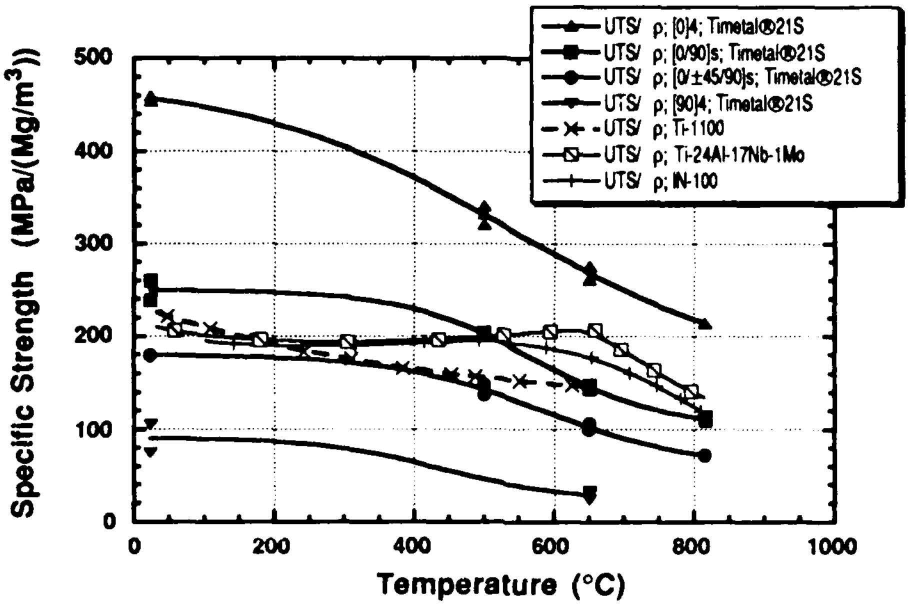

Fig. 7. Density-corrected ultimate strengths of SCS-6/TIMETAL®21S laminates compared with the ultimate strengths of more conventional aerospace materials.

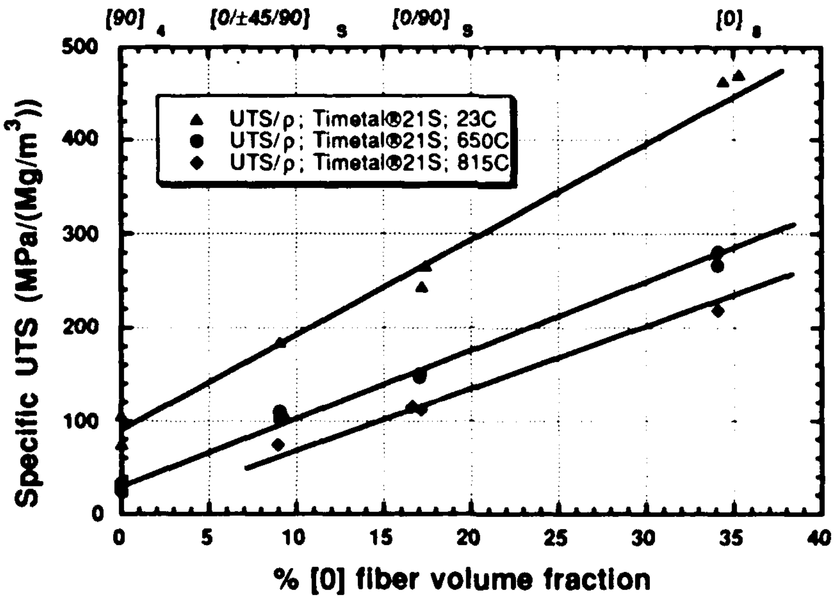

Fig. 8a. SCS-6/TIMETAL®21S laminate strength plotted versus volume fraction of [0] fibers.

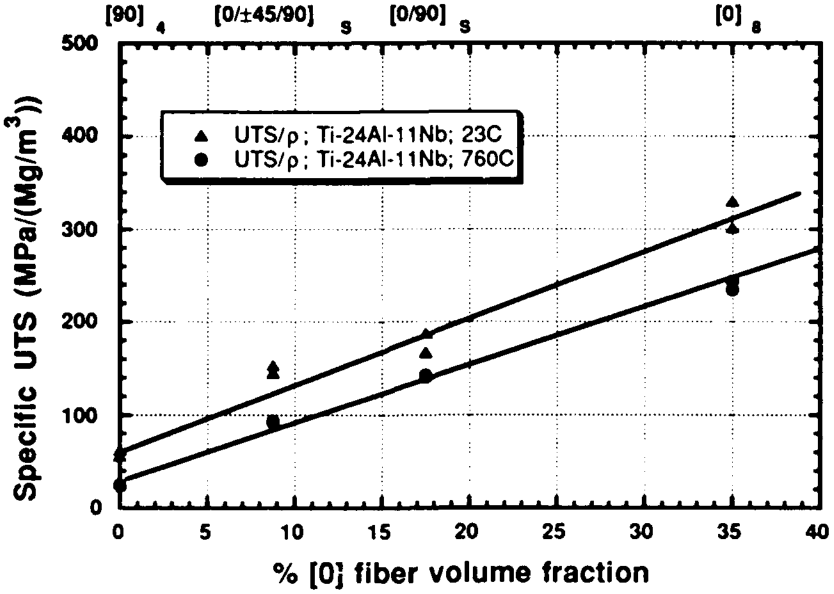

Fig. 8b. SCS-6/Ti-24Al-11Nb laminate strength plotted versus volume fraction of [0] fibers.

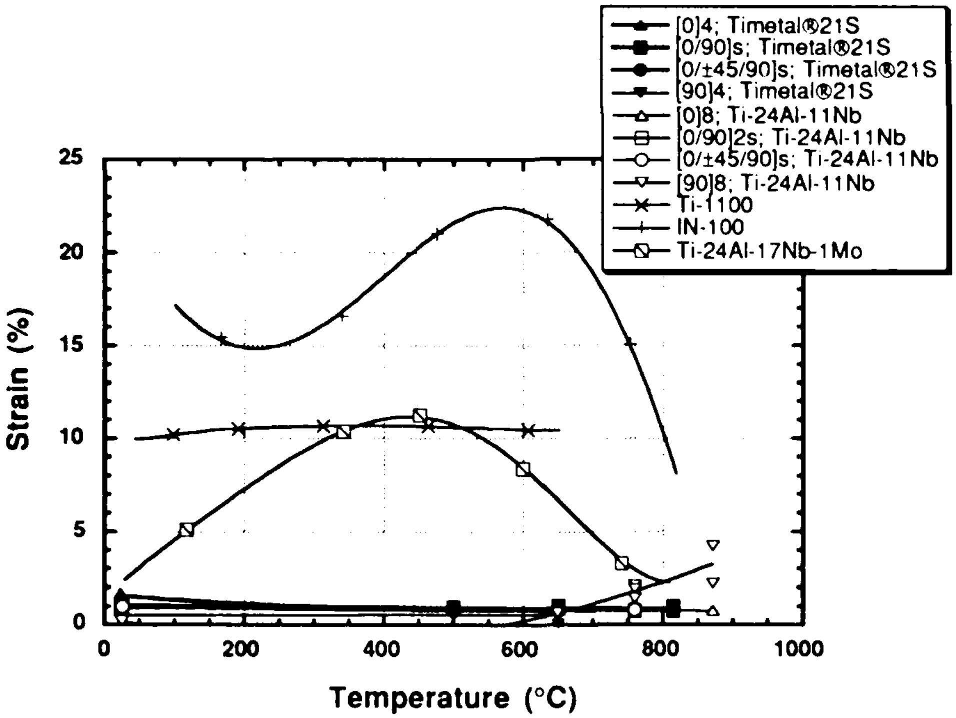

Fig. 9. Failure strain for the various materials.

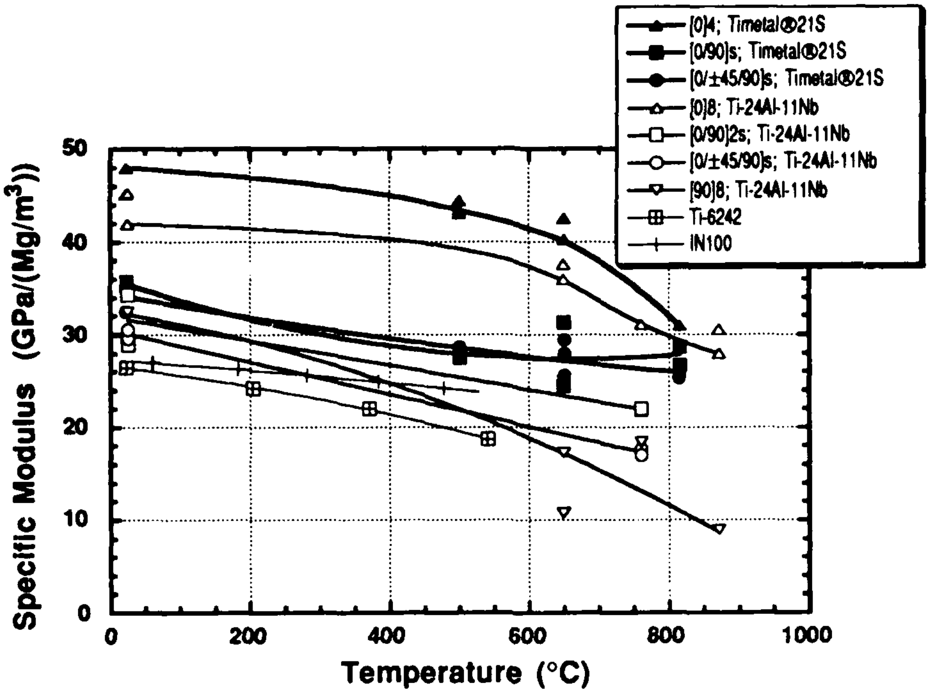

Fig. 10. Density-corrected Young's modulus for the various materials.

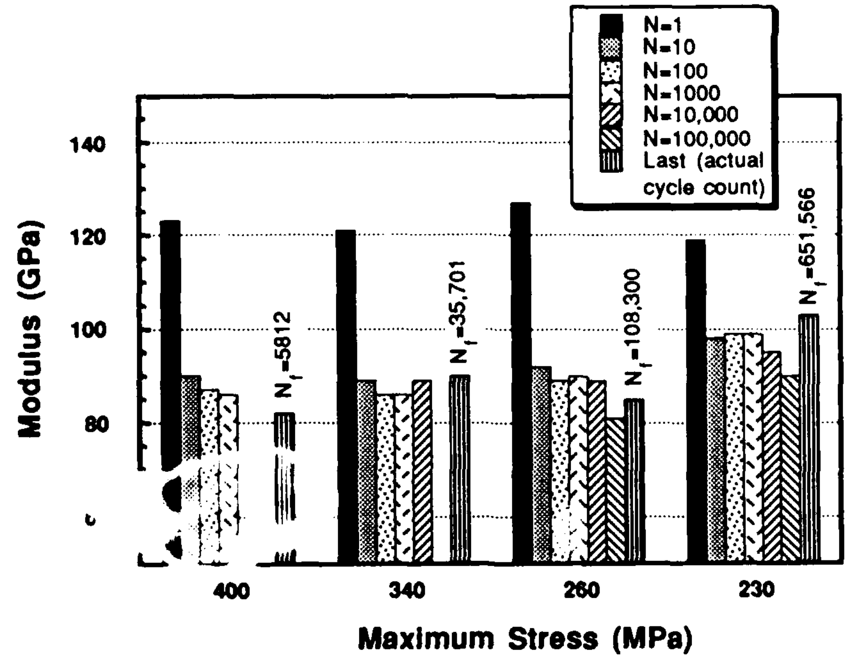

Fig. 11. Changes in elastic modulus during fatigue of [0/±45/90]s SCS-6/TIMETAL®21S; 650°C, 1 Hz, R = 0.1

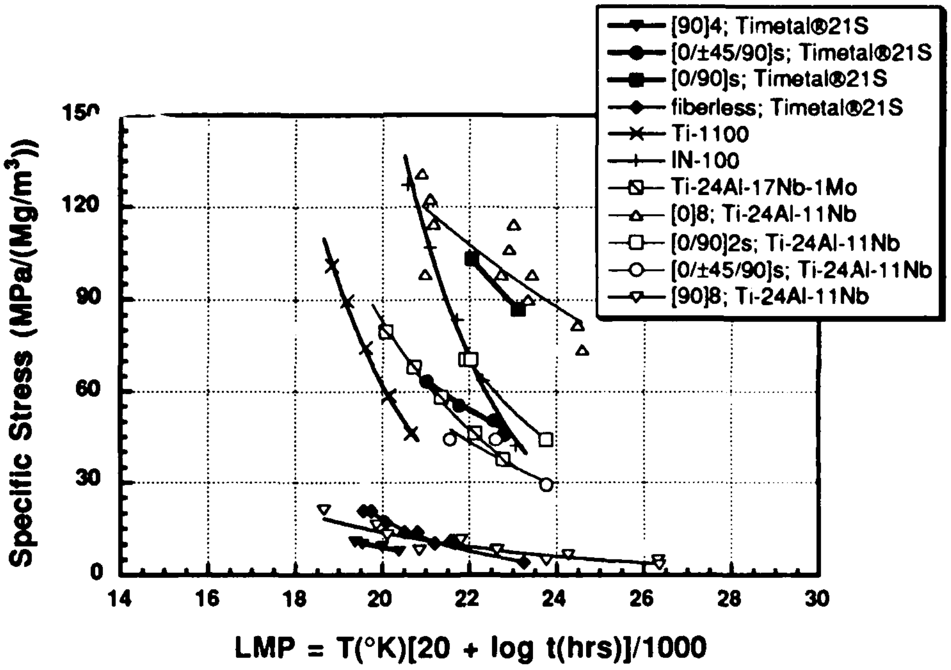

Fig. 12a. Density-corrected Larson-Miller plot of rupture strength for the various materials.

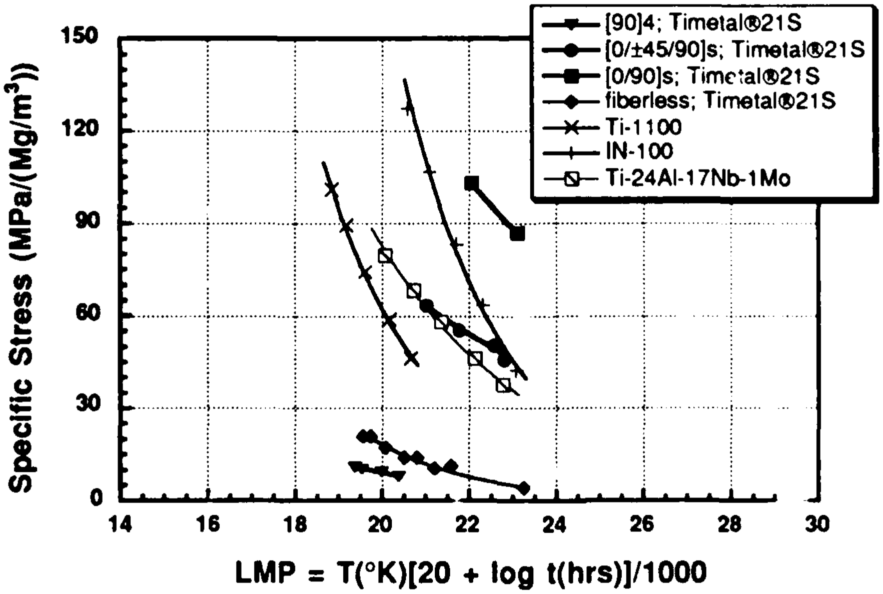

Fig. 12b. Density-corrected Larson-Miller plot of rupture strength for the various materials., omitting the SCS-6/Ti-24Al-11Nb composites.

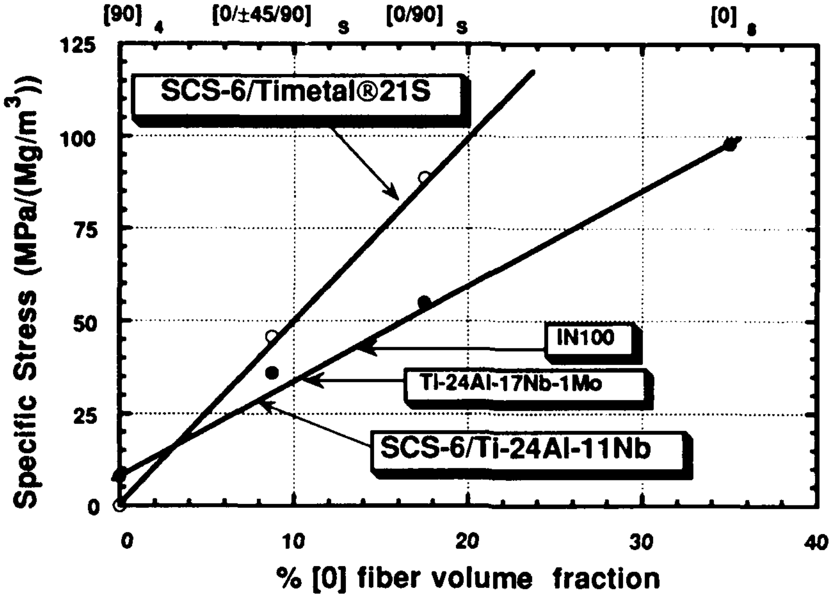

Fig. 13. Specific ruptu e stress corresponding to a Larson-Miller parameter of 23 in Fig. 12a.

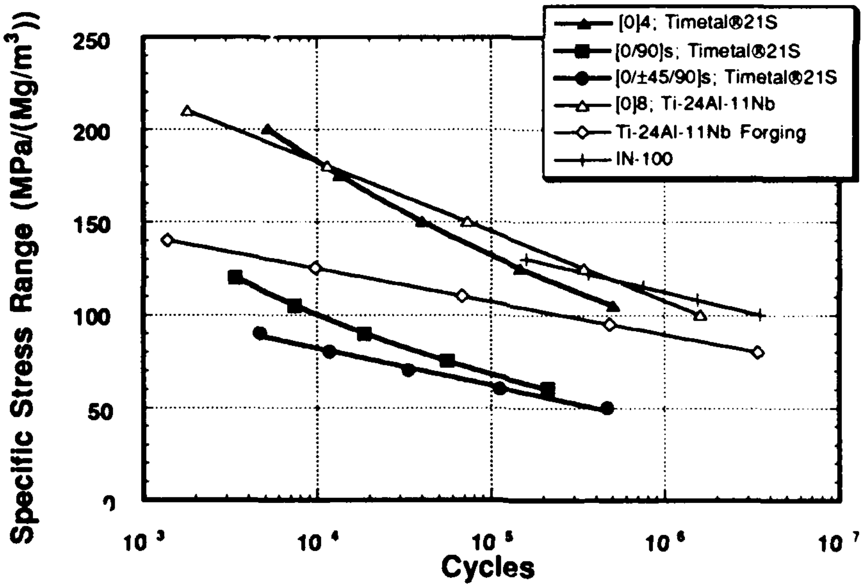

Fig. 14. Density-corrected fatigue stress range versus cycles-to-failure; 650°C, frequency ≈ 1 Hz, R ≈ 0.

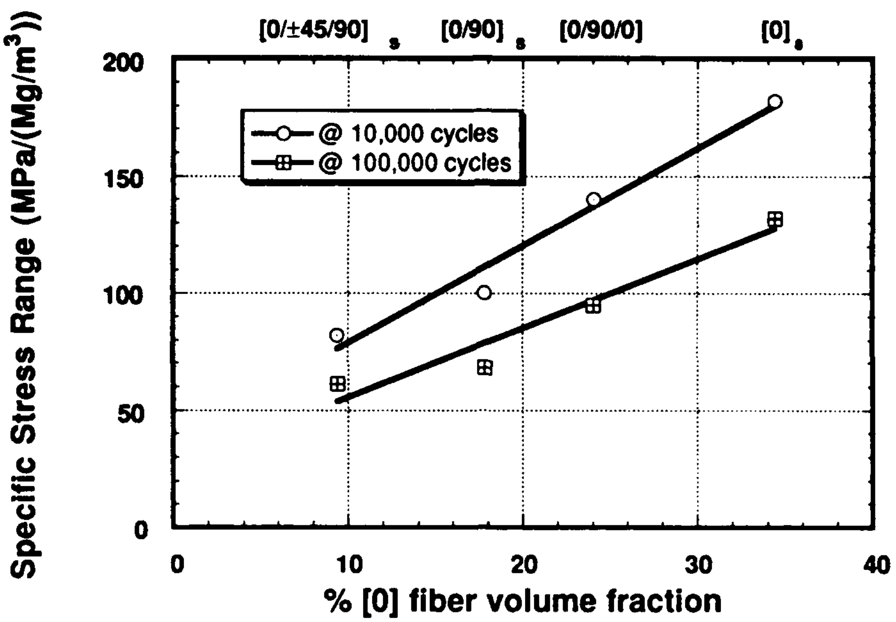

Fig. 15. SCS-6/TIMETAL®21S fatigue stress range versus volume fraction of [0] fibers.

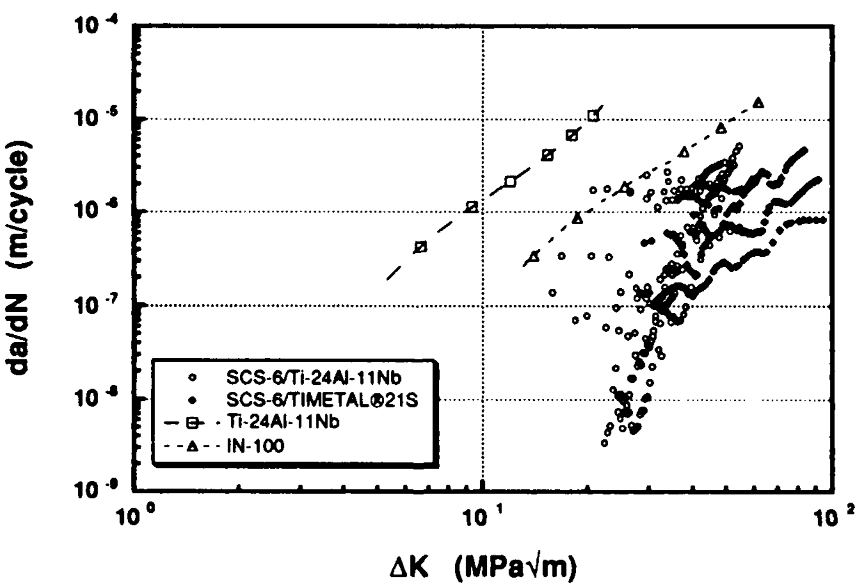

Figure 16. Comparison of fatigue crack growth behavior, 650°C, frequency of monolithic material tests = 0.2 Hz and 1 Hz for the composites, R= 0.1

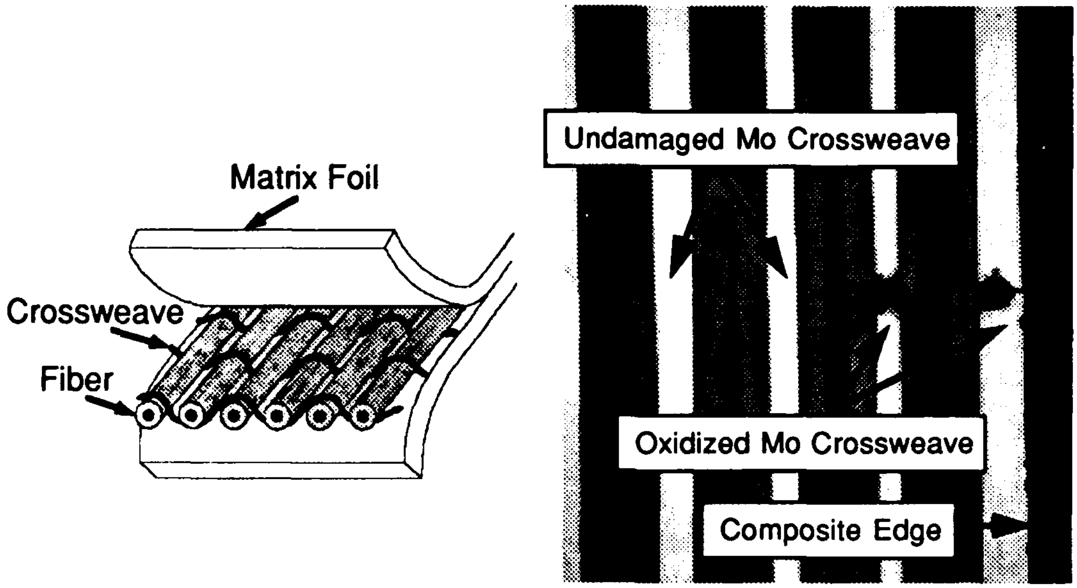
Matrix Foil
Crossweave
Fiber
Undamaged Mo Crossweave
Oxidized Mo Crossweave
Composite Edge

Fig. 17. Cross section of SCS-6/Ti-24Al-11Nb subjected isothermal exposure for two hours in air at 815°C showing oxidation of Mo crossweave and associated composite matrix cracking [3].

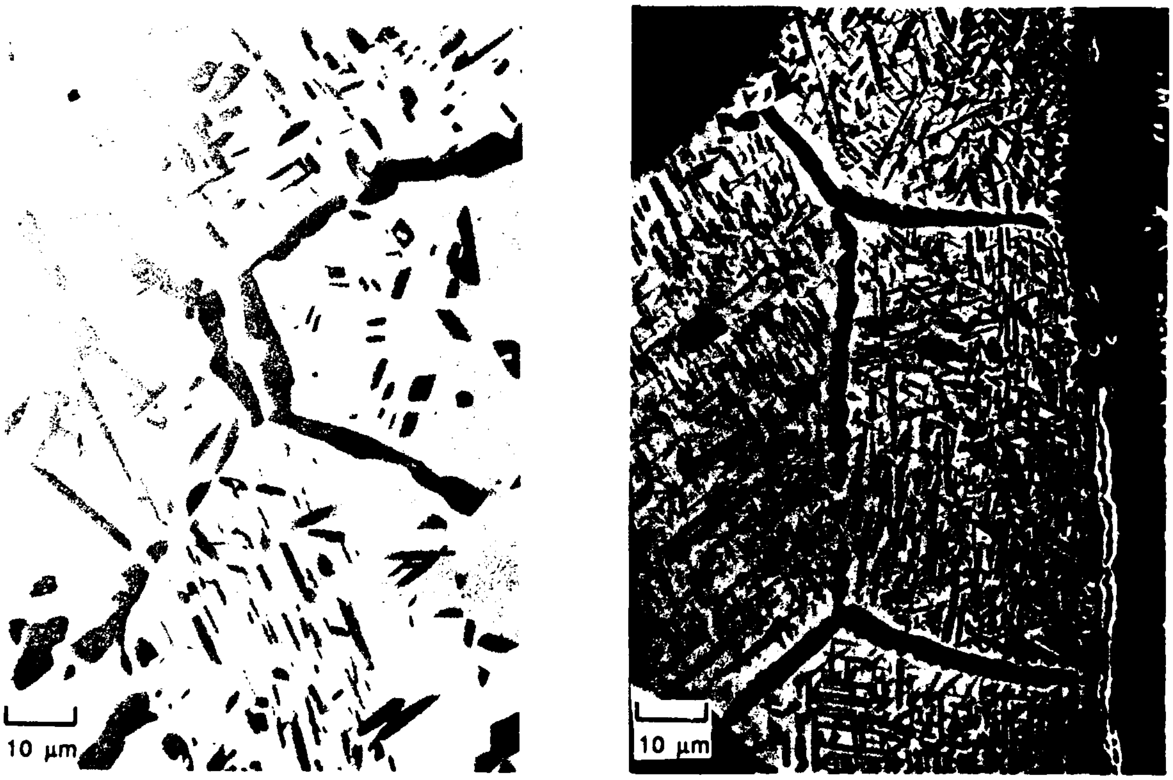

(a) (b)

Fig. 18. (a) Interior and (b) near-surface microstructures of $[0]_4$ SCS-6/TIMETAL®21S composite subjected isothermal exposure in air at 815°C for 500 ks.

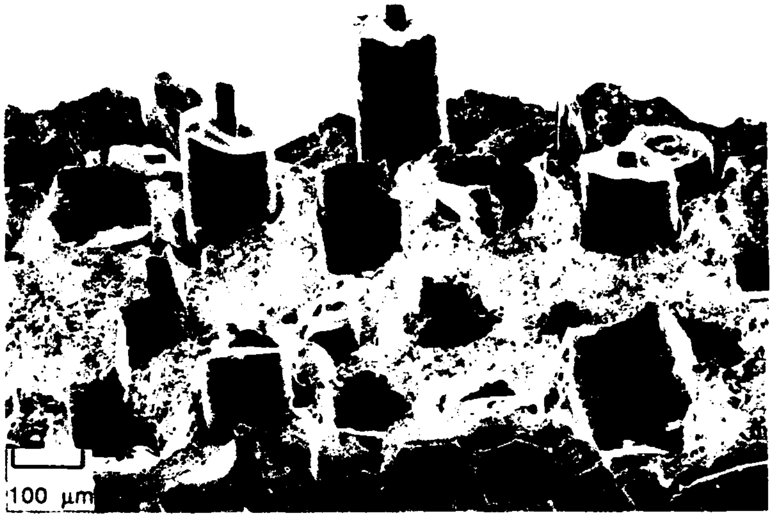

(a)

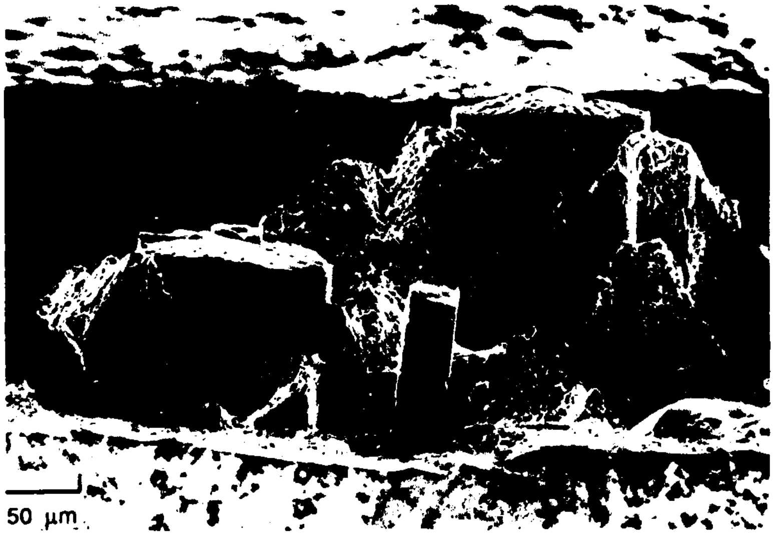

(b)

Fig. 19. Fracture surfaces of [0]4 SCS-6/TIMETAL®21S specimens: (a) Room temperature tensile test of an as-heat-treated specimen, and (b) a sample which had been thermally cycled for 500 cycles between 150 and 815 C.

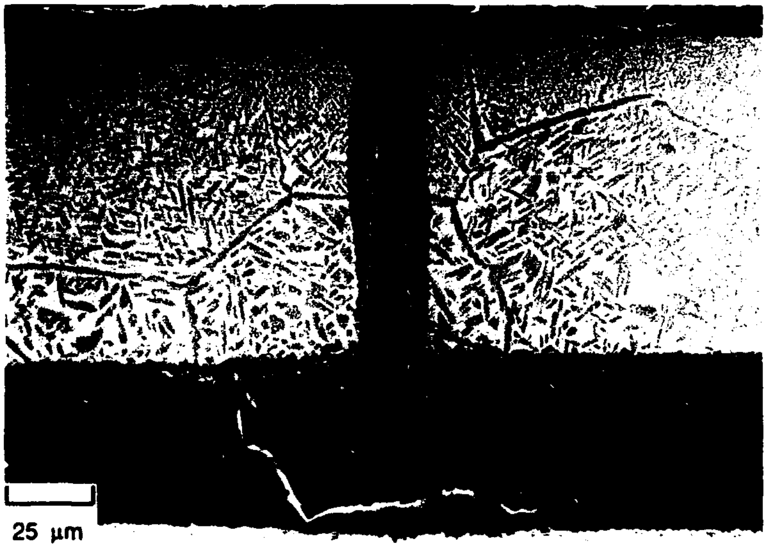

Fig. 20. A longitudinal section of [0]4 SCS-6/TIMETAL®21S showing the penetration of an oxide-filled crack which has progressed from the surface to the first fiber layer, resulting in severe fiber interface degradation by oxidation.

APPLICATIONS OF TITANIUM MATRIX COMPOSITE TO LARGE AIRFRAME STRUCTURE

by

Timothy M. Wilson
McDonnell Douglas Corporation
PO Box 516
St. Louis MO 63166
United States

ABSTRACT

Advanced Titanium Matrix Composite (TMC) materials are being developed for structures that must withstand high temperatures, possess high stiffness and be lighter. Scale-up of the TMC material system from the laboratory environment to large structural components has required significant advancements in design, manufacturing and assembly technology. Numerous large scale, TMC components have been developed, fabricated and tested to verify the feasibility of structural/material concepts for hypersonic vehicles. These articles include thick laminate TMC wing structure, minimum gage TMC fuselage sections, and integrated TMC fuselage/cryogenic tank structure. A summary of the development and testing of these articles is presented in this paper.

INTRODUCTION

Titanium Matrix Composites (TMC) are being used on large structural components to reduce weight and survive repeated exposure to elevated temperature environments. The development of a new material system like TMC from basic laboratory research to large structural applications requires three basic steps as shown in Figure 1; 1) requirements definition, 2) material research and process development, and 3) large scale demonstration and validation. It can take 10, 15 or even 20 years of research and development before the material is proven viable. Eash step in the material development has many challenges, any one of which could undermine the material system if not properly addressed.

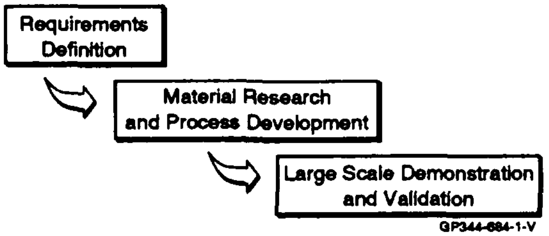
Requirements Definition
Material Research and Process Development
Large Scale Demonstration and Validation
GP344-684-1-V

Figure 1. Steps in TMC Material Development

Research on TMC has been in progress for many years, but it wasn't until 1986 that the material received serious attention. In this time period a significant effort to develop hypersonic vehicles was initiated. Hypersonic vehicles establish specific material requirements, such as temperature capability, material allowables, durability, environmental compatibility, thermal stability and desired product forms.

Once the requirements are defined, material research establishes the matrix composition and processing parameters. Scale-up from small samples to larger structural forms is an iterative process between the material scientist, producibility engineer and the structural designer. A significant amount of time is spent developing tooling and addressing product quality.

Large structures are assembled from smaller subcomponents or simple structural members. Assembly techniques for cutting, drilling, machining, and joining are established as a final part of the material development process. Once assembled the structures are tested under representative conditions to verify the performance of the material and structural concept.

HYPERSONIC VEHICLE REQUIREMENTS

The development of any new material system is typically driven by the requirements from a specific application. Although TMC has a wide range of possible uses, the principle application behind TMC research is the National Aerospace Plane (NASP) airframe.

The NASP is designed to takeoff and land from conventional runways using airbreathing propulsion concepts to achieve orbit. Because the airbreathing propulsion system operates more efficiently at high dynamic pressure (low altitude and high speed), the flight trajectory is very different from rocket powered vehicles or conventional aircraft, as shown in Figure 2. The result of operating in this flight regime is large structural loads, high temperatures, and large thermal gradients throughout the structure.

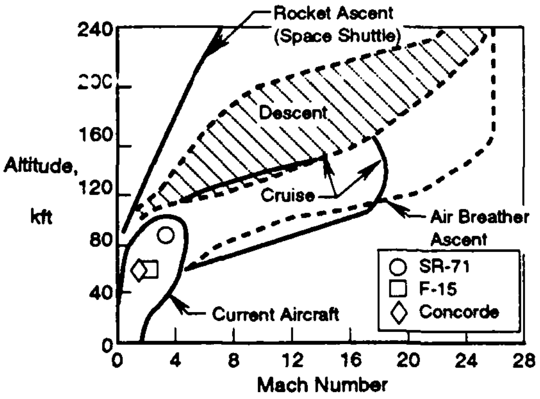

Figure 2. Typical Flight Trajectories for Hypersonic Vehicles

Design conditions for structural sizing of the airframe are selected from a combination of maneuver load factors, dynamic pressures and aerodynamic heating. Representative structural temperatures, shown in Figure 3, are used for establishing the requirements for active cooling, thermal protection systems and material selection.

Presented at an AGARD Meeting on 'Characterisation of Fibre Reinforced Titanium Matrix Composites', September 1993.

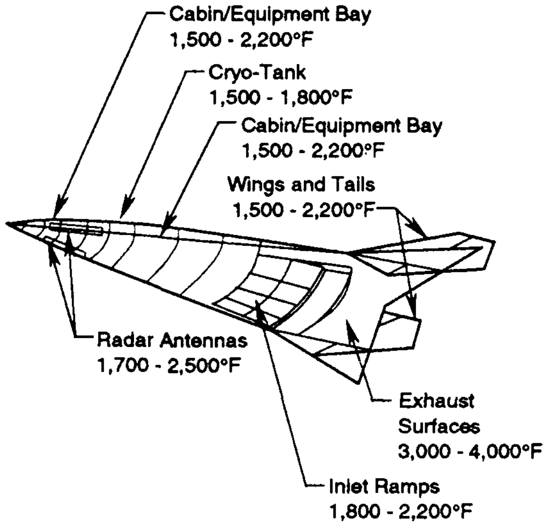

GP34-684-3-V

Figure 3. Representative Surface Temperatures

The critical challenge for the airframe is to meet all the environmental requirements at very low structural weight. Weight is more critical for hypersonic vehicles than conventional aircraft because of the low mass fraction required to achieve orbit and the sensitivity of the design to weight variances. Mass fraction is the ratio of the empty weight to Take-Off-Gross-Weight (TOGW) and determines how much usable propellant can be carried on the vehicle. Engines for hypersonic applications require large quantities of hydrogen propellant to generate sufficient thrust and Isp for a Single-Stage-To-Orbit (SSTO) mission. This coupled with the low density of hydrogen results in an airframe that is mostly propellant tanks that must have a very low structural mass fraction. Figure 4 shows a comparison of TOGW vs empty weight for conventional and hypersonic aircraft.

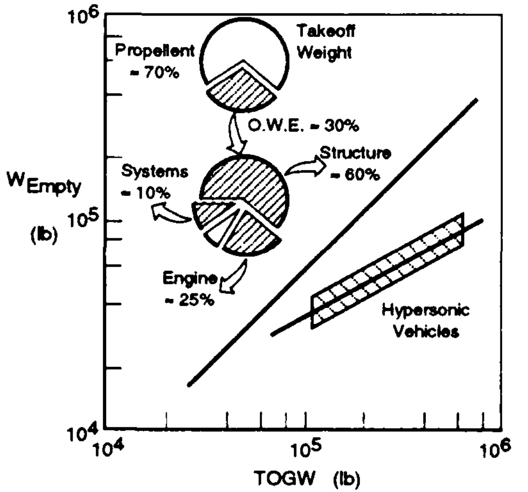

GP34-684-4-V

Figure 4. Weight Characteristics of Aircraft

Weight sensitivity is the rate-of-change of the mass fraction and is a measure of how the TOGW is affected by the empty weight. For example, a hypersonic vehicle may have a weight sensitivity of 10. This means that for every 1 pound increase in empty weight the TOGW will increase by 10 pounds. From Figure 4, conventional aircraft have a weight sensitivity slightly greater than 2. This is extremely important for hypersonic vehicles because a small reduction in structural weight (i.e., empty weight) can have a large affect on the overall size of the vehicle or significantly increase margin.

The primary design drivers for hypersonic airframes such as on NASP are weight and temperature. Candidate design concepts must address these two issues to satisfy overall mission requirements. But at the same time many underlying issues such as environmental reactions, material processing, and manufacturing must be understood before committing to a final concept.

STRUCTURAL CONCEPTS

Detailed structural concepts for hypersonic airframes are determined from iterating the structural arrangement with external environments. The structural arrangement defines internal load paths and the interfaces between airframe components. One of the critical structural interfaces is between the fuselage and the cryogenic propellant tanks.

Two fuselage / tank configurations are shown in Figure 5. The multi-bubble non-integral concept uses two independent structures to carry tank and fuselage internal loads. The tank pressure and cryogen inertia loads are carried with a stand-alone tank structure. Fuselage loads from external aerodynamic lifting forces are carried by the fuselage shell. A linkage system is used to thermally isolate the two components. The integral approach uses a single structure to carry both the tank and fuselage loads. Either configuration can be used in any fuselage shape, however, multi-lobed tanks are preferred for non-circular shapes and integral tanks work well with circular cross sections.

An important feature of the structural concept is thermal protection. By using thermal protection systems (TPS), the structural temperature of primary structure is lowered, allowing a wider range of materials to be considered. This result may or may not yield a more optimum design due to the additional TPS weight. However, certain areas of the fuselage must use a TPS system due to the extreme environments. The cold structure, integral tank concept shown in Figure 5 illustrates how TPS can be integrated with the fuselage/tank configuration.

Thermal stresses generated by temperature differences within the structure influences the concept selection. An illustration of how thermal stresses are induced is shown in Figure 6. A non-uniform temperature distribution across the fuselage occurs due to aeroheating and uneven thermal mass distribution caused by ring frames used to stiffen the fuselage. The frames are cooler than the fuselage shell causing a build-up of thermal load (Ny) at the interface. Load continues to rise with increased thermal gradients unless deformations (Δ) or buckling occur. A concept that allows this deformation without sacrificing primary load capability is used in areas of high thermal gradients.

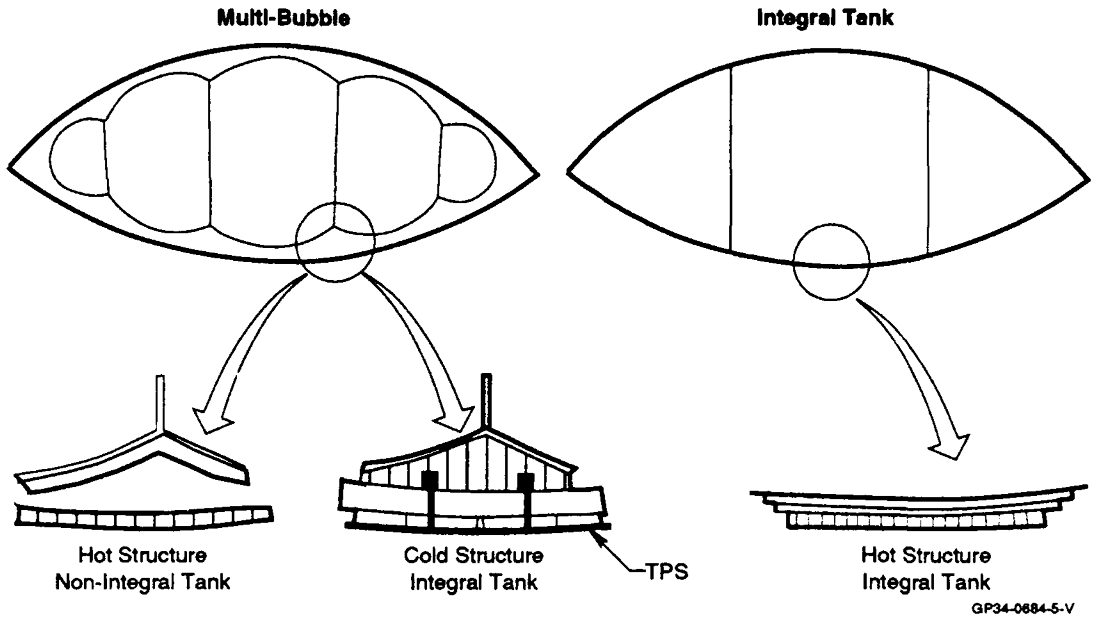
Multi-Bubble
Integral Tank
Hot Structure
Non-Integral Tank
Cold Structure
Integral Tank
TPS
Hot Structure
Integral Tank
GP34-0684-5-V

Figure 5. Fuselage / Tank Configurations

Detailed structural concepts for the fuselage shell are shown in Figure 7. The concepts vary from hat or blade stiffened structure to sandwich type construction. Each concept is evaluated using different materials and load conditions to establish a final structural/material concept. Design, fabrication and validation of the concept are demonstrated as part of the material development program.

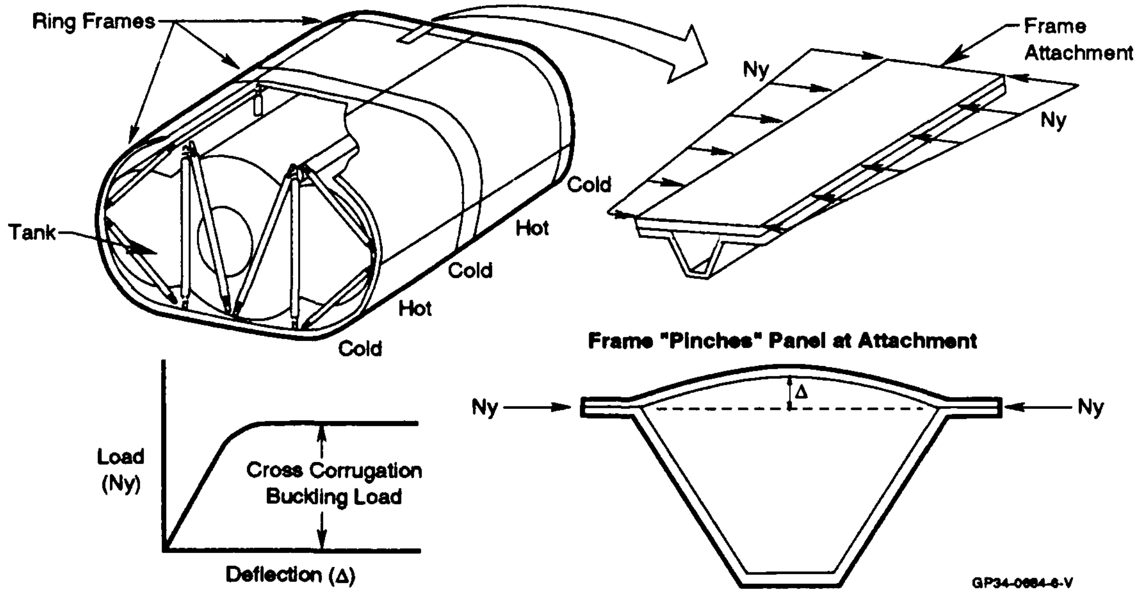
Ring Frames
Tank
Cold
Hot
Cold
Hot
Cold
Ny
Frame Attachment
Ny
Frame "Pinches" Panel at Attachment
Ny
Δ
Ny
Load (Ny)
Cross Corrugation Buckling Load
Deflection (Δ)
GP34-0684-6-V

Figure 6. Effects of Thermal Gradients

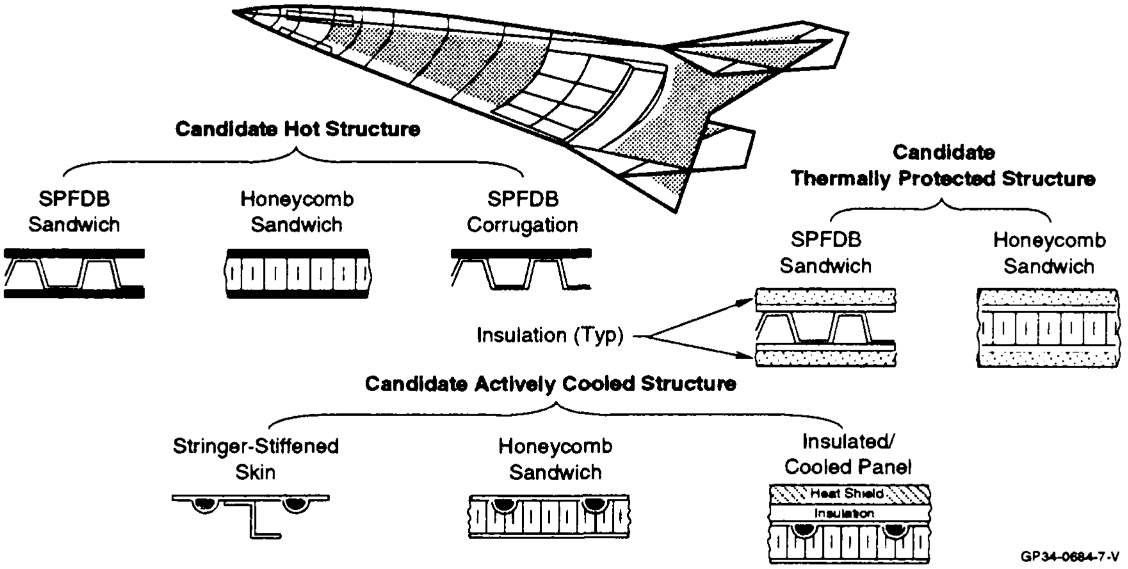

Figure 7. Detailed Structural Concepts

MATERIAL REQUIREMENTS

Material requirements are generated from a wide range of parametric studies performed at the vehicle and subcomponent level. Using automated structural optimization techniques, preliminary fuselage shell sizing can be done quickly for a large combination of structural concepts and candidate materials. Material sensitivities are also calculated using this approach such that critical material attributes like stiffness can be prioritized and guide material development. These studies also establish the benefits and risks associated with developing certain types of structural / material concepts. They also serve to anchor the material development program whose charter is to develop a usable material system and demonstrate the feasibility of the concept.

Candidate material / structural concepts evaluated for NASP encompassed conventional materials as well as advanced systems. Goal properties for advanced materials are established by evaluating the state-of-the-art in materials development, requirements and times required to develop new materials. TMC was the advanced material identified as most promising for NASP airframe structure applications. Figure 8 is a plot of specific strength as a function of temperature for several material systems. TMC exhibits distinct advantages in the 700°F to 1500°F temperature range over other materials. Based on these evaluations, a TMC hat stiffened concept was selected for further development.

PROCESSING DEVELOPMENT

With material requirements and product forms defined from applications studies, material research begins at the constituent level to select a matrix alloy and reinforcing fiber. As various formulations are examined, processing parameters are refined to obtain a consolidated material that satisfies the requirements. Regardless of how good the material characteristics, it must be formed into the required structural shapes to be usable for large applications. Therefore, significant research is focused on fabrication and manufacturing procedures. Some of the more challenging structural shapes are shown in Figure 9.

TMC material research and process development was accomplished under three activities. The first was the NASP Materials and Structures Augmentation Program (NMASAP) which was a companion program to the main NASP initiative and involved 5 national contractors working on a variety of advanced materials including TMC. The second was the risk reduction portion of the NASP program focused on critical, high risk structure. The third was internal research and development by McDonnell Douglas to develop company wide expertise with Titanium Matrix Composites. All of the large structural demonstration articles discussed in this paper are associated with these three programs.

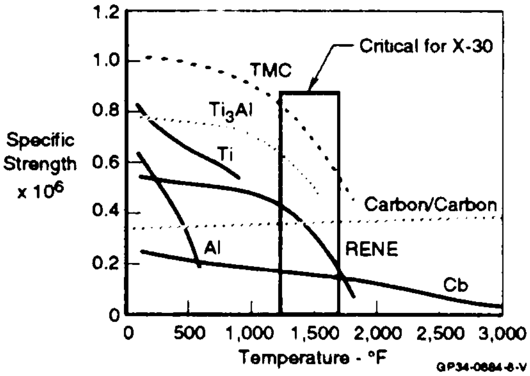

Figure 8. Advanced and Conventional Material Comparison

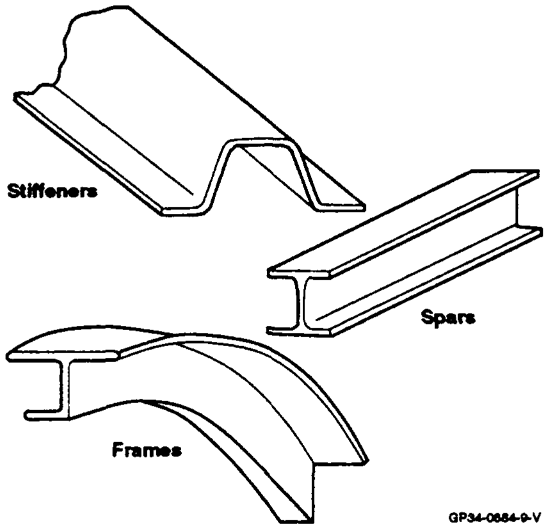

Figure 9. Structural Shapes Required for NASP

MATERIAL RESEARCH

The constituents of TMC are the titanium matrix and reinforcing fibers. The initial focus of the NMASAP program was to select appropriate matrix materials and reinforcing fibers to meet NASP requirements. Seventeen matrix formulations including both Beta alloys and Ti aluminides were evaluated. The evaluation criteria, shown in Figure 10, concentrated on specific material attributes important for high temperature applications. Considering all of the desired attributes, the Beta or Timet™ 21S alloy as the preferred matrix for a 1500° F TMC material system.

Attention Was Focused First on Matrix Alloy Selection

Compositions	Number	Selection Criteria
• ß	5	• Tensile Properties
• α-2 Strengthened α	1	• Thermal Stability
• α-2	9	• Creep Strength
• γ	2	• Fiber Compatibility
Total = 17		• Oxidation Resistance

Beta 21S Was Final Choice

GP34-0684-10-V

Figure 10. Matrix Selection Criteria

Previous experience showed that the Textron SCS-6 fiber would meet NASP elevated temperature strength and stiffness requirements. However, a key issue is preventing fiber / matrix interaction. Titanium is highly reactive and at elevated temperatures will essentially destroy unprotected fibers. The SCS-6 fiber coating survived repeated exposures to NASP temperature environments with no degradation and was selected as the baseline fiber for all development structures. Other fibers with smaller diameters also met the acceptance criteria for NASP. The smaller fiber is important because of it's direct relationship to minimum gage laminates. Therefore, the small diameter SCS-9 and Sigma fibers are used in some of the demonstration hardware. A comparison of large and small diameter fibers is shown in Figure 11.

Three Silicon Carbide Fibers Were Compared

	Diameter (In.)	Tensile Strength (KSI)	Modulus (msi)	Density (Lb/In.^{3})
SCS-9 (1)	0.0032	500	47	0.09
Sigma (2) 1240	0.004	500	60	0.1
SCS-6 (1)	0.0056	500	58	0.11

(1) Textron Speciality Materials, Lowell MA
(2) British Petroleum, Hampshire UK

GP34-0684-11-V

SCS-9 and SCS-6 Were Selected

Figure 11. Reinforcing Fiber Properties

TMC LAMINATE PROCESSING

A general approach for combining matrix and fibers into a consolidated TMC laminate is shown in Figure 12 and consists of 5 basic steps.

The first step is layup. A "foil / fiber" method of layup was used in all demonstration hardware that will be discussed later. In this method, the matrix material is rolled into thin foil sheets and cut into foil plys which correlate to the final part dimension. Fibers are woven into unidirectional flat mats and plys are cut depending on the final orientation required in the consolidated laminate. Cutting the fiber and foil for small parts is typically done by hand as shown in Figure 13 , but is not well suited for high rate production or consistent quality. Therefore, automated cutting techniques, shown in Figure 13, using numerically controlled chisel cutters were successfully developed and used. Once cut, the foil and fiber plys are collated in sequence to obtain the desired fiber orientation in the consolidated part.

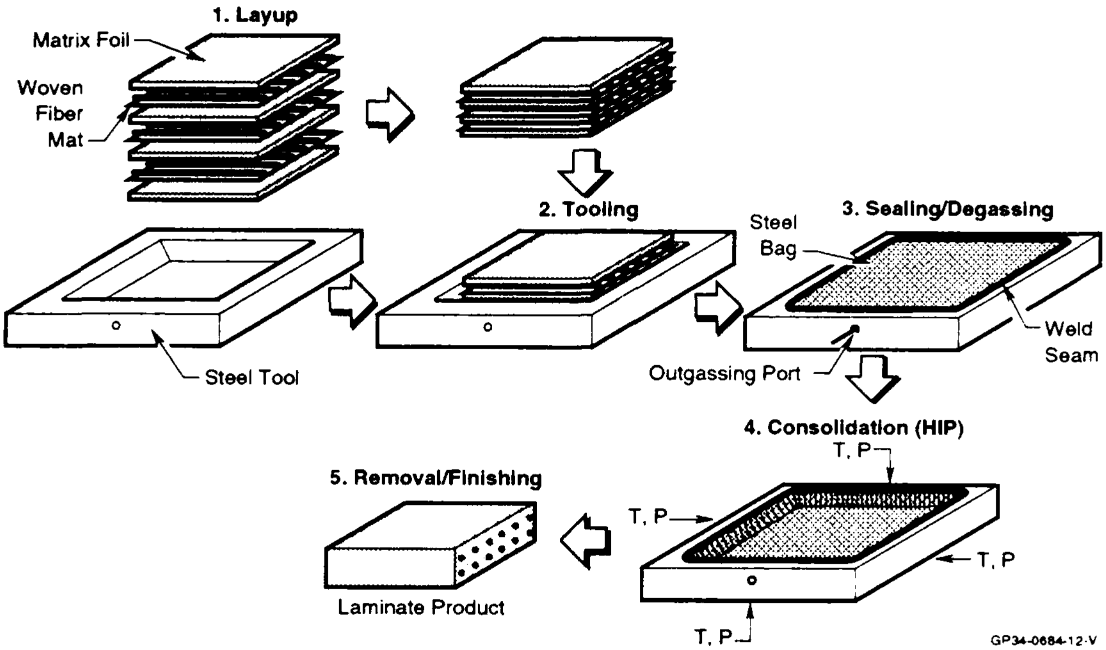
1. Layup
Matrix Foil
Woven Fiber Mat
2. Tooling
Steel Tool
Steel Bag
3. Sealing/Degassing
Weld Seam
Outgassing Port
4. Consolidation (HIP)
T, P
T, P
T, P
T, P
5. Removal/Finishing
Laminate Product
GP34-0684-12-V

Figure 12. TMC Processing Steps

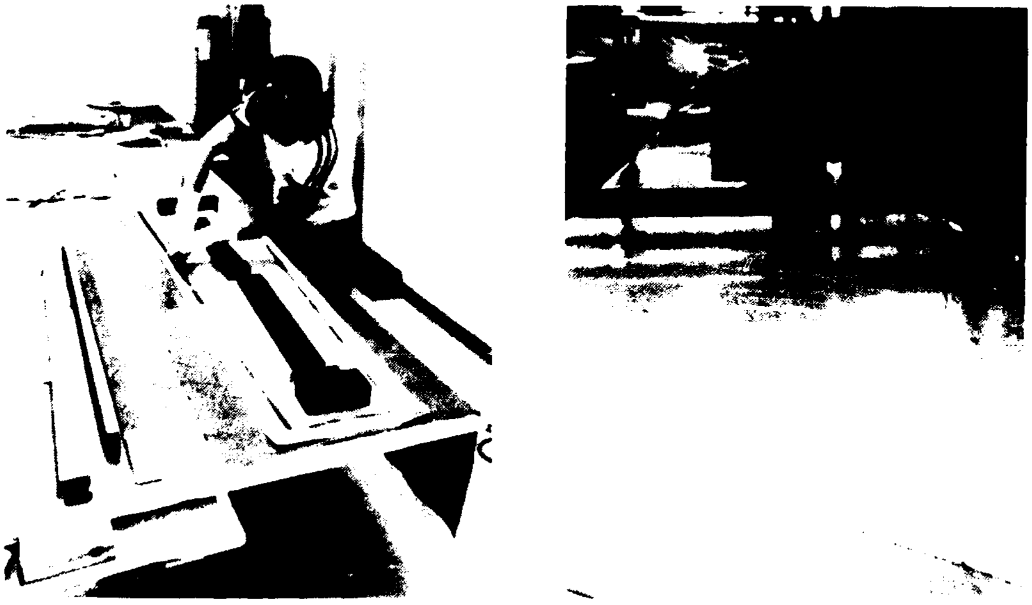

Conventional Hand Cutting

Improved Numerically Controlled Cutting

Figure 13. Cutting Techniques Used for TMC Processing

The second step in the process is to place the stack of foil / fiber plys in the tool. The tooling approach is critical in fabricating top quality TMC parts. Many tooling concepts and layup procedures were evaluated and refined to establish the sequence shown in Figure 14. Hard steel tooling with symmetric laminate stacks is used to prohibit significant tool warping that occurs with one sided tooling concepts. Since the tool and laminate stack expand differently with temperature, buffer or slip sheets (coated with a "stop off" material to prevent bonding) are placed on both sides of the laminate stack. The complete stack is held in place by a steel bag or bladder welded to the tool.

Depending on the final shape of the part, this step can be very simple as with a flat laminates or very difficult requiring tooling aids for complex parts. A foil/fiber stack is being formed into a C-channel tool in Figure 15. The photo on the left shows the preformed steel bladder and the green stack prior to forming and the right photo shows the greenstack formed into the tool with the bladder in place for welding.

Tooling and Bagging Method for TMC Laminates Provides Reliable Consolidation

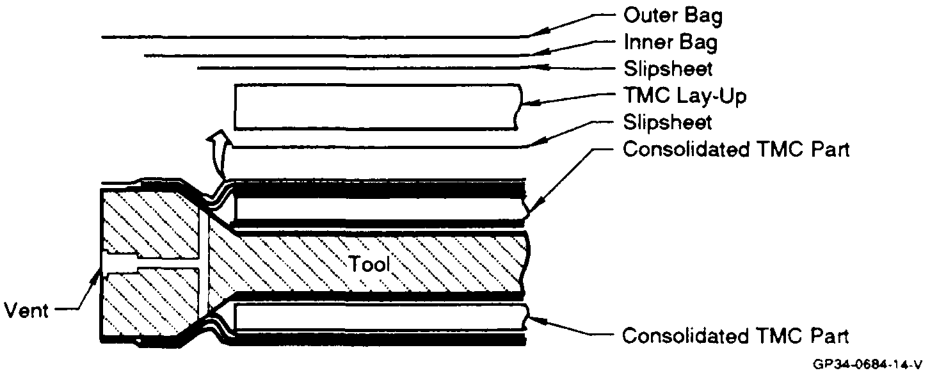

Figure 14. TMC Tooling Stack

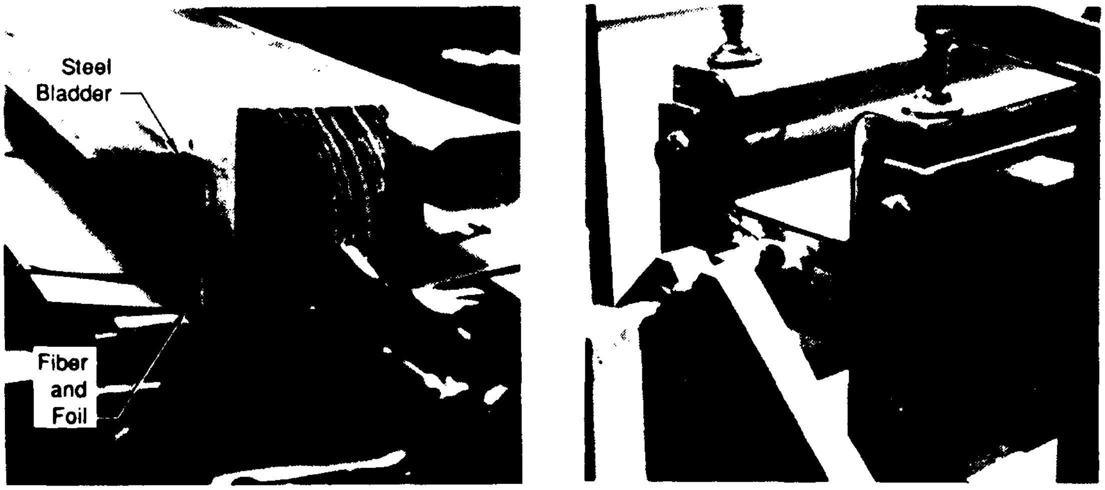

Fiber and Foil Before Pressing Into Consolidation Tool

Fiber, Foil and Bladder In Place and Ready For Welding

Figure 15. Forming of a TMC C-Channel

The third step is sealing / degassing. Sealing the bladder or bag to the tool forms a pressure tight cavity that can be evacuated through a vent port in the steel tool Degassing or removing all of the volatiles from the cavity is required for good consolidation and to prevent contamination of the laminate.

The fourth step is consolidation. Consolidation of TMC is done under high temperature and pressure using a hot isostatic press (HIP) unit.

Temperature and pressure are phased to obtain good consolidation and to minimize the wear and tear on the HIP. Temperatures are slowly increased from room temperature to avoid any excessive distortions caused by thermal gradients in the tool. Pressure is kept relatively low during the heat-up process and is increase to over 15,000 psi at the end of heat-up cycle and held for a prescribed time period. Most of the pressure is relieved and the HIP is allowed to cool. At room temperature, the consolidated laminate and tool are removed from the HIP.

The fifth and final step is removal and finishing. At the extreme conditions during consolidation, the bladder or bag is formed to match the outer contour of the laminate and flows into any creases or crevasses. Bags are removed by machining or grinding the bag welds and exposing areas where the "stop off" prevented diffusion bonding of the tool and bag. Once accomplished, the bag is lifted off of the laminate stack. Slip sheets are also removed and the laminate is wiped clean with solvent. The laminate or part is now ready for assembly operations.

MANUFACTURING AND ASSEMBLY OPERATIONS

Operations required to prepare TMC parts for final assembly are no different than for any other built-up structure. Parts must be cut or trimmed into final blueprint dimensions, joined by either fasteners, spotwelded, or brazed to make subcomponents and finally assembled together into the final assembly. However, methods used to accomplish these tasks are not so conventional because of the abrasive nature of TMC. Improper cutting not only damages tools, but can damage the part as well.

Several methods of trimming and cutting are used. The abrasive waterjet, shown in Figure 16, uses a high pressure stream of water with suspended abrasive particles to cut TMC. The jet is mounted on a multi-axis head that makes continuous straight or curved cuts. As an example, Figure 17 hows a TMC angle being cut into a "saw tooth" or crenelated pattern for a curved TMC ring frame. Multiple parts with identical geometries are produced at cutting rates of up to 30 inches per minute, making this technique suitable for high production rate applications. The integrity of the cut surface is also very good as shown in Figure 18.

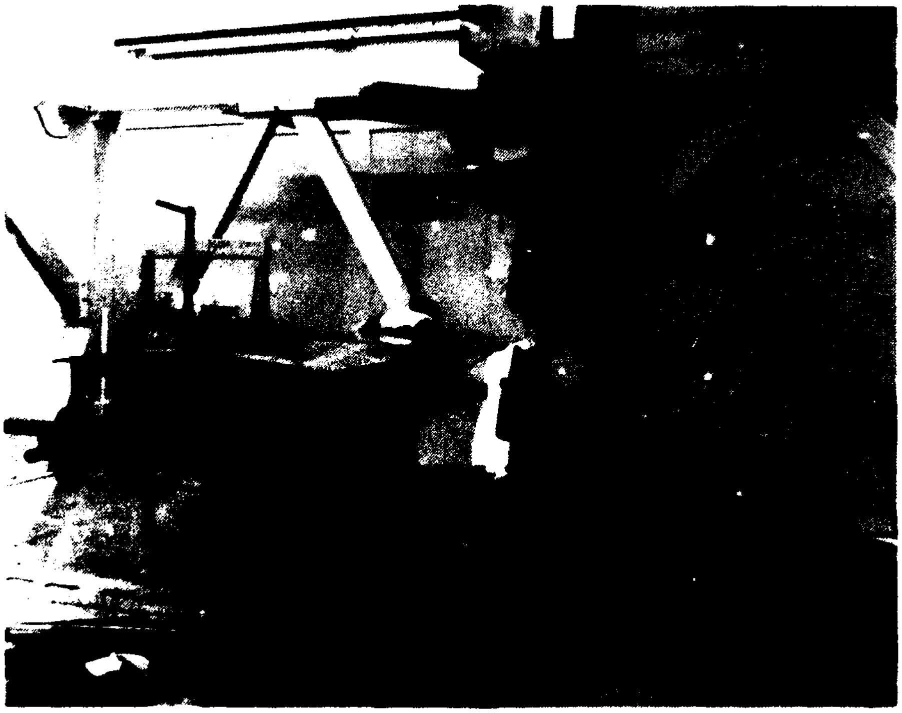

Figure 16. Multi-Axis Waterjet Cutter

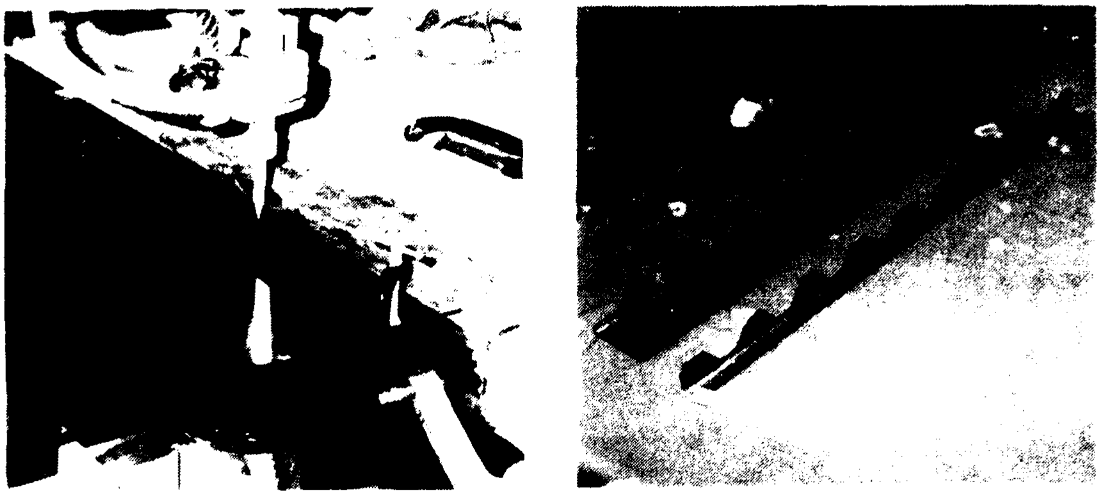

Cutting Crenelated Pattern In TMC C-Channel

Two Finished Components For TMC I-Beam

GP34-0684-17

Figure 17. Waterjet Cutter in Operation

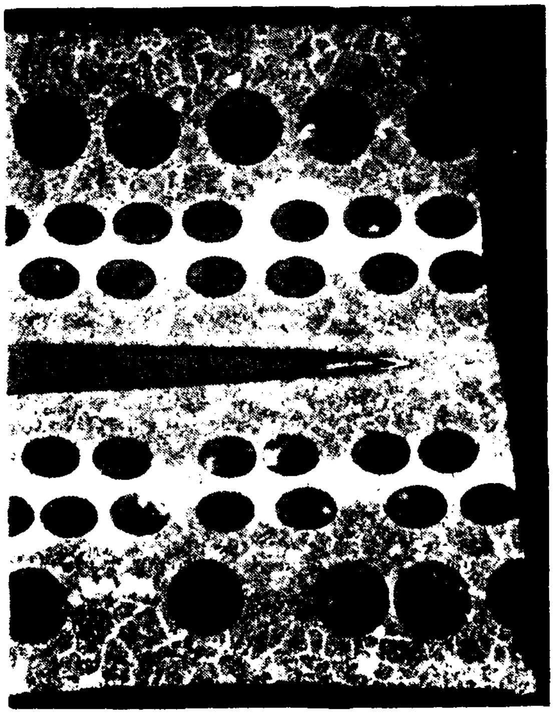

GP34-0684-18

Figure 18. Cut Surface from a Waterjet

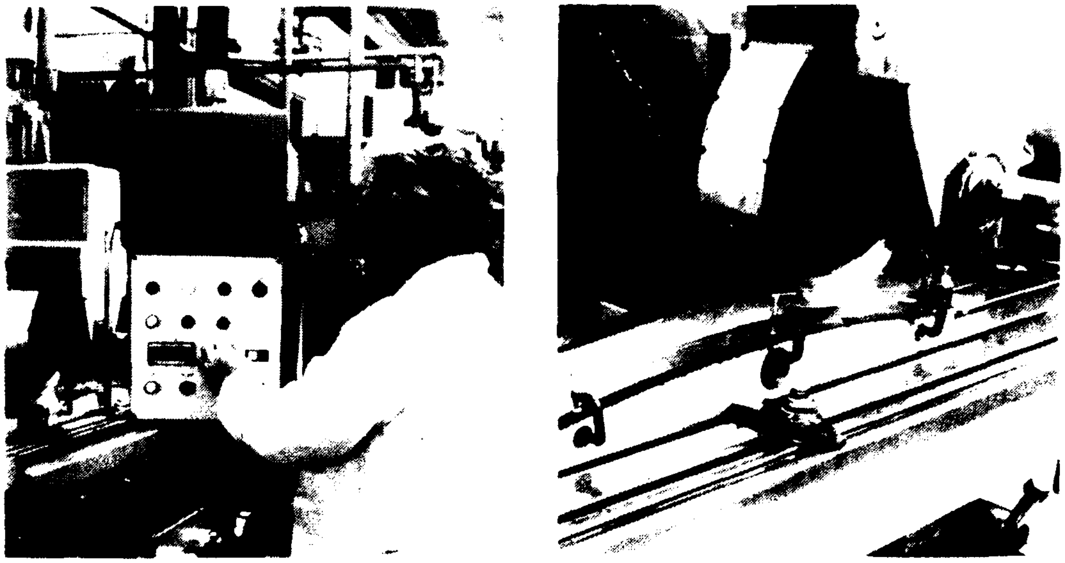

Diamond Wheel
Mounted On A Horizontal Mill

Trimming Short Flange of
Curved I-Beam

Figure 19. Diamond Wheel Cutter Set-Up

The diamond cutting wheel, shown in Figure 19, is another method used to produce excellent cuts in TMC. The diamond wheel is mounted on a horizontal mill and cutting is done at controlled speeds and feeds by moving the part through the wheel. Only straight cuts are made using this method due to set-up procedure on the mill. Cutting rates are usually slow because this is basically a grinding process and excessive heat is generated. This method produces very precise cuts as shown in Figure 20, and is used for very thick parts.

Wire electrical discharged machining (EDM) is a very flexible method for cutting complex forms of TMC. EDM is considered a non-contact cutting method which removes material through melting or vaporization by high frequency electric energy. Since no contact is made between the cutting medium and the part, very small radii are possible. This method is useful when orientation or clearance preclude the use of the waterjet due to backspray. Figure 21 shows the EDM unit cutting a 16-ply TMC spar for the MDC Wing Torque Box article. The finished part shown in Figure 22 required cutting the cap web joint with a very tight radius. A photomicrograph of the joint shows a uniform, good quality cut.

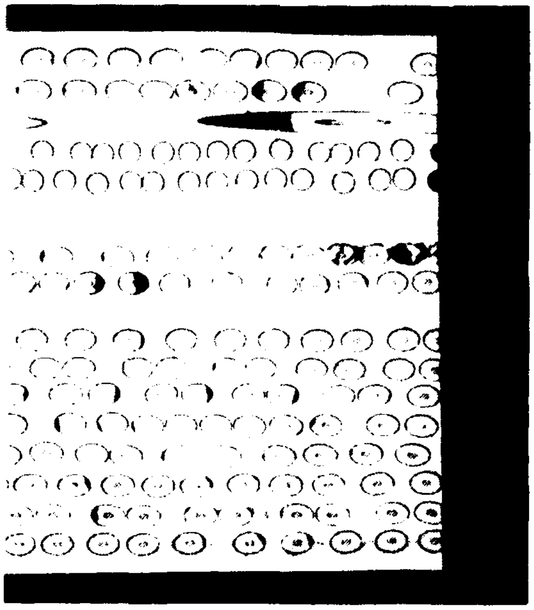

GP34 0684 22

Figure 20. Cut Surface from Diamond Wheel

Machine Area

Cutting Through Flange of Canted I-Beam

GP34-0684-21

Figure 21. EDM Cutting of A Wing Intercostal

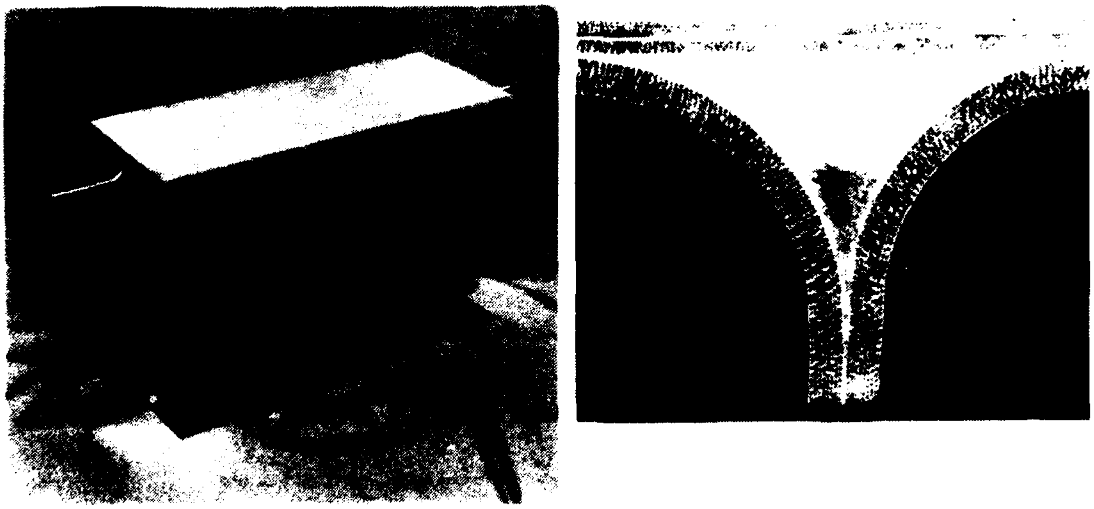

TMC Spar For Stabilator Torque Box

GP34-0684-22

Figure 22. Completed Part Cut With EDM

HOLE PREPARATION

Several methods are used to cut fastener holes in TMC. For thin laminates with few holes, conventional high speed steel or cobalt twist drills can be used, but significant tool wear requires frequent drill replacement. On large structure with numerous holes through thick and thin laminates two methods are used: hole punching and diamond core drilling.

Hole punching works well on thin laminates and at fastener locations near the edge of the part. Hole punches are pneumatic operated and required rigid support to limit part deflection and minimize hole distortion. Panels for the Integrated Fuselage/Cryotank article are being punched in Figure 23. Machines are stationery and part size is typically limited due to the "throat" size of the machine. Thick laminates deflect as the punch penetrates the material causing nonuniform holes or excessive material damage around the hole. The thickest laminate punched, shown in Figure 24, is a 24 ply SCS-6/Ti 15-3 part. The figure shows metal smearing and fiber damage at surface of the hole after punching. The damaged area is removed by secondary reaming operations to achieve final hole dimensions. Several passes and several reamers may be required during this process.

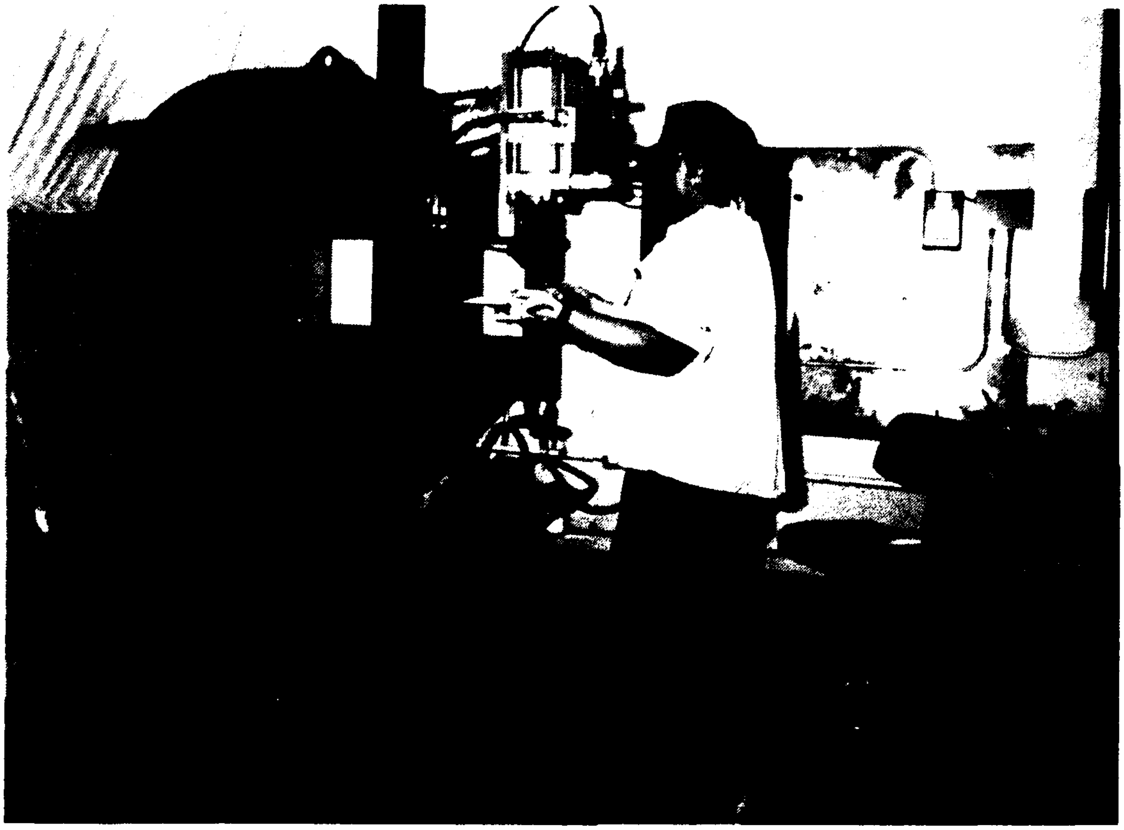

GP34 0684 23

Figure 23. Hole Punching of Integrated Fuselage/Cryotank Panels

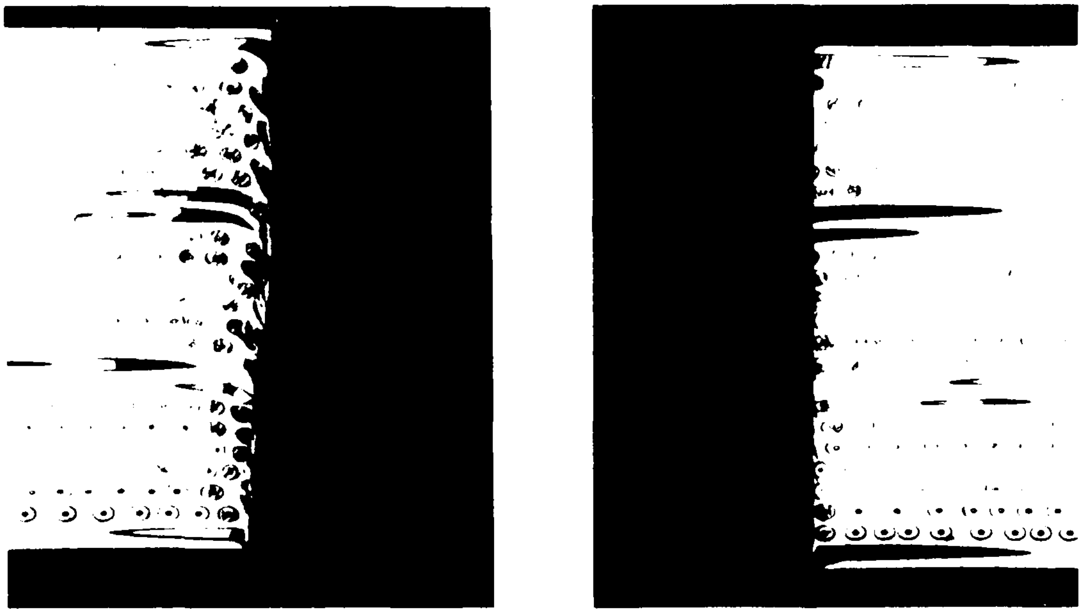

As Punched

After Reaming

GP34-0684-24

Figure 24. Hole Integrity From Punching and Reaming Operations

Neither conventional twist drills or punching will consistently produce high quality holes in thick TMC laminates. Diamond core drills are used for these applications. The core drills are tubular with a diamond matrix built up on one end similar to diamond grinding wheels. As the drill rotates, the diamond edge cuts the TMC and material is removed from the tube. This procedure is used on other MMC materials, but special modifications to the core drill design, drill motors and procedures has yielded better cutting efficiency and hole quality for TMC. This method is adaptable to multiple drill set-ups, shown in Figure 25, for large TMC structure. Aluminum drill templates are designed to hold several drills at one time, allowing the operator work on more than one hole at a time. Hole quality from this method is excellent as shown in Figure 26. Hole tolerances can be held to +/- .006 inches for a 32 ply TMC laminate.

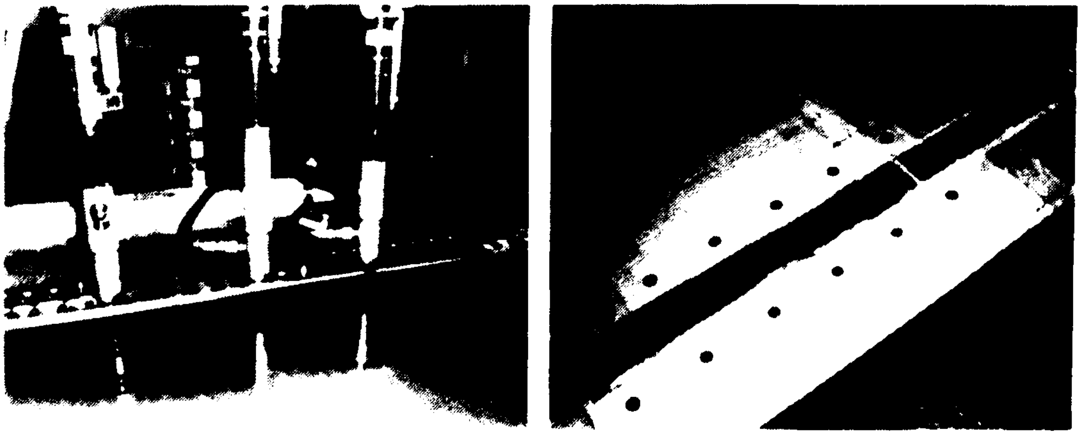

Uses Conventional Rigid Set-Up

Close-Up of Drilled Holes

Figure 25. Multiple Drill Set-Up Used on Large Assemblies

SPOT WELDING AND BRAZING

While mechanical fastening is a principle method used for assembly other techniques of joining TMC structures are feasible. Two methods, spotwelding and brazing, are useful for subcomponent fabrication and preclude much of the hole drilling required on large structure.

The spotwelding process consists of clamping two pieces of TMC together with electrodes, discharging electrical current through the electrodes causing local heating and joining of the two pieces. Parameters such as clamping force, electrode diameter, and amperage have significant effect on the integrity of the spotweld "nugget". Nugget size and quality is directly related to the strength and durability of the joint. Since the process requires a rigid set-up, the part size is limited by the "throat" dimension of the spotweld machine. Shown in Figure 27 is a typical machine used for spotwelding and Figure 28 shows a close-up of a hat stiffened panel from the Integrated Fuselage/ Cryotank article.

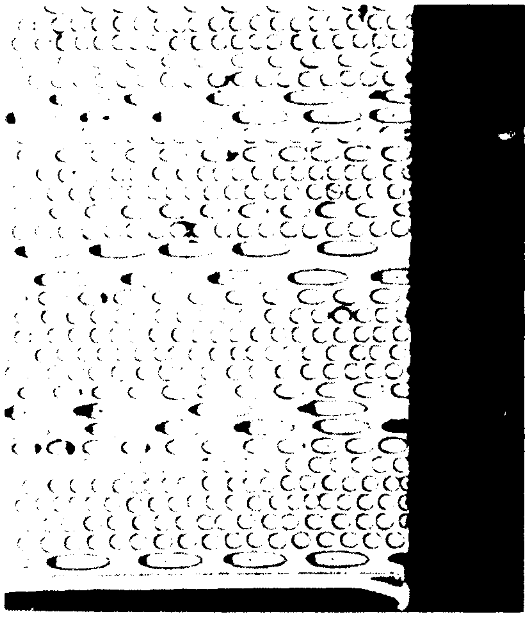

Figure 26. Core Drill Holes Are Good Quality

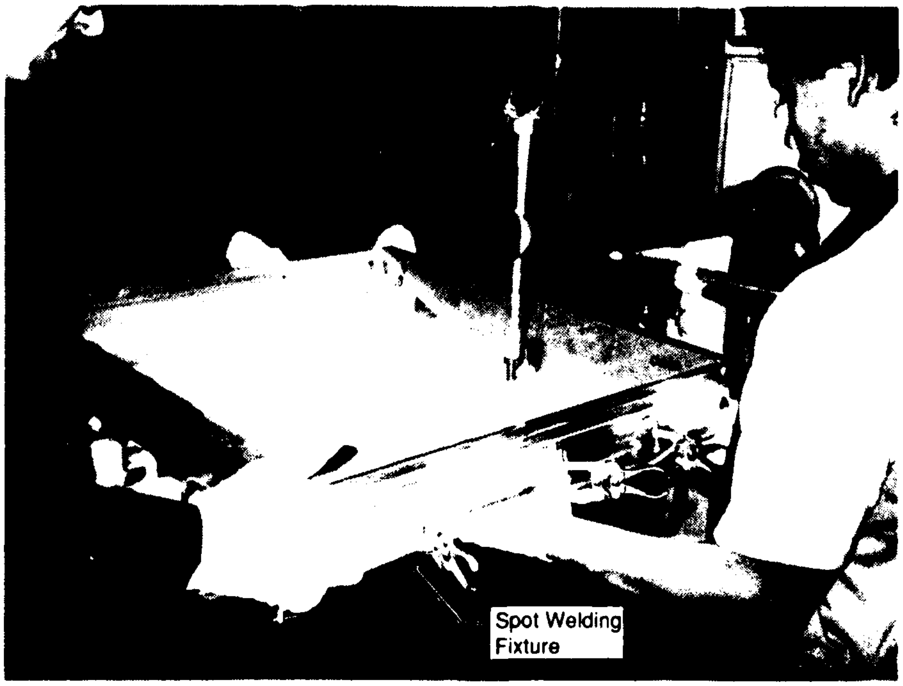

Figure 27. Spotwelding of Hat Stiffened Panels

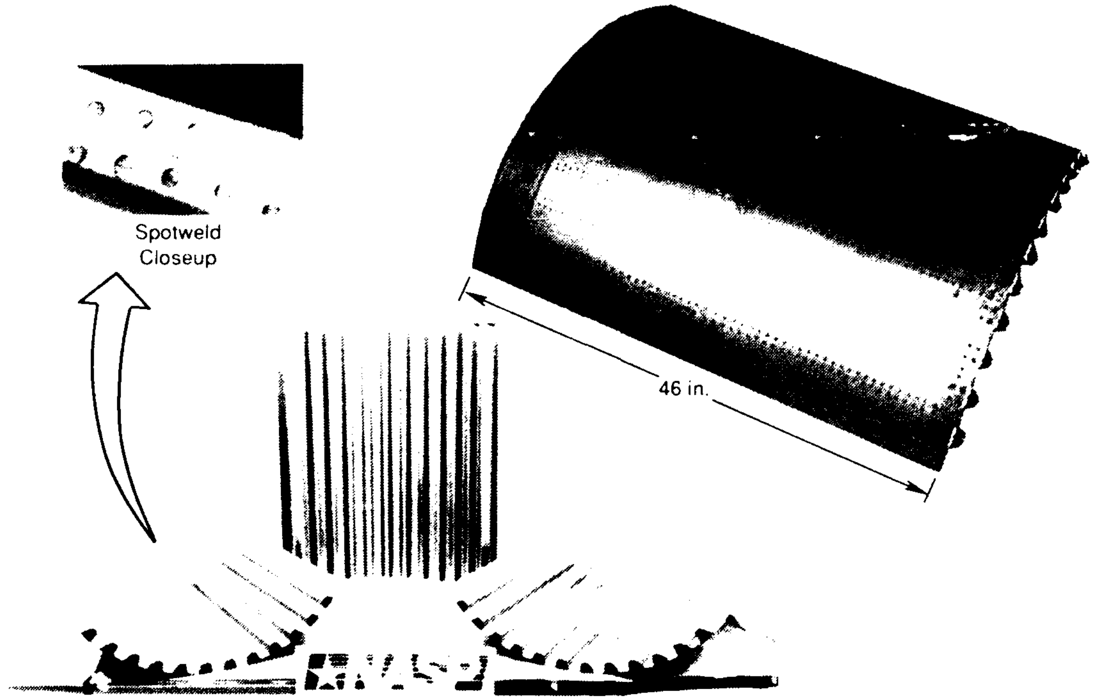

GP34-0684-28

Figure 28. Typical Panels Welded Using Spotwelding Techniques

Brazing is more complex than spotwelding, but produces higher strength joints. A brazing process consists of sandwiching foil of monolithic material in between two TMC parts and applying high temperature and pressure. Special fixtures are required to maintain part location throughout the braze operations, especially at high temperature when bonding occurs. The braze fixture used for the hat stiffened panels of the Lightly Loaded Splice Subcomponent is shown in Figure 29. Moldline contour is maintained by the massive lower tool and hats are securely held against the skin by large cross-bars and shims made from superalloy material. Processing parameters such as maximum temperature and soak time are selected to generate good braze flow and joint strength. The photomicrograph, Figure 30, shows a good, homogeneous braze joint and excellent wettability from this process.

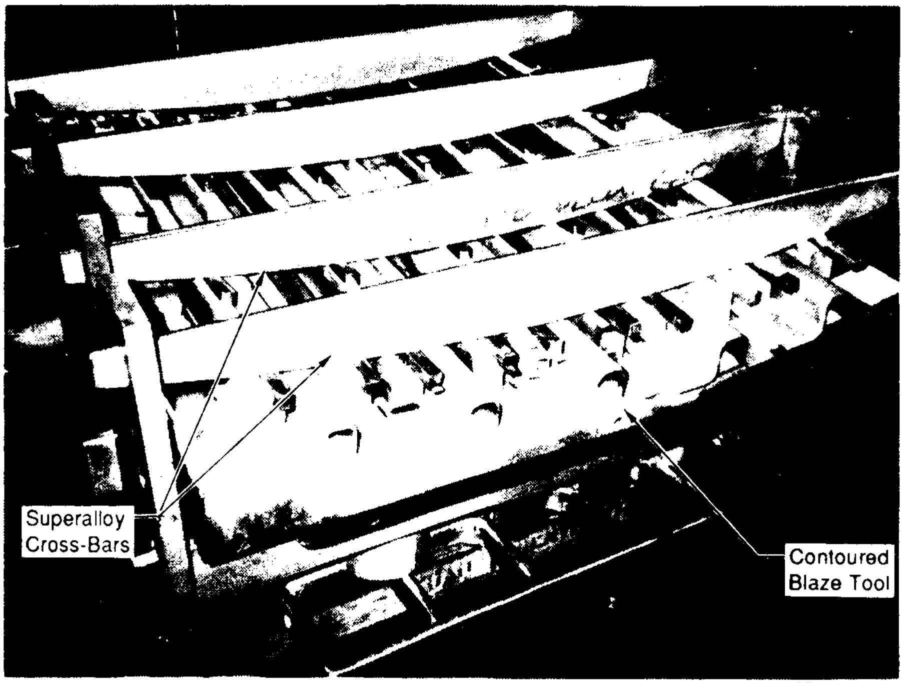

Figure 29. Typical Braze Fixture Set-up

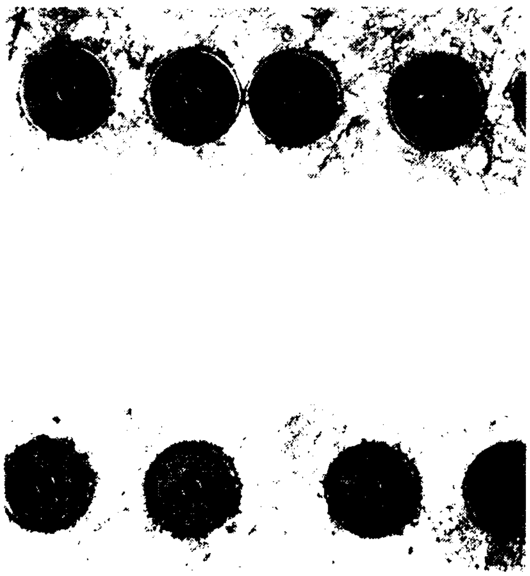

Figure 30. Good Quality Brazing Has Been Demonstrated

LARGE SCALE DEMONSTRATION VALIDATION

The design, analysis, fabrication and testing of demonstration hardware is an integrated process between requirements and process development. McDonnell Douglas along with the NASP team has successfully fabricated and tested several large scale TMC articles shown in Figure 31. These articles range in size from flat subcomponent panels to large fuselage assemblies and demonstrate all of the processes discussed earlier.

BUCKLING PANELS

Early in the TMC development process hat stiffened structure was identified as a candidate structural concept in which local buckling was the critical failure mode. One of the first risk reduction efforts was to design, fabricate and test a series of articles to characterize buckling of flat panels. Panel geometry was selected to be representative of either a fuselage section or wing skin. The general geometry, shown in Figure 32, was two foot square with a hat depth of 1.25 inches. This geometry was determined by structural optimization using temperatures and loads from the vehicle and TMC material properties.

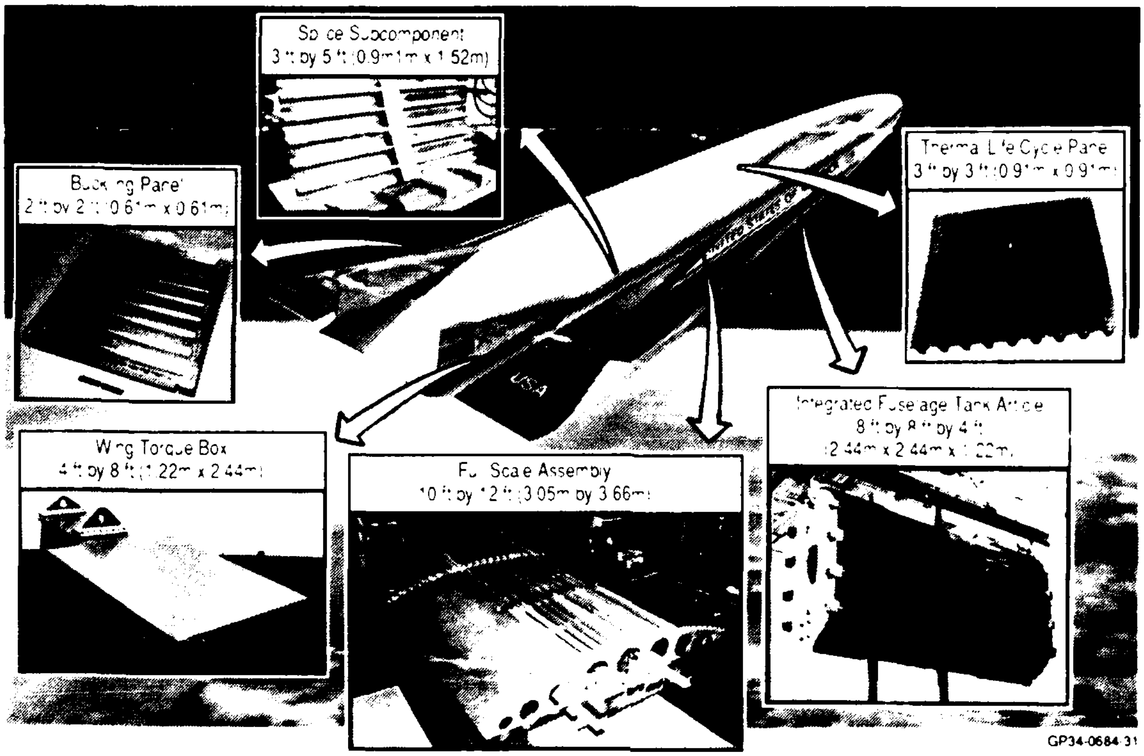
Splice Subcomponent
3 ft by 5 ft (0.91m x 1.52m)
Buckling Panel
2 ft by 2 ft (0.61m x 0.61m)
Thermal Life Cycle Panel
3 ft by 3 ft (0.91m x 0.91m)
Integrated Fuselage Tank Article
8 ft by 8 ft by 4 ft
(2.44m x 2.44m x 1.22m)
Wing Torque Box
4 ft by 8 ft (1.22m x 2.44m)
Full Scale Assembly
10 ft by 12 ft (3.05m by 3.66m)
USA
GP34-0684-31

Figure 31. Large Airframe Structures Fabricated from TMC

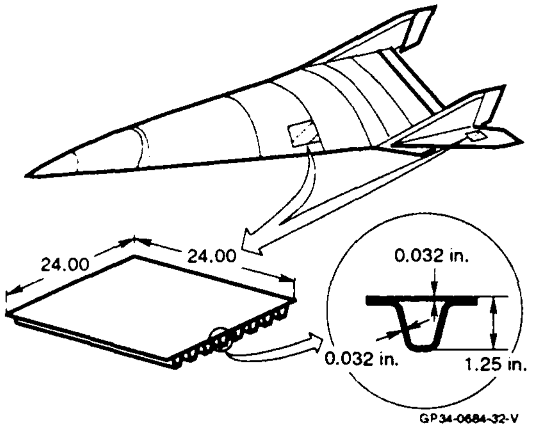
24.00
24.00
0.032 in.
0.032 in.
1.25 in.
GP34-0684-32-V

Figure 32. Buckling Panel Geometry

A monolithic, Ti-6Al-4V panel was fabricated and tested to gain confidence in analysis and testing methods. Although the test temperature was significantly less with this panel than TMC, general thermal/structural response trends were determined. Testing was designed to subject the panel to uniform temperatures and gradients that simulated vehicle conditions. One of the significant challenges in the airframe design is large thermal stresses induced by temperature differences between the hot fuselage skin panels and the cooler fuselage ring frames. Frames were simulated by load introduction hardware attached at the end of the hats. Edge conditions were controlled with frame members designed to prevent out of plane deformation. Test results showed very good correlation to prediction as illustrated in Figure 33. Mid-panel strains are plotted as a function of load along with nonlinear predictions made with the ABAQUS finite element solver. Initial buckling was predicted at 31,000 lbs and the indicated test buckling load was 29,300 lbs or within 7%. Post buckling strength was considerable with the panel capability over 200% of the initial elastic buckling load.

A panel with identical geometry, shown in Figure 34, was fabricated from SCS-6/ Ti 15-3-3 TMC. The skin and hats were constructed using the foil/fiber process and joined by spotwelding. Testing was completed for temperatures up to 1200°F in combination with both axial and transverse mechanical loading. High temperature strain instrumentation was erratic at maximum temperature. Data at temperatures less than 1000°F showed good correlation to pre-test prediction. The transverse load capability or in-plane loads perpendicular to the hat stiffeners was greater than expected. Load paths in this direction are critical due to the build up of thermal stress from thermal surface gradients.

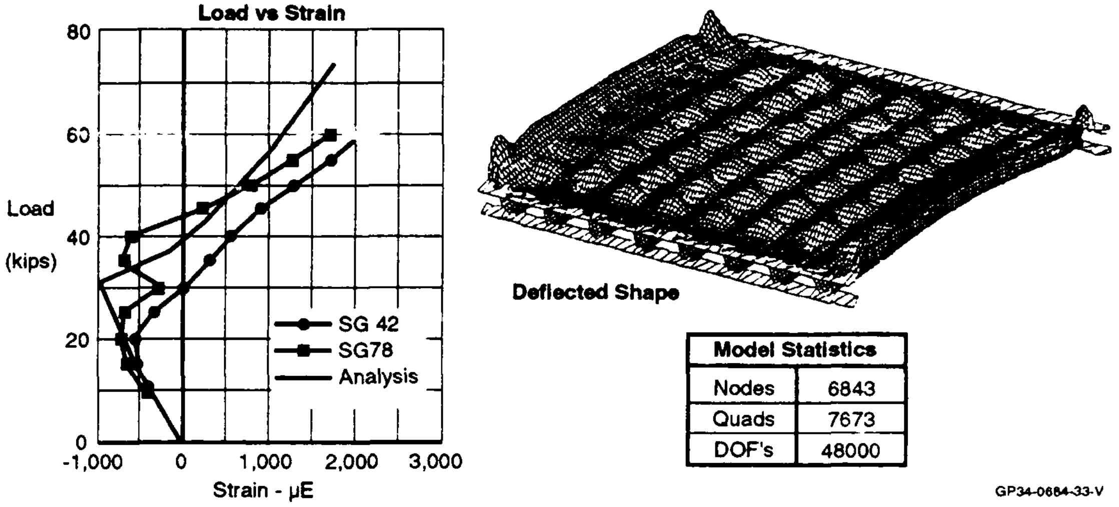

Model Statistics	
Nodes	6843
Quads	7673
DOF's	48000

Figure 33. Monolithic Titanium Panel Test Results

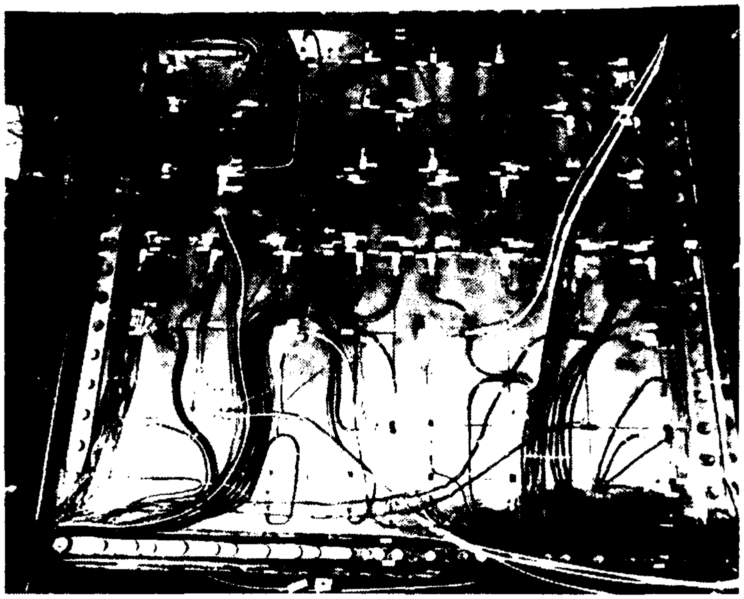

Figure 34. TMC Buckling Panel With Instrumentation

The final buckling panel test article was designed to address the evolving material and design development. The Brazed Beaded Beta Buckling (BBBB) panel, shown in Figure 35, used the Beta or Timet™ 21s matrix system with SCS-9 fibers and hat stiffeners were brazed to the skin. The key design change from the TMC buckling panel was longitudinal skin beads aligned above the hat stiffeners. From the flat panel testing, significant stiffness in the transverse direction was observed causing a build up thermal stress at elevated temperature and was relieved when the skin deformed into a wave pattern. Beads are used to eliminate the transverse thermal stresses and control the deformations. An added benefit is that the initial axial buckling load is increased. This panel is currently under test at Dryden Research Test Facility in Edwards, CA. Initial results from room temperature testing match pre-test predictions within 5%.

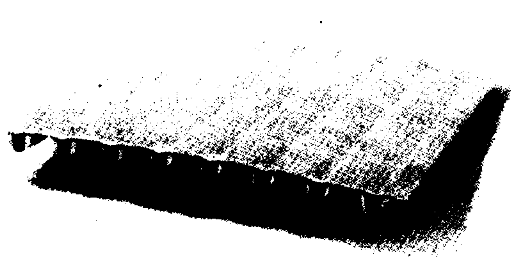

Figure 35. Brazed Beaded Beta Buckling Panel

THERMAL LIFE CYCLE (TLC) PANEL

The Thermal Life Cycle panel is designed to simulate a typical fuselage skin panel joint and demonstrate the durability of TMC. The 3 ft by 3 ft panel is comprised of two hat stiffened panels joined by a midframe splice. Panel components are shown in Figure 36. The hat stiffened panels are approximately 1.5 inches and stiffeners are spaced about every 3.5 inches. The SCS-6/ Ti 15-3-3 TMC components are spotwelded together. The midframe joint consists of two splice plates, one attached to the skin side of the panels and the other connected to the hat side. In addition to providing load path continuity across the joint, the splice plates serve as the frame caps. An inverted hat is used as the shear web of the frame and is connected to the upper and lower caps. This configuration is identical to the fuselage design of the Integrated Fuselage/Cryotank article.

Two main objectives were successfully demonstrated during the test program conducted at Wright Lab in Dayton Ohio. First, in plane shear loads were applied to verify that the midframe joint was adequate. The joint performed as expected and no anomalies were noted. Secondly, repeated exposure to an ascent heating profile was investigated. Since the article was not protected with an oxidation resistant coating, elevated temperature testing was conducted in a helium environment. The article was cycled over 100 times to 1300° F. The majority of the high temperature instrumentation did not survive but the panel looked very good. A slight surface waviness very similar to pre-test predictions could be seen. Some cracks were also identified in the spotweld nuggets.

LIGHTLY LOADED SPLICE SUBCOMPONENT (LLSS)

The 2.5 foot by 5 foot Lightly Loaded Splice Subcomponent, shown in Figure 37, is another article which represents a typical fuselage joint between two hat stiffened panels. Critical design features demonstrated in this article are an all TMC curved frame, smooth moldline transition, hat and skin joggles, combined SCS-6 and SCS-9 fibers, brazed hat/skin panels and oxidation coating. The midframe splice, illustrated in Figure 38, is the most complex joint of any TMC demonstration hardware. The curved frame consists of several preformed TMC parts that are diffusion bonded together to form the 80 inch radius frame. Moldline smoothness across the joint is critical to avoid excessive temperatures from aeroheating. Joggles in the skins, hats and the upper splice plates are required along with countersunk fasteners to achieve this requirement. Shear clips are used to provide good shear continuity from the hat stiffeners to the frame. The Beta or Timet™ 21s matrix is used throughout the article and is combined with either SCS-6 or SCS-9 depending on structural component requirements. Hats are brazed to skin panels resulting in a 80 inch radius curved panel using the process describe previously. A protective coating was applied on

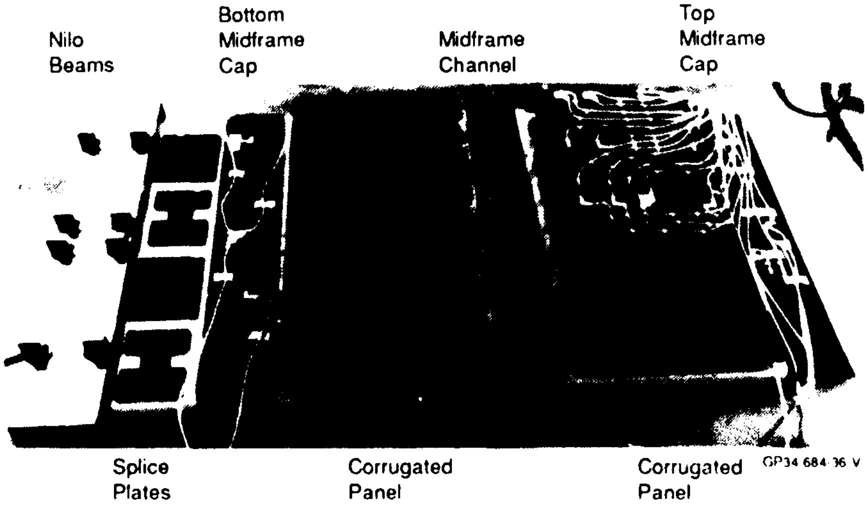

Figure 36. Thermal Life Cycle Panel Components

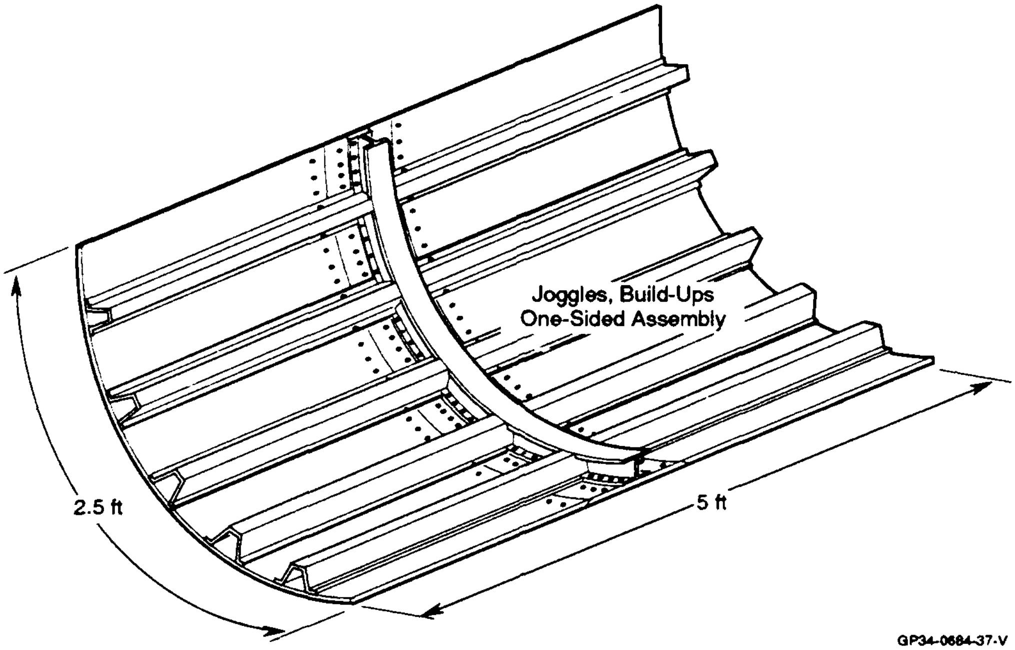
Joggles, Build-Ups
One-Sided Assembly
2.5 ft
5 ft
GP34-0684-37-V

Figure 37. Lightly Loaded Splice Subcomponent Represents NASP Fuselage

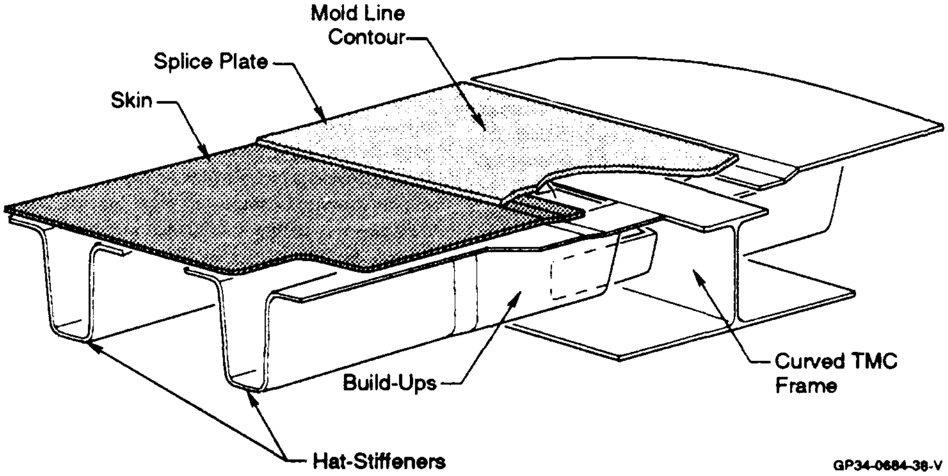
Mold Line Contour
Splice Plate
Skin
Build-Ups
Curved TMC Frame
Hat-Stiffeners
GP34-0684-38-V

Figure 38. Frame Splice Provides Smooth Moldline

all surfaces to prevent oxidation at elevated temperature. Final assembly is accomplished from one-side access, as shown in Figure 39, to demonstrate vehicle assembly.

Testing of the article under axial compression load and transient thermal conditions is complete with the exception of the test to failure. Accomplishments of this testing are summarized in Figure 40. Over 66 tests have been completed representing combined thermal/mechanical flight conditions. A maximum temperature of 1500° F was achieved with no adverse effects. The article was subjected to ultimate mechanical load at two design conditions, 990°F and 1140°F, with no observed damage. Deflections and strains were low as expected with a critical failure mode of local buckling.

GP34-0684-39

Figure 39. LLSS Final Assembly Using One Sided Access

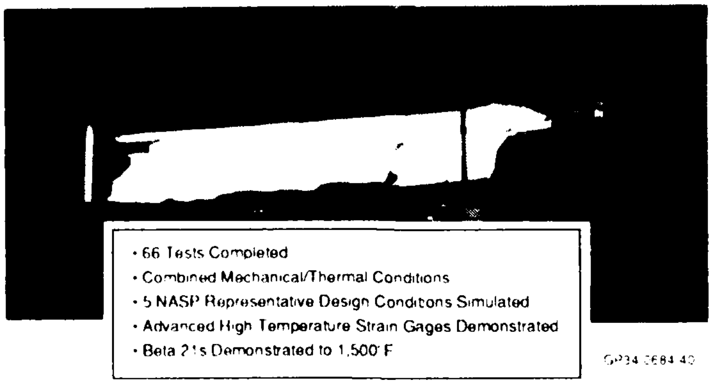

- 66 Tests Completed
- Combined Mechanical/Thermal Conditions
- 5 NASP Representative Design Conditons Simulated
- Advanced High Temperature Strain Gages Demonstrated
- Beta 21s Demonstrated to 1,500°F

GP34-0684-40

Figure 40. LLSS Accomplishments

MAJOR ASSEMBLIES

One major TMC assembly is currently in work and two have completed assembly and test. They are the TMC Wing Torque Box developed under MDC IRAD, the Full Scale Assembly (FSA) designed and in fabrication as part of the NASP Phase 2D effort, and the Integrated Fuselage/Cryotank Article designed and built in a cooperative effort between NASP and MDC and tested under the NASP Phase 2D program.

TMC WING TORQUE BOX

The TMC Wing Torque Box is an all TMC, built-up structure representing the root section of a highly loaded aerosurface, as shown in Figure 41. A Ti 15-3-3 matrix material is reinforced with SCS-6 fibers. It is the largest, thick laminate TMC structure ever built measuring 8 feet long by 4 feet wide, with a depth varying from 14 inches at the root to 5 inches at the tip. Internal stiffening is provided by provided by 4 inboard/outboard spars, shown in Figure 42. Two 8 foot main spars located in the center of the article run root to tip and two 5 foot edge spars close out the leading and trailing edges. A 9-bay "box" is formed by intercostals between the main and edge spar members. Large one piece TMC skins with a thickness varying from .22 inches to .14 inches are attached on the upper and lower surfaces to form the complete structure.

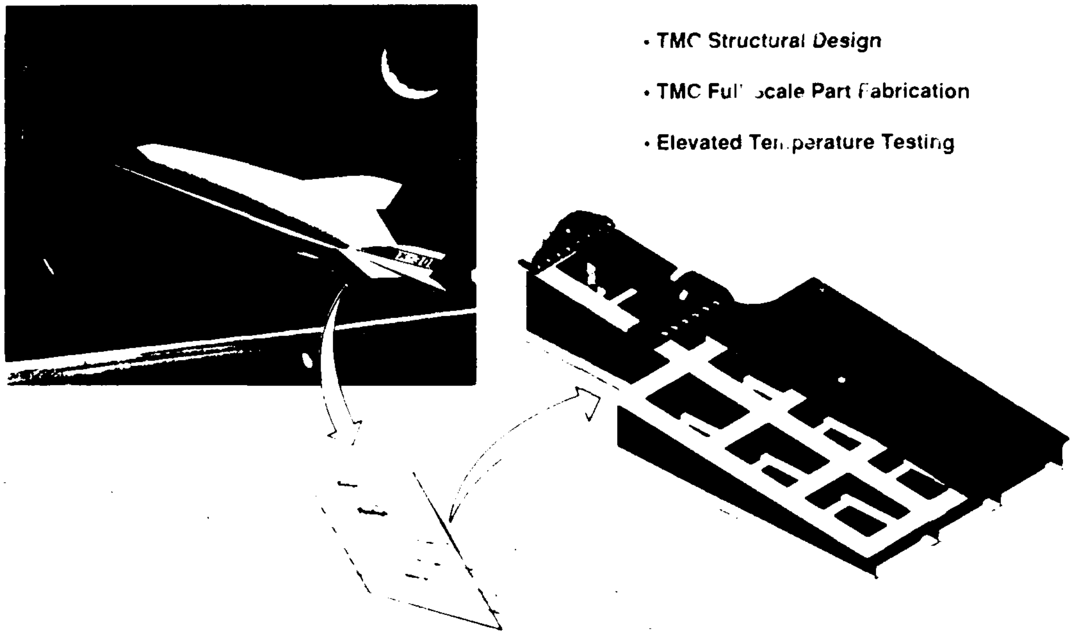
• TMC Structural Design
• TMC Full Scale Part Fabrication
• Elevated Temperature Testing

Figure 41. TMC Wing Torque Box Represents Wing Root Section

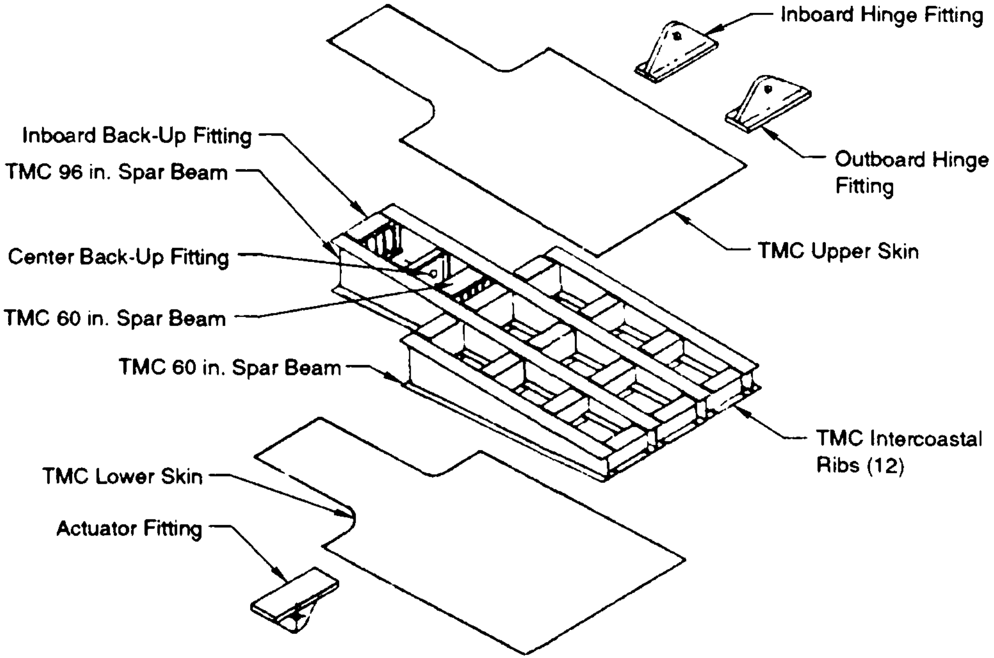
Inboard Hinge Fitting
Inboard Back-Up Fitting
TMC 96 in. Spar Beam
Outboard Hinge Fitting
Center Back-Up Fitting
TMC Upper Skin
TMC 60 in. Spar Beam
TMC 60 in. Spar Beam
TMC Intercoastal Ribs (12)
TMC Lower Skin
Actuator Fitting
GP34-0684-42-V

Figure 42. Wing Torque Box Components

Many of the TMC fabrication process steps previously described were developed and refined for this article. Spars and intercostals are I-beam configuration and are fabricated using a two step process similar to the one used on the LLSS curved TMC frame. Webs of the spars are formed with two C-channels placed back-to-back, and additional laminates are placed on top of the channels to create the I-beam caps. Extra titanium foil is inserted between mating surfaces to facilitate good bonding. The spar is diffusion bonded in the same HIP unit used to consolidate the TMC laminates. Spars and intercostals are cut and trimmed using the waterjet, diamond wheel, and EDM processes described earlier. Over 1000 mechanical fasteners are used to join spars, skins, and intercostals.

Figure 43 shows the test set-up at Wright Lab for combined mechanical and elevated temperature testing. Testing was designed to complete room temperature testing first to efficiently utilize low temperature instrumentation before proceeding to high temperature conditions. The article failed at 100% design limit loads at room temperature. Shown in Figure 44 are strains in the radius area where the failure initiated. The interaction of stress concentration effects around the spindle region resulted in excessive strains and caused the failure. Insufficient material characterization in early design phases also contributed to the failure. A smaller version of the article with different boundary reactions is currently being developed and testing of the modified article is scheduled for next year.

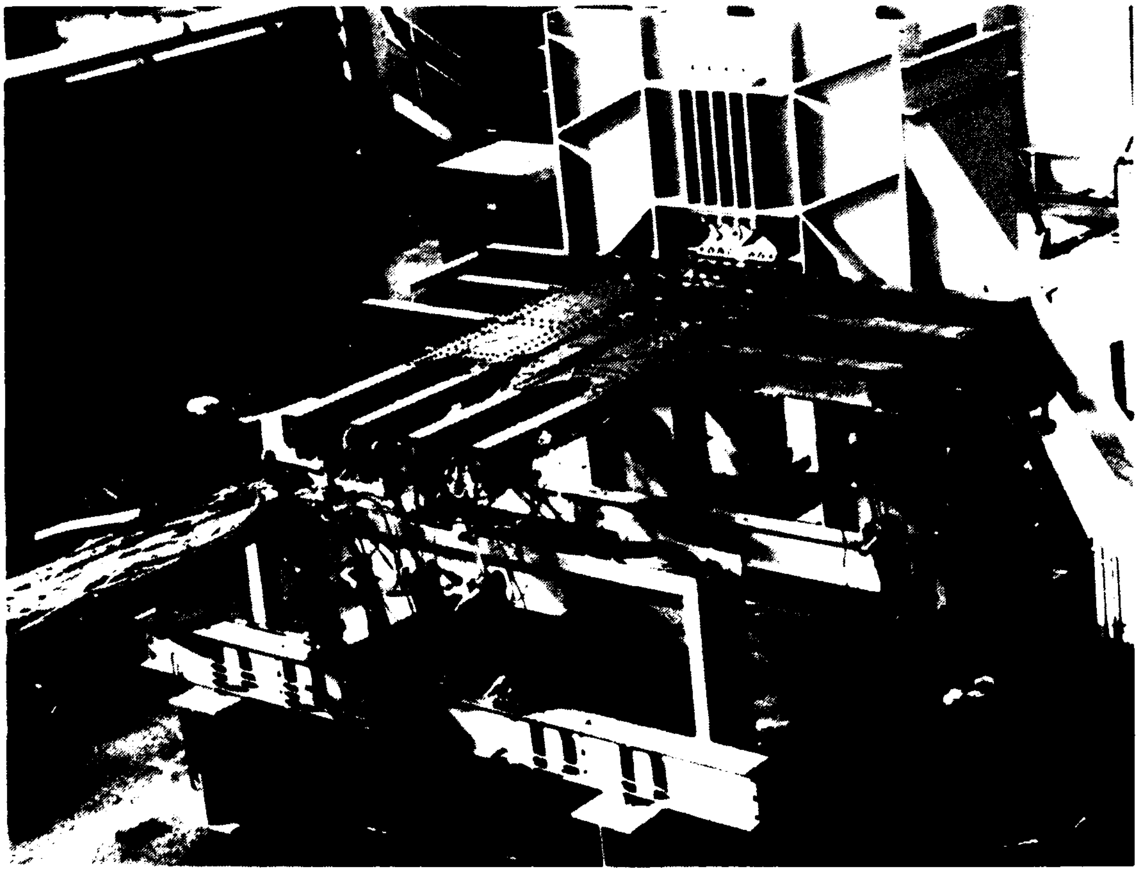

Figure 43. Test Set-Up for TMC Wing Torque Box at Wright Lab

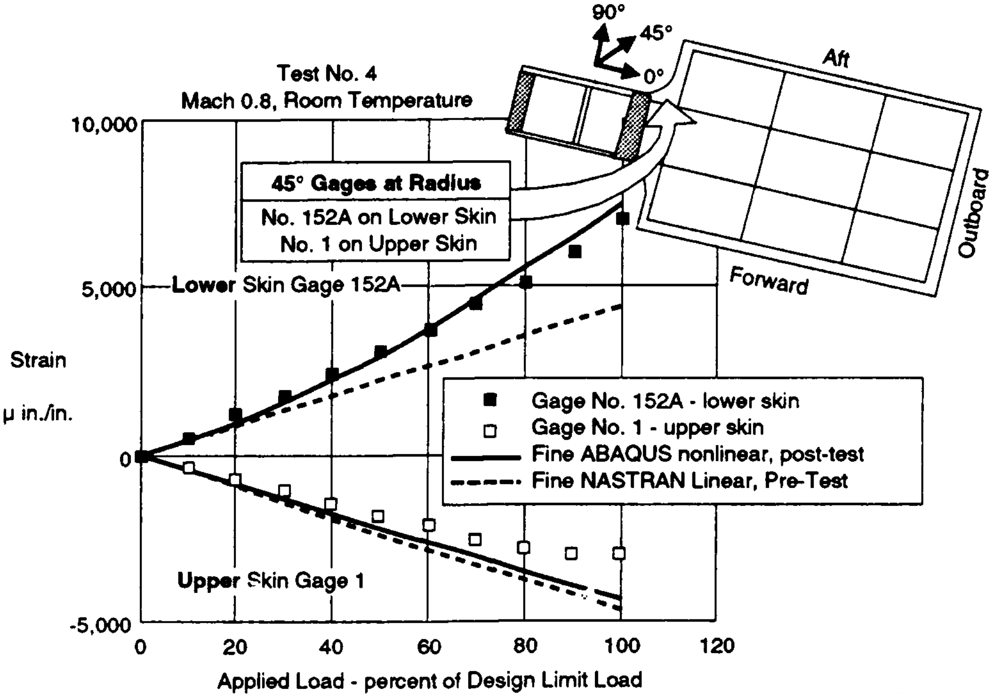

Figure 44. Strains in Corner Radius of Wing Torque Box

FULL SCALE ASSEMBLY (FSA)

The Full Scale Assembly is the latest TMC article being developed by the NASP program. The article is representative of a full scale section of the upper fuselage measuring 10 feet wide by 12 feet long and demonstrates two different frame concepts. A manufacturing breakdown of the article shown in Figure 45 depicts the number, shape and size of assembly components. Hat stiffeners are joined to skins with spotwelding. Large, 8 foot long panels, shown in Figure 46, are used to demonstrate an integral frame concept where a build-up in the skin serves as the upper frame cap. The joint between the 8 foot sections and the 4 foot sections is a more typical splice. The joint is shown in Figure 47 as well as the link fitting which provides interface to the cryogenic tank through thermal isolation links. The link fitting access holes are covered by structural TMC access plates or covers.

One significant challenge addressed with this article is the scale-up of large thin laminate TMC. The 4 foot by 8 foot skins consist of various build-ups of SCS-6 and SCS-9 / Beta or Timet™ 21s TMC. A large portion of the skin is a 3 ply laminate. Anomalies caused by separation of the fibers during processing, referred to as "fisheyes" have been observed. Modification of processing parameters and improvements in layup methods have eliminated the "fisheyes" in test laminates and a full scale skin is in production.

As large articles like the FSA are produced, assembly techniques are being refined and lessons learned for the use on the vehicle. Figure 48 shows the assembly tool used for the FSA. This tool is modular and not only serves at the final assembly platform but is also used as a spotweld jig for individual panels. Drilling techniques used on the LLSS and TMC Wing Torque Box will be used on the FSA.

The FSA will be tested under combined mechanical/thermal conditions representative of flight environments. Test planning and fixture development work is ongoing at Wright Lab in Dayton, Ohio.

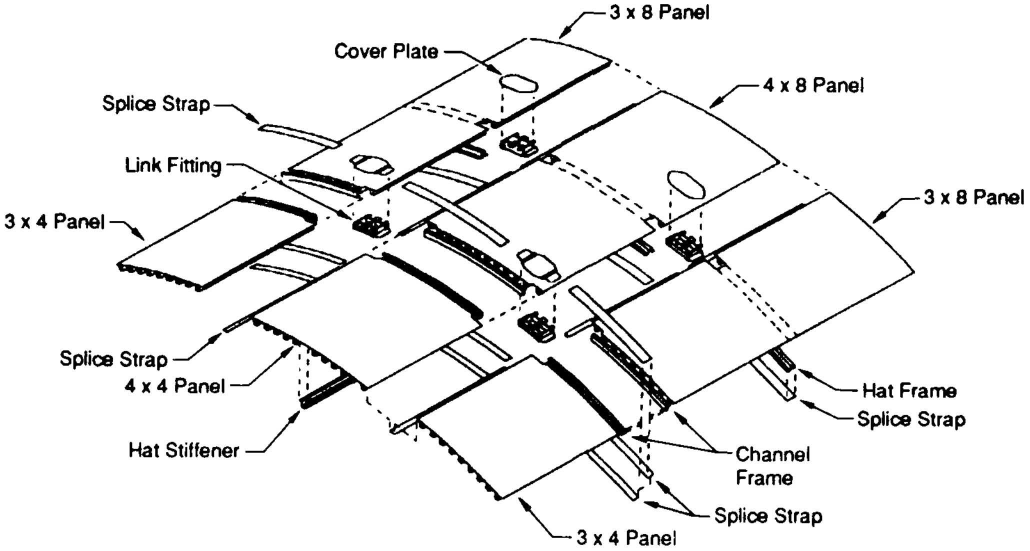
3 x 8 Panel
Cover Plate
4 x 8 Panel
Splice Strap
Link Fitting
3 x 8 Panel
3 x 4 Panel
Splice Strap
4 x 4 Panel
Hat Frame
Splice Strap
Hat Stiffener
Channel Frame
Splice Strap
3 x 4 Panel
GP34-0684-45-V

Figure 45. Full Scale Assembly Manufacturing Breakdown

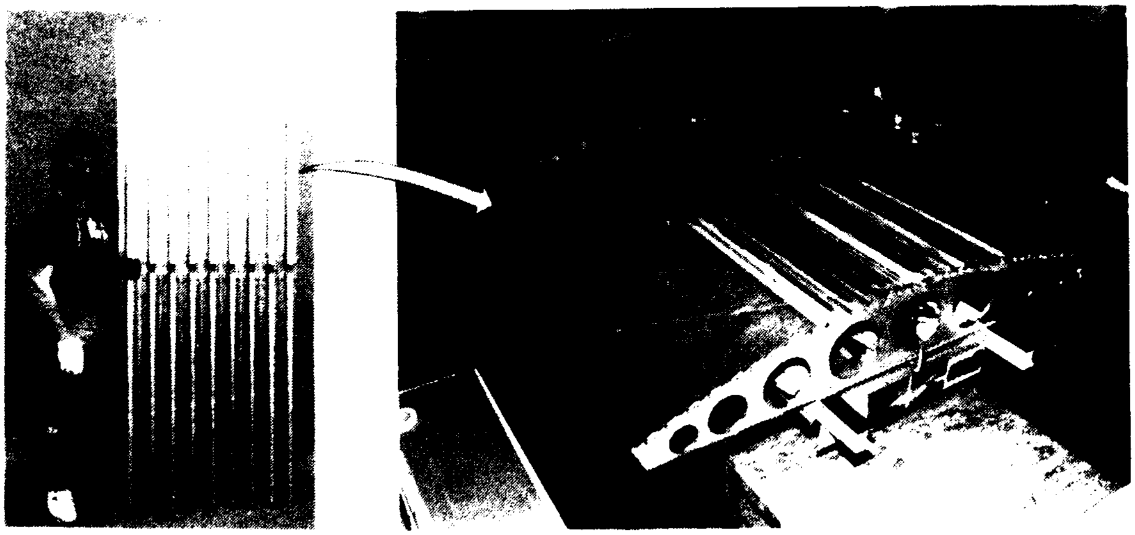
Hat Stiffened TMC Panel
3 ft by 3 ft

TMC Panels/Hats In Assembly Jig

GP34-0684-46

Figure 46. Spotwelded Full Scale Assembly Panels

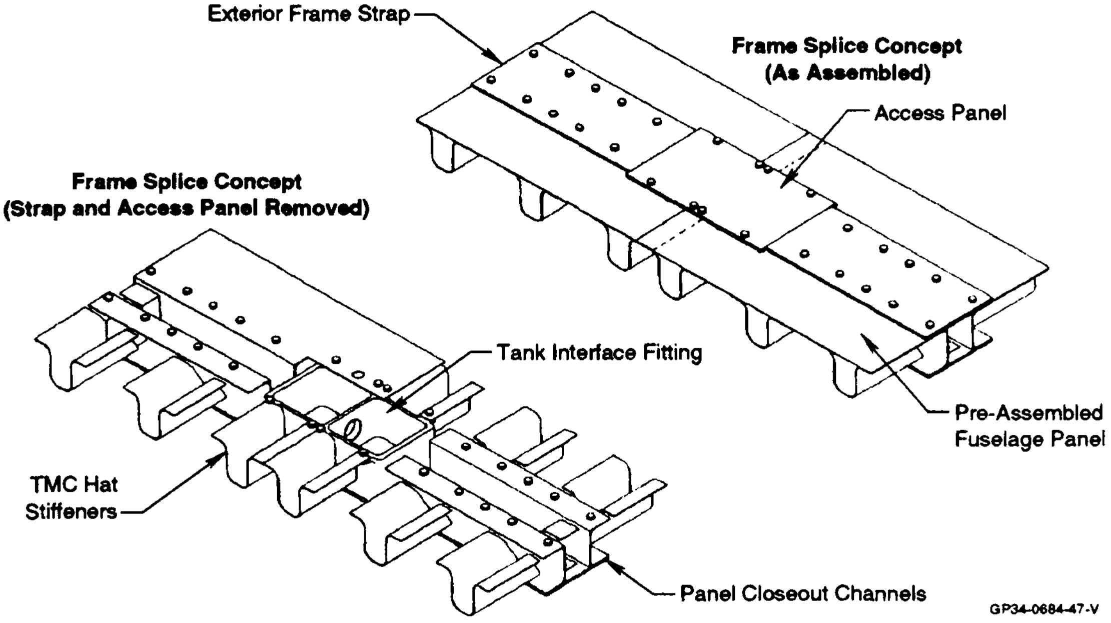
Exterior Frame Strap
Frame Splice Concept
(As Assembled)
Access Panel
Frame Splice Concept
(Strap and Access Panel Removed)
Tank Interface Fitting
Pre-Assembled
Fusealge Panel
TMC Hat
Stiffeners
Panel Closeout Channels
GP34-0684-47-V

Figure 47. Full Scale Assembly Joint Addresses Critical Requirements

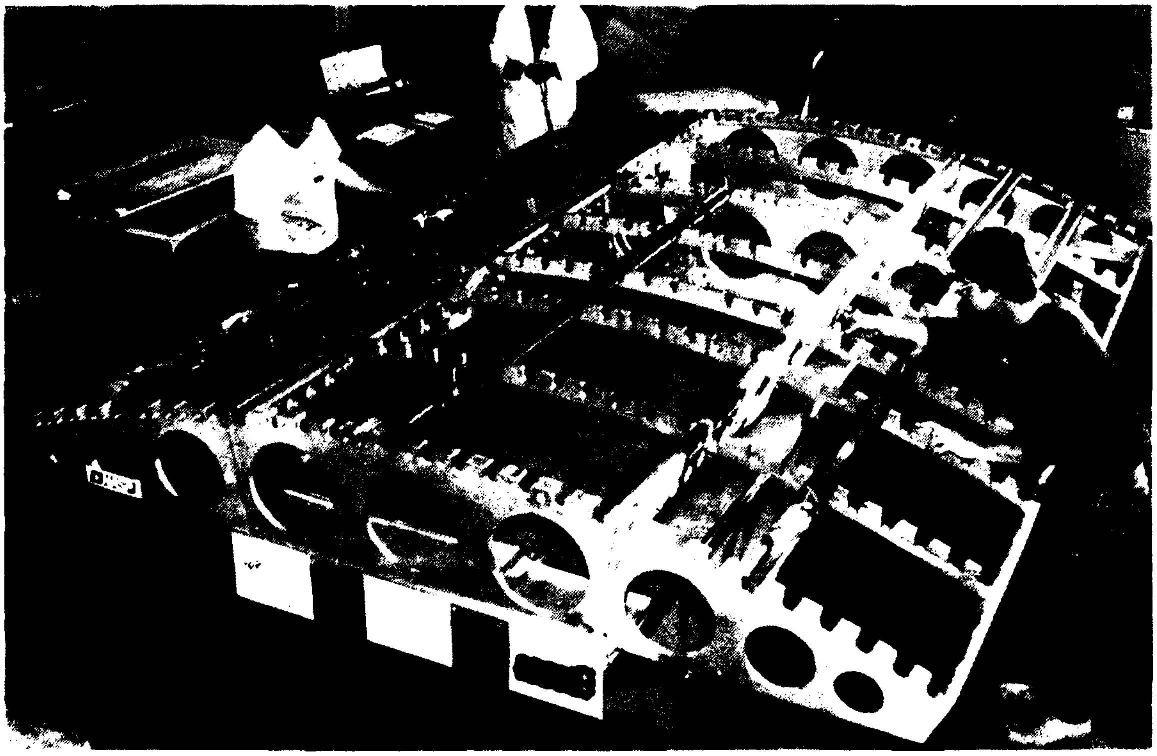
GP34-0684-48

Figure 48. FSA Assembly Tool and Spotwelding Jig

INTEGRATED FUSELAGE/CRYOTANK ARTICLE (IFTA)

The principle demonstration article developed for the NASP program is the Integrated Fuselage/Cryotank article designed and fabricated by McDonnell Douglas and tested under the NASP Phase 2D program. The article is representative of an airframe section including a TMC fuselage and carbon/epoxy cryogenic tank which are integrated as shown in Figure 49. The fuselage component shown in Figure 50 measures approximately 8 feet long by 8 feet wide and 4 feet high and is built-up from eight curved TMC skins and four flat skins. More than one hundred TMC hat stiffeners were fabricated and attached to the skins with spotwelds. An internal view of the fuselage is shown in *Figure* 51. The Ti 15-3-3/SCS-6 TMC material system was used for this article.

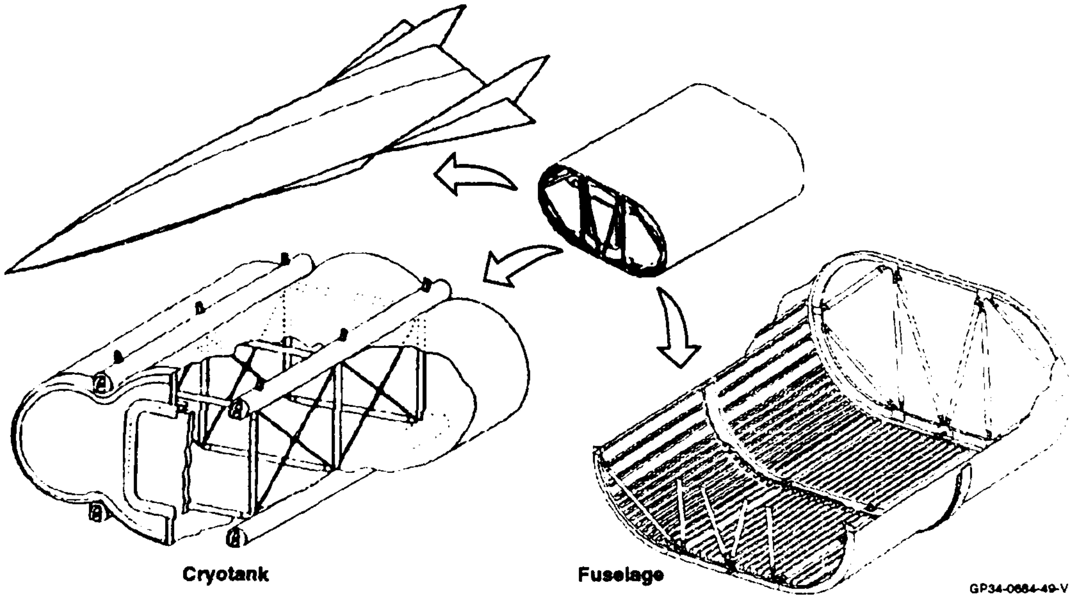
Cryotank
Fuselage
GP34-0684-49-V

Figure 49. Fuselage and Cryotank Are Integrated

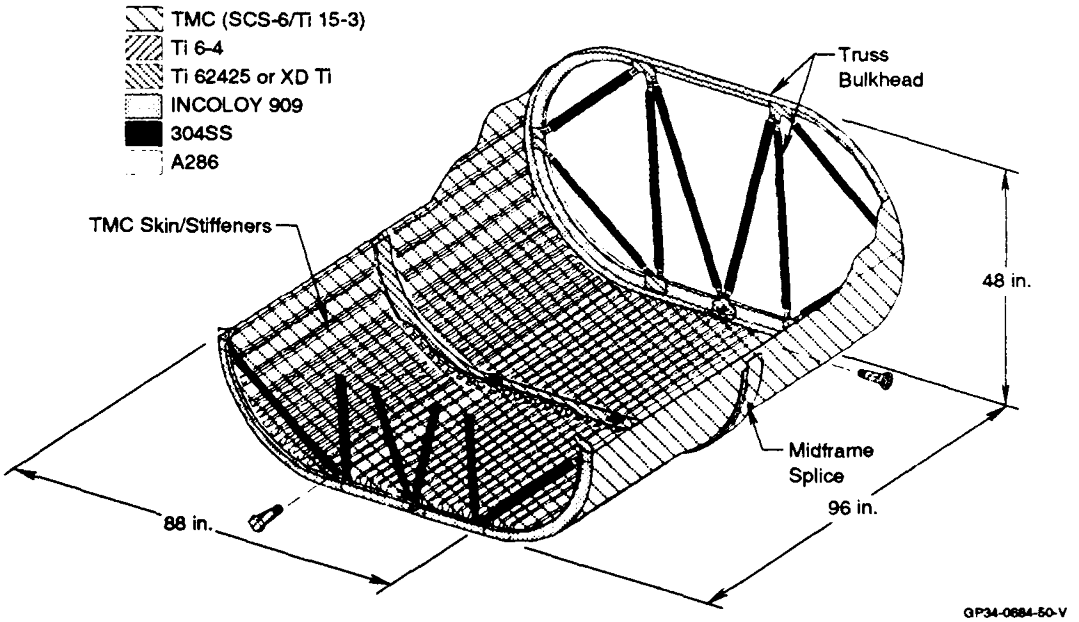
TMC (SCS-6/Ti 15-3)
Ti 6-4
Ti 62425 or XD Ti
INCOLOY 909
304SS
A286
Truss Bulkhead
TMC Skin/Stiffeners
48 in.
Midframe Splice
96 in.
88 in.
GP34-0684-50-V

Figure 50. Fuselage Material Distribution

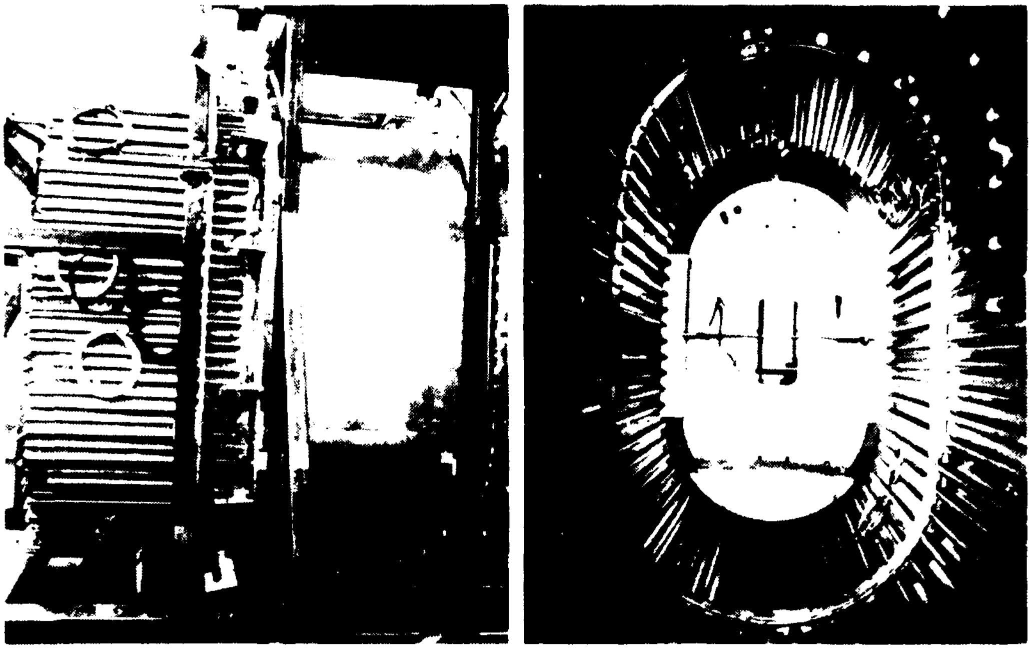
GP34-0684-51

Figure 51. Internal And External Views of IFTA Fuselage

The midframe region of the article was identical to the Thermal Life Cycle panel and represented a typical panel to panel splice as shown in Figure 52. Fasteners holes were prepared by punching and reaming along with drilling. The majority of the TMC was thin (less than 8 plys) and did not present major assembly problems. Final assembly of the panels required large assembly jigs to hold accurate tolerances. Especially since the panels had to be mate drilled, removed for painting, and re-assembled. An additional complexity was the insertion of the cryogenic tank into the fuselage. This procedure was accomplished by mounting the assembly jig on rails which allowed one end of the fuselage to be moved. The tank is shown ready for insertion in Figure 53.

The article was tested under combined thermal / mechanical / cryogenic conditions that represented critical design environments. The TMC fuselage shell was heated to 1300° F while the cryogenic tank contained over 900 gallons of liquid hydrogen at -420°F. The result was the most realistic test for a NASP system yet. Testing of this complexity required the integration of many operational system as shown in Figure 54. These systems were designed and implemented at the McDonnell Douglas Cryogenic Test Facility located at Wyle Labs in Norco CA.

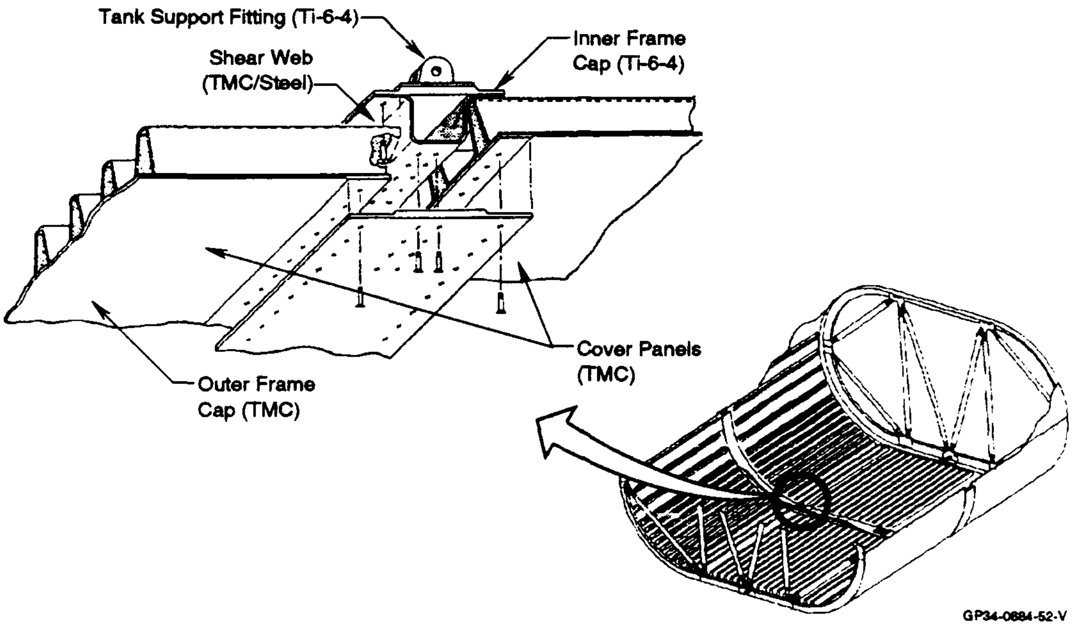
Tank Support Fitting (Ti-6-4)
Shear Web (TMC/Steel)
Inner Frame Cap (Ti-6-4)
Cover Panels (TMC)
Outer Frame Cap (TMC)
GP34-0684-52-V

Figure 52. Frame Splice Joint Used In IFTA Fuselage Article

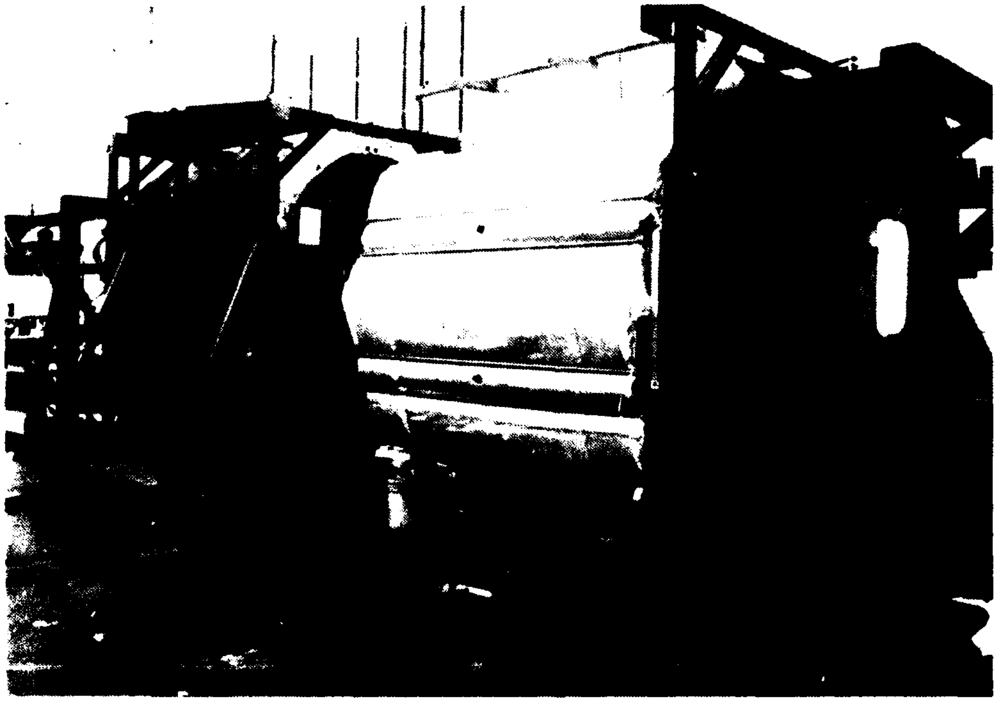
GP34-0684-53

Figure 53. Cryotank Ready for Insertion Into TMC Fuselage

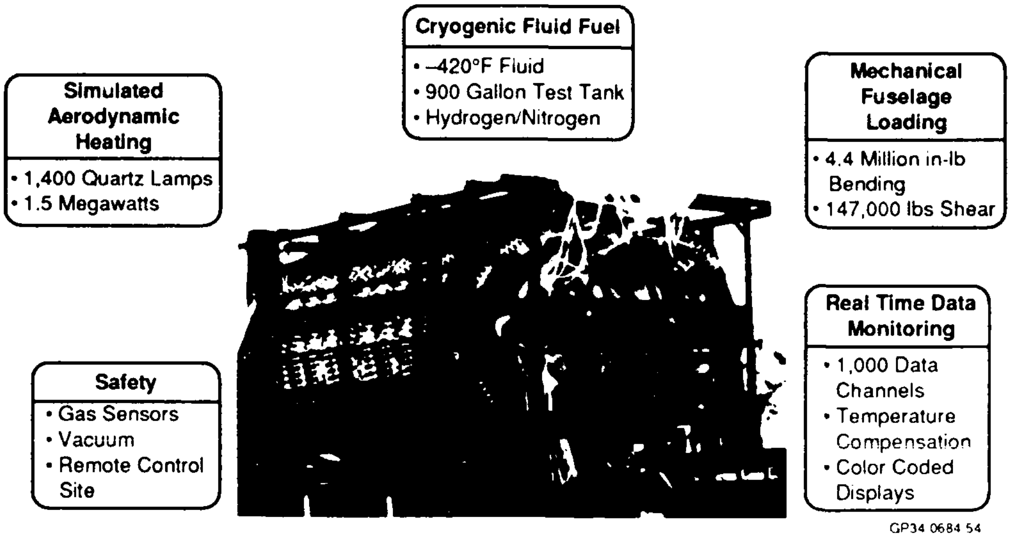
Cryogenic Fluid Fuel
• –420°F Fluid
• 900 Gallon Test Tank
• Hydrogen/Nitrogen
Simulated Aerodynamic Heating
• 1,400 Quartz Lamps
• 1.5 Megawatts
Mechanical Fuselage Loading
• 4.4 Million in-lb Bending
• 147,000 lbs Shear
Real Time Data Monitoring
• 1,000 Data Channels
• Temperature Compensation
• Color Coded Displays
Safety
• Gas Sensors
• Vacuum
• Remote Control Site
GP34 0684 54

Figure 54. Systems Required for Integrated Testing

Testing verified that the TMC hot structure fuselage shell concept could meet NASP requirements as a complete system. The stiffened structure performed well under both thermal and mechanical load conditions. Mechanical response correlated with pre-test predictions and analysis tools, shown in Figure 55, while elevated temperature conditions followed expected trends, but could not be quantitatively correlated due to poor instrumentation performance. Spotweld attachments showed no indication of failure from visual inspection, but more detailed NDE is planned.

A summary of the testing accomplishment is presented in Figure 56.

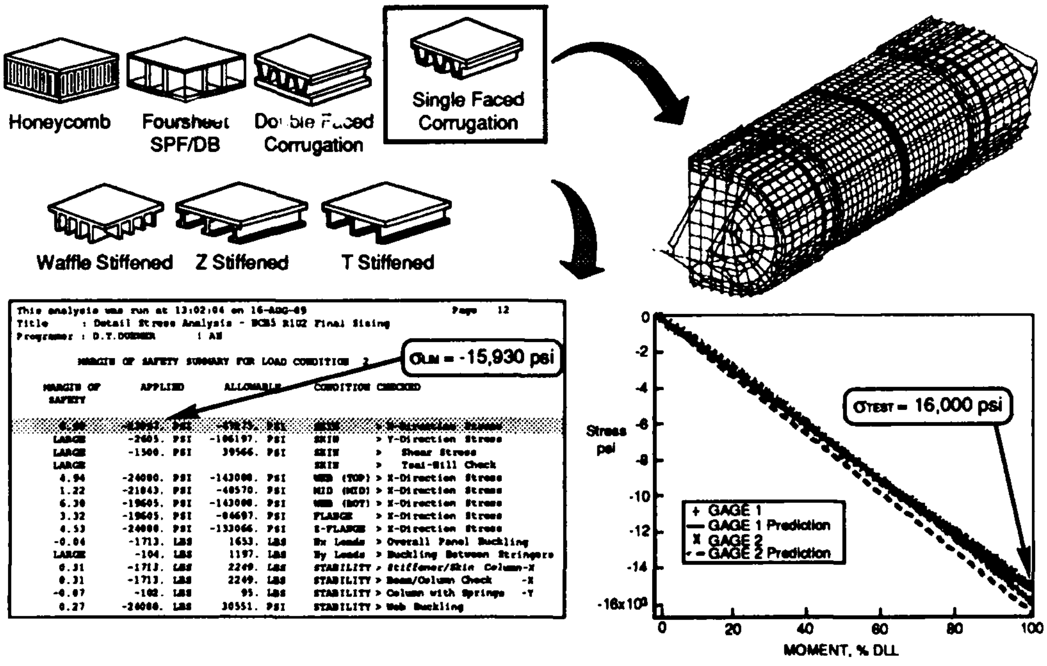

```
This analysis was run at 13:02:04 on 16-AUG-89                Page   12
Title      : Detail Stress Analysis - BCB5 R102 Final Sizing
Programmer : D.T.[illegible]        ! AB

       MARGIN OF SAFETY SUMMARY FOR LOAD CONDITION  2

  MARGIN OF      APPLIED       ALLOWABLE      CONDITION CHECKED
   SAFETY

[illegible]
    LARGE        -2605. PSI   -106197. PSI   SKIN       > Y-Direction Stress
    LARGE        -1500. PSI     39566. PSI   SKIN       >   Shear Stress
    LARGE                                    SKIN       >   Tsai-Hill Check
     4.94       -24080. PSI   -143000. PSI   WEB (TOP) > X-Direction Stress
     1.22       -21043. PSI    -48570. PSI   MID (MID) > X-Direction Stress
     6.30       -19605. PSI   -143000. PSI   WEB (BOT) > X-Direction Stress
     3.32       -19605. PSI    -84697. PSI   FLANGE     > X-Direction Stress
     4.53       -24000. PSI   -133066. PSI   Z-FLANGE   > X-Direction Stress
    -0.04        -1713. LBS      1653. LBS   Nx Loads   > Overall Panel Buckling
    LARGE         -104. LBS      1197. LBS   Ny Loads   > Buckling Between Stringers
     0.31        -1713. LBS      2249. LBS   STABILITY > Stiffener/Skin Column-X
     0.31        -1713. LBS      2249. LBS   STABILITY > Beam/Column Check    -X
    -0.07         -102. LBS        95. LBS   STABILITY > Column with Springs  -Y
     0.27       -24000. LBS     30551. PSI   STABILITY > Web Buckling
```

Figure 55. Analysis Correlation to IFTA Test Results

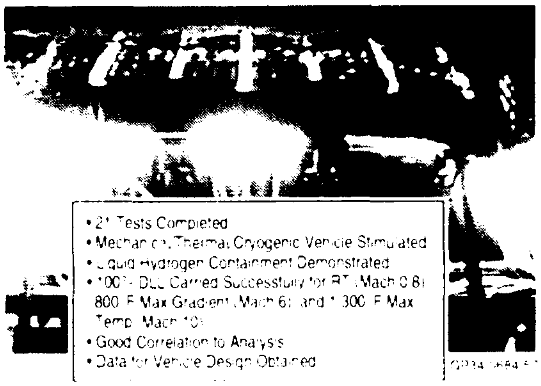

- 21 Tests Completed
- Mechanical/Thermal/Cryogenic Vehicle Simulated
- Liquid Hydrogen Containment Demonstrated
- 100% DLL Carried Successfully for RT (Mach 0.8), 800 F Max Gradient (Mach 6) and 1300 F Max Temp (Mach 10)
- Good Correlation to Analysis
- Data for Vehicle Design Obtained

Figure 56. IFTA Testing Accomplishments

CONCLUSIONS

Titanium Matrix Material systems are candidates for large structures to achieve high payoff results. The benefits of TMC are high temperature capability at very low weight with good reliability. Development has progressed from small coupon samples for materials research to simple structural forms such as hat stiffeners with final applications large enough to be used as subassemblies for hypersonic vehicles. Design and analysis methods have produced feasible designs. Manufacturing research has developed techniques and processes to successfully fabricate and assemble complex structures. Testing has validated design performance and in certain circumstances identified areas where even lighter weight concepts are possible. The overriding issue facing TMC material systems illustrated in Figure 57, is not performance, but cost. New procedures that will significantly lower TMC cost are needed to make the system viable for more applications.

Summary of Titanium Matrix Development

- Advantages of TMC Are Low Weight and High Temperatures
- Foil/Fiber Processing Is Widely Used for Large Structures
- TMC Manufacturing Techniques Exist and Are in Use
- Large Hardware Demonstrates Material Scale-Up
- Mechanical/Thermal Testing Validates Structural Capabilities

GP34-0684-58-V

Figure 57. TMC Development Conclusions

SCS-6™ FIBER REINFORCED TITANIUM

by

Jim Henshaw
Textron Specialty Materials
2 Industrial Avenue
Lowell
Massachusetts 01851
United States

1.0 Introduction

The low weight structurally efficient "SCS-6™ Fiber Reinforced Titanium," as produced by Textron Specialty Materials, is a material awaiting the development of production applications. A multitude of airframe and engine parts have been produced for test and developmental purposes and a production facility has been established to fabricate preforms, intermediary products and component shapes.

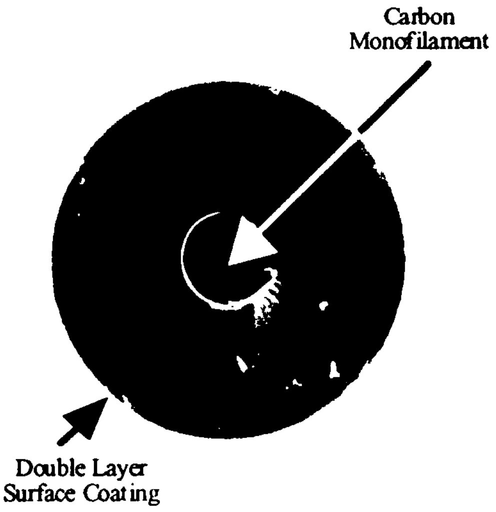

Figure 1
Cross Section of a 140 Micron
Diameter SCS-6 Filament

• • • • • • • • • • • • • • • •

2.0 The SCS-6™ Reinforcing Fiber

As discussed herein the continuous fiber reinforced titanium utilizes a 140 micron diameter silicon carbide monofilament. This fiber, designated as SCS-6™ and specifically constructed for reinforcement of titanium, is produced by the conventional chemical vapor deposition (CVD) using an especially fabricated 33 micron diameter carbon substrate filament that acts as a nucleation site for the growth of the silicon carbide material in the CVD reactor. Through speed, deposition rate and other factors control the resultant filament diameter. *Figure 1* illustrates the cross section of the 140 micron diameter SCS-6 fiber, showing the carbon monofilament substrate, the various graduated layers of silicon carbide, and the well known double layer surface coating. This surface coating has two purposes, (a) to essentially heal the irregular surface of the crystalline beta silicon carbide and hence increase its strength, and (b) to act as a sacrificial layer to aleviate stress concentration effects resulting from the fiber to matrix chemical reactions that occur during high temperature consolidation. The strength of the fiber is controlled to a minimum average of 500 ksi, while demonstrating a typical individual average strength of (600 ksi) and a coefficient of variation of (13.9%). A histogram for a particular filament production period is illustrated in *Figure 2*. For those who prefer the Wiebull analysis, this data converts to a Wiebull modulus of 9 at a 99% confidence level.

Presented at an AGARD Meeting on 'Characterisation of Fibre Reinforced Titanium Matrix Composites', September 1993.

Figure 2

HISTOGRAM of SCS-6 FIBER
AUGUST-SEPTEMBER 1992

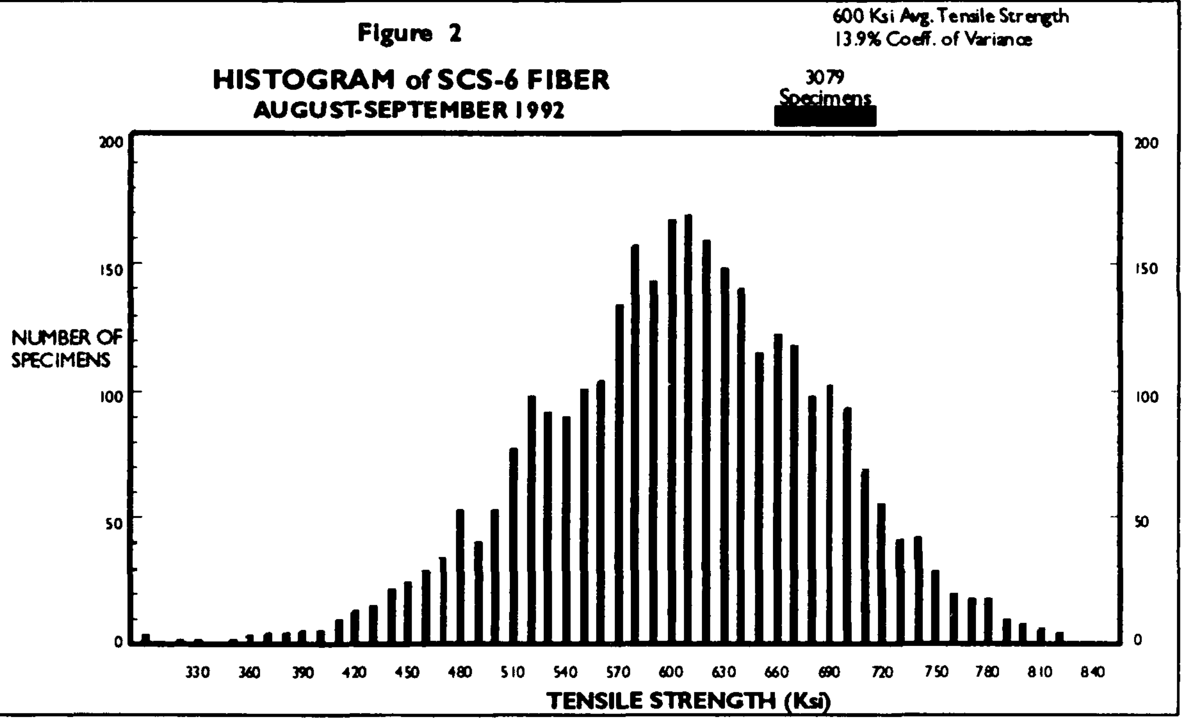

A particular attribute of the titanium composite material is its ability to retain its high strength at elevated temperature. An important factor here is the high temperature capability of the SCS-6 fiber, where as shown in *Figure 3*, high strength is retained to above 1000°C-- above the requirement for the conventional titanium alloys as well as for the developing family of titanium aluminides.

As indicated also in *Figure 3*, the silicon carbide vapor deposited monofilament is capable of further development. In the case illustrated a higher temperature capability has been obtained which together with improvements in creep strength will prove attractive for ceramic composite materials. Also other filament diameters are being produced experimentally. *Figure 4* shows various experimental filaments that are being produced in diameters ranging from 50 microns to 180 microns. In some cases reducing the diameter of the carbon monofilament to 20 microns.

Currently the Textron silicon carbide fiber production plant is capable of producing more than the minimum quantities of fiber needed to satisfy present day research and development requirements. The capability of the plant in its present configuration is over 1000 lbs of SCS-6 per year. This can be increased to to over 10,000 lbs/year by relative minor additions to the gas recovery systems and the addition of the necessary modular reactors.

• • • • • • • • • • • • • • • •

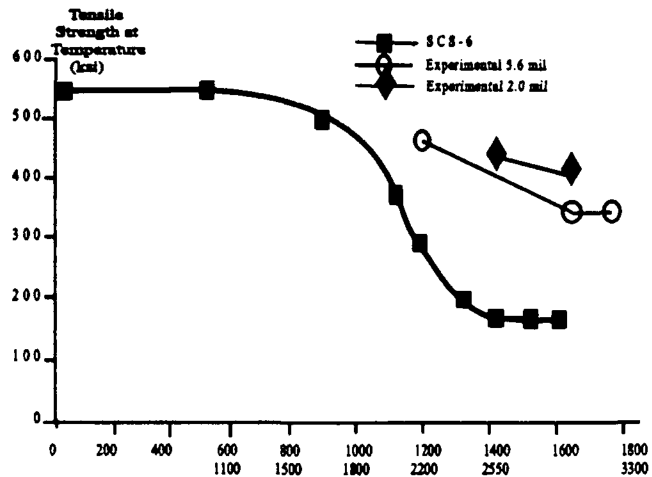

Figure 3
Fiber Tensile Strength at Temperature

3.0 *Titanium Composite Fabrication*

As a result of many years of development effort, SCS-6 Titanium composite fabrication techniques are well established. In general the techniques are directed at the solid state high temperature/high pressure consolidation process. Here the fiber is immersed in, or layered within, titanium metal and by the process of pressure and heat the titanium is bonded to the fibers to form a quasi homogeneous material. Three methods of applying heat and pressure are used for fabrication of SCS-6 Titanium shapes. These are illustrated in *Figure 5*. The most common consolidation technique used to-date is Hot Isostatic Pressing. In this case, using a shaped tool, a pressure membrane and a vacuum environment, the fiber and titanium metal are subjected to the hot isostatic gas pressure which acts on the thin membrane to consolidate the composite to shape. Alternatively; two direct mechanical pressing techniques are available, using either

Figure 4
Experimental Silicon Carbide Fibers

50 Micron Diameter

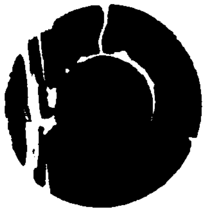

75 Micron Diameter

112 Micron Diameter

180 Micron Diameter

Figure 5
SCS-6/Titanium
Consolidation Methods

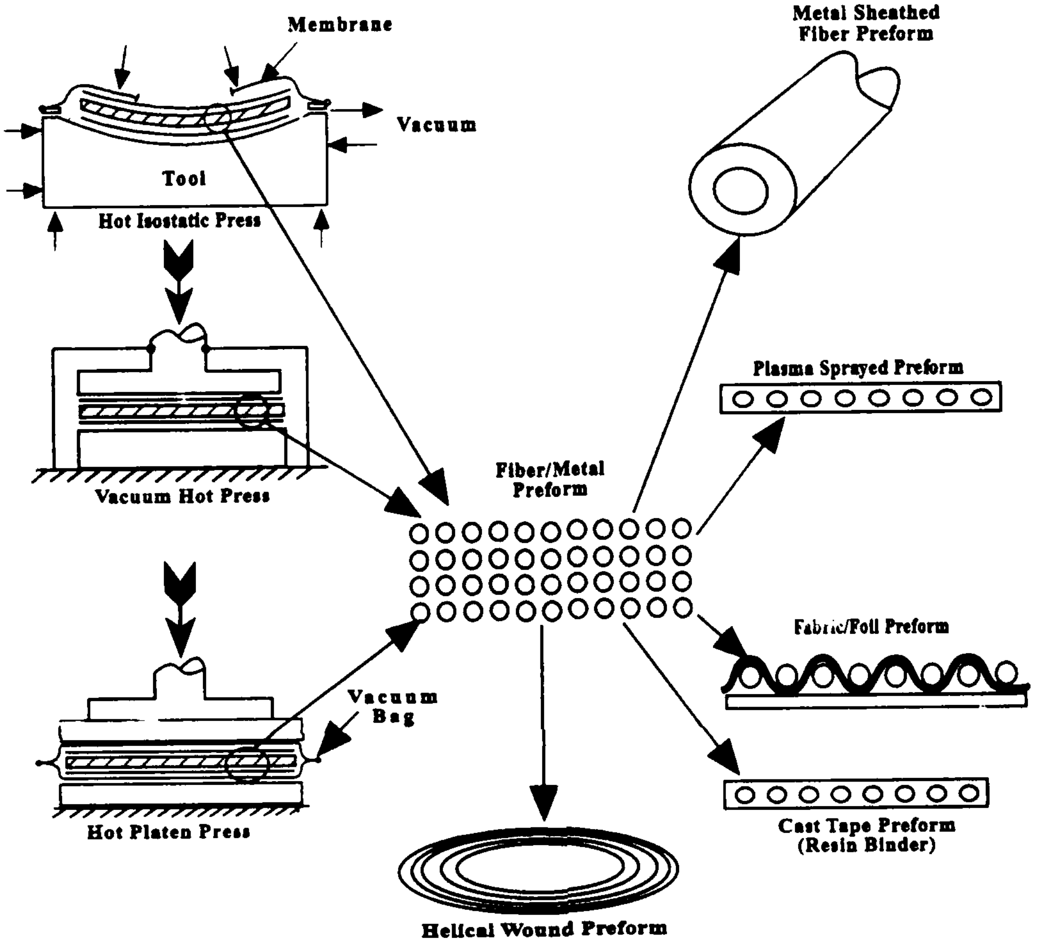
Membrane
Vacuum
Tool
Hot Isostatic Press
Vacuum Hot Press
Vacuum Bag
Hot Platen Press
Fiber/Metal Preform
Metal Sheathed Fiber Preform
Plasma Sprayed Preform
Fabric/Foil Preform
Cast Tape Preform (Resin Binder)
Helical Wound Preform

a vacuum sealed chamber with radiant heaters or a resistively heated platen press where the composite is sealed in a vacuum membrane enclosure.

As stated previously the HIP process is as of to-date the most universally used composite fabrication technique. This is primarily due to ease of molding large complicated shapes as well as the potential for low cost where one HIP run can accomodate a large number of parts. However, the direct mechanical pressing technique offers in some cases a lower cost approach for smaller simpler shapes that require less total pressing tonnage.-- Specifically engine disks and blades.

For each of the fabrication techniques described above, a method of collecting the metal and the fiber together in a preform is used so as to facilitate installation of material into the mold or press. Various type of preforms are available as shown in Figure 5. In each case they: represent varying stages of preform development, or are developed for reduction of fiber movement during consolidation, or directed at the fabrication of specific shapes. The most commonly used preforms to-date are the foil-fabric and the plasma sprayed tape. Each of these are capable of producing large area sheet preforms and have been used extensively for production of many shapes. Plasma spray techniques have also been used to directly deposit the metal onto the fibers for insitu construction of irregular or thick walled shapes. Recently a competing cast tape prepregg has been devloped using titanium powder embedded in a resin binder to produce a very pliable sheet material similar to an organic prepreg.

The sheathed or coated fiber approach (sometimes called the fat fiber approach), where the metal is deposited onto the fiber by the sputtering or electron beam evaporation methods, is in the early stages of development. This is proving very useful for single filament winding techniques that can be used for the fabrication of rings or for the production of complex surfaces. Finally the helically wound preform is available in a number of variations (using specially wound "fabric with titanium foil" or "filaments layed into spirally grooved titanium foil") for fabrication of thick walled rings.

Whereas the originally produced SiC Titanium composite shapes utilized only the standard 6.4 titanium alloy, much progress has been made with a number of other systems. *Table 1* summarizes the experience to-date with various alloys, their associated preforms and compositing experience.

• • • • • • • • • • • • • • • •

TMC Materials & Processes Status
Table 1

	Established	Development	Experimental	Comments
SCS-6/Woven Preform Fabric Crossweave Materials				
- Ti-6-4	X			
- Mo	X			
- Nb/Ti	X			
- B-21S			X	• Fabrication Experiments
Plasma Sprayed Preform				
- Ti-6-4		X		
- Ti-6-2-4-2	X			
- Ti-14-21	X			
- Adv. Alpha-2 & Beta Alloys			X	
- Orthorbombic			X	
Cast Tape Preforms				
- Alloy C			X	
- 6 2 4 2			X	
Fabric/Foil Compositing	X			
- SCS-6/Ti-6-4	X			
- SCS-6/Ti-15-3	X			
- SCS-6Beta-21S	X			
- SCS-6/Ti-6-2-4-2	X			
- SCS-6/Ti-14-21			X	• Inconsistent Results
- SCS-6/Adv. Alpha-2 & Beta Alloys			X	
Plasma Spray Compositing				
- SCS-6/Ti-6-4		X		• Panels Fabricated
- SCS-6/Ti-6-2-4-2		X		• Panels & Shapes Fabricated
- SCS-6/Ti-14-21		X		• Panels & Shhapes Fabricated
- SCS-6/Adv. Alpha-2 & Beta Alloys			X	• Good Initial Results
- SCS-6/Orthorhombic			X	• Poor Results
Cast Tape Compositing				
- SCS-6/Ti Alloy C			X	• Good Initial Results

4.0 Fabricated Shapes

During the last two years or so. over 4,000 lbs of SCS-6 Titanium composite shapes have been fabricated for development and test purposes. They, as shown in *Table 2*, range from large flat and curved

SCS-6/Titanium Fabricated Shapes
Table 2

Shape		Comments
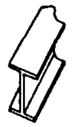	I-Beams	• Up to 13 feet long, 10 inches deep • Tapered flanges & height • Tapered thicknesses • 0°±45° caps and webs
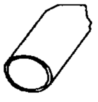	Cylinders	• 8 feet long, 4 inches dia. compression tubes • 1 inches dia., 12 inches long engine links and power shafts • 4 feet long, 4 inches dia. turbine power shafts
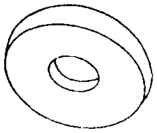	Disks	• Helical wound disks for reinforcement of turbine compressor disks • 10 inches dia., 0.20 thick
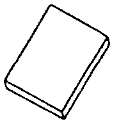	Flat Plates	• 11 feet x 8 feet x 0.2 inches thick • Many fiber architectures • Tapered thicknesses
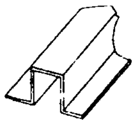	Panel Stiffeners	• 8 feet long • 0° • 0°±45° • 0°±30°
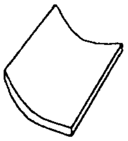	Curved Plates	• 4 feet x 8 feet x 0.05 inches thick • Many fiber architectures • Tapered thicknesses

plates to complicated shapes such as turbine disks, hat shaped stiffeners and long tapered height/tapered thickness wing spar beams.

• • • • • • • • • • • • • • •

5.0 TMC Production Facility

A 50,000 square foot facility has been recently established at Textron by the National Aerospace Plane program office for production of SCS-6 titanium shapes. In this dedicated facility are all, except a HIP, of the facilities and equipment necessary for production of titanium composite shapes. Included are:

- Fabric weaving looms
- Laser jet foil and fabric preform cutter
- Clean rooms for composite preform assembly
- Tool preparation rooms
- Computer controlled tool welding equipment
- Five axis water jet cutter for tool breakdown
- Offgassing equipment
- Three dimensional co-ordinate equipment
- Acid Cleaning facility
- XRay & Ultrasonic NDT equipment
- CAD support equipment
- Vacuum Hot Press

PROCESSING OF TITANIUM MATRIX COMPOSITES

E A Feest & J Cook
AEA Technology
B528.10 Harwell Laboratory
Didcot, Oxon OX11 0RA, UK

SUMMARY

European experience in the processing of monofilament reinforced Ti matrix composites is briefly reviewed. Results on fibre coating developments on foil-and PVD-based processing routes are presented. Issues addressed include fibre handling, fibre property measurement, residual stresses in fibre and matrix, fibre coating formulation and deposition, MMC consolidation and composite properties. Progress towards economically viable matrix deposition via sputter ion plating is reported.

1. INTRODUCTION

This contribution aims to bring together elements of recent European experience in the processing of monofilament reinforced titanium-based matrix components. Emphasis is given to projects and initiatives in which the authors have had a direct involvement and to results which have not been previously published. It thus makes no claim to be a comprehensive review of current processing options, for which the reader is referred elsewhere (eg. Ref 1).

2. EUROPEAN INITIATIVES IN THE 1980's

The initial stimulus for development was, as elsewhere, centred on potential aerospace applications such as aero gas turbine compressor components or hypervelocity plane structural components. These are characteristically high technical risk, high pay-off applications and thus it was not surprising that most significant development was centred on projects involving national aerospace research establishments in countries where there were existing industrial engine manufacturing interests or planned aerospace plane initiatives.

Silicon carbide monofilament was considered to be a key enabling material which would form the basis for the fibre optimisation and MMC process development activities which would be required as precursors to any materials evaluation programmes. In the early 1980's US-sourced monofilament was not freely available for such activities. However, a monofilament source was being developed in Germany through the initiative of Dr P E Gruber, first at the Forschungsinstitut Berghof and then, with Berghof's demise, at his own company Sigma Composite Materials. At this time the Sigma product had good strength and stiffness properties, but was not appropriate for incorporation or use in titanium-based matrices. Other technologies required for a successful MMC development were also being pursued. These included MMC consolidation studies, eg. at DLR (eg. Ref 2), interfacial reactions, eg. at the Univ. of Bordeaux (eg. Ref 3) and fibre coating developments eg. at ONERA. Potential end users were also testing US-sourced MMC material with a view to addressing design issues. In general, however, these studies were being carried out in isolation rather than as an integrated project aimed at industrial exploitation.

In 1985 the CEC's BRITE programme provided a framework for accelerating the development of a European source of titanium-based matrix MMC. A consortium comprising laboratories capable of mobilising all the necessary technologies together with a group of sponsoring companies with ultimate interest in supply or use was assembled to bid for a project on "The control of fibre matrix interactions in SiC/Ti MMC". The make-up of this consortium, the way it was assembled and logic behind its formulation have been presented elsewhere (Ref 4). The main working laboratories in the original consortium were:

Harwell Laboratory, project prime, (now AEA Technology)
ONERA
DFVLR (now DLR)
Sigma Composite Materials

Funding was 45% from the CEC and 55% from 14 subscribers from 4 countries, and including potential makers, users and competitors.

The main results of the arising project, P1204, are summarised in the following section. Further details are given in Ref 5.

Presented at an AGARD Meeting on 'Characterisation of Fibre Reinforced Titanium Matrix Composites', September 1993.

3. BRITE PROJECT P1204

3.1 Mission

The project was aimed at developing and evaluating on the laboratory scale an improved version of the Sigma fibre for use in titanium-based matrices. Clearly this involved a number of inter-related milestones related to identifying degradation mechanisms, postulating and evaluating means of overcoming degradation and developing coating and consolidation processes. It also aimed to produce and evaluate larger scale composites. The latter objective was dropped at the mid-point review in order to concentrate all available resources on the fibre development task.

3.2 Preliminary scoping

Key findings were:

- confirmation of the need for an interfacial barrier
- clarification of the significance of the W/SiC interaction within the fibre
- measurement of high levels of residual elastic strain within the fibre and matrix constituents
- the importance of handling damage and test method standardisation in fibre testing.

Experimental contributions to these findings included those described below.

Concerning the need for an interfacial barrier, Auger scans showed that the Avco SCS-6 coating prevented Ti reaching the underlying SiC at 900°C whereas reaction zones were evident between uncoated Sigma fibre and Ti alloy matrix at 850°C. Fibre testing and MMC fractography indicated the importance of a weak interface within the 'coating' regions of the fibre to decouple the load bearing component of the fibre from failure in the coating during handling and service. The formation of a self-diffusion barrier layer of fine grained TiC at the interface between Ti matrix alloy and an outer coating of pyrocarbon appeared to be an important contribution to fibre survival. The beneficial effect of a pyrocarbon coating alone was confirmed in the experiments summarised in section 3.4 below. Some indications on matrix composition dependence were given by the observations of preferential attack of carbon rich coatings when in contact with the β, as opposed to α, phase of an adjacent Ti-6Al-4V matrix

It was necessary to investigate the kinetics of the W/SiC reaction to indicate its potential influence on service performance and also, more pressingly, to ensure that it did not distort the significance of the experimental results on coating assessment and selection. Vacuum heat treatment experiments on uncoated Sigma fibres showed that whereas thermal exposure at 600°C had no significant degrading effect on tensile strength, appreciable drops in mean tensile strengths were observed after similar exposures at 900°C. This degradation was initially attributed to a possible reaction between the W core and the SiC CVD deposit. Since the temperatures were within the regions envisaged for both composite consolidation and CVD retro-coating within the project, further investigations were undertaken to determine the extent of reaction between the W core and SiC deposit. In one study amorphous SiC was sputter ion plated on the tungsten heater of a high temperature x-ray chamber and the evolution of x-ray patterns was monitored as a function of thermal exposure. Some reaction product started to form at 810°C after 10 minutes holding time and Fig 1 shows the temperature and time dependence of the reaction kinetics measured in this way. These experiments were backed up by tensile tests on uncoated Sigma fibres which had been vacuum heat treated for 1 hour at 1000°C. Optical fractography of the break ends of the fractured fibres showed however that all the fracture initiation sites were identified with surface defects and none with the W core/SiC deposit interface. Thus, whilst some W/SiC is initiated at as low as 810°C, the reaction becomes rapid only at temperatures greater than ~1000°C and therefore was not of concern for the retro-coating temperatures envisaged in the project.

Because of the integrated nature of the work in the different laboratories involved in this project a rigorous intercomparison exercise was carried out on the test methods used by three of the laboratories. Initial experiments showed the need to avoid the use of jigs with stiff compliance and hence sensitivity to misalignment. Key results are summarised in Table 1. Similar results were obtained on other fibre variants. A gauge length sensitivity was evident as expected. Sampling size effects were also measured by two techniques both of which indicated that 20 was an adequate sample size from which to determine valid strength values. This intercomparison exercise highlighted the sensitivity of the uncoated Sigma fibre to handling damage. Experiments simulating the handling sequence encountered before the effect had been isolated showed that a ~40% decrease in fibre strength could result from such handling.

Given the large thermal expansion mismatch between fibre and matrix and the high MMC consolidation temperatures, large residual stresses in fibre and matrix are to be expected. These were measured using neutron diffraction experiments on composite, monolithic matrix alloy and unincorporated fibre. Experimental points for shift of a matrix alloy peak are shown in Fig 2. The study showed, as expected, residual compressive strain (and therefore stress) in the fibres and tensile stress in the matrix. The latter was at a significant level compared with the yield strength of Ti-6Al-4V. These results have a bearing on the interpretation of mechanical test data and on the prediction of service performance particularly under the anticipated thermal cycling regimes.

3.3 Prediction of protective coating systems

A thermodynamic assessment based on published thermodynamic data was carried out to predict the phases that can co-exist at temperatures relevant to MMC fabrication and use, taking account of the influence of relevant matrix alloying elements. The results were summarised in the form of predominance area diagrams, such as that shown in Fig 3, from which predicted reaction zone sequences were derived as illustrated by Fig 4 which represents the situation for both carbon-rich and stoichiometric SiC fibre surface formulations . These diagrams were used as the starting point for a detailed thermodynamic study for recommending promising coating interlayers for protecting the Sigma fibre in a Ti-6Al-4V matrix. Key requirements were that components should have a high chemical stability and that at least one of the elements in the compound should have a very low solubility in Ti. Two coating interlayer systems were recommended: a titanium carbide based system and a titanium boride based system, see (Fig 5). Both use a carbon layer immediately on the surface of the fibre prior to the layer of carbide or boride. The coating systems were designed to provide a structure in which each layer of the coating was in equilibrium at its interfaces with the adjoining layers - a coating structure with a minimised tendency to react. Chemical potential gradients will however still cause the elements to diffuse as indicated in Fig 5. In the case of the boride-based system the carbon layer was not needed for thermodynamic reasons; it was included to provide an interface that would protect the fibre surface from reactive chemical species (titanium) during coating and provide a weak interface to allow the fibre, when necessary, to detach itself from the coating. In the titanium carbide based system the carbon layer was also needed to take part in the reaction dynamics. Of the two systems the boride one had the greater promise because of a lower solubility in titanium of boron compared with carbon, and a lower rate of diffusion of boron in titanium and TiB_2 compared with carbon in titanium and TiC. Coatings development within the programme was therefore aimed at trying to accomplish the recommendations laid out in this thermodynamic study.

3.4 The efficacy of carbon coatings

During the coating development aimed at the recommended duplex coating systems, single layer carbon coatings were investigated. At this stage four coating processes were under investigation, viz: low pressure CVD (retro), high pressure CVD (on line and retro) and PVD (retro). The low pressure CVD carbon produced a 7% drop in fibre strength on coating; the fibre experiencing an elevated temperature at the start of the deposition process. The lower temperature PVD and high pressure CVD processes both demonstrated the beneficial effects of carbon coating on the intrinsic properties (mean failure strength) of the fibres and also on the resistance to degradation on heat treatment. Carbon coating alone also improved resistance to degradation by titanium. For example the high pressure CVD carbon produced a 17% increase in fibre strength on coating with a 1.25μm thick layer and a 70% rule of mixtures composite strength (cf. 40% for similar composite using uncoated fibre). Key results of thermal exposure tests are summarised in Table 2. These experiments showed that even a sub-micron adherent carbon layer substantially enhanced the intrinsic quality of the Sigma fibre and also improved its resistance to thermal exposure in N_2 and Ti vapour. Handleability, as demonstrated by resistance to self-abrasion, was greatly improved even with an extremely thin (50nm) coating of carbon. Some degree of protection against reaction with a titanium-based matrix could be achieved by allowing a natural TiC reaction zone to form around the carbon coated fibre.

3.5 The efficacy of duplex coatings

Whilst the developments of carbide and boride coatings by CVD techniques were set in train, the responsibility for demonstration of the effectiveness of the duplex layer concept fell to the PVD process because of its relative versatility and comparatively low development time. Preliminary experiments had examined the comparative suitability of reactive sputtering (carbon introduced via introduction of an argon methane gas mixture) and dual dc sputtering (carbon introduced by sputtering from solid graphite cathode plates). The latter was used for the duplex carbide system experiments because it was compatible with the initial carbon deposition stage and because of its comparatively simple rig configuration. It had the additional advantage of being compatible with a system for depositing the matrix alloy around the coated fibre. A sputter ion plating (SIP) coating rig was therefore modified to comprise two interconnected coating chambers, one for the C/TiC coating sequence and the second for overcoating with Ti-6Al-4V matrix alloy.

Composite wires produced in this manner achieved 90% of rule of mixtures mean strength after heat treatment under conditions simulating representative consolidation heat treatment schedules. In general heat treatment times in excess of 1 hour however caused embrittlement of the matrix and reduced strength of the composite wire. Fibres coated with the C/TiC sequence were also consolidated into composite monotape tensile samples and these achieved tensile properties at least as good as those of monotapes processed using a similar volume fraction of Avco SCS-6 fibre.

The boride-based protective coating system was demonstrated using a high pressure CVD technique. The depositions of a boron-rich TiB_2 layer onto a carbon-coated continuous fibre produced a mean fibre strength of 3.73 GPa. When consolidated to form a 0.35 volume fraction Ti-6Al-4V composite plate the strength was 76% of the rule of mixtures value.

3.6 MMC consolidation

In parallel with the fibre coating developments, various MMC consolidation routes were explored on the laboratory scale in order to demonstrate the success of the fibre developments whilst bearing in mind the requirement for larger scale production. Effort was soon concentrated on just two processes

- planar hot pressing of matrix foil/fibre lay-ups
- hot isostatic pressing (HIP) of precursor composite wires.

The foil/fibre process imposed strict demands on foil thickness uniformity and, in order to achieve a fibre volume fraction approaching 0.4, profiled foils were used. Four profiling techniques were evaluated. Electrical discharge machining was found to be most suitable for laboratory scale processing although inappropriate for industrial scale-up. Composites with excellent fibre distribution and strength approaching 80% of rule of mixtures values were achieved in this way.

The HIP route experiments demonstrated that the process was capable of producing good fibre distributions and high (0.4) volume fractions which, with appropriate control of matrix interstitial contamination levels, can achieve rule of mixtures strength values.

4. SUBSEQUENT PROCESS AND PRODUCT DEVELOPMENT

Clearly the most direct industrial development of the concepts demonstrated in the above BRITE project occurred through the establishment of the Sigma operation within BP Metal Composites - BP having bought out Sigma's SiC fibre technology midway through the project. BP Metal Composites has productionised some of the coating concepts and developed a scaled up foil based MMC processing route using advanced fibre placement technology and HIP consolidation. This product development is dealt with elsewhere in this Workshop (Ref 6 on processing and properties and Ref 7 on product uniformity and test technique development).

The authors are aware of two other current process development thrusts involving major industrial participation. One is centred on the scale up by DRA of their EBED (electron beam evaporation and vapour deposition) route for producing matrix-coated fibres (Ref 1). The other is centred on the further development of AEA's SIP (sputter ion plating) route for both protective coating development and matrix coating of fibres. Both of these initiatives involve developments aimed at titanium aluminide matrix composites.

Of the other candidate processes for industrial commitment, spray processing (notably low pressure plasma spraying) has received the most developmental attention. This is because of the conceptual simplicity of the process and the existing investment in spray processing facilities required for mainstream barrier coating development work. Current limitations relate to the practicalities of achieving the required homogeneity and composition of matrix formulation together with the required accurate placement of fibre.

A possible difference between the European and US routes to industrial investment in this field of materials development is that the European experience to date has been characterised by bottom up involvement into general collaboration initiatives (eg. BRITE and EUCLID on the European scale or LINK on the national scale) whereas major mission initiatives (eg. NASP and IHPTET) have provided a strong industrial focus in the US. This has made European progress particularly dependent on the entrepreneurial initiatives of the likes of Sigma Composite Materials and BP Metal Composites.

5. PROCESS DEVELOPMENTS BASED ON SPUTTER ION PLATING

The SIP work which was the cornerstone of the coatings systems demonstration work reported in section 3 above was introduced into the work programme as an experimental expedient to provide proof of concept results on a timescale far shorter than would have been possible using compound specific CVD routes. This was because there was available equipment and expertise at AEA as a result of continuing investment in the technology since its invention in the 1970's (Ref 8).

The SIP input into the BRITE project (Ref 9) demonstrated the following potential for the process in the content of the development of titanium-based matrix composites:

- it is a versatile R&D tool for rapidly screening potential coatings systems (during the project it provided the first demonstrations of the enhanced thermal stability imparted by carbon coating and the viability of the C/TiC duplex coating system as a barrier to attack by titanium-based matrices, and was also a key step in elucidating the significance of the W/SiC interaction);
- it is a means of depositing matrix alloys on the fibre wire in a manner consistent with the impurity constraints imposed by titanium-based matrices and with the potential for compatibility with a process for retro-coating the protective coating sequence on the fibre.

Limitations of the process, as employed in the BRITE project, included the constraint that continuous fibre could not be coated in the rig configuration used and deposition rates were unacceptably low for industrial application.

In the light of the above experience AEA has continued to invest in the development of this technology both through internal investment and collaborative initiatives. The main directions of this investment have been:

- increasing the deposition rate on fibres
- achievement of continuous fibre coating
- application to the development of intermetallic matrix composites.

Concerning deposition rates, those deployed in batch processing for the activities described in section 3 above were ~4μm/hr. Subsequent reconfiguration from cathode planar plate co-sputtering to hollow cathode achieved an increase in deposition rate to ~90μm/hr. Fig 6 shows a fibre coated at this deposition rate.

Current industrial collaborative work within the LINK Programme framework in the UK is focussed on coating a continuous fibre at still higher deposition rates via increased power levels and changed cathode configuration. The project aims to develop a high performance TiAl based precursor composite and to provide experience for supply and exploitation.

A processing route involving SIP matrix deposition, wire preform winding and HIPing is particularly suitable in this case because:

- the processing route has greater flexibility in design options and fabrication than do processing routes limited to plate product;
- it is particularly suited to matrix formulations, such as Ti-based intermetallics where interstitial impurity level control is paramount and the range of acceptable processing and consolidation routes is limited.

CONCLUSIONS

Recent developments in the field of titanium based MMC have demonstrated the value of international, interlaboratory collaboration in accelerating progress. The technical value of techniques such as thermodynamic prediction for coating selection and PVD for coating prototyping were highlighted in the quest for a viable MMC system. Sputter ion plating plus hot isostatic pressing is a primary processing route for composite systems such as monofilament-reinforced titanium aluminides where non-planar shapes may be required and matrix impurity control is critical to performance.

ACKNOWLEDGEMENTS

The authors wish to acknowledge the contributions to the work reported above of their colleagues at AEA Technology and their partners in the BRITE Project 1204 Consortium. The internal investment work reported was funded by the Corporate Research and Applications Development Programme of AEA Technology.

REFERENCES

1. Partridge PG, Ward-Close CM, "Processing of advanced continuous fibre composites: Current practice and potential developments" Int. Met. Rev 38, 1, 1993, pp1-24.

2. Le Petitcorps Y, Thesis, Univ. of Bordeaux I (1985).
3. Leucht R, Dudek HJ, Ziegler G, Proc DVM, Dortmund, 1981, pp 203-214.
4. Feest EA, Proc. First BRITE Technology Days, CEC DG XII, Brussels, Dec. 1987, pp 131-135.
5. Cook J, Feest EA, "Control of fibre matrix interactions in SiC/Ti MMC" Report No. EUR 13614, CEC Luxembourg, 1991.
6. Robertson J, "Manufacture and properties of silicon carbide filament reinforced TMCs", Paper 7 of these proceedings, 1993.
7. Tweed JH, "Prestandardisation work on fracture and fatigue testing", Paper 20 of these proceedings, 1993.
8. Dugdale RA, "Improvements in or relating to vapour deposition apparatus", UK Pat. 1,500,701.
9. Cook J, Knights CF, Rickerby DS, "Coated filaments for composites", UK Pat. 2,237,031.

Testing Laboratory	1		2			3	
Test Gauge Length	25mm	40mm	25mm	40mm	40mm*	25mm	25mm**
BRITE 'Standard' Sigma fibre							
Mean tensile strength (GPa)	3.57	3.53	3.58	3.46	2.29	3.11	2.79
Standard deviation (GPa)	0.41	0.29	0.33	0.30	0.30	0.51	0.58
Coeff. of variation (%)	11.6	8.2	9.22	8.67	13.10	16.40	20.79
US source fibre							
Mean tensile strength (GPa)	3.43	3.41	3.67	3.40	2.13	3.60	3.75
Standard deviation (GPa)	0.42	0.38	0.48	0.59	0.42	0.36	0.38
Coeff. of variation (%)	12.2	11.1	13.08	17.35	19.72	10.01	10.13

** Initial tests using stiff compliance jig.

* Fibre lengths cut up in laboratory 1, mailed to laboratory 2, repacked and mailed for testing in laboratory 3 to illustrate propensity to handling damage.

Table 1. Comparative tensile test results on SiC fibres

Fibre Coating	Temp (°C)	Time (hr)	Conditions	UTS (GPa)
None	900	1	Control	4.07
	900	1	Ti	1.53
	1000	1	Control	3.60
	1000	1	Ti	0.87
	1000	12	N_2	3.20
Carbon	900	1	Control	3.70
	900	1	Ti	3.89
	1000	1	Control	3.74
	1000	1	Ti	3.63
	1000	12	N_2	3.73
C/TiB_2	900	1	Control	3.25
	900	1	Ti	3.21
	1000	1	Control	3.18
	1000	1	Ti	3.06
	1000	12	N_2	2.17*

* A surface reaction of TiB_2 was observed (TiB_2/N_2 is thermodynamically unstable at 1000°)

Table 2 Comparison of mean tensile strengths for Sigma fibre in the uncoated, carbon-and carbon plus titanium- coated condition following thermal exposure in various atmospheres.

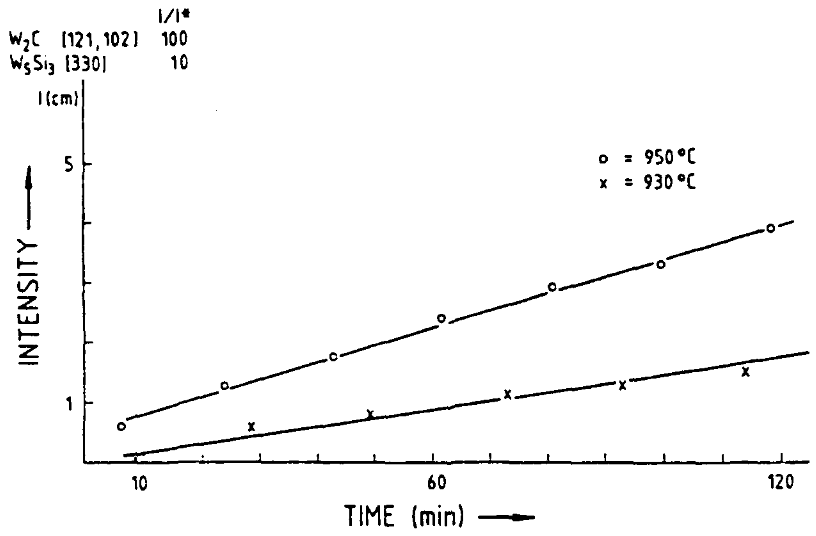

Fig 1. Intensities of the reaction products W_2C and W_5Si_3 formed between W and SiC as a function of annealing time at 930°C and 950°C (Ref. 5)

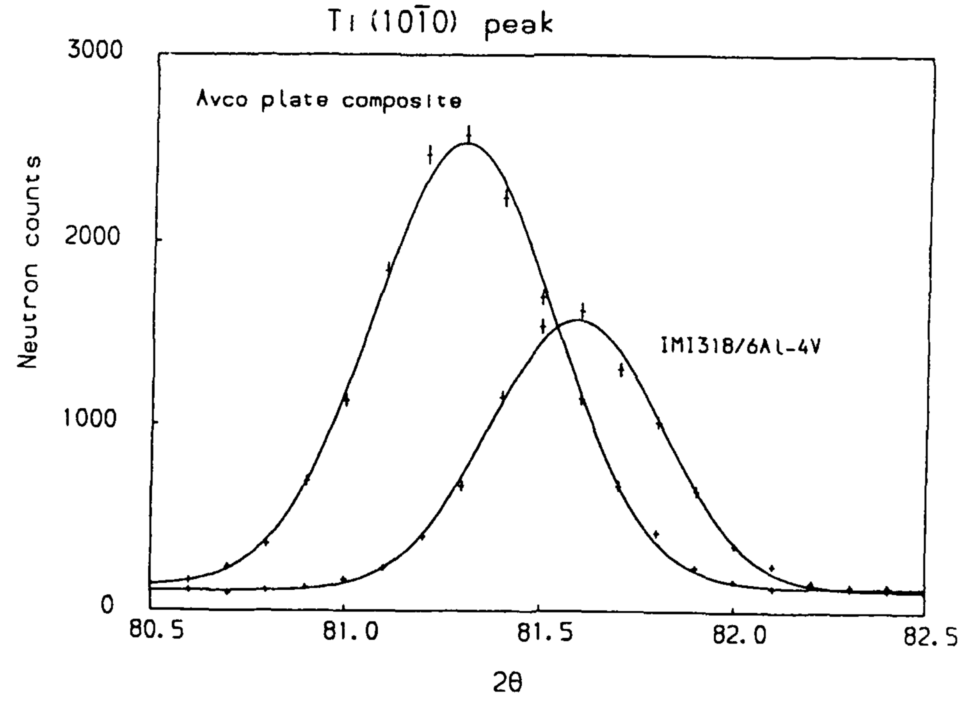

Fig 2. Comparison between matrix (10$\bar{1}$0) Bragg peak positions in MMC plate and unreinforced alloy (Ref. 5)

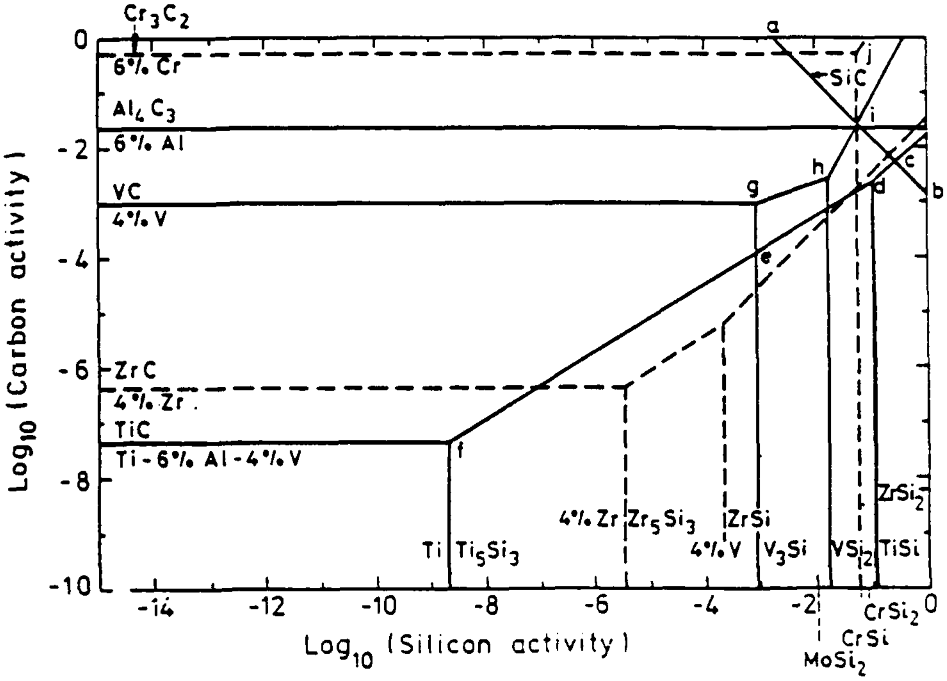

Fig 3. Predominance area diagram for carbides and silicides in Ti alloys at 12OOK (Ref. 5)

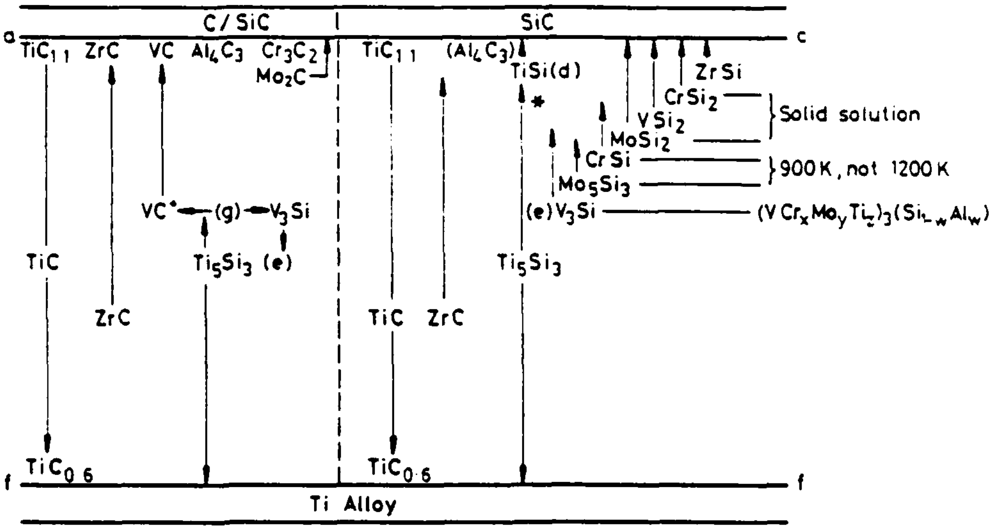
C/SiC
SiC
a
c
$TiC_{1\,1}$
ZrC
VC
Al_4C_3
Cr_3C_2
Mo_2C
$TiC_{1\,1}$
(Al_4C_3)
TiSi(d)
ZrSi
$CrSi_2$
VSi_2
$MoSi_2$
CrSi
Mo_5Si_3
(e)V_3Si
Solid solution
900K, not 1200K
$(VCr_xMo_yTi_z)_3(Si_{1-w}Al_w)$
VC^*
(g)
V_3Si
TiC
Ti_5Si_3 (e)
ZrC
TiC
ZrC
Ti_5Si_3
$TiC_{0\cdot6}$
$TiC_{0\cdot6}$
f
f
Ti Alloy

• $VC_{0\cdot88}$

* $M_{6-x}Ti_xSi_5$ compounds exist

The letters a,c,(d),(e),f and (g) refer to positions on Fig 3

Tin, present in some Ti alloys, does not form a carbide or a silicide.

M	x
V	0 - 4
Cr	2 - 4
Mn	2 - 3

Fig 4. Thermodynamically predicted reaction zones between Ti alloys and SiC (C-rich and stoichiometric)(Ref.5)

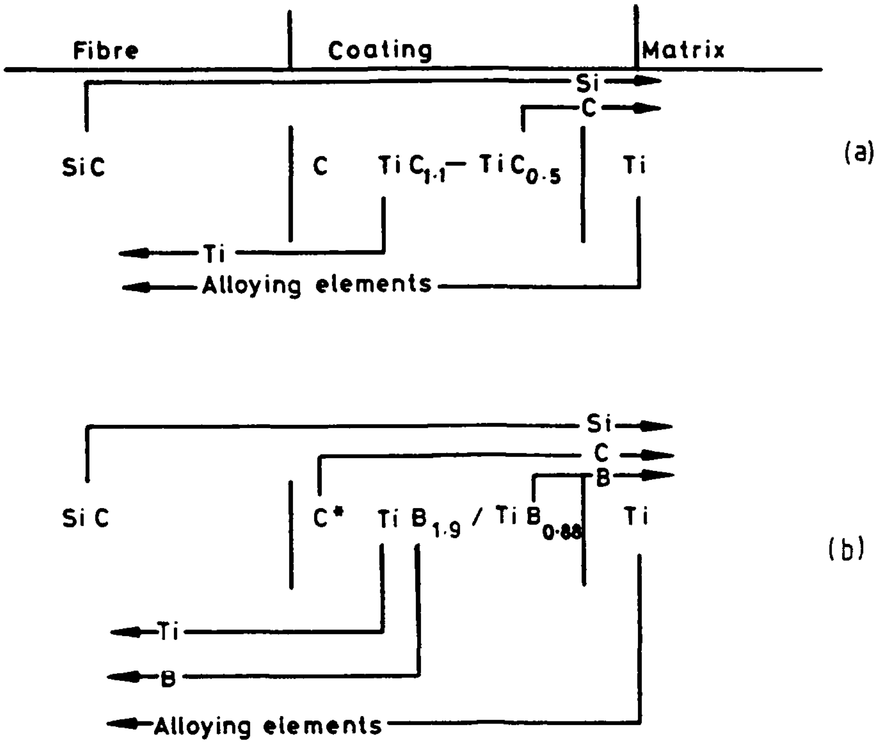
Fibre
Coating
Matrix
Si
C
SiC
C
$TiC_{1.1} - TiC_{0.5}$
Ti
(a)
Ti
Alloying elements
Si
C
B
Si C
C*
$TiB_{1.9} / TiB_{0.88}$
Ti
(b)
Ti
B
Alloying elements

* This carbon need not be present on thermodynamic grounds.

Fig 5. Proposed structures of least reactive coatings to protect SiC in a Ti matrix. (a) carbide-based system, (b) boride-based system. Arrows indicate directions of elemental diffusion (Ref. 5)

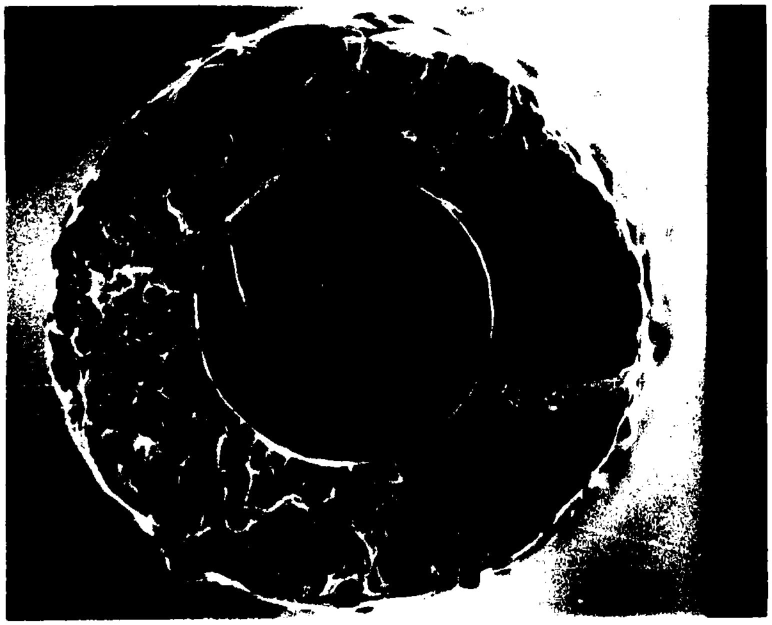

Fig 6. Scanning electron micrograph of MMC wire precursor prepared by high rate sputter ion plating of titanium alloy matrix on SiC monofilament.

COMPOSITES BASED ON TITANIUM WITH EXTERNAL AND INTERNAL REINFORCEMENT

by

A.I. Khorev
Chief of Scientific Laboratory
Russian Institute of Aviation Materials (VIAM)
17 Radio Street
107005 Moscow
Russia

The possibility of the efficient increase of the specific elasticity modulus and the specific strength of materials as well as aerospace vehicles by means of developing composites based on titanium with external and internal reinforcement was considered.

High-strength titanium matrices in the form of foil for composites with internal reinforcement; cylindrical shells and ball vessels of titanium alloys for structures with external reinforcement were developed (Fig. 1).

High-strength titanium alloys with $\alpha+\beta$ -(VT6, VT14, VT16, VT23) and β -structure (VT15, VT19) were developed as well as the thermomechanical parameters for the production of foil with a thickness of 0,08 mm, ensuring the possibility of obtaining, for example, on VT23 alloy, or σ_B = 1000 MPa in the as-annealed condition and σ_B = 1200 MPa in the heat-treated condition.

The technological parameters of heat and thermomechanical treatments of cylindrical and spherical vessels of titanium alloys with $\alpha+\beta$ - and β-structure, ensuring a structural strength of σ_{Bs} = 1000 - 1500 MPa, were established.

Cylindrical and welded vessels of VT 14 alloy were manufactured in accordance with different technologies. Fig. 2 shows the dependence of the structural strength (σ_{Bs}), calculated by the destructive internal pressure, on the ultimate strength of the material (σ_B). Each curve reflects this dependence for the vessels, made by one technology and heat treated under different conditions. Fig. 3 - shows the fractured vessels of VT 14 alloy. The welded vessels of higher-strength VT 23 alloy were fractured at σ_{Bs}, higher by 150 - 200 MPa, compared to those of VT 14 alloy in the annealed and heat - treated conditions. The maximum strength (σ_{Bs} = 1450 MPa) was obtained on welded vessels of VT 23 alloy with the thickening in the weld zone (Fig. 4).

The cylindrical non-welded vessels made of VT 15 β-alloy with the use of heat and thermomechanical treatments (Fig. 5).

According to the efficiency of mechanical properties and structural strength increase for the vessels, made of β-alloys, the methods of thermomechanical treatment can be placed as follows : heat treatment, high temperature, low temperature mechanical treatment, high - temperature + low - temperature mechanical treatment.

The schemes of making ball vessels of VT 23 alloy are shown in Fig. 6. Plastics were used for external reinforcement (Table 1).

The results of hydraulic tests for internal pressure of the vessels of VT 23 alloy, braided with plastic are shown in Table 2.

The composites with internal reinforcement, consisting of titanium alloys foil (Table 3) and high-strength and high modulus fiber (Table 4).

The parameters of compositions bonding are optimized (Fig. 7) ensuring the effective increase of the material strength and elasticity modulus.

Presented at an AGARD Meeting on 'Characterisation of Fibre Reinforced Titanium Matrix Composites', September 1993.

Table 1

Properties of Materials for External Reinforcement

Material	d kg/cm^2	E, MPa	σ_B, MPa	δ, %	σ_B/d km
1. BM1 glass fiber reinforced plastic	1900	60000	1800	3	95
2. BHP glass fiber reinforced plastic	1900	62000	2000	3,5	105
3. VNIVLON plastic	1150	70000	1300	3	113
4. Carbon fiber reinforced plastic	1125	220000	800	0,7	64
5. Boron fiber reinforced plastic	2000	230000	1200	0,55	60

Table 2

Vessels of VT 23 Alloy with External Reinforcement

Heat Treatment Condition	Type of Plastic	σ_{BS} of the shell, MPa	σ_{BS} of equivalent to titanium, MPa	σ_{BS}, eg d mater km
Annealing	BMI	1100	1800-1900	41-42
"	BMP	1100	1800-1850	40-41
Quenching + ageing	BMI	1400	1950-2000	43-44
"	BMP	1400	2150-2200	48-49
"	VNIVLON	1400	2160-2250	48-50
"	CFRP	1400	1570-1800	35-40
"	BFRP	1400	1450-1800	32-36

Table 3

Titanium Alloys Foil

Alloy	Thickness μm	σ_B MPa
VT 1-00	80	300
VT 6C	100	830
VT 16	100	800
VT 23 (annealing)	80	1000
VT 23 (quenching + ageing)	80	1200

Table 4

Reinforcing Fiber with a Diameter of 90-100 μm

Material	σ_B MPa	E MPa	d kg/m^3
SiC	1800	42000	3500
B/SiC	2300	40000	2700

Table 5

Properties of Composites with Internal Reinforcement

Composition constituents		Composites properties			
Alloy	20% fiber	σ_B MPa		E MPa	d kg/cm^3
		20°	500°		
VT 23	SiC	980	720	185000	4100
VT 16	SiC	950	580	185000	4100
VT 6C	SiC	820	520	185000	4000
VT 1-0	SiC	500	320	185000	4000
VT 23	B + SiC	990	610	195000	3600
VT 16	"	900	530	195000	3600

Conclusions

1. High-strength titanium alloys (VT 23, VT 19, etc.) production processes for foil, cylindrical and spherical vessels have been developed.
2. Cylindrical vessels of VT 23 alloy with external reinforcement by glass fibre reinforced plastic are promising for wide application.
3. High-strength foil of VT 23 alloy for composites internal reinforcement has been developed.
4. Work to improve the fiber quality, decreasing the extrusion temperature and developing the special extrusion equipment is necessary.

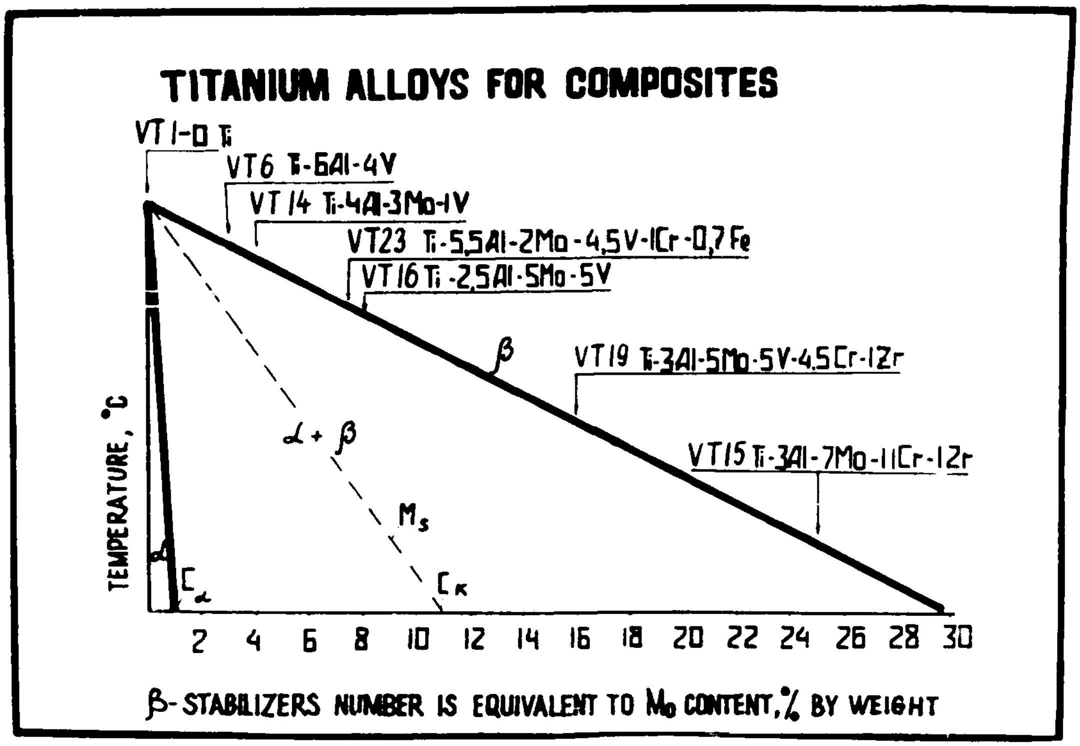
TITANIUM ALLOYS FOR COMPOSITES
VT1-0 Ti
VT6 Ti-6Al-4V
VT14 Ti-4Al-3Mo-1V
VT23 Ti-5,5Al-2Mo-4,5V-1Cr-0,7Fe
VT16 Ti-2,5Al-5Mo-5V
β
VT19 Ti-3Al-5Mo-5V-4,5Cr-1Zr
VT15 Ti-3Al-7Mo-11Cr-1Zr
α + β
Ms
Cκ
α
Cα
TEMPERATURE, °C
2 4 6 8 10 12 14 16 18 20 22 24 26 28 30
β-STABILIZERS NUMBER IS EQUIVALENT TO Mo CONTENT,% BY WEIGHT

Fig.1

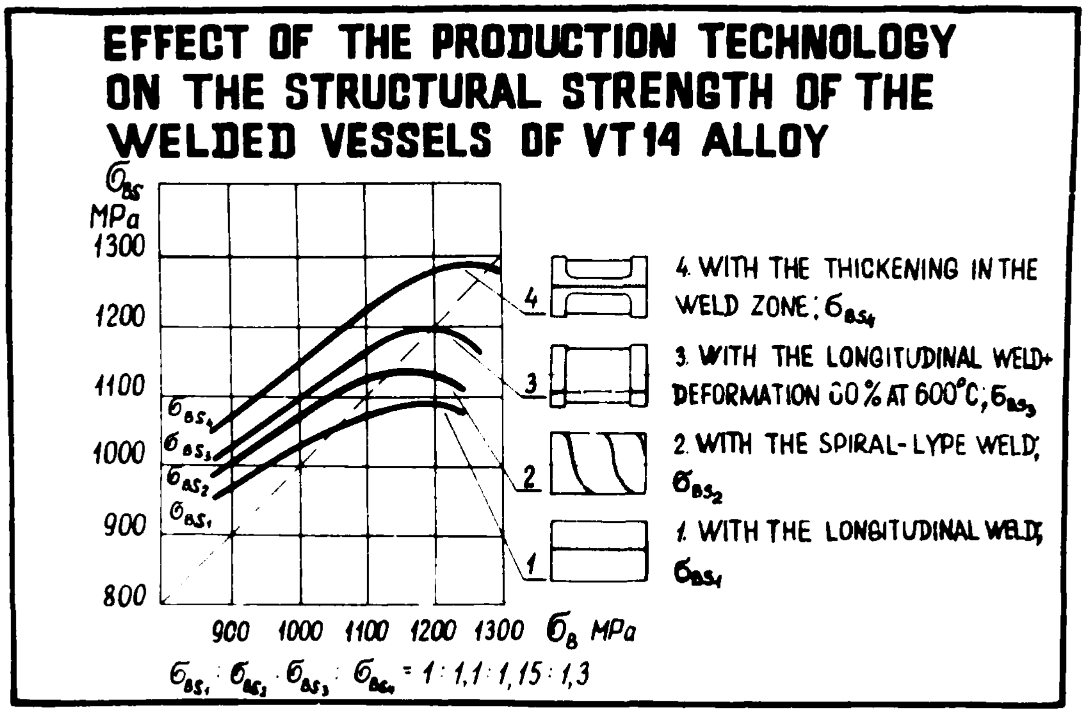
EFFECT OF THE PRODUCTION TECHNOLOGY ON THE STRUCTURAL STRENGTH OF THE WELDED VESSELS OF VT14 ALLOY
σBS MPa
1300
1200
1100
1000
900
800
σBS4
σBS3
σBS2
σBS1
900 1000 1100 1200 1300 σB MPa
σBS1 : σBS2 : σBS3 : σBS4 = 1 : 1,1 : 1,15 : 1,3
4
3
2
1
4. WITH THE THICKENING IN THE WELD ZONE; σBS4
3. WITH THE LONGITUDINAL WELD+ DEFORMATION 60% AT 600°C; σBS3
2. WITH THE SPIRAL-LYPE WELD; σBS2
1. WITH THE LONGITUDINAL WELD; σBS1

Fig 2

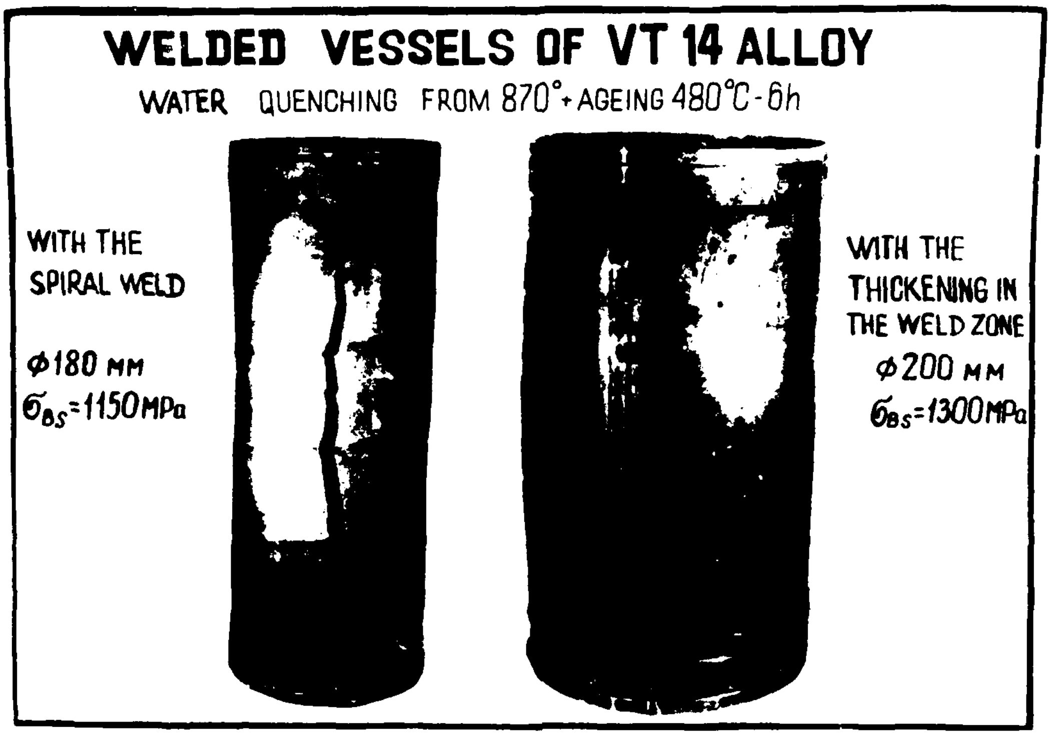
WELDED VESSELS OF VT 14 ALLOY
WATER QUENCHING FROM 870°+AGEING 480°C-6h
WITH THE SPIRAL WELD
ϕ180 MM
σ_{BS}=1150MPa
WITH THE THICKENING IN THE WELD ZONE
ϕ200 MM
σ_{BS}=1300MPa

Fig 3

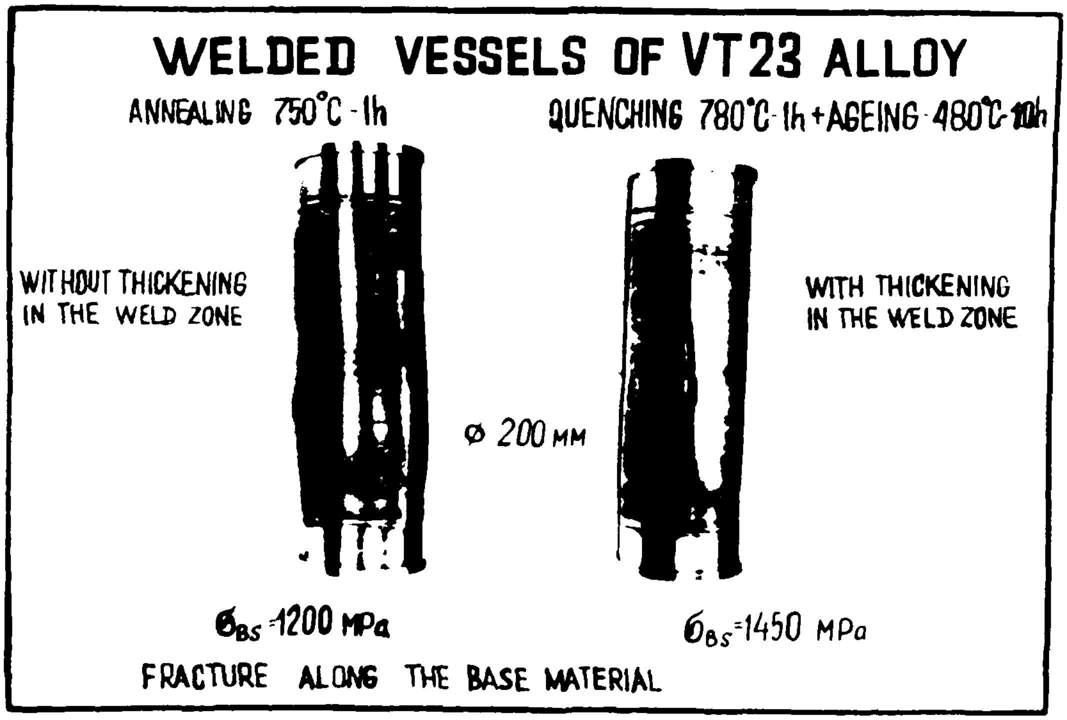
WELDED VESSELS OF VT23 ALLOY
ANNEALING 750°C-1h
QUENCHING 780°C-1h+AGEING 480°C-10h
WITHOUT THICKENING IN THE WELD ZONE
WITH THICKENING IN THE WELD ZONE
ϕ 200 MM
σ_{BS}=1200 MPa
σ_{BS}=1450 MPa
FRACTURE ALONG THE BASE MATERIAL

Fig 4

THERMOMECHANICAL TREATMENT VESSELS OF VT 15 ALLOY

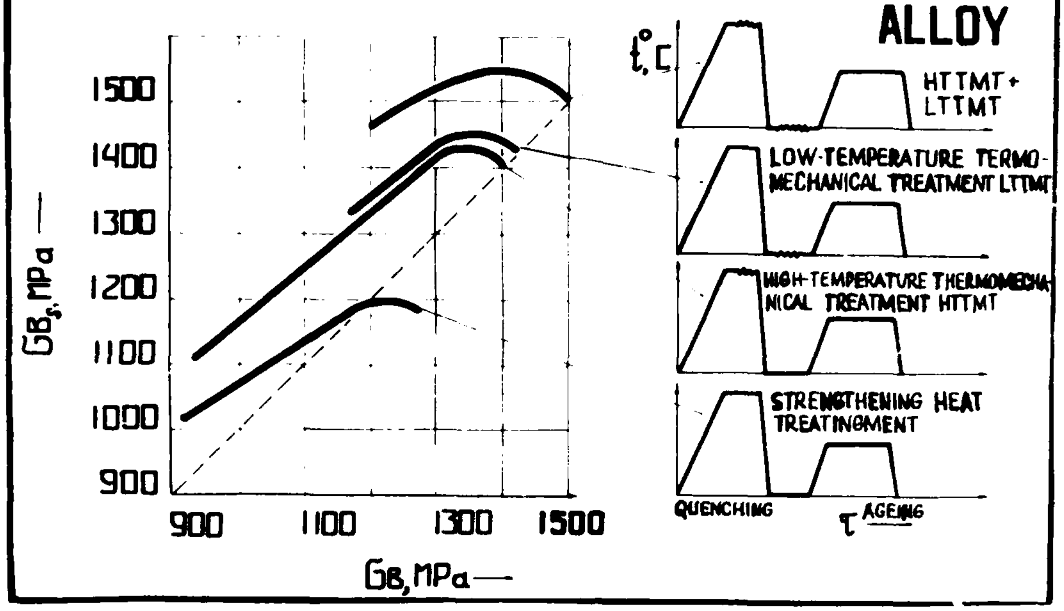

Fig.5

VESSELS OF VT23 ALLOY

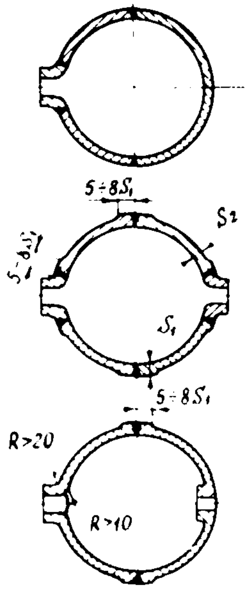

MADE OF SHEETS WITH
σ_{BS} = 1100 MPa

MADE OF SHEETS WITH THE
THICKENING IN THE WELDS
ZONE, σ_{BS} = 1250 MPa

MADE OF THE THREE-DIMEN-
SIONAL HEMISPHERES WITH
THE THICKENING IN THE WELDS
ZONE, σ_{BS} = 1350 MPa

Fig 6

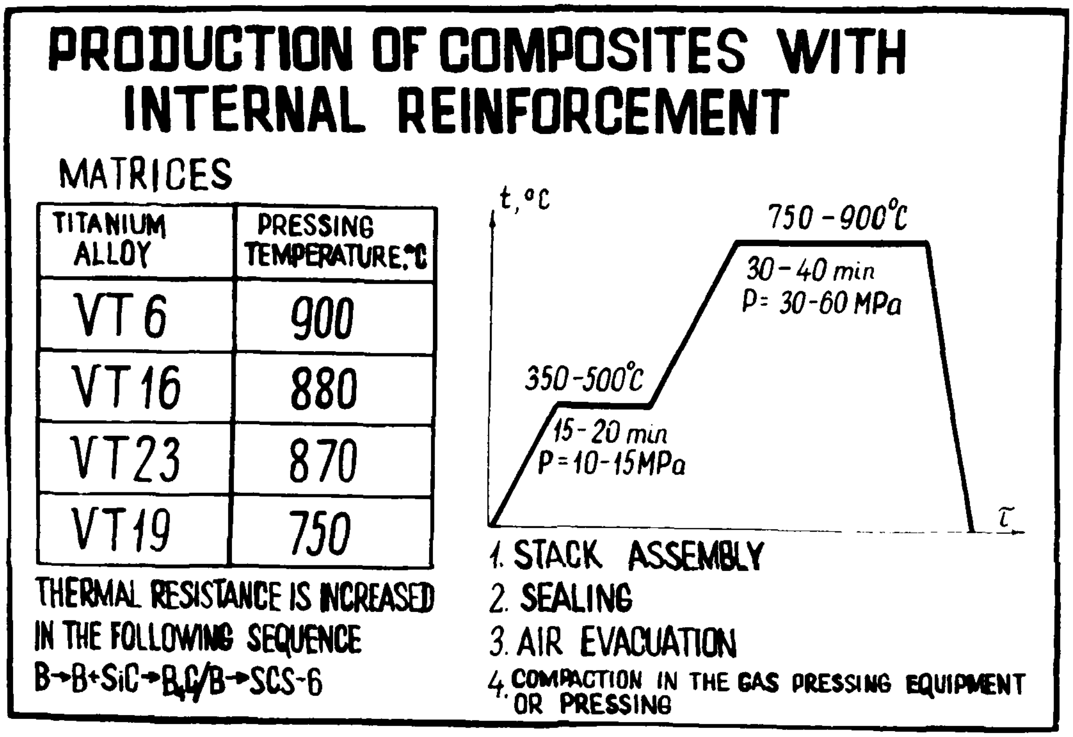

PRODUCTION OF COMPOSITES WITH INTERNAL REINFORCEMENT

MATRICES

TITANIUM ALLOY	PRESSING TEMPERATURE,°C
VT 6	900
VT 16	880
VT23	870
VT19	750

THERMAL RESISTANCE IS INCREASED IN THE FOLLOWING SEQUENCE

$B \rightarrow B+SiC \rightarrow B_4C/B \rightarrow SCS\text{-}6$

t,°C
750 - 900°C
30 - 40 min
P= 30-60 MPa
350-500°C
15 - 20 min
P=10-15MPa
τ

1. STACK ASSEMBLY
2. SEALING
3. AIR EVACUATION
4. COMPACTION IN THE GAS PRESSING EQUIPMENT OR PRESSING

Fig.7

Manufacture and Properties of Sigma Fibre Reinforced Titanium

J.G. Robertson
BP Metal Composites Limited
Research and Engineering Centre
Chertsey Road
Sunbury-On-Thames
Middlesex TW16 7LN
United Kingdom

1. Summary

Titanium Matrix Composites have long been known to offer potential for use in aeroengine components. The cost of producing the fibre and fabricating components has delayed large scale developments because of concern over long term component costs. The slow development pace has, in turn, kept the fibre and composite price high through low demand. Composite manufacturing routes using foil and filament wound fibre has been used for many years. The difficulties of maintaining a suitable fibre distribution during hot isostatic pressing and the availability of cheap foil have effectively put this technique on the shelf. However excellent fibre distributions have been achieved even in difficult geometries by a BP proprietary process . Mechanical properties comparable with the most expensive routes can be achieved with this, one of the cheapest manufacturing routes.

2. Introduction

Titanium Matrix Composites (TMCs) offer significant improvements in specific stiffness and strength over unreinforced alloys. The combination of high strength and stiffness available at elevated temperatures make them candidate materials for aeroengine structures. However there are a number of difficulties currently preventing thier widespread use. Cost of manufacture, limited design data, difficulties in designing with such anisotropic materials are but three. Their potential introduction is also delayed by the fact that the components offering the best structural efficiencies are also some of the most critical in the engine. Conservative design and lifing policies need to be adopted which will require considerable effort to develop sufficient confidence. This paper considers work carried out using Sigma monofilamnets incorporated into a titanium matrix using foil/fibre lay-up techniques.

3. Silicon Carbide Monofilament Manufacture

Figure 1 is a schematic representation of the fibre manufacturing process. This CVD technique for depositing silicon carbide onto a tungsten core has been in existance for about 15 years, first in Germany with Sigma Verbundverkstoffe and then in the UK with BP Metal Composites. The tungsten core is available cheaply in long lengths as it is a standard grade of lightbulb filament. This enables long lengths (upto 40km) of strong (3750 MPa) filament to be produced with a high modulus (400 GPa) and low coefficient of varience (5%). The tungsten core is therefore seen as offering key economic and performance advantages over carbon substrates.

However, at high temperatures (above about 1050°C) the silicon carbide can react with the tungsten core producing strength limiting defects in the filament. This reaction must be controlled both in the deposition process and during subsequent high temperature exposure. The CVD process has been designed to ensure that no degradation occurs during fibre production. The activation energy for the reaction is such that no degradation will occur during titanium composite processing. However, for intermetallic composite processing at high temperatures significant degradation can occur. To counter this potential problem, a 0.3μm coating has been deposited onto the tungsten core to control the reaction even after 75 hours at 1100°C (figure 2). BPMC is planning to develop this into a commercially available product.

4. Silicon Carbide Monofilament Coating

The uncoated monofilament, called SM1040, needs protection from the titanium matrix during composite fabrication and service life. BP has developed two coating systems which are retrosectively deposited onto the SM1040. Other coatings are being assessed.

-SM1140+ is a 4.5μm structured carbon coating deposited onto the silicon carbide surface.

-SM1240 is a 2μm duplex carbon/titanium boride coating.

The SM1140+ coating is designed to protect the fibre through many long aggressive consolidation cycles. Figure 3 shows the interface structure developed when SM1140+ is consolidated into a Ti-6-4 matrix. The titanium reacts with the carbon coating to form a titanium carbide reaction product which acts as a diffusion barrier layer. Further heat treatment of the composite results in slow growth of the reaction product following a diffusion controlled parabolic growth law [1].

Presented at an AGARD Meeting on 'Characterisation of Fibre Reinforced Titanium Matrix Composites', September 1993

SM1240 is a more economic fibre to produce and is suitable for most titanium alloys and consolidation cycles. Figure 4 shows the interface structure developed when SM1240 is consolidated into a Ti-6-4 matrix. Boron from the boron rich titanium boride diffuses into the titanium matrix forming titanium monoboride needles. Some of the remaining titanium boride coating forms a protective barrier of titanium monoboride. With further thermal exposure, the titanium boride layer is gradually consumed forming more rection product. Once the titanium is fully consumed the titanium can start to attack the carbon layer. Not until the carbon layer thickness is significantly reduced do the mechanical properties of the composite start to degrade significantly [2].

The chemical and mechanical properties of the coatings have been designed to prevent any brittle reaction products from degrading the perfolmance of the composite. The structure is designed to have layers that divert reaction product cracks away from the load bearing silicon carbide. The mechanical properties of the post-consolidated coating are critical in determining the performance of the composite.

5. Composite Manufacturing Routes

Many composite manufacturing routes are available. Each includes a technique for keeping the fibres separated while the gaps between them are filled with the titanium matrix. Filament winding, weaving and inserting spacers between neighbouring fibres have all been used to stop the fibre from moving. Plasma spaying, vapour deposition, foil or powder techniques have been used as a source of metal for the composite matrix. Hot Isostatic Pressing (HIPping), Uxiaxial Hot Pressing and Roll Bonding have all been used to consolidate the composite. There are advantages and disadvantages for each combination of techniques, for example, cost, shape specificity, fibre placement accuracy, capital outlay, alloy availability etc.

Figure 5 schematically shows the BPMC TMC fabrication process. While the whole route appears very similar to routes that have been used for many years, it differs in two significant ways. Hot Isostatic Pressing is used in conjunction with a technique that ensures that good fibre position is maintained before and during the HIPping operation. The fibres are prevented form moving prior to and during consolidation by the use of small quantities of titanium powder dispersed between the fibres. BPMC are in the process of patenting this process.

Filament winding was chosen because it offers a method of accurately controling the fibre position, allowing the volume fraction of the composite to easily adjusted. The accuracy of fibre placement is particularly important with smaller filaments and at higher volume fractions because the fibre spacings become smaller. The small spaces between neighbouring fibres are difficult to infiltrate, poor distribution makes it even more difficult. Lack of infiltration of the matrix will lead to critical defects in fatigue, flectural and transverse loading cases.

Foil has been used as it is a clean, simple source of titanium, however it is difficult to produce economically. Various manufacturing techniques have been used including hot rolling, cold rolling, isobaric rolling, plasma spraying, pack rolling and chemical milling. The cost of foil and its availability in the required alloy are critical factors determining whether the whole route is viable. Beta alloys are fairly easy to obtain and significant advances have been made with alpha/beta and near-alpha alloy foil production. Most fabrication work to date has concentrated on Ti-6-4, produced via several different techniques. Limited consolidation and evaluation experiments have also been carried out using near-alpha and beta alloys.

During the degassing phase of the procedure the binder undergoes a smooth depolymerisation and is removed via a vacuum system and cold trap. The powder remains in the lay up and actually bonds to the foils, effectively forming channels which prevent the fibres from rolling, moving or "swimming" prior to or during the HIP operation. Since the powder has essentially the same chemistry as the foil, it blends into the structure by diffusion bonding. The choice of which powder to use is determined by the particle size and contamination considerations. Large particles cannot lodge between neighbouring fibres and small ones can contain higher than acceptible quantities of contaminants. But, the volume fraction of powder used is so small that it need not significantly increase overall composite contamination. It is still necessary to design the the can and tooling carefully to allow for easy degassing and to maintain the position of the channels.

Hot Isostatic Pressing was chosen to ensure that an even load is applied to the composite during consolidation. Conventional uniaxial hot pressing suffers from the drawbacks that high temperature tooling either deforms (if metallic) or cracks (if ceramic) when under the pressures needed to ensure full consolidation. This means that frequent reginding or recasting is required. Also, to produce large parts (eg flat panels) the load required is greater than that available on most presses. HIPping can produce complex shapes using relatively cheap tooling. These would not work with conventional pressing techniques. The cost of HIPing is often quoted as a reason for avoiding the process. For one off processing it is expensive but for the large number of production parts contemplated, the process becomes economic. However it is important to ensure the canning and sealing techniques are reiliable when processing such valuable material.

Figure 6 shows the typical distribution of fibre within a composite made using the BPMC fabrication route. This quality of distribution can be maintained in thick sections, monosheets and more complex configurations (eg twisted cambered panels, tubes, rings, and sections incorporating unreinforced material). Figure 7 is a histogram showing the measured spacings of neighbouring fibres. The spacing of fibres within the same row can clearly be differentiated from fibre spacings between adjoining rows. The thickness of foils (100μm in this case) and the spacing of fibres within each row can be further tailored to achieve a near hexagonal array if that is required. However it is believed the most important feature is to minimise the occurance of touching fibres.

6. Mechanical Properties of Sigma Reinforced Titanium

Simple tensile tests were carried out on many panels produced using the BPMC technique described above. The tests were designed to use the minimum amount of material consistant with producing an accurate failure stress and reasonably accurate modulus and strain to failure. The specimen design and tabbing arrangement are given in figure 8. The composite was sectioned using 150mm diameter electroplated nickel/diamond discs rotating at 5000 rpm with a feed speed of 5mm per minute. An Instron 4505 testing machine with a 100 kN load cell, 2650-558 static averaging extensometers, 0-6mm tapered grips and data analysis by Instron Series IX software. The crosshead speed was 1mm/min and the gauge length 25mm.

Table 1 summarises the results from a range of panels produced using SM1240 and SM1140+ fibre reinforcing Ti-6-4. The tensile strengths given are conservative estimates of the population average because the results include tests that failed at the tab run out (approximately 1/3 of tests performed). The modulus is somewhat less accurate, strain gauges would have yielded higher quality information but were considered too time consuming for this number of tests. However, the scatter of results does indicate that when extensometer slippage occurs, the result is clearly not consistant and can be excluded. The strain to failure results must be treated similarly.

The longitudinal results suggest that the strength of the fibre is maintained in the composite. A crude "Rule of Mixtures" calculation can be carried out, using the fibre starting strength (measured as an average of 20 pulls at the beginning of each spool and 20 at the end of each spool), an estimate of the matrix strength and the volume fraction as measured by metallographic analysis. This gives figures of approximately 90% for both SM1240 and SM1140+. This estimate is crude but is approximately correct since the matrix is at yield when the fibres fail. However, it does not take into account "bundle" effects or residual stresses. Estimating the matrix strength is not simple as the alloy is not in a standard metalurgical condition.

$$\%ROM = \frac{UTS \times 100}{(Ff \times Vf) + (Ym \times Vm)}$$

%ROM = Rule of mixtures strength
Ff = Fibre failure strength
Ym = Matrix yield strength
UTS = Composite failure strength
Vf = Fibre volume fraction
Vm = Matrix volume fraction

A similar ROM calculation can be carried out for the modulus, the results are consistant with the quoted fibre modulus.

The transverse strengths are lower than unreinforced titanium matrix. This is to be expected as the engineered fibre matrix interface is deliberately fairly weak. Good fibre management is important in achieving a high transverse strength. BPMC produced laminate gives a higher than average transverse UTS. The residual tensile stress in the matrix between closely spaced fibres is high (the matrix is probably on the point of yielding). As the matrix yields, the fibre debonds within the interface. Matrix rupture starts as thin ligaments between closely spaced fibres fail. The strain to failure results show a high degree of scatter, to obtain a value at the top end, the thin ligaments must be avoided, therefore excellent fibre management is needed.

7. Discussion

Many other workers in the field are currently testing and developing test techniques using laminates produced by BPMC. Fatigue crack growth, low cycle fatigue, high temperature, creep, and compression testing are all underway and being reported elsewhere. Initial indications are that the material behaves very like SCS-6 reinforced titanium. The diferent fibre diameter and surface coatings do not seem to significantly affect the primary mechanical properties providing the coatings are deposited correctly. There are some applications where the smaller fibre diameter is desireable (SM1040 has half the cross-sectional area of SCS-6). Sigma fibre also appears to have a tighter distribution of strengths than SCS-6, probably due to the change in core. While the effect has yet to be quantified, it may well lead to more acceptable minimum performance. The precise failure mechanism under specific loading cases within components could be different but this effect should only be of secondary interest.

8. References

[1] Warwick,C.M. (1991) "The Interfacial Reaction between carbon-coated silicon carbide monofilament and Ti-6Al-4V". BP Branch Report No 138003, available on request from BP Metal Composites Ltd.

[2] Warwick,C.M. & Smith,J.E. "Interfacial reactions in titanium alloys reinforced with C/TiB- coated SiC monofilment". Proceedings of the 12th Riso International Symposium on Materials Science. Metal Matrix Composites - Processing , Microstructure and Properties. Denmark 1991.

Table 1
SIGMA Titanium Matrix Composite Tensile Test Summary

Alloy: Ti-6Al-4V
Fibre Type: SM1140+ or SM1240
Volume Fraction: 25-40%
Number of Ply: 6-8
Lay-up: Unidirectional
Fabrication Technique: Foil/Filament Wound Fibre/HIP
Testing Direction: Longitudinal
Test temperature: Room Temperature
Number of Panels in Test: 49
Number of tests: 142

Mean UTS:	1612 MPa	Average Standard Deviation:	45 MPa
Mean Young's Modulus:	210 GPa	Average Standard Deviation:	8 GPa
Mean Strain to Failure:	0.98%	Standard Deviation:	0.09%

	SM1240	s.d.		SM1140+	s.d.
Volume Fraction:	30-35%		Volume Fraction:	32-37%	
UTS:	1606 MPa	60 MPa	UTS:	1614 MPa	54 MPa
ROM%:	90%	3%	ROM%:	93%	4%
Modulus:	210 GPa	8 GPa	Modulus:	208 GPa	6 GPa
Failure Strain:	0.97%	0.07%	Failure Strain:	1.01%	0.13%

Transverse UTS: 550 MPa
Transverse Young's Modulus: 150 GPa
Transverse Strain to Failure: 1-3%

Longitudinal Poisson's Ratio:	0.26	Thermal Expansion Coefficient:	6.58 x 10-6/K
Transverse Poisson's Ratio:	0.17	Transverse Expansion Coef':	9.32 x 10-6/K
Density:	4.1 g/cc	(0-700°C)	

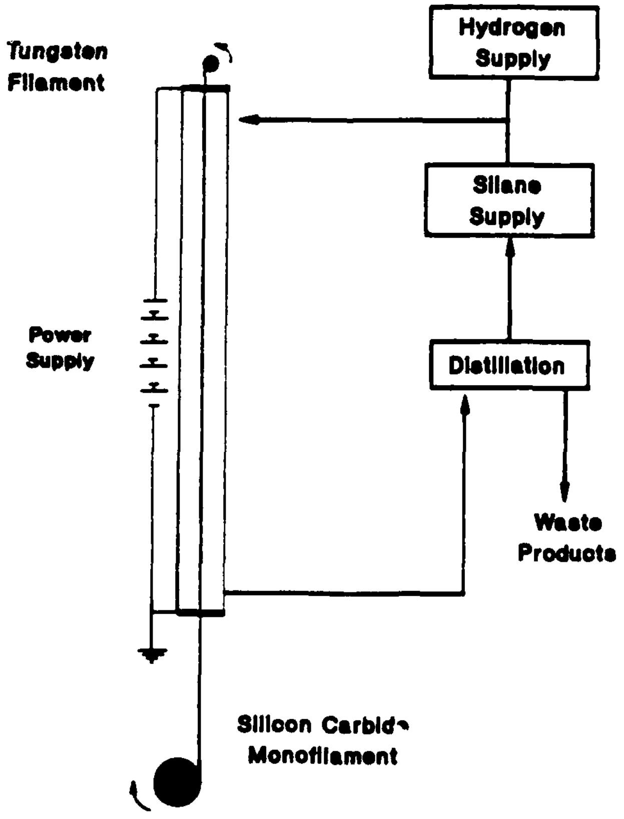
Tungsten Filament
Hydrogen Supply
Silane Supply
Power Supply
Distillation
Waste Products
Silicon Carbide Monofilament

Figure 1 Schematic of Sigma SiC SM1040 Monofilament Reactor

Figure 2 The effect of thermal exposure on W/SiC interface

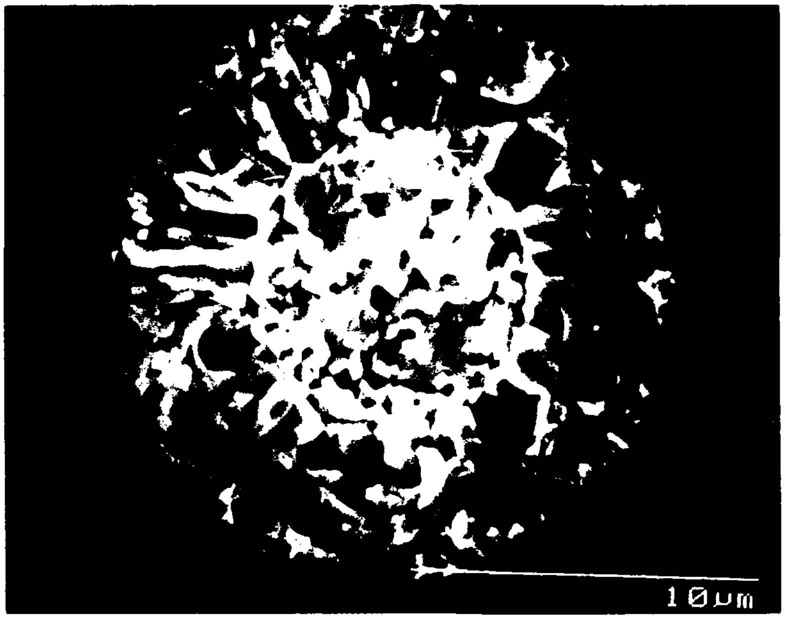

Uncoated tunsten core/silicon carbide
reaction after 100 hours at 1100°C.

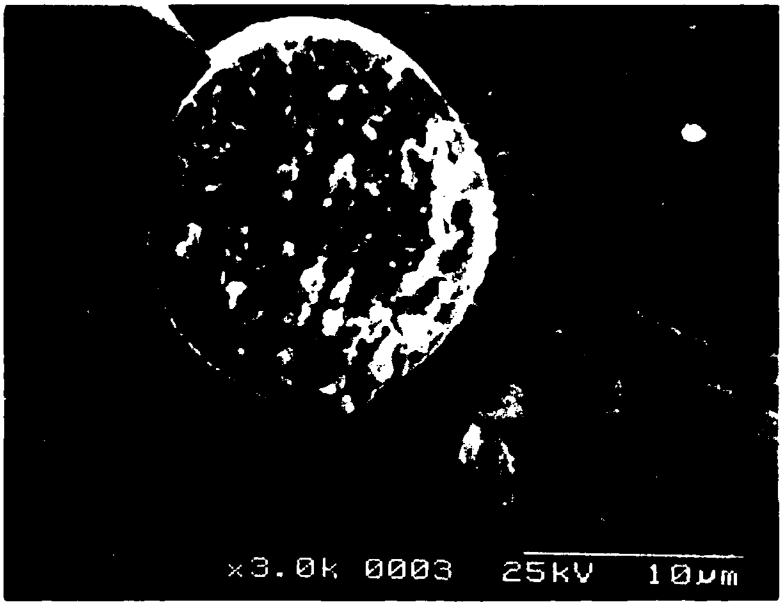
×3.0k 0003 25kV 10µm

Coated tungsten core/silicon carbide
reaction after 75 hours at 1100°C.

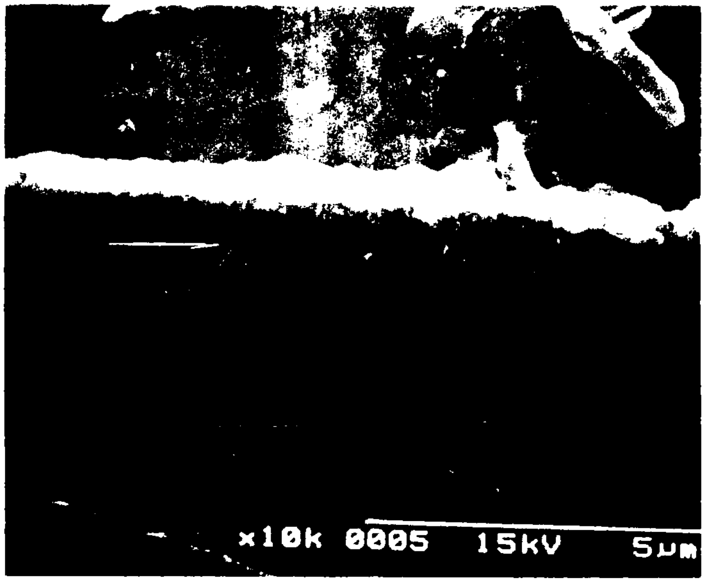
x10k 0005 15kV 5μm

Figure 3 SM1140+/Ti-6-4 Interface
4.5 μm carbon layer and reaction zone.

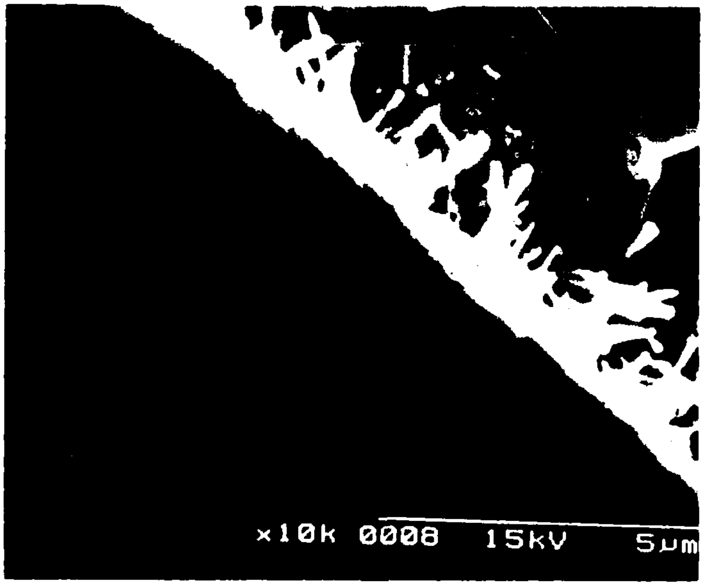
x10k 0008 15kV 5μm

Figure 4 SM1240/Ti-6-4 Interface
Carbon and TiBx layers, reaction zone and TiB needles

Figure 5.

Composite Panel Fabrication Route

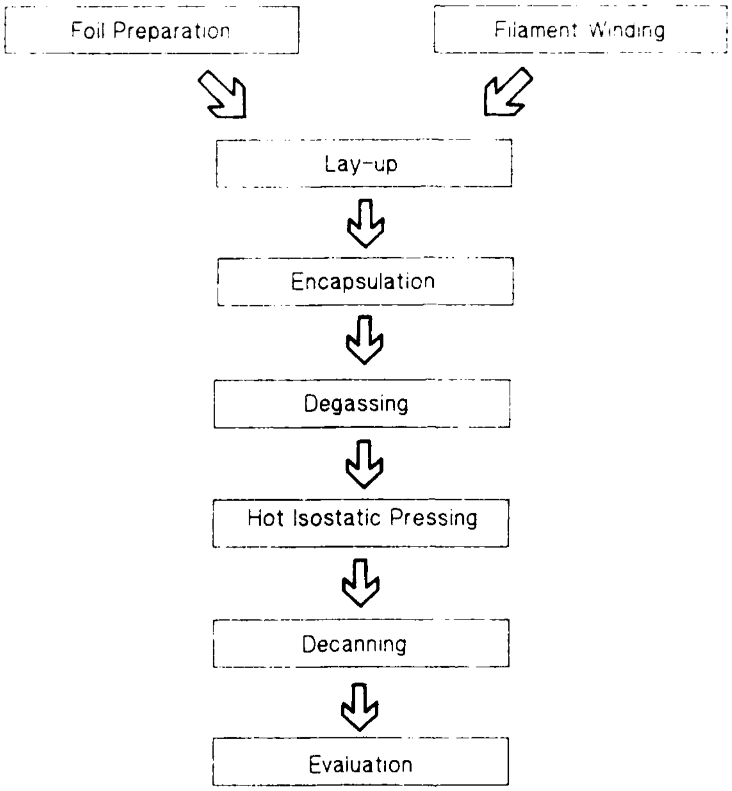
Foil Preparation
Filament Winding
Lay-up
Encapsulation
Degassing
Hot Isostatic Pressing
Decanning
Evaluation

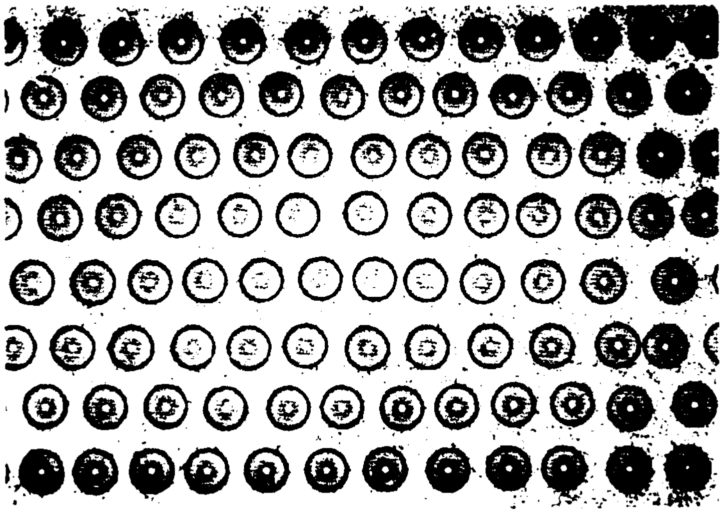

Figure 6 Ti-6-4/SM1240 composite microstructure.
The uniform fibre distribution is as achieved using
the BP proprietary foil/fibre lay-up process.

Figure 7 Histogram of nearest neighbour fibre spacings

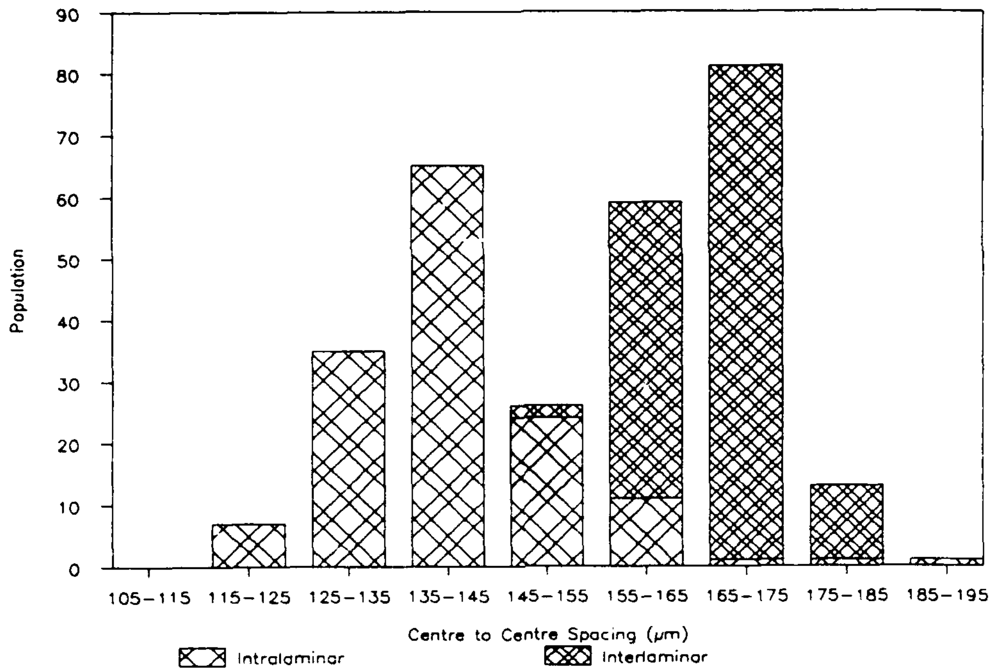

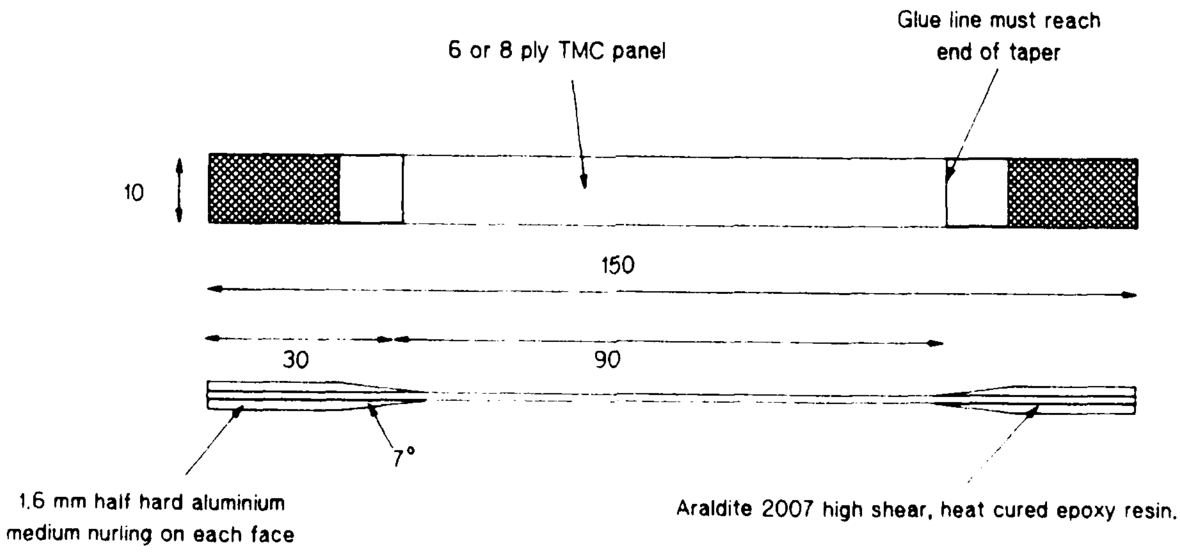
6 or 8 ply TMC panel
Glue line must reach end of taper
10
150
30
90
7°
1.6 mm half hard aluminium medium nurling on each face
Araldite 2007 high shear, heat cured epoxy resin.

Figure 8 TMC Tensile Test Specimen Design

PROPERTIES OF TMC PROCESSED BY FIBRE COATING AND HIPING

by

H.J. Dudek and **R. Leucht**
German Aerospace Research Establishment (DLR)
Institute for Materials Science
Linderhohe
51147 Köln
Germany

1. SUMMARY

SiC-fibre reinforced titanium alloys (Ti6Al4V and IMI834) were processed by fibre coating and hot isostatic pressing (HIPing). Composites with a well consolidated microstructure, with a fibre volume fraction between 0.2 to 0.6, with a narrow fibre distance distribution and a fine globular grain structure were obtained. Tensile properties according to the rule of mixture are measured with values of the ultimate tensile strength for the 0.4 SiC-Ti6Al4V-composite of 2.4 GPa at room temperature and for the 0.37 SiC-IMI834-composite of 1.3 GPa at 900^{0}C. Fatigue properties were measured under loading conditions of R =-1. Different crack initiation effects for different matrix properties and stress amplitudes were observed.

2. INTRODUCTION

An alternative method of TMC processing by hot pressing (or HIPing) of alternating layers of fibres and titanium foils is the hot isostatic pressing of SiC-fibres coated with the matrix material [***1-12***]. The fibre coating can be performed by a physical vapour deposition method or by plasma spraying. At DLR in Cologne three different deposition methods were applied and compared to each other to reveal the most suitable one for composite processing [***12***]. The coated fibres are bundled, introduced into a tube made from the matrix material, encapsulated in a stainless steel capsule, outgassed and hot isostatically pressed.

The fibre coating and HIPing method should have some advantages compared to the hot pressing(HIPing) of alternating layers of fibres and titanium foils. Applying fibre coating and HIPing no foils of the matrix material are needed, a better consolidation of the composites is expected and the processing of rotation symmetric parts by winding should be easier to perform [***5,11,13***]. In the present paper results of the characterization of composites, processed by fibre coating and HIPing at DLR are presented and advantages and disadvantages of this processing method are discussed.

3. EXPERIMENTAL

Two titanium alloys, the Ti6Al4V and the IMI834, were used for the deposition on the Textron SiC-SCS-6 fibres. The matrix was deposited on the fibre by electron beam evaporation (EB-PVD), magnetron sputtering and random arc. HIPing was performed at 900^{0}C at 1900 bar for 30 minutes. From the hiped material cylindrical samples were prepared by machining and investigated by metallography, scanning electron microscopy, chemical analysis, by determining the tensile properties at room and elevated temperatures and by fatigue experiments. The details of composite processing and characterization are described in [***9,12***].

4. COMPOSITE CHARACTERIZATION

In ***Fig.1*** SEM images of fracture surfaces of SiC-fibres coated with the Ti6Al4V matrix are shown. The fibre in ***Fig.1a*** was coated by EB-PVD and in ***Fig.1b*** applying magnetron sputtering. The grain size in the deposited coatings are a few micrometers only for both deposition methods. The lamellar structure of the coating in ***Fig.1b*** is typical for the magnetron deposition [***14***]. As can be seen from that image the thickness of the lamelles are of the order of a few micrometers.
The fibre volume content of the

Presented at an AGARD Meeting on 'Characterisation of Fibre Reinforced Titanium Matrix Composites', September 1993

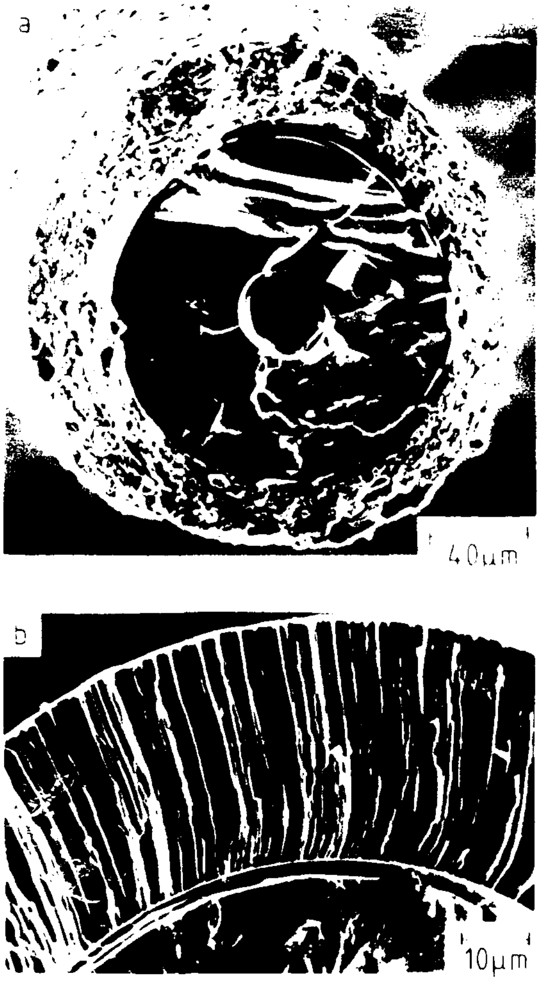

Fig 1 SiC-fibre coated with the Ti6Al4V-alloy by (a) EB-PVD and (b) magnetron sputter deposition

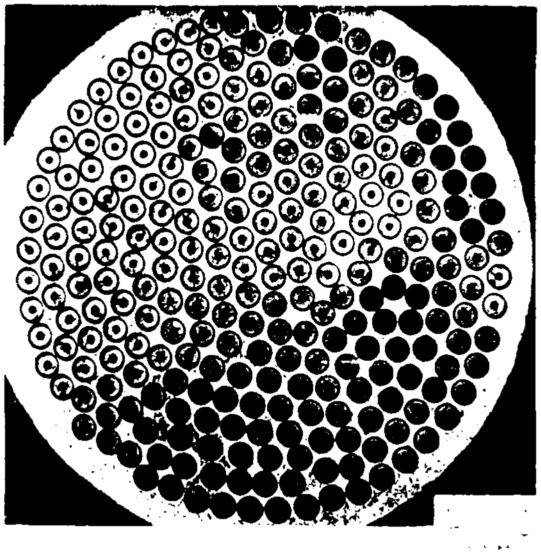

Fig.2 SiC-Ti6Al4V- composite with a fibre volume fraction of 0.57 (inside the reinforced region)

composite can be varied by the thickness of the matrix coating on the fibres. In *Fig.2* a composite with a fibre volume fraction of 0.57 [illegible] was determined from the fibre distance distribution shown in *Fig.3* [9]. V_f here considers only the inner part of the composite and neglects the outer unreinforced ring of the matrix material. In case the unreinforced material is included in the computation of V_f, a lower fibre volume fraction of 0.4[illegible] is obtained. In the following sections the lower V_f values including the unreinforced region are used to relate the mechanical properties to V_f.

Fig.3 shows a narrow fibre distance distribution with a very low fraction of fibres with small fibre distances. The fraction of

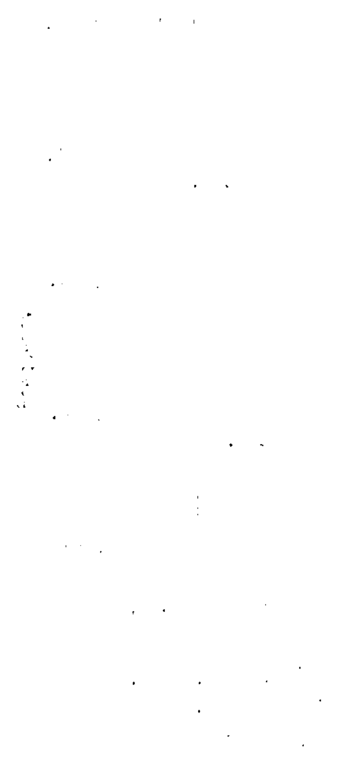

Fig.3 Frequency of fibre distances in the composite shown in Fig 2

fibres with distances lower than 10 µm is 1 percent. As can be concluded from **Fig.2**, fibres are in all cases completely surrounded by the matrix and a nearly hexagonal arrangement of them is obtained.

During HIPing the composite consolidation proceeds at a low deformation speed of the order of 0.1 µm/sec. Together with the small grain size of the matrix material of the coating, superplastic deformation is typical for this processing method[**15-17**]. In **Fig.4** the grain structure of the matrix is shown from a composite processed by applying magnetron sputtering as a deposition method. A mean grain size of 2 µm is measured. In samples processed applying EB-PVD and random arc grain sizes of 5 and 10 µm are obtained respectively [**12**].

Table 1 a comparison of the chemical composition of the coatings obtained by the three deposition methods with the as received alloy for the IMI834 is shown. For coatings obtained by random arc and EB-PVD the chemical composition deviates drastically from that of the target material. For both methods an expenditure melt metallurgical procedure is needed to process evaporation targets which results in a suitable coating composition. Only the magnetron sputtering results in nearly the same composition of the coating and the target material.

Applying magnetron sputter deposition, the danger of oxygen introduction into the alloy exists however. Using commercial magnetron sputter deposition equipments without an optimization of deposition conditions up to 10 000 ppm oxygen was measured in the coating material. An optimization of the sputtering process was performed with the aim to reduce the oxygen introduced into the alloy during coating under the conditions of an as low as possible fibre heating. Fibre heating has to be prevented be-

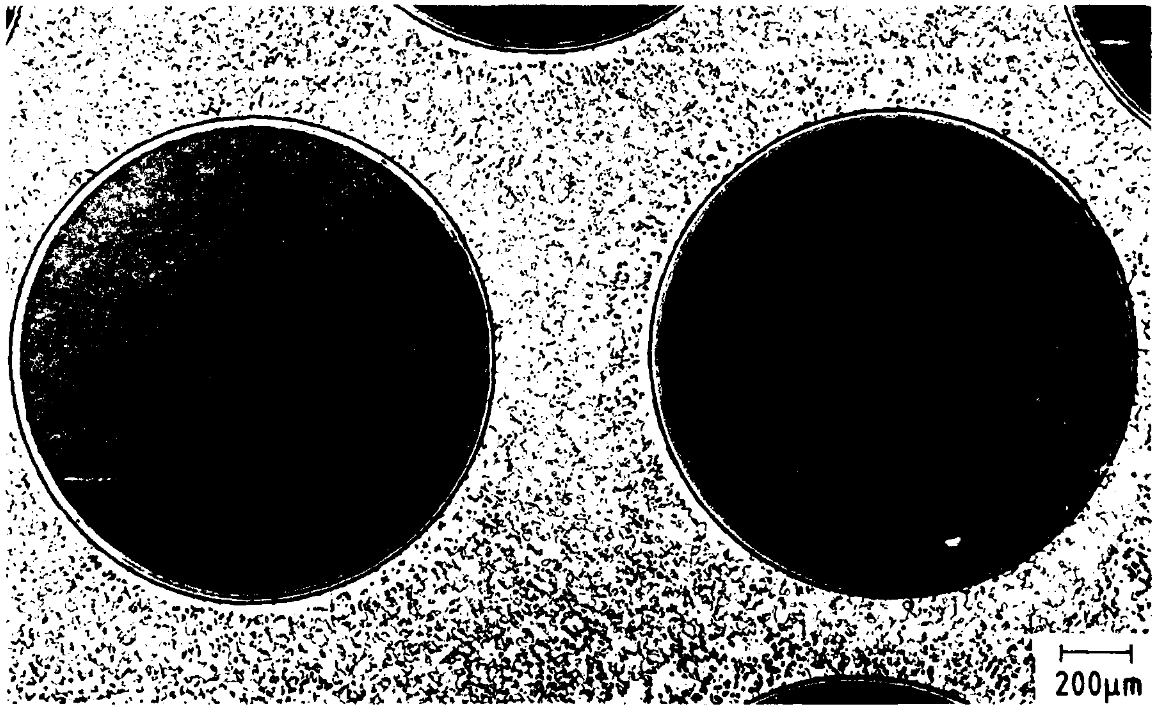

Fig.4. Globular grain structure in composites processed by fibre coating with matrix and HIPing. For the fibre coating the optimized magnetron sputter deposition was applied.

The vapour deposition of the matrix may cause a change of the chemical composition of the coating and an introduction of the oxygen (or hydrogen) from the residual gas pressure of the vacuum system can take place. Extensive investigations were performed to quantify these effects [**12**]. In cause a reaction of the titanium-alloy with the carbon coating may result in a fibre strength degradation [**18**]. Applying the optimal sputter deposition conditions an oxygen content lower than that of the other deposition methods was obtained [**12**]. The lowest value obtained up to now was 1000 ppm and there is still hope for a further reduction. In this paper only results of composites with an oxygen content lower than 2000 ppm will be discussed. A ductile matrix is obtained in this case. For the influence of the matrix embrittlement due to an incorporation of a high oxygen content in the matrix on the composite properties see [**9,12**].

5. MECHANICAL PROPERTIES

In ***Fig.5*** ultimate tensile strength and Young's modulus is shown as a function of the fibre volume fraction v_f. The shadowed area marks the predictions of the rule of mixture (the FWHM of the fibre strength distribution was used to predict strength and modulus). All measured values are inside the region predicted by the rule of mixtures. For a typical v_f = 0.4 an ultimate tensile strength of 2.4 GPa and a modulus of 220 GPa is measured. The elongation to failure is of the order of 1.3 % [**12**]. We refer the high

Table 1

Chemical composition of the Ti-IMI 834 coatings (in wt%)

Deposition	Elements					
method	Sn	Zr	Mo	Al	Nb	Fe
Target composition	4.9	3.6	0.5	5.8	0.7	0.03
Magnetron sputtering	3.1	4.6	0.6	6.4	0.8	0.05
EB-PVD	4.8	<0.05	<0.05	5.0	<0.05	--

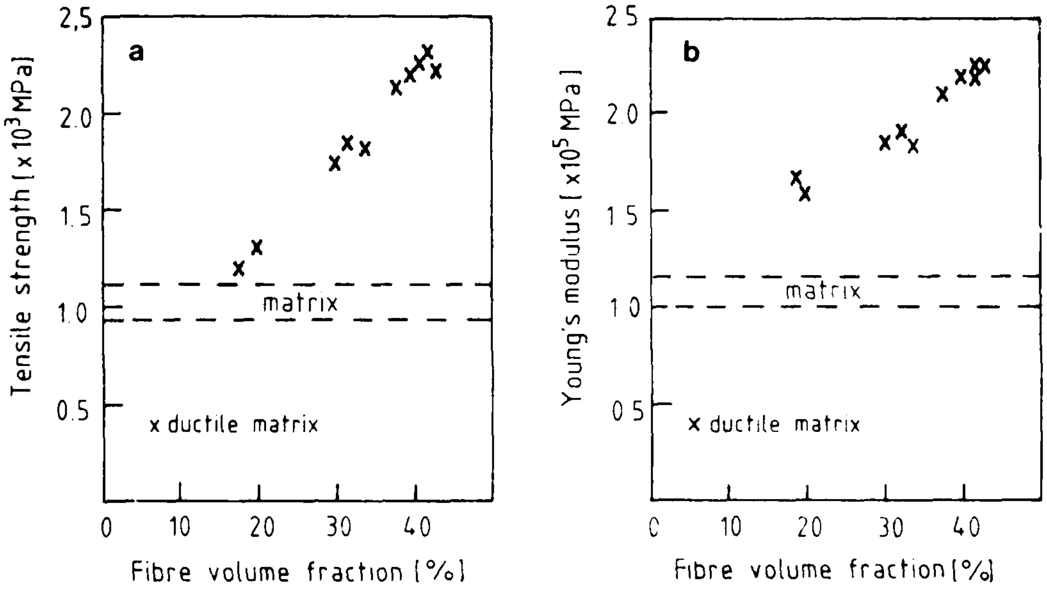

Fig.5 Ultimate tensile strength of the SiC-Ti6Al4V-composites (a) and Young's modulus (b) as a function of the fibre volume fraction. The shadowed area shows the predictions of the rule of mixture.

strength measured in our composites, compared to that of values obtained in composites processed by hot pressing of alternating layers of fibres and foils published in literature (e.g.[**19**]), to the nearly ideal composite consolidation and the small grain size of the matrix.

In ***Table 2*** some ultimate tensile test values of the SiC-IMI834-composites at different temperatures are shown. For an unreinforced IMI834 material at room temperature approximately 1 GPa is obtained. With increasing temperature the ultimate tensile strength decreases first slowly to values of 750 MPa at 500°C, and decreases rapidly above that temperature [**20**]. For the 0.37 SiC-IMI834 composites 1.3 GPa is measured even at 900°C. As can be seen from the fracture surface, ***Fig.6***, a ductile fracture with no necking of the reinforced region is obtained at test temperatures of 900°C.

Table 2

Ultimate tensile strength for SiC-IMI834-composites at different test temperatures

Fibre volume fraction [%]	Test temperature [°C]	Ultimate tensile strength [GPa]
0	RT	1.0
35	RT	2.0
37	300	1.92
42	400	2.13
40	500	2.05
39	600	1.83
37	700	1.60
35	800	1.27
37	900	1.29
42	970.	1.21

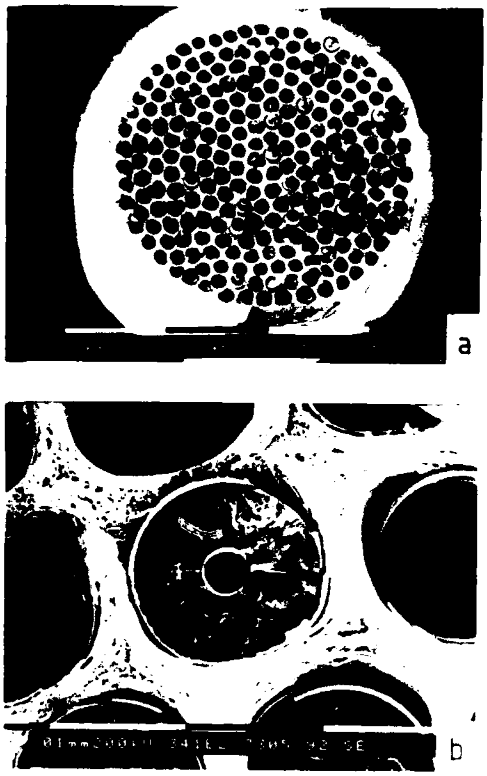

Fig. 6. Fracture surface of a SiC-IMI834-composite tested at 900°C, (a) overwiew and (b) detail

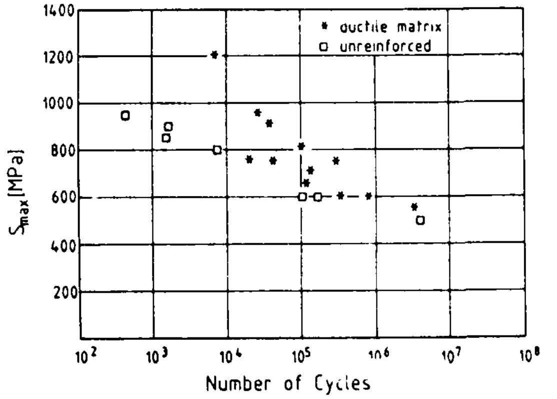

Fig. 7. Number of cycles to failure for different stress amplitudes for SiC-Ti6Al4V-composites with a fibre volume fraction of 0,32 compared with results of unreinforced material with the same sample geometry.

In ***Fig.7*** the fatigue behaviour for the 0.32 SiC-Ti6Al4V-composites obtained under symmetrical load conditions of R = -1 is compared with unreinforced material tested under the same sample geometry and load conditions. At high stress amplitudes of ±900 MPa the fatigue life is higher by more than one order of magnitude compared with the unreinforced material. At low stress amplitudes of ±600 MPa and lower, nearly the same values for the reinforced and unreinforced material are obtained.

The symmetrical sample geometry, the homogeneous fibre distribution and the complete fibre envelopment by the matrix allow the study of fatigue crack initiation effects in these composites. A detailed study will be published elsewhere [**21**]. In ***Fig.8*** an example is given of a metallographic section parallel to fibres of a 0.32 SiC-Ti6Al4V-composite loaded at a stress amplitude of ±600. Mainly fibre breaking during the fatigue loading of the composites is observed and the matrix remains mostly unchanged.For different matrix properties und different load amplitudes different crack initiation effects were observed in these composites: in a ductile matrix at high stresses crack initiation at the reaction zone fibre-matrix and at low stresses in the fibre was observed. In composites with a brittle matrix at high stresses crack initiation in the matrix and at low stresses at the sample surface was detected [**12,21**].

Fig.8. Metallographic section of a SiC-Ti6Al4V-composite parallel to the sample axis loaded at ±600 MPa showing the preferential breakage of fibres.

6. DISCUSSION AND CONCLUSIONS

Processing of composites by coating the SiC-fibres with marix and HIPing results in a material with a variable fibre volume fraction between 0.2 and 0.6 with a narrow fibre distance distribution and a low fraction of fibres with small distances. Applying optimized magnetron sputtering as a matrix deposition method a small globular grain size, nearly the same matrix composition in the composite material as in the target material and a low oxygen content is obtained. Ultimate tensile strength and Young's modulus values as predicted by the rule of mixture in the region between 0.2 and 0.5 are measured. The elongation to failure is 1.3 %. For the 0.37 SiC-IMI834 composite at 900°C ultimate tensile strength of 1.3 GPa were obtained. Fatigue life of 0.32 SiC-Ti6Al4V composites is higher by more than one order of magnitude than the unreinforced material for high stresses of the order of ±900 MPa and as high as the unreinforced material for stresses below ±600 MPa. Different crack initiation effects were observed in these composites during fatigue loading.

The high ultimate tensile strength of our composites is explained by the nearly ideal fibre distribution and the fine globular grain structure of the matrix. The increase of fatigue life is unsufficient compared to the unreinforced material when the high tensile strength of the composites is considered. A careful investigation of the crack initiation and propagation effects should however give informations on the methods for an increase of fatigue properties [**21**].

Some of the advantages of the processing method by fibre coating and HIPing can presently be predicted: Every matrix material which can be evaporated by PVD and consolidated by HIPing can be used for processing composites without the need of matrix foils. Nearly ideal composites with a small globular grain size are obtained. These are conditions to obtain tensile properties of composites according to the rule of mixture. Processing of building parts by winding of coated fibres should be easier compared with the method applying hot pressing of alternating layers [***5,10,11,13***].

As one can expect there are disadvantages of this processing method however. The fibre coating and HIPing method is up to now an expensive method of processing and some of the problems have not been solved until now. For an application to processing of parts by winding the problem of fibre breackage during the HIP process has to be solved [***11***].

Most of the unresolved problems are however common to those for the composites obtained by hot pressing (HIPing) of alternating layers of foils and fibres. Compared with the high tensile properties the fatigue properties of the composites are unsufficient. For application temperatures higher than 600^{0}C the carbon coating of the fibre has to be modified [18] and for a titanium aluminate as a matrix material the optimal processing conditions have not been determined until now [***20***].

Literature

[1] Dudek, H.J., R.Leucht, G. Ziegler: "Auger Electron Spectroscopy of the Interface of SiC Fiber Reinforced Titanium Alloys", Titanium Science and Technology, Proc. 5th Int. Conf. Titanium, Munich, 1984, Vol.3, p. 1773-1780

[2] Leucht, R., H.J. Dudek, G. Ziegler: "Einfluß von Zwischenschichten auf die Ausbildung der Reaktionszone in SiC-faserverstärktem Ti6Al4V", in "Haftung als Basis für Stoffverbunde und Verbundwerkstoffe", ed. W. Brockmann, DGM, Oberursel 1986, p.101-111

[3] Leucht, R., H.J. Dudek, G. Ziegler: "SiC - faserverstärkte Titanlegierung Ti6Al4V",Z.Werkstofftech. 18(1987)27-32

[4] Leucht, R., H.J. Dudek, G. Ziegler: "Thermal Stability of SiC Fibre Reinforced Ti6Al4V Alloys", Proc. EUROMAT Aachen 1989, p.

[5] Leucht, R. H.J. Dudek, G. Ziegler: "Laboratory Scale Processing of SiC-Ti6Al4V Composites", Proc. 4th Int. Conf. Fibre Reinforced Composites, Liverpool 1990. p.279-282

[6] Dudek, H.J., R. Leucht, G. Ziegler: "SiC-Fibre Reinforced Titanium Alloys: Processing, Interfaces and Mechanical Properties", Proc. 4th Eur. Conf. Comp. Mat., Stuttgart, 1990, p.339-344.

[7] Ward-Close, C.M., P.G. Partridge: "A Fibre Coating Process for Advanced Metal Matrix Composites",J.Mat.Sci.1990

[8] Ward-Close, C.M., P.G. Partridge, 7th World Conf. titanium, San Diego, June 28 - July 2, 1992

[9] Dudek, H.J., R. Leucht: "Titanium-Matrix Composites", in Advanced Aerospace Materials, ed.: H. Buhl, Springer Verlag, Heidelberg, 1992, p.124-139

[10] Dudek, H.J., R. Leucht: "Verfahren und Vorrichtung zum Beschichten von Fasern", Deutsches Patent DE 40 18340 A1

[11] Dudek, H.J., R. Leucht: "Verfahren zum Herstellen von faserverstärkten Bauteilen", Deutsches Patent DE 40 21547 A1

[12] Leucht, R., H.J. Dudek: "Properties of SiC-Fibre Reinforced Titanium Alloys Processed by Fibre Coating and HIPing", submitted to Mat. Sci. Engn. 1993

[13] Leucht, R., H.J. Dudek, G. Ziegler: "Processing of Parts Made of SiC-Fibre Reinforced Titanium Using Hot Isostatic Pressing (HIP)", Proc. 4th Eur. Conf. Comp. Mat., Stuttgart, 1990, p.393-398.

[14] J.A. Thornton, Ann. Rev. Mat. Sci. 7(1977)239

[15] A. Wisbey, P.G. Partridge, A.W. Bowen: "Superplastic deformation of Ti-6Al-4V extruded tube", J. Mat. Sci. 27(1992)3925-3931

[16] M.T. Salehi, J. Pilling, N. Ridley, D.L. Hamilton: "Isostatic diffusion bonding of superplastic Ti-6Al-4V", Mat. Sci. Engn. A150(992)1-6

[17] T.G. Langdon: "The physics of superplastic deformation", Mat. Sci. Engn. A137(1991)1-11

[18] Dudek, H.J., R. Leucht, R. Borath, G. Ziegler: "Analytical Investigations of Thermal Stability of the Interface in an SiC-Fibre Reinforced Ti6Al4V-Alloy", Microchim. Acta 1990-II, 137-148

[19] Handout of Textron Speciality Materials: "Continuous Silicon Carbide Metal Matrix Composites", Lowell, MA 01851, USA 1993

[20] R. Leucht, M. Peters, H.J. Dudek: Verbundwerkstoffe und Stoffverbunde, Chemnitz, 1992, in press

[21] H.J. Dudek, R. Leucht, J. Hemptenmacher: in preparation

Fibre-matrix interface properties in Ti-matrix composites : chemical compatibility and micromechanical behaviour

A. Vassel, R. Mévrel, J.P. Favre, J.F. Stohr
Materials Department, ONERA, BP 72
F 92322 Chatillon, France

ABSTRACT

Silicon carbide reinforced titanium alloys or titanium aluminides are challenging materials for engine discs applications in the temperature range 650-800°C. The main problems concerning fibre-matrix compatibility, i.e. fibre coating degradation through diffusion controlled mechanisms and fibre-matrix mechanical behaviour are reviewed based on recent studies.

It is also shown how two micromechanical tests, the fragmentation test and the push-out test may be correlated. With the help of a 1D shear-lag type model, taking fibre-matrix debonding into account, a good fit is obtained between measured and computed values of the fibre-matrix load-transfer mean shear-stress.

INTRODUCTION

Metal matrix composites appear to be good candidates to ensure a further temperature rise of compressor components. One of the main challenge for these materials will be to replace titanium alloys and superalloys for discs applications, the former being able to operate today at a maximum temperature of 550°C and the latter at 650°C. Titanium alloy matrix composites are expected to work at temperatures around 650°C while titanium alumide matrices are expected to allow a 100 or 150°C further rise in operating temperatures.

Three main problems have to be solved in a first step :

- the determination of the maximum operating conditions so as to allow an accurate control of the reaction between the fibre-coating and the matrix in order to maintain, during the component life, the efficiency of the mechanical fuse, i.e. the fibre coating ;

- the definition of reliable means of measuring the fibre-matrix interface characteristics so as to be able to proceed to non destructive testing of the composite at any time during its life ;

- the achievement of good links between the mechanical behaviour of these materials (strength, fatigue and thermal-fatigue behaviour) and the micromechanical parameters, essentially the fibre-matrix bond strength and glide properties.

1. ANALYSIS OF FIBRE-MATRIX INTERACTIONS

1.1. Microstructural investigations

1.1.1. *SCS-6/Ti-6Al-4V composite*

The interaction between the SCS-6 fibre and the Ti-6Al-4V matrix is well documented in the literature [1-7] and the main results are summarized below. The SCS-6 fibre (ø 140 µm) produced by Textron is made of SiC deposited by CVD on a carbon core. It possesses a 3 µm thick protective coating which is mainly composed of pyrocarbon.

During processing of the SCS-6/Ti-6Al-4V composite around 900°C, a partial consumption of the carbon layer takes place with the formation of different compounds. According to Rhodes and Spurling [2], the interaction zone consists of three layers of reaction products. The major reaction product is TiC which is sandwiched between an inner layer of a fine-grained mixture of TiC and Ti_5Si_3 and an outer layer of Ti_5Si_3. Titanium carbide develops more extensively than titanium silicide as a direct result of the composition of the fibre surface. Hall et al. [3,4] observed the same compounds in the reaction zone and they identified a Ti_5Si_4 silicide associated with Ti_5Si_3.

When titanium reacts with the coating , titanium carbide is formed in a first step. As long as the carbon coating is not entirely consumed, the titanium carbide plays the role of a diffusion barrier by preventing titanium from reacting with SiC. For longer durations, the reaction growth rate is controlled by the diffusion of titanium and silicon through the titanium carbide layer [5]. The alloying elements do not participate in the fibre-matrix reaction and an increase in the aluminium and vanadium concentrations has been found at the interface between the matrix and the reaction zone [5,6]. There is no evidence that new intermetallic compounds are formed, it rather appears that the alloying elements are simply combined substitutionally [3].

Growth of the reaction zone and consumption of the fibre surface layer are nonuniform with greater reaction occuring where the fibre contacts beta phase of the titanium matrix. This phenomenon appears to

Presented at an AGARD Meeting on 'Characterisation of Fibre Reinforced Titanium Matrix Composites', September 1993.

result from the higher diffusivity of carbon in the beta phase [2].

1.1.2. *SiC/Ti$_3$Al+Nb composites*

Analytical studies of fibre-matrix interactions were performed on SCS-6/Ti-14Al-19Nb and SM 1240/Ti-14Al-19Nb composites. The SM 1240 is a SiC fibre (ø 100 μm) with a tungsten core. Its protective coating, designed within the framework of a European collaborative programme, is composed of three layers : pyrocarbon (1 μm), TiB_2 (0.2 μm) and an external TiB_2+B coating (0.8 μm). Due to the difficulty in processing intermetallic matrix composites, such materials were simulated by sputtering a Ti-14Al-19Nb layer onto SiC fibres and heat treating in an inert atmosphere at temperatures representative of fabrication conditions. The experimental procedure is described elsewhere [8].

The fibre-matrix interaction on the SCS-6/Ti-14Al-19Nb system was studied using a submicron ion probe [9]. Ionic images after a thermal exposure of one hour at 1050°C are presented in Fig. 1. The C^- image illustrates the carbon coating of the SCS-6 fibre and the $TiO^-{*}C^-$ correlation image shows the extent of the interaction zone which is about 0.8 μm. It was checked that no silicon is present in the reaction zone. A detailed analysis of the fibre-matrix interface using TEM techniques has also been performed by Baumann et al. [10]. They found that the matrix had reacted only with a portion of the carbon-rich outer layer of the SCS-6 fibre in the as-consolidated condition. The reaction zone is composed of two concentric zones. The zone closest to the fibre consists of $(Ti,Nb)C_{(1-x)}$, $(Ti,Nb,Al)_5Si_3$ and some microporosity. There is a diffusion-generated Nb concentration through this zone. The zone adjacent to the matrix contains $(Ti,Nb)_3AlC$ and $(Ti,Nb,Al)_5Si_3$.

We have performed TEM investigations on the interaction zone of the SM 1240/Ti-14Al-19Nb composite. A micrograph of this zone in contact with the fibre is shown in Fig. 2. During the exposure at 1050°C, the external boron rich coating has been fully transformed to needle like precipitates which were identified as TiB_2 from electron diffraction patterns. These precipitates act as a diffusion barrier and the inner carbon layer remains intact. Fig. 3 is a micrograph of the reaction zone near the matrix. Here, long needles embedded in the Ti-14Al-19Nb aluminide can be observed. The combination of electron microdiffraction, EDS and EELS reveals that their composition is $(Ti_{0.7},Nb_{0.3})B$.

Recent investigations were carried out on the phase equilibria in the ternary Ti-Al-B system [11]. Titanium monoboride and titanium diboride are the two main compounds that can appear. It was shown that TiB_2 is stable above 30-40 at.% aluminium and/or 40 at.% boron. Accordingly, the presence of TiB_2 is expected near the fibre, the external layer containing a large proportion of boron, whereas a TiB type compound is likely to precipitate on the matrix side. Our observations agree with these thermodynamic considerations.

1.2. Kinetic parameters

The increase in reaction zone thickness as a function of the square root of time for two SiC/Ti$_3$Al+Nb composites are shown in Fig. 4. These plots show that in the temperature range 800-1050°C, the growth of the reaction zone is linear with the square root of time and this result is in agreement with previous work on SiC/Ti composites [13-16]. This indicates that the reaction zone growth kinetics is mainly controlled by diffusion and that it can be modelled with a parabolic growth law :

$$x = kt^{1/2}$$

where x is the reaction zone thickness, k is the temperature dependent rate constant and t is the isothermal exposure time. Furthermore, k can be expressed by the Arrhenius equation :

$$k = k_0 e^{-Q/2RT}$$

where k_0 is the pre-exponential factor, Q is the apparent activation energy, R is the gas constant and T is the exposure temperature. The values of Q and k_0 can be calculated by plotting the logarithm of the reaction zone thickness versus the reciprocal of the absolute temperature. These values are listed in Table 1 for several SiC/Ti composites. The activation energy varies from 206 to 269 kJ/mol depending on the systems and the laboratories.

The knowledge of the reaction kinetics at operating temperatures is an important parameter. Thermodynamic parameters determined for short exposures at high temperatures can be used to predict the extent of the reaction zone thickness for long term use of the composites at lower temperatures. Such a calculation was made for a 1000 hours exposure at 700°C (Table 2). It can be seen that for the SCS-6/Ti-6Al-4V composite which exhibits the highest reaction kinetics, the 3 μm thick pyrocarbon coating of the SCS-6 fibre is not totally consumed. The comparison between the Ti-6Al-4V and Ti_3Al+Nb matrices reveals the slower reaction rate when increasing the alloy additions and this effect can be mainly attributed to aluminium [6]. Also, it appears that the reaction kinetics is similar for the SCS-6 and the SM 1240 fibres although their coatings are of different nature, pyrocarbon and TiB_2+B respectively.

2. THE FIBRE-MATRIX INTERFACE AND THE MICROMECHANICS OF Ti MATRIX COMPOSITES

As already stated, most of the components made with a Ti-base matrix composite will be mainly used for aircraft engine applications. The concerned parts are compressor discs with either a flat or a drum shape for which the main loading originates from the centrifugal forces due to the high rotational speed of the engine. Therefore, due to the highly anisotropic loading, composites with a unidirectional (U.D.) reinforcement will be used for these components. The loading will be mainly the hoop stress together with combined thermal and low-cycle fatigue stresses ; the design of these components will be made in a first step on relying upon the elastic limit, which appears to be very close to the rupture stress in these composites with a high fibre volume fraction (> 30%). Prediction of the U.D. composite strength starting from the constituent properties, i.e. those of the fibres, the matrix and the interface between the fibre and the matrix, appears to be one of the major concern for the use of these materials.

2.1. Approach of a failure criterion for U.D. composites

The very first models developed for the prediction of the rupture stress are due to Rosen [17] and Zweben [18] in the mid-sixties. Both models made the assumption that the composite failure results from the concurrent rupture of single fibres linked by a tough matrix, where a penny shape crack is supposed not to grow. The rupture criterion has been derived based on the concept of the inefficiency length, i.e. the critical length over which a single fibre is reloaded from its broken ends. The predicted rupture stress is strongly dependent upon this inefficiency length. To get better strength predictions than those obtained with the shear-lag fibre reloading considered by Zweben [18], it is essential to take into account more realistic reloading mechanisms including fibre-matrix debonding :

- firstly, fibre-matrix debonding ensures that a matrix crack will not grow subsequently to the fibre failure, thus leading to stress concentrations on the neighbouring ones, as shown by J.A. Cornie et al [19].

- secondly, the consideration of a real fibre-matrix load-transfer shear-stress obtained through fragmentation tests measurements, and its evolution with temperature, allows a good fit between the measured and the computed values of the composite rupture-stress, Fig. 5 [20].

Moreover the composite failure simulation performed using a model material with 400 single fibres, (20 x 20) clearly reveals that :

- an increase in the fibre Weibull-modulus results in an increase in the composite rupture strength (Fig. 6a). It is worth mentioning that for the same mean rupture-stress of the fibres (4000 MPa for a gauge length of 5 mm), an increase in the fibre Weibull-modulus from 4 to 25 leads to a rise in the composite rupture-stress of more than 55%. On the opposite, a low fibre Weibull-modulus allows a larger number of single fibre ruptures before the composite failure (Fig. 6b, c, d) ;

- the influence of the fibre-matrix load transfer is even more important when the fibre Weibull modulus is low ; it vanishes for high Weibull modulus, i.e. when m ≥ 20, (Fig. 7) ;

- the limitation of the load transfer from the broken fibre to the next neighbouring ones is even less deleterious when the inefficiency length is low ;

- in titanium-alloys matrix composites the limiting factors of the fibre-matrix load transfer shear-stress appear to be linked to fibre-matrix debonding ; as shown by D. Jacques [21], two physical parameters are to be taken into account, the fibre-matrix bond-strength and the fibre-matrix friction stress over the fibre debonded length. Fig. 8 illustrates the reloading of a fibre from a broken end showing the friction stress, proportional to the thermal hoop stress, which is constant over the debonded length of the fibre, followed by the elastic reloading starting from the fibre-matrix bond strength.

This very first approach of a composite rupture-criterion does evidence the prime role of the fibre-matrix load transfer shear-stress, and that of the contributing physical parameters, the fibre-matrix bond strength and the friction stress over the debonded length. At the present time, two methods are available to reach those parameters : the fragmentation test which allows the measurement of the mean interfacial shear-stress and the push-out technique which permits the measurement of both the fibre-matrix bond strength and the fibre-matrix friction stress [22].

2.2. Fragmentation tests results

The processing of the fragmentation test, using single fibre specimens, has been described elsewhere and the data for the SCS-6/Ti-6Al-4V composite already reported [23 [illegible]. The Ti-14Al-21Nb aluminide sheets used in this study were kindly provided by Mrs Brindley from NASA Lewis. SCS-6/Ti-6Al-4V specimens were tested at room temperature whereas the SCS-6/titanium aluminide ones were tensile tested at 425 and 650° C due the very low elongation to rupture of this titanium aluminide at room temperature. Fig. 9 illustrates a typical fragmentation tensile curve for the SCS-6/Ti-14Al-21Nb composite at 425°C. Fragmentation of the fibre occurs in the elastic-plastic region with small load drops resulting from the successive ruptures of the SCS-6 fibre. The number of load drops fits the number of fibre ruptures observed after matrix dissolution. The maximum fibre-matrix load transfer shear stress is derived from the Kelly-Tyson relationship :

$$\tau_m = \frac{d\sigma_{fr}(l_c)}{2l_c}$$

where the critical length l_c is equal to 3/4 $<l>$, $<l>$ being the mean fragment length, and $\sigma_{fr}(l_c)$ the fibre strength of the fragment. The fibre strength is obtained from single filament tensile testing, these filaments being previously coated with the convenient matrix, using a PVD technique, and subsequently heat treated to simulate the processing cycle [26]. The measured values of the interfacial mean shear- stress τ_m have been plotted for both the Ti-6Al-4V and the Ti-14Al-21Nb matrix composites in Fig. 10. The τ_m values are quite similar for both composites whatever the matrix. Concerning the reloading mode, observations performed on broken test pieces reveal that in both cases fibre debonding occurs mainly within the coating itself or at the fibre-coating/metal or reaction zone interface. This is an indication of the role played by the fibre-matrix friction-stress in the fibre reloading.

2.3. Push-out tests results

Push-out tests have been performed at ONERA using SCS-6/Ti-6Al-4V unidirectional composites provided by Textron Specialty Metals Division. The experimental conditions have been reported elsewhere [22]. Both the decohesion stress τ_d and the friction stress τ_f have been derived from these tests using the following relationships (Fig. 11) :

$$\tau_d = \frac{F_d}{2\pi r(h-\alpha)}$$

where Fd is the load at decohesion, r the fibre radius, h the specimen thickness and α a fitting parameter obtained from tests with different fibre embedded lengths.

$$\tau_f = \frac{F_f}{2\pi rh}$$

where F_f is the applied force and h the embedded length of the fibre.

Table 3 collects the available results on push-out tests originating either from the literature [28-32] or from work done at ONERA [22]. A keen examination of the results shows a good agreement for both τ_d and τ_f values obtained in different laboratories, which is rather unusual for micromechanical testing [27]. As already mentioned, decohesion occurs both at the fibre-carbon coating interface and the coating-matrix interface (Fig. 12).

2.4. Correlation between push-out and fragmentation tests

As already mentioned, the fibre-matrix load-transfer mean shear-stress τ_m obtained from fragmentation tests and the fibre-matrix bond strength and friction stress derived from push-out tests cannot be directly compared. Nevertheless, as shown by D. Jacques [21] τ_m can be computed from τ_d values, provided that the fibre and matrix characteristics are known, and with the assumption that on the debonded length, the fibre glides relative to the matrix with a Coulomb type friction-stress. Taking the characteristics given in Table 4 for the two matrices, values of τ_m can then be computed, assuming that the stress distribution at the fibre end is the one given in Fig. 8.

A comparison of the computed and measured values of τ_m is given in Table 5 for both SCS-6/Ti-6Al-4V and SCS-6/Ti-14Al-21Nb composites. The agreement between the measured and the calculated values can be considered as pretty good. This first correlation attempt between interfacial characteristics obtained through two different tests appears quite promising in view of predicting the mechanical behaviour of this kind of composite.

3. DISCUSSION

Titanium-aluminide matrix composites processed with SCS-6 Textron fibres do exhibit a better thermal stability than Ti-6Al-4V matrix composites as evidenced from Table 2. It appears from these results that at 700°C the carbon coating layer should be consumed within 7000 hours, which corresponds to ultimate conditions for SCS-6/Ti-6Al-4V use. On the opposite, titanium-aluminide composites will be able to sustain much longer holding times -about one order of magnitude- without the carbon coating being fully destroyed. This better behaviour has been linked to a decrease of both the reactivity and diffusion rate when the aluminium content of the alloy is increased.

From another point of view, it has been shown that in the as-processed state, both composites do exhibit fibre-matrix debonding and fibre glide within its matrix sheath, the debonding occuring either at the fibre-coating or the coating-matrix interface. Moreover, a good fit has been obtained between the interfacial characteristics measured from fragmentation tests and those computed from push-out data, using or shear-lag unidimensional model taking into account only two parameters, the fibre-matrix bond strength and/or the friction coefficient between the fibre and the matrix.

Further development of this model should take into account :

- firstly a 2D modelling of the fibre reloading such as proposed by J.A. Nairn [33].

- secondly a fitting of the friction coefficient μ, which has been taken equal to 0.24 formerly, with the help of the friction-stress derived from push-out tests.

Conclusions

- SCS-6 Textron and SM 1240 BP fibres appear to be suitable reinforcements for titanium base matrix composites. For Ti-6Al-4V however, maximum use conditions are close to 700°C/6000 hours.

- A Ti_3Al type matrix (Ti-14Al-21Nb) appears less reactive with the carbon coating of the SCS-6 fibre. The SM 1240 and SCS-6 fibres exhibit similar reaction kinetics in that matrix.

- Micromechanical measurements using either the fragmentation or the push-out test performed on both Ti-6Al-4V or titanium aluminide (Ti-14Al-21Nb) matrix composites lead to values in agreement with those obtained in other laboratories. A simple shear-lag computation modelling taking into account fibre-matrix debonding and glide allows to calculate the fibre-matrix load-transfer mean shear stress from the push-out data. The correlation with the measured values appears quite good for both composites.

Acknowledgments

Thanks are due to DRET for the financial support of the different studies, the results of which have allowed the publication of this paper.

Literature

[1] R. Pailler et al., Revue de Chimie Minérale, t. 18 (1981), pp 520-543.

[2] C.G. Rhodes, R.A. Spurling, Recent Advances in Composites, ASTM STP 864, Philadelphia, 1985, pp. 585-599.

[3] I.W. Hall, J.L. Lirn, J. Rizza, J. of Materials Science Letters, 10 (1991), pp 263-266.

[4] I.W. Hall et al., J. of Materials Science, 27 (1992), pp 3835-3842.

[5] Y. Le Petitcorps et al., Proceedings of the ECCM 3 Conference, Bordeaux, France (1989), pp 185-191.

[6] W.D. Brewer, J. Unman, Nasa Technical Paper 96, August 1982.

[7] C. Jones, C.J. Kiely, S.S. Wang, J. of Materials Research, 5 (1990), pp 1435-1442.

[8] F. Brisset, A. Vassel, Proceedings of the International Symposium on Structural Intermetallics, TMS, Warrendale, PA (1993), to be published.

[9] G. Slodzian et al., C.R. Acad. Sc. Paris, t. 311 (1990), pp 57-64.

[10] S.F. Baumann, P.K. Brindley, S.D. Smith, Met. Trans. A, 21A (1990), pp 1559-1569.

[11] J.J. Valencia et al., Materials Science and Engineering, A144 (1991), pp 25-36.

[12] F. Brisset, Ph.D. Thesis, to be published.

[13] P. Martineau et al., "Developments in the Science and Technology of Composite Materials", ECCM, Bordeaux, France (1985), pp 725-731.

[14] W. Whatley, F.E. Wawner, J. of Materials Science Letters, 4 (1985), pp 173-175.

[15] S.M. Jeng, J.M. Yang, Proceedings of the Seventh Conference on Composite Materials, Pergamon Press (1989), pp 555-560.

[16] D.B. Gundel, F.E. Wawner, Scripta Metallurgica et Materiala, 25 (1991), pp 437-441.

[17] B.W. Rosen, "Fibre Composite Materials", Proc. Rog. Soc A319, p 69 (1970).

[18] C. Zweben and B.W. Rosen, J. Mech. Phys. Solids, 18, p 189 (1970).

[19] J.A. Cornie, A.S. Argon and V. Gupta "Designing Interfaces in Inorganic Matrix Composites" MRS Bulletin, April 1991, pp 32-38.

[20] L. Molliex, Ph. D. Thesis, to be published.

[21] D. Jacques, Ph. D. Thesis "Transfert de charge entre fibre et matrice dans les composites résine : comportement en traction d'un composite monofilamentaire", INPL, Nancy, mai 1989.

[22] J.P. Favre, C. Laclau and A. Vassel, to be published at Int. Conf. on Interfaces, Cambridge, Sept. 1993.

[23] Y. Le Petitcorps, R. Pailler and R. Naslain, Composite Sci. and Tech., 35 (1989), pp 207-214.

[24] A. Vassel, M.C. Merienne, F. Pautonnier, L. Molliex and J.P. Favre, 6th World Conf. on Titanium, Les Editions de Physique (Paris, 1989) pp 919-923.

[25] L. Molliex, J.P. Favre and A. Vassel, 1990, Int. Conf. on Titanium Prop. and Appl., (TDA, Dayton, 1990), Vol. 1, pp 180-188.

[26] F. Brisset et al., "Colloque Matériaux, Science et Industrie", Paris, june 1992, pp. 146.

[27] B. Derby et al., "Interfacial Phenomema in Composite Materials'91", Proceedings of the 2nd International Conference, 17-19 September 1991 in Leuven (Belgium), Ed. by Ignaas Verpoest and Frank Jones, pp 208-211.

[28] C.J. Yang, S.M. Cheng and J.M. Yang Scripta Met. et Materiala, 24 (1990), pp 469-474.

[29] J.I. Eldridge and P.K. Brindley J. Mat. Sci. Letters, 8 (1989), pp 14651-1454.

[30] P.K. Brindley, S.L. Draper, J.I. Eldridge, M.V. Nathal and S.M. Arnold, Met. Trans. A., 23A (1992), pp 2527-2540.

[31] M.C. Watson and T.W. Clyne, Acta Met. 40.1 (1992), pp 141-148.

[32] G.A. Cooper and M.G. Bader, 5th Eur Conf. on Comp. Mat. (ECCMS), A.R. Bunsel Edts EACM, Bordeaux (1992), pp 877-882.

[33] J.A. Nairn, Mechanics of Materials, 13 (1992), pp 131-154.

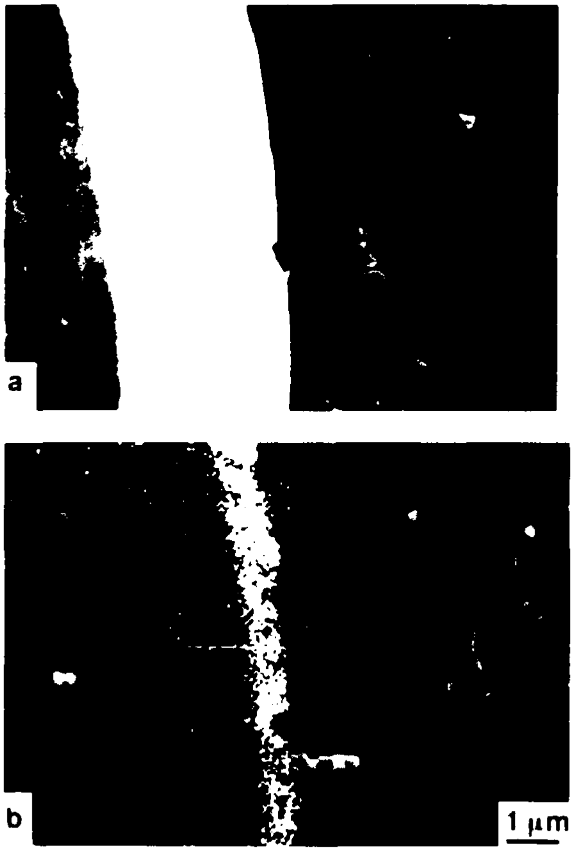

*Fig. 1 : Ionic images of SCS-6/Ti-14Al-19Nb interaction zone after one hour at 1050°C : a) C image, b) TiO *C correlation image.*

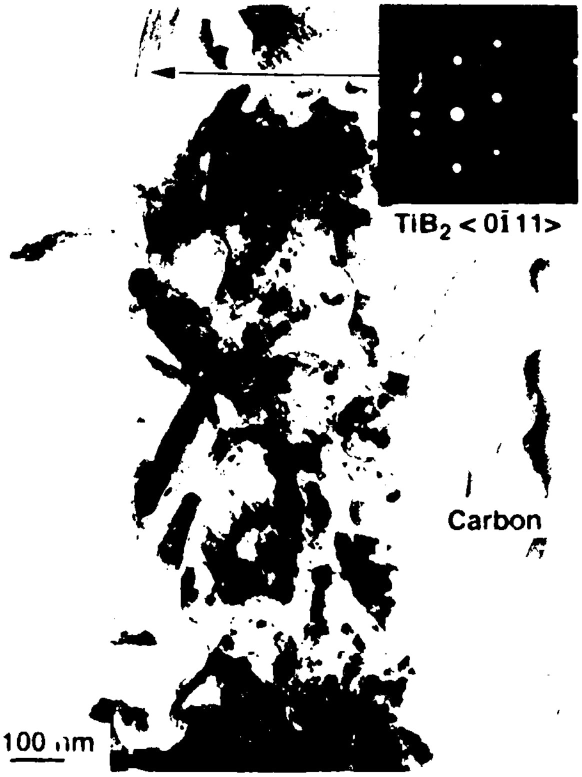

Fig. 2 : TEM micrograph of the SM 1240/Ti-14Al-19Nb interaction zone near the fibre after one hour at 1050°C. Note the presence of TiB_2 rod like precipitates.

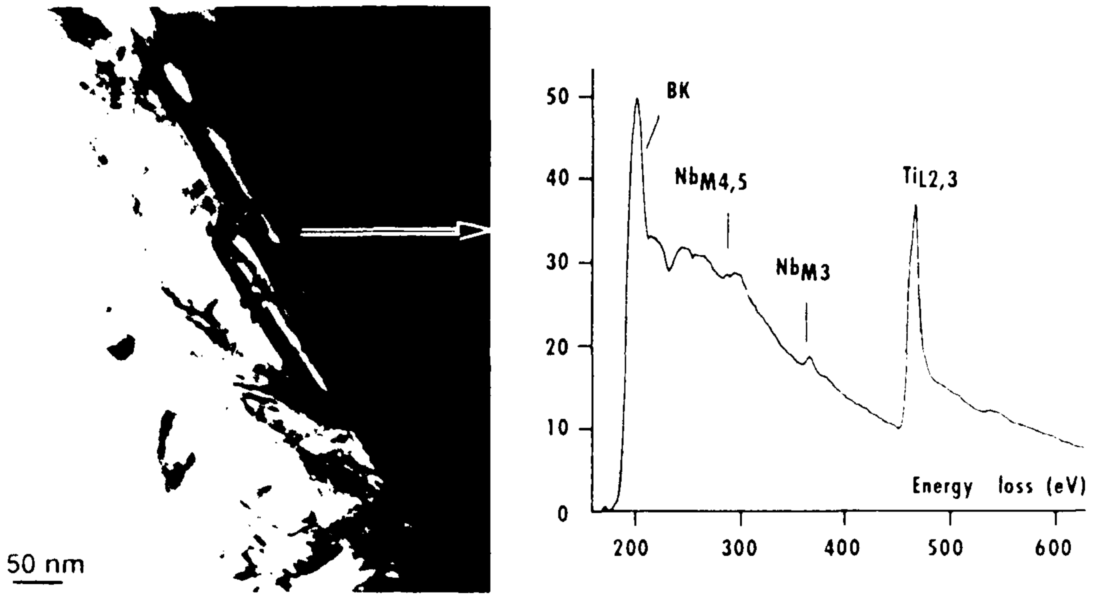

TEM image

EELS spectrum

Fig. 3 TEM micrograph of the SM 1240/Ti-14Al-19Nb [illegible] reaction zone near the matrix after [illegible] at 1050°C. [illegible] shown is an EELS spectrum of Ti-Nb-B [illegible]

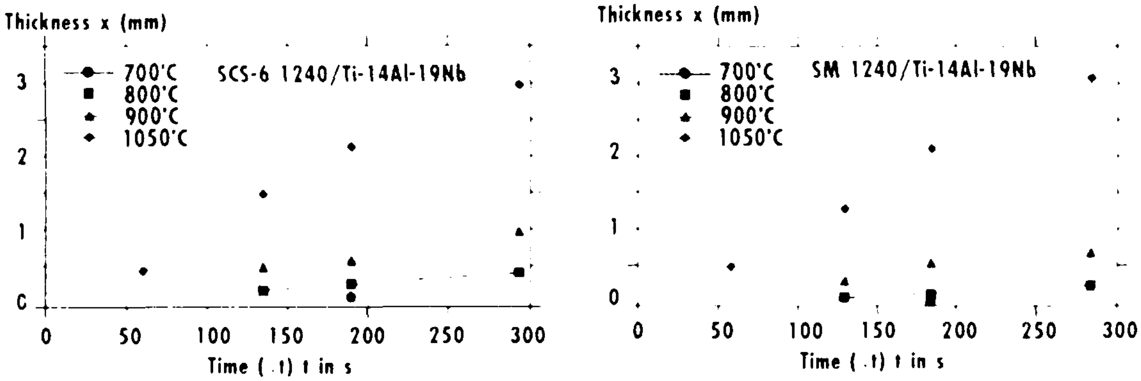

Fig. 4 The thickness of the reaction zone as a function of the square root of time (a) SCS-6/Ti-14Al-19Nb, (b) SM 1240/Ti-14Al-19Nb [2]

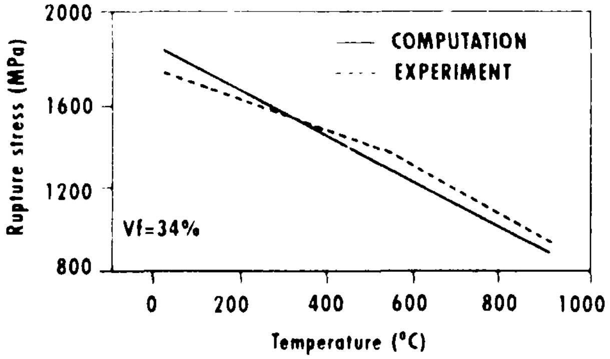

Fig. 5 R[illegible]

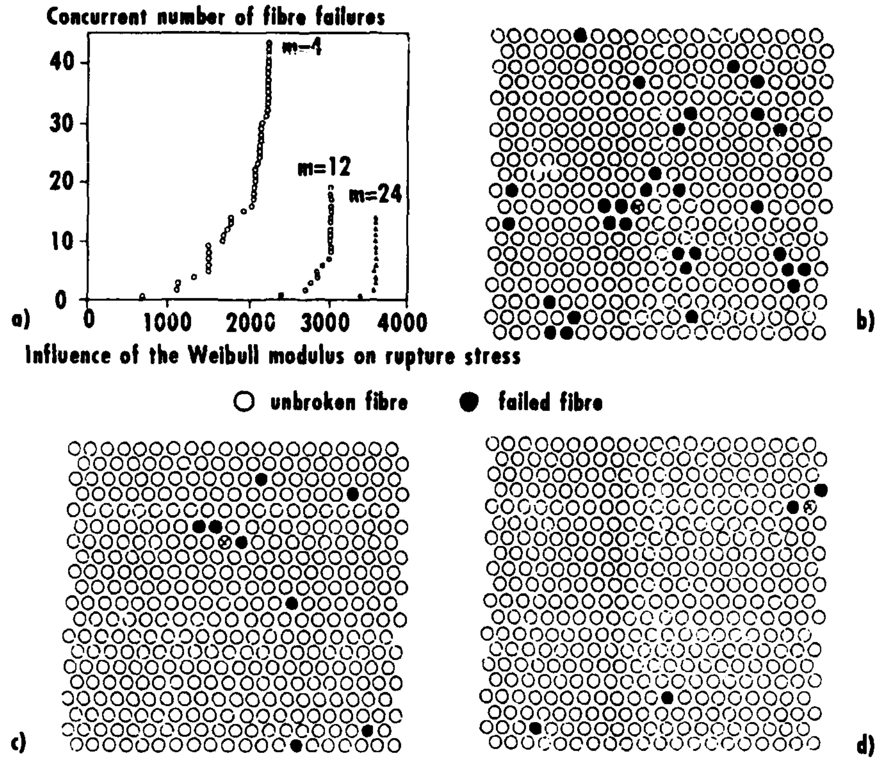

Fig. 6 : *Simulation of a 1D composite failure a) influence of the Weibull modulus on the composite rupture stress ; b), c), d) influence of the Weibull modulus on the number and the distribution of broken fibres prior to composite failure.*

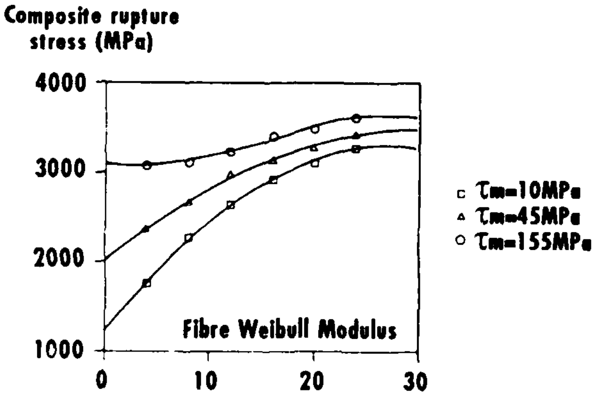

Fig. 7 : *Influence of the fibre-matrix load transfer shear stress on the composite rupture-stress for different Weibull modulus of the fibre.*

Fig. 8 : *Fibre-matrix interface shear-stress at a fibre broken-end.*

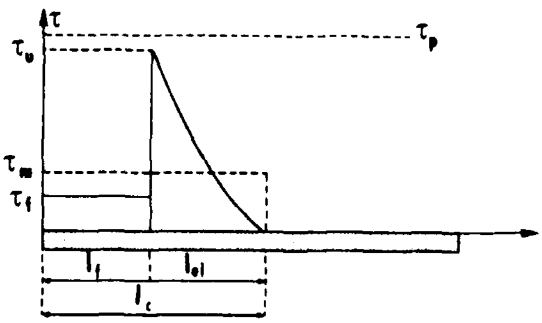

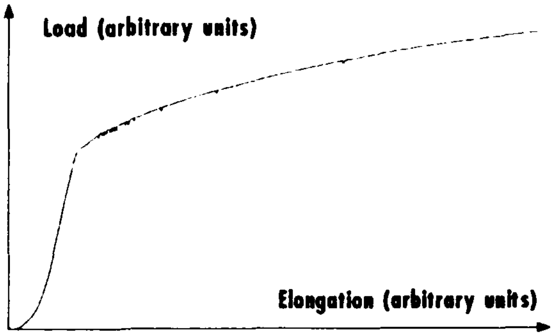

Fig. 9 : *Stress-strain curve for the tensile testing of a single fibre fragmentation specimen (SCS-6/Ti-14Al-21Nb composite, tested at 425°C).*

Fig. 10 : *Fibre-matrix load-transfer shear-stress as a function of temperature for both SCS-6/Ti-6Al-4V and SCS6/Ti-14Al-21Nb composites.*

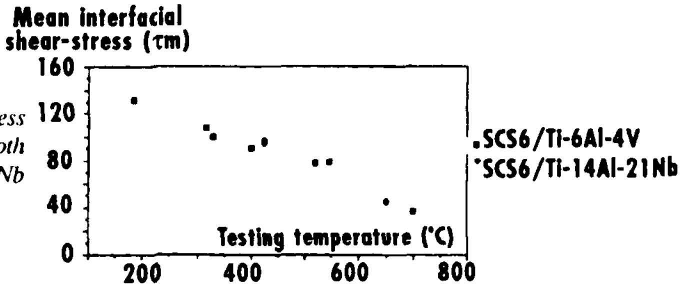

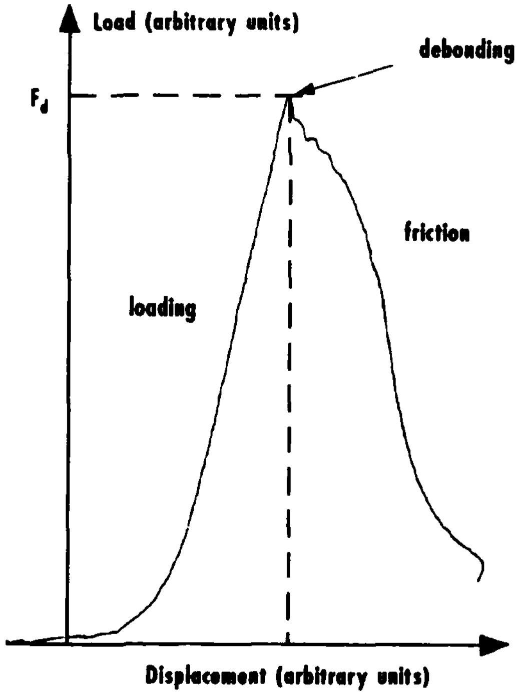

Fig. 11 : *A typical load-displacement curve (or load-time curve at a given indentor speed) for a SCS-6/Ti-6Al-4V composite.*

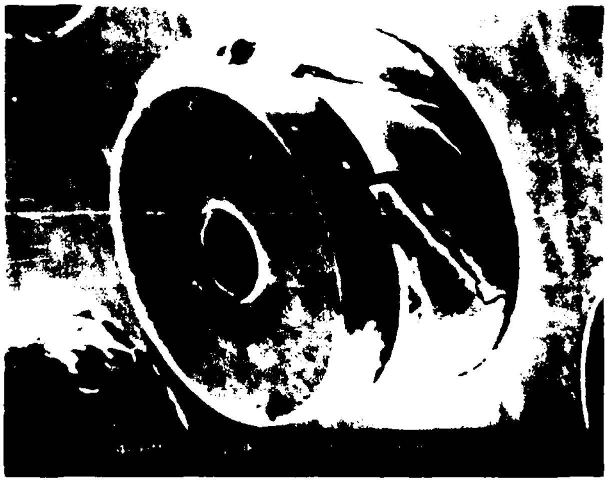

Fig. 12 : *SEM micrograph of a push-out fibre in a SCS-6/Ti-6Al-4V composite highlighting fibre-coating and coating-matrix debonding.*

***Table 1** : Q and k_0 values for various composites*

Q (kJ/mol)	$k_0.10^4$ (m/s$^{1/2}$)	Composite	Ref.
258	82	SiC/C/Ti-6Al-4V	[1]
207	6	SCS-6/Ti-6Al-4V	[13]
252	49	SCS-6/Ti-6Al-4V	[16]
206	1.3	SCS-6/Ti-14Al-19Nb	[12]
269	29	SCS-6/Ti-14Al-21Nb	[16]
221	5	SM 1240/Ti-14Al-19Nb	[12]

***Table 2** : Calculated reaction zone thickness after 1000 hours at 700°C*

Thickness (μm)	Composite	Ref.
2.1	SCS-6/Ti-6Al-4V	[16]
0.8	SCS-6/Ti-14Al-21Nb	[16]
0.7	SCS-6/Ti-14Al-19Nb	[12]
1.1	SM 1240/Ti-14Al-19Nb	[12]

***Table 3** : Push-out and fragnentation tests results on two composites SCS-6/Ti-6Al-4V and SCS-6/Titanium aluminide*

Composite	Processing conditions	Push-out tests		Fragmentation tests τ_m (MPa)	Ref.
		τ_d (MPa)	τ_f (MPa)		
SCS-6/Ti-6Al-4V	925°C/70 MPa/30 mn	156 ± 11	87.5	-	[28]
SCS-6/Ti-14Al-19Nb	"	115 ± 4	58.5 ± 2.3	-	
SCS-6/Ti-6Al-4V	895°C/80 MPa/30 mn	-	-	180	[238]
SCS-6/Ti-14Al-21Nb	-	119 ± 3	47.8 ± 2.5	-	[29]
SCS-6/Ti-14Al-21Nb	-	105 ± 11	57.5 ± 7	-	[30]
SCS-6/Ti-6Al-4V	as received	-	80	-	[31]
SCS-6/Ti-6Al-4V	as received	151 ± 6	-	192 ± 20	[22]
SCS-6/Ti-14Al-21Nb	925°C/40 MPa/30 mn			96 ± 15 *	
SCS-6/Ti-6Al-4V	as received	-	78	-	[32]

* *This test performed at 425°C, all others at room temperature*

Table 4 *: Characteristics of the matrix used for τ_m computation.*

Composite Characteristics	SCS-6/Ti-6Al-4V (20°C)	SCS-6/Ti-14Al-21Nb (425°C)
E_m (GPa)	115	87.3 [33]
ν_m	0.4	0.4
α_m (°C^{-1})	10.10^{-6}	10.10^{-6}

Table 5 *: Comparison of measured and computed values of the mean interfacial shear strengh τ_m*

Composite τ_m (MPa)	SCS-6/Ti-6Al-4V (20°C)	SCS-6/Ti-14Al-21Nb (425°C)
measured value	192 ± 20	96 ± 15
computed value	202	107

OXIDATION BEHAVIOR OF TITANIUM ALUMINIDE MATRIX MATERIALS

by

Jeffrey Cook
Eun U. Lee, William E. Frazier
Thu-Ha T. Mickle and **Jeffrey Waldman**
Naval Air Warfare Center, Aircraft Division
Warminster, PA 18974
United States

SUMMARY

Oxidation tests were performed on titanium aluminide alloys of three different compositions to determine their oxidation properties under isothermal and cyclic conditions. The TiAl/Ti_3Al alloy and the Al_3Ti exhibited roughly parabolic behavior between 900 and 1100°C, while the TiAl oxidized in a linear fashion. Rate constants and activation energies were calculated for each material, and based on these the rate-controlling processes and mechanisms were determined.

1. INTRODUCTION

Alloys based on the titanium rich portion of the aluminum-titanium phase diagram have been the subject of intense scientific and developmental work [1]. The benefits of the substantial engineering investment in alpha, super-alpha-two, and gamma titanium aluminides are now beginning to be realized: improvements have been made in ductility, toughness, elevated temperature strength, and deformation processing [2]. However, the exploration of the aluminum rich portion of the aluminum-titanium phase diagram is still in its infancy. The exploitation of titanium trialuminide based alloys as aircraft materials is of significant interest because of their high melting point (1350°C) [3], high elastic moduli (170 GPa), low density (3.35 gcm^{-3}), and elevated temperature strength [4,5]. In addition, their oxidation resistance is expected to be superior to that of the alpha-two and gamma titanium aluminides.

The oxidation of titanium aluminides at high temperatures is dominated by reaction kinetics rather than equilibrium thermodynamics. This is because the activity of oxygen in air is fixed, the supply of oxygen is virtually unlimited, and metal oxides are typically more thermodynamically stable than metals. Oxidation kinetics are related to a large number of variables, including diffusion rates, scale chemistry and morphology, and crystal structure.

The rate of oxidation is typically classified as logarithmic, linear, or parabolic [6,7]. Logarithmic oxidation is generally observed at temperatures below 400°C. Oxidation is initially very rapid but drops off to negligibly small values. Al_2O_3 growth on aluminum at room temperature is an example of logarithmic oxidation. Linear oxidation behavior is constant with time and thus independent of the quantity of gas or metal previously consumed in the reaction. Linear oxidation is dominated by surface or phase boundary processes. Parabolic oxidation is typically observed at high temperatures and indicates that a thermal diffusion process is rate-determining.

Mass transport in polycrystalline materials may be dominated by either bulk diffusion or by diffusion along grain boundaries and other short-circuit paths of low resistance. The activation energy for grain boundary diffusion is typically 0.5 to 0.67 that for lattice diffusion, and $D_{gb}/D_l \cong 10^5$. However, short-circuit diffusion only becomes significant at homologous temperatures below $0.6T_{mp}$ [7]. Application of this rule-of-thumb to polycrystalline Al_2O_3 and TiO_2 scales suggests that short-circuit mechanisms may become significant below 1120°C and 920°C respectively.

Ti_3Al, TiAl: A number of studies have been conducted to determine the oxidation properties of titanium aluminides[8-21]. Their oxidation behavior has been shown to be composition dependent. Protective Al_2O_3 oxide scales are reported to form only when the Al content of TiAl exceeds 57% [19]. Mckee and Huang [11] also examined the cyclic oxidation behavior of Ti-Al-X-Y alloys at temperatures between 850-900°C. Oxidation resistance was found to increase with aluminum content and with the additions of Nb and W, as well as with Cr additions of

Presented at an AGARD Meeting on 'Characterisation of Fibre Reinforced Titanium Matrix Composites', September 1993.

greater than 8%. This oxidation response was explained in terms of reduced Ti activity.

Al_3Ti: The oxidation response of cast Al_3Ti has been examined by Smialek and Humphrey [15]. They observed parabolic oxidation, controlled by α-Al_2O_3 formation, at temperatures greater than 1000°C. Anomalously high oxidation rates were observed at short times at temperatures below 1000°C. This was explained in terms of the internal oxidation of aluminum which had partitioned during solidification. The use of titanium trialuminide coatings for gamma and alpha-two titanium aluminides was studied by Subrahmanyam [13,14]. Al_3Ti coatings on Ti-14Al-24Nb decreased cyclic oxidation weight gains by at least a factor of 10. Work by Umakoshi, et al [12], and Hirukawa, et al, [18] showed that the oxidation rate of bulk Al_3Ti is lower than that of bulk TiAl by at least a factor of 30 at 1000°C.

The greater oxidation resistance of Al_3Ti compared to the lower aluminides is due in part to the tendency for aluminum to oxidize internally in the lower aluminides.[21] Wagner has theorized that the aluminum content of the aluminide must exceed a certain critical value, N_{Al}^{crit}, in order to prevent this internal oxidation [20,21,22]. Perkins, et al, [21] have found this value to be about 59% for TiAl.

The excellent oxidation resistance of Al_3Ti is also attributable in part to the nature of the TiO_2/Al_2O_3 oxide layer which forms. Al_2O_3 forms a dense, protective layer, which serves as a diffusion barrier against further oxidation. TiO_2, on the other hand, forms a porous layer of crystals which is only partially protective, and tends to spall. TiO_2 also has a higher diffusivity to oxygen than does Al_2O_3.

2. EXPERIMENTAL PROCEDURE

2.1. Materials and Materials Processing

Three different alloys were examined in this study, covering a range of compositions (see the Al-Ti phase diagram, Figure 1). These were a two-phase alloy containing Ti_3Al and TiAl, single-phase γ-TiAl, and Al_3Ti which ideally was also single phase. The compositions of these alloys are summarized in Table 1. The two-phase $TiAl/Ti_3Al$ material was obtained from Martin Marietta Laboratories, Baltimore, MD. Oxidation specimens were cut using a water-cooled diamond wafering saw. The preparation of γ-TiAl and Al_3Ti was accomplished at the NAWC using a Marko Materials Model 2T Melt Spinner. Castings, weighing 0.25 to 0.35 kg, were prepared in a water cooled copper hearth by arc melting. Oxidation specimens designated "as cast" were cut from these ingots by wire EDM. "HIPed" specimens were cut from arc-cast ingots after HIP consolidation.

2.2. Oxidation Tests

1) $TiAl/Ti_3Al$. Oxidation tests were conducted in air under isothermal conditions, at temperatures ranging from 400° to 1500°C and test times from 4 to 40 hours. Each specimen was weighed before and after exposure in order to determine the weight change due to oxidation. Surface oxide phases were identified using standard x-ray diffraction techniques.

2) γ-TiAl and Al_3Ti. Cyclic oxidation tests were performed on these alloys in order to determine the effects of rapid thermal cycling on the oxidation properties. Cycles consisted of a rapid heat-up (500°C/min) to temperature, a 55 minute hold at temperature, and a rapid cool-down outside the furnace for 5 minutes, and each test consisted of 144 or more cycles. An ATS 3310 furnace was used for the tests; an apparatus designed and constructed by the authors was employed to move the specimen in and out of the furnace. Oxidation tests were performed on both alloys in both the as-cast and the HIPed conditions at 900°C and 1100°C in air. Weight gains were measured at increasing intervals using a Sartorius microbalance having a precision of ±0.01 mg.

Isothermal oxidation tests were performed on these two alloys to determine their oxidation kinetics at constant temperature in air. Tests were performed on both the as-cast and the HIPed materials at 900°C, 1000°C, and 1100°C. Isothermal tests were conducted in a CM Rapid Temp furnace. Specimen weight was measured to ±0.01 mg every 24 hours for a period of 144 to 196 hours.

Compositional changes in the alloys and oxidation products were identified using scanning electron microscopy (SEM) and x-ray diffraction. A Rigaku DMAX-B unit with a $\theta/2\theta$ goniometer and an operating voltage of

40 kV was used for x-ray diffraction analysis. For the SEM study, an Amray 1000B was used at an accelerating voltage of 15-20 kV. The SEM was equipped with a Kevex Model 8000 EDS with an ultra-thin aluminum/parylene window.

3. RESULTS

3.1. TiAl/Ti_3Al

Above 1000°C, oxide products formed a thick white scale that tended to spall. Considerable internal cracking was also evident after exposure above 1000°C. This cracking occurred along the TiAl/Ti_3Al phase boundaries. Weight gain at all temperatures is approximately parabolic.

3.2. γ-TiAl

Cyclic: The cyclic oxidation weight gains for this alloy are shown in Figure 2a. Weight gain is linear at both 900° and 1100°C. At 900°C the weight gain is about 0.3 $mg/cm^2/hr$, while that at 1100°C is about 2.6 $mg/cm^2/hr$. At both temperatures, large volumes of yellow and white oxides were produced, which flaked off during each cool-down cycle.

Isothermal: Oxidation weight gain of this alloy under isothermal conditions is shown in Figure 2b. At both 900° and 1100°C, the weight gain appears to be parabolic, in contrast to the alloy's linear oxidation under cyclic conditions. The oxide product is thick, yellow, and adherent, and essentially free of visible cracks. Some cracking and spalling did occur, however, upon cooling to ambient temperature.

3.3. Al_3Ti

Cyclic: Cyclic weight gains for this alloy are shown in Figure 3a. At 1100°C, weight gain is initially parabolic, but overall is in between linear and parabolic. Average weight gain over 206 hours is 0.04 $mg/cm^2/hr$, or about 1/60 that for TiAl. At both temperatures, the oxide product is pale gray and powdery, and non-uniformly distributed.

Isothermal: Isothermal weight gains for this alloy are shown in Figure 3b. As in cyclic oxidation, weight gains are very low, averaging about 0.06 $mg/cm^2/hr$ over 168 hours, and are between linear and parabolic. The appearance of the oxide product is similar to that in the cyclic tests.

3.4. Effects of HIPing on Oxidation: The purpose of HIPing the cast γ-TiAl and Al_3Ti alloys was to reduce the level of porosity and micro-cracking present, which are believed to promote enhanced oxidation. HIPing was therefore expected to decrease oxidation weight gains as compared to the as-cast condition. Although in general HIPing appeared to reduce oxidation rate constants, the as-cast specimens revealed a wide variation in surface quality and porosity, and this appears to have affected the oxidation properties much more than the changes produced by subsequent HIPing. The effectiveness of HIPing to reduce surface oxidation is therefore unclear.

4. DISCUSSION OF RESULTS

In analyzing the oxidation properties of these materials, oxidation is assumed to proceed according to the equation:

$$W^n = kt + C \qquad (1)$$

where W is the weight gain per unit area after time t, and k is the rate constant. The units for k are $(mg/cm^2)^n/sec$. The n-exponent depends upon the mechanism which controls the oxidation rate; n=1 represents linear or interface-controlled oxidation, n=2 is parabolic or diffusion-limited oxidation, and 3 represents some form of exponential behavior, such as oxidation controlled by grain-boundary diffusion.

The oxidation of these materials was assumed to follow an Arrhenius-type temperature dependence, wherein

$$k = A \exp(-Q/RT) \qquad (2)$$

where A is a constant and Q is the activation energy for the rate-controlling process. By plotting ln(k) as a function of 1/T , a straight line whose slope is (-Q/R) is obtained.

4.1. TiAl/Ti_3Al

The oxide layer formed at 1000°C and above was found to consist of a thin inner layer of $TiO_2 + Al_2O_3$, and an outer layer of $TiO_2 + Al_2TiO_5$. This was not quite in agreement with the findings of Choudhury [9] and Mendiratta [10], who detected only TiO_2 in the outer layer. At 1100°C and higher, internal oxidation occurred. Aluminum oxidized selectively within the TiAl phase, forming parallel plates of Al_2O_3, while titanium oxidized within the Ti_3Al phase to form TiO_2 in a fine structure resembling fingerprints.

Parabolic rate constants (k_p) were calculated from weight gain per unit time at each temperature. Figure 4 is an Arrhenius plot showing k_p as a function of 1/T. From the slope of the resulting line, the activation energy for oxidation was found to be about 63 kcal/mole, which is approximately the same as that for bulk diffusion of oxygen through TiO_2. The activation energies for all three alloys tested are listed in Table 4, along with the likely rate-controlling mechanism.

4.2. γ-TiAl

Experiments by Meier, Perkins, et al [20] indicate that Al-Ti compounds containing less than 59 atomic % (45 weight percent) aluminum do not form a continuous Al_2O_3 scale, but rather a mixed Al_2O_3/TiO_2 layer under an initial layer of almost pure TiO_2. This was found to be the case in these experiments on near-stoichiometric TiAl, as well.

Cyclic Oxidation: As can be seen from Figure 2a, the cyclic oxidation behavior of TiAl is linear. During the hot portion of the cycle, the oxide formed is more or less adherent. However, upon cooling, it becomes detached and peels away due to the thermal expansion coefficient mismatch between the oxide and the TiAl, exposing the underlying TiAl to the next hot cycle. The SEM image in Figure 5 suggests that oxidation occurs through the selective oxidation of aluminum within the TiAl. This alumina formation depletes the surrounding TiAl of aluminum, eventually raising the activity of titanium high enough that the formation of TiO_2 becomes thermodynamically favorable.

Table 2 shows the calculated linear rate constants for the cyclic specimens at 900° and 1100°C. Although tests were conducted at only two temperatures, the ln(k) versus 1/T plot in Figure 6 suggests an activation energy of about 34 cal/mol. This is about 57% of the activation energy for bulk diffusion of oxygen through TiO_2, and also very close to the activation energy for grain boundary diffusion in Al_2O_3 (32 kcal/mol), suggesting that short-circuit diffusion may control oxide formation during the hot portion of the cycle. Parabolic behavior is not observed, however, due to the complete spallation of the oxide during each cooldown cycle.

Isothermal Oxidation: The isothermal oxidation behavior of TiAl differs from the cyclic behavior in that the oxide layer does not peel away, because no thermal cycling occurs. Therefore the oxide remains essentially adherent, and continues to grow in thickness as long as the specimen remains at temperature. The outer oxide layer is shown in the SEM image in Figure 7 to consist of islands of Al_2O_3 in a porous matrix of TiO_2. The outermost layer of the oxide is predominantly TiO_2, while thin layers within the oxide are either alumina-rich or titania-rich. These regions are believed to correspond to transient oxidation which occurred during the heat-up and cool-down cycles when the specimen was removed from the furnace for weighing.

Even with the adherent oxide, there is evidence of internal oxidation of aluminum at all test temperatures. At 900° and 1000°C, the internally oxidized zone consists of a two-phase outer region about 10 μm thick, consisting of plates of Al_2O_3 in aluminum-depleted TiAl, and a single-phase region underneath which was also found to be aluminum-deficient compared to the TiAl in unaffected areas. This lower layer may be Ti_3Al or simply titanium-rich TiAl. At 1100°C, the internal oxidation zone consists of a two-phase outer layer containing Al_2O_3 and a severely Al-depleted phase, and an inner two-phase layer in which the aluminum is depleted to a lesser degree (see Figure 5). The overall thickness of the zone is nearly 100 μm. The Al_2O_3 in the outer layer appears to form on preferred crystallographic planes within each TiAl grain.

It appears that the oxidation of TiAl begins with a brief initial transient period in which TiO_2 is the major product. Thereafter, oxidation proceeds via internal oxidation of aluminum, forming plates of Al_2O_3 in an increasingly aluminum-poor matrix. Meanwhile, this matrix is consumed from the outer surface inward; this explains the observed oxide morphology. The rate of titanium consumption is controlled by the rate of Al_2O_3 formation, in that the formation of alumina eventually raises the activity of titanium in the TiAl to the point where TiO_2 formation becomes favorable. The exponential behavior observed over a range of test times, however, indicates that the overall oxidation rate is controlled not by Al_2O_3 formation, but by the inward diffusion of oxygen through the oxide. This is supported by Figure 6, which shows the activation energy for oxidation to be about 28.8 kcal/mol (just under half the activation energy for bulk diffusion of oxygen through TiO_2) based on linear kinetics, or 57 kcal/mol based on parabolic kinetics. The rate of isothermal oxidation therefore appears to be controlled by some combination of short-circuit and bulk diffusion through TiO_2, with the latter expected to be dominant above 920°C. Note that the true behavior is roughly parabolic, but measuring the weight gains at successive intervals required the use of multiple specimens, so parabolic rate constants could only be estimated by assuming C in Equation 1 to be zero. Both linear and parabolic constants are shown in Table 2.

4.3. Al_3Ti

Al_3Ti has been noted by previous researchers for its ability to form a continuous Al_2O_3 coating, which acts as a barrier to the diffusion of oxygen and aluminum ions. Oxidation weight gains are therefore typically assumed to follow the parabolic form of Equation 1. The oxidation behavior of Al_3Ti appears to be strongly influenced by both its chemistry and the surface quality of the specimens. Thermodynamically, Al_2O_3 is expected to form preferentially to TiO_2; however, since Al_3Ti is ideally a line compound, the preferential formation of Al_2O_3 results in the formation of lower aluminides which are less oxidation resistant than Al_3Ti. The oxidation of Al_3Ti was therefore expected to proceed according to the reaction:

$$4\ Al_3Ti + 13\ O_2 \Rightarrow 6\ Al_2O_3 + 4\ TiO_2 \quad (3)$$

SEM/EDS examination suggests that TiO_2 is not present in significant amounts in the Al_2O_3 coating, and therefore may not contribute to diffusion processes. The lack of TiO_2 in the oxide may be a result of preferential Al_2O_3 formation, due to the reduced oxygen partial pressure at the oxidizing surface, once an Al_2O_3 layer has been established.

Cyclic Oxidation: When the cyclic oxidation data in Figure 3a is plotted as weight gain per unit area versus $(\text{time})^{1/2}$, the slope of a straight line drawn through the data points is then equal to the parabolic rate constant k_p. It was found that the slope is not constant in some cases, but rather decreases with increasing time. This suggests that either the rate constant decreases with time or the n-exponent in Equation 1 is actually greater than 2. The latter possibility is discussed in detail in Reference [23]. For these calculations, the former case is assumed, and k_p values are calculated based on the longer test times. These values are shown in Table 3. For cyclic oxidation, the activation energy Q was found to be about 35 kcal/mol (Figure 8), which is very close to the activation energy for short-circuit (grain boundary) diffusion of oxygen in Al_2O_3 or TiO_2. However, by differentiating Equation 1 with respect to time and converting the rate of weight gain into an inward flux of oxygen, it can be shown that the observed oxidation rate is much too high to be explained by even grain boundary diffusion. This calculation appears in a previous paper by the authors, and can be found in Reference [23]. It may be that the cyclic oxidation rate of Al_3Ti is controlled by the inward diffusion of molecular oxygen through cracks in the oxide layer, rather than lattice or short-circuit diffusion.

Isothermal Oxidation: Parabolic rate constants were determined for these tests in the same manner as for the cyclic tests. These k_p values are shown in Table 3. The rate constants for isothermal oxidation are slightly lower at 900°C than in cyclic oxidation, but somewhat higher at 1100°C. There is also a knee in the isothermal data at 1000°C, as can be seen in Figure 8, indicating a possible change in transport mechanism around that temperature. Below 1000°C, the activation energy is close to the value expected for grain boundary diffusion in Al_2O_3, while above 1000°C it is close to that for bulk diffusion in alumina. The observed oxidation rates, however, are still much higher than those predicted for diffusion control.

A partial explanation for the unusually high oxidation rates and rate constants in this material was found by comparing the oxide thickness inferred from weight gain with the actual thickness as measured from SEM images. The weight gain after 168 hours at 1100°C suggests that the thickness of the oxide should be 37 μm. However, micrographs clearly show that the outer oxide is only 4 μm thick. The remaining 90% of the weight gain was found to be the result of the internal oxidation of a second phase, which was identified previously as α-Al, and which constitutes 2.1 volume percent of the material. [24] If it is assumed that this phase oxidizes completely, the remainder of the observed weight gain is just enough to form a surface layer 3.7 μm thick. Similarly, the oxide coating after 24 hours at 1000°C was about 2μm thick, suggesting that about 22% of the second phase has oxidized.

Despite the large amount of internal second-phase oxidation, however, the oxidation rates are still much too high to be controlled by a bulk diffusion mechanism. If the assumption of parabolic behavior is retained, the discrepancy might again be due to the imperfect structure of the oxide, as was suggested previously.

SEM micrographs show that the Al_3Ti specimens contained considerable interconnected porosity, with a very rough and uneven surface. The latter would tend to hinder the formation of a continuous, protective oxide layer, while the former would allow molecular oxygen to get into the specimen, exposing to oxidation a total surface area which is probably much greater than the "ideal" surface area calculated from the dimensions of the specimen. In addition, the porosity exposes the 2.1% α Al phase to rapid internal oxidation, particularly at the higher temperatures. The total weight gain is therefore the sum of the internal weight gain and external scale formation, with the internal oxidation dominating until either the aluminum second phase is consumed or a truly protective external scale can form.

5. CONCLUSIONS

1. All of the alloys examined form a mixed oxide scale consisting primarily of Al_2O_3 and TiO_2.

2. Under identical conditions, TiAl oxidizes at a rate two orders of magnitude faster than Al_3Ti.

3. Partitioning of excess aluminum during solidification of Al_3Ti resulted in internal oxidation of the aluminum second phase. This internal oxidation accounted for 90% of the total weight gain.

4. The oxidation of TiAl/Ti_3Al is roughly parabolic at all temperatures, while the oxidation behavior of TiAl is linear. The oxidation behavior of Al_3Ti was fit to parabolic kinetic equations; however, the n exponents were generally greater than 2.

5. The oxidation kinetics of Al_3Ti are controlled by the short circuit diffusion of molecular oxygen through cracks and imperfections in the oxide scale.

ACKNOWLEDGMENTS

The authors are very grateful to Mrs. Mary E. Donnellan for her technical contributions to this work. Technical discourse with Mr. John B. Boodey was also very valuable. The financial support of ONR Code 11 is gratefully acknowledged as is the guidance of the program's Technical Monitor, Dr. Steven Fishman.

REFERENCES

1. E.L. Hall and Shyh-Chin Huang, "Microstructures of Rapidly-Solidified Binary TiAl Alloys, Acta Metallurgica et Materialia, Vol.38 No.4 (1990), 539-549.

2. J.D. Destefani, "Advances in Intermetallics," Advanced Materials & Processes 2 (1989), 37-41.

3. Binary Alloy Phase Diagrams, vol I, T.B. Massalski et al. editors, ASM, Materials Park, OH (1986), 175.

4. K.S. Kumar, "Review: Ternary Intermetallics in Aluminum-Refractory Metal-X(X= V, Cr, Mn, Fe, Co, Ni, Cu, Zn) Systems," Report MML JL 89-46, Martin Marietta Laboratories, Baltimore, MD (April 1989).

5. M. Yamaguchi, Y. Shirai, and Y. Umakaoshi, "Deformation Behavior of Single and Polycrystal Al_3Ti and $Al_3Ti$with Ternary Alloying Additions," Dispersion Strengthened Aluminum Alloys, ed. Y-W. Kim and W.M. Griffith TMS, Warrendale, PA, (1988), 721-740.

6. O. Kuaschewski and B.E. Hopkins, Oxidation of Metals and Alloys. Butterworths, London, 1953.

7. Per Kofstad, High-Temperature Oxidation of Metals. John Wiley, New York, 1966.

8. E.W. Lee and J. Waldman, "Oxidation of Two-Phase (TiAl + Ti_3Al) Alloy," Scripta Metallurgica 22 (1988) 1389-1394.

9. N.S. Choudhury, H.C. Graham, and J.W. Hinze, "Oxidation Behavior of Titanium Aluminides," in Proceedings of the Symposium on Properties of High Temperature Alloys, the Electrochemical Society, Princeton, NJ (March 1977), 668.

10. M.G. Mendiratta and N.S. Choudhury, "Properties and Microstructures of High-Temperature Materials," Air Force Materials Laboratory Technical Report AFML-TR-78-112 (August 1978).

11. D.W. Mckee and S.C. Huang, "The Oxidation Behavior of Gamma-Titanium Aluminide Alloys Under Thermal Cycling Conditions," Corrosion Science 33(12) (1992), 1899-1914.

12. Y. Umakoshi et al., "Oxidation Resistance of Intermetallic Compounds Al3Ti and TiAl," Journal of Material Science 24 (1989), 1599-1603.

13. J. Subrahmanyam, "Cyclic Oxidation of Aluminized Ti-14Al-24Nb Alloy". Journal of Materials Science 23 (1988), 1906-1910.

14. J. Subrahmanyam and J. Annapurna, "High Temperature Cyclic Oxidation of Aluminide Layers on Titanium". Oxidation of Metals 26(3/4) (1986), 275-285.

15. J.L. Smialek and D.L. Humphrey, "Oxidation Kinetics of Cast TiAl3," Scripta Metallurgica et Materialia 26 (1992), 1763-1768.

16. E.U. Lee and J. Waldman, Scripta Metallurgica et Materialia 22 (1988), 1389.

17. R.A. Perkins, K.T. Chiang, and G.H. Meier, "Formation of Alumina on Ti-Al Alloys". Scripta MET 21 (1987), 1505-1510.

18. K. Hirukawa, H. Mabuchi, and Y. Nakayama, "Oxidation Behavior of TiAl3-Based Alloys with the L12 Structure". Scripta MET 25 (1991), 1211-1216.

19. G.H. Meier, "Fundamentals of the Oxidation of High-Temperature Intermetallics". In Oxidation of High-Temperature Intermetallics, Ed. T. Grobstein and J. Doychak, TMS (1988), 1-16.

20. G.H. Meier, D. Appalonia, R.A. Perkins, and K.T. Chiang, "Oxidation of Ti-Base Alloys". In Oxidation of High-Temperature Intermetallics, Ed. T. Grobstein and J. Doychak, TMS (1988), 185-193.

21. R.A. Perkins and K.T. Chiang, "Formation of Alumina on Niobium and Titanium Alloys". In Oxidation of High-Temperature Intermetallics, Ed. T. Grobstein and J. Doychak, TMS (1988), 157-169.

22. M.G. Hebsur, et al, "Influence of Alloying Elements on the Oxidation Behavior of NbAl3". In Oxidation of High-Temperature Intermetallics, Ed. T. Grobstein and J. Doychak, TMS (1988), 171-183.

23. W.E. Frazier, J. Cook, and T. Mickle, "Evaluation of the Oxidation Response and Fiber-Matrix Compatibility in Aluminum-Rich Intermetallic Composites". NAWCADWAR Report No. 93083-60 (November 1993).

24. W.E. Frazier, J.E. Benci, and J.W. Zanter, "Microstructural Evaluation of As-Cast and Melt-Spun Al3Ti and Al3Ti Plus Copper". In Low Density, High Temperature Powder Metallurgy Alloys, Ed. W.E. Frazier and M.J. Koczak, TMS (1991), 49-69.

TABLE 1. Alloy Compositions (Wt.%)

Alloy	Aluminum	Titanium
$TiAl+Ti_3Al$	32.4	66.8
γ-TiAl	36	64
Al_3Ti	62.8	37.2

TABLE 2. γ-TiAl Oxidation Kinetics

			Rate Constant, k	
	Temp. °C	Condition	Linear	Parabolic
			(mg/cm^2hr)	(mg^2/cm^4hr)
Cyclic	900	As Cast	0.328	----
	1100	As Cast	2.674	----
Isothermal	900	As Cast	0.795*	16.5
		HIPed	0.852*	15.8
	1000	As Cast	2.225*	119
		HIPed	1.783*	76
	1100	As Cast	4.961*	625
		HIPed	5.032*	678

* - Based upon the total weight gain after 24 hours

TABLE 3. Al3Ti Parabolic Oxidation Parameters

	Temp. °C	Condition	Rate Constant
			kp (mg^2/cm^4hr)
Cyclic	900	As Cast	0.0052
	1100	As Cast	0.3324
		HIPed	0.0460
Isothermal	900	As Cast	0.0031
		HIPed	0.0014
	1000	As Cast	0.0095
		HIPed	0.0086
	1100	As Cast	0.8260
		HIPed	0.2460

TABLE 4. Summary of Activation Energies (Q) and Rate-Controlling Mechanisms

Alloy	Q (kcal/mole)	Rate-Controlling Mechanism
$Ti_3Al + TiAl$	63	Bulk diffusion thru TiO_2
γ-TiAl-Isothermal	59	Bulk diffusion thru TiO_2
γ-TiAl-Cyclic	34	Short circuit diffusion thru TiO_2 or TiAl
Al_3Ti-Isothermal	34-50	S.C. diffusion thru oxide (< 1000°C)
	100	Bulk diffusion thru Al_2O_3 (> 1000°C)
Al_3Ti-Cyclic	35	S.C. diffusion thru oxide

(Oxygen is assumed to be the diffusing species)

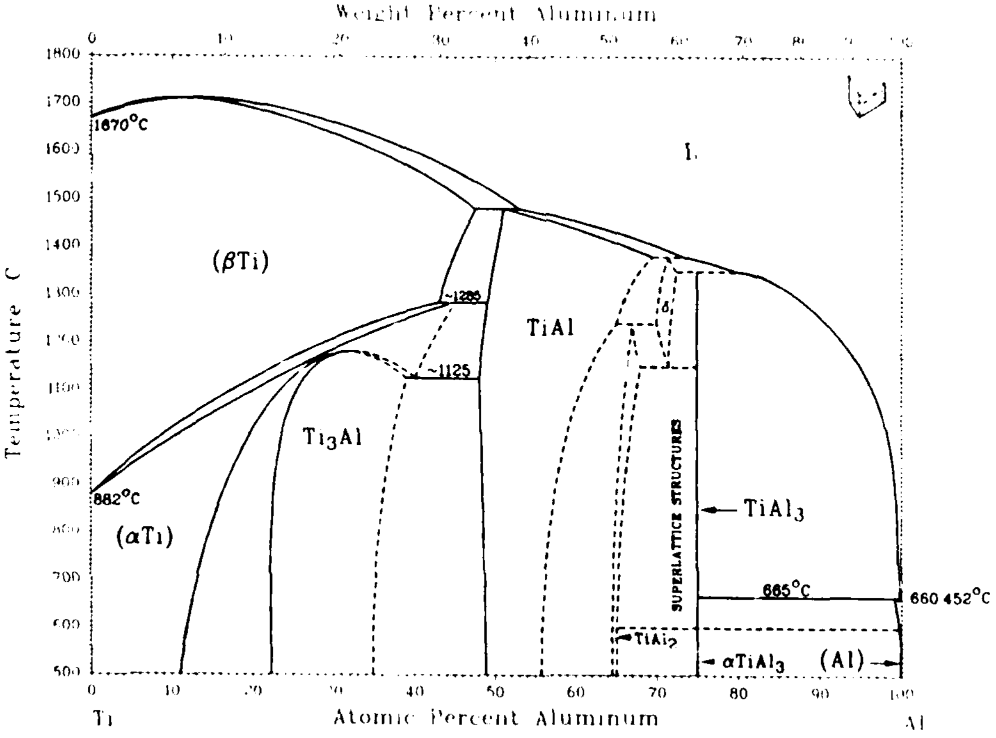

Figure 1. The Aluminum-Titanium Phase Diagram (from Ref. 3)

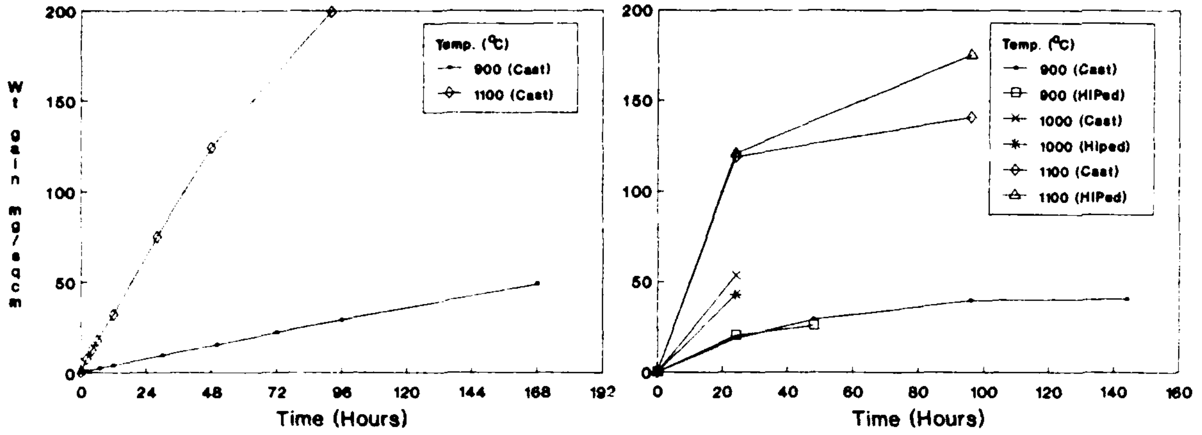

(a) (b)

Figure 2. Oxidation Weight Gains for γ-TiAl.
(a) Cyclic (b) Isothermal

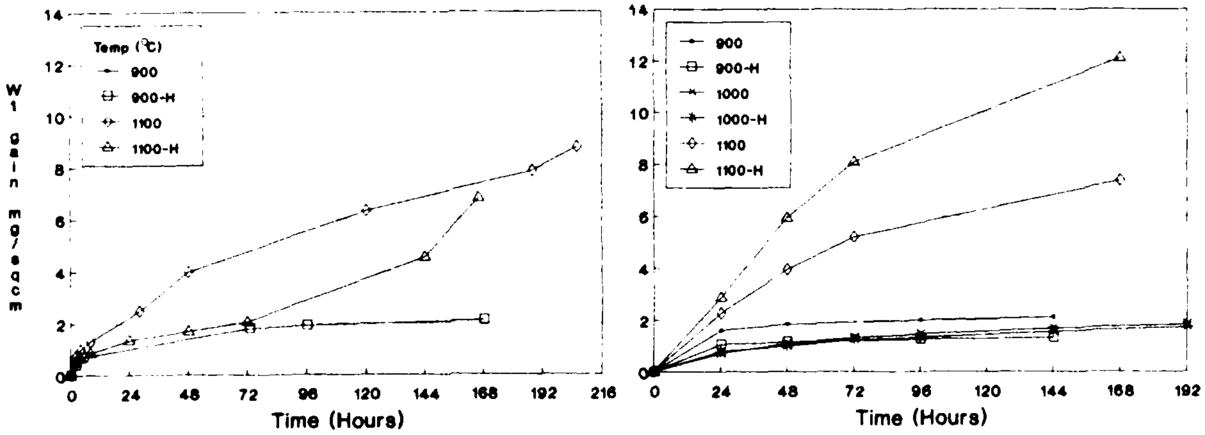

(a) (b)

Figure 3. Oxidation Weight Gains for Al_3Ti.
(a) Cyclic (b) Isothermal

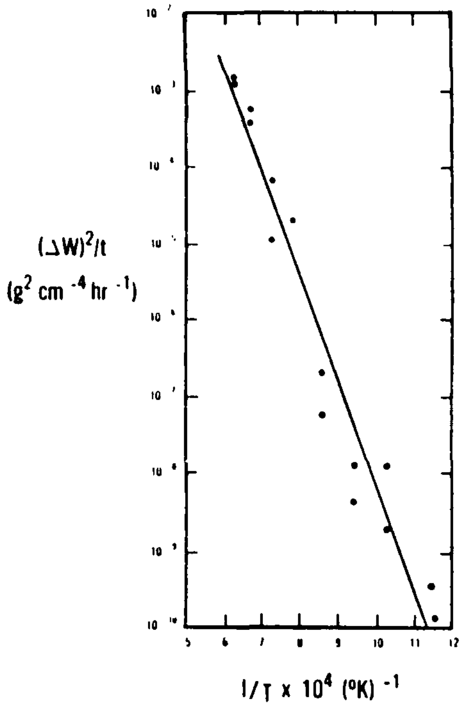

Figure 4. Oxidation Kinetics - TiAl/Ti3Al.

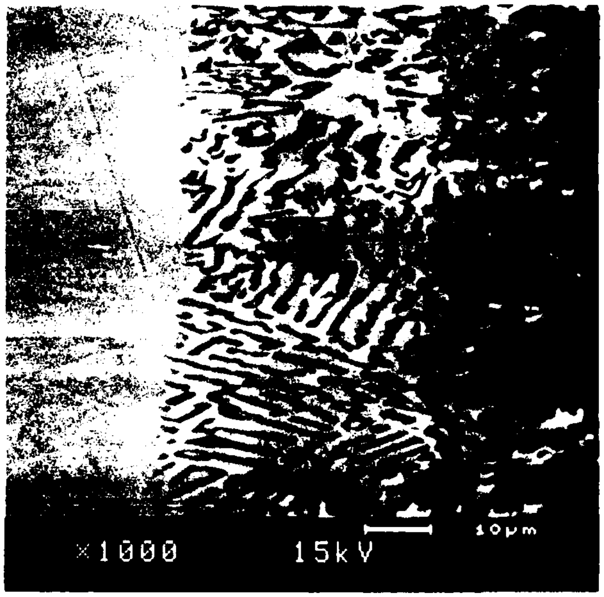

Figure 5. SEM Image Showing Internal Alumina Formation in γ-TiAl.

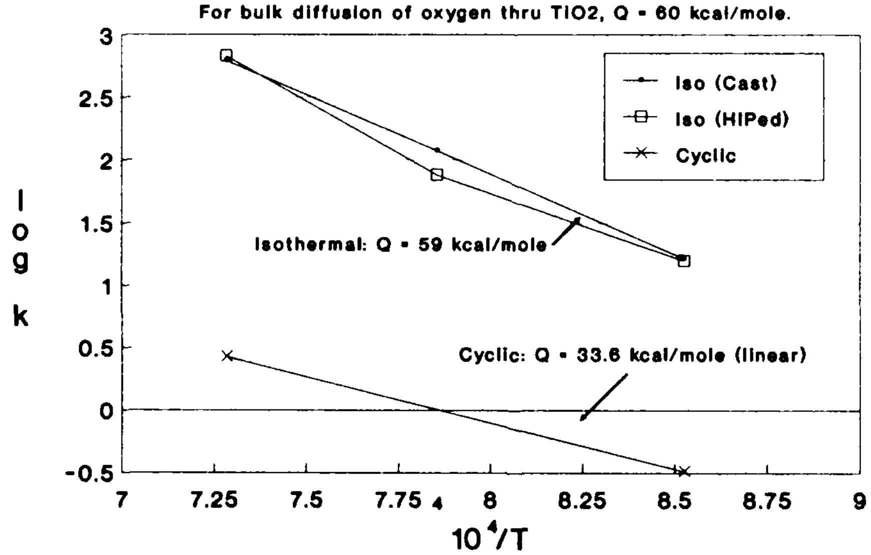

Figure 6. Oxidation Kinetics - γ-TiAl.

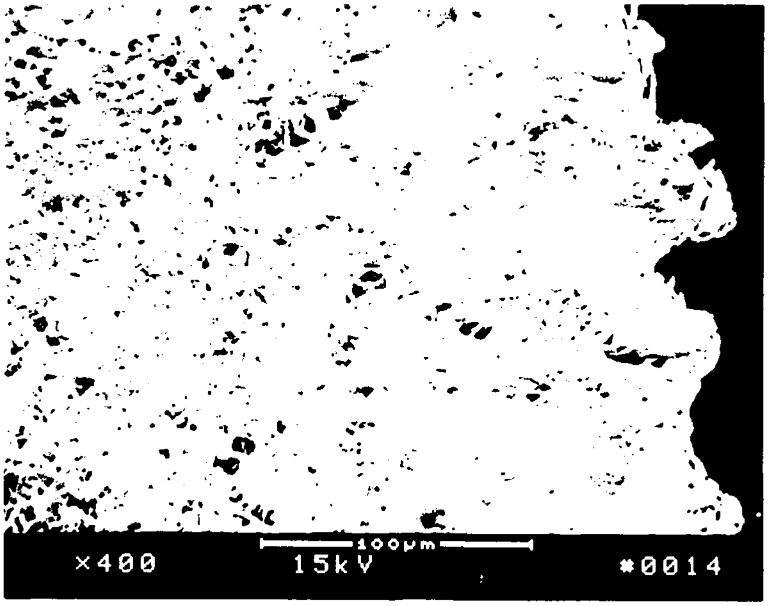
×400
100µm
15kV
*0014

Figure 7. Outer Oxide Layer Formed on γ-TiAl at 1100°C. Dark Plates are Alumina, Light Regions are TiO_2.

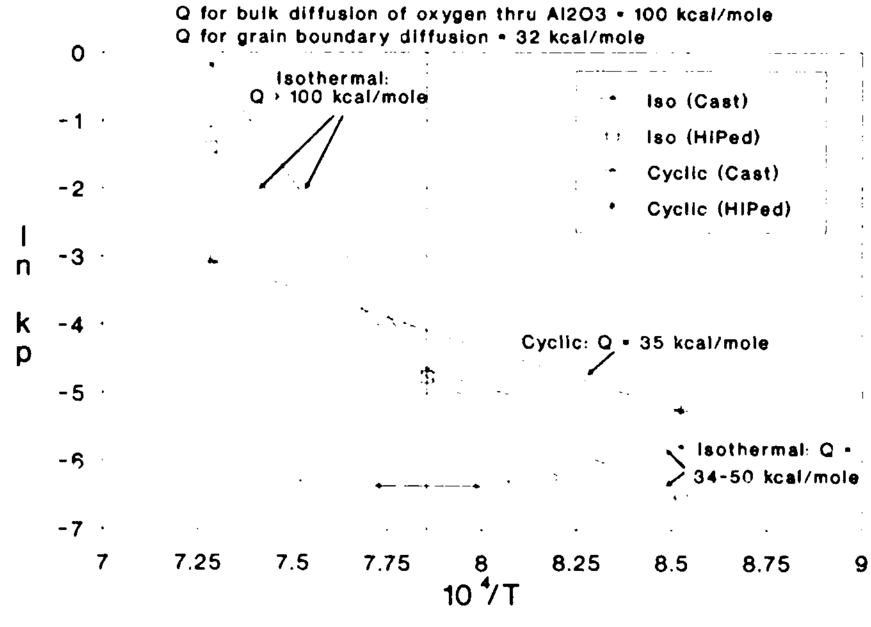

Figure 8. Oxidation Kinetics - Al_3Ti.

METHODOLOGIES FOR THERMAL AND MECHANICAL TESTING OF TMC MATERIALS

George A. Hartman
Dennis J. Buchanan
The University of Dayton Research Institute
300 College Park
Dayton, Ohio 45469-0128
USA

SUMMARY

An overview of test techniques currently being used at the Air Force Materials Directorate/MLLN laboratories for elevated temperature testing of TMC materials is presented. Methods for test system alignment/specimen gripping, specimen heating, temperature measurement, and displacement measurement are discussed in detail. In some cases, the interdependence of choices made in each of these areas is also discussed. A description of a complete system used to perform a variety of thermal and mechanical tests on TMC materials is presented Selected results from tests using this system with TMC materials are presented.

INTRODUCTION

Both structural and propulsion systems of hypersonic vehicles require application of materials with relatively low density, high modulus, and good elevated temperature strength and endurance. Although traditional materials are being considered, increasing emphasis is being placed on developing new materials with the desired characteristics. Continuous reinforced titanium matrix composites (TMCs) have been identified as one class of materials that have the potential to satisfy hypersonic vehicle design requirements.

The process of evaluating the mechanical and thermal behavior of TMC materials presents certain challenges. For example, these materials are typically costly to produce - at least in the development stage. Thus, it is often necessary to limit specimen size so that the maximum number of test results can be obtained from a given supply of material. This reduced specimen size may make it impossible to use conventional test methodologies and thus, new methodologies appropriate to TMCs may need to be developed.

This paper addresses methodologies developed by University of Dayton and Air Force researchers to address four of the many issues that require special attention when testing TMC materials. The four methodologies selected for discussion include test system alignment/specimen gripping, specimen heating, temperature measurement, and displacement measurement. Each of these methodologies are described in detail in the next section.

EXPERIMENTAL METHODOLOGIES

Test system alignment/specimen gripping

Most of the currently available TMC materials exhibit limited ductility. The ductility limit is sometimes due to the matrix material but more often is fixed by the failure strain of the fibers. The most common fibers currently in use are SiC fibers which exhibit failure strains less than 0.01mm/mm. This limited ductility means that accurate test system alignment and specimen gripping methods are required since it is not possible to rely on specimen yielding early in the test to rectify any bending that may initially be present.

Test system alignment and specimen gripping are, in general, addressed as a single issue in mechanical test systems. This is because the practical concerns involved in developing methodologies to address the two issues are tightly linked. Even so, the two issues have separate requirements that must be independently considered to achieve satisfactory results.

Methods of test system alignment for uniaxial testing must address the following three requirements:

1 the three rotational degrees of freedom (DOF) of each grip must be aligned at the point of contact between the specimen and grip,
2 the two transverse translational DOF of each grip must be aligned at the point of contact between the specimen and grip, and
3 the remaining (axial) translational DOF must be parallel to the axis of symmetry of the specimen when the specimen is installed in the grips.

Figure 1 illustrates a grip system that meets these requirements.

The requirements for specimen gripping vary with the specimen geometry, however, for the purposes of this discussion we will concentrate on flat-plate type specimens since this is the most common form in which TMCs are tested. For the flat plate geometry, the

Presented at an AGARD Meeting on 'Characterisation of Fibre Reinforced Titanium Matrix Composites', September 1993.

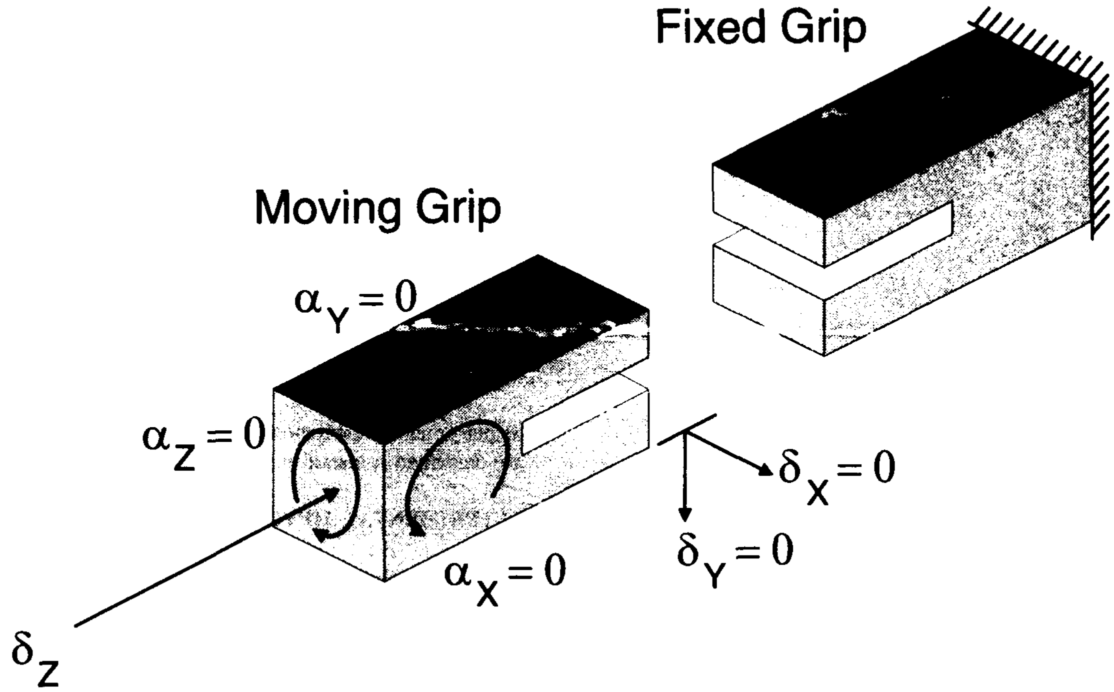

Figure 1. Schematic of Grip System That Meets the Kinematic Requirements for Unidirectional Alignment.

specimen gripping methodology must meet the following requirements:

1 the grips must provide sufficient traction on the specimen surfaces to prevent slipping under the test loads,

2 the transverse clamping forces must not crush the specimen or cause premature failure in the grip region, and

3 a method must be available to ensure that the longitudinal axis of symmetry of the specimen is parallel to the axial DOF of the grips as discussed above.

The fixed-grip system developed in-house for use with TMCs addresses these issues explicitly, i.e., direct measurements or physical constraints are used to meet the requirements. This is in contrast to methods which use strain-gaged specimens in conjunction with elastic material response relationships as an indicator of grip misalignment. Although the latter method is commonly used, it involves assumptions regarding specimen symmetry and material homogeneity that the explicit alignment method avoids. Figure 2 illustrates the steps used in explicitly aligning the grip system.

As in many commercial grip systems, the transverse forces used to clamp the specimen are adjusted by varying the hydraulic pressure applied to the clamping cylinders. To improve the traction between the grip inserts and the specimen, inserts may be coated with Surfalloy®. For most TMCs tested in the Materials Directorate MLLN laboratory, Surfalloy-coated inserts are not needed to provide sufficient traction without crushing the specimen.

Alignment of the specimen in the grips is accomplished by placing each end of the specimen a fixed distance from the lateral edge of the grip using a depth gage. Alignment in the out-of-plane direction is inherent in the grip design due to the floating yokes and double-cantilever grip body. The yokes ensure that equal forces are applied to each of the grip arms and the use of a monolithic grip body ensures that each cantilever arm deflects an equal amount. In addition, the deflections are kept to a minimum using inserts whose thickness is chosen based on the specimen thickness. Specimens are thus positioned within the grips using the same reference surfaces that were initially used to align the grip system. This method ensures that the axis of symmetry of the specimen is parallel to the axial DOF of the grips. Direct measurements of specimen misalignment yield an effective tolerance of ±0.0015rad for this system.

Figure 3 shows a typical bending strain check obtained from one of the test stations utilizing the fixed-grip system. As can be seen from the data, the bending strains are less than 2% at an axial strain of 0.00025mm/mm. The modulus values computed from strains taken from each of the four specimen sides vary by less than 1.5%.

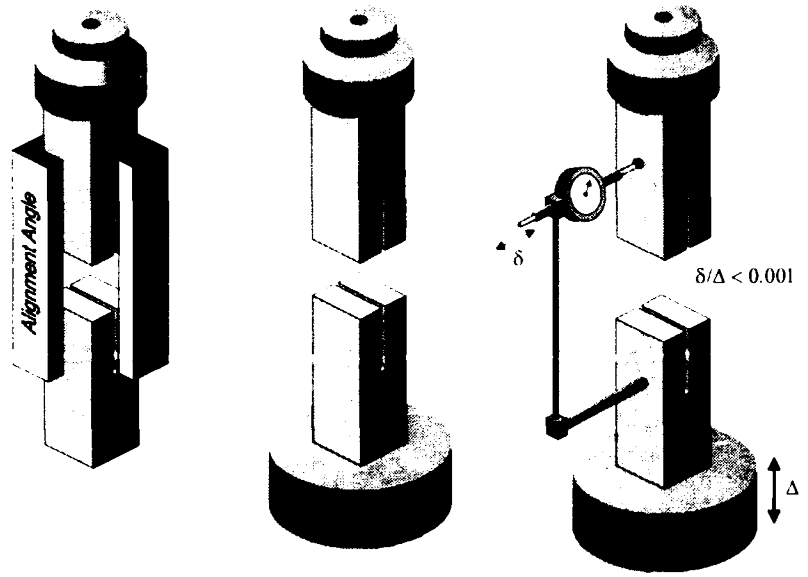

Upper Grip is Fixed to Load Cell
Lower Grip is Free to Move
Alignment Angles are Attached

Lower Grip is Fixed in Wood's Metal
Alignment Angles are Removed

Lower Grip is Translated
Dial Indicators are Used to Verify That
the Translation is in the Grip Z-direction

Figure 2. Schematic of the Steps Used to Align the Grip System.

Specimen Heating

Since the candidate composite materials are intended for use at elevated temperatures, it is essential that their behavior be characterized at representative service temperatures. Operating temperatures of over 800°C are projected for some of the TMCs.

There are several challenges to overcome in heating TMC specimens for the required mechanical tests. First, the limited amount of material available for many emerging TMCs and the desire to perform some tests in compression dictate that specimens be as short as possible. Second, tests requiring temperature cycling such as strain-control thermomechanical fatigue (TMF) must be performed. Third, the specimen is typically mounted between two thermally massive grips. Thus, it is necessary to heat and cool a relatively short specimen as rapidly as possible while maintaining a uniform spatial temperature field in the specimen gage length. It is generally not desirable to heat the grips along with the specimen due to the large power input required and the non-uniform temperature distributions produced by the large thermal mass of the grips relative to the specimen.

Induction heating has been successfully used in-house for isothermal testing, however, our experience indicates that it is very difficult to maintain uniform spatial temperature gradients during thermal cycling. This is due to two factors:

1 the inability of a single induction power source to independently vary the energy input to various points on the specimen throughout the thermal cycle, and

2 the large test section aspect ratios typical of MMC TMF tests.

The test section aspect ratio is defined as the ratio of gage length to characteristic transverse dimension. For typical tubular and cylindrical low-cycle fatigue (LCF) and monolithic alloy TMF specimens, the test section aspect ratios are less than 2 and single-zone controls like induction heaters are appropriate. Many of the TMC TMF tests, however, are performed on specimens with aspect ratios as large as 25. These large aspect ratios make it especially difficult to maintain uniform temperature fields because of reduced thermal conduction paths between distant points on the specimen.

To meet these challenges, a multi-zone quartz-lamp heating system [1] is being used that allows dynamic adjustment of the energy input at up to four zones on the specimen. Using the specially designed reflector shown in Figure 4, the lamp energy can be directed to localized regions on the specimen. Uniform spatial temperature fields can be generated by controlling the temperature at multiple points on the specimen using independent closed loop controllers. In a typical 360s thermal cycle from 425 to 815°C, temperature measurements showed less than 5°C gradient on the specimen. Temperatures as high as

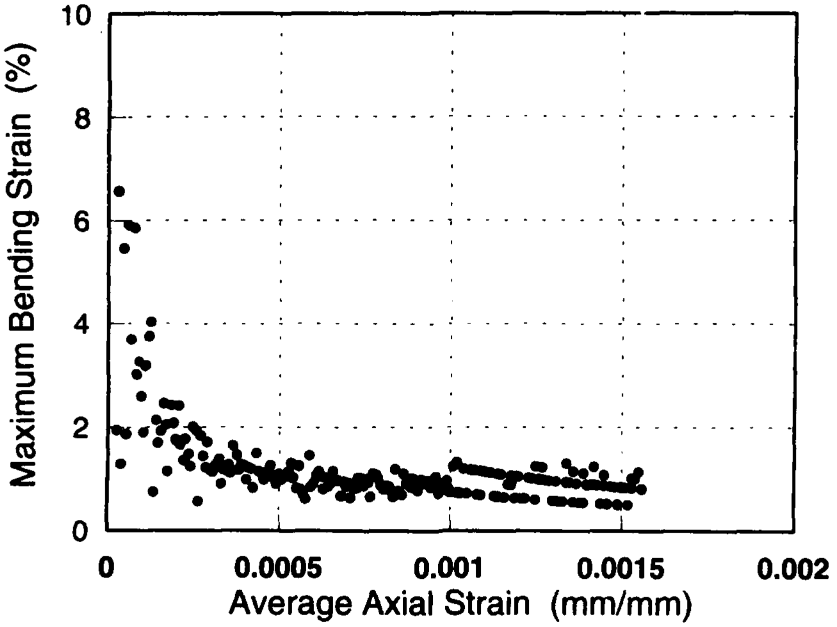

Figure 3. Grip Alignment Data for Grip System on MMC Test Station #12.

1500°C have been obtained using this unit. Higher temperatures are possible by changing the shape of the reflector interior.

The in-house test systems are constructed in such a way that the long axis of the specimen is horizontal. This aids in reducing thermal gradients by restricting convection heat transfer (the chimney effect) to the short transverse axis of the specimen.

Specimen cooling, when necessary, is performed using forced air jets to provide more cooling than necessary during decreasing portions of the thermal cycle. The multi-zone heating system is then used to provide make-up heat as needed to maintain the desired thermal cycle.

Temperature Measurement

One of the disadvantages of multi-zone heating equipment is that multiple temperature measurement devices must be used to control the various zones. Thus, it is important to find a robust and convenient way of monitoring temperature at selected locations on the specimen. Various methods were considered for the in-house program, however, spot-welded thermocouples (TCs) were found to be the most effective method.

There are several benefits to spot-welded TCs. First, the intimate contact provided by direct welding avoids TC bead radiation errors that can be significant in high radiation environments such as in the quartz-lamp heating unit. Second, properly attached TCs stay in the same location relative to the specimen, even under high displacement conditions. Third, TCs can be accurately located on the specimen using spot-welding techniques.

A significant disadvantage to direct welded TCs is the specimen damage associated with the welding process. The relative importance of this damage depends on the existing defects or damage in the test article and the type of data that will be collected during the test.

First, if the weld damage is small compared with the existing defects or damage then the weld will have little effect on the test results. Minimizing the weld damage can be accomplished by using small diameter TC wire and low weld energy. TC wires of 0.13mm diameter and weld energies of 4-5J are used in-house to produce a minimum of weld damage.

Second, if the type of data to be collected is not affected by weld damage then spot-welded TCs may be acceptable. For example, it is possible to perform low-cycle fatigue tests using welded TCs provided that test data is not required past the point where cracks begin to form at the weld site. In this case, it may be possible to obtain all of the necessary data before the weld damage progresses to a significant degree.

In practice, spot welded TCs have rarely produced premature failure of TMC specimens subjected to high-cycle fatigue, tensile, TMF, or creep test conditions

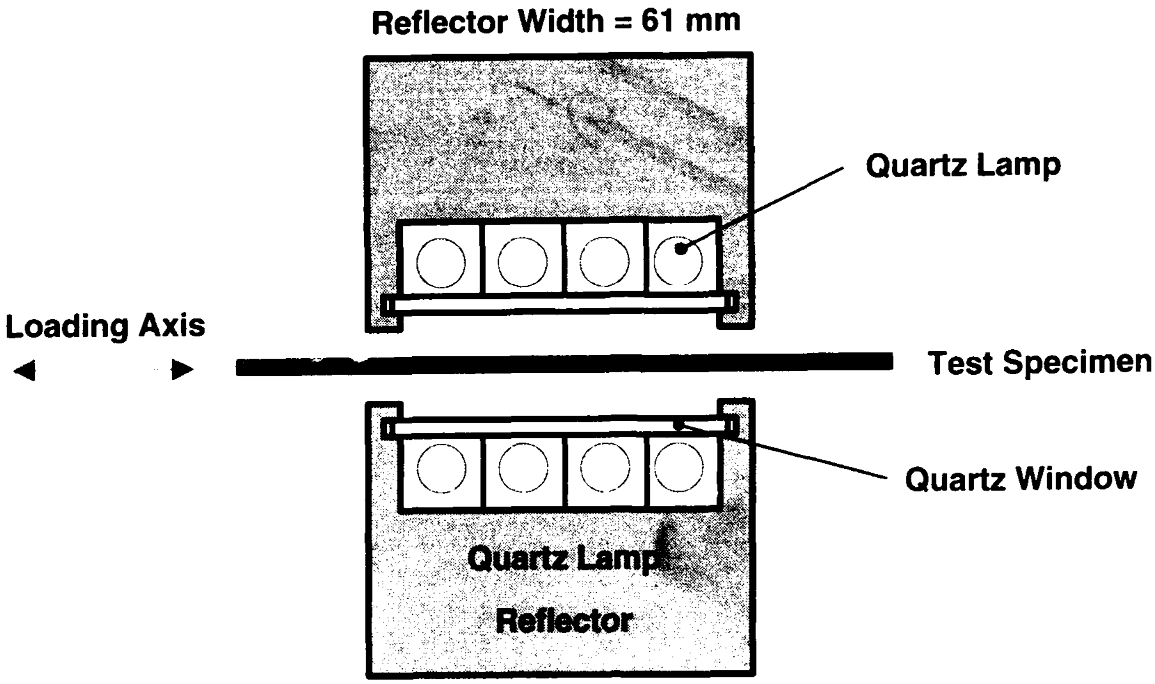

Figure 4. Specially Designed Quartz Lamp Reflectors.

during in-house tests. This experience has been obtained from hundreds of tests under the various conditions. The author speculates that the lack of weld damage effects on specimen life is due to:

1. the extremely limited weld damage produced by small TC wires and low weld energy, and
2. the relatively large existing damage in TMC specimens due to exposed fiber ends, broken internal fibers, and damage in the fiber-matrix interface

Displacement Measurement

Conventional elevated-temperature extensometers have worked well on tests of monolithic materials under conditions similar to those used with TMCs and, initially, there seemed to be no compelling reason to switch to another technique. The small size of many MMC specimens, however, means the high contact force of conventional elevated-temperature extensometers can produce significant specimen damage in some situations.

When using an elevated temperature extensometer in a vertical system, the weight of the extensometer must be counterbalanced by the same contact forces that press the extensometer against the specimen (Figure 5). Counterbalancing the weight of the extensometer is accomplished by adjusting the angle of these contact forces or the difference between the forces on each rod. This adjustment becomes increasingly difficult as the magnitude of the contact forces are reduced. This problem has been circumvented in the current project because, as described above, the longitudinal axis of the specimen is horizontal in the test frame. Since the rigid body translation of the extensometer will now be in a horizontal direction, vertical forces at the extensometer measurement head can be applied to counterbalance the weight of the extensometer independent of any rigid body translation. Thus, the forces used to press the extensometer against the specimen can be drastically reduced since all these forces must do is maintain contact between the points of the extensometer rods and the specimen throughout the test. Contact forces as low as 15g per rod have been successfully used in conjunction with conventional elevated-temperature extensometers for TMC testing in the in-house systems

INTEGRATED SYSTEM

A number of TMC test systems incorporating the methodologies and components described in the preceding sections have been assembled. Figure 6 is a photograph of one of the systems with an MMC specimen in place.

The systems utilize standard servohydraulic controls and actuators as well as commercial load cells with high lateral stiffness. Anti-rotation devices are fitted to the hydraulic actuators to restrict rotation of the moving grip about the loading axis.

Translation stages are provided to allow precise positioning of the lamp heaters prior to testing. These

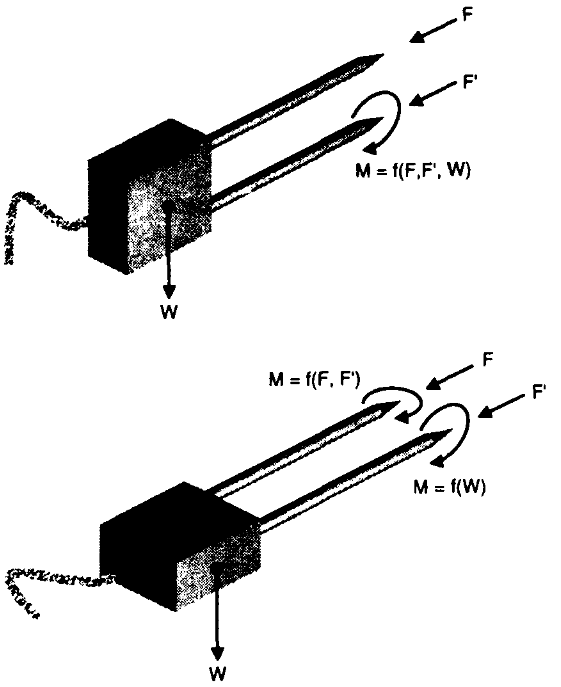

Vertical Orientation

Moments from the contact forces and the weight force are in the same plane and are coupled.

Horizontal Orientation

Moments from the contact forces and the weight force are in orthogonal planes and are decoupled.

Figure 5. Effect of Extensometer Orientation on Coupling of Contact and Weight Forces.

stages also allow the lamps to be moved out of the way for specimen loading and instrumentation.

A commercial pneumatic-to-hydraulic intensifier is used to provide up to 70MPa pressure to the grip cylinders. This translates to a maximum of approximately 45kN of transverse force at the grip insert faces. This clamping force, sometimes in conjunction with Surfalloy® coated grip inserts, has proven to be sufficient for all of the MMC testing performed in-house.

Mechanical waveform generation, thermal waveform generation, data acquisition and analysis, and general test control functions are performed by the Material Analysis and Testing Environment (MATE) test automation system [2].

TEST RESULTS

A large number of tests have been performed using the systems described in this paper and it is inappropriate to discuss here every type of test performed. Several selected sets of data from different types of tests are presented, however, to illustrate the flexibility of these systems in testing MMC materials and the types of data that can be obtained using them.

Isothermal Fatigue Crack Propagation Test Results

A number of fatigue crack propagation tests have been performed under isothermal conditions on TMC materials using the MMC test systems. Figure 7 shows the data obtained from one of these tests on a modified single edge tension (MSE(T)) geometry. This geometry is equivalent to the ASTM SE(T) with the pin loading condition replaced by a fixed displacement loading condition. Appropriate compliance, DC electric potential, and stress intensity equations were derived so that automated methods could be used to control the test and acquire the data. The purpose of this test was to study the relationship between the compliance crack length, the DCEP crack length, and the observed bridging of the fracture surface by fibers.

Isothermal High-Cycle Fatigue Test Results

Figure 8 contains data from an isothermal fatigue test run under nominally elastic conditions. Note that even though nominally elastic conditions were used, the shapes of the hysteresis loops indicate the accumulation of damage as the test proceeds. Tests of this type are being used to study the various damage mechanisms present and when each becomes significant. In addition to the hysteresis loop data, acoustic emission information is often gathered from these tests to obtain additional information about the damage mechanisms.

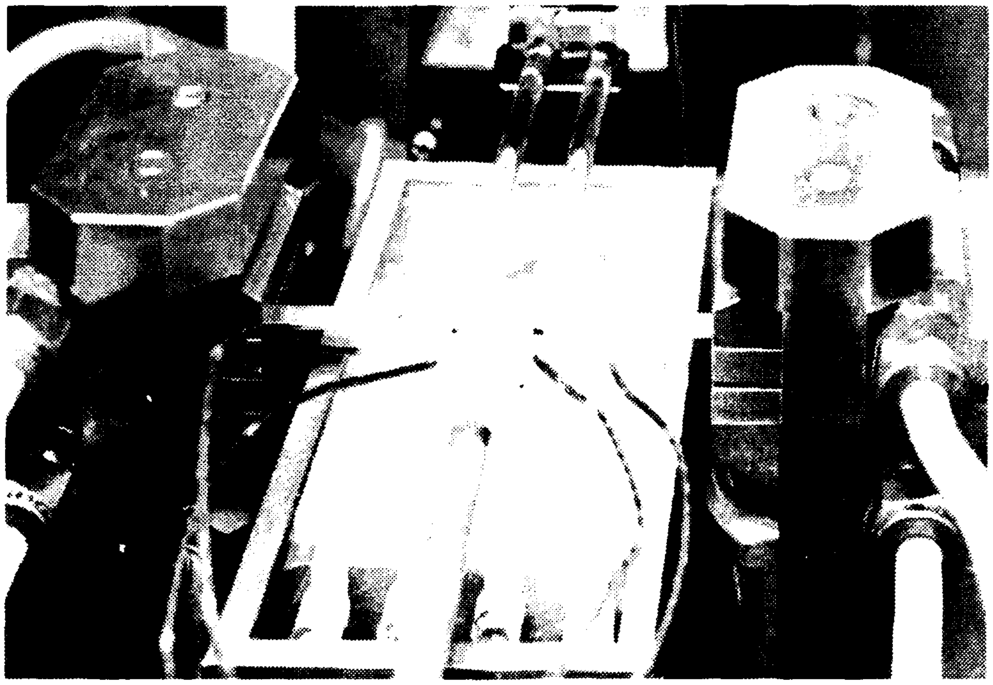

Figure 6. Photo of MMC Test Station Showing Grip and Quartz Lamp Heating Systems.

TMF Test Results

The most complex types of tests performed using the MMC test systems include the TMF and TMF crack propagation tests. Here, the operator may independently specify arbitrary mechanical and thermal waveforms for the system to impose on the specimen. To accurately impose these waveforms, the temperatures and loads at each endpoint in the cycle are continually adjusted to obtain the desired waveform shapes. In addition, the phase between the thermal and mechanical cycles is adjusted using a pattern matching algorithm to ensure that the cycles are imposed using the phase angle specified by the operator. At the same time as the waveform adjustments are being performed, hysteresis loop data is acquired, analyzed, stored, and displayed. DC electric potential information is also acquired for the crack propagation tests.

Figure 9 contains some representative imposed cycle and maximum/minimum displacement data from one of the TMF tests. Note that the thermal and mechanical waveforms are well defined both in amplitude and phase. Although the displacements include the thermal expansion due to the temperature cycle, the trends in the maximum and minimum values can be used to help identify the types of damage mechanisms at work.

REFERENCES

[1] Hartman, G. A., "A Thermal Control System for Thermal/Mechanical Cycling," Journal of Testing and Evaluation, JTEVA, Vol. 13, No. 5, September 1985, pp. 363-366.

[2] Hartman, G. A., Ashbaugh, N. E., and Buchanan, D. J., **"A Sampling of Mechanical Test Automation Methodologies used in a Basic Research Laboratory,"** *Automation in Fatigue and Fracture: Testing and Analysis*, ASTM STP, American Society for Testing and Materials, Philadelphia, 1992.

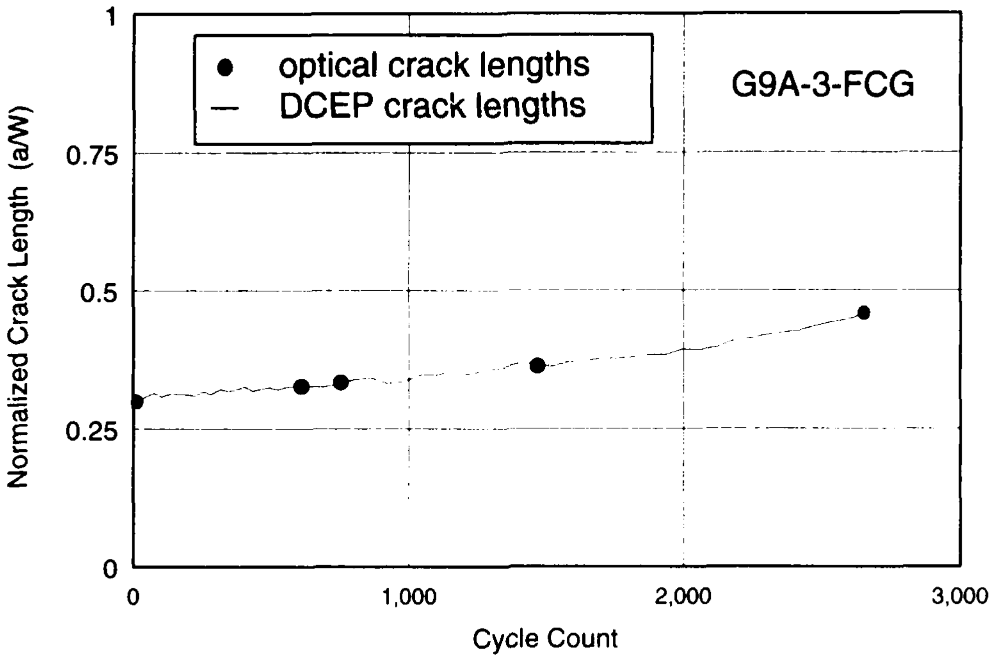

Figure 7. **MMC Fatigue Crack Propagation Data Obtained With the MMC Test System.**

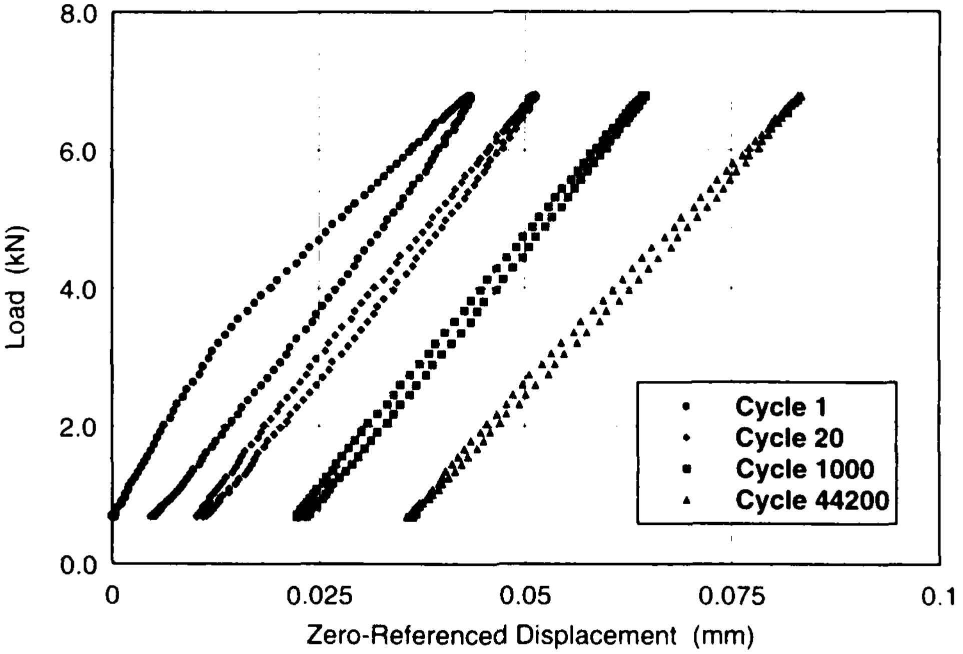

Figure 8. **MMC High-Cycle Fatigue Hysteresis Loop Data.**

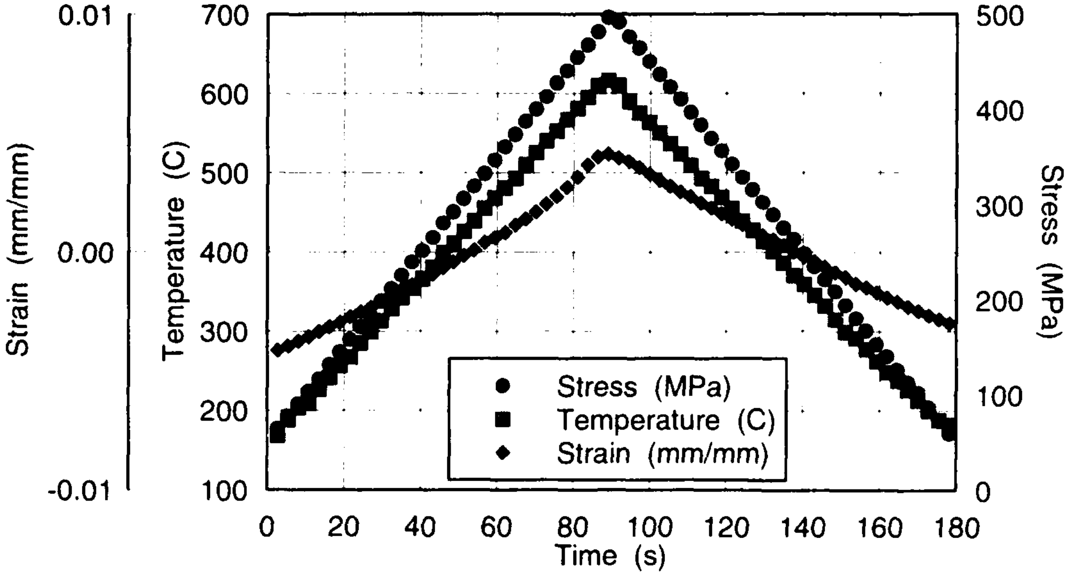

Figure 9a. Thermal and Mechanical Cycles From an MMC TMF Test.

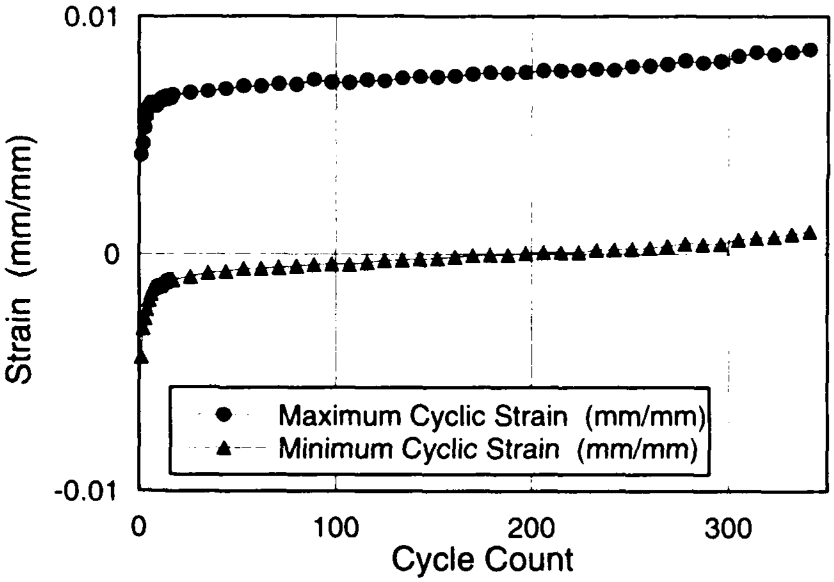

Figure 9b. MMC Maximum and Minimum Strain Data From a TMF Test.

Ultrasonic Nondestructive Characterization methods for the Development and Life Prediction of Titanium Matrix Composites

Prasanna Karpur[1], **David A. Stubbs**[1]
Research Institute, University of Dayton
300 College Park Avenue
Dayton Ohio 45469-0127, USA

Theodore E. Matikas [2], **Mark P. Blodgett**
Materials Directorate, Wright Laboratory
Wright-Patterson Air Force Base
Ohio 45433-7817, USA

S. Krishnamurthy [3]
Universal Energy Systems, Inc.
4401 Dayton-Xenia Rd.
Dayton, OH

1. SUMMARY

Titanium matrix composites (TMCs) are currently being developed for high strength and high stiffness applications with improved elevated operating temperature behavior. In order to provide guidelines for the development of new TMCs with the desired properties and to ensure reliable use, a thorough understanding of material behavior is required which necessitates the development and use of appropriate nondestructive evaluation (NDE) methods. This work outlines the concurrent use of NDE during composites development as well as material behavior studies of TMCs. The paper presents results based on various ultrasonic techniques developed in the Materials Directorate, Wright Laboratory of the US Air Force for the evaluation of different aspects of development and use of TMCs to tailor the properties for a particular application.

During the design and development of fiber reinforced TMCs, there is a need to design and control the formation of the fiber-matrix interphase so that the composites behave as per the material design criteria. As a result, it is essential to understand how the fiber and matrix interact. Further, such a 'designed property' approach is critical to both the cost and the performance of these materials. However, for any 'designed property' approach to be successful, it is imperative to have a method of interface characterization during the developmental stages of the composite. There is also a need for a nondestructive method of evaluating the microstructure of the matrix material so that the processing parameters can be suitably adjusted to obtain the desired failure behavior due to the microstructure of the titanium alloy. Life prediction for TMCs has unique needs for the understanding of failure mechanisms and material behavior. In particular, during the study of the elevated temperature interfacial degradation in environmentally exposed titanium matrix composites, it is essential to have a nondestructive characterization tool to monitor the initiation and progression of internal damage of the composites. In addition to the needs discussed above, it is essential to ensure that the composite panels that are to be tested are devoid of any manufacturing problems such as poor consolidation, fiber swimming, voids, etc. Otherwise, the results of tests for life

---

[1] On-site contracts, WL/MLLP (Contract No F33615-89-C-5612 P. Karpur) and WL/MLLN (Contract No F33615-91-C-5606 D. Stubbs), Materials Directorate, Wright Laboratory, WPAFB, OH 45433-7817.

[2] National Research Council Associate

[3] On-site contracts, WL/MLLM , (Contract No F33615-92-C-5663), Materials Directorate, Wright Laboratory, WPAFB, OH 45433-7817.

Presented at an AGARD Meeting on 'Characterisation of Fibre Reinforced Titanium Matrix Composites', September 1993.

prediction will reflect the data scatter due to manufacturing defects rather than only due to the material properties.

In this paper, we present a collection of various methods of ultrasonic nondestructive evaluation of TMCs useful for applications during material design, development, and life prediction studies. First, a novel approach for the evaluation of the elastic properties and behavior of the fiber-matrix interface will be provided by introducing a mechanical parameter called the interfacial shear stiffness coefficient which can be measured using ultrasonic shear wave reflectivity technique. In addition, a Scanning Acoustic Microscopy (SAM) method will be presented to clearly demonstrate the ability for the monitoring of the matrix cracking and the initiation, growth, and accumulation of interfacial degradation. It will be shown that the SAM can be effectively used to delineate the impact of stress, temperature, and duration of exposure of the fiber-matrix interface in TMC test specimens with different stress concentration geometry that have been subjected to cyclical mechanical loading with either isothermal exposure to temperature, or superimposed cyclical thermal loading (in-phase or out-of-phase with mechanical loading). Also, methods of prescanning the samples for fiber swimming, embedded manufacturing anomalies, etc. will be discussed. Finally ultrasonic imaging of fiber breaks of a few micrometers width in model composites will be presented.

2. INTRODUCTION

The use of titanium matrix composites (TMCs) as structural composites requires a good characterization and evaluation of nascent composite systems in research and developmental stages. Such a need for the characterization necessitates a concurrent developmental approach involving several fields of expertise so that it can be verified [1]. Such multidisciplinary interactions make it possible to evaluate (a) the compatibility of different types of matrix materials with different types of fibers including the effect of different types of fiber coating on the load transfer between the matrix and the fiber, (b) the effect of processing conditions such as temperature, pressure, environmental gases used during fabrication, duration of processing, etc., (c) the suitability of the overall mechanical properties for the intended application, (d) the material behavior and life prediction studies to evaluate failure modes and life expectancy under use conditions, and (e) the quality of composite panels being made for the above studies.

A successful development and use of a new class of materials such as TMCs require the use of suitable nondestructive evaluation (NDE) methods. However, nondestructive evaluation techniques have been historically used only in organic matrix composites to detect processing flaws, inherent defects, and also in metallic materials for the detection of damage such as cracks. A proper utilization of the traditional NDE methods for a material such as TMC requires suitable modifications and adaptations of the existing NDE methods. Techniques that have been traditionally used in a macroscopic or global level are visual, ultrasonic C-scan, X-ray, eddy current, dye penetrants, acoustic emission, and magnetic particle inspection. In addition, a new trend in the use of NDE for material characterization is becoming more important and critical during the developmental stages of a new class of materials. Innovative ultrasonic nondestructive methods for property evaluation and characterization in microscopic and localized levels can enhance the composite development process.

The objective of this paper is to describe the role of ultrasonic nondestructive evaluation in materials development for both innovative methods of (local) micro-property characterization and global quality assurance so that the composite being designed can be evaluated through various stages of development such as material selection, life prediction, material behavior, fracture mechanics, etc. The nondestructive methods developed during the initial stages of the design of the composite system can also be used after the development in order to: (a) assure that the composite panel is free of defects while the designed properties are being achieved during production, and (b) detect the degradation of initial properties because of use. The paper will first present novel and innovative methods of ultrasonic nondestructive characterization of TMCs during the developmental stages of the composites followed by a brief discussion on modified traditional techniques for global inspection of TMCs.

3. MICRO-PROPERTY EVALUATION DURING THE DEVELOPMENT OF TMCs

In order to design a composite with suitable properties for the intended application, the development of the composite system should progress from a global sense to a microscopic approach. For example, during the initial stage of design, materials will have to be selected for optimum chemical compatibility to avoid global problems such as warping, corrosion, high temperature resistance, etc. In the next stage of design, the composite system will have to be evaluated for macroscopic anomalies such as porosity, lack of consolidation, fiber swimming, etc. Thus, in this stage of development, there is a need for optimization of the material processing parameters. However, since the changes in the processing parameters could introduce global problems of warping, etc., there is a necessity for iterative material selection and processing parameter modulation until the global and macroscopic design are achieved to satisfaction. The final step (with the necessary feed back) of composite development would be the control of the local properties such as the chemically formed interphase region between the fiber and the matrix materials. Nondestructive evaluation can play a critical role in all the stages of the development of a composite.

3.1 Ultrasonic Evaluation of Lack of Consolidation

Materials such as TMCs which are based on reactive matrices with high melting temperatures are processed by solid state diffusion bonding of matrix foils, powders or sprayed deposits with reinforcements. For example, the processing of continuously reinforced composites by the foil-fiber-foil method typically involves diffusion bonding of rolled matrix alloy foils with reinforcing fibers in the form of woven mats with a cross weave to hold the fibers in place. The foils and the fiber mats are stacked alternately and consolidated by vacuum hot pressing or hot isostatic pressing. The processing conditions are to be carefully selected in order to achieve complete consolidation and produce acceptable composite material. While higher temperatures and longer processing times may enable consolidation, they can promote undesirable reactions at the fiber/matrix interface and also cause high residual stresses after the composite is cooled to ambient temperature. On the other hand, lower processing temperatures can lead to fiber damage as well as incomplete consolidation.

In practice, optimum processing conditions are determined through preliminary diffusion bonding experiments using small samples. The initial processing temperatures are chosen on the basis of known flow characteristics of the matrix alloy at different temperatures and strain rates. The consolidation of these samples is checked by metallographic examination of polished sections. However, the use of metallography alone is generally inadequate since consolidation often occurs nonuniformly within the sample. A normal incidence longitudinal wave method has been used to map the extent of poor consolidation between the foils [2]. The technique is rapid, easy to use and capable of detecting consolidation problems as small as a few tens of microns. The fact that the technique is nondestructive makes it feasible to evaluate the integrity of the samples so that they can be used for further tests such as fragmentation, push-in, push-out, etc. The detection of improper consolidation is demonstrated in Figure 1 wherein a model titanium alloy based composite (Ti-24Al-11Nb/SCS-6) fabricated by the foil-fiber-foil approach is shown.

3.2 Ultrasonic Evaluation of Matrix Microstructure

Conventional titanium alloys can be classified as near alpha, alpha + beta or meta stable beta compositions. A variety of microstructures with different phase morphologies can be obtained depending on the alloy composition and processing conditions. All these alloy classes have been investigated to develop matrices for the fiber reinforced metallic composites. For example, published work includes composites based on the two-phase alloy (Ti-6Al-4V), the near alpha alloy (Ti-1100), and the metastable beta alloys such as Ti-15-3 and Timetal 21S. More recently, there has been considerable interest in compositions based on Ti alloys containing much higher levels of aluminum and niobium leading to the formation of ordered intermetallic compounds based on alpha-2 and orthorhombic phases which appear to provide improved mechanical properties and oxidation resistance.

While different types of matrix microstructures have been experimented for the TMCs, existence of multiple types of grain structure in the composite, especially near the fiber-matrix interface region might be undesirable for certain types of TMCs. Also, changes in the microstructure of the matrix from region to region of the sample

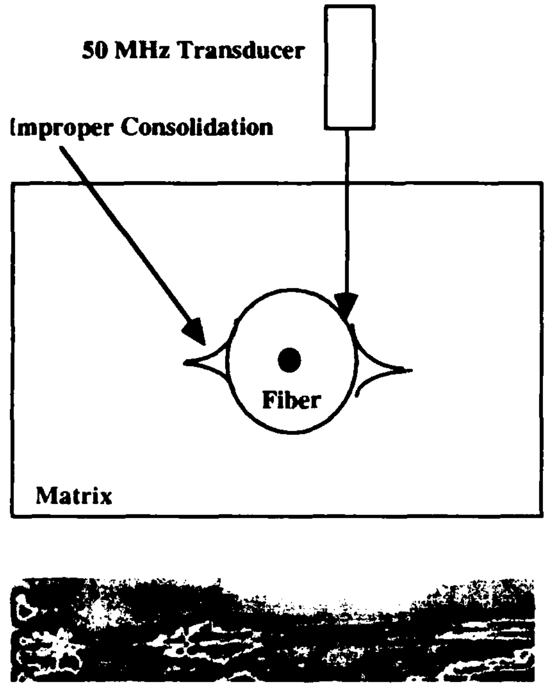

Figure 1 Ultrasonic Evaluation of Lack of Consolidation. The image at the bottom was obtained using a 50 MHz focused transducer as shown on the top.

might introduce zones of stress concentration resulting in reduced overall strength of the composite system. Thus detection, monitoring and control of the microstructure of the composite matrix is essential to obtain overall mechanical behavior of the composite. Ultrasonic NDE provides an excellent tool to detect the existence of anisotropy in the matrix. Figure 2 demonstrates the application wherein Figure 2 a is the image of a single fiber embedded in finer homogeneous equiaxed alpha + beta Ti-6Al-4V matrix microstructure (morphology obtained from metallography). Figure 2 b shows the image when the matrix microstructure was coarser plate-like alpha + beta morphology due to the presence of interstitial impurities during the processing of the composite. Similarly, the ultrasonic image of three fiber embedded in Ti-6Al-4V matrix is shown in Figure 2 c. The matrix was consolidated at a temperature slightly above beta-transus. Under metallography, the matrix regions away from the fibers show coarse alpha plates and elongated beta phase while the matrix adjacent to the fibers shows equiaxed alpha plus beta structure which was stabilized by carbon diffusion from the fiber.

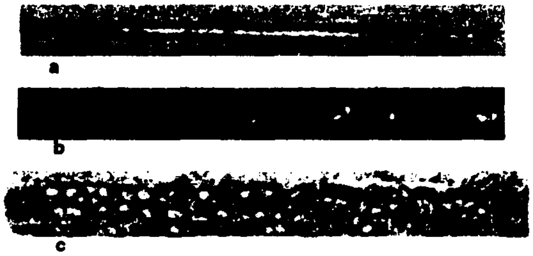

Figure 2 (a) Image of Single Fiber embedded in Homogenous Ti-6Al-4V Matrix with fine equiaxed alpha+beta microstructure. (b) Single Fiber Image in Ti-6Al-4V Single Fiber. (c) Ti-6-4 Three Fibers.

3.3 Interface Analysis

The properties of a composite system are dominated and determined by the properties and the behavior of the interface between the fiber and the matrix materials. It is at the interface that the load transfer takes place and the crack resistance exists. As a result, the characterization of the interface is of great interest to the researchers who are developing the composite materials. Many investigators have employed a number of experimental techniques including fiber pull-out, fiber push-out, and fiber fragmentation tests [3-7] to characterize the interface. These techniques are 'destructive' in nature. There are nondestructive methods of interfacial analysis being developed [8] to be used in conjunction with the destructive tests as well as by themselves [9-11] in a completely nondestructive mode. The following sections will outline three modes of ultrasonic NDE wherein the first method will show the use of ultrasound in conjunction with the fiber fragmentation technique. The second method will be a completely nondestructive method of interface characterization using ultrasonic shear wave back reflectivity technique (SBR). The third method outlines an ultrasonic 'Scanning Acoustic Microscopy (SAM)' technique to evaluate the fiber-matrix interfacial degradation [11] due to elevated temperature effects.

3.3.1 Ultrasonic Imaging of Fiber Fragmentation Samples

In the fiber fragmentation test, a composite sample made of a single fiber embedded in a ductile matrix is subjected to tensile loading along the fiber axis. When the tensile stress, which is transferred from the matrix to the fiber by shear, exceeds the local fiber strength, the single fiber breaks successively into smaller fragments until the fragments become too short to enable further increase in stress level. Using arguments based on shear lag analysis, Kelly and Tyson [3] showed that the critical length of fiber for load transfer, L_c, is a function of the interfacial shear stress according to the equation

$$\tau_i = \sigma_f \frac{d}{2 L_c} \qquad (1)$$

where τ_i is the shear stress, σ_f is the tensile strength of the fiber of critical length and d is the fiber diameter.

The Ti-6Al-4V/SCS-6 and Ti-14Al-21Nb/SCS-6 composite samples were fabricated by diffusion bonding two matrix alloy sheets with a single fiber between them. The processing method consisted of vacuum hot pressing at 925°C/5.5 MPa/30 min. followed by hot isostatic pressing at 1010°C/100 MPa/2 hr. The consolidated samples were machined into 1.5 mm thick sheet tensile specimens with 19.05mm x 6.35 mm gage sections. All samples were examined by microfocus x-ray radiography to ascertain proper alignment of fiber parallel to the tensile specimen axis. Tensile tests were conducted on a servohydraulic machine in laboratory air at ambient temperature using a nominal strain rate of $2 \times 10^{-4}\ s^{-1}$ for Ti-6Al-4V/SCS-6 and $1 \times 10^{-4}\ s^{-1}$ for Ti-14Al-21Nb/SCS-6 specimens. Subsequent to ultrasonic imaging, metallographic examination of the fiber fragments was conducted by using optical microscopy and SEM [8].

Tensile tested specimens for fragmentation were ultrasonically imaged using a 25 MHz focused transducer (0.25" dia, 0.5" focus) in the pulse-echo mode. The ultrasonic wave front was incident on the composite at an angle of 24° (which is between the first and the second critical angles). As a result, vertically polarized shear waves were incident on the interface between the fiber and the matrix. Back-reflected ultrasound was gated for imaging. Since the wave front was incident at an angle, the received signal was either low amplitude due to back-scattering from the material texture or a very strong amplitude due to the back-reflection from the cylindrical fiber (when the wave front was perpendicular to the fiber circumference). As a result, the dynamic range of the image of the fiber was excellent. Also, the wave front was slightly defocused (0.06") in to the fiber interface. The reasoning for the defocus will follow in a later section of this paper. Figure 2 shows the schematic of the shear wave interrogation approach.

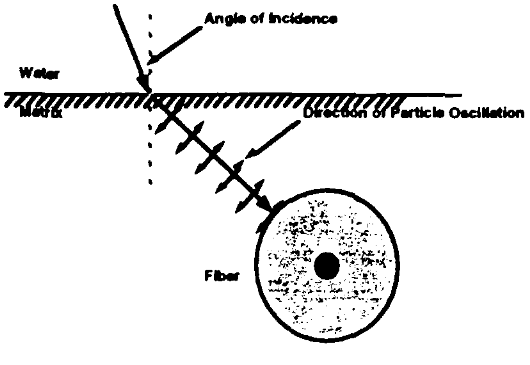

Figure 3 Ultrasonic Experiment Setup

Figure 4-a shows an example of the 'before loading' image of a SCS-6 fiber embedded in a type of Titanium Aluminide matrix (Ti-6Al-4V). Figure 4-b shows the fiber after loading. Since the average fiber size is about the same as the diameter of the fiber, the interface has successfully transferred the load to the fiber.

Figure 4-c shows a SCS-6 fiber embedded in Ti-14Al-21Nb matrix after loading. Since the average fiber size is more than three times the diameter of the fiber, the interface has not efficiently transferred the load to the fiber. In both the 'after-test' images, in addition to the main breaks, we can also observe smaller pieces due to secondary breaks. The presence of such secondary pieces have been corroborated by metallography [8, 12].

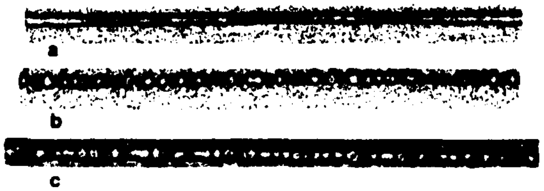

Figure 4 (a) Ultrasonic Image of an untested single fiber sample. (b) Fiber Fragmentation Image in Ti-6Al-4V sample with SCS-6 Fiber. (c) Fiber Fragmentation Image in Ti-14Al-21Nb (or Ti-24Al-11Nb by atomic %) sample with SCS-6 Fiber.

3.3.2 Ultrasonic Shear Wave Back Reflectivity Technique (SBR)

An ultrasonic back-reflectivity technique has been developed [9, 10] to complement other existing techniques for the characterization of the interfacial behavior in fiber reinforced model composites. These techniques may be: (1) destructive: fiber "pull-out" and "push-out" tests [13]; the "fiber fragmentation" technique implemented by subjecting the model composite to axial loading to induce the fragmentation of the fiber and by measuring the size of the fragments which would be linked to the "interfacial load transfer behavior" [3, 8, 12]; (2) nondestructive: ultrasonic imaging of the fiber fragmentation, in conjunction with advanced signal processing techniques[14].

The ultrasonic characterization of the interface is achieved by the analysis of the back-reflected signal from the fiber-matrix interface [9, 10]. The advantages of the ultrasonic back-reflectivity technique are several: (i) the method is completely nondestructive and facilitates the use of the same sample for the tests (fatigue and creep) other than the interface analysis, (ii) the technique can provide the distribution and variation of the interfacial properties along the length of the fiber thereby facilitating better process control, and (iii) the interface can be monitored for degradation and changes during fatigue tests for life prediction.

The goal of this study was to develop a theoretical model which will aid in the determination of various experimental parameters such as the frequency of ultrasound and angle of incidence while providing the vital relationship necessary to interpret the future experimental results. The theoretical model considers the reflection of an ultrasonic wave front from a single fiber embedded in a homogeneous isotropic matrix.

Model

Figure 3 shows the geometry of the problem: a plane wave $\exp[i(\omega t + \kappa_1 zi)]$ is obliquely incident at an angle θ on a model monofilament composite immersed in a fluid and in a plane normal to the axis of the fiber.

For the development of the theoretical model, the composite is simulated by an infinitely extended plate consisting of an isotropic matrix with an embedded cylindrical isotropic and homogeneous fiber (which is justified at the wavelength of interest - frequency < 50MHz). Further, since the ultrasonic beam is assumed to be incident on the composite such that the refracted wave is always normal to the fiber circumference (back-reflection interrogation technique), without the loss of the generality, the cylindrical fiber can be replaced with an infinitely extended homogeneous isotropic layer of thickness equal to the diameter of the fiber. Although it is relatively easy to model the fiber as a cylinder and use the Bessel function response of the cylinder, the present formulation of a plate will not deviate substantially from the reflected amplitude at the center of the main lobe of the Bessel function (the center of the main lobe of the Bessel function is the only point of interest for this study because the ultrasonic beam is normally incident to the circumference of the cylindrical fiber). Effects of attenuation and diffraction can also be considered in the model if the matrix and the fiber thicknesses are significant. However, since the matrix is relatively thin (approximately five times the wavelength) for this application, the effect of attenuation and diffraction are omitted here.

The interface between the matrix and the fiber is modeled by: (i) assuming continuity of normal and shear stresses and normal displacements at the interface, and (ii) by allowing the discontinuity of shear displacements at the interface. It is assumed that the vibration is transmitted instantaneously from one medium to the other by weightless springs with an equivalent rigidity of N_n [GPa/μm].

The interfacial stiffness coefficient, N_n, of the matrix-fiber boundaries (upper and lower) can be generally different around the circumference, due to the fabrication conditions or due to the use of different material for each matrix plate. Thus, consider two different coefficients N_n and $\tilde{N}_n$, one for each interface. Accordingly, the interface conditions are:

$$\{\sigma^P\} = 0 \quad \{\sigma^T\} = 0 \quad [u^P] = 0 \tag{2}$$

$$\sigma^T = N_n\ [u^T] \quad \text{or} \quad \sigma^T = \tilde{N}_n\ [u^T]$$

where the superscripts P and T denote the normal and tangential displacements/stresses respectively; the square brackets denote the jump of a function across the interface, and the curly brackets denote the vectorial resultant of stresses at the interface. The linearity of equation (2) is based on the assumption of small amplitudes of vibrations which is justified for ultrasonic applications wherein the amplitudes of displacements are around a few Angstroms.

The back-reflection coefficients for the shear interrogation is dependent on:

- the properties of the matrix (density, ρ_2, longitudinal, c_{2L}, and shear, c_{2S}, velocities)
- the properties of the fiber (density, ρ_3, longitudinal, c_{3L}, and shear, c_{3S}, velocities)
- the diameter of the fiber (d')
- the angle of incidence (θ)
- the frequency (f) of interrogation, and
- the interfacial stiffness coefficients (N_n, $\tilde{N}_n$)

The stiffness coefficient is dependent on the wave type because of the different mechanism of stress transfer for compressional or shear displacement waves as discussed in earlier publications [9, 10]. Further details of this modeling and the results can be obtained from these papers.

3.3.3 Scanning Acoustic Microscopy

Scanning Acoustic Microscope was developed by Quate et al., [15] to image integrated circuits. The most important contrast phenomenon in a SAM is the presence of Rayleigh waves which are leaking toward the transducer and are very sensitive to local mechanical properties of the materials being evaluated. The generation and propagation of the leaky Rayleigh waves are modulated by the material properties, thereby making it feasible to image even very subtle changes of the mechanical properties.

A SAM transducer is schematically shown in Figure 5. The transducer has a piezoelectric active element situated behind a delay line made of silica crystal oriented such that the 1-1-1 axis is parallel to the direction of sound propagation. The thickness of the active element is suitable to excite ultrasonic signals with a nominal frequency of 50 MHz when an electrical spike voltage is delivered to the piezoelectric element. The silica delay has a spherical acoustical concave lens (Fig. 5) which is ground to an optical finish. The numerical aperture (NA - ratio of the diameter of the lens to the focal distance) is 1.25 for the transducer used for this study. An NA of more than 1 or F number (focal distance/diameter of the lens) less than 1 is essential for the SAM technique to effectively generate and receive surface waves in the sample being imaged.

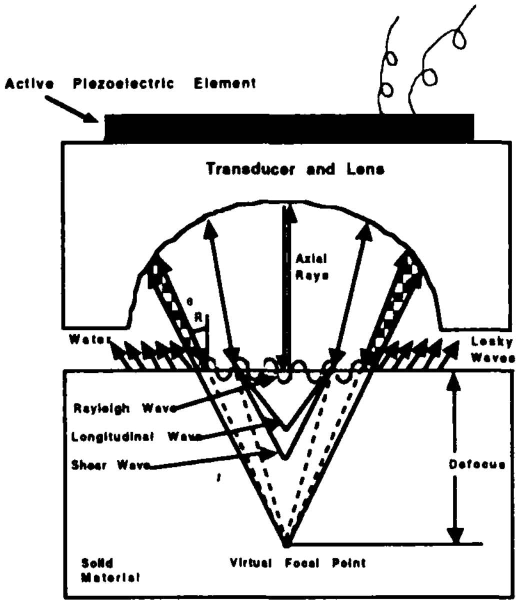

Figure 5 Schematic of a Scanning Acoustic Microscope Transducer

The principle of operation of a SAM transducer is based on the production and propagation of surface acoustic waves (SAW) as a direct result of a combination of the high curvature of the focusing lens of the transducer and the defocus of the transducer into the sample [15, 16]. The sensitivity of the SAW signals to the surface and the subsurface features depend on the degree of defocus and has been well documented in the literature as the V(z) curves [17]. The defocus distance also has another important effect on the SAW signal obtained by the SAM transducer: the degree of defocus dictates whether the SAW signal is well separated from the specular reflection or interferes with it. Thus, depending on the defocus, the SAM technique can be used either to map the interference phenomenon in the first layer of subsurface fibers or to map the surface and subsurface features (reflectors) in the sample.

The SAM was used in conjunction with several on-going material behavior investigations [11, 18-20] to evaluate the extent of damage accumulated during the respective test procedures. Specimens were removed during or after testing and evaluated using the SAM. Thus, composite materials composed of a range of different matrix materials could be evaluated. All the samples are titanium matrix composites reinforced with a silicon-carbide based fiber, commercially designated SCS-6, that has a double pass carbon rich coating. The matrix material was a Beta processed titanium alloy, Ti-15Mo-3Nb-3Al-0.2Si (weight percent). The composites were manufactured using the foil-fiber-foil process.

SAM Results

One benefit of the SAM is that it provides a nondestructive indication of the extent of interfacial damage. To demonstrate its utility, a notch (hole) fatigue experiment was periodically interrupted and the specimen scanned using the SAM to evaluate the development of damage during the life of the specimen. After each SAM evaluation, the specimen was returned for further fatigue cycling. The fatigue cycling was terminated after the third interruption at 9.66 X 10^5 cycles. For this test, the composite consisted of t a cross-ply lay-up of fibers in the [0/90]s configuration. Prior to testing, a SAM image was made of the specimen to establish the initial integrity of the material. The pre-testing image is shown in Fig. 6a and shows no damage to the interfaces prior to testing. After the initial scan, the specimen was isothermally fatigued at 650°C with a maximum remote stress of 200 MPa applied at 1 Hz along the fibers with reference to the image in Fig. 6a. The fatigue test was stopped after 1.54 X 10^5 cycles or approximately 43 hours at temperature. The specimen was removed from testing and imaged using the SAM. The resulting image is shown in Fig 6b. In this figure, the damage (as indicated by the high contrast regions) originates at the top and bottom of the hole and proceeds away from the hole along the fibers. The shorter crack on one side of the hole is only beginning to develop an affected zone and is barely visible in the ultrasonic image although the crack extends about three fiber diameters at the surface. Figure 6c is the SAM image after an additional 9.66 X 10^4 cycles were applied for a total of 2.51 X 10^5 cycles and total time of 70 hours at temperature. In this figure, the cracks on each side of the hole can be clearly seen. To substantiate the indications made by the SAM, the outer layer of matrix material was etched away using a saturated solution of tartaric acid in 10% bromine in methanol. Metallography showed excellent correlation with the SAM images [11]. Further details can be obtained from the literature [11].

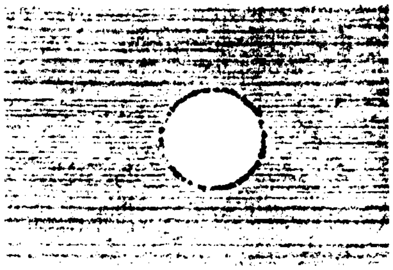

Figure 5 a. SAM Image of the Untested Sample

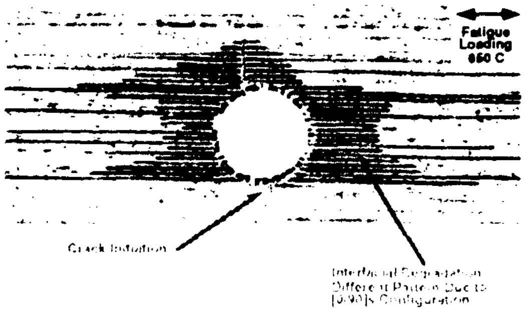
Fatigue Loading 650 C
Crack Initiation
Interfacial Separation Different Pattern Due to [0/90]s Configuration

Figure 5 b. SAM Image of the Sample after the first interruption.

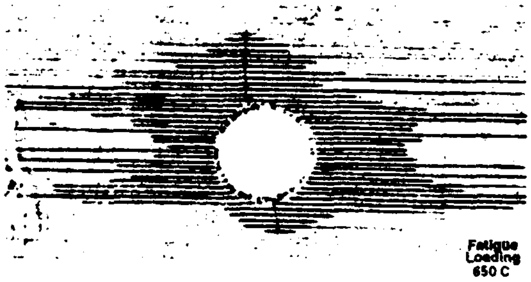

Figure 5 c. SAM Image of the Sample after the third and final interruption.

4. GLOBAL NONDESTRUCTIVE EVALUATION OF TMCs

A modified through-transmission reflection plate inspection technique can be effectively used to evaluate the TMCs. In this technique, one ultrasonic transducer is used to send ultrasound into and through the specimen.

The ultrasound transmitted through the specimen reflects off a glass reflector plate and travels back through the TMC specimen. Ultrasonic energy reflected back through the specimen is received by the transducer and detected by the ultrasonic instrument. The reflector plate technique is very sensitive to any change in material acoustic impedance which is a function of the Young's modulus, density, and Poisson's ratio. Hence the technique provides a map of variations in material integrity. Consequently, areas of reduced transmission should have some correlation with damage in the composite. Also, since the amplitude data that is recorded comes from ultrasound that has passed through the material twice, the technique is very sensitive to changes in acoustic impedance.

A technique capability assessment was conducted in the Materials Directorate [21] to evaluate the correlation between NDE data and specific tensile and fatigue properties in a titanium matrix composite. The ultimate goal was to use the NDE techniques to quantitatively assess the integrity of MMCs. The titanium matrix composite used for the study consisted of silicon carbide (SCS-6) fibers in a Ti-15Mo-2.6Nb-3Al-0.2Si matrix (designated Timetal 21S). The fiber diameter is nominally 0.142 mm. All specimens were fabricated using the foil-fiber-foil technique and hot isostatic processing. None of the specimens had any type of coating.

A horizontal fatigue test frame incorporating a pneumatic ram was used for applying cyclic loads to the test specimens. A 20 kN load cell was used and loads were controlled to within 0.1 kN (typically 1 MPa for these specimens). Specimens were positioned horizontally in precisely aligned, hydraulically actuated, rigid grips [22]. Gripping pressure was 60 MPa. The applied load cycle was controlled by a PC using control software developed by the University of Dayton [23]. Strain data was acquired using high temperature extensometers with 110 mm long quartz rods. Typical displacement resolutions were 0.0004 mm.

A TMF test was developed that combined both in-phase and out-of-phase TMF tests into one compound cycle [21]. The cycle is shown in Figure 6. The total cycle time was 360 seconds for the specimens tested. In actual testing the temperature was ramped from 150 °C to 638 °C in the first 90 seconds of the cycle. During the second 90 seconds the temperature was ramped to the maximum temperature of 650 °C. Ramping the temperature set points during the second 90 seconds resulted in the "isothermal" portion of the cycle where the actual specimen temperature was maintained between 640 and 650 °C and assisted in maintaining a proper phase relationship with the load profile.

Reflector plate scans of all of the specimens were obtained before the fatigue tests Low ultrasonic transmission could result from voids, delaminations, or fractured fiber groups sufficient to scatter ultrasound. With the motivation to quantify the NDE results, a simple "damage assessment" parameter was constructed to quantify the ultrasonic data using the principle that the amount of ultrasonic attenuation is related to the degree of disorder within the specimen. Additionally, in the direction perpendicular to the axis of mechanical loading, it seems reasonable to assume that there is an inverse relationship between the extent of the disorder and the strength and/or fatigue life of the composite. Finally, since the cyclic stress on the fibers is highest in the region of highest temperature, where oxidation and cracking of the matrix are more likely to occur, the abnormalities within the heated portion of the specimen should dominate failure. Thus only the NDE indications from the heated region, ±15 mm from the center,

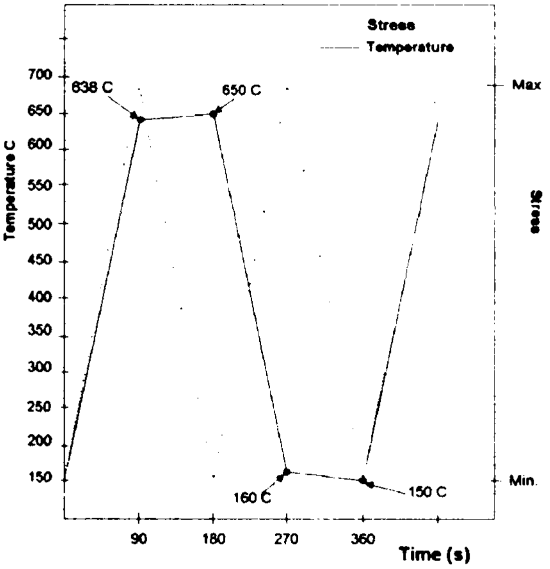

Figure 6 Load and temperature profiles during the thermomechanical fatigue tests.

Table 1 Data Showing the Dependence of Percent Life as a Function of Damage Parameter

Specimen #	Ply Config.	Test Type	Ultrasonic Attenuation (dB)	UT-detected defect length (l/width)	Damage Parameter	% UTS or % Life
91-379	$[0/90]_{2S}$	Tension	8.5/7	0.1 / 0.9	7.2	73%
91-366	$[0/90]_{2S}$	Tension	6 /12/18	0.3 / 0.2 / 0.5	13.2	40%
91-361	$[0/90]_{2S}$	Tension	8.5 / 14	0.25 / 0.65	11.1	39%
91-367	$[0/90]_{2S}$	Tension	20	1	20	13%
91-380	$[0/90]_{2S}$	TMF	18/12	0.2 / 0.2	6	80%
91-368	$[0/90]_{2S}$	TMF	18/12	0.17 / 0.17	5.1	32%
91-358	$[0/90]_{2S}$	TMF	8.5	0.55	4.6	26%
91-360	$[0/90]_{2S}$	TMF	9.5/13.6	0.5 / 0.5	11.6	16%
92-098	$[0/90]_S$	TMF	0	0	0	100%
92-099	$[0/90]_S$	TMF	2.5	0.25	0.6	91%
92-100	$[0/90]_S$	TMF	3.3	1	3.3	89%
92-126	$[0/90]_S$	TMF	7	1	7	45%
92-127	$[0/90]_S$	TMF	7/6	0.35 / 0.65	6.4	50%

were analyzed. A simple damage parameter was developed [21]:

$$DP = UTA \cdot \frac{DL}{W} \qquad (1)$$

where DP = Damage parameter, UTA = Ultrasonic attenuation, DL = Defect length, and W = Specimen width. Applying this algorithm to the ultrasonically detected abnormalities in the heated portion of the specimens produced the data shown in Table 1. From the table, it is apparent that This technique, when properly calibrated, can be a useful tool for screening advanced metal matrix composites, thus preventing the use of defective material in mechanical property evaluations. Further details can be found in the literature [21].

5. CONCLUSIONS

Ultrasonic evaluation of TMCs is an integral part of the developmental process of the composite systems. Ultrasound can be an effective tool during all the phases of development. For example, proper consolidation can be verified while ensuring the formation of suitable microstructure of the matrix material. Also, the elastic behavior of the interface between the matrix and the fiber can be quantified using ultrasound. Acoustic microscopy can be effective to evaluate the interfacial degradation due to the exposure to elevated temperatures and load. Global ultrasonic nondestructive evaluation is essential to either reject samples with poor initial properties or to determine their remaining life due to the extent of manufacturing defects.

6. REFERENCES

1. T. E. Matikas, and P. Karpur, Ultrasonic Nondestructive Evaluation as a Tool for the Development of Aerospace Structural Ceramic Composites, *NATO/AGARD 76th Meeting of the Structures and Meterials Panel*, Antalya, Turkey, 1993, (in print).

2. S. Krishnamurthy, T. E. Matikas, P. Karpur, and D. B. Miracle, Evaluation of the Processing of Fiber-Reinforced Metal Matrix Composites Using Ultrasonic Methods, to be submitted to *Journal of Composites Science and Technology*, (1993).

3. A. Kelly, and W. R. Tyson, Tensile Properties of Fiber-Reinforced Metals: Cu-W and Cu-Mo, *J. Mech. Phys. Solids*, **13**, (1965), pp. 329-350.

4. S. Ochiai, and K. Z. Osamura, Multiple Fracture of a Fiber in a Single Tungsten Fiber-Copper Matrix Composite, *Metallkde*, **77**, (1986), pp. 255-259.

5. I. Roman, and R. Aharonov, Mechanical

Interrogation of Interfaces in Monofilament Model Composites of Continuous SiC Fiber-Aluminum Matrix, *Acta Metall. Mater.*, **40**, (1992), pp. 477-485.

6. A. Vassel, M. C. Merienne, F. Pautonnier, L. Molliex, and J. P. Favre, A Method to Evaluate the Bonding Between Fiber and Matrix in Ti-Base Composite, Sixth World Conference on Titanium, Les Ulis Cedex, France, 1988, pp. 919-923.

7. Y. L. Petitcorps, R. Pailler, and R. Naslain, The Fiber/Matrix Interfacial Shear Strength in Titanium Alloy Matrix Composites Reinforced by SiC or Boron CVD Filaments, *Composites Science and Technology*, **35**, (1989), pp. 207-214.

8. P. Karpur, T. E. Matikas, and S. Krishnamurthy, Matrix-Fiber Interface Characterization in Metal Matrix Composites Using Ultrasonic Imaging of Fiber Fragmentation, *American Society for Composites*, Pennsylvania State University, University Park, PA, 1992, pp. 420-429.

9. T. E. Matikas, and P.Karpur, Matrix-Fiber Interface Characterization in Metal Matrix Composites Using Ultrasonic Shear-Wave Back-Reflection Coefficient Technique, *Review of Progress in Quantitative Nondestructive Evaluation*, **12B**, La Jolla, California, 1992, pp. 1515-1522.

10. T. E. Matikas, and P. Karpur, Ultrasonic Reflectivity Technique for the Characterization of Fiber-Matrix Interface in Metal Matrix Composites, *Journal of Applied Physics*, **74 (1)**, (1993), pp. 228-236.

11. P. Karpur, T. E. Matikas, M. P. Blodgett, D. Blatt, and J. Jira, Nondestructive Crack Size and Interfacial Degradation Evaluation in Metal Matrix Composites Using High Frequency Ultrasonic Microscopy, *ASTM Symposium on Special Applications and Advanced Techniques for Crack Size Determination*, Atlanta, 1993, (in print).

12. P. Karpur, T. Matikas, S. Krishnamurthy, and N. Ashbaugh, Ultrasound for Fiber Fragmentation Size Determination to Characterize Load Transfer Behavior of Matrix-Fiber Interface in Metal Matrix Composites, *Review of Progress in Quantitative NDE*, **12B**, La Jolla, California, July 19-24, 1992, pp. 1507-1513.

13. R. J. Kerans, and T. A. Parthasarathy, Theoretical analysis of the fiber pullout and pushout tests, *J. Am. Ceramic Soc*, **74 (7)**, (1991), pp. 1585-1596.

14. L. L. Mann, T. E. Matikas, P. Karpur, and S. Krishnamurthy, Supervised Backpropagation Neural Networks for the Classification of Ultrasonic Signals from Fiber Microcracking in Metal Matrix Composites, *IEEE Ultrasonics Symposium*, **1**, Tucson, Arizona, 1992, pp. 355-360.

15. C. F. Quate, A. Atalar, and H. K. Wickramasinghe, Acoustic Microscopy with Mechanical Scanning - A Review, *Proceedings of the IEEE*, **67**, (1979), pp. 1092-1114.

16. H. L. Bertoni, Rayleigh Waves in Scanning Acoustic Microscopy, *Rayleigh-Wave Theory and Application*, **2**, The Royal Institution, London, 1985, pp. 274-290.

17. K. K. Liang, G. S. Kino, and B. T. Khuri-Yakub, Material Characterization by the Inversion of V(z), *IEEE Transactions on Sonics and Ultrasonics*, **SU-32**, (1985), pp. 213-224.

18. J. R. Jira, and J. M. Larsen, Fatigue of Unidirectional SCS-6/Ti-24Al-11Nb Composite Containing A Circular Hole (Part II), *companion paper submitted to Metallurgical Transactions A, Carnegie Mellon University, Pittsburgh PA 15213 (Metall. Trans.)*, (1993), (in print).

19. R. John, J. R. Jira, J. M. Larsen, and N. E. Ashbaugh, Fatigue Crack Growth In Unidirectional SCS-6/Ti-24Al-11Nb Composite Containing A Circular Hole (Part II), *companion paper submitted to Metallurgical Transactions A, Carnegie Mellon University, Pittsburgh PA 15213 (Metall. Trans.)*, (1993), (in print).

20. D. Blatt, "Fatigue Crack Growth of Metal Matrix Composites Under Thermomechanical Loading", Ph.D. (under preparation), Purdue University (1993).

21. D. A. Stubbs, S. M. Russ, and P. T. MacLellan, Examination of the Correlation Between NDE-detected Manufacturing Anomalies in MMCs and Ultimate Tensile Strength of Thermomechanical Fatigue Life, *ASTM Second Symposium on Cyclic Deformation, Fracture and Nondestructive*

Evaluation of Advanced Materials, Miami, Florida, November 16-17, 1992, (in print).

22. G. A. Hartman, and S. M. Russ, "Techniques for Mechanical and Thermal Testing of Ti_3Al/SCS-6 Metal Matrix Composites", in *Standard Technical Publication 1032*(American Society for Testing and Materials, Philadelphia, 1989) pp. 43-53.

23. G. A. Hartman, and N. E. Ashbaugh, A Fracture Mechanics Test Automation System for a Basic Research Laboratory, *Applications of Automation Technology to Fatigue and Fracture Testing*, **ASTM STP1092**, 1990, pp. 95-112.

Metal Matrix Composites - Analysis of Simple Specimens and Model Components under Creep and Fatigue Loading

G.F. Harrison
B. Morgan
P.H. Tranter
M.R. Winstone

Defence Research Agency, Pyestock, Farnborough,
Hampshire, GU14 0LS, UK

1 SUMMARY

The paper presents the results of a limited test programme to establish the mechanical behaviour of titanium Metal Matrix Composite (MMC) laboratory specimens under tensile, Low Cycle Fatigue (LCF) and creep loading conditions at 600°C. Using a micromechanical model, finite element stress analyses have been undertaken to evaluate local stresses under the various loading conditions. Good agreement was obtained only after the inclusion of procedures to calculate the residual stresses induced in cooling from the composite consolidation temperature to the test temperature.

Additionally, as part of a collaborative component evaluation study, model discs manufactured by Rolls-Royce plc have been subjected to spin testing. These LCF results have been correlated via a macromechanical model which accounts for the orthotropic behaviour of the MMC reinforced region of the disc.

2 INTRODUCTION

Advanced aeroengine gas turbine designs require lighter and stronger materials capable of operating at temperatures above those experienced in current engines and beyond the capabilities of existing titanium and nickel superalloys. MMC's offer the design engineer the potential of stiffer, lighter materials capable of operating above the temperature limits of existing materials and hence provide the opportunity for radical innovative designs. Of all the identified aeroengine applications for MMC's, the components showing the greatest potential benefit are the compressor and turbine discs. In such components, material added outside the disc free hoop radius, although it may reduce local stresses in the rim or the blade, is not self supporting. Consequently inertia forces rise and the overall loadings increase. The conventional solution to this is to enlarge the cob region thus increasing overall disc weight. Design studies based on the use of MMC materials show that when a whole engine stage is replaced in MMC, weight reductions well in excess of 50% may be possible. Published design studies by Pratt & Whitney[1] indicate that rotor speeds in such components can be increased by up to 10%, gas path temperatures by up to 130 K and rotor weight reduced by up to 60% relative to current designs. In these designs, the large cross sections of conventional disc designs with their thick rims, long diaphragms and bulky cob regions are replaced by simple ring cross sections which incorporate circumferentially orientated silicon carbide fibres for reinforcement.

In addition to their potential in disc applications, the higher specific moduli of composite materials offer advantages for other lightweight component designs. The increased stiffness of reinforced titanium alloys is arousing interest in future large fan/aerofoil designs. The lower coefficient of expansion introduced by the fibres should also enable the improved maintenance of blade tip clearances and hence should lead to improved in-service efficiencies. Other possible uses include main engine and auxiliary power take-off shafts. These options offer significant benefits for overall improved performance. Nevertheless before they can be successfully introduced, considerable work still has to be done to ensure quality assurance, component integrity and to develop effective lifing methodologies.

3 METAL MATRIX COMPOSITE MATERIALS

MMC's may be manufactured by the fibre-foil route in which layered sequences of titanium alloy foil and silicon carbide fibres are consolidated via hot isostatic pressing. In this procedure significant debulking can occur and hence there is considerable scope for

Presented at an AGARD Meeting on 'Characterisation of Fibre Reinforced Titanium Matrix Composites', September 1993.

fibre movement. Various proprietary methods are used to minimise the effects but DRA has developed a highly successful Physical Vapour Deposition (PVD) technique in which the matrix alloy is deposited directly onto the fibre[2]. The coated fibre can be more easily handled and compacted with potentially less fibre damage, improved fibre distribution and higher fibre volume fractions. Although composite materials offer the direct weight savings discussed above, due to their different mechanical behaviour, these new materials cannot be used as direct substitutes in current metallic designs. Additionally, such future designs will require to be extensively evaluated because of the failure critical nature of the components involved, ie discs and blades. In this connection it has been necessary to develop both micromechanical modelling techniques which are being used to assess composite behaviour at the individual fibre matrix interface level and macromechanical techniques to translate the local fibre level response into bulk or global composite response within the surrounding material.

DRA has been in the field of advanced materials development and in particular PVD exploitation and MMC materials for some considerable time, but has only recently become involved in the mechanical assessment of these materials for engine component usage rather than as novel research alloys. To this end it is involved in collaborative testing and evaluation of MMC laboratory specimens and model components and sponsors research activities both within industry and UK Universities. The presentation will address the interpretation of the results of current testing and modelling activities at DRA and will briefly refer to some results from earlier sponsored work.

The material used in the laboratory testing programme is SiC fibre (SM1240)/Ti matrix (Ti 6-4) composite supplied by BP Metal Composites. A typical specimen cross section is shown in Fig 1. The measured fibre volume fraction was found to be nominally 34%. The material was supplied mostly as 6-ply unidirectional composite panels of nominal thickness 1.0 mm produced by vacuum hot pressing a lay-up of foil and fibre mats. The titanium foils were 100 μm thick and the fibres were produced by the Chemical Vapour Deposition (CVD) of SiC onto a 15 μm diameter tungsten filament to produce a final diameter of approx 96μm. Onto this is then deposited a 1.0 μm carbon coating followed by a 1.0μm hyperstoichiometric titanium boride (TiB_x x>2) coating, thus producing a final diameter of 100-101 μm. In this double coated form, the role of the carbon layer is to isolate the fibre and hence to minimise the formation of brittle high temperature reaction products. In addition this coating is considered to alleviate the effects of rough fibre surfaces and to reduce the overall scatter in fibre strength. The outer layer is intended to inhibit reactions between the matrix and the carbon. The model disc components were manufactured by Rolls-Royce plc from Textron SiC SCS-6 fibre reinforced Ti 6-4 monolayers.

4 SPECIMEN TEST PROGRAMME

Although the primary target for introducing metal matrix composites is directed at significantly lighter, higher temperature capability rotating components, it is essential to ensure that adequate ambient temperature properties are maintained.

The experimental programme included longitudinal and transverse loaded tensile testing at temperatures up to 600°C and repeated tension LCF and static creep testing at 600°C. The laboratory testing was conducted using a closed loop servohydraulic test machine with specially adapted water cooled hydraulic grips. Blanks were cut from unidirectional panels using electro discharge machining. Test pieces were ground to a final size of 150 mm x 12 mm and degreased prior to the attachment of aluminium or glass fibre tabs. The initial gauge length was set at 20 mm and extension was measured using a capacitance extensometer. Heating was achieved using a specially designed three zone platinum wound furnace capable of temperatures in excess of 600°C with a gradient along the gauge length of not more than 2°C. A continuous data logging system was used to monitor strain and load and an x-y recorder allowed stress-strain hysteresis loops to be plotted during the test.

The LCF tests used a triangular wave loading sequence to a constant maximum load and were conducted at 600°C and a frequency of 0.1 Hz.

4.1 Tensile Behaviour

The results of the tensile tests are summarised in Table I. Typical stress-strain responses for the longitudinal specimens are shown in Fig 2 and transverse specimen results in Fig 3[1].

4.2 Static Creep and High Temperature Low Cycle Fatigue Behaviour

Currently only the longitudinal testing at 600°C has been completed. Typical total strain-time responses are shown in Fig 4 and the lives to failure are presented as conventional creep rupture plots in Fig 5. For ease of comparison the times-to-failure of the high temperature LCF tests (at 0.1 Hz) are presented on the same figure. It can be seen immediately that even at 600°C and with a Ti 6-4 matrix which has an extremely poor creep resistance, the material is much more sensitive to cyclic rather than static loading.

5 FINITE ELEMENT MODELLING

Even the simplest unidirectional long fibre metal matrix composite components, show complex non-isotropic response to applied load. Unfortunately, it has been found to be computationally impractical to model individually the thousands of fibres present in 3-dimensional composite structures. To overcome this problem, combinations of micromechanical and macromechanical modelling have been developed. The reinforced metal matrix composite region is treated as a single composite block whose behaviour is determined by the material models developed to characterise the response of individual fibres and small groups of fibres in their matrix material.

The unit cell used in the micromechanical modelling used dimensions compatible with the material shown in Fig 1. In the current stress analysis the coating/fibre interface has not been modelled separately and for the longitudinal tests the coating/matrix interface is assumed to be a perfect bond. The MARC non-linear finite element code was used for the stress analysis and generalised plane strain elements were used. Appropriate boundary conditions were applied to the model edges to simulate a regular distribution of fibres and matrix.

In modelling the transverse tests, the fibre matrix interface is taken to be extremely weak and matrix flow around the fibres and the associated shear forces are assumed to be controlled by the friction coefficient of the surfaces. It has been established that the value selected for the friction coefficient did not have a significant influence on the results and a value of 0.1 was selected in subsequent analyses. Special gap elements were used to represent the interface and to prevent surface interpenetration.

At the outset it was recognised that in cooling down from the fabrication temperature, the large differences in coefficients of thermal expansion between the fibre and the matrix will lead to thermal strains and stresses and that on cooling, significant residual stresses can be present in the composite. Hence, in order to model the tensile tests, it was necessary to calculate the level of the induced thermal stresses using a thermal loading option and temperature dependent tensile and thermal expansion data. Residual stress levels are highly temperature dependent and at 20°C the maximum axial stress in the matrix is calculated to be about 380 MPa with a corresponding compressive residual fibre stress of about 840 MPa. In the analysis of the creep and high temperature LCF tests, a user defined creep option was employed. For the matrix material, a standard Norton type creep law was employed with material specific values for the equation constants taken from Nimmer[4]. In addition, for the transient loading cases, a strain hardening equation of state was applied. In all the analyses the silicon carbide fibres were assumed to behave elastically throughout the loading sequences.

6.0 ANALYSIS OF RESULTS

6.1 Longitudinal Tension

In Fig 6, the predicted longitudinal behaviour is compared with the experimental stress-strain curve of Fig 2. It can be seen that agreement is satisfactory. As shown in Table I, over the temperature range 20° to 600°C the simplest analysis, namely the rule of mixtures, accurately models the temperature dependent composite moduli. At 20°C, yielding initiates at very low strains due to the high matrix tensile residual stresses followed by the almost linear response of the MMC as progressively more of the load is carried by the fibres. In the DRA analysis which includes the residual stress distribution associated with the original cooling down from the consolidation temperature, the results suggest that the matrix material does indeed yield close to the identified knee. In complementary work supported by DRA[5], a series of tests were performed in which the specimen was loaded to strain levels of 0.2%, 0.4%, 0.6% and 0.9% and unloaded before proceeding to the higher strain levels. The measured elastic modulus was found to decrease progressively although the measured values were found to be approximately 10% lower than the predicted modulii. This is now attributed to the effects of fibre breakage such that as the load carrying capability of the fibres is compromised this is reflected in the observed reduced stiffness. At 600°C although the residual stress levels are very low, the response is similar to that observed at lower temperature since the matrix yield stress at this temperature is also significantly lower than at 20°C.

6.2 Transverse Tension

The predicted stress-strain curves under transverse tension and the corresponding test data are shown in Fig 7. In the complementary work referred to earlier[5], unloading and reloading tests similar to those described by Johnson[6] and by Nimmer[4] were conducted in order to investigate coating/fibre interface debonding. On first loading, the knee in the stress-strain loading curve is attributed to the applied stress necessary to overcome the interfacial bond strength. On subsequent loadings the knee occurs at lower applied stress levels and the difference in these values is attributed to the magnitude of the interfacial bond strength. Taking into account the maximum interfacial radial stress concentration factor of 1.4, this gives an interfacial strength of approximately 50 MPa. This is in reasonable agreement with the room temperature value of 67 MPa obtained for Ti 6-4/SiC by the micro hardness push out test[5].

6.3 Static Creep

The 600°C longitudinal static creep tests have been analysed using a Norton exponential creep law with values for the material specific constants taken from work of Nimmer[4]. Currently tests are being completed to enable analysis using the standard DRA Graham and Walles techniques[7]. The application of this titanium creep equation in a creep micromechanical analysis allows the rate of stress redistribution within the composite to be identified. Fig 8 shows predictions of typical peak maximum Von Mises stress distributions in both the matrix and the fibre during the test. For the same loading conditions, in Fig 9, stress distributions are shown for time zero (t = 0) and for time just prior to failure $(t = t_f)$. In Table II the fibre stresses at initial loading and at creep rupture are identified for the 4 creep tests at 600°C.

6.4 High Temperature Low Cycle Fatigue

Table III provides initial and final stresses for the four fatigue loaded tests. Comparison with table and examination of Fig 5 show that despite the poor creep resistance of the Ti 6-4 matrix material, even at 600°C the MMC is significantly poorer under LCF loading at 0.1 Hz than under the static loading associated with creep. The MMC response to fatigue loading is considerably more complex than to creep loading and Fig 10 shows typical stress-strain responses in a) the fibre and b) the matrix during selected triangular loading cycles predicted as the test progresses. The predictions were achieved using the micromechanical model and assuming the matrix creep model and strain hardening hypothesis.

Table III also shows that immediately prior to failure the nominal stress levels in the remaining ligaments have increased due to cracks propagating from the specimen edge. Full transient analyses of the stress redistributions, in which it is necessary to take account of concentration effects at the tip of the cracks, have not yet been completed. However, simple calculations based on the final applied stresses yields fibres stresses close to their tensile limit.

7 METALLOGRAPHY OF FAILURE PROCESSES UNDER CREEP AND LCF LOADING

The micrograph in Fig 11a shows a typical creep failure region in a creep test at a stress of 750 MPa and a test temperature of 600°C. Fig 11b is a longitudinal section through the fracture surface. It can be seen that fibre cracking is extensive and occurs at relatively regular intervals along the fibres. In some places it appears that significant interface debonding leads to large local fibre movement and in such cases this is sufficient to alleviate the requirements for the regular cracking observed elsewhere. Away from the fracture surfaces, as shown in Fig 11c, only the regular fine cracking is observed.

With regard to LCF loading, Fig 12a shows a typical failure (700 MPa at 600°C). It can be seen that there is significantly less fibre pull-out than for creep loading. This is clearly shown in Fig 12b which is a section through the crack initiation region. This micrograph also illustrates that with crack initiation under fatigue loading, fibre cracking is limited to the crack plane but just prior to final failure more widespread multiple cracking of the fibres occurs. Again, in contrast to the creep situation, as illustrated in Fig 12c, away from the immediate vicinity of the cracking plane, fibre cracking does not occur. Thus, it is now suggested that when the matrix experiences only limited plasticity, fibre breakage will be slight and additionally the shear stresses around the ends of the broken fibres will be able to reload the fibres to their full stress levels in very short lengths. However with greater matrix yielding (or nonlinear deformation), the shear stresses around the fibre breaks are more dispersed and hence a longer end length is required to reload the fibres. Fig 12d confirms that even at 600°C, cracks within the matrix show typical fatigue growth.

These findings are consistent with the results of the stress redistribution analyses and suggest that final metal matrix composite failure at elevated temperature is associated with fibre overload and that environmental degradation makes only secondary contributions to the failure event although it may be important in the development of crack initiation and early growth.

8 MODEL DISC

Fig 13 is a photograph of the Rolls-Royce plc metal matrix composite model disc which was tested in the DRA disc spinning facility. The "top-hat" areas above the lobes being simply for attachment to the spin rig and the lobes being dimensioned to provide appropriate loadings. The inner ring between the lobes and the bore surface contains the reinforcement and was manufactured with the fibres lying in the hoop direction. The ring was consolidated and diffusion bonded to the Ti 6-4 material used in the remainder of the disc.

8.1 Test Results

An overspeed disc burst test was undertaken to assess the strength of the material in a representative component form and to confirm that basic laboratory specimen tensile properties can be maintained. The burst speed of 26,700 rpm was achieved after about 30 seconds. The cyclic tests were conducted at 3 cycles per minute and the tests were continued until complete failure of the disc. Based on average room temperature tensile failure data on SCS-6/Ti 6-4, the disc showed a 7% higher than predicted burst speed. Under such loading conditions, radial and axial stresses are low and failure is dominated by circumferential hoop stresses.

In Fig 14, the disc spinning LCF results are indicated in conjunction with room temperature longitudinally loaded metal matrix composite minimum property data supplied by Rolls-Royce plc. It can be seen that the disc results are typical of average laboratory data indicating that the disc manufacturing route has had no detrimental effect on the material.

8.2 Stress Analysis

Since it is not practical to model every fibre individually a global analysis model has been developed. In this approach the component model treats the metal matrix composite area as a homogeneous orthotropic material with circumferential and radial/axial materials data supplied from the specimen elasto-plastic micromechanical model used to characterise the composite response to both longitudinal and transverse loading. Currently analysis of the reinforced region is limited to the elastic case with an elasto-plastic capability used for the remainder of the disc. The repetitive symmetry of the disc design required only a 1/24th segment to be modelled. Standard "cake-slice" boundary conditions were applied (hoop displacements constrained to radial planes of the slice faces).

To aid in the assessment of this reinforced disc, a theoretical overspeed analysis was performed on an equivalent monolithic Ti 6-4 disc which predicted an initial yield speed of 17,760 rpm. In the reinforced disc, the orthotropic macromechanical analysis predicts yielding at a similar location is delayed until a speed of over 22750 rpm although a full elasto-plastic analysis would predict a lower value for MMC matrix yielding.

Although the material has been identified primarily for elevated temperature applications, the analyses also indicate that even at room temperature there is a significant advantage of the composite over base matrix material behaviour. Fig 14 also includes some room temperature LCF specimen results for Ti 6-4 for comparison. Indeed, at the same rotational speed, the lower density metal matrix composite disc is calculated to have about a 10% lower 'average' stress level or alternatively, for the same 'average' stress level an MMC disc can be run about 7% faster.

9 IMPLICATIONS FOR FUTURE COMPONENT DESIGNS

The correlation between the disc spinning results and laboratory LCF data is encouraging and allows general conclusions on component behaviour to be drawn from 600°C laboratory LCF results. The data presented in Fig 5, has been reanalysed in terms of cycles to failure and has also been added to this figure. It can be seen that for usable lives of about 10^4 cycles to failure there is only about a 10% fall in material capability relative to 20°C behaviour.

The inherent fatigue resistance in the maximum principle hoop direction is highly encouraging although problems may arise from environmental interactions, coating fibre interface reactions and design problems associated with disc and blade attachment. The immediate problem now being addressed at DRA is the high temperature transverse loading capability of the material since maximum principle radial stress levels could be a design limitation.

10 FINAL COMMENTS

Conventional FAA and JAR 'safe life' regulations are based on the life-to-first-engineering-crack concept and are clearly inappropriate for composite components. However, the adoption of damage tolerant methodologies, in which the life declared is based on the release of a portion of the identified safe crack growth life, do appear to hold certain attractions. In such a damage tolerant lifing approach it will be necessary to identify, either from proven process control or by inspection, a maximum initial flaw size that may never be exceeded in a component. Available results suggest that if initial levels of stress intensity range can be kept sufficiently low, even in the presence of defects, eventual crack arrest may still occur. In service, thermal stress effects are always likely to be present and will therefore have to be considered in conjunction with traditional mechanical loading to ensure that fatigue failure of the fibres would not eventually occur. Nevertheless it is tempting to suggest that such materials could provide the opportunity for truly damage tolerant designs.

ACKNOWLEDGEMENTS

The authors gratefully acknowledge the supply of the MMC discs by Rolls-Royce plc as part of a collaborative programme and useful discussions with M Hartley and P Doorbar of Rolls-Royce plc.

REFERENCES

1 T E Farmer, "Damage tolerance concepts for advanced engines", AIAA-88-3165, 24th Joint Propulsion Conf, Boston (1988)

2 P G Partridge & C M Ward-Close, "Processing of advanced continuous fibre composites: current practice and potential developments", *International Materials Reviews, 38*, No 1 (1993)

3 A J Yarrow, "The development of mechanical test methods for fibre reinforced titanium matrix composites", DRA report TR93042 (1993)

4 R P Nimmer et al, "Micromechanical modelling of fibre/matrix interface effects in transversely loaded SiC/Ti 6-4 metal matrix composites", *Jnl of Composites Technology & Research, 13, No 1,* 3-13 (1991)

5 D S Li & M R Wisnom, "Micromechanical modelling of unidirectional fibre reinforced titanium matrix composites", *University of Bristol,* DRA Contract Final Report (1992)

6 W S Johnson, "Damage development in titanium metal matrix composites subjected to cyclic loading", Fatigue and Fracture of Inorganic Composites, Cambridge (1992)

7 G Harrison & G Tilly, "The static and cyclic creep properties of three forms of a cast nickel superalloy", Int Conf on Creep and Fatigue in Elevated Temperature Applications, ASME (1973)

© British Crown Copyright
1993 / DRA
Published with the permission of
the Controller HMSO

Fibre Orientation	Temperature °C	Modulus		Tensile Strength MPa	Failure Strain %
		Measured	Rule of Mixtures		
0°	20	200	210	1612	0.98
	300	196	-	1348	0.82
	600	191	188	1093	0.74
90°	20	165	210	499	1.0
	600	108	188	156	>2.5

Table I Summary of longitudinal and transverse tensile data for the Metal Matrix Composite SiC/Ti 6-4

Nominal Applied Stress MPa	Predicted Fibre Stress at $t=0$ MPa	Predicted Fibre Stress at $t=t_r$ MPa
750	1643	2264
800	1758	2400
830	1841	2412
870	1940	2395

Table II Maximum initial and final fibre stresses under creep loading at 600°C

Peak Applied Stress MPa	Reduction in Area at End of Test %	Nominal Reduced Area Stress MPa	Initial Fibre Stress from FEA MPa	Calculated Final Fibre Stress MPa
645	12	722	1380	1800
700	8	753	1513	1897
790	5	831	1738	2127
885	5	931	1978	2413

Table III Initial and final fibre stresses under Low Cycle Fatigue loading at 600°C

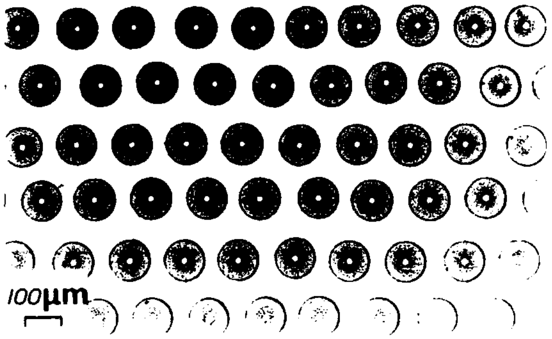

Fig 1 Typical fibre distribution in SiC/Ti 6-4

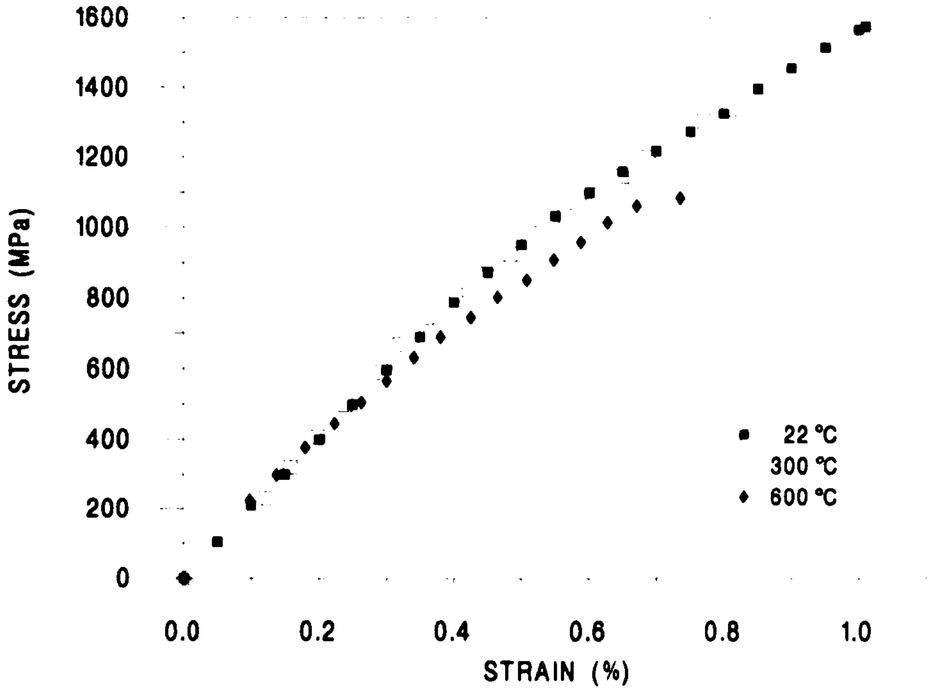

Fig 2 Tensile behaviour of longitudinally loaded specimens at temperatures up to 600°C

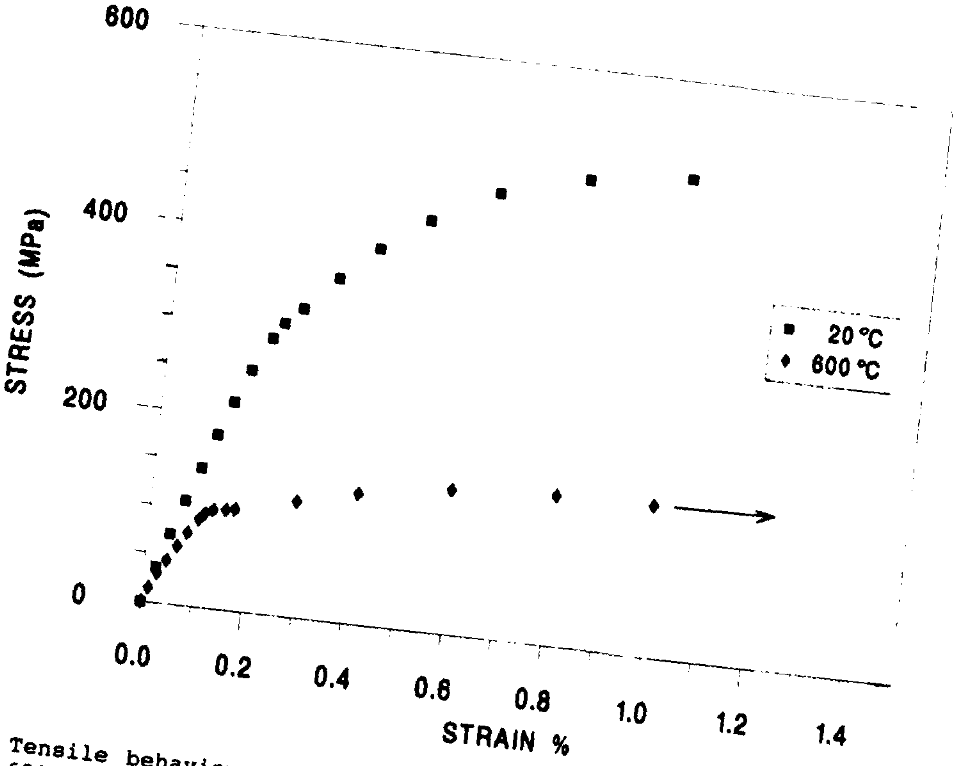

Fig 3 Tensile behaviour of transversely loaded specimens at temperatures up to 600°C

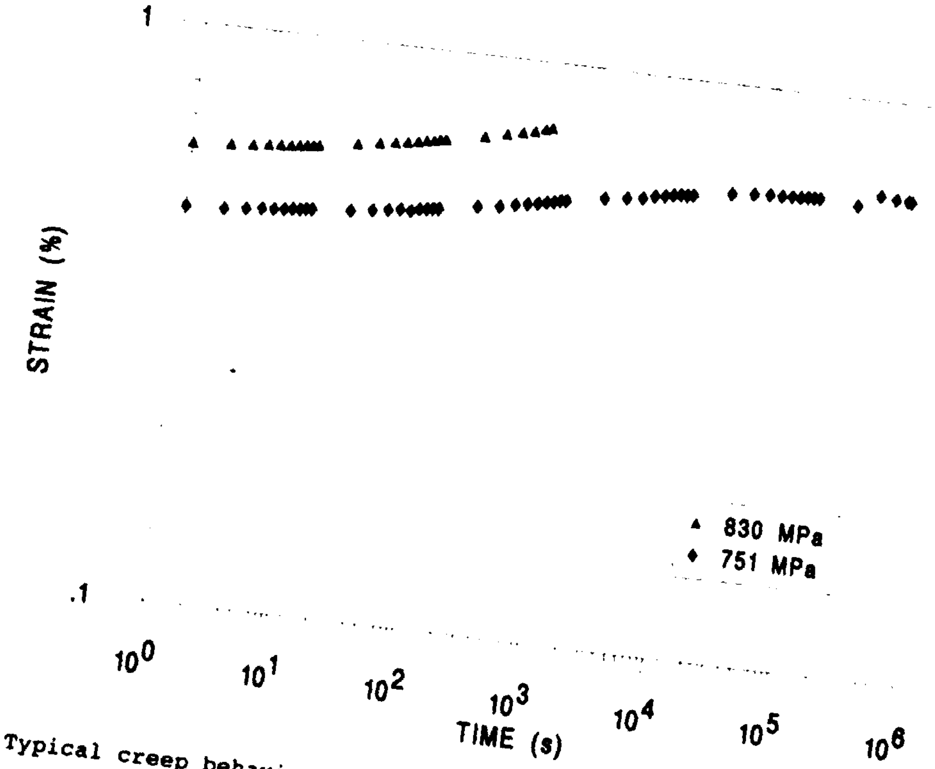

Fig 4 Typical creep behaviour under longitudinal loading at 600°C

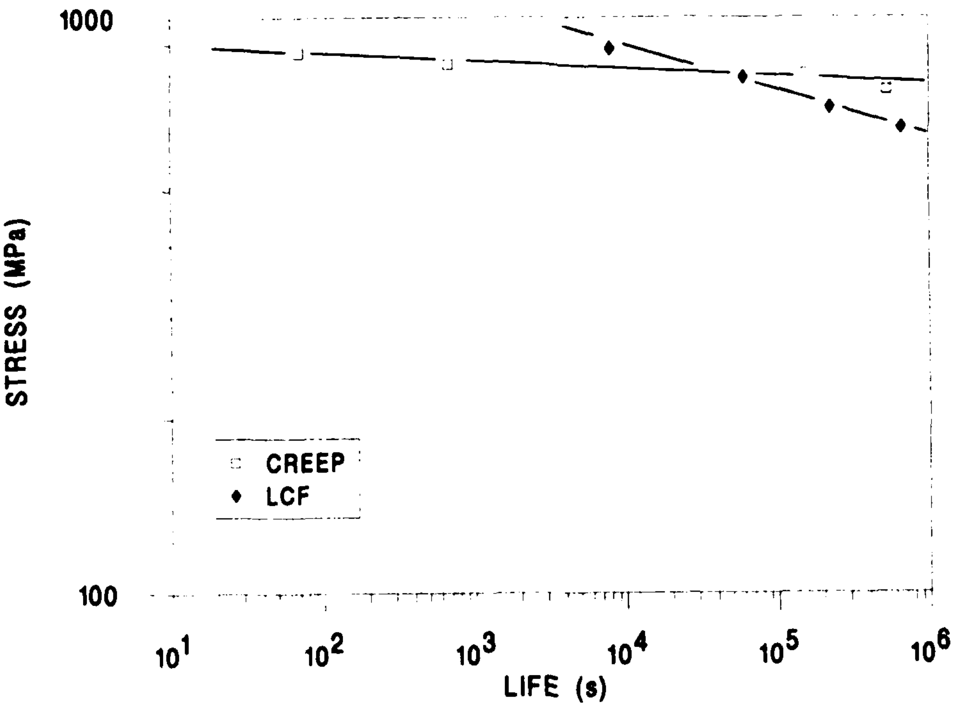

Fig 5 Creep rupture and LCF (0.1 Hz) lives at 600°C

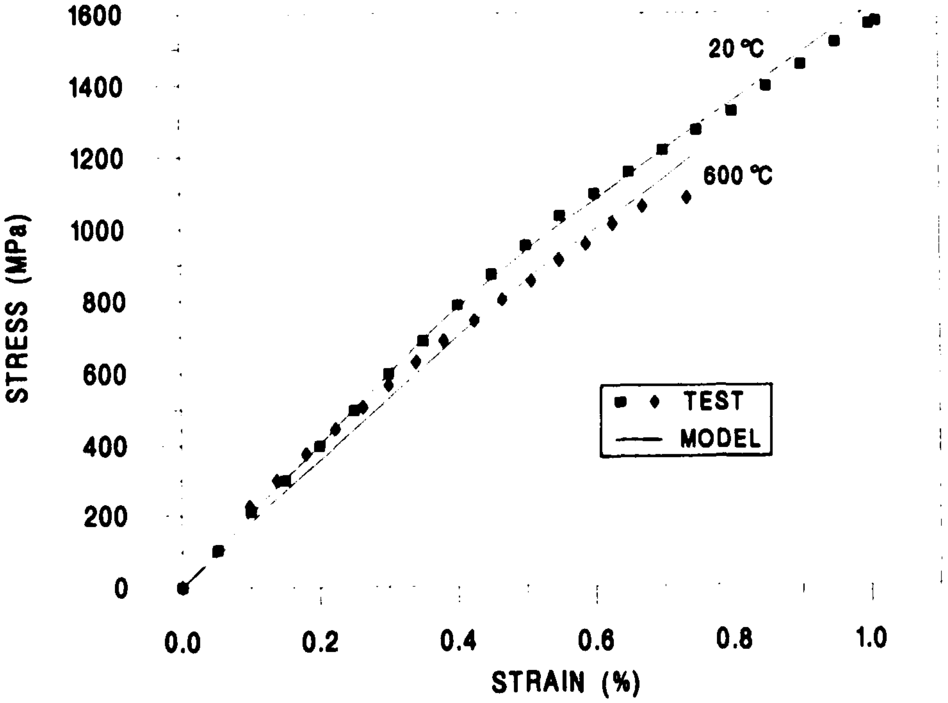

Fig 6 Comparison of experimental and predicted tensile behaviour for longitudinal loading at 20 and 600°C

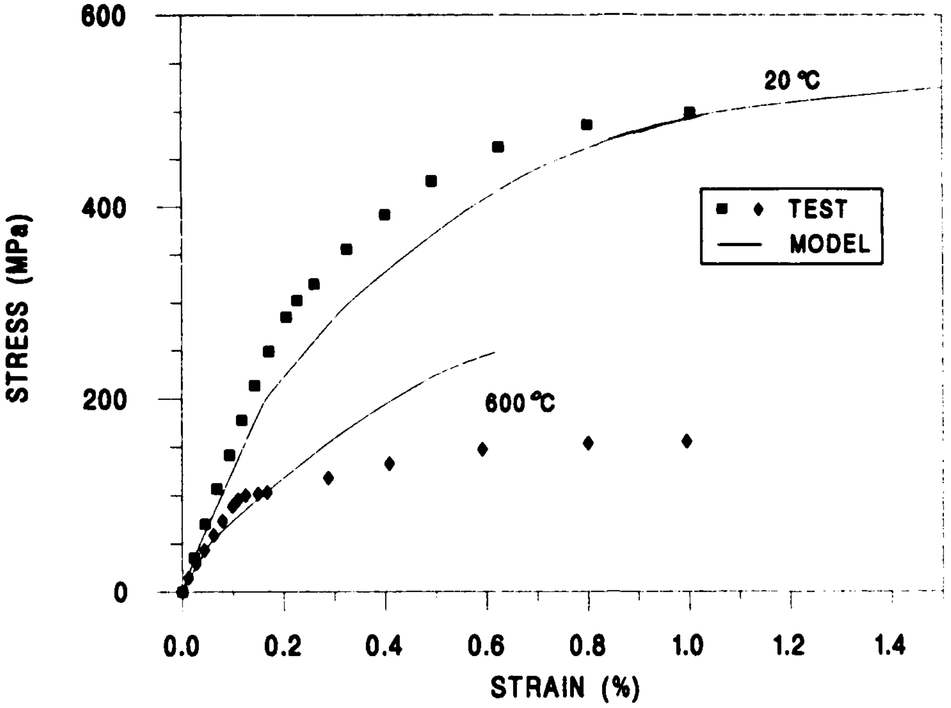

Fig 7 Comparison of experimental and predicted tensile behaviour for transverse loading at 20 and 600°C

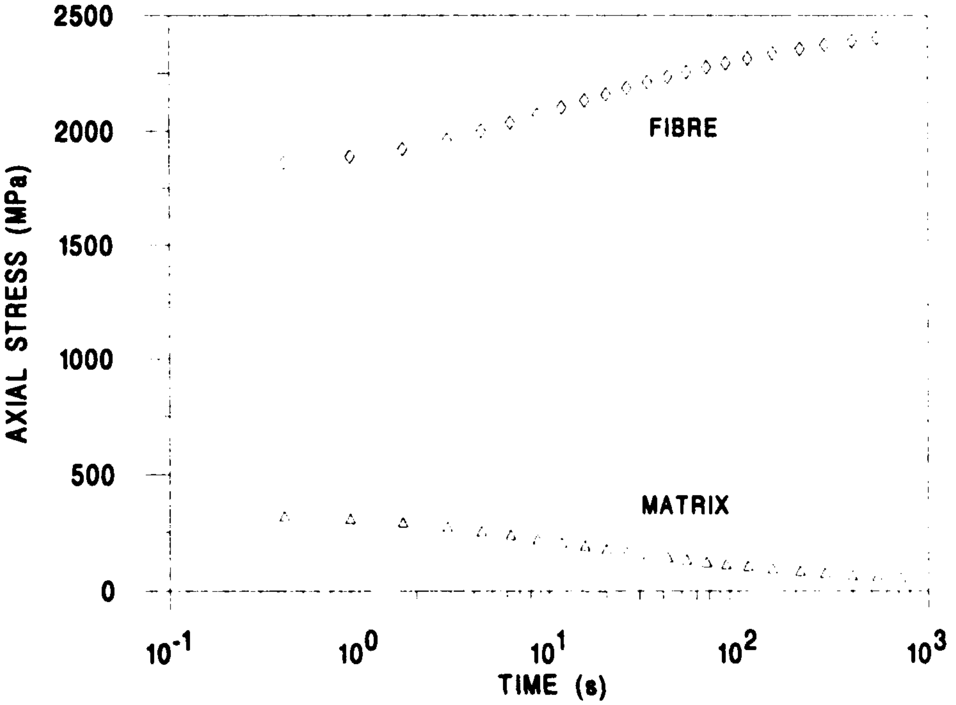

Fig 8 Typical predicted peak axial fibre and matrix stress variation during a creep test (830 MPa and 600°C)

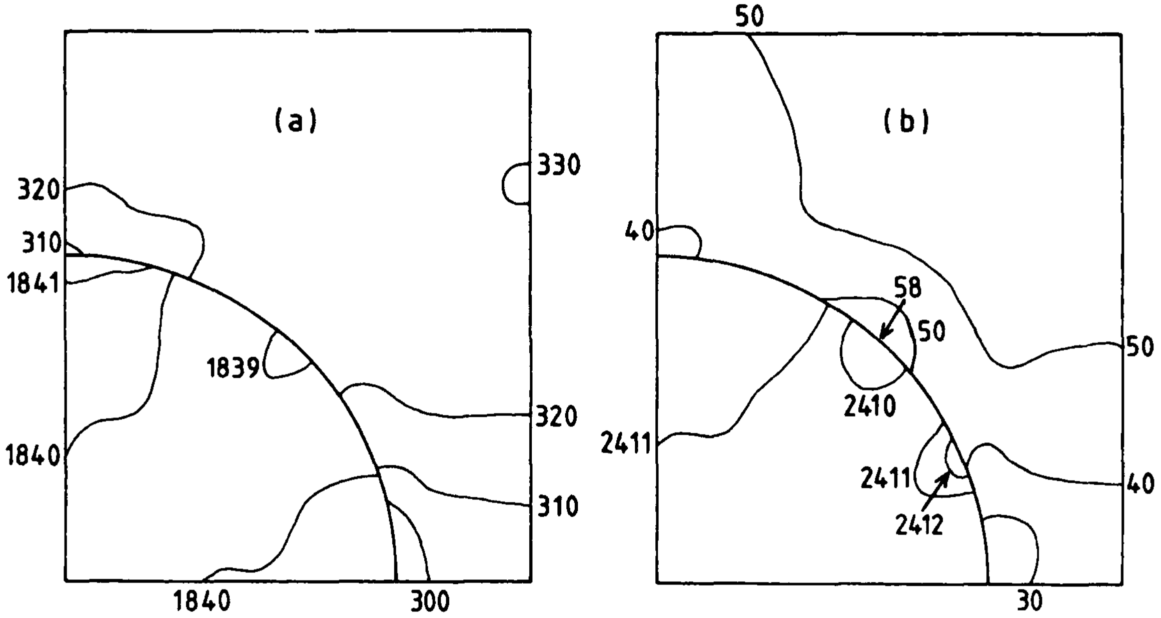
(a)
320
310
1841
1839
1840
330
320
310
1840
300
(b)
50
40
58
50
50
2410
2411
2411
2412
40
30

Fig 9 Predicted axial stress distributions at a) time = 0 and b) time = just prior to rupture (830 MPa and 600°C creep test)

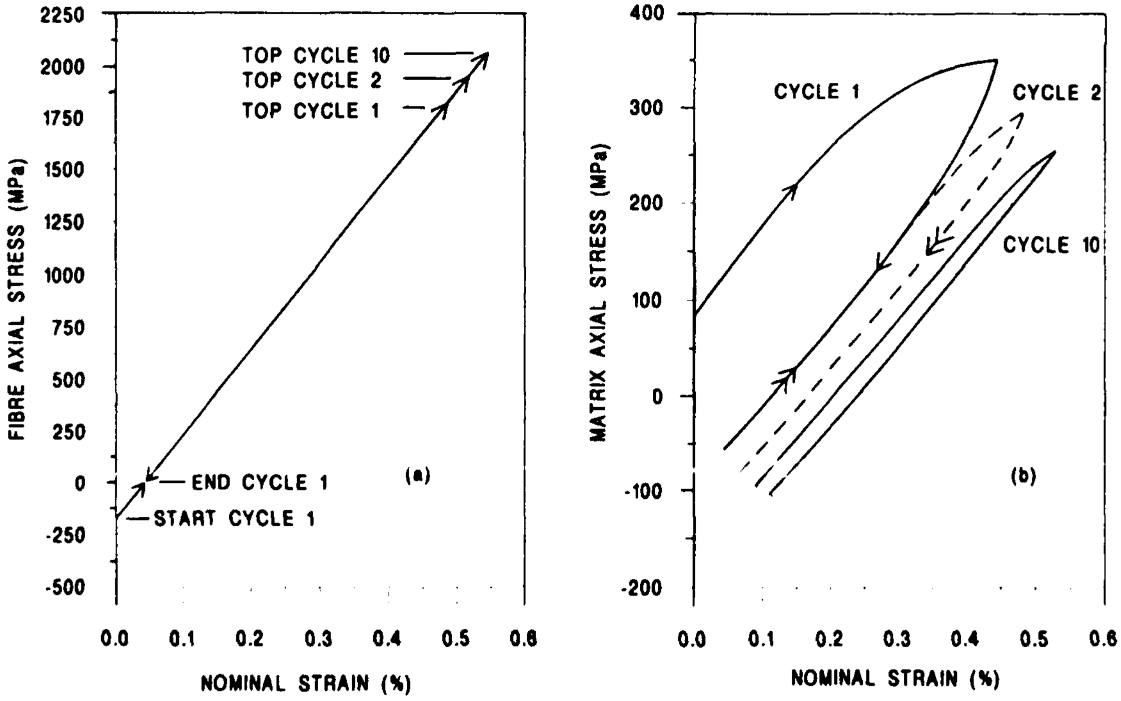

Fig 10 Predicted peak stress-strain responses in a) the fibre and b) the matrix for selected cycles during 790 MPa triangular LCF test at 600°C

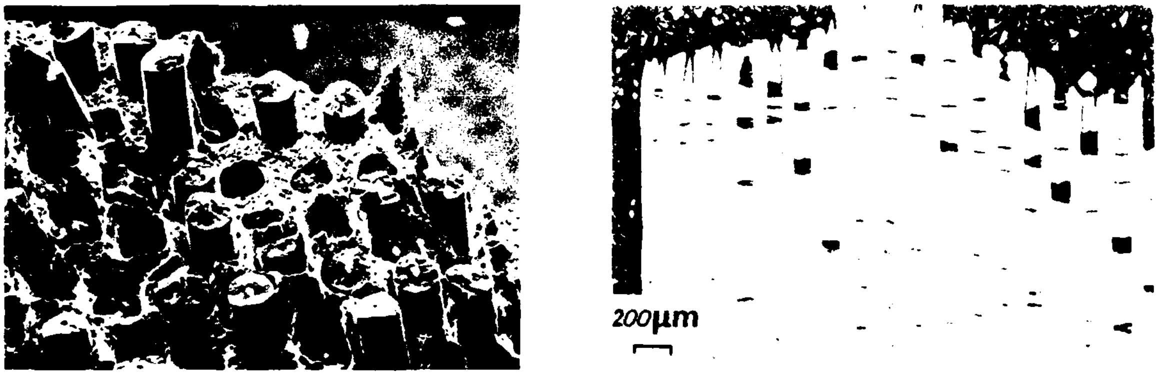

a) Typical creep fracture surface

b) Cross-section through typical creep fracture surface

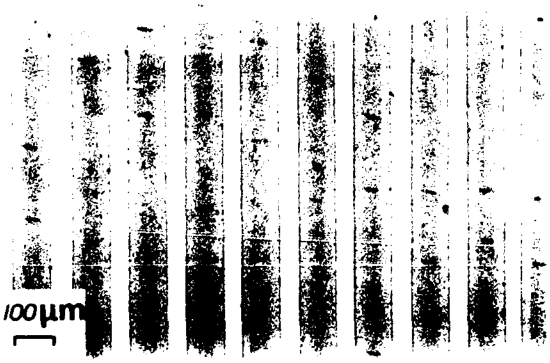

c) Cross-section through creep specimen at a site more than 1 cm below the fracture surface

Fig 11 Typical creep failure in specimen tested at 600°C

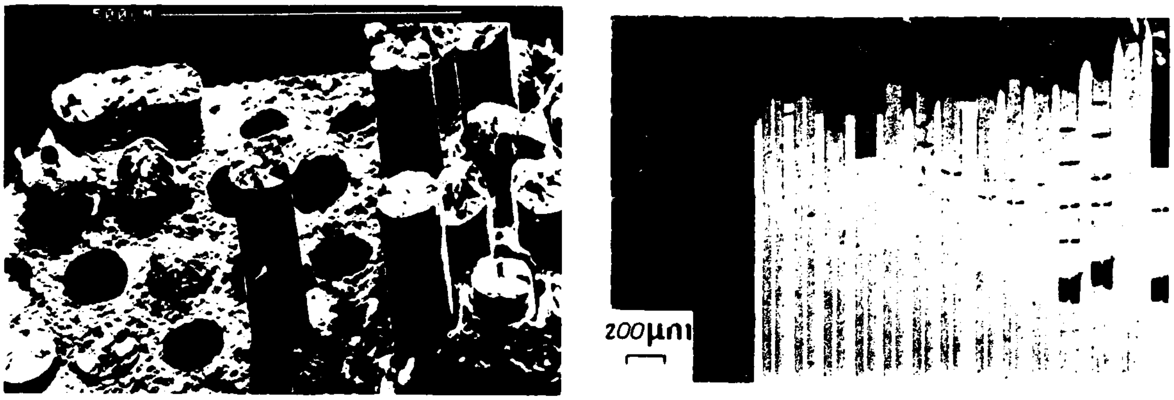

a) Typical fatigue fracture surface (crack initiation site)

b) Cross-section through typical LCF fracture surface

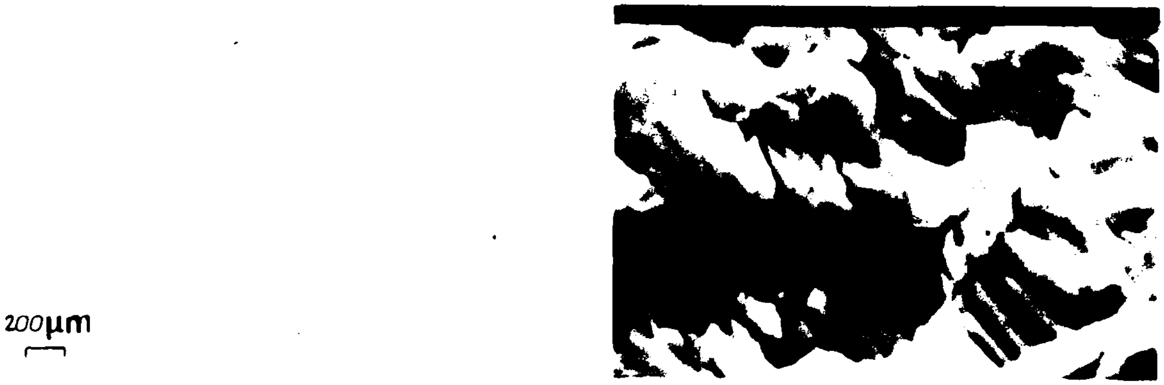

c) Cross-section through LCF specimen at a site 1 cm below the fracture surface

d) Fatigue striations found in matrix material

Fig 12 Typical fatigue failure in specimen tested at 600°C

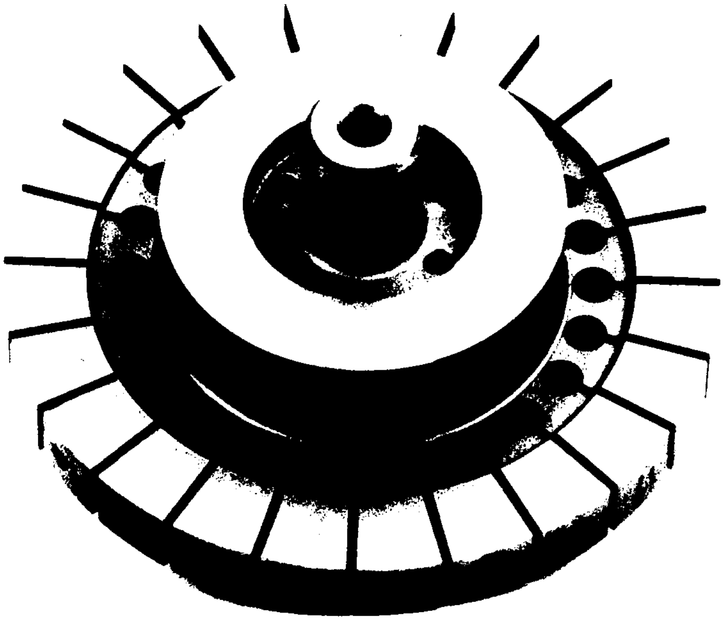

Fig 13 View of model disc manufactured by Rolls-Royce plc

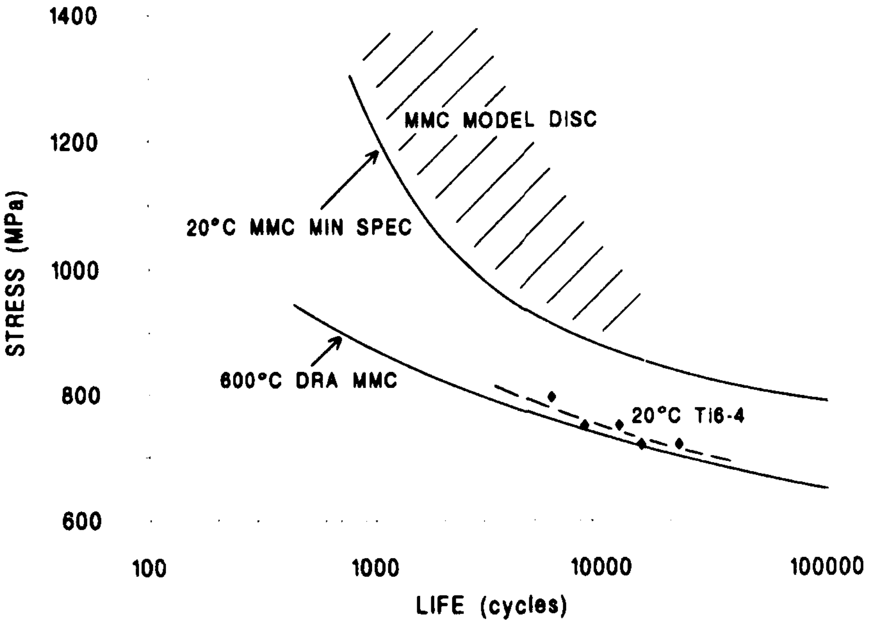

Fig 14 20°C LCF data for MMC specimens with minimum disc data and some typical Ti 6-4 data superimposed

RESIDUAL STRENGTH AND LIFE PREDICTION TECHNIQUES FOR Ti MMC

by

J. Harter
Wright Laboratory
Wright-Patterson AFB
Dayton, OH 45433-7817
United States

D. Harmon
McDonnell Douglas Corporation
McDonnell Aircraft Company
St. Louis, MO

R. Post
CSA Engineering
Palo Alto, CA

SUMMARY

To date, the fatigue crack growth behavior of metal matrix composites (MMC) has been generally limited to data obtained from relatively small coupons (approx. 150mm x 25mm). Although self similar crack growth has been observed in some cases, many observers have noted various complex crack growth phenomena. Behaviors such as fiber bridging and extensive crack branching have been reported in several papers (Ref 1-4). The purpose of this paper is to present the results of several static and crack growth tests on larger titanium based MMC center cracked coupons (406mm x 63.5mm). The use of larger specimens has allowed for more observations during stable crack growth and is much more representative of actual applications.

LIST OF SYMBOLS

σ	stress
σ_f	fiber stress
σ_{ult}	ultimate stress
da/dN	crack growth rate
ΔK	stress intensity range
R	min to max stress ratio
CCT	center cracked tension

1 INTRODUCTION

To date, nearly all material characterization testing for titanium matrix composites (TMCs) has been conducted using relatively small specimens (approx. 150 x 25 mm). This is primarily due to cost and availability issues. As part of an effort to characterize the damage tolerance of MMCs, the United States Air Force Flight Dynamics Directorate is conducting a program using larger test specimens. The goal of the effort is to obtain damage tolerance data for Beta 21s/SCS-6 MMC and develop a realistic life prediction model for room and elevated temperature use. The project is well underway and room temperature data are available for both [0/90]s and [0/±45/90]s laminates.

2 TEST PLAN AND PROCEDURES

The room temperature test plan is given in TABLE 1.0. As may be seen, the matrix is fairly small owing to the cost and availability issues noted above. Static and crack growth testing was conducted on MTS servo-hydraulic testing machines using state-of-the-art, low noise analog controllers. The first tests were conducted on small (150 x 19 mm) coupons to determine ultimate strength of the [0/90]s and [0/±45/90]s laminates. The results are shown in TABLE 2.0. A vacuum aging procedure was planned for the larger test specimens and crack growth tests were performed on small edge cracked specimens (approx. 150 x 25 mm) to determine the effect of the aging process. The specimens were sent to Refrac Systems, Phoenix, AZ for aging. The aging process was: 621 degrees C for 8 hours at less than 1.0E-04 Torr. The test showed at least a factor of four (4) improvement in crack growth life on the edge crack specimens. An image of one of the edge cracked specimens is given in FIGURE 1.0.

Crack growth testing for the larger specimens (406 x 63.5 mm) was performed at a cyclic frequency of four (4) Hz. A typical specimen is shown in FIGURE 2.0. Electric potential drop monitoring techniques were used to provide a means of crack length monitoring, however, visual measurements were taken at approximately 0.5 mm intervals as monitored. The electric potential drop method was used only to place a test on hold for a visual measurement. The method proved to be unreliable compared to visual methods and was never used to record crack lengths. Visual measurements were made using a microscope and graduated mylar tape above the crack plane. The tape was graduated to 0.127 mm. The crack length vs. cycle data were curve fit to obtain smoothed data at approximately 0.05 mm crack length intervals. These smoothed data points were then used to determine the da/dN vs. ΔK data. In all cases, the secant method was used to determine da/dN. The corresponding ΔK values were calculated using the classic center cracked plate solution with the secant finite edge correction at the midpoint of two adjacent data points. An example of the smoothing technique may be seen in FIGURE 3.0. It should be noted that in cases where crack growth extension at a given load level was slowed due to apparent fiber bridging, the load level was

Presented at an AGARD Meeting on 'Characterisation of Fibre Reinforced Titanium Matrix Composites', September 1993.

increased to overcome the effect. The testing was performed over a five day week, 24 hours a day; however, test support was not available over weekends. Tests were not conducted over weekends due to potentially long hold times and potential power (electric and/or hydraulic) failures. In certain cases, loads were increased as many as two (2) times during the test to meet the five (5) working day time constraint.

3 RESULTS

The results of the ultimate strength tests are given in TABLE 2.0. The results tend to agree with results obtained for these laminates by other investigators (Ref 5).

The results of the room temperature crack growth rate testing were extremely significant. The specimens were large enough to show stable crack growth prior to failure. Data shown in FIGURE 4.0 compares the results between raw and smoothed data for a typical test. The smoothed data provides a much clearer view of the crack growth behavior of the material. A composite plot of da/dN vs. ΔK for the [0/90]s laminate is presented in FIGURE 5.0. Data are available for R = 0.05, 0.3, and 0.5. Originally, six (6) tests were planned, however, an accidental overload occurred in one of the R=0.3 tests which caused the loss of one of the fragile 4 ply specimens. A composite plot for the [0/±45/90]s laminates is given in FIGURE 6.0. A sufficient quantity of the eight (8) ply material was available so that spare specimens were used as required. In this case, an extra test was performed for R=0.05. Although the data are limited, especially in the case of the [0/90]s data, several features should be noted. First, apparent fiber bridging is indicated where da/dN is decreasing with increasing ΔK. Second, the "bridging" effect is repeated, as expected, after the maximum applied load was increased. The decreasing apparent ΔK effect is preceded by a noticeable rate increase. The magnitude of the increase is variable, but consistent. Load increases are indicated where there is a discrete jump in the value of ΔK for a given set of data points. Finally, one of the most interesting trends from the data is the stable crack growth region where no fiber bridging is apparent. This is clearly visible in FIGURE 6.0. The data in this region is typical of what is seen in isotropic materials where self similar crack growth is the standard. The data seems to support the existence of "laminate" fracture toughness.

4 DISCUSSION

A significant amount of crack growth rate testing has been conducted on Beta 21s/SCS-6 material. Almost all of the testing has been performed on very small specimens (25mm wide or less). While fiber bridging has been noted by several investigators (Ref 1), the region of stable crack growth seen in these tests would be difficult to observe in small specimens.

Previous experimental studies on Ti-15-3/SCS-6 have indicated that MMCs, in general are notch insensitive (Ref 6). Room temperature crack growth tests were performed where cracks have extended completely through the matrix with no fiber failures. When residual strength tests were performed on the specimens, the result correlated very well with the fiber ultimate strength (σ_{ult} - when corrected for fiber volume and number of zero degree plies). This indicates that it may be relatively easy to obtain engineering approximations to fiber stresses in these types of materials and then apply the results to determine an effective ΔK.

$$\Delta K_{eff} = \Delta K_{applied} - \Delta K_{bridged}$$

The data in figures 5.0 and 6.0 show spikes in all data sets in varying degrees. Observations made during the tests seem to indicate that these "spikes" are due to crack arrest mechanisms inherent in MMCs. Prior to the spikes, the cracks showed very little opening displacement from visual observation. At the times when these "spikes" occurred, the cracks were open enough at maximum load to show fibers. A weak fiber/matrix interface strength could provide a sufficient damping effect to a propagating fiber failure. It is reasonable to assume that a material with a strong fiber/matrix interface would exhibit notch sensitivity AND much lower fracture toughness (without these spikes). More information is clearly required.

Crack growth in the stable region was accompanied by regular noise from the specimens. The noise was clearly audible as a snapping type of sound - failing fibers. The fibers were apparently failing as the crack progressed. It is easy to suggest that the local fiber stresses (σf) exceeded their ultimate strength (σ_{ult}) as the cracks grew around them. However, this is only based on the regularity of the sounds and the fact that no further da/dN reductions were seen.

5 CONCLUSIONS

The fiber bridging effect is certainly at work in this case. Future work is required to develop an engineering solution to the issue of an effective ΔK on a macroscopic level. Work is underway to perform additional tests on the material using strain gages in the crack plane to monitor changes in deflection before and after significant fiber failures. These data may provide the information needed for the engineering solution.

These data show very clearly that this material exhibits a "laminate" fracture toughness value. This is very important in the determination of residual strength and life for these types of MMCs.

REFERENCES

1. Marshall, D.B., Cox, B., and Evans, A.G., "The Mechanics of Matrix Cracking in Brittle Matrix Fiber Composites", Acta Metalurgica, Vol 11, pp. 2013-2121, 1985.

2. John, R., Kaldon, S.G., and Ashbaugh, N., "Applicability of Fiber Bridging Models to Describe Crack Growth in Unidirectional Titanium Matrix Composites", Titanium Matrix Composites Workshop, La Jolla, CA, 2-4 June 1993.

3. Ahmad, J., and Santhosh, U., "An Estimate of the Effect of Fiber Bridging on Crack Driving Force", WL-TR-92-4035, 1992.

4. Jira, J.R., John, R., Larsen, J.M., and Ashbaugh, N.E., "Notch Fatigue and Crack Growth in Titanium Matrix Composites", NIC Steering Committee Meeting, Pratt & Whitney, W. Palm Beach, FL, 26-27 January 1993.

5. Buchanan, D., "Material Characterization of Titanium Matrix Composites", NIC Steering Committee Meeting, Pratt & Whitney, W. Palm Beach, FL, 26-27 January 1993.

6. Harmon, D., Finefield, D., Harter, J., and Buchanan, D., "Differences in Fatigue/Fracture Behavior of Woven Mat and Acrylic Binder in the SCS-6/Ti-15-3 Composite", Journal of Composite Technology and Research, Fall 1993.

TABLE 1.0 : Room Temperature Test Matrix

Laminate	Specimen	Type	Replicates
[0/90]s	σult	Static	4
[0/±45/90]s	σult	Static	2
[0/90]s	CCT	da/dN	6
[0/±45/90]s	CCT	da/dN	8

TABLE 2.0 : Laminate Ultimate Strength Data

Laminate	Min (MPa)	Max (MPa)	Ave (MPa)
[0/90]s	1103	1263	1209
[0/±45/90]s	1034	1044	1039

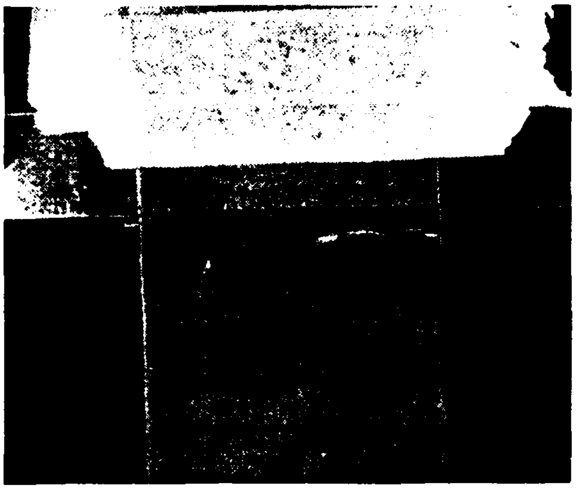

FIGURE 1.0 : Typical Edge Crack Specimen Used to Assess Aging Process

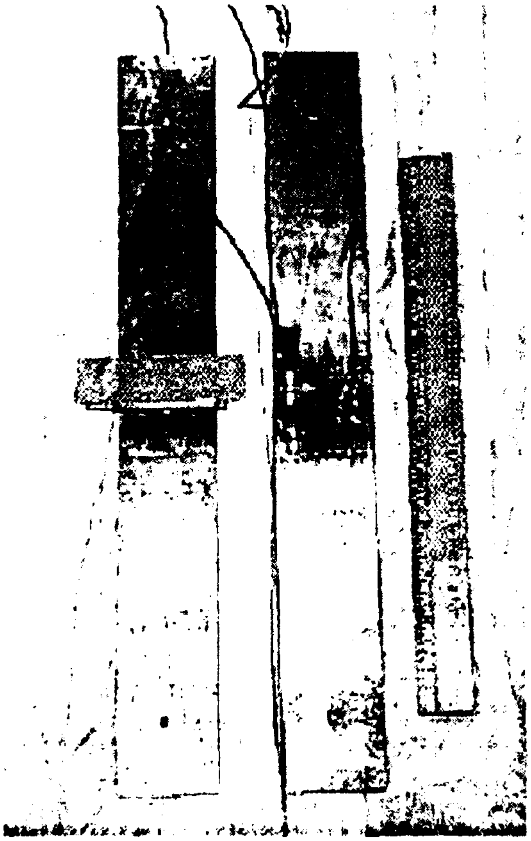

FIGURE 2.0 : Front and Rear View of CCT Specimen

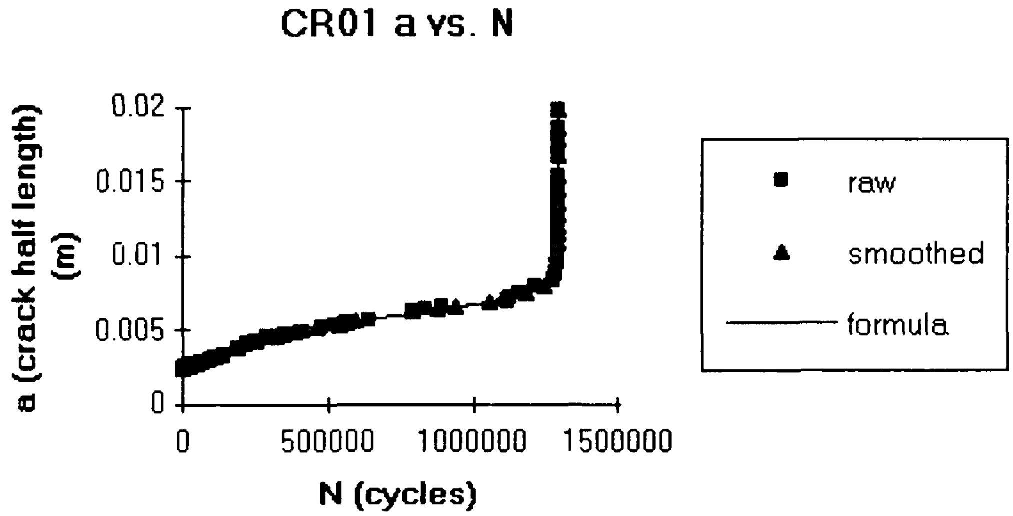

FIGURE 3.0 : Example of Crack Length vs. Cycle Curve Fitting

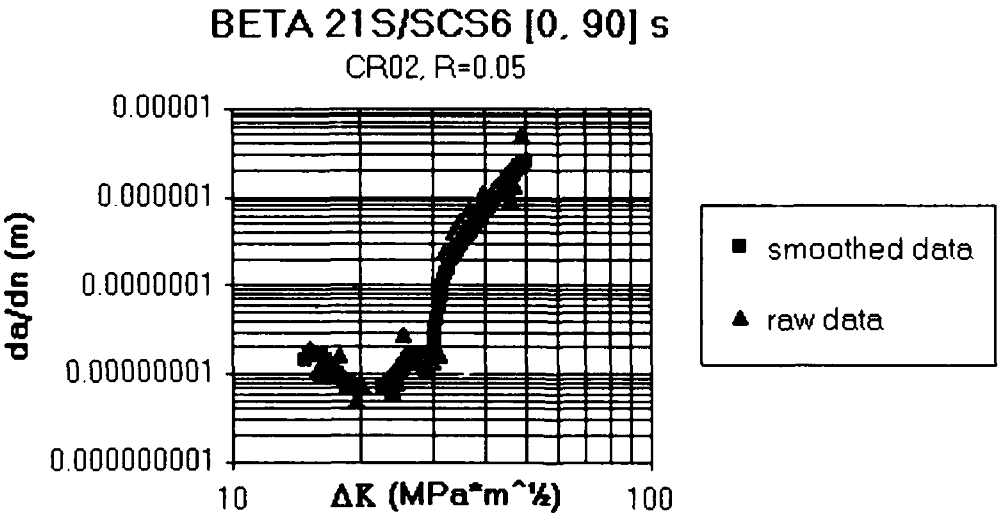

FIGURE 4.0 : Comparison of Smoothed vs. Raw Crack Growth Rate Data

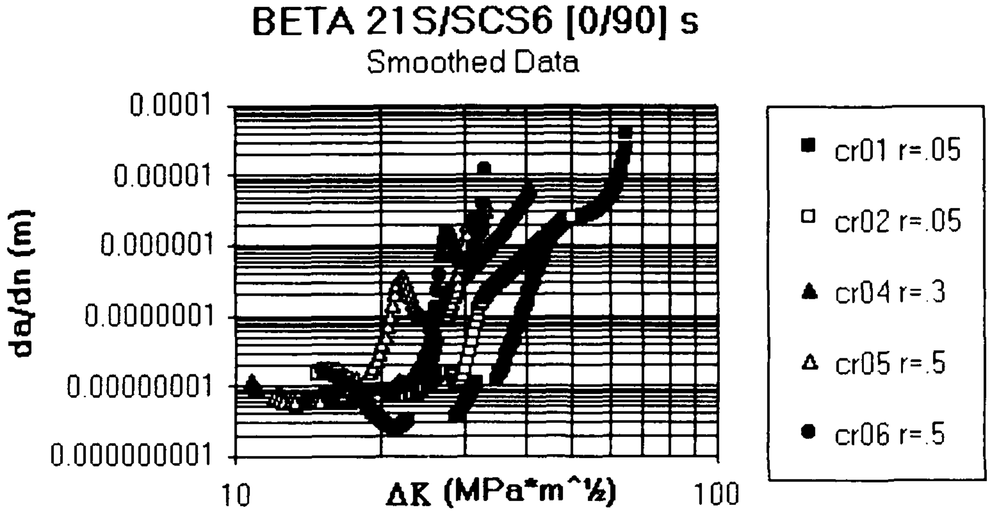

FIGURE 5.0 : Room Temperature Crack Growth Rate Data for [0/90]s Specimens

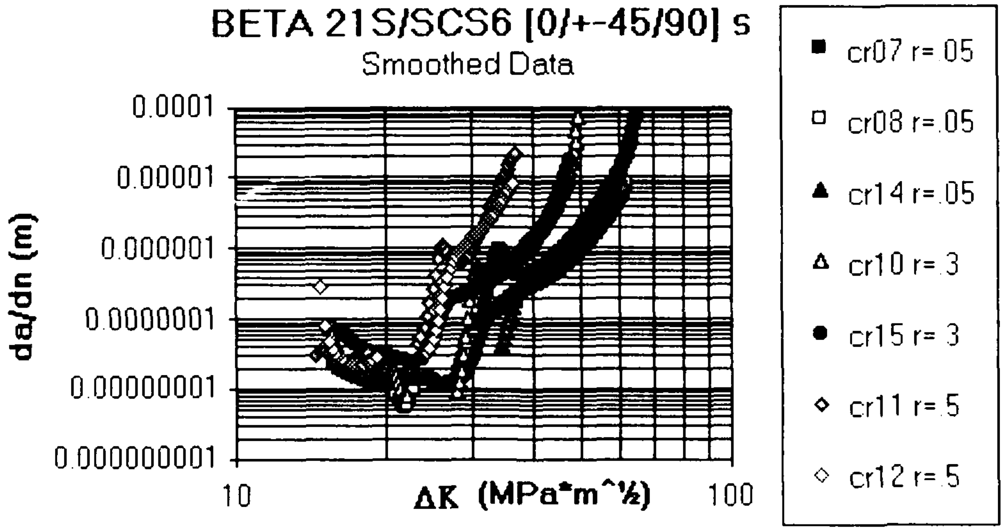

FIGURE 6.0 : Room Temperature Crack Growth Rate Data for [0/±45/90]s Specimens

PROCESS/COMPOSITE CONCURRENT TAILORING OF SiC/Ti COMPOSITES

by

C.C. Chamis and D.A. Saravanos
Structures Division
21000 Brookpark Rd, MS 49-8
NASA Lewis Research Center
Cleveland, Ohio 44135
United States

SUMMARY

Recent work on the prediction of optimal processing and material characteristics for improved fatigue behavior of MMCs/IMCs is summarized. The method is incorporated into the MMLT (Metal Matrix Laminate Tailoring) code. Excellent correlations between predictions for the isothermal fatigue life of the SCS-6/Ti-24Al-11Nb composite and experimental data are obtained at various temperatures and stress ranges. Finally, the optimal processing conditions for *improved isothermal fatigue life* of the composite are evaluated and the attained isothermal fatigue life improvements are shown.

INTRODUCTION

Fatigue endurance is a primary consideration for high-temperature metal and intermetallic matrix composites (MMCs/IMCs), as these materials are expected to sustain aggressive mechanical and thermal cyclic loads. Yet, the inherent heterogeneity of these composites, in terms of differing thermomechanical properties, may severely degrade their fatigue performance[1]. Fatigue life is typically reduced by either the presence of microcracks in the matrix due to residual stresses after processing, or by interactions between the residual stresses, the inelastic behavior of the metallic matrix, post-fabrication loads and environmental effects. Consequently, the development of analytical capabilities is required enabling: (1) reliable/robust predictions of the thermomechanical fatigue (TMF) life of MMCs/IMCs and (2) optimal process/material synthesis for explicitly improving the fatigue life of the composite.

Previous work has addressed the reduction of residual stresses in MMCs, as an indirect approach to improve fatigue life, by tailoring either the processing, the composite parameters, or an interphase layer (fiber coating) in unidirectional MMCs[2]. Yet, the reduction of residual stresses is a quantitative criterion only, as does not account for either the complex thermomechanical interactions between matrix and fibers during cyclic loading, or for the various combinations of mechanical and thermal cyclic loads. Instead, the introduction of life prediction capabilities into the synthesis cycle allows for the concurrent synthesis of both process and material, and ensures explicit improvements in fatigue performance. Additional advantages of this technique are the automatic identification of significant residual stresses in connection with the critical failure modes of the composite, and the optimal control of their evolution irrespectively of the applied loads and TMF cycle.

Consequently, this paper presents recent extensions in the capabilities of the MMLT (Metal Matrix Laminate Tailoring)[3] code to address the previous crucial problems. The code entails the capability to predict and maximize the isothermal fatigue life of IMCs/MMCs. The method was applied on a ceramic silicon carbide fiber (SCS-6)/titanium aluminide (Ti-24Al-11Nb) matrix composite. This intermetallic matrix composite system was selected for its significance as a candidate high-temperature material and the availability of experimental data regarding its fatigue performance. Excellent isothermal life predictions were obtained at both room and elevated temperatures. The robustness of the method in low-, intermediate- and high-cycle fatigue conditions was validated. Additionally, optimal processing temperatures and consolidation pressures were predicted which maximize the isothermal life at room and elevated temperatures. The remaining sections summarize the approach and present the obtained results.

METHOD

A typical thermomechanical life cycle of a MMC, from fabrication to failure at cyclic loading conditions (Fig. 1) is simulated. The constituents are hot-pressed at elevated temperatures, then both temperature and pressure are reduced to ambient conditions (70° F and 0 psi). A cyclic mechanical load is subsequently applied at constant temperature (isothermal fatigue). Thermal strains are developed during the complete processing-loading phase, which act as mean strains and directly affect the fatigue performance of the material. The strain distribution in the composite is also affected by changes in the mechanical properties of the constituents due to temperature and inelastic effects.

The complicated thermomechanical response of the composite during the previously described thermomechanical cycle is simulated using incremental inelastic micro- and macromechanics encoded in METCAN[4]. The mechanics include temperature effects, the inelastic response of the constituent materials, and the residual stress/strain build-up based on the representative unit cell shown in Fig. 2. The constitutive relations were further extended to represent the effect of mechanical cycles N_F on the maximum allowable cyclic strain of the constituents. The maximum elastic $\epsilon_{a,el}^{max}$ and inelastic $\epsilon_{a,in}^{max}$ cyclic strains[5] of the matrix are calculated using the multi-factor equation. The exponents and reference intercepts are calculated from calibrations with experimental data. The fibers were assumed elastic, thus, only the elastic counterpart of the maximum cyclic strain was calculated.

The optimization problem for the direct improvement of the fatigue life is formulated as the direct maximization of the fatigue life (expressed by the number of cycles) of the composite for a specified isothermal cyclic load. Static strain constraints are imposed on the fiber and matrix microstrains to eliminate failures during the fabrication and loading phases. Additional constrains are imposed on the cyclic microstrains of each constituent. Specifically, the cyclic microstrains ϵ_a in the matrix should not exceed the sum of the maximum cyclic elastic and inelastic strains as proposed by Saltsman and Halford[5], while the fiber cyclic strains should not exceed their maximum elastic strain limit. The numerical solution of this non-linear programming problem is obtained with the method of feasible directions[6]. The described methodology including the mechanics and the optimization algorithm was encoded into the MMLT (Metal-Matrix Laminate Tailoring) code.

It is pointed out, that the previous formulation can be applied in two different ways:

(1) For predicting the fatigue life of the composite, under fixed processing and material parameters. In this case, the life is maximized until some of the cyclic strain constrains are activated. The resultant maximum number of cycles corresponds to the life of the composite for the given isothermal fatigue conditions. The associated mode(s) of failure, in terms of constituent, microregion, and direction, are also calculated.

(2) For predicting the optimal processing and material parameters which will improve the fatigue life of the composite. In this case, the life of the composite at the initial set of processing and material parameters is predicted, and a search is initiated until the best combination of process/material characteristics is achieved. In this manner, the residual microstresses and the inelastic response of the constituents are optimally controlled to achieve the desired objective of maximum fatigue life.

RESULTS AND DISCUSSION

Applications of the method on a SCS-6/Ti-24Al-11Nb composite were performed. The temperature and stress factors in the constitutive multi-factor equations were calibrated with reported uniaxial monotonic loading data for the Ti-24Al-11Nb alloy[7], and the SCS-6 fiber[8,9]. The elastic and inelastic strain intercepts, and the corresponding exponents of maximum cyclic strains were calculated from experimental isothermal fatigue data at room temperature[8,9,10]. It should be noted that the constituent properties represent average values from different sources and experimental configurations were modelled as accurately as possible.

Life Predictions. The life prediction capability of the method was first evaluated. The predicted and measured[8] isothermal fatigue life of a unidirectional SCS-6/Ti-24Al-11Nb composite (0.35 FVR) at 70°F (23° C) is shown in Fig. 3. The obtained agreement with measured values is excellent. Moreover, the method has succeeded in capturing both low-, intermediate-, and high-cycle fatigue regions, which illustrates the robustness of the method. The corresponding predicted failure mechanisms in the composite for each region are also shown in Fig. 3. These are, longitudinal fiber breakage (F11) in low cycles, mixed longitudinal matrix failure in the C microregion (C11) for the intermediate cycle range, and longitudinal matrix failure in the A microregion (A11) for the high cycle realm.

Isothermal fatigue life predictions at 1200°F (650°C) where also obtained (Fig. 4). As seen in Fig. 4, the results correlate very well with reported experimental data form various sources[9,10]. Again the predictions have captured the low-cycle, intermediate-cycle, and high-cycle ranges, as well as, the associated failure mechanisms. The predictions slightly overestimate the life at high cycles, because oxidation is a factor there. Note that all data shown in Fig. 4, correspond to fatigue experiments in air environment. Bartolotta[11] and others have noted that environmental effects, such as oxidation, increase the rate of degradation at elevated temperatures. Oxidation effects in the matrix will be included in future work.

Optimal Processing Conditions. Optimal processing characteristics which improve the isothermal fatigue life of a SCS-6/Ti-24Al-11Nb composite (0.35 FVR) were also predicted. The resultant increases in isothermal fatigue life at ambient conditions are shown in Fig. 5, and are compared to the predicted life for the initial fabrication process. The predicted life of the composite in the ideal situation of zero residual stresses (processing effects were neglected) is also shown to establish the maximum range for improvements in fatigue life. Considering this range, the obtained fatigue life enhancements seem significant. The resultant optimal consolidation pressure histories at points 1,2, and 3 (see Fig. 5) increased drastically, yet, different pressure profiles were predicted for each point. Considering the various failure modes associated with the three fatigue regions, these differences in optimal processes are justified, as each optimization case has targeted different residual stresses in the composite. The last observation demonstrates the capability of the method to identify and subsequently reduce the critical residual stresses in the composite. The resultant changes in temperature profiles were small.

Slightly lower life improvements were obtained for the isothermal fatigue at 1200°F (650°C) (see Fig. 6). The lower improvements were attributed to the presence of lower residual stresses in the material. However, similar trends were predicted in the corresponding optimal consolidation pressure profiles. The different trends are similar to the ones obtained at room conditions and correspond to the previously discussed different failure modes at low, intermediate and high cycles.

CONCLUSIONS

The development of a methodology to predict optimal process and material characteristics for improved fatigue behavior is developed and incorporated into the MMLT code[3]. Excellent correlations between predictions for the isothermal fatigue life of the SCS-6/Ti-24Al-11Nb composite and experimental data were obtained. The accuracy of the method at various temperatures and cycling ranges was also validated. Finally, optimal processing conditions for improved isothermal fatigue life of the composite were evaluated.

REFERENCES

1. Castelli, M. G., and Gayda J. "An overview of Elevated Temperature Damage Mechanisms

and Fatigue Behavior of a Unidirectional SCS-6/Ti-15-3 Composite," *NASA TM 106131*, 1993

2. Saravanos, D. A., Morel, M. R., and Chamis, C. C. "Concurrent Tailoring of Fabrication Process and Interphase Layer to Reduce Residual Stresses in Metal Matrix Composites," *SAMPE Quarterly*, Vol. 22, No. 4, 1991, pp 36-44.

3. Morel, M. R., Saravanos, D. A. and Murthy, P. L. N. "Metal Matrix Laminate Tailoring (MMLT) Code: User's Manual," *NASA TM 106052*, 1993.

4. Murthy, P., L., N, Hopkins, D. A., and Chamis, C. C., "Metal Matrix Composite Micromechanics: In-Situ Behavior Influence on Composite Properties," *NASA TM 102302*, 1989.

5. Saltsman, J. F. and Halford, G. "Life Prediction of Thermomechanical Fatigue Using Total Strain Version of Strainrange Partitioning (SRP)," *NASA TP 2779*, 1988.

6. Vanderplaats, G. N, "ADS - A Fortran Program for Automated Design Synthesis," *NASA CR 177985*, 1985.

7. Deluca, D. P., and Cowles, B. A. "Fatigue and Fracture of Titanium Aluminides," *WRDC-TR-89-4136*, Wright Research and Development Center, 1989.

8. Gambone, M. L. "Fatigue and Fracture of Titanium Aluminides," WRDC-TR-89-4145, *Wright Research and Development Center*, 1990.

9. Brindley, P. K., Draper, S. L., Eldridge, J. I., Nathal, M. V., and Arnold, S. N. "The Effect of Temperature on the Deformation and Fracture of SiC/Ti-24Al-11Nb," *Metallurgical Transactions*, Vol 23A, No. 9, 1992.

10. Nicholas, T., Russ, S. and Cheney, A. "Frequency and Stress Ratio Effects on Fatigue of Unidirectional SCS/Ti-24Al-11Nb Composite at 650°C," *Fatigue '93*, Editors, J. P. Bailson and J. I. Dickson, 1993.

11. Bartolotta P.A., "Fatigue Behavior and Life Prediction of a SiC/Ti-24Al-11Nb Composite Under Isothermal Conditions," *NASA TM-105168*, 1991.

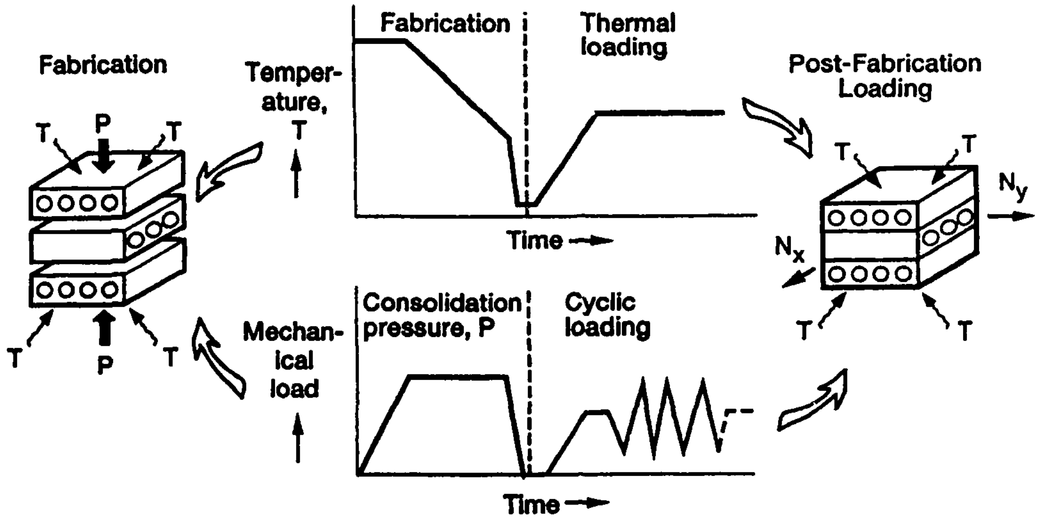
Fabrication
T
P
T
T
P
T
Temper-
ature,
T
Fabrication
Thermal
loading
Time
Post-Fabrication
Loading
T
T
N_y
N_x
T
T
Mechan-
ical
load
Consolidation
pressure, P
Cyclic
loading
Time

Fig. 1 Typical fabrication and loading phases

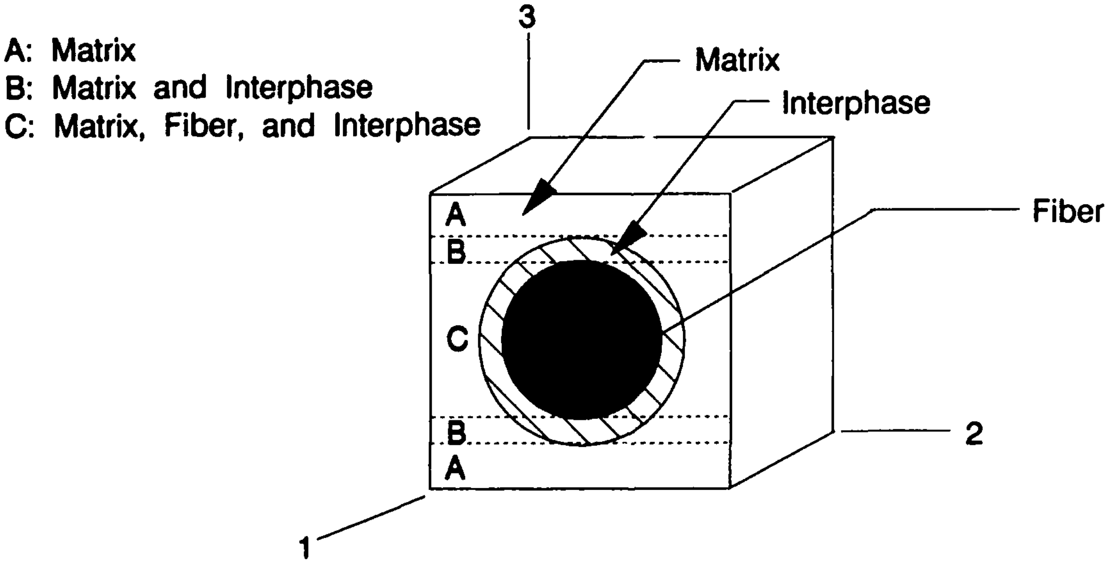
A: Matrix
B: Matrix and Interphase
C: Matrix, Fiber, and Interphase
3
Matrix
Interphase
Fiber
A
B
C
B
A
2
1

Fig. 2 Representative unit cell

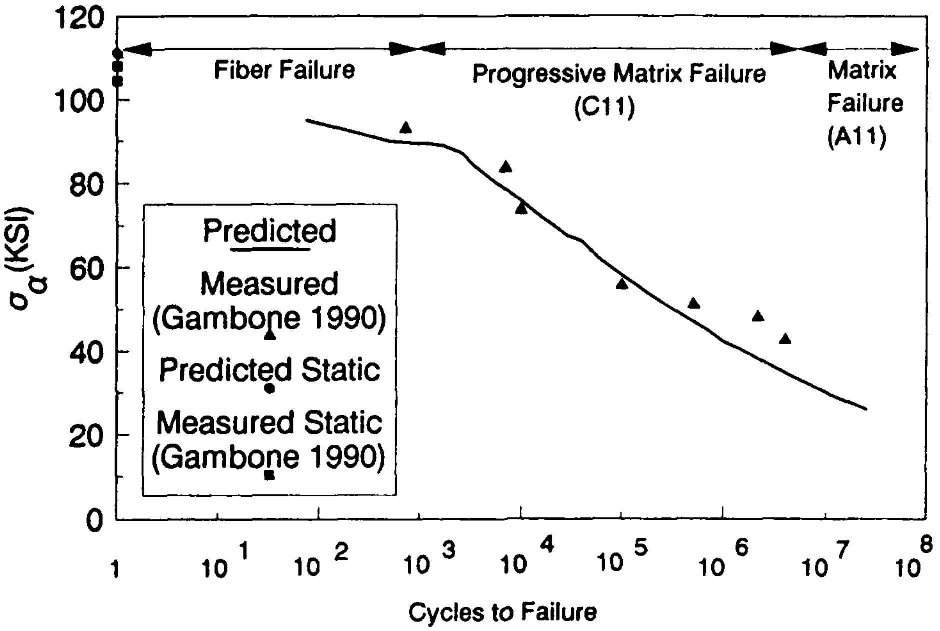

Fig. 3 Predicted Isothermal Fatigue Life (23 deg. C, R=0.1)

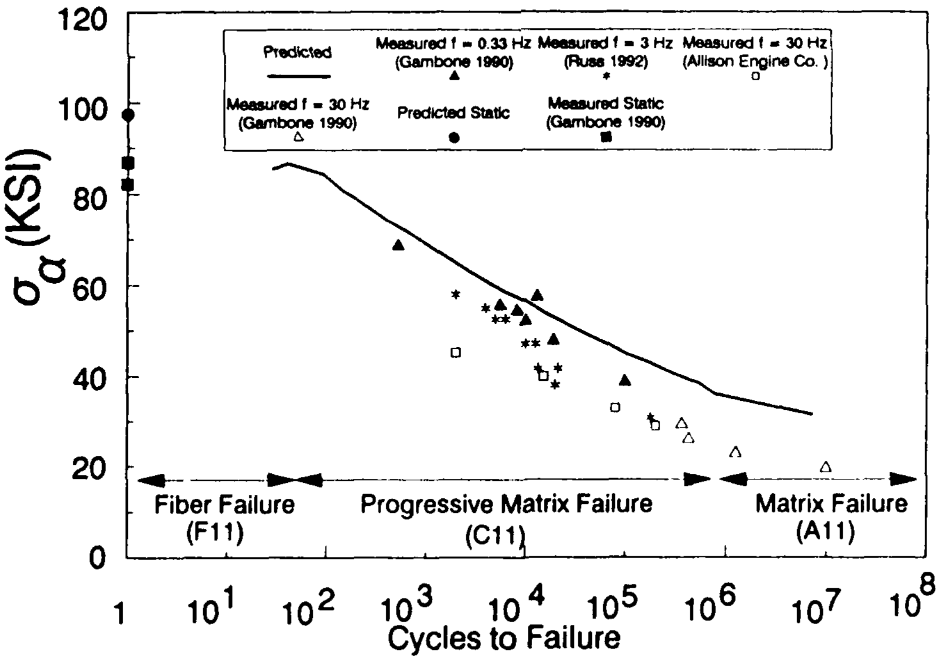

Fig. 4 Predicted Isothermal Fatigue Life (650 deg. C, R=0.1)

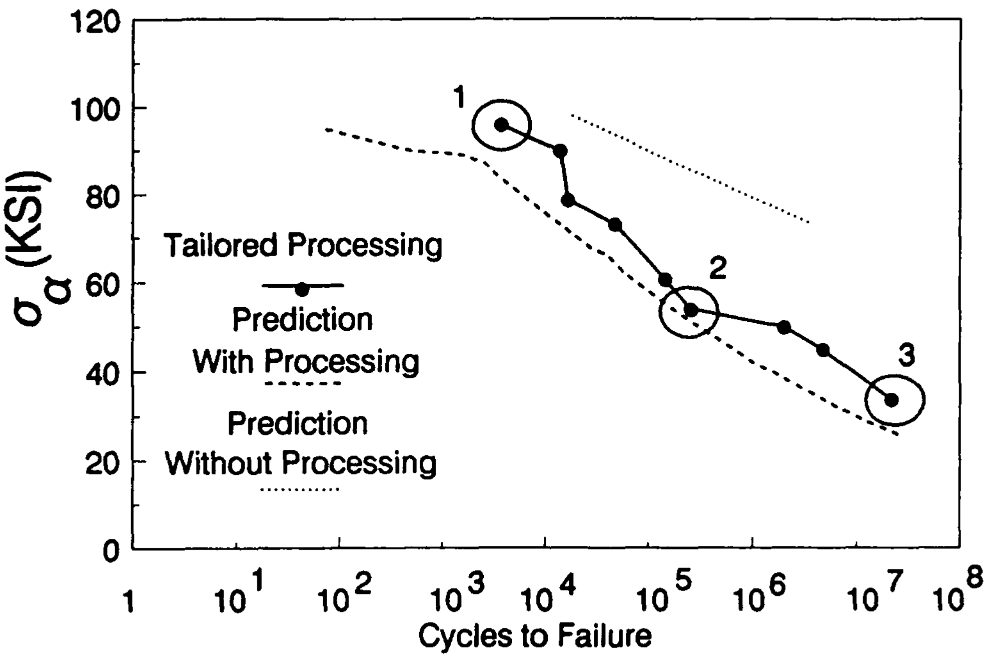

Fig. 5 Effect of processing optimization on fatigue life (T=23 deg C, R=0.1)

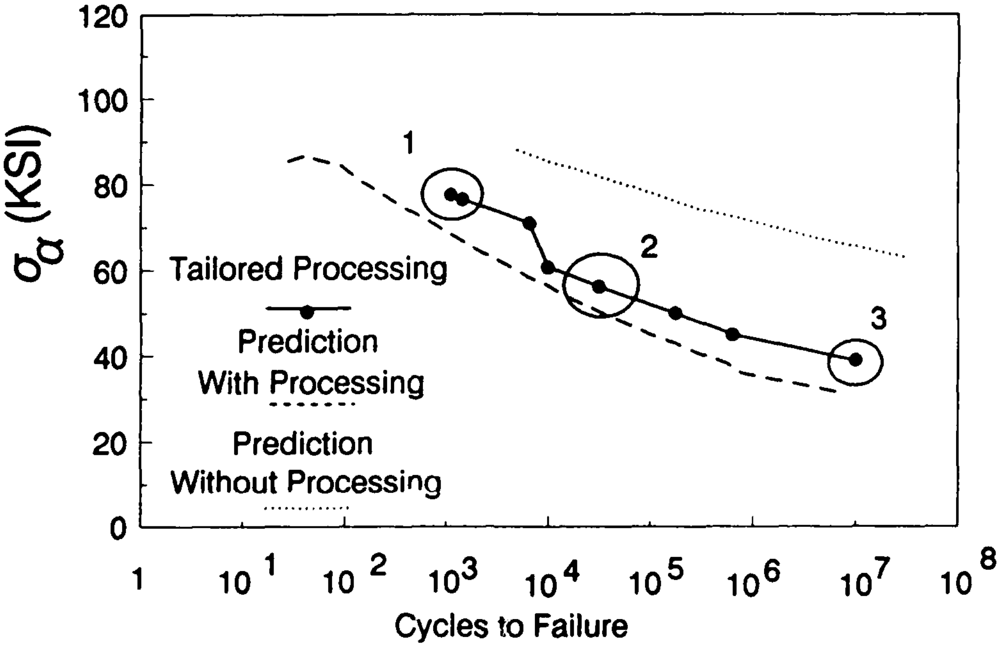

Fig. 6 Effect of processing optimization on fatigue life (T=650 deg C, R=0.1)

Micromechanical Modeling of Damage Growth in Titanium Based Metal-Matrix Composites

James A. Sherwood
Howard M. Quimby
Department of Mechanical Engineering
University of Massachusetts at Lowell
One University Avenue
Lowell, MA 01854
USA

1. Abstract

The thermomechanical behavior of continuous-fiber reinforced titanium based metal-matrix composites (MMC) is studied using the finite element method. A thermoviscoplastic unified state variable constitutive theory is employed to capture inelastic and strain-rate sensitive behavior in the Timetal-21s matrix. The SCS-6 fibers are modeled as thermoelastic. The effects of residual stresses generated during the consolidation process on the tensile response of the composites are investigated. Unidirectional and cross-ply geometries are considered. Differences between the tensile responses in composites with perfectly bonded and completely debonded fiber/matrix interfaces are discussed. Model simulations for the completely debonded-interface condition are shown to correlate well with experimental results.

2. Introduction

The aerospace, automotive and gas-turbine industries all share the never-ending quest for lighter and stronger materials suitable for use in increasingly demanding high-temperature environments. The performance of nickel-based superalloys, which have been the past material of choice for high-temperature environments, has peaked. The development of composite materials that have reduced weight and increased strength relative to the nickel-based superalloys is critical to achieving the goal of higher operating temperatures, long-life and reduced weight. One such composite system is the titanium-based silicon-carbide fiber reinforced metal-matrix composite.

To accurately predict the complex thermomechanical response for this class of composite materials, the rate- and temperature-dependent properties of the constituents must be considered in the model. Adding to the complexity of the composite-material model is the lack of a complete understanding of the behavior at the fiber-matrix interface. The nature of the interface bond is a combination of mechanical and chemical bonding, and the contribution of each is not well defined.

The use of a unit cell in the finite element method is common for investigating the stress state on the microscale. This approach assumes that the respective thermomechanical properties of the matrix and fiber can be characterized individually. The individual constituents can then be used together in the finite element model such that the overall response of the composite can be simulated.

In addition to the material properties of the constituents, the finite element model should also consider the fiber-matrix interface bond and the immediate surrounding region. While discrete characterization of the interphase region may not be crucial to the overall macroscopic response of the composite, it is important to consider the state of the fiber-matrix interface bond. At a minimum, the finite element model of the composite should be able to simulate perfect bonding of the fiber and matrix as well as complete debonding of the constituents. It is also desirable to simulate partial debonding and the evolution of the strength of the interface during composite loading. One goal of this study is to investigate the role of the interface-bond strength on the predicted thermomechanical macroscopic response of the composite, Timetal-21s/SCS6.

In the past five years, many experimental and numerical research efforts have been directed toward titanium-based composites. Experimental research still represents the major portion of the effort. However, numerical techniques have been established as a viable means of composite analysis, and their use is becoming more common. Numerical studies typically employ a constitutive theory with the ability to capture the plastic and time-dependent behaviors inherent to the matrix in some composite materials. Several comprehensive constitutive theories have been developed in the past, and new theories continue to emerge [1-5]. Most of the theories share common ingredients in that they use some plastic-flow rule in cooperation with evolution equations for state variables and hardening rules. Constitutive models are often implemented into finite element codes in the form of user-supplied material models and/or incorporated into stand-alone composite analysis packages.

Several researchers have completed numerical and experimental investigations of the microscopic and macroscopic thermomechanical behaviors of titanium-based fiber-reinforced composites. The numerical investigations all required some a priori assumptions about the interfacial bond strength. Many computational works have considered the fiber-matrix interface as completely bonded, e.g. Kroupa, et al. [6], Aboudi [7], Santhosh and Ahmad [8], Gosz, et al. [9], and Arnold, et al. [10]. While others have considered the interface as completely debonded or strong, e.g. Grady and Lerch [11], Nimmer, et al. [12], and Mital and Chamis [13]. Still other studies have considered it in between perfectly bonded and debonded, i.e. weak, e.g. Lissenden et al. [14], Eggleston and Krempl [15], Mital et al. [16], Majumdar, et al. [17]. In addition other analyses of Ti-based composites have been completed and are worthy of attention [18-26]. The evolution and effect of fiber-matrix debonding is a major concern in composites which are loaded transversely to the fiber direction [27].

Presented at an AGARD Meeting on 'Characterisation of Fibre Reinforced Titanium Matrix Composites', September 1993

The goal of this paper is to use the unit cell in the finite element method to investigate the macroscopic response of the composite due to tensile loadings at 23 and 650°C. The influence of the residual stresses developed during the consolidation process are addressed. Unidirectional $[0]_4$ and cross-ply $[0/90]_s$ lay-ups are considered. The effect of perfect and imperfect fiber/matrix interfaces and rate-dependent matrix behavior on the response are investigated.

3. Constitutive Theories for the Fiber and Matrix

A unified constitutive theory was used in this study to model the matrix thermomechanical behavior. The theory was chosen for its ability to model the nonlinear time-dependent behavior. The model was proposed by Ramaswamy and Stouffer [28] and is based on the theoretical development of Bodner and Partom [29]. Sherwood and Boyle [30] implemented the theory into the ADINA finite element program [31] in the form of a user-supplied material model for two- and three-dimensional analyses. Ramaswamy, et al demonstrated that the model had the ability to accurately predict the tensile, creep and cyclic behavior of René 80 over a wide range of temperatures. In addition, Sherwood and Stouffer [32] used the model in analyses of René 95. Boyle [33] used the model to investigate the thermomechanical response of a titanium-matrix composite. Sherwood and Fay [34] demonstrated its ability to accurately capture material response to nonproportional loadings.

Material constants are derived from experimental testing of monolithic matrix materials. The work of Sherwood and Doore [35] has streamlined the process of finding the necessary temperature- and rate-dependent material constants. The state variables Z and Ω_{ij} represent changes in the microstructure and describe the isotropic and kinematic hardening contributions, respectively. An extensive review of the Ramaswamy-Stouffer constitutive theory is presented in [33] and is readily available in other references [36]. Thus, a detailed review of the theory will not be reproduced here. Rather, the following equations summarize the constitutive theory.

The flow rule is represented by

$$\dot{\varepsilon}^{I}_{ij} = D_0 \exp\left(-\frac{1}{2}\left(\frac{Z^2}{3K_2} \right)^{n} \right) \frac{S_{ij} - \Omega_{ij}}{\sqrt{3K_2}} \tag{1}$$

where K_2 is analogous to J_2 and is given by

$$K_2 = \frac{1}{2}(S_{ij} - \Omega_{ij})(S_{ij} - \Omega_{ij}) \tag{2}$$

with the back-stress-evolution equation

$$\dot{\Omega}_{ij} = \dot{\Omega}^{E}_{ij} + \dot{\Omega}^{I}_{ij} \tag{3}$$

expressed in terms of the elastic component

$$\Omega^{E}_{ij} = f_1 S_{ij} \tag{4}$$

and the inelastic component

$$\dot{\Omega}^{I}_{ij} = f_1 \dot{\varepsilon}^{I}_{ij} - \frac{2}{3} f_3 \frac{\Omega_{ij}}{\Omega_s} \sqrt{\frac{2}{3} \dot{\varepsilon}^{I}_{ij} \dot{\varepsilon}^{I}_{ij}} \tag{5}$$

The back-stress-recovery equation is

$$\Omega_s = -B \left(\frac{\sqrt{3J_2}}{\sigma_o} \right)^{r} (\Omega_s - \Omega_{CRP}) \tag{6}$$

The drag-stress evolution is described by

$$\dot{Z} = m(Z_1 - Z)\dot{W}^{I} - A_1 (Z - Z_2)^{p} \tag{7}$$

The value of D_o is typically assumed to be 10^4 and is temperature independent. The remaining material constants n, f_1, f_3, B, r, m, Z_1, Z_2, A_1 and p are temperature dependent.

Timetal-21s, the matrix material, was developed by TIMET to be roughly equivalent to the Ti-15V-3Cr-3Sn-3Al (atomic percent) material with much improved oxidation resistance. Previously designated Ti-β21s, Timetal-21s is characterized by a high melting point, low density and improved oxidation resistance due to the removal of the vanadium (V). The exact chemical composition is proprietary information. The temperature-dependent material constants used is the present study were developed by Doore, and are given in Table 1. These material constants were derived from neat material test data supplied by the University of Dayton Research Institute (UDRI) and the NASA Lewis Research Center (NASA LeRC). A complete discussion of the material-constant-determination methodology is presented in [36].

The Textron Specialty Materials SCS-6 silicon carbide fiber is the reinforcement constituent used in the composites under investigation. The fiber behavior is such that a thermoelastic material model can be used to capture the fiber in the composite analyses. Table 2 summarizes the material constants for the fiber.

In Tables 1 and 2, the secant coefficients of thermal expansion (CTE) were adjusted to correspond to a reference temperature equal to that for the consolidation of composite. The consolidation temperature is proprietary information and can not be presented here. The CTE reference temperature is the temperature at which the thermal strains are equal to zero.

4. Finite Element Modeling

The fully three-dimensional finite element model of the SCS-6/Timetal-21S $[0]_4$ system is the first in a series of models used to numerically investigate the macroscopic behavior of the composite. The Timetal-21s composites considered in this work have a fiber-volume fraction of 33%. The three-dimensional model is used to capture changes in the stress state that occur during consolidation and the subsequent external load application.

A square unit cell of a unidirectional composite is shown in Figure 1. The unit cell is representative of a typical section of the composite that is not influenced by edge effects. Figure 1 also shows the two planes of symmetry that are present in the unit cell. Symmetry boundary conditions can therefore be

Temp °C	CTE $10^{-6}/°C$	n	Z_o MPa	E MPa	f_1	f_3	Ω_{SAT} MPa
23	9.49	1.40	703	113681	660350	0.6971	661
260	10.45	1.20	737	106116	49664	0.8081	537
482	11.24	1.05	760	93674	23609	0.7669	384
650	11.79	0.95	781	68065	20439	0.2811	79
760	12.11	0.65	805	65362	19067	0.2758	43
815	12.27	0.55	807	64010	19007	0.2739	33

Table 1. Timetal-21s material constants as a function of temperature

Temperature °C	Elastic Modulus MPa	Poisson's Ratio	Fiber CTE 10-6/°C
21.1	393000	0.25	3.93
93.3	390000	0.25	3.97
204.4	386000	0.25	4.04
315.6	382000	0.25	4.12
426.7	378000	0.25	4.20
537.8	374000	0.25	4.29
648.9	370000	0.25	4.38
760.0	365000	0.25	4.45
871.1	361000	0.25	4.53
1093.3	354000	0.25	4.56

Table 2. Material properties of SCS-6 fibers in Timetal-21S matrix composites

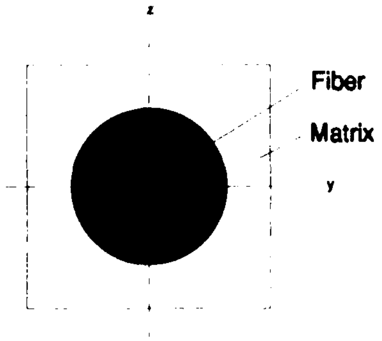

Figure 1 Unidirectional composite unit cell and lines of symmetry

used in a finite element model to capture the behavior of an entire unit cell with a mesh which is only one-quarter of the total cell geometry. The finite element models in this paper take advantage of these symmetries

The finite element mesh of the unidirectional $[0]_4$ composite in Figure 2 represents one-quarter of a square unit cell. The fiber is modeled using 48 elements, and the matrix is modeled with 32 elements This mesh density was determined in a previous study [33] to be suitable for use in three-dimensional composite analyses. All elements employ the 20-node THREEDSOLID element formulation in ADINA The thickness of the model was chosen to yield the optimum aspect ratio for the matrix elements and represents an average of the matrix element side lengths A step change in material properties occurs at the fiber-matrix interface

The fiber-matrix interface bond was characterized as either perfectly bonded or completely debonded The perfect bond was modelled by the fiber and the matrix elements sharing the nodes on the interface A complete fiber-matrix-interface debond was modeled using the contact-surface option

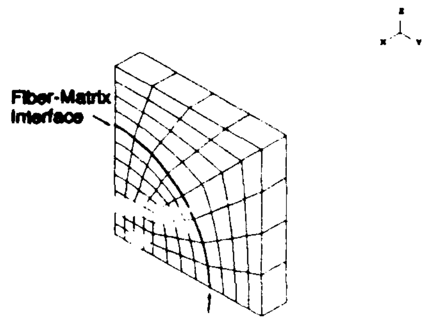

Figure 2 Finite element model of the unidirectional $[0]_4$ composite system.

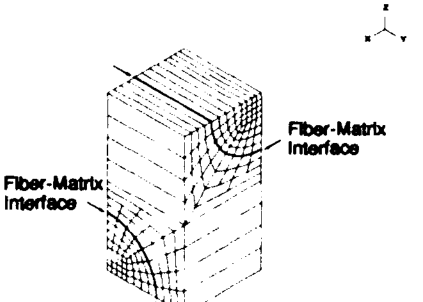

Figure 3 Finite element model of the $[0/90]_s$ cross-ply composite system

in ADINA. This approach required pairs of coincident nodes at the interface. One node is used in the element connectivity of the matrix and the other for the fiber. The contact surface permits compressive loads normal to the surface to be transmitted across the interface without violating compatibility between the fiber and matrix. To properly define the contact, the midside nodes were deleted from the element faces on which contact surfaces were applied. Finite element contact algorithms are typically not equipped to handle midside element nodes. The ADINA contact algorithms require that midside nodes be removed if compatibility between contacting surfaces is to be strictly enforced. The coefficient of friction between the two surfaces was set to zero in keeping with the zero-bond-strength assumption. This assumption is consistent with that of other composite modeling efforts [8,17,33].

Symmetry boundary conditions are imposed on the three negative faces of the model. The orientation of the fiber coincides with the x-axis. The displacements of nodes on the negative x-face are confined to the y-z plane. The displacements of nodes on the negative y-face are confined to the x-z plane. Similarly, the displacements of nodes on the negative z-face are confined to the x-y plane. All nodes belonging to the positive x-face are constrained to have the same axial displacements. This boundary condition is used to obtain the behavior in a nominal layer of the composite and satisfy compatibility. The nodes belonging to the positive y-face are constrained to have the same y-displacements. Similarly, the nodes belonging to the positive z-face are constrained to have the same z-displacements. The latter two boundary conditions serve to satisfy compatibility requirements. The modeling of the perfectly debonded fiber-matrix interface introduces some difficultly in the definition of the boundary condition for the x-displacement of plane sections to remain plane. This difficulty is particular to ADINA and is addressed in the Appendix.

It is important to note that use of the above boundary conditions in the modeling of imperfect fiber-matrix interfaces can introduce physically unrealistic behaviors. The above boundary conditions used to capture the response of a nominal layer of the composite will artificially hold the fiber in place when complete interface separation occurs. This behavior is physically unreasonable as complete interface separation would allow the fiber to move independently of the matrix. Thus, these boundary conditions carry the inherent assumption that due to varying gripping along the length of the fiber, the fiber is never free to move independently from the matrix.

The finite element mesh of the $[0/90]_s$ composite in Figure 3 represents 1/16 of a unit cell and takes advantage of the symmetry found in a complete $[0/90]_s$ unit cell. The fiber is modeled using 96 elements and the matrix is modeled with 54 elements. The mesh density is based upon that used in the three-dimensional $[0]_4$ modeling. However, the computational resources required to complete the $[0]_4$ modeling were significant. This fact had to be considered when developing the $[0/90]_s$ models.

The depths of the finite elements used in the cross-ply model were extended to lengths equal to the length of a side of one-quarter of a unidirectional unit cell. Finite elements used in the transition between the [0] and [90] fiber orientations were degenerated to allow mating of [0] and [90] unit cells which make up the complete cross-ply model. The mating of the [0] and [90] unit cells is accomplished using 20-nodded THREEDSOLID elements located at the midpoint of the two fiber orientations. Most elements employ the 20-nodded THREEDSOLID element formulation. The exception occurs with the use of 12 degenerated 16-nodded THREEDSOLID elements used to complete the [0] to [90] transition. The correlation of the numerical and experimental results presented later justify the appropriateness of the cross-ply model presented here. The displacement boundary conditions are analogous to those used for the unidirectional model. The model also considered the weak and strong interface conditions as described previously for the unidirectional model

5. Analysis Conditions

A series of strain-rate control simulations were performed for each of the interface bond conditions. The composites were subjected to the manufacturing process followed by a strain-rate control tensile test at either 23 or 650 C. The manufacturing process assumed a one-hour linear cooldown from the consolidation temperature to room temperature. For tensile tests performed at 23 C, the pull was done immediately following the manufacturing process. For the 650 C tensile tests, a reheat from room temperature to 650 C was performed before pulling. For the unidirectional composite, the material response was investigated for displacement loads in and normal-to the fiber direction. The cross-ply pull was such that it was in line with the 0 -fibers and normal to the 90 -fibers. To explore the influence of the residual stresses resulting from

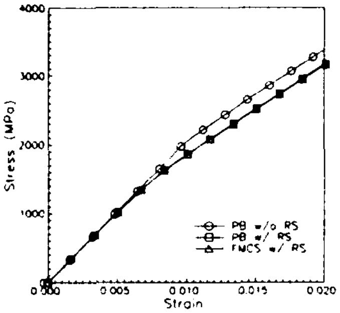

Figure 4 0° lamina response at 23°C.

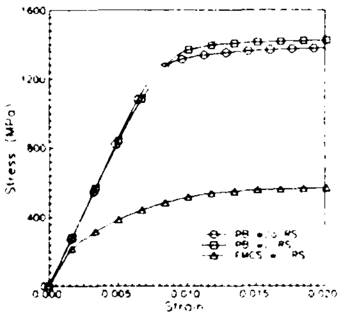

Figure 5 90° lamina response at 23°C.

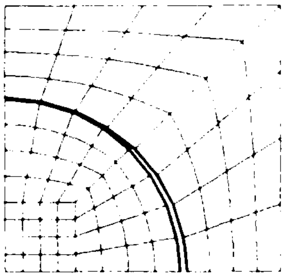

Figure 6 Fiber/matrix debonding in a unidirectional composite loaded normal to the fiber direction

the manufacturing process on the overall response, some tensile tests were run without first simulating the manufacturing process.

6. Unidirectional Composite Results

The numerical investigations of the unidirectional composite system were conducted as outlined above. The effect of the residual stresses on the overall response was minimal. Figure 4 shows the unidirectional composite response to the axial loading at 23°C. The highest stress level is observed in the system with a perfect bond and no residual stresses (PB w/o RS). Although it is unrealistic to expect such a case to exist following consolidation, this model represents an upper limit of the composite response. The inclusion of the residual stresses due to consolidation with the perfect bond (PB w/ RS) results in a reduction of the overall stress level. This reduction is a direct result of the initiation of matrix yield at lower strains due to the tensile residual stresses in the fiber direction. The inclusion of the fiber/matrix contact surface with the residual stresses (FMCS w/ RS) yields the same result as that without fiber/matrix contact. This result is expected as a direct result of the boundary condition that constrains the fiber and matrix to move together in the axial direction such that the axial face remains plane.

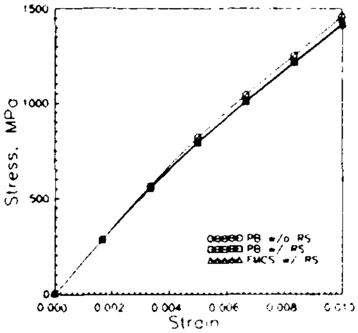

Figure 7 0° lamina response at 650°C.

The unidirectional composite response for a displacement load normal to the fiber is shown in Figure 5. In this figure it is observed that the residual stresses serve to increase the overall stress response of the system when perfectly bonded unidirectional specimens are transversely loaded. The matrix stress state following consolidation is tensile in the fiber direction. The resulting 3-D state of stress requires the application of additional stress in the lateral direction to counter the tensile stress in the fiber direction before yielding can occur. This stress is more than would be necessary in a stress-free matrix. The response of the completely debonded composite to the transverse load is far less than the bonded specimens due to the inability of the debonded matrix to transfer loads to the fiber. The resulting response is essentially controlled by the mechanical behavior of the matrix material. Figure 6 shows the fiber/matrix debonding observed in unidirectional systems transversely loaded in the y-direction.

The results of the unidirectional tests conducted at 650°C closely parallel the behavior observed at room temperature in the same system. The elevated-temperature stress-strain response for the composite is naturally less than the room temperature response. However, the predicted tensile behavior is much the same for each of the loading conditions considered. Figure 7 shows the results of the elevated-temperature response for loading in the fiber direction. Once again it is observed that the highest stress is observed in the perfectly bonded interface model without residual stresses. However, the inclusion of the residual stress state in both the perfectly bonded and debonded analyses has only a small effect on the overall response as compared to what was observed at room temperature. At the elevated temperature the matrix residual stress resulting from the thermal mismatch

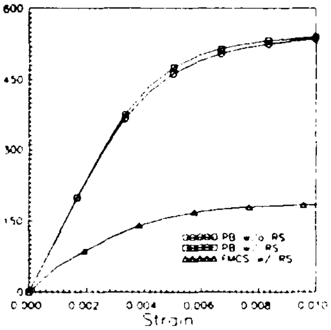

Figure 8 90° lamina response at 650°C

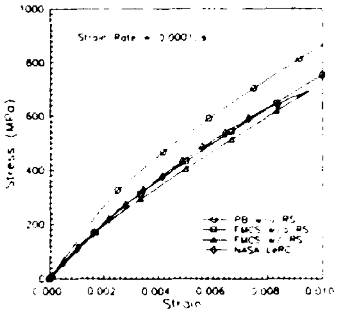

Figure 10 FEM and experimental [0/90]$_s$ laminate response at 650°C

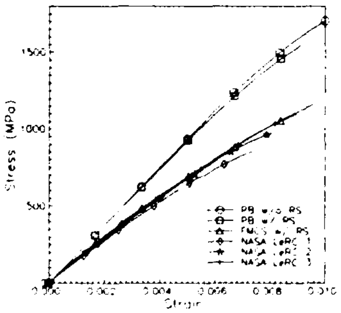

Figure 9 FEM and experimental results of [0/90]$_s$ laminate response at 23°C

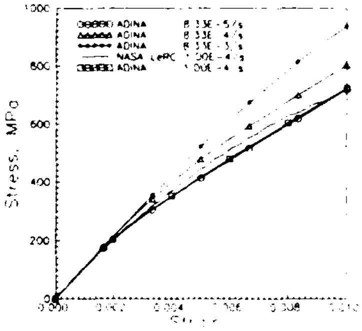

Figure 11 FEM and experimental [0/90]$_s$ laminate response at 650°C as a function of strain rate

of the fiber and matrix has been reduced. It is noted that the elevated temperature response is largely fiber dominated. Figure 8 shows the results of the unidirectional composite responses to the transverse loading at 650°C. Not unlike the behavior observed at room temperature, the inclusion of the residual stress in the perfectly bonded model increases composite stress levels relative to the residual-stress-free model. The debonded model with residual stresses shows once again a significant drop in the stress-strain response due to the inability to transfer tensile matrix loads to the fiber.

7. Cross-Ply Composite Results

The [0/90]$_s$ cross-ply composite system was investigated at 23 and 650°C as discussed previously. Figure 9 shows the results of the evaluations completed at 23°C. The perfectly bonded cross-ply composite responses, with and without residual stresses, at 23°C are quite similar. The effect of the residual stresses on the response of the perfectly bonded composite is a slight decrease in stress level caused by matrix yielding at a lower strain than would occur in their absence. In an overall sense, the matrix residual stresses developed during the consolidation process have a detrimental effect. This reduction can be interpreted as the onset of yielding in the 0° direction is greater than the increase in yield strength in the 90° direction. The perfectly debonded model with residual stresses shows the least stress level of all in the set of simulations. A comparison of the three analytical results with experimental data provided by the NASA Lewis Research Center indicates the completely debonded analysis is the most realistic. The good correlation at 23°C between the experimental data and the analytical model of [0/90]$_s$ system with completely debonded interfaces and with the inclusion of residual stresses may be indicative that the actual material interfaces are very weak following consolidation, i.e. the bond is essentially only a mechanical one.

Figure 10 shows the results of the cross-ply analyses conducted at 650°C and a strain rate of 1×10^{-4} s^{-1}. At this elevated temperature, the response is rate-dependent. The results exhibit the same behavior observed during the room temperature analyses. However, the more distinct separation between the perfectly bonded models with and without residual stresses is once again indicative of the weakened matrix at elevated temperature and the increased role of the fiber. As before, the completely debonded model with residual stresses shows the lowest stress level. The agreement between the analytical and experimental results is essentially as good as was observed at 23°C. The shape of the experimental stress-strain curve indicates an evolution of damage. This damage evolution may be due to the development of microcracks and microvoids in the matrix material. It may also be a consequence of fiber-matrix debonding.

Figure 11 shows the results of the cross-ply analyses at 650°C as a function of strain rate. All these simulations include the residual stresses developed during consolidation and completely debonded interfaces. The simulations predict that the stress level is a function of the applied strain rate. The simulation and experimental data at 1×10^{-4} s^{-1} correlate fairly well. Thus, it can be concluded that to properly model the material response a strain-rate sensitive constitutive theory should be used.

8. Conclusions

Three-dimensional finite element models were used to investigate the influence of residual stresses and interface bond condition on the macroscopic response of two composite layups. The thermomechanical behavior in $[0]_4$ and $[0/90]_s$ layups of the composite system is a function of residual stresses and the level of fiber-matrix interface bonding. Depending on the direction of the applied tensile load, the residual stresses developed during cooldown from the consolidation temperature will either slightly increase or decrease the macroscopic stress-strain response as compared to the same response in the absence of these residuals. The influence of a debonded interface as given by the loss of any chemical bonding is a major when the applied strain is normal to a fiber.

For the titanium-based metal matrix considered in this study, the use of a completely debonded fiber-matrix interface matched experimental data at 23 and 650°C very well. This correlation suggests that the interface is significantly weak following the consolidation process for the composite system investigated in this study.

The composite response at 650°C was shown to be strain-rate dependent. Thus, the use a rate-dependent constitutive theory is critical for numerically investigating the thermomechanical response of the composite.

9. Acknowledgements

The authors wish to express their appreciation to Dr. Michael Castelli of NASA Lewis Research Center for providing the experimental data. The authors wish to thank Drs. Theodore Nicholas and Lt. Col James Hansen of Wright Laboratory for their support. This work was completed under NASA Grant NCC3-218. The University Licensing Program and useful discussions with Dr. Jan Walczak of ADINA R&D, Inc. are also appreciated.

10. References

1. Robinson, D. N., Duffy, S. F., and Ellis, J. R., "A Viscoplastic Constitutive Theory for Metal-Matrix Composites at High Temperature," Thermal Stress, Material Deformation, and Thermo-Mechanical Fatigue, H. Sehitoglu and S. Y. Zamrik, eds., ASME, pp. 49-56, 1987

2. Robinson, D. N., and Duffy, S. F., "Continuum Deformation Theory for High Temperature Metallic Composites," ASCE Journal of Engineering Mechanics, Vol. 116, pp. 832-844, 1990

3. Sun, C. T. and Chen, J. L., "A Simple Flow Rule for Characterizing Nonlinear Behavior of Fiber Composites," Journal of Composite Materials, Vol. 23, pp. 1009-1020, 1989

4. Aboudi, J., "Closed Form Constitutive Equations for Metal Matrix Composites," International Journal of Engineering Science, Vol. 25, No. 9, pp. 1229-1240, 1987

5. Majors, P. S., and Krempl, E., "A Recovery of State Formulation for the Viscoplasticity Theory Based on Overstress," High Temperature Constitutive Modeling - Theory and Application, MD-Vol. 26/AMD-Vol. 121, ASME, pp. 235-250, 1991

6. Kroupa, J. L., Sherwood, J. A., Ashbaugh, N. E., Quimby, H. M., and Boyle, M. J., "Comparison of Responses of a MMC Using Classical and Unified Constitutive Matrix Behaviors," Titanium Matrix Composites, Proceedings from the Titanium Matrix Composite Workshop held at the Harry Gray Conference Center, Orlando, Florida 6-8 November 1991, WL-TR-92-4035, pp. 410-429, 1992

7. Aboudi, J., "The Effective Thermomechanical Behavior of Inelastic Fiber-Reinforced Materials," International Journal of Engineering Science, Vol. 23, No. 7, pp. 773-787, 1985

8. Santhosh, U., and Ahmad, J., "Metal Matrix Composite Response Under Biaxial Loading," MD-Vol. 40, Constitutive Behavior of High-Temperature Composites, B. S. Maumdar, G. M. Newaz, and S. Mall, eds., ASME, pp. 53-66, 1992

9. Gosz, M., Moran, B., and Achenbach, J. D., "Matrix Cracking in Transversely Loaded Fiber Composites with Compliant Interphases," AMD-Vol. 150 AD-Vol. 32, Damage Mechanics in Composites, D. H. Allen and D. C. Lagoudas, eds., ASME, pp. 133-140, 1992

10. Arnold, S. M., Robinson, D. N., and Bartolotta, P. A., "Unified Viscoplastic behavior of Metal Matrix Composites," Constitutive Behavior of High-Temperature Composites, MD-Vol. 40, B. S. Majumdar, G. M. Newaz and S. Mall, eds., ASME, pp. 17-25, 1992

11. Grady, J. E. and Lerch, B. A., "Evaluation of Thermomechanical Damage in Silicon Carbide/Titanium Composites," AIAA Journal, Vol. 29, pp. 992-997, 1991

12. Nimmer, R.P., Bankert, R.J., Russell, E.S., Smith, G.A., and Wright, P.K., "Micromechanical Modeling of Fiber/Matrix Interface Effects in Transversely Loaded SiC/Ti-6-4 Metal Matrix Composites," *Journal of Composites Technology and Research*, JCTRER, Vol. 13, No. 1, Spring 1991, pp. 3-13.

13. Mital, S. K., and Chamis, C. C., "Fiber Pushout Test: A Three-Dimensional Finite Element Computational Simulation," ASTM Journal of Composites Technology & Research, JCTRER, Vol. 13, No. 1, pp. 14-21, 1991

14. Lissenden, C. J., Pindera, M.-J., and Herakovich, C. T., "Response of SiC/Ti Tubes Under Biaxial Loading in the Presence of Damage," AMD-Vol. 150/AD-Vol. 32, Damage Mechanics in Composites, D. H Allen and D. C. Lagoudas, eds., ASME, pp. 73-90, 1992

15. Eggleston, M. R., and Krempl, E., "Modeling the Transverse Creep of Titanium-Based Metal Matrix Composites," AMD-Vol 150/AD-Vol. 32, Damage Mechanics in Composites, D. H. Allen and D. C. Lagoudas, eds., ASME, pp. 313-326, 1992

16. Mital, S. K., Lee, H.-J., and Murthy, P. L. N., "Computational Simulation of Matrix Microslip Bands in SiC/Ti-15 Composite," MD-Vol. 40, Constitutive Behavior of High-Temperature Composites, B. S. Maumdar, G. M. Newaz, and S Mall, eds., ASME, pp. 67-75, 1992

17. Majumdar, B S., Newaz, G. M., and Brust, F W. "Constitutive Behavior of Metal Matrix Composites," MD-Vol. 40, Constitutive Behavior of High-Temperature Composites, B. S. Maumdar, G. M. Newaz, and S. Mall, eds., ASME, pp. 77-90, 1992

18. Mirdamadi, M., and Johnson, W. S., "Stress-Strain Analysis of a $[0/90]_{2s}$ Titanium Matrix Laminate Subjected to a Generic Hypersonic Flight Profile," Titanium Matrix Composites, Proceedings from the Titanium Matrix Composite Workshop held at the Harry Gray Conference Center, Orlando, Florida 6-8 November 1991, WL-TR-92-4035, pp. 348-371, 1992

19. Murthy, P. L. N., and Chamis, C. C., "Interfacial Microfracture in High Temperature Metal Matrix Composites," Titanium Matrix Composites, Proceedings from the Titanium Matrix Composite Workshop held at the Harry Gray Conference Center, Orlando, Florida 6-8 November 1991, WL-TR-92-4035, pp 391-409, 1992

20. Lagoudas, D. C., and Huang, C.-M., "Damage Evolution in the Gauge Theory with Applications to Fibrous Composites," AMD-Vol. 150/AD-Vol. 32, Damage Mechanics in Composites, D. H. Allen and D. C. Lagoudas, eds., ASME, pp. 91-102, 1992

21. Bao, G., "A Micromechanics Model for Damage in Metal Matrix Composites," AMD-Vol. 142/MD-Vol. 34, Damage Mechanics and Localization, J W Ju and K. C Valanis, eds., ASME, pp. 1-12, 1992

22. Faruque, M. O., and Wu, H., "Damage Mechanics Based Constitutive Model: Application in Crash Analysis of Aluminum Components," AMD-Vol 142/MD-Vol 34, Damage Mechanics and Localization, J. W. Ju and K C Valanis, eds., ASME, pp. 41-52, 1992

23. Kuo, W.-S., and Chou, T.-S., "Modeling of Damage in Ceramic-Matrix Cross-Ply Composites," AMD-Vol 142 MD-Vol 34, Damage Mechanics and Localization, J. W. Ju and K C Valanis, eds., ASME, pp 97-107, 1992

24. Suresh, S., and Needleman, A., "Analyses of Deformation and Ductility in Metal-Ceramic Composites," AMD-Vol. 150/AD-Vol. 32, Damage Mechanics in Composites, D. H. Allen and D. C. Lagoudas, eds., ASME, pp. 191-212, 1992

25. Averill, R. C., and Reddy, J. N., "Geometrically Nonlinear Analysis of Laminated Composite Shells Using a Macro-Micro Cumulative Damage Model," AMD-Vol. 150/AD-Vol. 32, Damage Mechanics in Composites, D. H. Allen and D. C Lagoudas, eds., ASME, pp. 255-273, 1992

26. Mall, S., Hanson, D. G., Nicholas, T., and Russ, S. M., "Thermomechanical Fatigue Behavior of a Cross-Ply SCS-6/β21-S Metal Matrix Composite," MD-Vol. 40, Constitutive Behavior of High-Temperature Composites, B. S. Maumdar, G. M. Newaz, and S. Mall, eds., ASME, pp. 91-106, 1992

27. Karlak, R.F., Crossman, F.W. and Grant, J.J., 1976, "Interface Failures in Composites," *Proceedings, 105th AIME Annual Meeting*, T.T. Chiao and D.M. Schuster, ed., Metallurgical Society of AIME, New York, NY, Vol III, pp. 119-130.

28. Ramaswamy, V. G., Stouffer, D. C., and Laflen, J. H., "A Unified Constitutive Model for the Inelastic Uniaxial Response of René 80 at Temperatures between 538 C and 982 C," ASME Journal of Engineering Materials and Technology, Vol. 112, No. 3, pp. 280-286, 1990

29. Bodner, S. R., and Partom, Y., "Constitutive Equations for Elastic Viscoplastic Strain *Hardening* Materials," ASME Journal of Applied Mechanics, Vol. 42, pp. 385-389, 1975

30. Sherwood, J. A., and Boyle, M. J., "Investigation of the Thermomechanical Response of a Titanium-Aluminide/Silicon-Carbide Composite Using a Unified State Variable Model in ADINA," Computers and Structures, Vol. 40, No. 2, pp. 257-269, 1991

31. ADINA-A Finite Element Program for Automatic Dynamic Incremental Nonlinear Analysis, Report ARD 89-1, ADINA R&D, Inc., Watertown, MA, 1989

32. Sherwood, J. A., and Stouffer, D. C., "A Phenomenologically Based Constitutive Model for Rene 95," ASME Journal of Engineering Materials and Technology, Vol 114, No 4, pp 340-347, 1992

33. Boyle, M. J., "Investigation of the Thermomechanical Response of a Metal-Matrix Composite Using a Unified Constitutive Theory and the Finite Element Method," Thesis, University of New Hampshire, 1991

34. Sherwood, J. A., and Fay, E. M., "Application of a Unified Constitutive Theory to the Nonproportional Multiaxial Strain Deformation of 1045 Steel," *ASME Journal of Engineering Materials and Technology*, Vol. 114, pp 147-155, 1992

35. Sherwood, J.A. and Doore, R.J., "Estimating the Material Parametrss for Timetal-21s in the Ramaswamy-Stouffer Constitutive Model," (in preparation), 1993

36. Doore, R. J., "A Methodology for Estimating Material Parameters for the Ramaswamy-Stouffer Constitutive Model," Thesis, University of New Hampshire, 1992

11. Appendix

The use of a contact surface in ADINA requires the definition of a target surface and a contactor surface. In this case, the face of the matrix at the interface is defined as the target and the face of the fiber at the interface is defined as the contactor. However, ADINA does not allow displacements to be prescribed for nodes belonging to a contactor surface. Thus, fiber-element nodes located at the fiber-matrix interface and on the positive x-face of the model could not be constrained to have the same axial displacements as other nodes on the face. The failure to constrain these nodes would have resulted in an analysis that did not represent the behavior of a nominal layer of the composite.

The appropriate constraint of the contactor nodes was achieved through the use of short and rigid beam elements. The two-nodded beam element in ADINA is a 12 degree-of-freedom (DOF) element allowing displacements and rotations at each node. All rotational DOF's were inactive when used in conjunction with the THREEDSOLID element type. The short and rigid beam elements were defined as outward normals to the positive x-face of the model using the contactor nodes of the fiber and partner nodes located slightly above the positive x-face. The rigid beam element modulus was set to 4 ×10^7 MPa and is roughly two orders of magnitude stiffer than the SCS-6 fiber at room temperature. This value of the modulus was chosen because it is sufficiently large to truly represent a stiff member without impacting the stability of the overall finite element solution. The partner nodes to the contactor nodes used to define the beam elements were all constrained to have the same axial displacements as the other nodes on the positive x-face as shown by Figure 12. This figure provides a close-up view of the fiber-matrix interface region. Thus, by use of the rigid beam elements, the contactor nodes had axial displacements consistent with the modeling of a nominal layer of the composite.

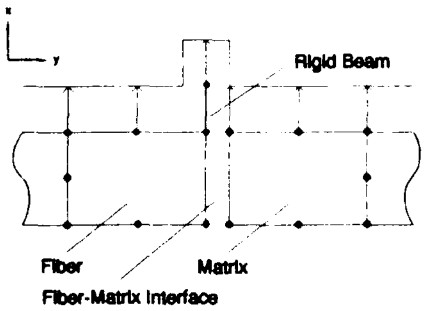

Figure 12 Schematic of rigid beam element used to satisfy axial compatibility

CRACK GROWTH UNDER CYCLIC LOADING IN FIBRE REINFORCED TITANIUM METAL MATRIX COMPOSITES

P Bowen
School of Metallurgy and Materials/IRC in Materials for High Performance Applications,
The University of Birmingham, Edgbaston, Birmingham, B15 2TT, UK

ABSTRACT

This review paper considers the experimental characterisation of crack growth from unbridged defects in fibre reinforced titanium metal matrix composites subjected to cyclic loading by the use of fracture mechanics parameters. The conditions under which parameters such as the nominal applied stress intensity range, ΔK_{app}, the nominal maximum stress intensity factor, K_{max}, and the effective stress intensity range, ΔK_{eff}, are of use, and their experimental measurement are considered. Effects of fibre fracture, stress intensity factor range, mean stress, loading configuration (bending versus tension), test temperature, and fibre-matrix interfacial strength on fatigue crack growth resistance are highlighted. Finally, a possible approach to the prediction of crack arrest in such composites is outlined.

1. INTRODUCTION

At present, there is considerable interest in silicon carbide fibre reinforced titanium metal matrix composites for use in aerospace applications at elevated temperatures. In the longer term, matrix alloys based on titanium aluminides may offer the potential for use at temperatures of upto 900°C, but for the present there are lower temperature applications where more conventional titanium alloys are suitable for use as the matrix phase. These composites are expensive to produce and to justify their use it is essential to utilise their mechanical properties fully. Commercially available unidirectionally reinforced materials at ambient temperatures may have longitudinal tensile strengths in excess of 1600 MPa, and they can exhibit fatigue lifetimes of better than 10^4 cycles when stressed at upto 75% of their longitudinal tensile strength.

Under such envisaged loading conditions it is imperative to establish their "fitness for purpose" and reliability. Indeed, to utilise their potential fully it is necessary to develop realistic methods of assessment of damage and validated lifing procedures. It is natural, in view of their envisaged substitution for monolithic alloys in many cases, to consider the use of fracture mechanics parameters including the fracture toughness, stress intensity factor range, and integrated crack growth rates for the prediction of fatigue life. *Such parameters are not usually applied to characterise damage in fibre reinforced composites, but it is important to recognise that many studies have established in these titanium MMCs that localised dominant cracks can develop under cyclic loading* (1-6). Examples are shown in Figure 1. Such observations give confidence that a fracture mechanics based approach may be of use provided that effective crack-tip stress intensities can be determined, and such evaluation is the subject of many numerical micromodels (7-13). In such models the influence of bridging length scale" must be considered carefully (6, 14-16).

The purpose of this paper is to address some of the issues that relate to the characterisation and predictive modelling of crack growth resistance from an initial unbridged defect subjected to cyclic loading. In particular the experimental determination of factors that control crack growth resistance will be considered.

2. EXPERIMENTAL STUDIES

2.1. Materials

Commercially available titanium alloy/silicon carbide fibre composite systems: Ti-15-3/SCS6; Ti-6Al-4V/SCS6; Ti-6Al-4V/SM1240; and Ti-β215/SCS6 have all been studied. Details of all systems are given elsewhere (3-6, 16-20). Here, it is noted that all composites reinforced with SCS6 fibres have a nominal fibre volume fraction of 0.35, while those reinforced with SM1240 fibres have a nominal volume fraction of fibres of 0.31. In the metastable β systems ageing treatments have been found to increase the interfacial strength. In most cases unidirectionally reinforced materials only have been considered, but initial tests on cross-ply laminates are now in progress and results obtained on the Ti-6Al-4V/SCS6 cross ply laminate system reinforced to a nominal fibre volume fraction of 0.35 are also reported.

2.2. Fatigue crack growth resistance curves

To date, most tests have been confined to single-edged-through thickness notch testpieces in bending, but comparisons for some systems have now been made with single-edged notch testpieces in tension-tension loading. Initial normalised notch depths of between 0.05 and 0.25 have been considered, where the notch depth is normalised to the testpiece width. Crack growth was monitored using the direct current potential difference technique. In many cases, care is required to establish appropriate calibration curves of normalised potential to normalised crack depth because of the small size of testpiece under consideration (5).

Tests have usually been performed using a constant cyclic load range, ΔP. Therefore, the nominal applied stress intensity range, ΔK_{app}, increases with increases

Presented at an AGARD Meeting on 'Characterisation of Fibre Reinforced Titanium Matrix Composites', September 1993.

in fatigue crack length. Crack growth resistance curves can be usefully represented under such testing conditions by plotting crack growth rate per cycle, da/dN, versus either ΔK_{app} or total crack length. Servo-hydraulic testing machines, operating at test frequencies of up to 10Hz, have been used throughout these programmes. Since these tests in bending require very low loads, the largest load-cell employed was rated to 10kN. [Under tensile - tensile loading a 100kN load cell has been utilised. Note that hydraulic grips are required to perform tests under cyclic tensile loading on these materials]. Load ratios of both R=0.5 and R=0.1 (where $R=P_{min}/P_{max}$ and P_{min}, P_{max} are the minimum and maximum loads applied over the fatigue cycle respectively) have been considered.

A methodology of evaluating crack arrest for a given geometry of specimen and initial unbridged defect has also been developed (16,25). It involves, for a given mean stress and a single composite system, testing a range of initial ΔK_{app} values until crack arrest (defined as $da/dN \leq 10^{-8}$ mm/cycle) has been achieved under a constant cyclic load range. It is important to note that multiple tests are required since once the crack is bridged by fibres then comparisons between testpieces are valid only if the testpiece geometry (including unbridged to bridged scaling length) is similar and even then great care is necessary.

2.3. In-situ determination of fibre fracture during cyclic loading

Early studies deduced the onset of fibre fracture from audible emissions and rapid voltage excursions observed during crack growth (4, 21). Such events have now been quantified by the in-situ use of both acoustic emission and direct optical observation of the failure of (surface) fibres during cyclic loading. A commercially available PAC LOCAN AE analyser has been used, and under the conditions of use, fibre fracture is characterised by amplitudes of ≥ 90dB. Details of this system and analysis are given elsewhere (22, 23).

2.4. Evaluation of fibre-matrix interfacial strength

Early studies employed micro-hardness push-out tests, (5, 19) but recently a continuous load-displacement fibre push-out test has been developed at the University of Birmingham. A remote high resolution optical telescope and video recording system have been used to monitor the behaviour of the individual fibres during the push-out tests. Details are given elsewhere, (20) but here it is sufficient to note that such a system allows both the debonding shear stress and the frictional shear stress of the (debonded) interface to be evaluated.

In general for the systems studied to date the value of the frictional shear stress appears to be higher than that of the debonding shear stress.

The wide range of assessment techniques employed during these studies have allowed micromechanisms of crack growth in fibre reinforced composites to be elucidated, and they have also highlighted many important factors for controlling crack growth resistance. A selection of some of these results is now presented.

3. GENERAL CHARACTERISATION OF THE FATIGUE CRACK GROWTH RESISTANCE CURVE

In monolithic Ti-6Al-4V material (manufactured by a foil-foil processing route similar to that used for many of the composites under study here), a characteristic fatigue crack growth resistance curve is obtained, see Figure 2. For $\Delta K \geq 4.5$ MPam$^{1/2}$, the curve can be represented well by a Paris-Erodgan relationship of the form $da/dN = CK^{m}$, where C and m are numerical constants, equal to 9.2 10^{-9} mm/cycle and 3.12 respectively (for ΔK in MPam$^{1/2}$).(11)

In sharp contrast for the Ti-6Al-4V/ SM1240 composite system, the dependence of crack growth rates observed experimentally da/dN is shown versus total crack length, Figure 3, for an initial ΔK_{app} of 7.5 MPam$^{1/2}$. At this stress intensity range, crack growth rates decrease with increases in fatigue crack length until crack arrest is obtained, despite the increase in nominal stress intensity range with fatigue crack length increase (because these tests are performed at constant cyclic load range).(11)

Such observations are quite general in all systems studied to date, where crack growth increments per cycle, da/dN, usually decrease initially with crack length increase ahead of the initial unbridged defect. Examples are given in Figures 3 - 6. These decreases in crack growth rates are despite an increase in nominal applied stress intensity range, ΔK_{app}, with crack length increase. An explanation for this unusual crack growth behaviour is given by considering optical sections through interrupted fatigue crack growth tests, see Figure 1. The micromechanism of crack growth is well characterised by initial crack growth through the matrix which breaches (debonded) fibres in its wake. In studies to date no fibres have been observed to fail ahead of the growing fatigue crack tip). The bridging fibres then reduce the effective stress intensity at the growing crack tip, ΔK_{eff}, and if no (or very few) fibres fail then crack growth rates decrease eventually to crack arrest defined here by $da/dN \leq 10^{-8}$mm/cycle. The balance between sub-critical crack growth and catastrophic failure will be governed primarily by the number of fibres remaining intact within the crack wake, see Figure 1 and Table 1. In all tests performed to date crack growth either arrests eventually or catastrophic failure occurs (defined by the symbol ☆ in all Figures).

A second general feature of all tests to date is that the failure of discrete fibres often sharply increases local crack growth rates, see Figure 7, where the failure of fibres has been identified unequivocally by acoustic emission techniques. (For reference a complete amplitude distribution for events detected during this test is given in Figure 8). Note to measure such local increases in crack growth rate it is essential to monitor crack growth rates by continuous potential difference techniques. Further examples are given in Figure 9, and Figure 10 (following monotonic overloads to fracture individual fibres). The sharpest increases in local fatigue crack growth rates are observed at near crack arrest growth rates, and the magnitude of these growth rate excursions is also in part determined by the precise secant method employed to determine crack growth rates. These observations indicate that to model these systems the fibres must be considered as discrete entities (11-13). Moreover, many tests have illustrated that fibres may fail after extended cycling in near crack arrest regions, (see Figure 4) and which may plausibly be interpreted as a result of changes to fibre-matrix interfacial regions with cycling.

The paper now considers some specific experimental observations which indicate controlling features of these composite systems when subjected to cyclic loading in the presence of a through-thickness unbridged defect.

3.1. *Effects of test temperature*

In tests performed to date at elevated temperatures crack growth rates usually increase relative to those measured at room temperature(17, 18). However, a full picture of the influence of test temperature on testpiece life and/or crack arrest has yet to emerge, and it is expected in part to depend upon the influence of test temperature on the fibre-matrix interfacial strength. Certainly in systems which can age during testing pronounced effects of test temperature and test frequency are observed, see Figures 11 and 12 respectively for Ti-15-3/SCS6 composites in the solution treated condition. For an initial ΔK_{app} level of 16 MPam$^{1/2}$ crack arrest is observed at room temperature only, Figure 11. As the test temperature is increased, crack growth towards arrest is interrupted by sharp-crack growth rate excursions, and catastrophic testpiece failure occurs eventually. In general, crack growth rates increase with increased test temperature and catastrophic failure occurs at decreased crack length, see Figure 11. This is reflected clearly in the number of cycles to failure as a function of test temperature, see Table 2. More subtle effects of test frequency are also observed at the test temperature of 500°C, see Figure 12. In general, the poorer crack growth resistance of the composites that is displayed at elevated temperatures requires both faster matrix crack growth rates and easier fibre fracture (consistent with an increased fibre-matrix interfacial strength on ageing), but further work is required to establish such observations fully.

For Ti-6Al-4V/SCS6 composites such effects of elevated temperature on crack growth behaviour are less clear, see Figure 13. Crack growth rates are once more increased at the test temperature of 550°C relative to their respective room temperature values, and lower test frequencies promote increased crack growth rates. However, in this system catastrophic failure occurs at a longer crack length at the elevated temperature. Note that this observation is rationalised by the fact that crack bifurcation away from the maximum mode I opening direction occurs at the test temperature of 550°C for this composite system alone and is consistent with a reduced effective fibre-matrix interfacial strength at this elevated temperature(26).

These preliminary observations indicate the potential complexity of the behaviour of these composites at elevated temperatures. Some confidence in the repeatibility of the types of testing carried out here can be gained from Figure 14 and Table 2 which indicates only a factor of two difference in total life for similar testpieces, and closely similar crack growth resistance curves are observed for all three testpieces.

3.2. Effects of fibre-matrix interfacial strength

After peak ageing the interfacial strength of the β21S/SCS6 composite system increases significantly, compared with solution-treated or as-processed conditions. Values of the debonding shear stress increase from approximately 80 to 120MPa, and values of the frictional shear stress (after debonding) increase from 100 to 180 MPa. Moreover, the number of cycles to failure decreases sharply from a minimum of 1,800,000 for as-processed and solution treated conditions to 88,000 for the peak aged condition. These studies are reported elsewhere, (20) but here it is noted that the initial stress intensity factor range was sufficient to promote fibre failure in all conditions. Under these circumstances an increase in interfacial strength would be expected to increase the incidence of fibre failure and hence to promote earlier catastrophic failure, because the fibres will be more highly stressed as a result of more efficient load transfer.

3.3. Effects of loading geometry

Figure 4 suggests that crack arrest can occur more readily under cyclic tensile loading than under cyclic three point bending, for tests performed under identical initial ΔK_{app} conditions. However, this can be shown to be a function primarily of the rate of increase in stress intensity range with crack increment by matching the rate of nominal ΔK_{app} increase for each geometry. (This is achieved simply by load range shedding for the tensile geometry and load range increases for the bending geometry after appropriate crack depth increments).

Under such conditions, similar crack growth behaviour can be produced for each testpiece geometry, and this illustrates the usefulness of even nominal stress intensity parameters in characterising crack growth in *geometrically similar testpieces* (24).

In this context the influence of testpiece size is expected to introduce further significant effects and is the subject of continuing studies.

3.4. Effects of mean stress

In general, two different regimes of behaviour can be distinguished under equivalent ΔK_{app} conditions, and they appear to depend upon whether increased mean stress promotes major instances of fibre failure. In situations where crack arrest will eventually occur at both mean stresses Figure 5, the influence of mean stress can be seen only to promote crack growth to longer crack lengths (i.e. an increased number of load cycles occur prior to arrest). This may be the result of minor instances of fibre failure, but is more likely in general to be simply a consequence of decreased threshold values, ΔK_{th}, which often result in monolithic alloys at increased mean stress (17). In other examples, cracks can grow towards arrest at low mean stress conditions, $R = 0.1$, but can grow to catastrophic failure under equivalent ΔK_{app} conditions at high mean stress, $R = 0.5$, see Figures 6 and 15. In such situations little effect of the higher mean stress is observed on crack growth rates prior to catastrophic failure. In general, bridging fibre failure is deduced to occur more readily at high mean stress because they will be required to resist greater local crack opening displacements during the load cycle. *However, an important feature is that as each fibre is stressed more highly it will exert a higher clampback stress across the crack surfaces in the wake of the crack provided it does not fail i.e. it is both more potent at shielding the crack-tip and closer to reaching its fibre fracture stress in tension.* Such considerations are inherent to numerical and analytical micromodelling studies and are discussed elsewhere(6, 11-13). In sumary, care is required to assess the effects of mean stress in these fibre reinforced composites.

3.5. Effects of initial applied stress intensity range

For a given depth of initial unbridged crack (notch) examples of the influence of ΔK_{app} on crack growth resistance are shown in Figures 16 and 17. In both systems, crack growth rates are similar initially for both levels of ΔK_{app}, but then crack arrest is observed for the lower applied stress intensity range only. Such observations indicate the delicate balance than can sometimes exist between promoting crack arrest and catastrophic failure in these composites(4,17).

Recently, further systematic studies have considered both effects of mean stress and initial applied stress intensity range for a constant initial unbridged defect size and a single composite system(16,25). These studies have resulted in a simple model for the prediction of fibre failure for testpieces of a specific geometry and for the given composite system (Ti-6Al-4V/SM1240). This is reported elsewhere in more detail (16), but some of the results are also summarised in Table 3. Since crack arrest occurs if few fibres fail, then provided K_{max} values (where K_{max} is the maximum nominal stress intensity factor applied over the fatigue cycle) after the first row of breached fibres are kept below 27.5 $MPam^{1/2}$ then crack arrest will be predicted, and is consistent with the experimental observations in this single system. It is of interest to note that such values of K_{max} that can be tolerated vary with composite system for testpieces of identical geometry, and are greatly reduced for a 0/90 cross-ply laminate (which has only half the number of 0^{o} bridging fibres present for an equivalent increment of crack depth), see Table 4.

It is important to note that such an approach implicitly includes a bridging scale length argument because the crack depth increment to breach the first row of fibres will be constant for a given fibre architecture. Thus the model can account easily for the experimental observations, Figure 18, that a smaller initial unbridged normalised crack depth, a_o/W (where W is the testpiece depth), can be more damaging than a larger unbridged defect when tested under an identical initial stress intensity range ΔK_{app} (≈ 18 $MPam^{1/2}$). This is simply because the fixed absolute increment of crack depth required to breach the first row of fibres will produce a larger increase in K_{max} for the smaller initial crack. The approach has clear potential to produce crack arrest maps.

4. GENERAL DISCUSSION

Several factors that may control crack growth resistance have been demonstrated experimentally. Although no unique relationship between an applied nominal stress intensity factor range and crack growth rate can be defined, it is hoped that the use of parameters such as ΔK_{app} and K_{max} to characterise crack growth resistance for specific testpiece geometries has been illustrated. Moreover, the beginning of a predictive model to address crack arrest has been outlined. It considers the failure of fibres to be controlled primarily by the level of K_{max} applied after they have been breached by matrix crack growth (a quantitative description will require local crack opening displacements under load and detailed numerical micromodelling), and the extent of fibre failure determines the integrity of the composite.

This approach, in principle, can be applied to a wide range of fibre architectures, crack sizes, shapes and geometries of testpiece (components). It avoids many of the problems inherent to the modelling of actual crack growth rates prior to catastrophic failure, but further work is required to establish if such crack arrest maps are unduly pessimistic with respect to lifing of actual components.

The degree of complexity inherent to crack growth resistance in these materials should not be underestimated. Effects of interfacial strength, mean stress, testpiece geometry and initial applied stress intensity factor range on crack growth resistance under cyclic loading will always be significant if they alter the balance of the number of bridging fibres that fail for any given crack depth increment. Great care is needed if fracture mechanics concepts are to be applied to the reliability of components containing a range of crack shapes and sizes, and the approach will require both predictive modelling and experimental validation. It forms the basis of much current research work within the group.

5. CONCLUSIONS

Dominant localised fatigue cracks are produced from unbridged defects in fibre reinforced titanium alloy composites subjected to cyclic loading. The growth of these cracks can be characterised by the use of fracture mechanics parameters and their experimental measurement has been considered. Crack growth resistance is controlled by the number of intact fibres bridging behind the growing fatigue crack-tip in its wake. Effects of test temperature, interfacial strength, applied stress intensity factor range, mean stress and testpiece geometry on crack growth resistance will be marked if the balance of the number of bridging fibres that fail for a given increment of matrix crack growth is altered. For specific testpiece geometries and fibre architecture, the onset of fibre failure appears to be controlled by the maximum nominal stress intensity factor applied over the fatigue cycle.

6. ACKNOWLEDGEMENTS

The author is indebted to many members of the fracture and fatigue group at the University of Birmingham. Particular thanks are due to D C Cardona (now at Rolls-Royce plc), P J Cotterill, J F Knott, M Strangwood and K Takashima together with C Barney, K M Fox, A R Ibbotson and J G Pursell. All studies have been supported by SERC, with additional funding from Rolls-Royce plc, Derby and BP Research Limited, Sunbury. The support of M V Hartley at Rolls-Royce plc has been invaluable to many of the programmes. The provision of facilities both within the IRC in Material for High Performance Applications and the School of Metallurgy and Materials is also gratefully acknowledged. Several of the studies were initiated in collaboration with Dr C J Beevers and his death in September 1992 is noted with sadness.

7. REFERENCES

1. W S Johnson, "Mechanical Fatigue of Advanced Materials", Eds RO Ritchie et al, Santa Barbara, January 1991, pp 357-377, MCE Publications.
2. D Walls, G Bao and F Zok, "Mechanical Fatigue of Advanced Materials", Eds R O Ritchie et al, Santa Barbara, January 1991, pp 343-356, MCE Publications.
3. C Barney, C J Beevers and P Bowen, J Composites, 24, pp 229-234, 1993.
4. P Bowen, A R Ibbotson and C J Beevers, "Mechanical Fatigue of Advanced Materials", Eds R O Ritchie et al, Santa Barbara, January 1991, pp 379-394, MCE Publications.
5. P Bowen, P J Cotterill and A R Ibbotson, "Test Techniques for Metal Matrix Composites", Ed N D R Goddard, IOPP, London, pp 82-96, 1990.
6. P Bowen, "The Processing, Properties and Applications of Metallic Materials", Eds M H Loretto and C J Beevers, Birmingham, September 1992, pp 697-718, MCE Publications.
7. B Budiansky, J W Hutchinson and A G Evans, J Mech Phys Solids, 34, pp 167-189, 1986.
8. D B Marshall, B N Cox and A G Evans, Acta Metall, 33 pp 2013-2021, 1985.
9. D B Marshall and B N Cox, Acta Metall, 35, pp 2607-2619, 1987.
10. R M McMeeking and A G Evans, Mechanics of Materials, 9, pp 217-227, 1990.
11. D C Cardona, C Barney and P Bowen, J Composites, 24, pp 122-128, 1993.
12. P Bowen, D C Cardona and A R Ibbotson, Mat Sci Eng A, 153, pp 628-634, 1992.
13. D C Cardona and P Bowen, "Theoretical Concepts and Numerical Analysis of Fatigue", Ed C J Beevers, May 1992, Birmingham, MCE Publications (awaiting publication).

14. B N Cox, Acta Metall et Mater, 39, pp 1189-1201, 1991.

15. B N Cox and C S Lo, Acta Metall et Mater, 40, pp 69-80, 1992.

16. C Barney, D C Cardona and P Bowen, ICCM9, Madrid, July 1993.

17. P J Cotterill and P Bowen, J Composites, 24, pp 241-247 1993.

18. A R Ibbotson, C J Beevers and P Bowen, J Composites, 24, pp 241-247, 1993.

19. K M Fox, P J Cotterill, M Strangwood and P Bowen, Proc 7th World Conf on Titanium, San Diego, July 1992, to be published.

20. K M Fox and P Bowen, ICCM9, Madrid, July 1993.

21. A R Ibbotson, C J Beevers and P Bowen, Scripta Metall et Mater, 25, pp 1781-1786, 1991.

22. K Takashima and P Bowen, 3rd Int SAMPE Symposium, Chiba, Japan, December 1993,

23. J G Pursell, K Takashima and P Bowen, 3rd Int SAMPE Symposium, Chiba, Japan, December 1993.

24. P J Cotterill and P Bowen, submitted for publication, Mat Sci Tech, 1993.

25. P Bowen, ICCM9, Madrid, July 1993.

26. J Gayda Jr., T P Gabb and A D Freed, NASA Technical Memorandum TM-101984, April 1989.

Number of Bridging Fibres Remaining Intact	K_{max} (nominal) (MPa√m)	Type of Event
8	39	Catastrophic Failure
12	64	Catastrophic Failure
26	66	No Growth
21	80	No Growth
16	51	No Growth
7	64	Catastrophic Failure

Table 1. The importance of the number of bridging fibres intact in the crack wake on stable/unstable crack growth transitions (Ti-6Al-4V/SCS6)(4,21).

		25°C	200°C	350°C	500°C
R = 0.1	10.0 Hz	Crack arrest		1 354 700	
R = 0.5	10.0 Hz	Crack arrest	697 800	323 600	38 400
				201 900	
				167 200	
	2.0 Hz				12 000
	0.5 Hz			147 000	16 200

Table 2. Comparison of the numbers of cycles to specimen failure for tests conducted at different temperatures, load ratios and frequencies for an initial $\Delta K_{app} \sim 16$ MPam$^{1/2}$ (Ti-15-3/SCS6)(17).

Stress Ratio	initial ΔK (MPa√m)	initial K_{max} (MPa√m)	K_{max} after 1st row fibres (MPa√m)	Test Result
0.5	12.1	24.2	25.8	Crack Arrest
0.5	13.8	27.6	29.8	Catastrophic Failure
0.1	22.3	24.8	27.5	Crack Arrest
0.1	25.0	27.8	30.2	Catastrophic Failure

Table 3. Effects of mean stress; initial ΔK_{app}, K_{max}; K_{max} after the first row of fibres; on crack growth resistance (Ti-6Al-4V/SM1240)(16).

Material	K_{max} after first row of fibres (MPam $^{1/2}$)	Test Result
Ti-6Al-4V/SCS6	22.5	Crack arrest
	28.8	Catastrophic failure
Ti-β21S/SCS6	39.6	Crack arrest
	40.6	Catastrophic failure
	45.6	Catastrophic failure
Ti-15-3/SCS6	35.0	Crack arrest
	42.2	Catastrophic failure
Ti-6Al-4V/SCS6 (0/90 laminate)	15.0	Crack arrest
	19.8	Catastrophic failure

Table 4. Comparison of experimental observations of crack growth behaviour related to K_{max} after the first row of breached fibres(16,25).

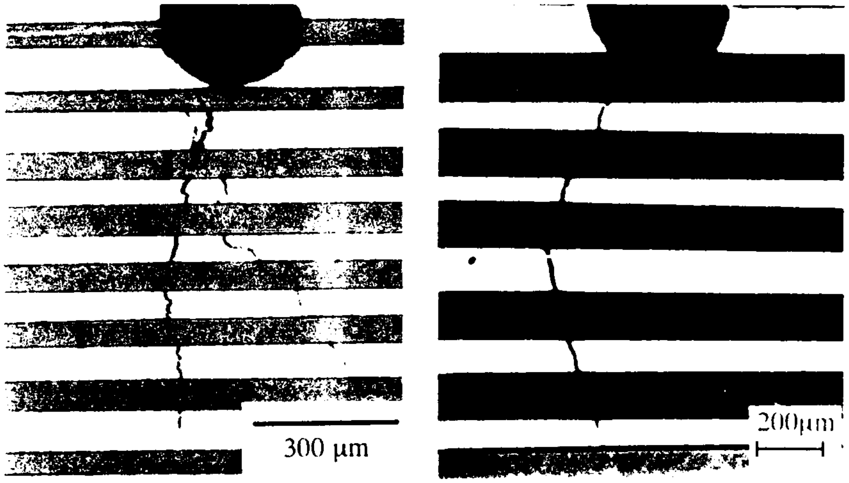

Figure 1. Optical micrographs of sections through interrupted fatigue crack growth:
(a) Ti-6Al-4V/SCS6; (b) Ti-15-3/SCS6.

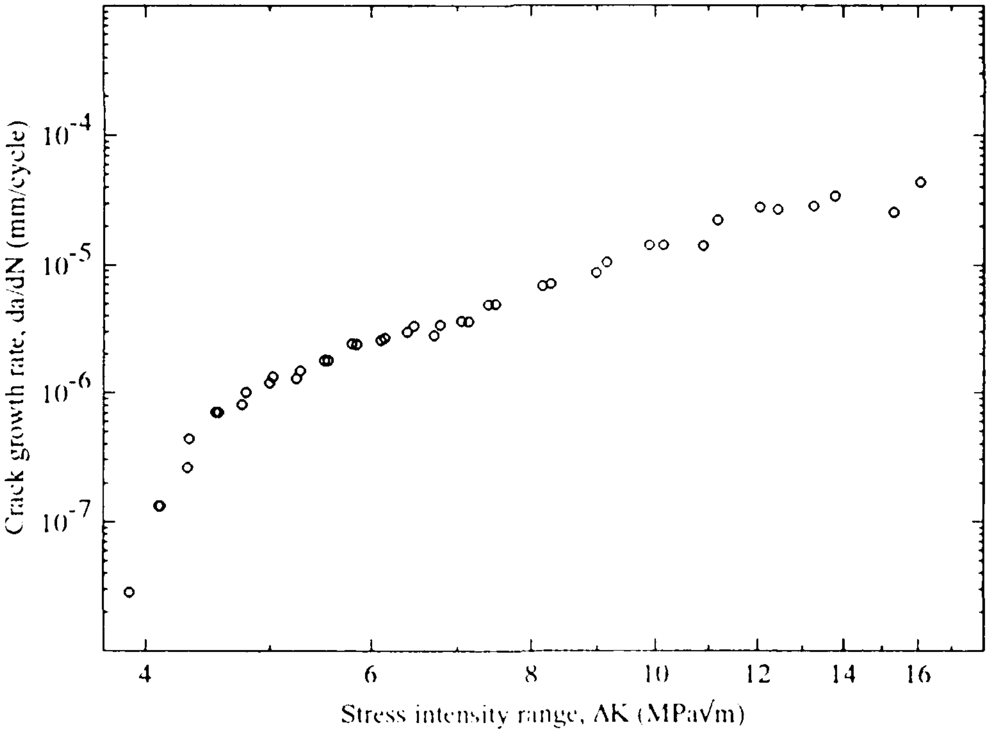

Figure 2. Crack growth resistance curve: da/dN versus ΔK, R=0.1, ν=0.5Hz. Monolithic Ti-6Al-4V alloy, ambient temperature.

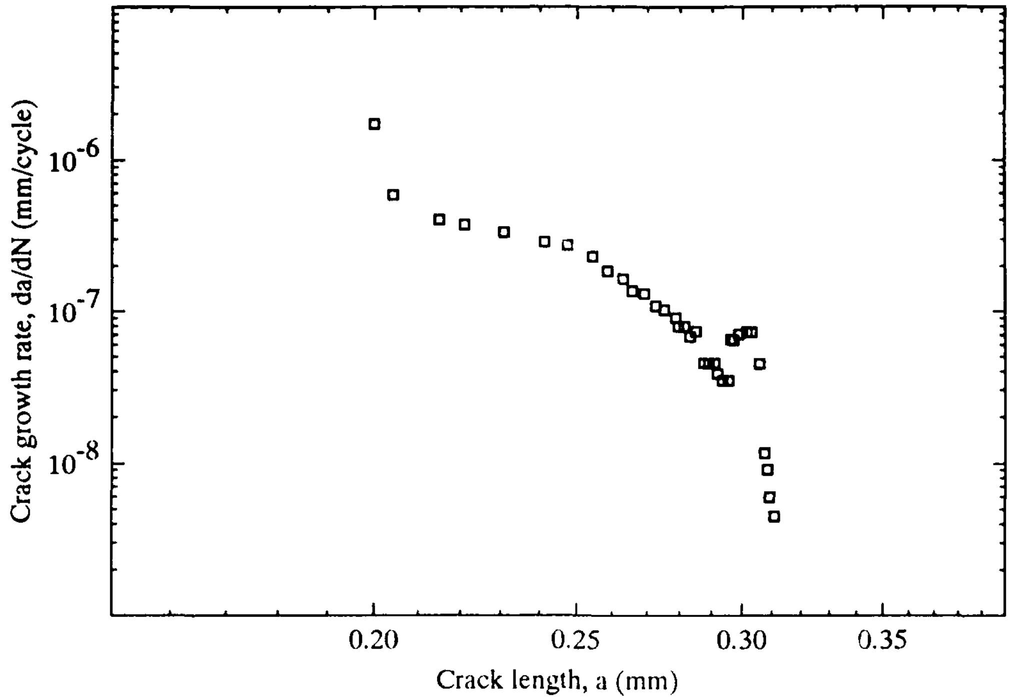

Figure 3. Crack growth resistance curve: da/dN versus crack length for initial ΔK_{app} = 7.5MP√m, R=0.5, υ=10Hz. Ti-6Al-4V /Sigma composite, ambient temperature.

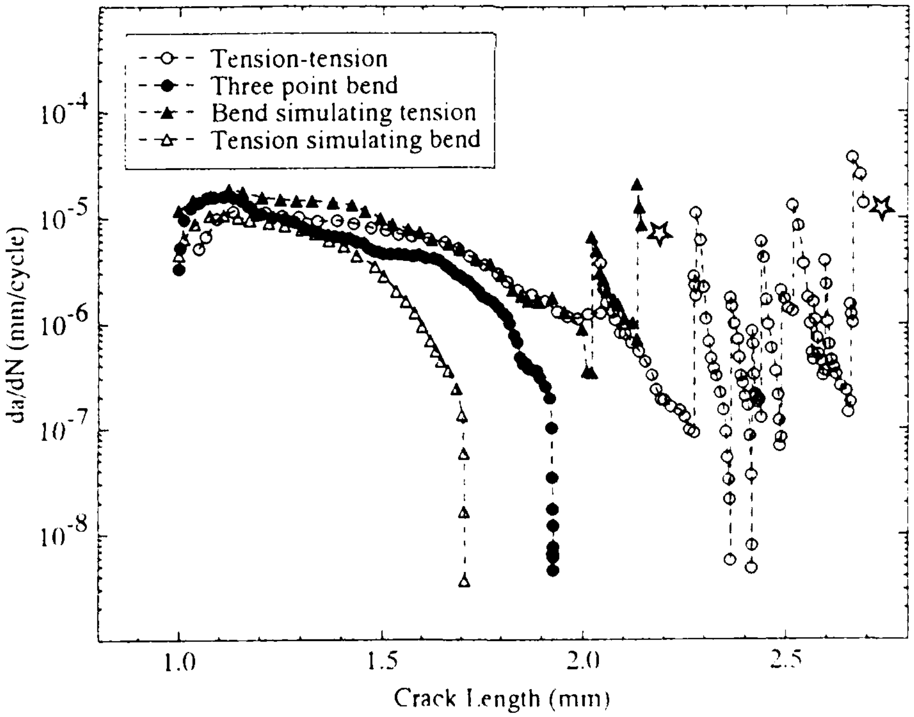

Figure 4. Crack growth resistance curves: da/dN versus total crack length for initial ΔK_{app} 17MPam$^{1/2}$, R=0.5, v=10Hz. Ti-15-3/SCS6 composite, solution treated, and tested at ambient temperature under cyclic bending and cyclic-tension.

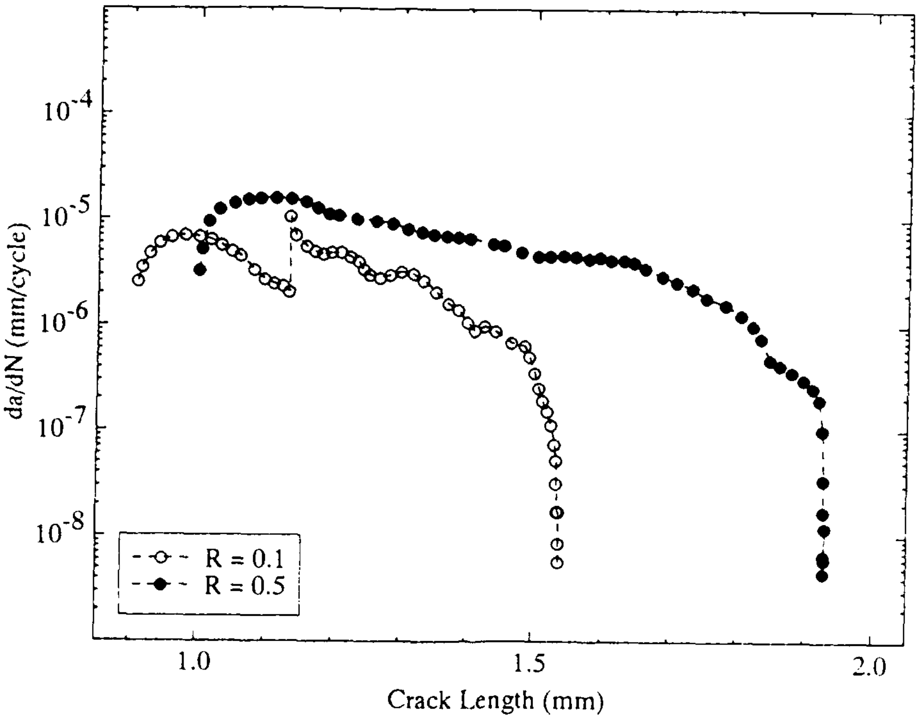

Figure 5. Effect of load ratio on crack growth resistance curves: da/dN versus crack length for initial $\Delta K_{app} \approx 16$ MPa√m, υ=10Hz. Ti-15-3/SCS6 composite, soution treated condition ambient temperature.

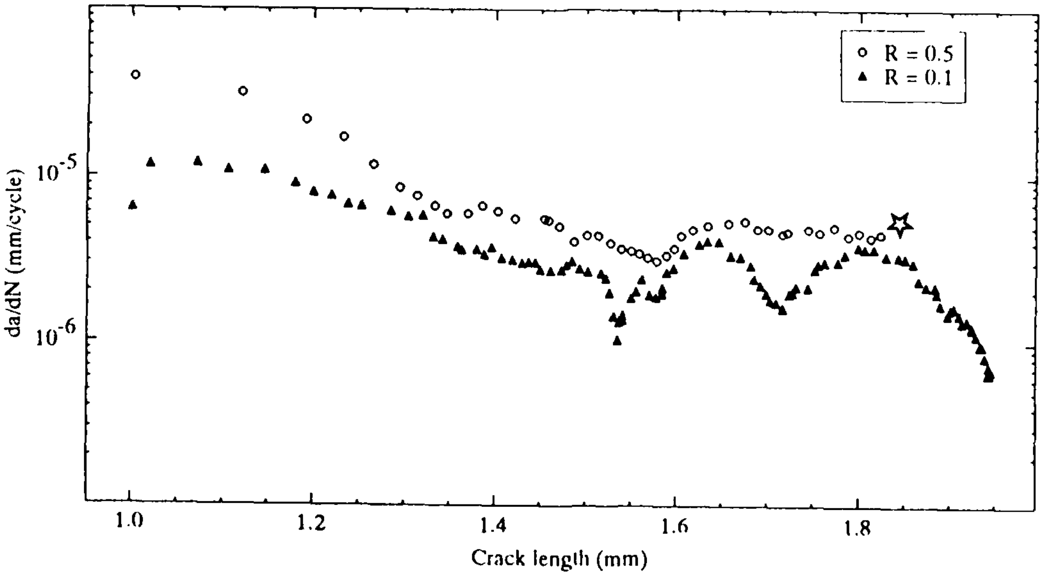

Figure 6. Effect of load ratio on crack growth resistance curves: da/dN versus crack length for initial $\Delta K_{app} \approx$ 18MPa√m, υ=0.5Hz. Ti-6Al - 4V / SCS6 composite, ambient temperature.

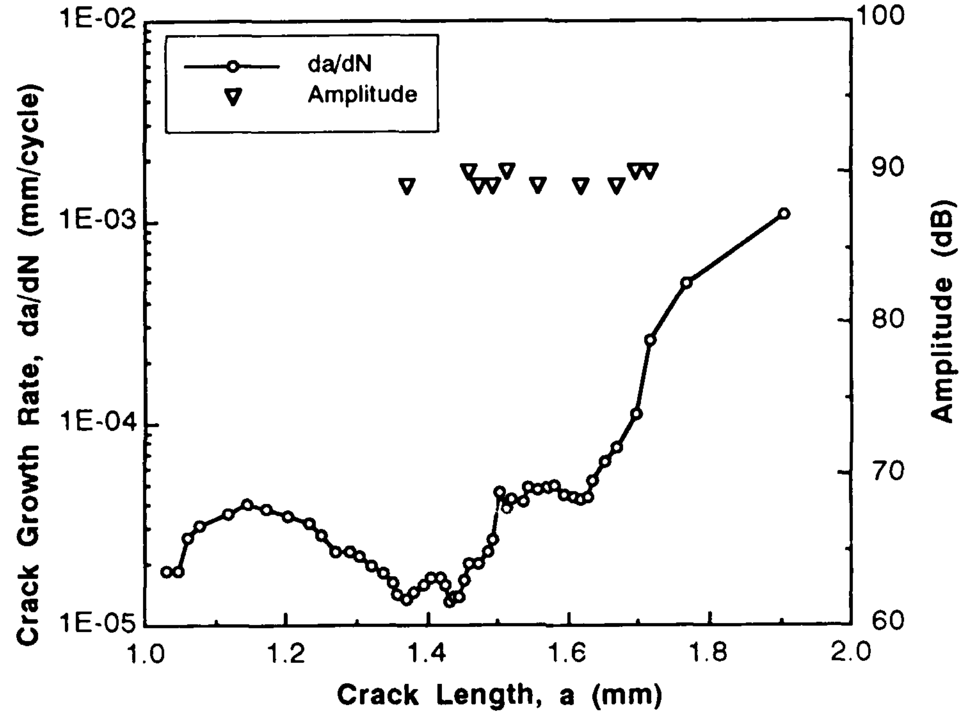

Figure 7. Crack growth resistance curve: da/dN versus nominal ΔK_{app} for initial ΔK_{app} 18MPam$^{1/2}$, R=0.1, υ=0.5Hz. Ti-6Al-4V/SCS6 0/90 cross-ply laminate, tested at ambient temperature. Individual fibre failures measured using AE events are arrowed.

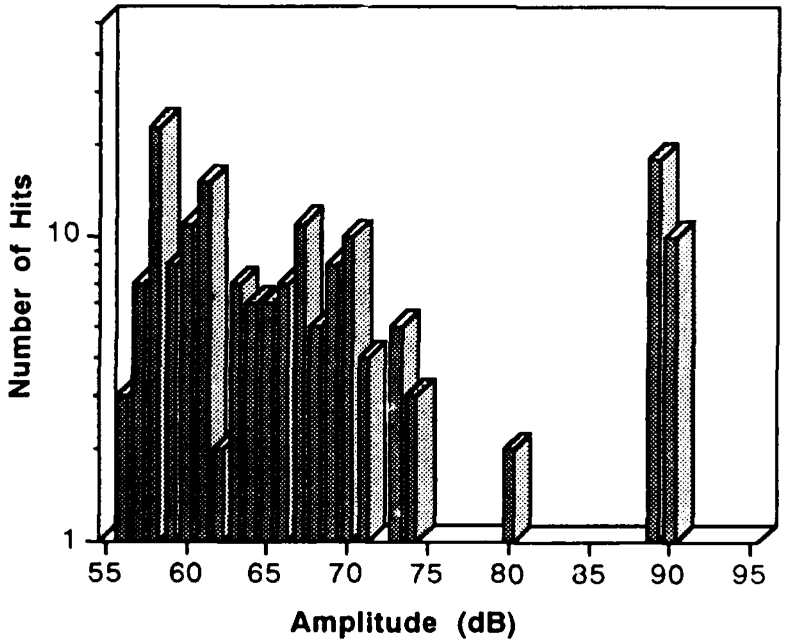

Figure 8. Acoustic emission amplitude spectrum measured after failure for the 0/90 cross-ply laminate.

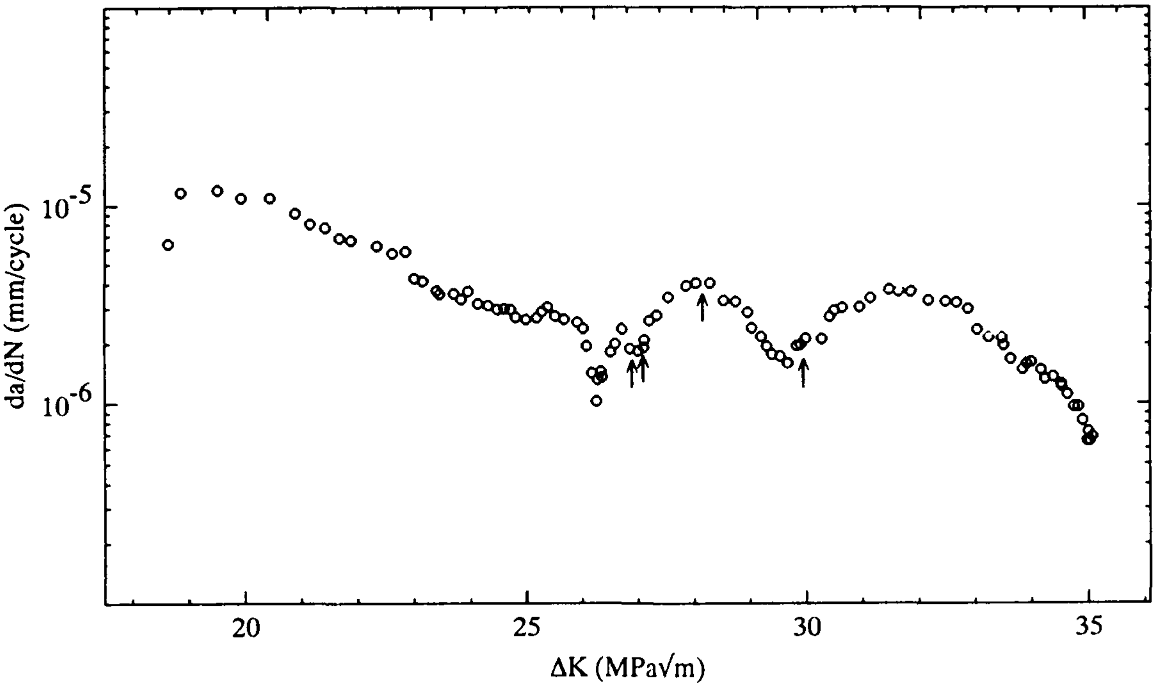

Figure 9. Effect of local fibre failure (arrowed) on crack growth resistance curves: da/dN versus ΔK_{app}, υ=0.5Hz, R=0.1, Ti-6Al - 4V / SCS6 composite, ambient temperature.

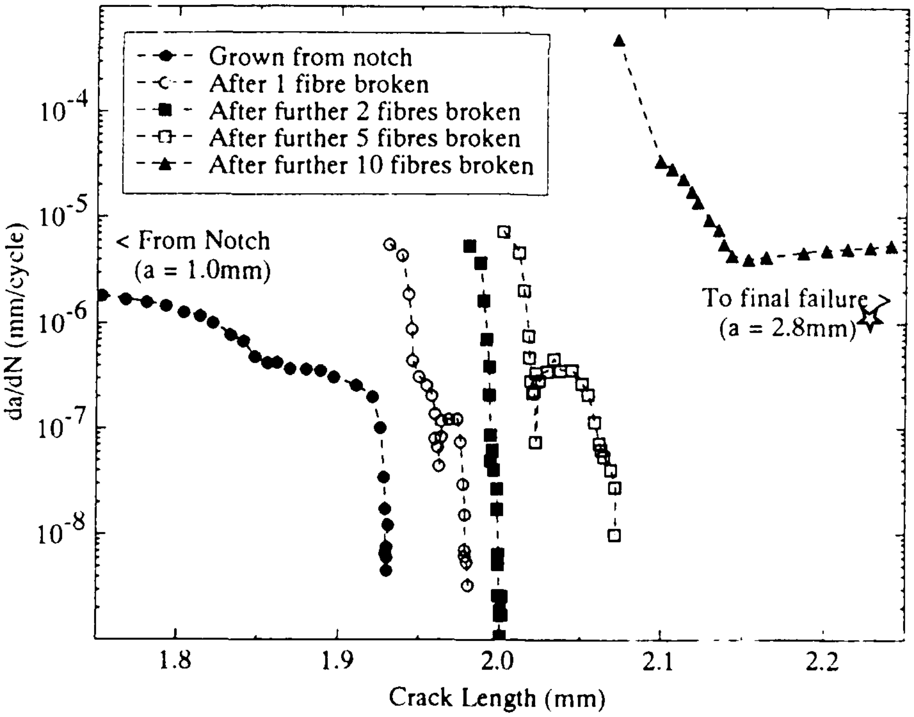

Figure 10. Effect of monotonic overloads on crack growth resistance curves: da/dN versus crack length, R=0.5, υ=10Hz. Ti-15 - 3 / SCS6 composite, ambient temperature, solution treated condition.

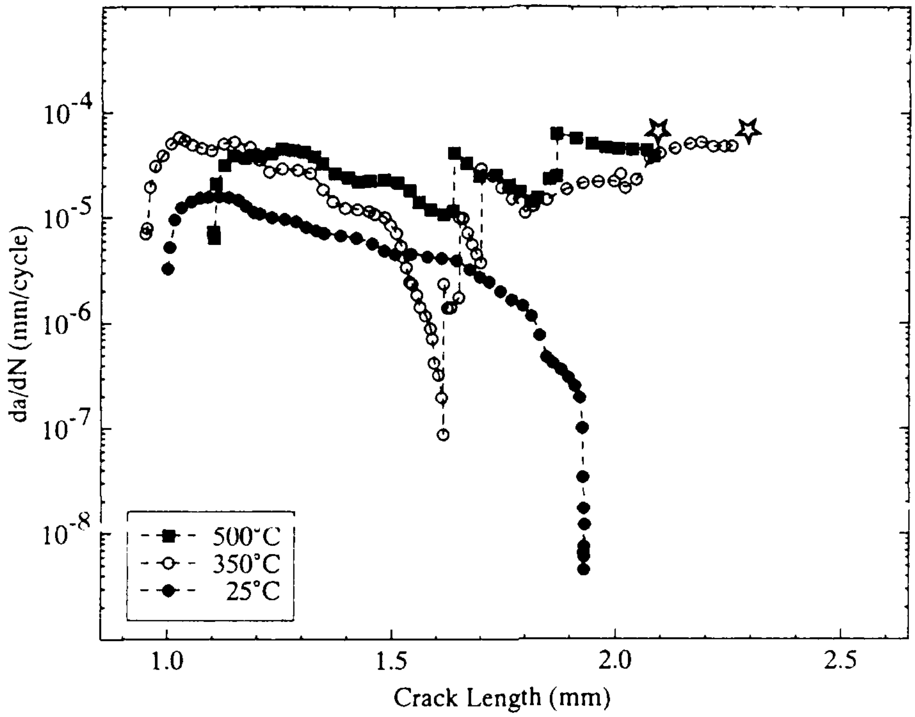

Figure 11. Crack growth resistance curve: da/dN versus crack length for initial $\Delta K_{app} \approx$ 16MPa√m, R=0.5, υ=10Hz, for a range of test temperatures. Ti- 15-3 / SCS6 composite, solution treated condition.

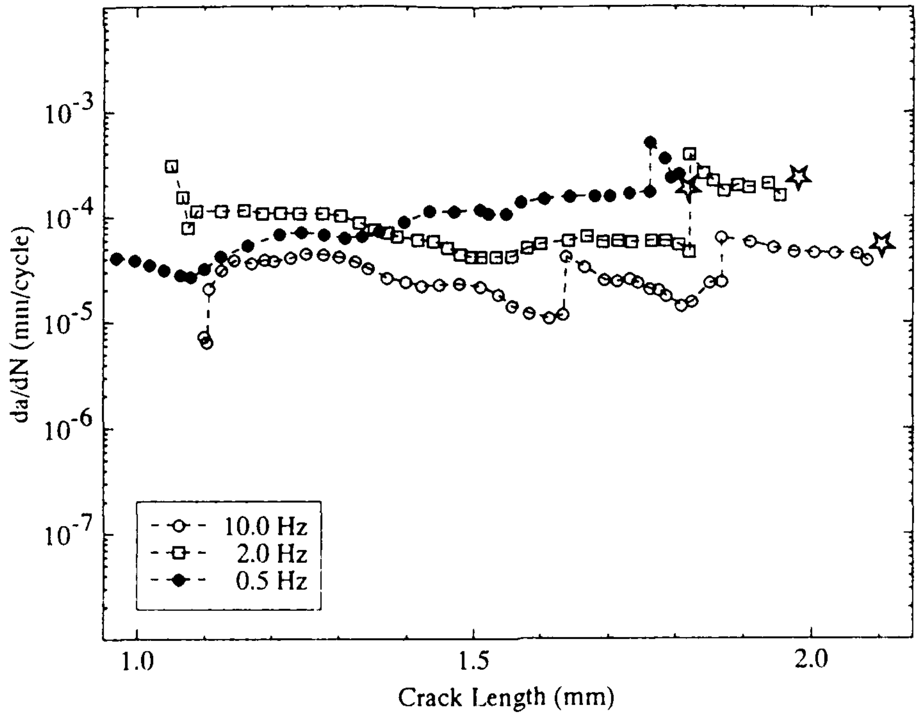

Figure 12. Effect of frequency on fatigue crack growth rates measured at 500°C, R=0.5, for initial $\Delta K_{app} \approx$ 16 MPa√m. Ti-15-3/SCS6 composite, solution treated condition.

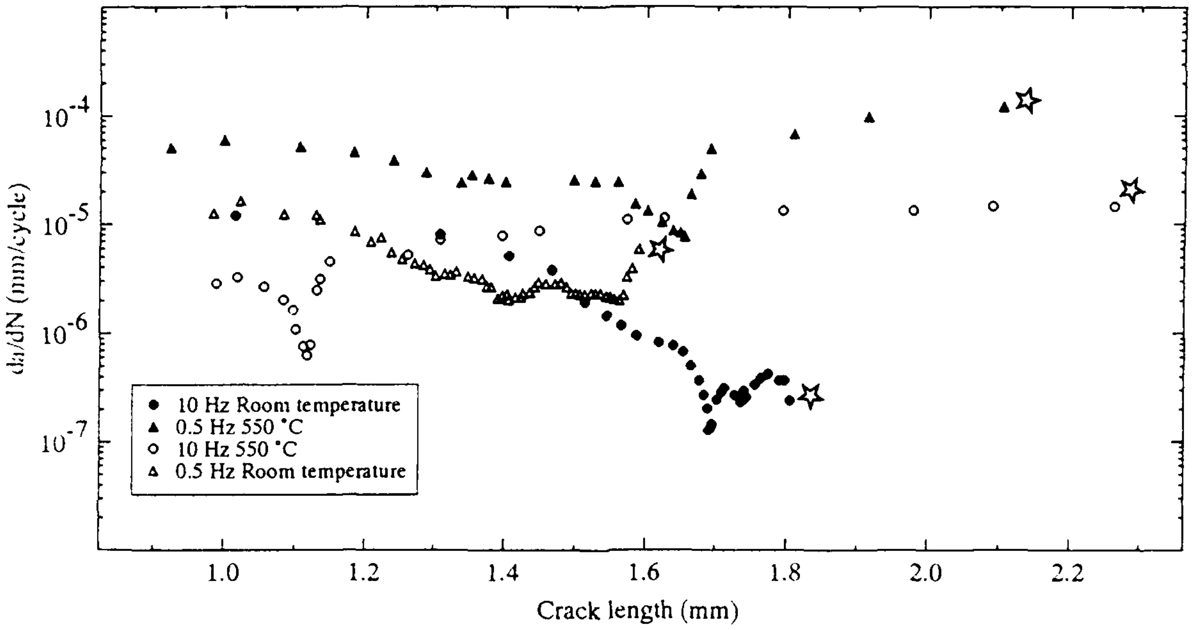

Figure 13. Crack growth resistance curves: da/dN versus crack length for initial $\Delta K_{app} \approx 23\mathrm{MPa}\sqrt{m}$, R=0.1, for ambient temperature and 550°C. Ti-6Al - 4V / SCS6 composite.

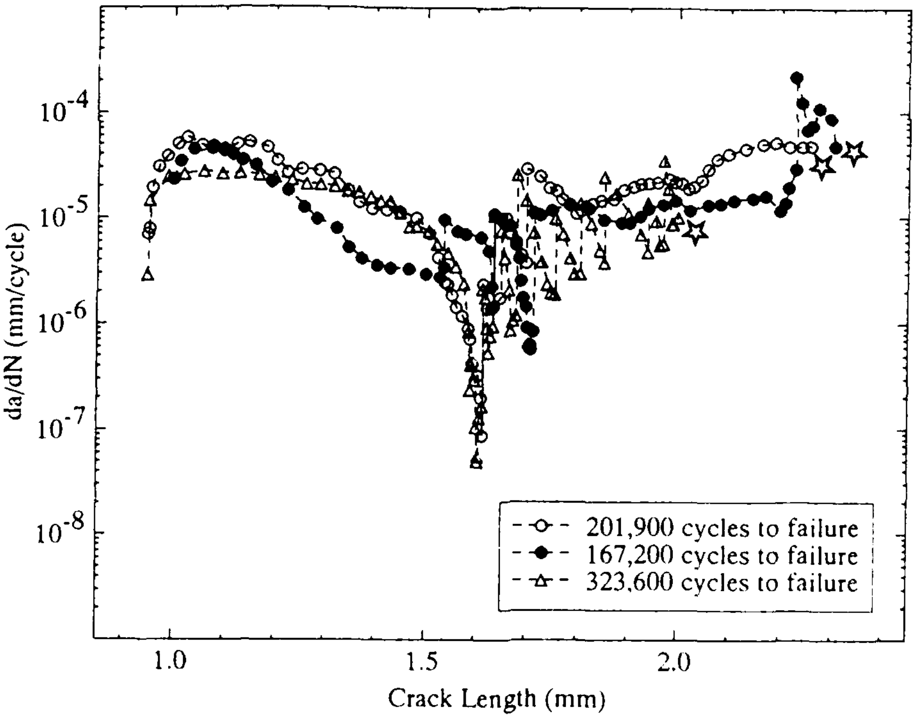

Figure 14. Variation in fatigue crack growth rates measured in three different specimens tested under identical conditions at 350°C,R=0.5, ν=10Hz for an initial $\Delta K_{app} \approx 9.6\ \mathrm{MPa}\sqrt{m}$. Ti-15-3/SCS6 composite, solution treated condition.

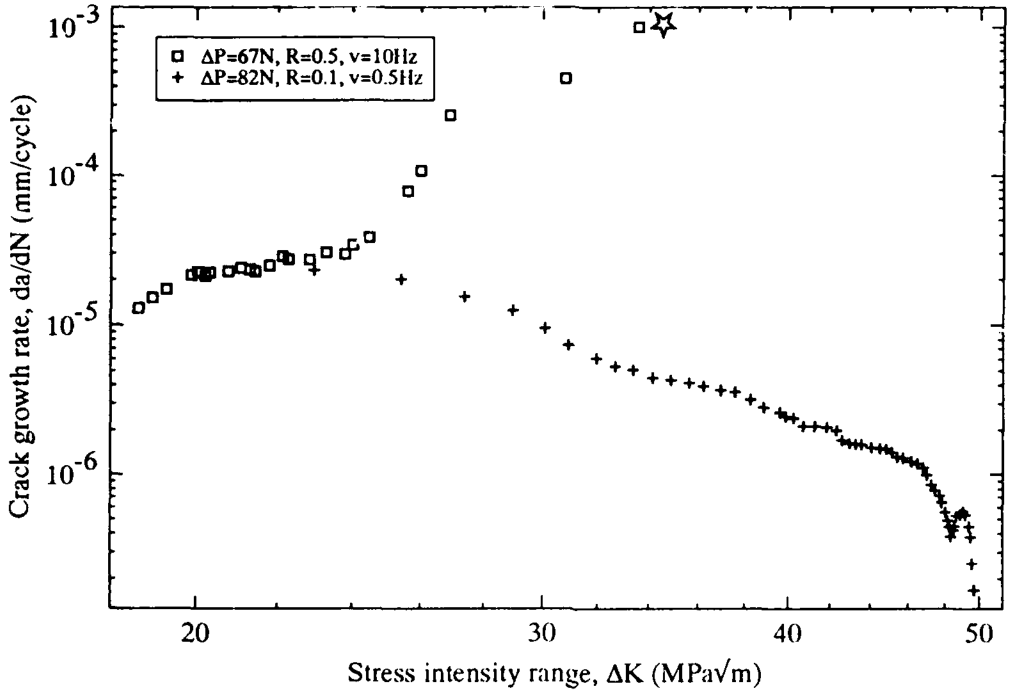

Figure 15. Effect of load ratio on crack growth resistance curves; da/dN versus ΔK_{app} υ=10Hz. Ti-6Al - 4V / Sigma composite, ambient temperature.

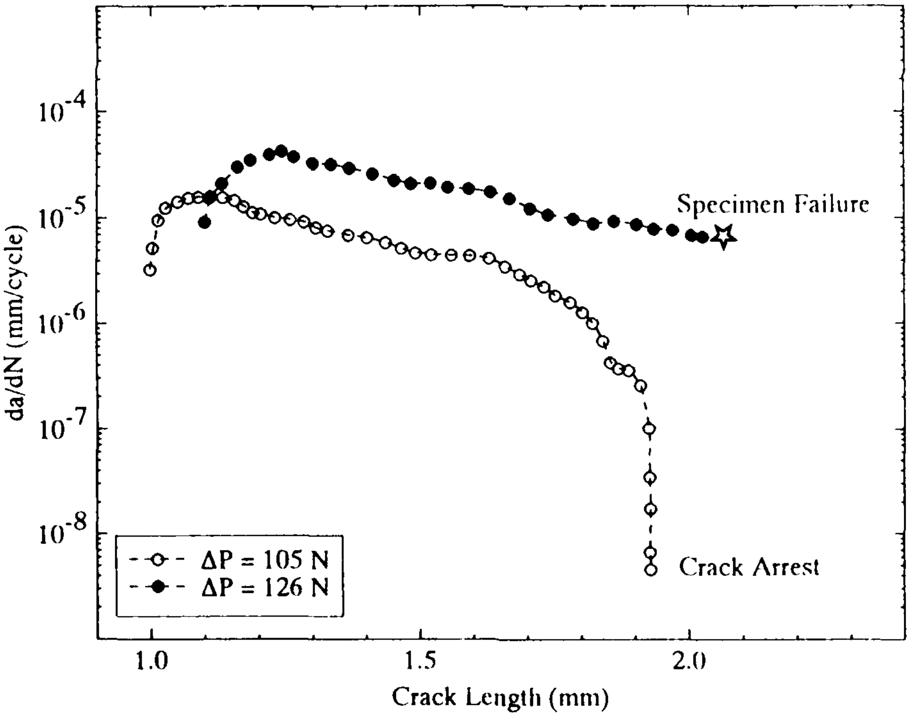

Figure 16. Effect of initial ΔK_{app} on crack growth resistance curves: da/dN versus crack length for R=0.5, υ=10Hz. Ti-15-3 /SCS6 composite, solution treated condition, ambient temperature. The curves correspond to initial ΔK_{app} = 16 and 19 MPa√m respectively.

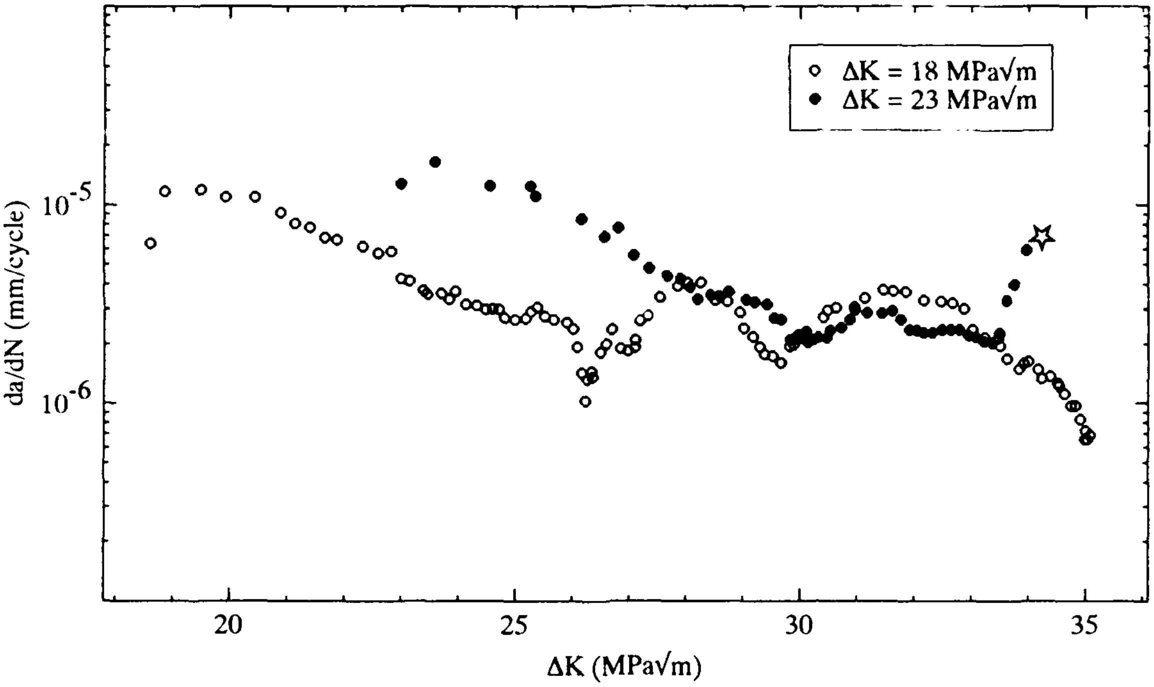

Figure 17. Effect of initial ΔK_{app} on crack growth resistance curves: da/dN versus ΔK_{app} for R=0.1, υ=0.5Hz. Ti-6Al - 4V / SCS6 composite, ambient temperature.

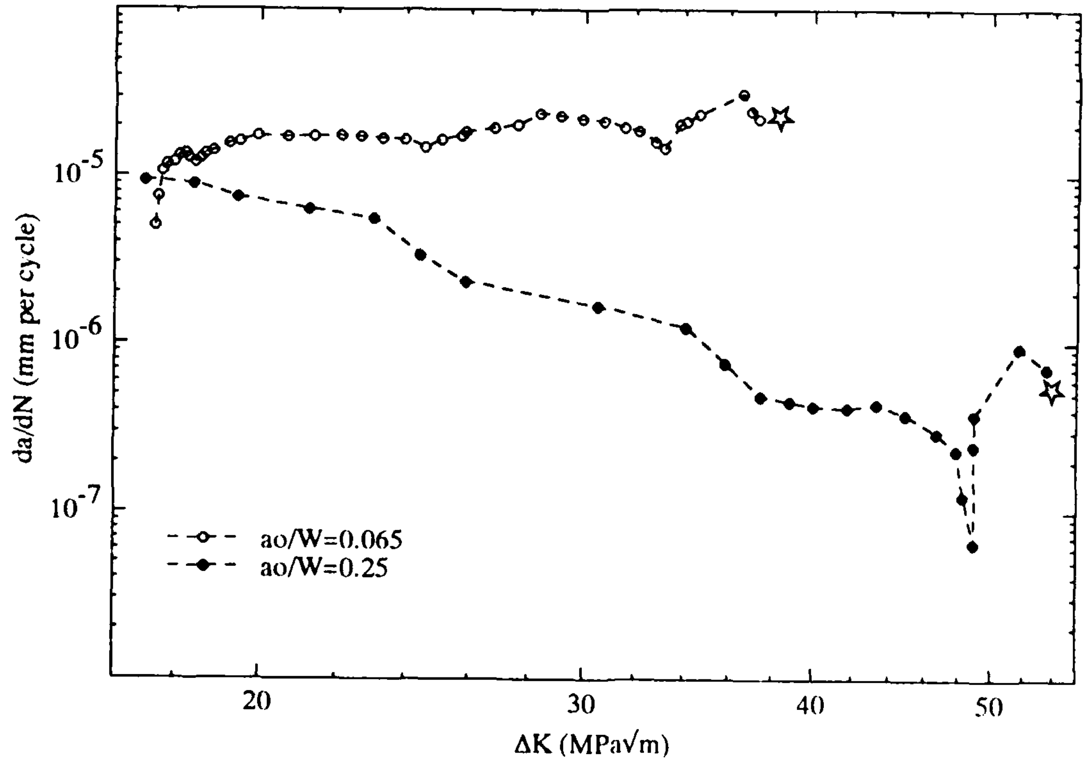

Figure 18. Effect of initial unbridged crack length on crack growth resistance curves: da/dN versus ΔK_{app}, υ=10Hz, R=0.5 Ti-β21S / SCS6 composite, ambient temperature.

Prediction of Thermal and Mechanical Stress-Strain Responses of TMC's Subjected to Complex TMF Histories

W. S. Johnson and M. Mirdamadi
NASA Langley Research Center
MS 188E
Hampton, VA 23681
USA

1. SUMMARY

This paper presents an experimental and analytical evaluation of cross-plied laminates of Ti-15V-3Cr-3Al-3Sn (Ti-15-3) matrix reinforced with continuous silicon-carbide fibers (SCS-6) subjected to a complex TMF loading profile. Thermomechanical fatigue test techniques were developed to conduct a simulation of a generic hypersonic flight profile. A micromechanical analysis was used. The analysis predicts the stress-strain response of the laminate and of the constituents in each ply during thermal and mechanical cycling by using only constituent properties as input. The fiber was modeled as elastic with transverse orthotropic and temperature-dependent properties. The matrix was modeled using a thermo-viscoplastic constitutive relation. The fiber transverse modulus was reduced in the analysis to simulate the fiber-matrix interface failures. Excellent correlation was found between measured and predicted laminate stress-strain response due to generic hypersonic flight profile when fiber debonding was modeled.

2. INTRODUCTION

Titanium metal matrix composites, such as Ti-15V-3Cr-3Al-3Sn (Ti-15-3) reinforced with continuous silicon-carbide fibers (SCS-6), are being evaluated for use in hypersonic vehicle structure where high strength-to-weight and high stiffness-to-weight ratios are critical. This material system has the potential for applications up to 650°C. However, at temperatures above 400°C, titanium exhibits significant viscoplastic behavior. Since the operating temperatures of hypersonic vehicles airframe structure surface are well above 400°C, the viscoplastic behavior of the titanium must be accounted for in an analytical evaluation of titanium metal matrix composites (TiMMC).

The objectives of this research are to (1) experimentally determine the stress-strain response of a $[0/90]_{2s}$ SCS-6/Ti-15-3 laminate due to the thermomechanical fatigue (TMF) that will occur during hypersonic flight profile testing and (2) verify an analytical method to predict the measured laminate stress-strain response, including fiber-matrix interface failure.

Mirdamadi, et al. [1], used an analysis to predict the stress-strain response of unidirectional SCS-6/Ti-15-3 laminates subjected to simple in-phase and out-of-phase TMF loading. Good agreement between experiment and prediction was found. This paper summarizes results for a more complex laminate, $[0/90]_{2s}$, with a more complicated TMF loading history [2].

3. MATERIAL AND TESTING PROCEDURE

A $[0/90]_{2s}$ SCS-6/Ti-15-3 laminate with a fiber volume fraction of 0.385 and a thickness of 1.68-mm was used in the present study. The SCS-6 fibers are continuous silicon-carbide fibers having a 0.140-mm diameter. The composite laminates were made by hot-pressing Ti-15-3 foil between tapes of unidirectional SCS-6 silicon-carbide fibers held in place with molybdenum wires. The Ti-15-3 matrix material is a metastable beta titanium alloy. Long exposures at elevated temperatures can lead to the precipitation of an α-phase which may alter the macroscopic mechanical behavior of the Ti-15-3 [3]. Therefore, the matrix and the composite in the present study was heat treated at 650°C for one hour in air followed by an air quench to stabilize the matrix material. This heat treatment was the

Presented at an AGARD Meeting on 'Characterisation of Fibre Reinforced Titanium Matrix Composites', September 1993.

same heat treatment used by Pollock and Johnson [4]. After the heat treatment, the viscoplastic material properties of the Ti-15-3 matrix at room temperature, 316°C, 482°C, 566°C, and 650°C were determined previously [1]; additional properties were also determined at 427°C [2]. It was assumed that the matrix properties remained the same from room temperature to 150°C and that the fibers remained elastic with temperature-dependent properties [2].

TMF spectrum testing was conducted on straight-sided rectangular specimens, 152-mm x 12.7-mm x 1.68-mm, cut using a diamond wheel saw. Brass tabs (10-mm x 30-mm x 1-mm) were placed between the end of the specimen and the grips to avoid specimen failure in the serrated grips. The brass tabs were not bonded to the specimens but were held in place by the grips.

A TMF test capability was developed to conduct hypersonic flight profiles. The temperature and the load spectrum of a generic hypersonic mission flight profile are shown in Figure 1. The letters shown in Figure 1 will be used later for comparison with stress-strain results. As shown in the figure, the flight profile consists of both isothermal and non- isothermal load cycling at 1 Hz with hold times at different temperatures. The thermal loading rates during heating and cooling were 2.8°C/sec and 1.4°C/sec, respectively.

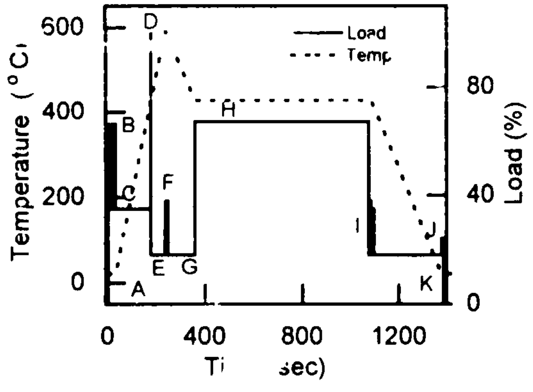

Figure 1. Generic hypersonic flight profile.

The TMF test setup consisted of a 100-kN servo-hydraulic test frame with water-cooled grips, a load profiler, a 5-kW induction generator controlled by a temperature profiler, and a nitrogen supply tank. The load and temperature spectra are independently controlled by load and a temperature profilers. The temperature profiler was modified to accept a command signal from the load profiler to initiate temperature spectrum at any desired point in the load profile. More details on the TMF test setup are given in [2]. Axial strains were measured on the edge of the specimen using a high temperature water-cooled quartz rod extensometer with a 25-mm gage length. An eight channel analog/digital PC based data acquisition system was used to record and store the test data. Prior to the flight profile test, the specimen was subjected to the temperature profile alone to ensure thermal stability and synchronization with the load profiler command.

4. ANALYTICAL METHOD

The stress-strain response of the $[0/90]_{2s}$ laminate was predicted using a micromechanics analysis. The VISCOPLY code, developed by Bahei-El-Din, is based on constituent properties. The program uses the vanishing fiber diameter (VFD) model [5] to calculate the orthotropic properties of a ply. The ply properties are then used in a laminated plate analysis [6] to predict the overall laminate stress-strain response. Both the fiber and the matrix can be described as thermo-viscoplastic materials. The viscoplastic theory used in the VISCOPLY program was developed by Bahei-El-Din [7] for high temperature, nonisothermal applications and is based on the viscoplasticity theory of Eisenberg and Yen [8]. The theory used in the VISCOPLY program assumes the existence of an equilibrium stress-strain curve which corresponds to the theoretical lower bound of the dynamic response. The theory further assumes that the elastic response is rate-independent and that inelastic rate dependent deformation takes place if the current stress state is greater than the equilibrium stress. A more detailed description of the theory can be found in Reference 2.

Combinations of thermal and mechanical loads can be modeled. Sequential jobs can be run for varying order and rate of load and temperature. Fiber and matrix average stresses and strains and the overall composite response under thermomechanical loading conditions are calculated. Although not used in the current work, the program has the capability to model the fiber as a viscoplastic material with transverse orthotropic properties.

A simple procedure was used to analytically simulate the fiber-matrix interface failure known to occur in the SCS-6/Ti-15-3 material. In room temperature fatigue tests [9], a distinct knee was observed in the stress-strain response at stress levels well below the yield stress of the matrix material. In the first cycle, this knee was found to correspond to the stress required to overcome the thermal residual stresses and fail the fiber-matrix interface in the off-axis plies. In subsequent fatigue cycles, the knee was observed at a lower stress level, the stress required to overcome the thermal residual stresses in the matrix. To simulate the fiber-matrix interfacial failure, the transverse modulus of the fibers in the 90° plies was reduced for stress levels above the stress level corresponding to the observed knee in the stress-strain response of the $[0/90]_{2s}$ laminate at room temperature. In elevated temperature fatigue tests, however, no knee was apparent in the stress-strain response [4] and it was assumed that fiber-matrix interfacial failure occurred upon loading. Thus, the fiber transverse modulus in the 90° plies was reduced at the start of loading for temperatures above 400°C.

5. RESULTS AND DISCUSSION

In this section, the experimental and analytical results are presented. The isothermal stress-strain response of the $[0/90]_{2s}$ laminates is analyzed to assess the effects of fiber-matrix separation and loading rates. The experimental results and the theoretical predictions for the flight profile are presented.

5.1 Isothermal Laminate Behavior

First, the appropriate reduction of the transverse modulus of the fibers in the 90° plies to simulate the fiber-matrix interface failure was determined. At room temperature the fiber-matrix interface failure occurred at a stress level of 70 MPa determined from the knee in the experimental stress-strain curve [2]. At 427°C, it was assumed that the fiber-matrix interface failed instantly upon loading. The experimental and predicted stress-strain response of the SCS-6/Ti-15-3 $[0/90]_{2s}$ laminate at 427°C (stress rate of $\dot{S} = 1250$ MPa/s) is shown in Figure 2. The VISCOPLY correlations are shown for various ratios of the fiber transverse modulus to the fiber axial modulus (E^f_t / E^f_a) in the 90° ply ranging from 1.0 to 0.001. Multiplying the 90° fiber transverse modulus by a factor of 0.1 produced very good correlations at 427°C. The room temperature correlations for $E^f_t / E^f_a = 0.1$ were also fairly good [2]. Therefore, a multiplication factor of 0.1 was used to model fiber-matrix interface failure at all temperatures. This reduction factor may be dependent on, fiber volume fraction, processing parameters, fiber-matrix interface strength, and fiber and matrix properties.

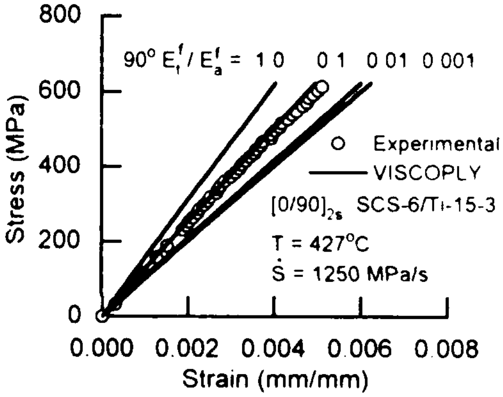

Figure 2. Effect of reducing 90° fiber transverse modulus on VISCOPLY predictions

Next, the effect of loading rate on the predictions was examined. Figure 3 shows the composite experimental stress-strain response during the second cycle (i.e., subsequent to the fiber-matrix interface failure of the 90° plies) at a stress rate of 10 MPa/sec at 650°C [4]. Included in the figure are the VISCOPLY predictions with fiber-matrix interface failure of the 90° plies ($E^f_t / E^f_a = 0.1$). The VISCOPLY prediction at a rate of 900 MPa/sec is also shown. The 900 MPa/sec rate corresponds to the loading rate used in the hypersonic flight profile. As seen in the figure VISCOPLY accurately predicted the initial elastic modulus but was somewhat less accurate at higher stress levels. The predicted maximum strain was 7% smaller than observed experimentally. The VISCOPLY prediction at the rate of 900

MPa/sec resulted in a nearly linear stress-strain response. These comparisons demonstrate the effect of the matrix rate-dependent behavior on composite stress-strain response.

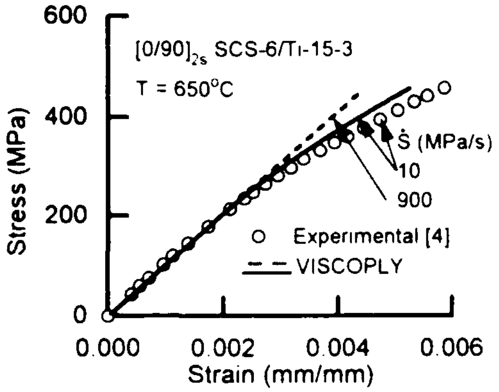

Figure 3 Prediction of stress-strain response of composite at 650°C

5.2 Flight Profile Behavior

In this section, the stress-strain response of the laminate subjected to the flight profile shown in Figure 1 will be analyzed and compared to experimental results. Predictions will be made assuming perfect bonding of the fiber-matrix interface in the 90° plies and assuming failure of the 90° fiber-matrix interfaces. For clarity, during the rapid cycling segments of the flight profile (e.g., segments B, F, I and J in Figure 1). only the first loading and last unloading cycle will be shown in the figures.

One test was conducted applying only the thermal history of the flight profile shown in Figure 1. The measured thermal strains and the VISCOPLY predictions are shown in Figure 4. The measured thermal strains match the applied temperature profile previously shown in Figure 1 indicating excellent control of the heating and cooling rates. The thermal strain of the laminate was accurately predicted by VISCOPLY.

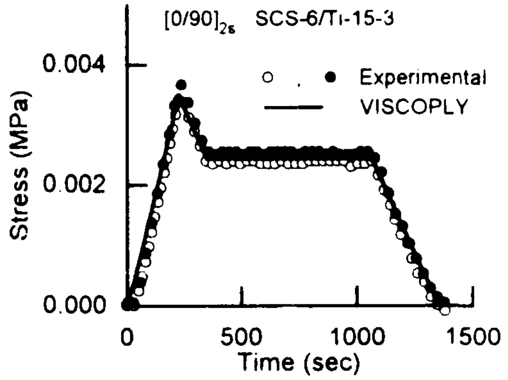

Figure 4. Predicted and experimental thermal strains as a function of time.

The specimen was then subjected to the full thermal and mechanical flight profile shown in Figure 1 at 100% stress equal to 420 MPa. The stress-strain response of the fifth repetition of the flight profile is shown in Figure 5. The letters placed at various locations on the stress-strain response can be referenced back to Figure 1 to find the associated point in the flight profile. The horizontal portions of the predictions and the experimental data indicate an increase in strain due solely to temperature changes while the mechanical loads were held constant. The VISCOPLY predictions assumed perfect fiber-matrix interface bonding. As seen in Figure 5, VISCOPLY predicted a stiffer response than was observed experimentally. The predictions of the cyclic loads shown at locations F and I

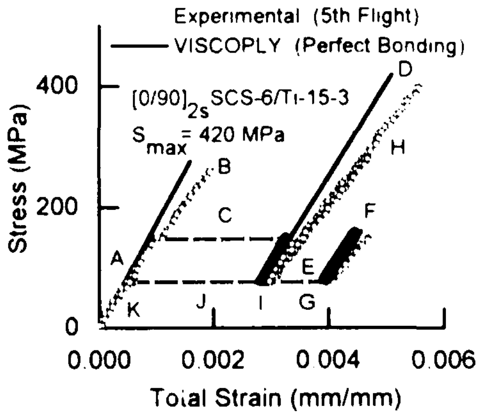

Figure 5 VISCOPLY prediction of composite response to the flight profile

appear broad because the temperature was changing. The experimental and predicted creep strain during hold period at H was very small. Predictions of the composite response under the flight profile made with simulated interface failure of the 90° plies are shown in Figure 6. The prediction agreed well with the experimental behavior when the interface failure was modeled as previously discussed.

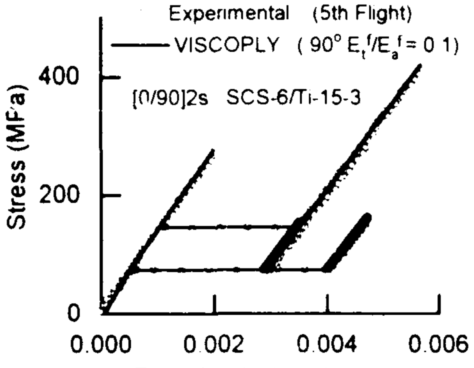

Figure 6. VISCOPLY prediction of composite response to the flight profile

If the fatigue behavior of the laminate is to be well understood and prediction methodology developed, the behavior of the composite constituents must be understood. Previous work by Johnson, et al. [9] showed good correlation between the stress range in the 0° fiber and the number of cycles to failure of the laminate at room temperature. More recently, Mirdamadi, et al. [1] used the 0° fiber stress range calculated from a micromechanics analysis to compare the TMF data of Castelli, et al. [10], Gabb, et al. [11], and the isothermal fatigue data of Pollock and Johnson [4]. They determined that for a given condition, the fatigue strength of the 0° fiber was controlled by a combination of temperature, loading frequency, and time at temperature. Furthermore, for a given temperature, loading frequency, and time at temperature, the stress range in the 0° fiber controlled the fatigue life. Bigelow and Johnson [12] and Bakuckas, Johnson, and Bigelow [13] accurately predicted the static strength of virgin specimens and fatigued specimens by monitoring the 0° fiber stress. Therefore, the 0° fiber stress (or strain) plays a major role in the static and fatigue strength of TiMMC. Under isothermal loading conditions, the 0° fiber strain is equivalent to the overall composite axial strain. However, under non-isothermal loading conditions, where the load and the temperature are cycled, determination of the 0° fiber stress is not straight forward and micromechanics-based models are required to predict the 0° fiber stress. Figure 7 shows the VISCOPLY predictions of the 0° fiber stress as a function of time during the flight profile. This prediction was made assuming fiber-matrix interface failure in the 90° plies. Such predictions are important when analyzing the fatigue behavior of the composite and could be used in a failure criteria.

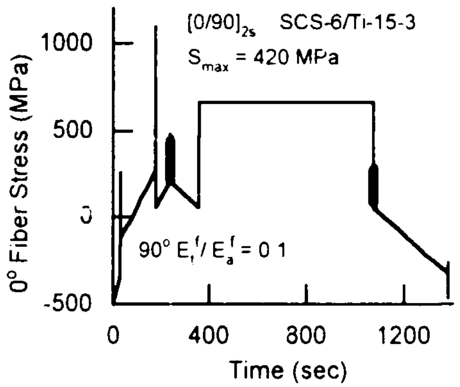

Figure 7 VISCOPLY prediction of 0° fiber stress under flight profile.

6. CONCLUSIONS

A TMF test capability was developed to simulate a generic hypersonic flight profile. The VISCOPLY analysis was used to predict the stress-strain response of the $[0/90]_{2s}$ SCS-6/Ti-15-3 laminate subjected to the flight profile loading. The following conclusions were made:

o In this material system, fiber-matrix interface failure must be modeled for accurate predictions. Fiber-matrix interface failure was modeled in VISCOPLY program by multiplying the 90° fiber transverse modulus by a factor of 0.1.

o The mechanical response of these composites is rate-dependent at elevated temperatures. The VISCOPLY analysis can predict such dependence.

o VISCOPLY accurately predicted the composite stress-strain response for a complex TMF loading profile.

7. REFERENCES

1. M Mirdamadi, W. S. Johnson, Y. A. Bahei-Fl-Din, and M. G. Castelli., "Analysis of Thermomechanical Fatigue of Unidirectional Titanium Metal Matrix Composites," *Composite Materials: Fatigue and Fracture, Fourth Volume*, ASTM STP 1156, W. W. Stinchomb and N. E. Ashbaugh, Eds., 1993, pp. 591-607..

2. W. S. Johnson, M. Mirdamadi and Y. A. Bahei-El-Din, "Stress-Strain Analysis of a $[0/90]_{2s}$ Titanium Matrix Laminate Subjected to a Generic Hypersonic Flight Profile", *Journal. of Composite Technology and Research*, Vol. 15, No. 4, Winter 1993.

3. H. W. Rosenberg, "Ti-15-3: A New Cold-Formable Sheet Titanium Alloy," *Journal of Metals*, 35(11)(1986), 30-34.

4. W. D. Pollock and W. S. Johnson, "Characterization of Unnotched SCS-6/Ti-15-3 Metal Matrix Composites at 650°C," *Composite Materials: Testing and Design (Tenth Volume)*, ASTM STP 1120, Glen C. Grimes, Ed., American Society for Testing and Materials, Philadelphia, (1992), 175-191.

5. G. J. Dvorak and Y. A. Bahei-El-Din, "Plasticity Analysis of Fibrous Composites," *Journal of Applied Mechanics*, 49 (1982), 327-335.

6. Y. A. Bahei-El-Din, "Plasticity Analysis of Fibrous Composite Laminates Under Thermomechanical Loads," *Thermal and Mechanical Behavior of Ceramic and Metal Matrix Composites*, ASTM STP 1080, J. M. Kennedy, N. H. Moeller, and W. S. Johnson, eds., American Society for Testing and Materials, Philadelphia (1990), 20-39.

7. Y. A. Bahei-El-Din, R. S. Shah, and G. J. Dvorak, "Numerical Analysis of the Rate-Dependent Behavior of High Temperature Fibrous Composites," *Symposium on Mechanics of Composites at Elevated and Cryogenic Temperatures*, ASME Applied Mechanics Division Meeting, Columbus, Ohio, June 16-19 (1991), 67-78.

8. M. A. Eisenberg and C. F. Yen, "A Theory of Multiaxial Anisotropic Viscoplasticity," *ASME Journal of Applied Mechanics*, 48 (1981), 276-284.

9. W. S. Johnson, S. L. Lubowinski, and A. L. Highsmith, "Mechanical Characterization of Unnotched SCS-6/Ti-15-3 Metal Matrix Composites at Room Temperature," *Thermal and Mechanical Behavior of Metal Matrix and Ceramic Matrix Composites*, ASTM STP 1080, J.M. Kennedy, H.H. Moeller, and W.S. Johnson, eds., American Society for Testing and Materials, Philadelphia (1990), 193-218.

10. M. G. Castelli, P. A. Bartolotta, and J. R. Ellis, "Thermomechanical Fatigue Testing of High Temperature Composites: Thermomechanical Fatigue Behavior of SiC (SCS-6)/Ti-15-3," *Composite Materials: Testing and Design (Tenth Volume)*, ASTM STP 1120, Glen C. Grimes, ed., American Society for Testing and Materials, Philadelphia, (1991), 70-86.

11. T. P. Gabb, J. Gayda, and R. A. MacKay "Isothermal and Nonisothermal Fatigue Behavior of a Metal Matrix Composite," *Journal of Composite Materials*, 24 (1990), 667-686.

12. C. A. Bigelow and W. S. Johnson, "Effect of Fiber-Matrix Debonding on Notched Strength of Titanium Metal Matrix Composites," *Fracture Mechanics: 23rd Symposium*, ASTM STP 1189, R. Chona, Ed., 1993, pp. 696-712.

13. J. G. Bakuckas, Jr., W. S. Johnson, and C. A. Bigelow, "Fatigue Damage in Cross Plied Titanium Metal Matrix Composites Containing Center Holes," NASA TM-104197, NASA Langley Research Center, February (1992).

PRE-STANDARDISATION WORK ON FATIGUE AND FRACTURE TESTING OF TITANIUM MATRIX COMPOSITES

J H Tweed, J Cook, N L Hancox, R J Lee and R F Preston

AEA Technology
B528.10, Harwell
Didcot, Oxon, OX11 0RA, UK

SUMMARY

This paper presents work on development of test techniques for S-N fatigue, fatigue crack growth and fracture toughness of titanium matrix composites. Work has concentrated on 8 ply unidirectional Ti-6-4/SM1240 from BP Metal Composites with some preliminary work on 8-ply unidirectional Ti-6-4/SCS-6 from Textron Speciality Materials. For S-N fatigue testing, an approach, used successfully for the Textron material, consistently gave failures in the tab region for BP material.

Transverse fracture toughness of Ti/SiC sheets has been determined using a double cantilever beam test. Care has to be taken to restrain specimen twisting. For two BP materials, the transverse fracture toughness correlates with the static strength values.

1. INTRODUCTION

Fibre reinforced metals are currently being considered in the UK for aero-engine, airframe and defence applications. Materials of interest are monofilament reinforced titanium and multifilament reinforced aluminium. In order to encourage designers to consider the use of metal composites, the UK Department of Trade and Industry has funded programmes of pre-standardisation work for mechanical properties of metal matrix composites. The current three year programme is being jointly undertaken by the National Physical Laboratory, Teddington and AEA Technology, Harwell and covers static, dynamic and fracture related properties of particulate and fibre reinforced metals.

For each material class a three stage approach is being taken to test method development. Initial test development is being undertaken on a single, commercially available material chosen to exhibit high material homogeneity. Robustness of selected test techniques is then being assessed using a range of other MMCs and finally the correlation between test data and component design will be considered.

This paper presents initial results of the pre-standardisation work on fatigue and fracture properties of titanium matrix composites (chosen as representative of fibre reinforced metals). This is thus intended as an interim statement which also presents current and future trends in the work programme.

2. CHARACTERISATION OF MATERIAL UNIFORMITY

Work in this programme has primarily used an 8-ply unidirectional Ti-6-4/SM1240 composite from BP Metal Composite produced in 1992 (six plates, each about 300mm x 300mm). Two cross ply plates (300mm x 300mm) have also been examined. Some early work used a Textron Ti-6-4/SCS-6 8-ply unidirectional composite produced in the mid 1980's (3 plates, each about 300mm x 300mm). Material uniformity has been assessed by X-radiography, ultrasonic C scanning, ultrasonic point determination of velocity and attenuation, metallography and matrix hardness testing.

X-radiography apparently gives resolution of individual Textron fibres (though this may be apparent rather than real, as 8-plys are being examined simultaneously). For the BP material, individual fibres are more difficult to resolve (despite their W cores) though a fibrous texture is evident on the radiographs. This indicates a possible slight misalignment of the fibre layers in the material. One area of fibre drift at the edge of a BP cross-ply plate was easily detectable.

Ultrasonic C scanning is sensitive to surface flatness, and hence slight ridging around groups of Textron Fibres leads to strong contrast (Figure 1(a)). For unidirectional and cross-ply BP plates, the contrast is uniform across the plates (Figures 1(b), 1(c) - each grey level corresponds to 2dB attenuation).

Ultrasonic determination of longitudinal and shear wave velocities (polarised along two plate axes) and attenuation have been made at 14-18 points on each plate. For the BP plates and one Textron plate, the longitudinal velocities are shown in Figure 2(a) and the shear velocities in Figure 2(b). The longitudinal velocities of the BP plates reflect their slightly lower volume fraction of SiC compared with the

Presented at an AGARD Meeting on 'Characterisation of Fibre Reinforced Titanium Matrix Composites', September 1993.

Textron material. Five of the unidirectional (UD)BP plates have similar mean velocities. One UD plate and the two cross ply plates have a slightly higher velocity. The shear velocities follow similar trends to the longitudinal velocities. For the Textron material the two shear wave velocities are distinct, whilst for all the BP plates they are not, again, possibly reflecting a lower SiC content than for the Textron plate.

Typical micrographs for the BP and Textron materials are in Figure 3. The more recent BP material shows a very good fibre distribution and material integrity with little or no fibre touching or lack of matrix bonding between fibres, features which are evident in the Textron material.

Matrix hardness in the BP and Textron materials is similar (Figure 4).

3. FATIGUE TESTS

Applications being considered for fibre reinforced metals frequently require resistance to cyclic, mechanical and thermal loads. The thermal performance of composite components is to be included in a new programme in the UK and hence the current programme is concentrating on property determination at ambient temperatures.

Initial work was undertaken on the Textron material and used a parallel sided specimen of 150mm x 10mm with a 100mm gauge length. Profiled steel end tabs were adhesively bonded to the specimen. Specimens were tested at 5Hz and a stress ratio, R, (minimum load/maximum load) of 0. For both static and dynamic tests, failures were generally in the gauge length (Figure 5), and are hence considered to be valid for use in design ie. the test technique did not bias the test result.

When an identical technique was used for BP Ti-6-4/SM1240, failures were systematically found at the end of the tabs even for static tests. This was found to be the case for a number of end tab materials and in studies at two laboratories. This is thought to be due to one of two causes:

- The BP material is thinner (1.3mm compared with 1.8mm for the Textron material) and hence the stress concentration at the end of the tabs may be greater leading to an increased probability of failure at the end tabs, rather than in the gauge length.

- The BP material may be more uniform than the Textron material (this is corroborated by the better fibre distribution for the BP material - Figure 3) and hence the stress concentration at the tabs may be more significant compared with the variation in material properties, again tending to favour failure at the end tab, rather than in the gauge length.

Three studies are currently in progress to seek to address these issues:

- A finite element study to predict the stress concentrations at the end of adhesively bonded end tabs for the two materials.

- An experimental study using laser moiré interferometry to seek to quantify the stress concentrations in the end tab region and in the profile region for profiled specimens.

- An experimental study to assess the validity of profiled specimens (using profiles from ASTM D 3552 and from Rolls Royce plc).

4. FRACTURE TESTS

For some service applications, designers wish to assess the integrity of fibre reinforced metals in the presence of crack life defects. These may be present between fibre layers or transverse to the fibre direction. Such cracks may appear under cyclic loading and may lead to fracture of the component under static loads.

Tests for interlaminar fracture toughness of polymer composites are being developed where specimens are produced with an artificial delamination to act as a crack starter. For fibre reinforced metals, an analogous technique may be very difficult. A simpler approach for unidirectional materials is to use a double cantilever beam specimen with a through thickness starter notch to assess material toughness parallel to the fibre direction. To date specimens have been used with overall dimensions of 130 x 30 x t mm (where t is the plate thickness) with an initial notch depth of 30mm. The thinner specimens, in particular, need to be restrained from twisting during loading. Crack growth has been observed using a travelling microscope and specimen compliance measured as a function of crack length to give fracture surface energy vs crack length. This has been determined for a Textron material and two BP materials (one known to have low strength (this was provided as an experimental material and not a production material)).

Results for the three materials are in Figure 7.

The effect of anti-twist guides is shown in Figure 7(a). Twisting of the cantilever beams can lead to additional deflection and an apparently low compliance (and hence toughness). This effect increases with crack length. An initial anti twist guide is a small piece of steel plate with a machined slot ~ 40mm long x 2mm wide. This slotted steel guide is slid over the specimen to rest close to the loading line. Further optimisation of this arrangement is required.

The BP and Textron materials are compared in Figure 7(b). The Textron material was not restrained from twisting, though this may be less of an issue than for the BP material because of its greater thickness. The Textron material shows an initial drop in toughness, perhaps due to the influence of the notch (a chevron notch was used for the BP materials to ease crack initiation). Both materials then show an increase in transverse toughness with crack length, possibly due to crack bridging by fibres eg. Figure 8.

Two strength levels of BP material are compared in Figure 7(c). The low strength of one panel is attributed to greater shear strength of the fibre/coating/matrix system and hence less ability to decouple the fibre from the matrix in the presence of cracks. This would correlate with increased transverse toughness for the low strength material, which is, indeed, observed.

Work on fracture tests is continuing to develop a specimen with a matrix crack bridged by SiC fibres, for both static and fatigue crack growth assessment.

5. CONCLUDING REMARKS

1. Ti-6-4/SM1240 from BP Metal Composites has been demonstrated to have high uniformity by non-destructive testing and metallography.

2. A, S-N fatigue test technique which gives gauge length failures for a Textron Ti-6-4/SCS-6 unidirectional 8-ply material, systematically gives tab end failures for a BP Ti-6-4/SM1240 unidirectional 8-ply material.

3. A double cantilever beam technique can provide through thickness failure energies for unidirectional fibre reinforced metals, though beam twisting needs to be restrained for thin materials.

ACKNOWLEDGEMENTS

This work is funded by the UK Department of Trade and Industry as part of its Measurement Technology and Standards programme. Helpful discussions are acknowledged with colleagues at the National Physical Laboratories and in UK industry.

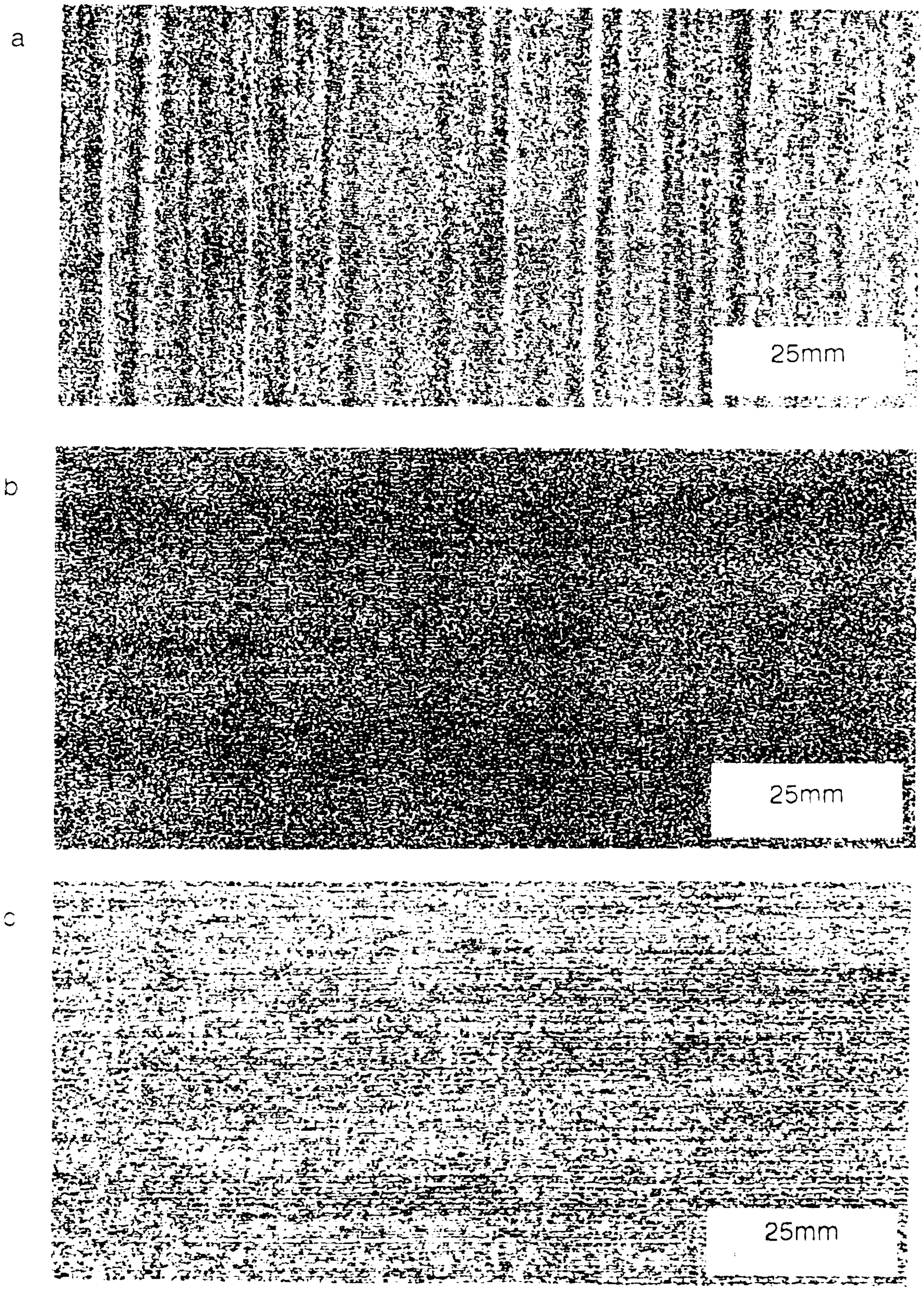
a
25mm
b
25mm
c
25mm

Figure 1 Ultrasonic C scans

(a) Textron plate 86 373
(b) BP unidirectional plate SW321
(c) BP cross ply plate SW44B

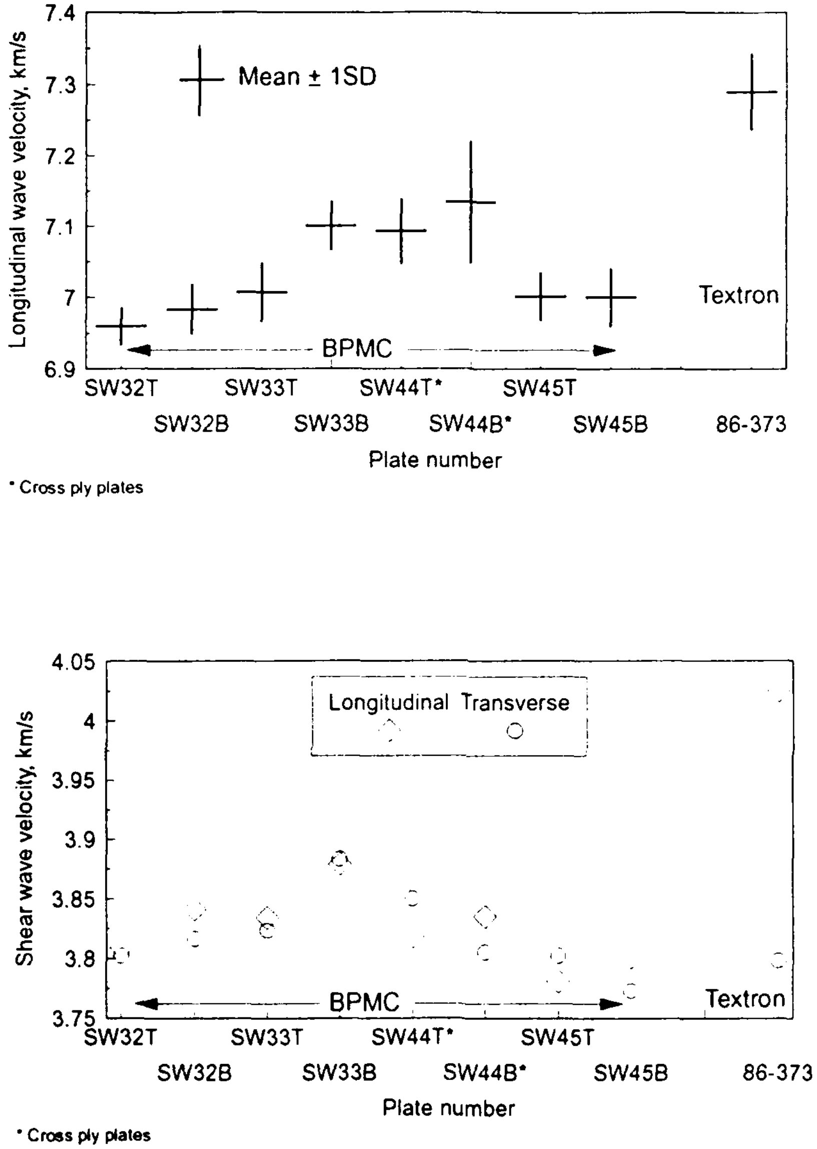

* Cross ply plates

* Cross ply plates

Figure 2. Ultrasonic velocities for BP plates and 1 Textron plate

(a) longitudinal through-thickness velocity
(b) shear through-thickness velocities

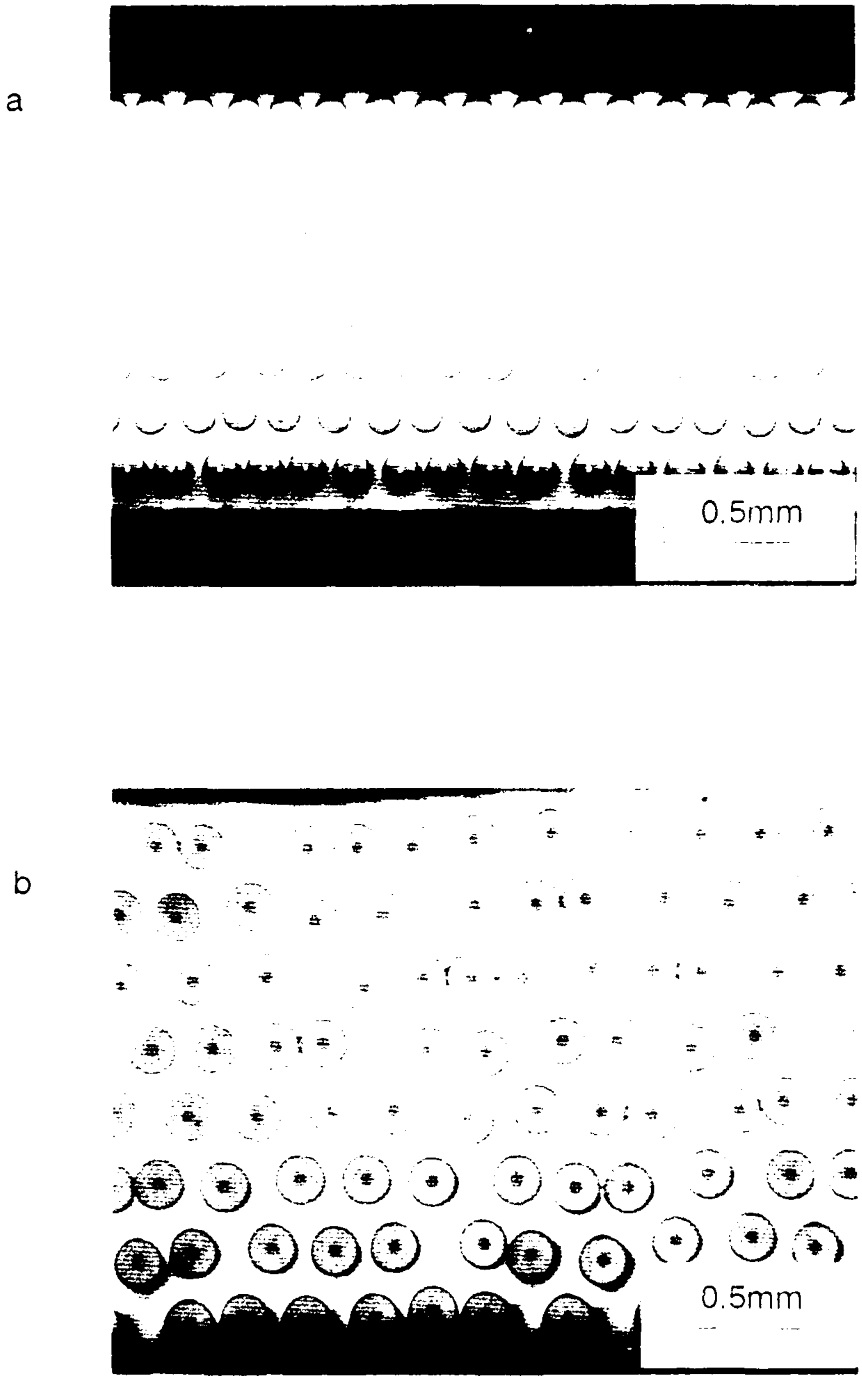
a
0.5mm
b
0.5mm

Figure 3 Optical micrographs of

(a) BP Ti-6-4 SM1240
and (b) Textron Ti-6-4 SCS-6

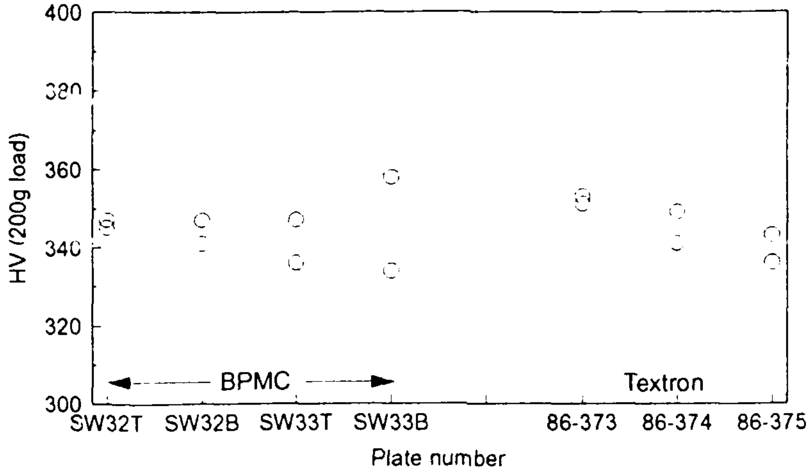

Data points from opposite plate corners

Figure 4. Matrix hardness in the BP and Textron materials.

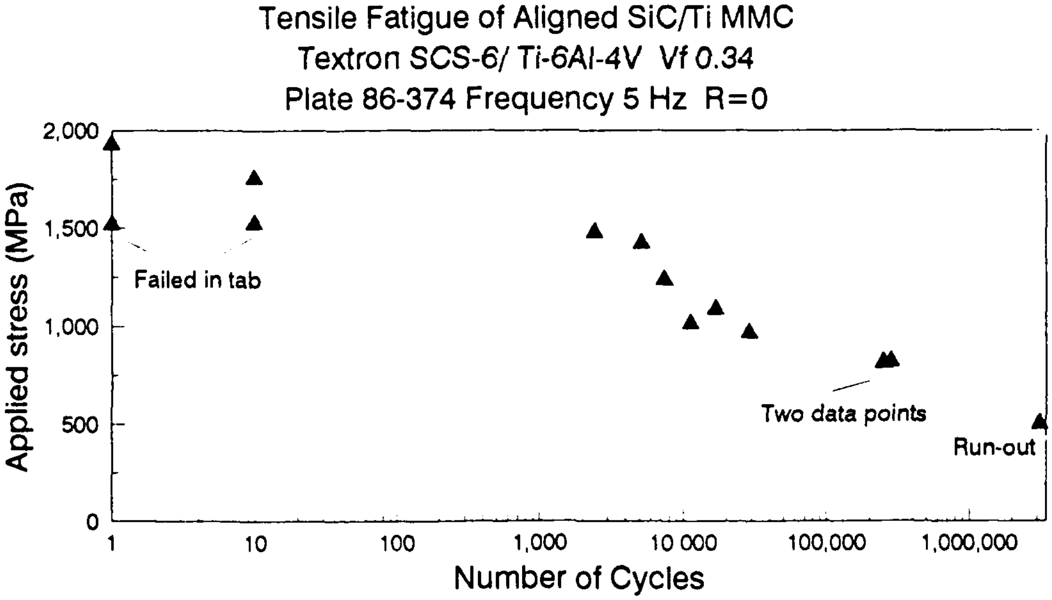
Tensile Fatigue of Aligned SiC/Ti MMC
Textron SCS-6/ Ti-6Al-4V Vf 0.34
Plate 86-374 Frequency 5 Hz R=0

Straight sided tensile coupon - Steel tabs
Gauge length 100 mm width 10 mm

Figure 5. S-N curve for Textron Ti-6-4/SCS-6

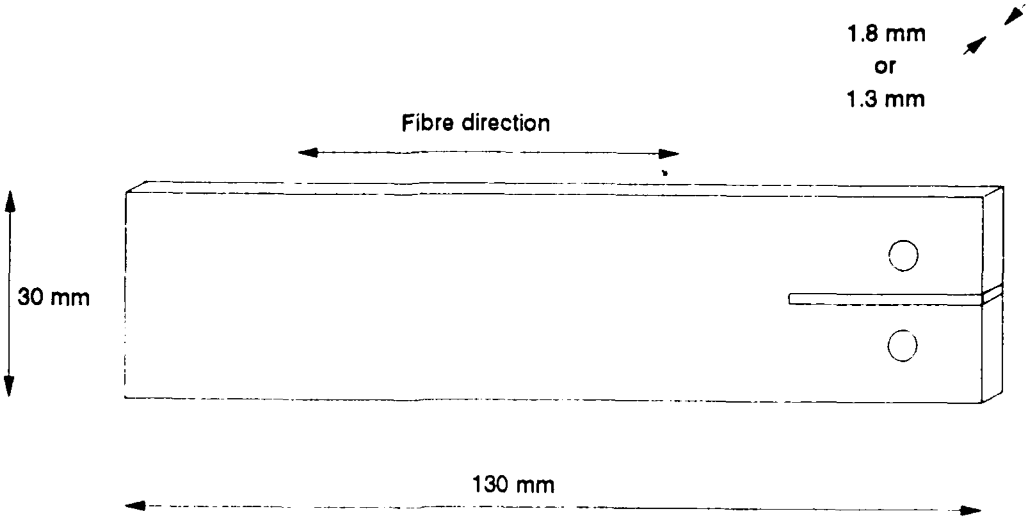
1.8 mm
or
1.3 mm
Fibre direction
30 mm
130 mm

Figure 6. Double cantilever beam specimen

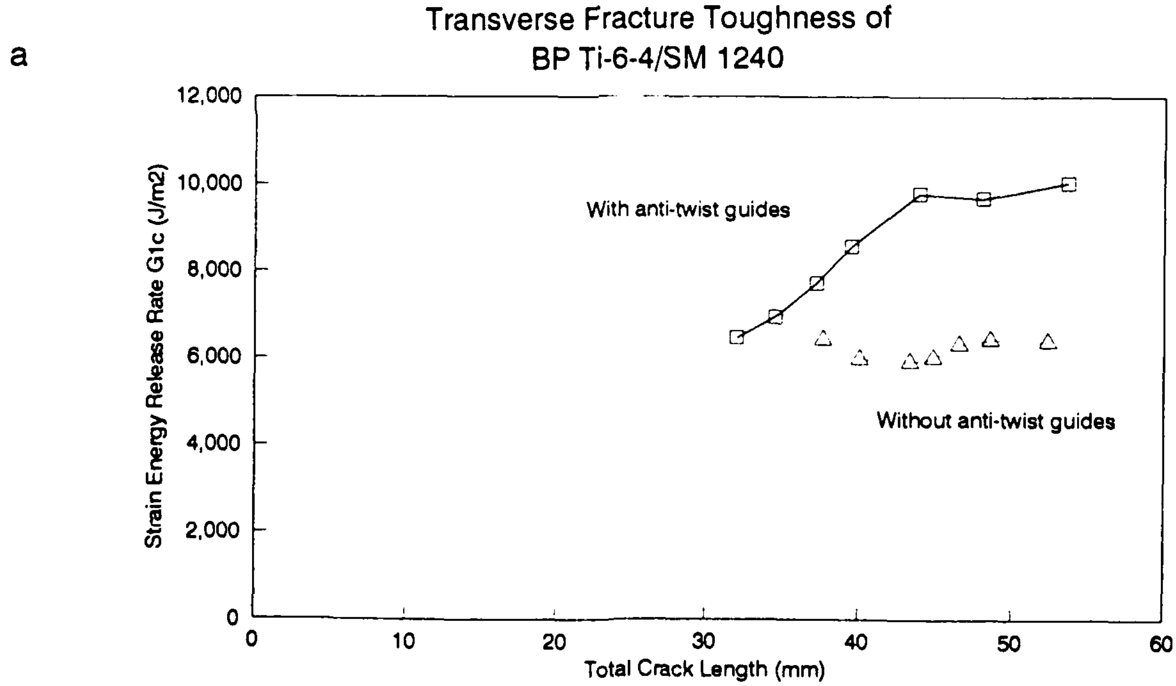

Figure 7. Fracture surface energy vs crack length for Ti/SiC materials.

(a) Effect of anti-twist guides

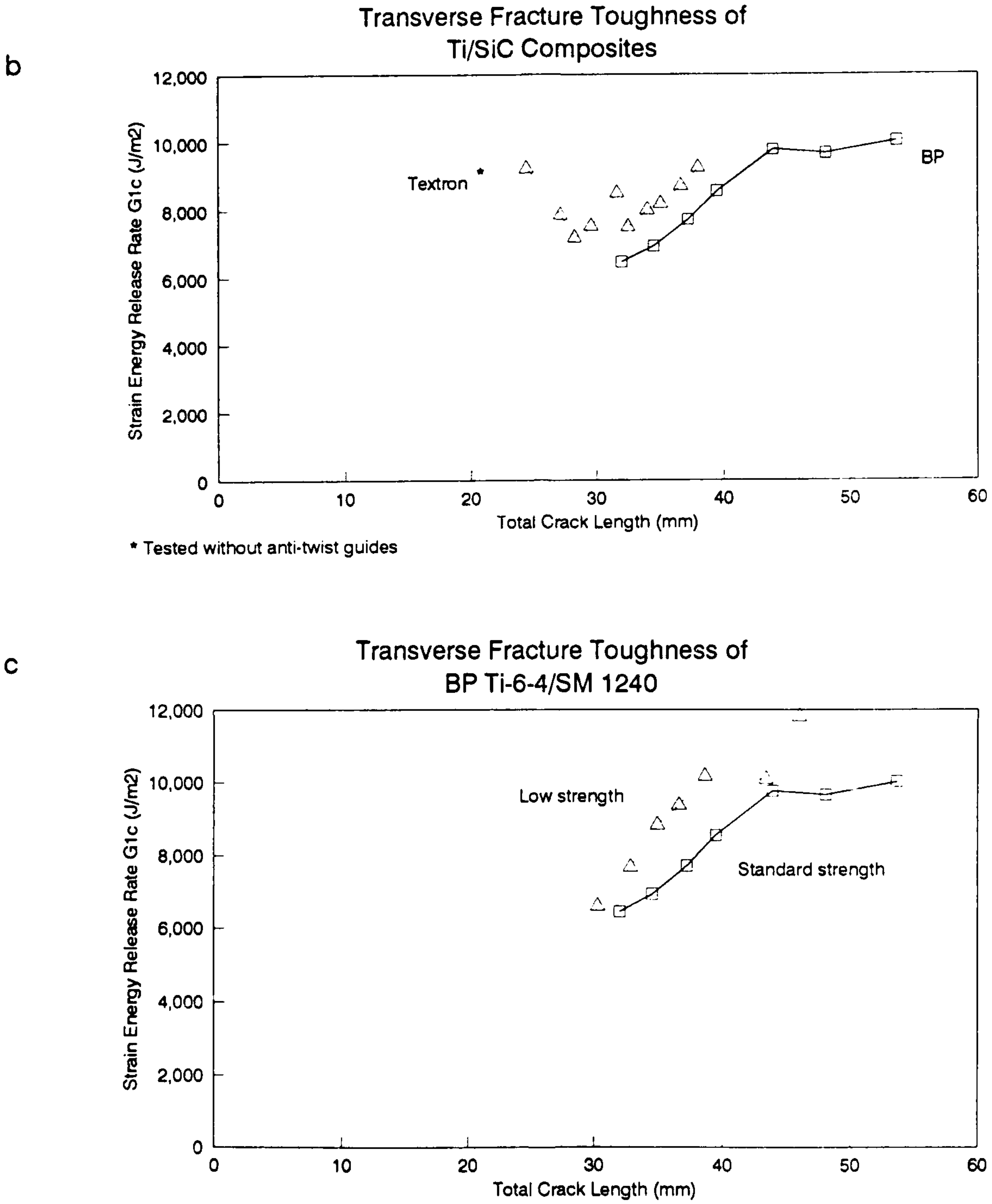

Figure 7. Fracture surface energy vs crack length for Ti/SiC materials.

- (a) Effect of anti-twist guides
- (b) Comparison of BP and Textron materials
- (c) Comparison of low strength and standard strength BP materials

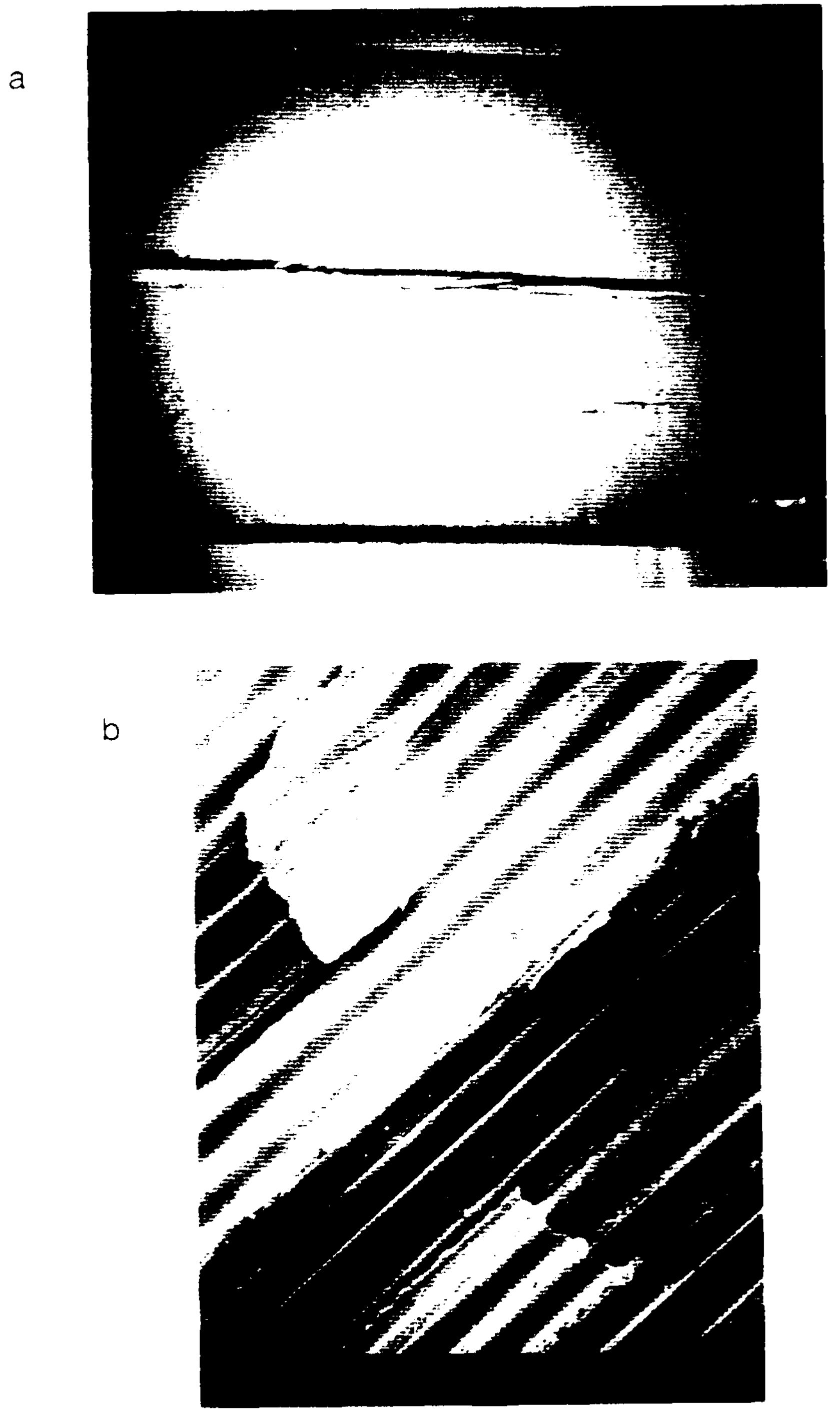

Figure 8 Crack bridging by fibres in a failed Textron sample

(a) Macrograph
(b) SEM micrograph of both halves of the fracture surface

ASTM and VAMAS Activities in Titanium Matrix Composites Test Methods Development

W. S. Johnson
NASA Langley Research Center
MS 188E
Hampton, VA 23681
USA

D. M. Harmon
McDonnell Aircraft Company
P.O. Box 516
St. Louis, MO 63166
USA

P. A. Bartolotta
NASA Lewis Research Center
MS 49-7
Cleveland, OH 44135
USA

S. M. Russ
USAF Wright Laboratories
WL/MLLN
WPAFB, OH 45433
USA

1. INTRODUCTION

Titanium matrix composites (TMC's) are being considered for a number of aerospace applications ranging from high performance engine components to airframe structures in areas that require high stiffness to weight ratios at temperatures up to 400°C. TMC's exhibit unique mechanical behavior due to fiber-matrix interface failures, matrix cracks bridged by fibers, thermo-viscoplastic behavior of the matrix at elevated temperatures, and the development of significant thermal residual stresses in the composite due to fabrication, standard testing methodology must be developed to reflect the uniqueness of this type of material systems.

The purpose of this paper is to review the current activities in ASTM and VAMAS that are directed toward the development of standard test methodology for titanium matrix composites.

2. ASTM ACTIVITY

A metal matrix composite (MMC) round robin test program was conducted with the objective of defining proper test procedures for unnotched static tension and fatigue testing. This work was conducted in the ASTM Subcommittee D30.07 on Metal Matrix Composites chaired by Steve Johnson and vice-chaired by Dave Harmon. The static portion of this test program was conducted by Task Group D30.07.01 on Tensile Testing chaired by Paul Bartolotta. The fatigue portion of this work was conducted by the Task Group D30.07.02 on Fatigue Testing chaired by Steve Russ.

Currently, the expense associated with the fabrication of these materials prohibits extensive testing at one location. Therefore, to properly characterize the material behavior it is necessary to rely on data produced by other researchers and available in the open literature. There are many research programs sponsored by the government and industry to study and understand these materials. Comparison of data from various sources is difficult without formal testing guidelines. Specific factors addressed in this study were lab-to-lab variability and specimen design (straight sided (SS) vs. dog bone (DB)).

The test program was conducted on SCS-6/TiMetal 21S with three laminate lay-ups:

Presented at an AGARD Meeting on 'Characterisation of Fibre Reinforced Titanium Matrix Composites', September 1993.

$[0]_3$, [0/90/0], and $[0/\pm 45/90_C]_S$. Static and fatigue tests were conducted at room temperature (RT) and 480°C (900°F) (Table 1). Since material was limited, only six test laboratories were able to participate in the testing. Labs were chosen based on past MMC testing experience. The six labs were GE Aircraft Engines, McDonnell Douglas, University of Virginia, NASA-Lewis Research Center, Rockwell International, and Wright Laboratories.

2.1 Material and Fabrication

The TiMetal 21S matrix material was donated to ASTM through the NASP Materials and Structures Augmentation Program sponsored by Wright Laboratories. All of the MMC was consolidated by Textron Specialty Materials using procedures and tooling developed under NASP by McDonnell Douglas and Textron. In addition to the MMC panels, Textron also provided two neat matrix panels.

Panel C-scans did not show any major delaminations or voids. All six panels were sent to McDonnell Douglas for specimen fabrication. All specimens were machined using a high speed abrasive water jet cutter.

The composites were tested in the as-fabricated condition. The specimens were not thermally aged prior to testing.

Both straight edge and dog bone specimens were fabricated using the drawings shown in Figures 1 and 2. The specimen configurations had a gage section width of 10 mm (0.39 in) for unidirectional and 0°/90° lay-ups and 15 mm (0.591 in) for the $[0/\pm 45/90_C]_S$ lay-up. The radius of curvature for the dog bone specimen was 386 mm (14.5 in).

2.2 Test Procedures

A set of test instructions were provided to each test lab. These instructions were based on past industry test experience, and applicable ASTM standards. Some of the applicable test standards include:

1) ASTM E 21-79, Standard Recommended Practice for Elevated Temperature Tension Tests of Metallic Materials,

2) ASTM E 466-82, Standard Practice for Conducting Constant Amplitude Axial Fatigue Tests of Metallic Materials,

3) ASTM D 3039-76, Standard Test Method for Tensile Properties of Fiber-Resin Composites, and

4) ASTM D 3479-76, Standard Test Methods for Tension-Tension Fatigue of Oriented Fiber, Resin Matrix Composites.

The following experimental techniques were used in this round robin:

Strain Measurement - Extensometry and strain gages were used for all room temperature tests for comparison purposes. All elevated temperature tests used extensometry.

Heating Method - The heating method was left to the discretion of the test lab. All methods chosen were required to be capable of heating the specimen to 480°C (900°F) at a rate between 3°C/second (5°F/second) and 11°C/second (20°F/second). All elevated temperature test specimens were to be held at temperature for 20 minutes prior to applying load. During the test the temperature must not vary more than 3°C (5°F). These guidelines were obtained from ASTM E 21.

Temperature Measurement - Thermocouples were affixed to the specimen using procedures which did not damage the surface of the composite coupon. The exact procedure was left to the discretion of the individual labs. For example, in lieu of welding a thermocouple directly to the test coupon, the thermocouple may be tack welded to a strip of nichrome ribbon and then wrapped around the test coupon.

Static Tension Strain Rate - 0.010±.002 /min.

Fatigue Tests - Load controlled sinusoidal waveform, Stress Ratio R = 0.1, Cycle Frequency = 1 Hz, Stress level were provided and were estimated to result in a life between 10,000 and 100,000 cycles.

Room temperature modulus was measured for all static tension specimens prior to testing. 0.05% strain (500 micro-inch/inch) was not to be exceeded when making this measurement.

Room temperature modulus was measured for all fatigue specimens prior to testing. 20% of fatigue stress level was not to be exceeded when making this measurement. Failure was defined as complete specimen fracture.

2.3 Tensile Test Results

For each lay-up, the participants were given two dog bone and two straight sided specimens to be tensile tested at temperatures of 20° and 480°C. This provided the study with sample sizes of six specimens for every test condition. The round robin's success ratio was quite high since, out of a possible total of 72 tensile tests, only one [0/90/0] DB specimen test at 20°C was questionable and was left out of subsequent analysis. Several statistical analytical techniques were used to see if tensile properties were influenced by specimen geometry or laboratory test techniques.

Tensile properties are presented in Tables 2-4 for $[0]_3$, [0/90/0], and $[0/\pm45/90_C]_S$ lay-ups respectively. In these tables, the composite's modulus at test temperature (E_{TT}), ultimate tensile strength (UTS), and strain at failure (E_f) are presented with respect to temperature and specimen geometry. In general, for all three lay-ups, E_{TT} and E_f sample means were similar for both specimen geometries with the greatest discrepancies being associated with the 480°C E_{TT} for the [0/90/0] lay-up and 480°C E_f for the $[0/\pm45/90_C]_S$ lay-up. As for the UTS values, larger differences between population means and larger standard deviations (more scatter) were observed for each case. However, through subsequent statistical analysis (via several Student's *t* tests), there was enough statistical evidence to support the fact that both geometries have identical population means for all of their tensile properties. Therefore, for this study, specimen geometry did not affect the tensile properties.

The only attribute that specimen geometry played a role in was fracture location. For the DB specimens, failures typically occurred at or near the start of the radius (from the specimen's test section). Failure locations for the SS specimens appeared to be scattered throughout the specimen length with 15% of the specimens failing at or near their gripping location. Temperature influenced the failure locations with the majority of fractures occurring within the test sections for the 480°C tests. As for the 20°C test, the SS specimens had the most failure location scatter while the DB specimens failed near or within the test section.

Typically, fracture locations did not influence tensile properties. Figures 3 and 4 illustrates this point by presenting UTS of $[0]_3$ and E_f of [0/90/0] data with respect to fracture location. In these figures solid symbols denote 480°C data and open symbols indicate 20°C data. The dotted vertical line represents the beginning of the 25.4 cm test section. From these figures, it is shown that regardless of fracture location tensile properties such as UTS can range between ± 100-150 MPa and for E_f between ± 0.25% from their respective means.

Lab-to-lab variability was investigated by conducting several analysis of variance (ANOVA) studies. In these studies, the means of each laboratory's tensile results were compared regardless of specimen geometry since it was shown that specimen geometry did not affect tensile properties. For each property, ANOVA tables were constructed to test the null hypothesis (each laboratory had the same average value for the tensile property in question) against an alternative hypothesis (at least two laboratory had averages that were significantly different). Results from these ANOVA studies show that there were only three cases where there is enough statistical evidence to support that at least two laboratories have different tensile property averages. These cases were as follows; i) E_f at 20°C for the $[0]_3$, ii) UTS at 20°C for the [0/90/0], and iii) UTS at 20°C for the $[0/\pm45/90_C]_S$. Note, the 480°C tensile properties for all of the laboratories had statistically similar averages.

Figures 5-7 graphically illustrates the lack of lab-to-lab variability in the tensile results. The histographs were constructed by normalizing all of the tensile properties, UTS, E_{TT}, and E_f, with respect to their individual means (by doing this all of the properties can be plotted on the same graph). Therefore, a normalized value of 1 on these figures represent a perfect correlation with the mean of a property. The symbols "1-6" represents the laboratories' identification number. The only definite trend observed in these figures [illegible] that most of laboratory 6's tensile data [illegible] away from their respective averages. This suggests that laboratory 6's test methods might differ enough from the other five laboratories to affect their tensile properties. However, the data appears to follow a *normal* distribution and perhaps laboratory 6's data spread is just an intrinsic occurrence.

2.4 Fatigue Test Results

Unnotched fatigue results from six participating laboratories were analyzed to determine the statistical significance of specimen geometry, lab-to-lab variability, and interactions including composite lay-up. Two specimen designs were evaluated, dog bone versus straight sided, for three lay-ups at two temperatures, Table 5. Each laboratory conducting 12 tests per temperature. Stress levels were predetermined with a goal of achieving fatigue lives ranging between 10,000 and 100,000 cycles. All tests were conducted under load-control with a sine wave, a frequency of 1 Hz, and a stress ratio of 0.1.

One of the six laboratories only participated in the 480°C testing, therefore, a separate analysis was conducted for each temperature. An analysis of variance is reported for the log of cycles-to-failure, log(N), normalized to account for the variance between the averages of the three lay-ups. Normalizing was performed at each temperature by multiplying log(N) by the ratio of total average of all the tests of all 3 lay-ups to the average of all tests for the specific lay-up. Figures 8 and 9 are histograms of the normalized data at room temperature and 480°C, respectively, demonstrating that a normal distribution was obtained for log(N) at both temperatures.

2.4.1 *Room Temperature Analysis*

Only five laboratories participated in the RT (approx. 20°C) fatigue testing, and a total of 60 tests were performed. A three-factor analysis of variance was conducted on log(N). The three factors were (A) laboratory, (B) specimen geometry, and (C) lay-up. From the ANOVA table, Table 6, only factor A was found to be statistically significant below the 5% level, with a P value of 0.007. This is interpreted as the following: if the null hypothesis is true (i.e., there is no difference between the five labs), the observed variance would occur only

0.7% of the time due to randomness. Figure 10 compares the results depicting the mean, ±1 standard deviation, and the range (minimum and maximum) for all five labs. Labs 2 and 5 have slightly higher averages than 1, 3, and 4. Although the scatter is fairly large for each lab, and visually it is difficult to discern a significant difference, the analysis of variance , taking into account the effects of the other factors and interactions, suggests the differences noted between the means is real, and not due merely to random scatter.

According to the ANOVA table, the factor of specimen design is not significant (P value of 0.875). This was further supported by comparing the means visually. Figure 11 shows the collective data for both the dog bone and straight sided geometries with the means being nearly identical. Figure 12 displays a comparison of averages for each lay-up. Small differences were observed for each lay-up, however, there was no consistency as to which design results in the longer lives, further suggesting a lack of a significant difference based on specimen geometry at RT.

2.4.2 *480°C Analysis*

All six laboratories participated in the 480°C fatigue testing, and results from 71 tests are reported (one test prematurely failed as a result of a power outage). Similar to the RT fatigue, a three-factor analysis of variance was conducted on log(N). The three factors were (A) laboratory, (B) specimen geometry, and (C) lay-up. From the ANOVA table, Table 7, both factors A and B are observed to be statistically significant below the 0.5% level.

The data for each lab are displayed in Figure 13 and illustrate that lab 6 has the highest average, lab 3 has the lowest, and the other 4 labs are very comparable. Similar to the RT data, the scatter is fairly large for each lab, and visually it is difficult to determine a significant difference. However, the analysis of variance, taking into account the effects of the other factors and interactions, suggests the differences noted between the means is real.

The data comparing the averages for the two specimen designs is presented in Figures 14 and 15. For the elevated temperature tests a significant difference is noted with dog bone specimens having longer lives for all three lay-ups over the straight sided specimens, Figure 15. It is observed that the difference is considerably larger for the lay-ups containing off-axis plies.

3. VAMAS ACTIVITY

In October 1992 The Versailles Project on Advanced Materials and Standards (VAMAS) Steering Committee approved the proposed test activities and created Technical Work Area (TWA) 15 on Metal Matrix Composites. Steve Johnson of NASA Langley Research Center (USA) serves as Chairman while Neil McCartney of the National Physical Laboratory (UK) ser[illegible]s Vice-chairman. This activity emphasizes collaboration on pre-standards measurement research, intercomparison of test results, and consolidation of existing views on priorities for standardization action. To date representatives from the following countries have expressed a desire to participate in TWA 15: USA, UK, Germany, France, Spain and Japan.

The initial focus of TWA-15 activities has been to conduct static and fatigue round robin testing on both whisker and particulate aluminum matrix composites at room and elevated temperature. The U. S. Air Forces' Title III program is providing the test materials. The National Research Institute for Metals (Japan) and NPL (UK) will machine the specimens.

TWA 15 members have expressed an interest in working the TMC systems. To date our efforts have been directed toward finding free or affordable TMC's to test. We intend to closely coordinate future ASTM and VAMAS activities in the TMC area. The next VAMAS TWA 15 meeting will be March 21, 1994, at Hilton Head Island, South Carolina, USA, in conjunction with the ASTM symposium entitled *Life Prediction Methodology for Titanium Matrix Composites.*

4. SUMMARY

An ASTM sponsored round robin test program was conducted on a titanium matrix composite to identify effects of specimen geometry and lab-to-lab variability on unnotched tension and fatigue test data. The material chosen for the round robin was SCS-6/TiMetal 21S. Six test labs participated. These labs represented industry, academia, and government. All labs used the same test procedures although different methods of heating and specimen tabbing were allowed.

Static test results showed little variation for each of the three lay-ups considered. Failure locations changed with specimen design, but tensile properties did not. Statistical studies were performed and showed no significant lab-to-lab variability.

Fatigue tests results were different depending on the temperature. Specimen geometry did not effect the fatigue lives at room temperature, but did effect lives at elevated temperature. Fatigue tests conducted on dog bone specimens lasted longer than those conducted on straight sided specimens at 480°C. Additionally, there was statistical evidence to suggest that there was lab-to-lab variability for the room temperature and 480°C tests. However, due to the large scatter observed, it is visually difficult to discern a significant difference. Scatter bands could perhaps be narrowed with additional testing.

The results of this test program indicate the following:

1) Either dog bone or straight sided specimens are adequate for tensile testing on unidirectional, crossplied, and other lay-ups and should not produce significant differences in measured properties.;
2) Either a straight-sided or dog-bone specimen geometry should be specifically identified in any test standard or test report; and
3) Further study is required to identify differences in lab fatigue test techniques which may have contributed to the statistically observed variability in life.

Efforts will be made to coordinate future ASTM and VAMAS round robin testing activities involving TMC's. A major concern for future testing activities is obtaining the TMC material.

Laminate	Temperature	Tension # tests		Fatigue # tests	
		SS	DB	SS	DB
$[0]_3$	20°C	1	1	2	2
	480°C	1	1	2	2
[0/90/0]	20°C	1	1	2	2
	480°C	1	1	2	2
[0/±45/90c]s	20°C	1	1	2	2
	480°C	1	1	2	2

Table 1. Round Robin Test Matrix (Per Lab)

$[0]_3$		TEMPERATURE			
		20 °C		480 °C	
		DB	SS	DB	SS
E_{TT}	mean	186.1	186.2	169.7	170.2
	s	15.8	12.7	8.2	8.1
(GPa)	max	214.0	204.0	181.0	180.6
	min	174.5	173.6	159.0	158.6
UTS	mean	1583.3	1620.8	1253.3	1303.1
	s	98.1	78.0	33.2	78.9
(MPa)	max	1751.0	1729.3	1288.0	1379.0
	min	1472.7	1486.8	1199.3	1200.9
E_f	mean	0.99	1.00	0.90	0.95
	s	0.11	0.10	0.08	0.11
(%)	max	1.11	1.12	1.03	1.10
	min	0.81	0.83	0.78	0.76

Table 2. Static Test Results - $[0]_3$

[0/90/0]		TEMPERATURE			
		20 °C		480 °C	
		DB	SS	DB	SS
E_{TT}	mean	152.3	152.6	129.4	133.4
	s	5.6	8.4	7.1	10.2
(GPa)	max	160.9	160.4	141.0	141.0
	min	145.3	136.6	120.2	114.0
UTS	mean	1234.9	1222.7	940.9	890.3
	s	55.4	62.9	46.8	59.8
(MPa)	max	1320.0	1295.0	983.1	998.0
	min	1180.3	1153.6	867.1	820.0
E_f	mean	1.01	0.96	0.86	0.80
	s	0.12	0.04	0.05	0.05
(%)	max	1.21	1.01	0.91	0.88
	min	0.89	0.91	0.76	0.74

Table 3. Static Test Results - [0/90/0]

$[0/\pm45/90_C]_S$		TEMPERATURE			
		20 °C		480 °C	
		DB	SS	DB	SS
E_{TT} (GPa)	mean	149.6	149.7	126.4	124.9
	s	5.3	12.1	20.1	13.2
	max	158.0	161.7	145.1	137.4
	min	142.0	131.0	89.0	103.0
UTS (MPa)	mean	906.5	900.0	656.9	679.6
	s	40.4	10.4	50.0	57.4
	max	944.1	915.5	727.0	737.4
	min	832.6	885.2	602.0	599.6
E_f (%)	mean	1.03	0.93	0.94	1.13
	s	0.17	0.05	0.21	0.13
	max	1.35	0.98	1.11	1.27
	min	0.86	0.83	0.55	1.01

Table 4. Static Test Results - $[0/\pm45/90_C]_S$

Temperature °C	Lay-up	Specimen Design	Max Stress MPa	Replicates
20	$[0]_3$	Dog Bone	625	2
20	$[0]_3$	Straight	625	2
20	[0/90/0]	Dog Bone	525	2
20	[0/90/0]	Straight	525	2
20	$[0/\pm45/90c]_s$	Dog Bone	325	2
20	$[0/\pm45/90c]_s$	Straight	325	2
480	$[0]_3$	Dog Bone	600	2
480	$[0]_3$	Straight	600	2
480	[0/90/0]	Dog Bone	460	2
480	[0/90/0]	Straight	460	2
480	$[0/\pm45/90c]_s$	Dog Bone	280	2
480	$[0/\pm45/90c]_s$	Straight	280	2

Table 5. Fatigue Test Matrix

Source	Degrees of Freedom	Sum of Squares	Mean Squares	F-test	P value
Labs (A)	4	0.27524	0.06881	4.348	0.007
Specimen Design (B)	1	0.0004	0.0004	0.025	0.875
AB Interaction	4	0.10651	0.02663	1.682	0.18
Lay-up (C)	2	0	0	0	1
AC Interaction	8	0.20581	0.02573	1.626	0.159
BC Interaction	2	0.06207	0.03104	1.961	0.158
ABC Interaction	8	0.1783	0.02229	1.408	0.234
Error	30	0.47483	0.01583		

Table 6. ANOVA Table for 3-factor Analysis of Variance on log(N), normalized, RT.

Source	Degrees of Freedom	Sum of Squares	Mean Squares	F-test	P value
Labs (A)	5	0.79418	0.15884	4.57	0.003
Specimen Design (B)	1	0.32661	0.32661	9.396	0.004
AB Interaction	5	0.08997	0.01799	0.518	0.761
Lay-up (C)	2	0.00051	0.00026	0.007	0.993
AC Interaction	10	0.83867	0.08387	2.413	0.027
BC Interaction	2	0.08874	0.04437	1.276	0.292
ABC Interaction	10	0.33306	0.03331	0.958	0.495
Error	35	1.21659	0.03476		

Table 7. ANOVA Table for 3-factor Analysis of Variance on log(N), normalized, 480°C.

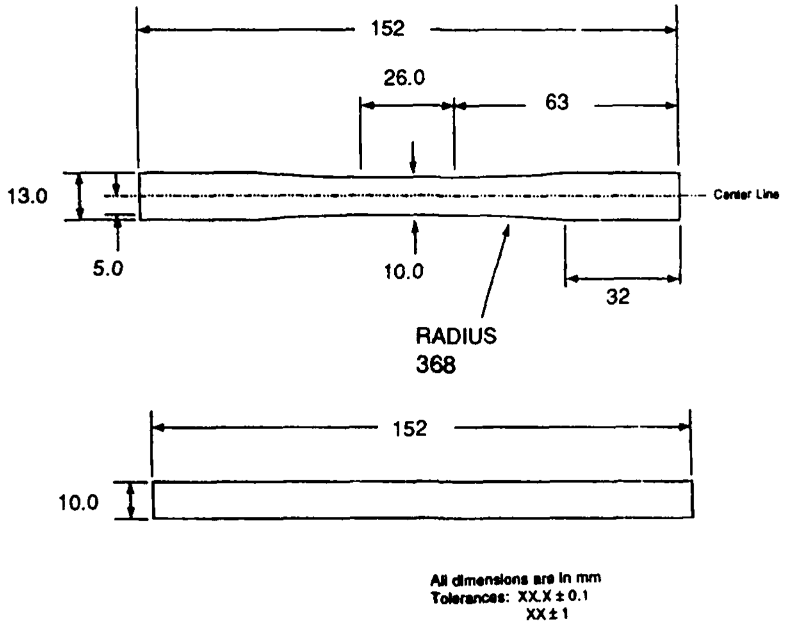
152
26.0
63
13.0
Center Line
5.0
10.0
32
RADIUS
368
152
10.0
All dimensions are in mm
Tolerances: XX.X ± 0.1
XX ± 1

Figure 1. Unidirectional and Crossplied Specimen Design

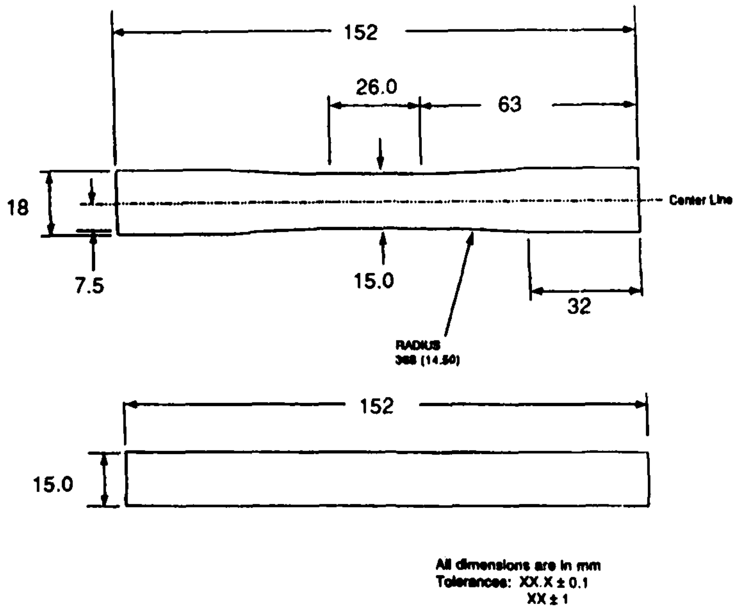
152
26.0
63
18
Center Line
7.5
15.0
32
RADIUS
368 (14.50)
152
15.0
All dimensions are in mm
Tolerances: XX.X ± 0.1
XX ± 1

Figure 2. Near Quasi-Isotropic Specimen Design

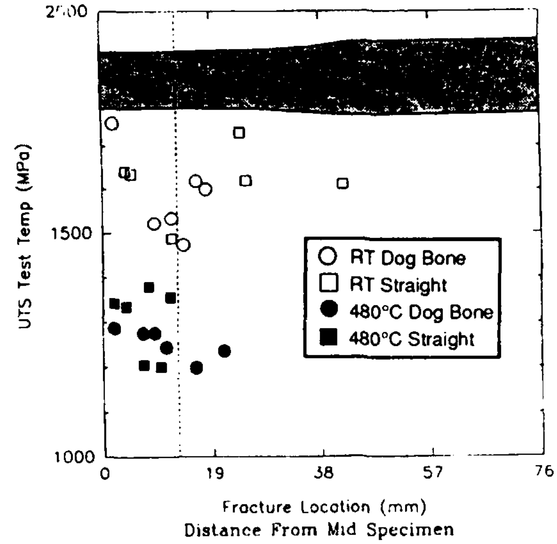

Figure 3. Ultimate Tensile Strength vs. Fracture Location, $[0]_3$

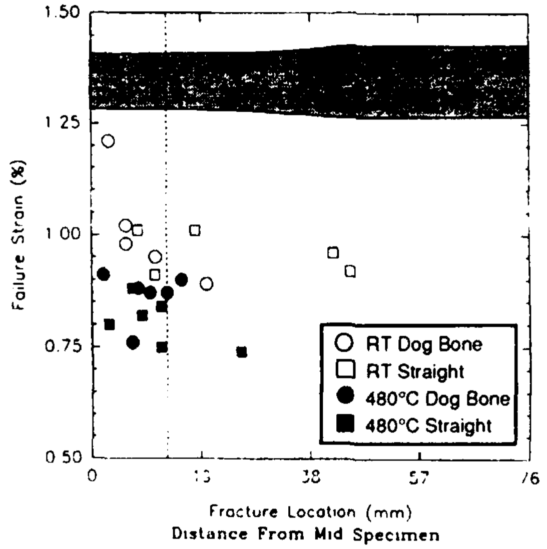

Figure 4. Failure Strain vs. Fracture Location, [0/90/0]

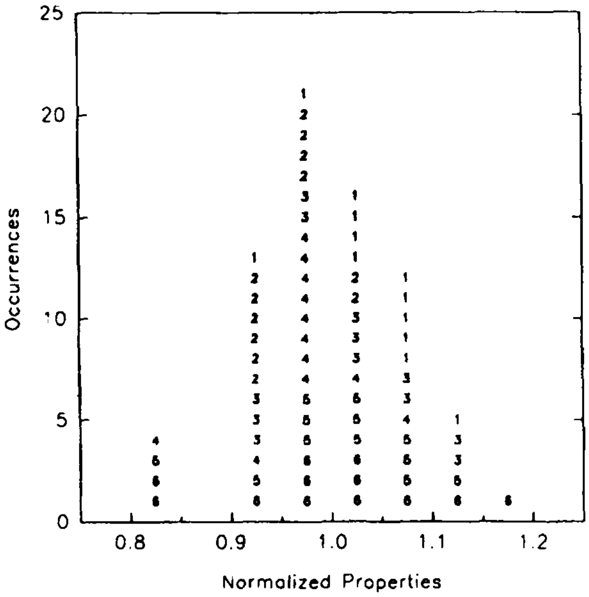

Figure 5. Distribution of Normalized Properties - [0]3

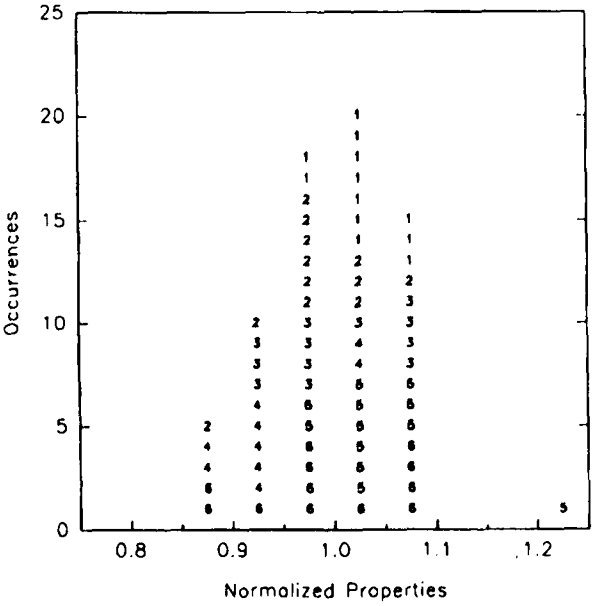

Figure 6. Distribution of Normalized Properties - [0/90/0]

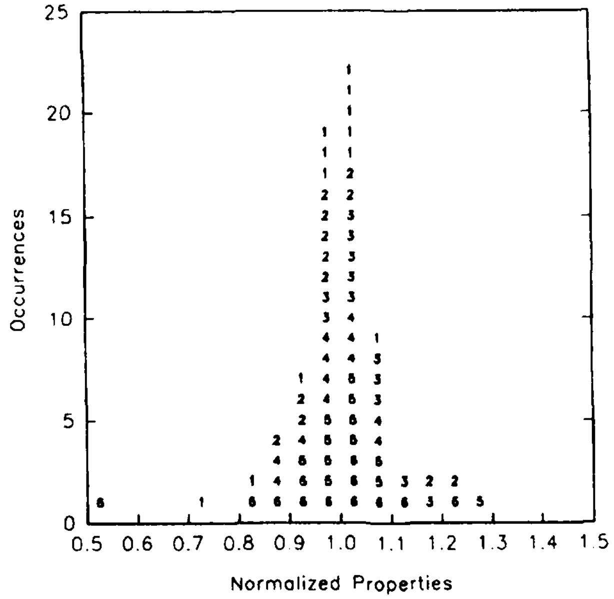

Figure 7. Distribution of Normalized Properties - [0/±45/90C]S

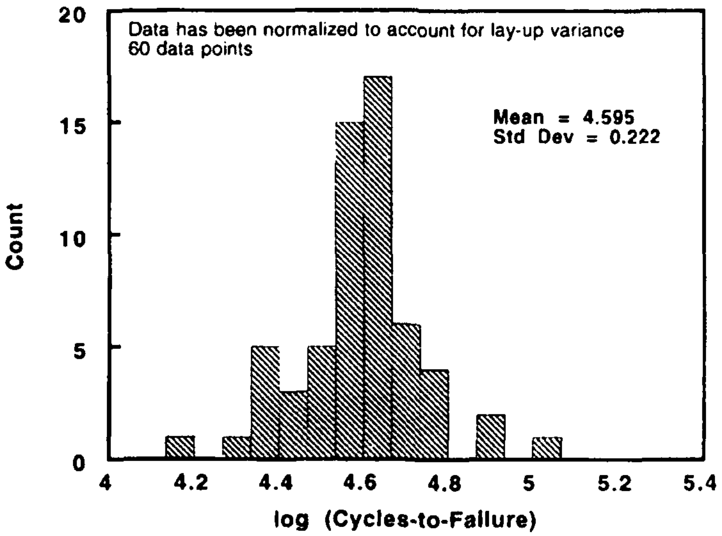

Figure 8. Histogram of Room Temperature Fatigue Data

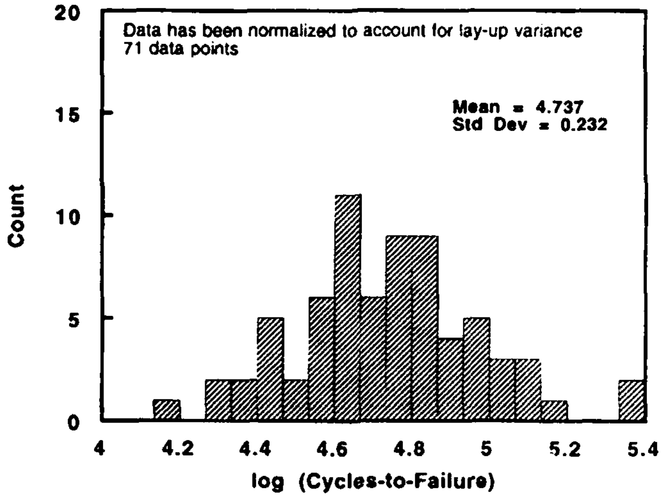

Figure 9. Histogram of 480°C Fatigue Data

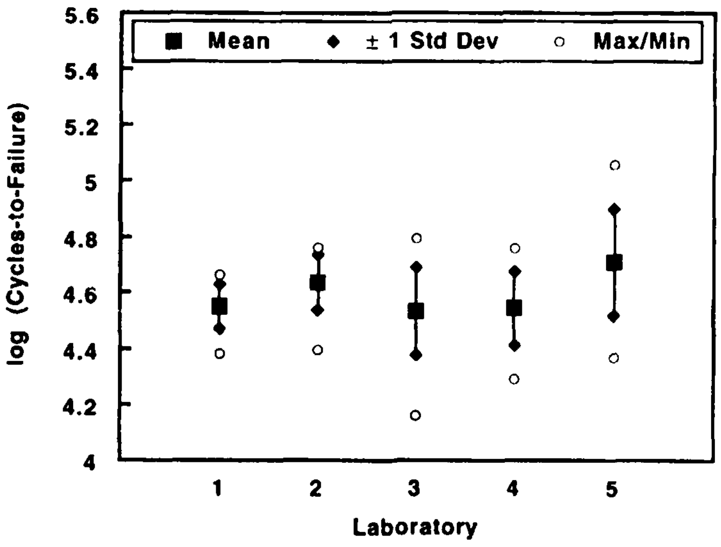

Figure 10. Lab to Lab Variability of Room Temperature Fatigue Data

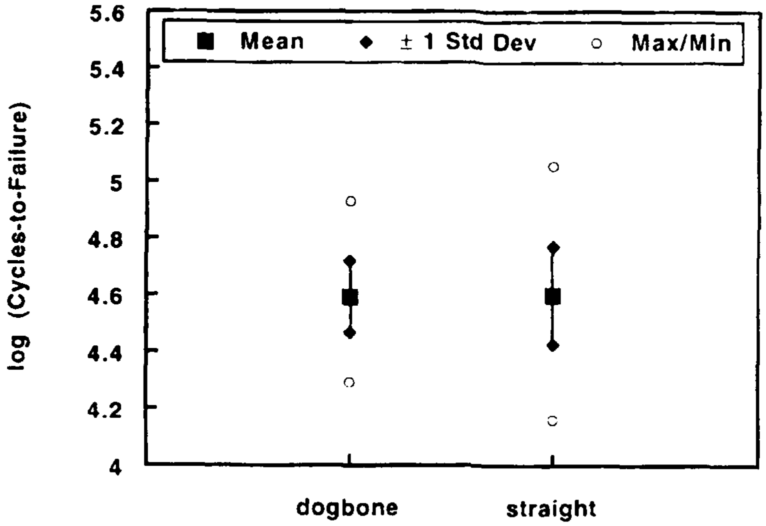

Figure 11. Effect of Specimen Design on Room Temperature Fatigue Data

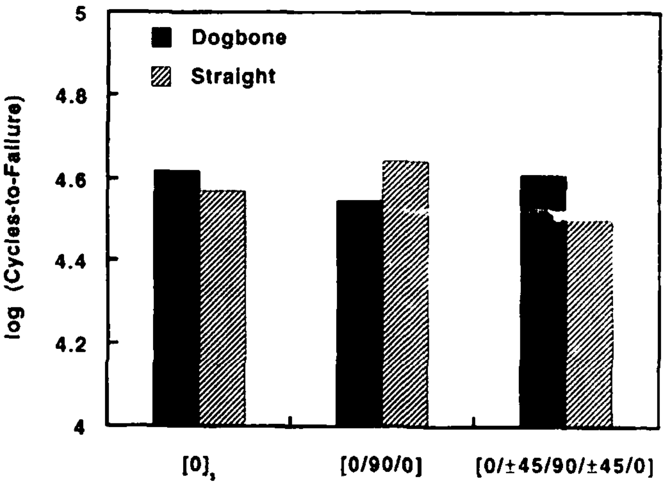

Figure 12. Effect of Specimen Design and Lay-up on Room Temperature Fatigue Data

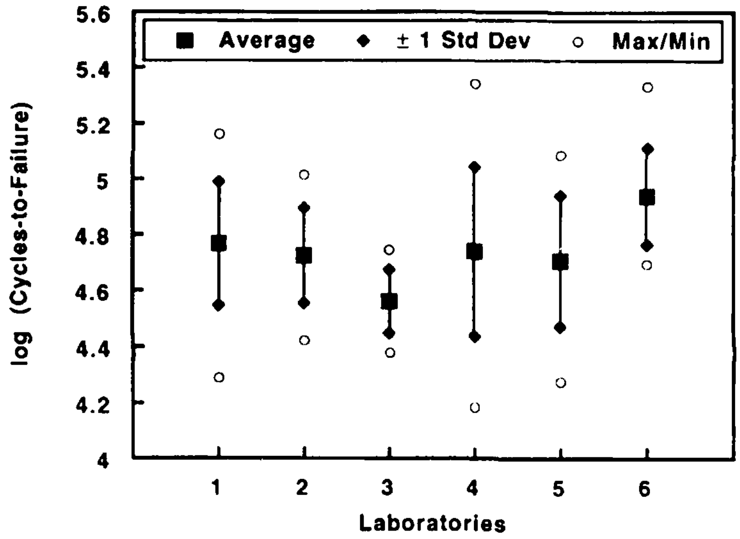

Figure 13. Lab-to-Lab Variability of 480°C Fatigue Data

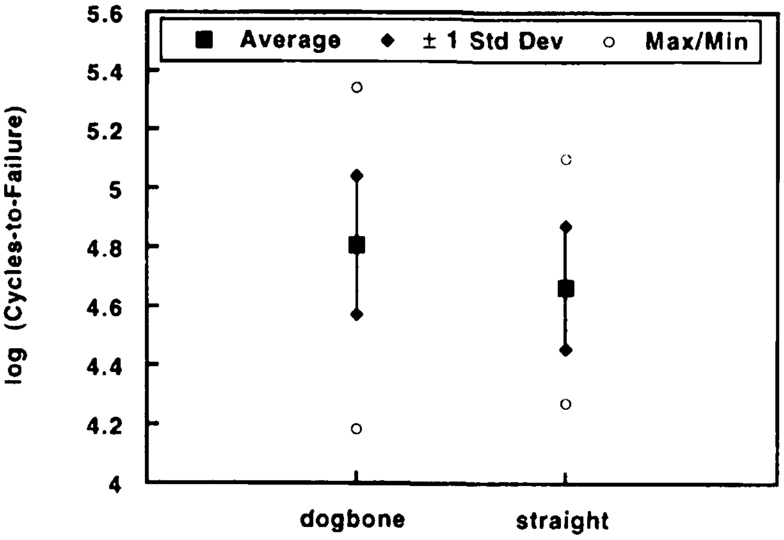

Figure 14. Effect of Specimen Design on 480°C Fatigue Data

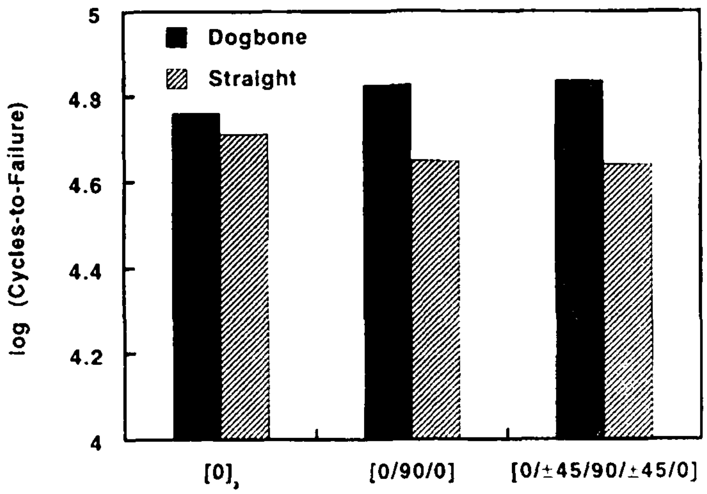

Figure 15. Effect of Specimen Design and Lay-up on 480°C Fatigue Data

DEVELOPPEMENT DE METHODES D'ESSAIS MECANIQUES POUR CMM A BASE TITANE (TRACTION-FATIGUE OLIGOCYCLIQUE)

par

B. Dambrine
SNECMA
BP 81
91003 Evry Cedex
France

M. Hartley
Rolls-Royce
PO Box 31
Derby DE2 8BJ
United Kingdom

INTRODUCTION

Les objectifs de performances fixés pour la prochaine génération de moteurs militaires (rapport poussée/masse ≈ 15) conduisent à des conditions extrêmes d'utilisation des alliages de titane pour les disques de compresseur, tout en ne permettant pas de respecter les objectifs de masse. Les matériaux composites à matrice métallique (matrice base titane renforcée par des fibres longues en carbure de silicium) montrent des propriétés de raideur, de résistance et de tenue en température prometteuses pour la réalisation de disques de compresseur [1].

Une bonne connaissance du comportement des Composites à Matrice Métallique base titane (CMM-Ti) est une condition préalable à l'établissement et la validation des méthodes de calcul de durée de vie des composants.

La première étape consiste en l'étude du comportement en traction et en fatigue oligocyclique sur éprouvettes à l'échelle du laboratoire. Dans la suite, on trouvera les éléments qui ont conduit au développement de ces essais

Matériaux testés

Deux matériaux ont servi de support à cette étude :

- Le premier, élaboré par TEXTRON SMD, est constitué de fibres SiC SCS6 (*ϕ=140µm) préalablement revêtues* d'alliage de titane 6242 (TiAl-2SN-42r-2Mo) déposé sous vide par procédé plasma. Le matériau est élaboré par compaction à chaud de huit couches de préimprégné plasma. La fig (1) montre la répartition des fibres dans une coupe transversale, le taux volumique de fibres obtenu est de 33%.
- Le second, élaboré par SNECMA, est constitué de fibres BP SM1240 (ϕ=104µm) tissées et maintenues par un fil de chaine en titane et d'une matrice TA6V sous forme de feuillard d'épaisseur 100µm. Le composite est obtenu à la presse par compaction d'un empilage de fibres et de feuillards pour obtenir un taux volumique de fibres de l'ordre de 33%. La figure (2) montre une coupe transversale du matériau obtenu. La principale différence entre ces deux matériaux, hormis le diamètre des fibres, réside dans la nature de l'interphase.

La fibre SCS-6 est revêtue de 3 µm de carbone pyrolitique alors que la fibre SM1240 es revêtue d'un dépôt composé d'une couche de carbone de 1,2 µm et 0,8 µm de TiB2. Cependant les aléas de production liés à la C.V.D conduisent en fait à un dépôt de bore dont la cohésion est faible. Au cours du compactage, ce dépôt migre entre les feuillards et une partie réagit pour former TiBx ($1 \leq x \leq 2$) qui affaiblit la liaison entre feuillards et fibre-feuillard. Cette contamination peut expliquer la relative faiblesse des caractéristiques mesurées sur ce matériau

Définition des essais de traction

Les critères retenus pour définir une éprouvette de traction sont les suivants

-La partie utile doit être de section rectangulaire pour pouvoir être usinée à partir de plaques.
-La rupture doit se localiser dans la partie utile
-La même géométrie doit pouvoir être testée à température ambiante et à haute température (600°C)
-Les chants doivent pouvoir être revêtus pour éviter l'oxydation dans les essais à chaud.

Les premiers essais sur éprouvette rectangulaire ont conduit systématiquement à l'amorçage au ras des mors (figure. 3). Pour éviter ce problème il a été décidé d'étudier une éprouvette sur laquelle des talons en TA6V sont rapportés par brasage. Pour optimiser la géométrie des talons, des simulations numériques ont été effectuées, les différentes géométries étudiées sont présentées sur la figure 4.

HYPOTHESES DE CALCUL

Maillage et modèle mathématique

Pour chaque géométrie un calcul plan a été réalisé avec le module ASEF (Analyse Statique Linéaire) du Code de Calcul par éléments finis SAMCEF.

Compte-tenu des symétries existantes, on a uniquement maillé une demi-éprouvette avec des éléments de volume torique isoparamétriques en déformation plane.

Conditions de chargement

On impose sur les deux faces extérieures des talons à la fois un déplacement constant (sens 1) et une pression uniforme représentative de celle exercée par les mors de serrage (sens 2). on peut alors visualiser la distribution des contraintes normales (σ_{11}, σ_{22}) et les contraintes de cisaillement σ_{12},

Données matériaux

Toutes les caractéristiques mécaniques nécessaires à la modélisation numérique sont connues :

SiC/Titane
E1 = 190 000 MPa
E2 = E3 = 135 000 MPa
G12 = G13 = 56 000 MPa
v12 = v13 = 0,21
v23 = v32 = 0,30

Titane
E = 115 000 MPa
v = 0,3

x = 1 = sens de sollicitation et des fibres SiC
y = 2 = sens orthogonal à 1 (2=3 i.e. le plan (2,3) est isotrope)

RESULTATS

Les distributions de contraintes normales (σ_{11}, σ_{22}) et de cisaillement σ_{12} pour les différentes géométries sont représentées sur les figures 6 à 8. Toutes ces grandeurs

Presented at an AGARD Meeting on 'Characterisation of Fibre Reinforced Titanium Matrix Composites', September 1993.

sont ramenées à la valeur nominale σ_{11N}, calculée dans la partie utile de l'éprouvette (ou zone d'homogénéité des contraintes σ_{11}). Nous détaillons ci-après l'analyse des résultats en essayant de comprendre les mécanismes essentiels entrant en jeu dans le comportement global de l'éprouvette.

A propos de σ_{11}
Une surcontrainte de traction apparaît dans le composite au niveau du raccord entre les talons et la partie utile de l'éprouvette pour les quatre géométries (figure 6) ; celle-ci peut atteindre $1{,}02 \bullet \sigma_{11N}$. Cet effet disparaît pour un talon avec congé de raccordement circulaire tangent au composite. Ceci donne à penser que la forme du congé est primordiale.

En pratique, il paraît difficile de réaliser une tangente aussi précise, c'est pourquoi la figure 6 indique ce que l'on obtient pour une marche d'environ 0,15 mm (géométrie 4) ; il n'y a toujours pas de zone critique.

A propos de σ_{12}
On observe un cisaillement dans les talons de titane (figure 7) , il est maximal au niveau de la partie la plus épaisse du talon (fin du congé dans le sens des x positifs), atteignant 38% de σ_{11N} pour la géométrie 2.

Ceci s'explique par la déviation ,dans le congé, des efforts qui suivent le bord libre en générant par la même occasion un glissement de matière (ou une contrainte de cisaillement). Une plastification locale du talon n'est donc pas impossible ; elle aurait cependant peu d'effet sur le comportement d'ensemble de l'éprouvette

On note que la géométrie 2 est la moins favorable de toutes ; elle présente en effet deux zones de cisaillement important dans les talons, sans oublier que les valeurs relatives de σ_{12}/σ_{11N} sont les plus importantes. Enfin, il n'y a pas de grandes différences entre les géométries 3 et 4

A propos de σ_{22}
Une contrainte σ_{22} de compression existe dans le composite au dessus du niveau du congé de raccordement (figure 8) ; celle-ci est la conséquence d'une contraction du titane dans le sens 2 probablement due à la différence des modules entre les deux matériaux.

La compression sens 2 atteint environ 5% de σ_{11N} pour les quatre géométries ce qui est relativement faible ; l'équilibrage de la zone précédente est réalisée par une zone de traction sens 2 comprise entre la partie utile et la fin du congé ; σ_{22} peut alors atteindre 31% de σ_{11N} et dépend en général de la forme du congé. Ainsi, les géométries 3 et 4 sont les plus favorables, alors que l'on pourrait craindre un éventuel décollement des talons pour les géométries 1 et 2.

Conséquences
Les principaux critères pénalisants mis en évidence sont donc la surcontrainte de traction σ_{11}, une localisation du cisaillement σ_{12} et une traction σ_{22} (équivalente à du pelage) dans l'éprouvette

Nous donnons dans le tableau 1 les valeurs extrêmes obtenues pour les contraintes dans le plan (1,2) ; par ordre d'importance nous retenons les critères de dimensionnement suivants :

$\sigma_{11}/\sigma_{11N} \leq 1$ au niveau du raccord entre talons et Composite

σ_{12}/σ_{1} tend vers zéro dans les talons.

Si l'on veut obtenir une rupture en traction dans la partie utile du composite, il faut retenir la géométrie 3 (ou 4 en pratique). Ce sont elles qui fournissent les écarts mini-maxi les plus faibles, exception faite de la géométrie 1 pour σ_{22}/σ_{11N}. D'autre part, les géométries 3 et 4 peuvent être améliorées en augmentant le rayon du congé de raccordement des talons ; cependant les surcontraintes σ_{11} observées étant très faibles et n'ayant pas lieu au début du raccord composite-métal proprement dit, cela nous a paru inutile.

RESULTATS EXPERIMENTAUX

Des essais de traction à température ambiante ont été effectués sur barreau parallélépipédique et sur éprouvettes à talons brasés (géométrie 4). Pour la réalisation de ces dernières, divers modes de réalisation ont été testés.:

Sur la figure (9), les talons sont rapportés par brasage (TiCuNi) en étant soit pré-usinés soit usinés ensuite. Cette technique nécessite un cycle de température supplémentaire d'une demi-heure à 900°C environ qui peut se montrer endommageant pour le composite, et des doutes existent sur la tenue mécanique de la brasure [2] ..

La deuxième technique utilisée consiste à presser le CMM en remplaçant les feuillards extérieurs de TA6V par des plaques du même matériau , une fois le composite réalisé, on effectue une découpe puis une rectification des éprouvettes afin d'obtenir dans la partie utile une épaisseur de TA6V identique à celle des feuillards externes d'une plaque de CMM standard. on réalise ainsi une éprouvette à talons sans cycle de brasage et assurant une meilleure continuité de la matière. la figure (10) illustre la fabrication de ces éprouvettes.

Des éprouvettes rayonnées, dont la géométrie est présentée figure (11) ont également été testées, car elles ont également été utilisées dans la littérature [3]. Si ces éprouvettes doivent convenir à température ambiante, les fibres débouchantes dans le rayon de raccordement constituent des sites privilégiés pour l'oxydation du carbone à haute température ,ce risque d'entraîner des ruptures prématurées .

Les resultats obtenus sont consignés dans le tableau II et montrent clairement que les éprouvettes sans talons ou à talons brasés ne permettent pas d'accéder aux caractéristiques de résistance du matériau.

L'éprouvette rayonnée ne permet pas d'obtenir une rupture dans la partie utile et les résultats sont inférieurs à ceux de l'éprouvette à talons cocuits qui permet d'obtenir 70% de ruptures conformes.

FATIGUE OLIGOCYCLIQUE

Les problèmes rencontrés en fatigue oligocyclique sont de même nature qu'en traction : comment amarrer l'éprouvette dans les mors tout en localisant la rupture dans la partie utile ?

Pour les essais à température ambiante, on a utilisé une éprouvette rayonnée pris en mors hydraulique telle que décrite dans la littérature [4] (figure 11) et qui doit éviter toute rupture dans les mors. Un calcul a évalué la surcontrainte de traction à 2 % à la naissance du rayon.

Les essais de fatigue ont été effectués sur machine servo hydraulique MTS équipée de mors hydrauliques d'une capacité de serrage de 20KN. Les conditions d'essais sont les suivantes :

- fréquence : 0,25 Hz,
- cycle trapézoïdal avec temps de maintien de 1 s aux mini et maxi de charge
- rapport de charge R = σmini/σmaxi = 0,1

A haute température, l'utilisation de mors hydrauliques refroidis a été rendue possible par l'emploi d 'un four à résistances simple zone FECRALLOY d'une hauteur de 60 mm. Les variations de température dans la zone utile de l'éprouvette sont limitée à +/- 5°C à 600°C grâce à l'utilisation d'écrans au de part et d'autre du four.

Deux séries d'essais ont été effectués à température ambiante et à 600°C sur des éprouvettes prélevées dans une plaque en SCS6/TA6V pressée par Textron SMD les résultats des deux séries d'essais sont présentés sur la figure (12).

L'observation des éprouvettes rompues amène les commentaires suivants :

A température ambiante, la rupture est amorcée dans le congé de raccordement. Sur les fractographies (fig 13) prises dans la zone de rupture, on observe les sites d'amorçages privilégiés que sont les fibres débouchantes à la surface de l'échantillon.

A haute température, on fait les mêmes observations sur les sites d'amorçage, la rupture étant localisée dans la zone de chauffage.

Des essais sur éprouvettes à chant-poli n'ont pas permis d'éviter l'amorçage sur les fibres débouchantes. les valeurs obtenues doivent donc être considérées comme une borne inférieure

CONCLUSIONS

Les essais de traction et de fatigue oligocyclique ont mis en évidence les points suivants

-Les éprouvettes parallélépipédiques sans talons ou avec talons rapportés par brasage ne permettent pas d'accéder aux caractéristiques réelles du matériau testé

-L'éprouvette rayonnée permet d'approcher ces caractéristiques en utilisant des plaques disponibles sur le marché. la présence de fibres débouchantes étant toutefois un problème important car celles-ci deviendront des sites privilégiés d'amorçage en fatigue et d'oxydation à haute température.

- L'éprouvette à talons cocuits permet de mesurer les caractéristiques intrinsèques du matériau.
La validation de cette géométrie est actuellement en cours pour les essais de fatigue oligocyclique à haute température.

BIBLIOGRAPHIE

[1] *Ph. DOOBAR* "Metal matrix Composites in Aeroengines"
15è colloque matériaux pour l'Aéronautique et l'Espace
Paris-Juin 83 - pp 209-226

[2] *E. HOFFMAN, R. BIRD, D. DICUS,* "Effect of braze processing on the microstructure and mechanical properties of SC6/β 21s titanium matrix composites.
AIAA Fourth international aerospace planes conference
1-4 dec. 1992 - ORLANDO

[3] M.L. GAMBONE "Fatigue and fracture of titanium aluminides" WRDC-TR-89-4145

[4] J. GAYDA, T.P. GABB, A.D. FREED "The isothermal fatigue behaviour of a unidirectionnal SiC/Ti composite and the Ti-Alloy matrix NASA-TM-101984

	σ11/σ11N		σ12/σ11N		σ22/σ11N	
	Mini	Maxi	Mini	Maxi	Mini	Maxi
Géométrie 1	-0,006	1,013	-0,217	0,217	-0,166	0,353
Géométrie 2	-0,006	1,021	-0,356	0,356	-0,151	0,818
Géométrie 3	-0,006	1,002	-0,200	0,200	-0,168	0,482
Géométrie 4	-0,006	1,016	-0,205	0,205	-0,166	0,508

Tableau 1 : Valeurs mini-maxi des contraintes ramenées à la contrainte nominale σ11N

Sans talons parallélépipédiques	*Eprouvettes talons brasés*	*Eprouvettes rayonnées*	*Talons cocuits*
Rupture ras des mors	Rupture ras du talon	Rupture dans le rayon	70% rupture en partie utile 30 % rupture au ras du rayon
σ rupture moyenne 1280 MPa	σ rupture moyenne 963	σ rupture moyenne 1350 MPa	σ rupture moyenne 1480 MPa

Tableau 2

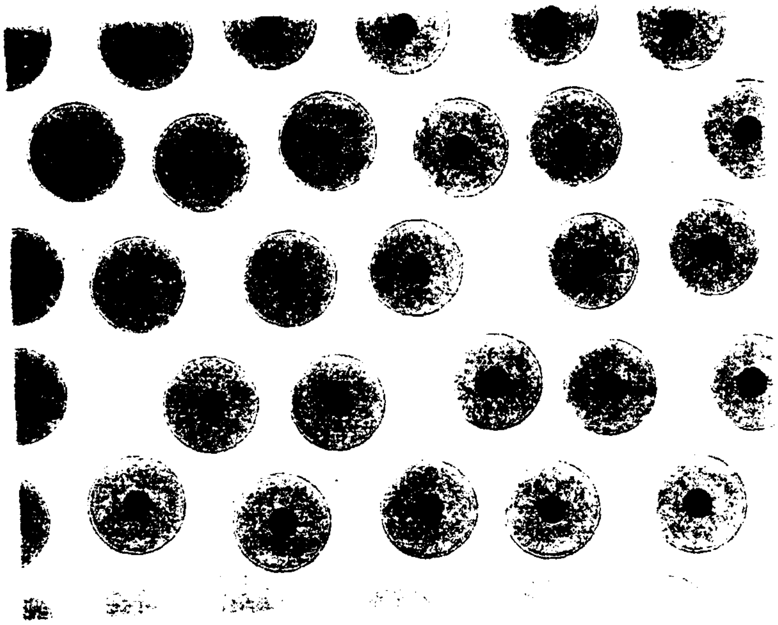

Figure 1 : Coupe transversale SCS-6 / TA6V

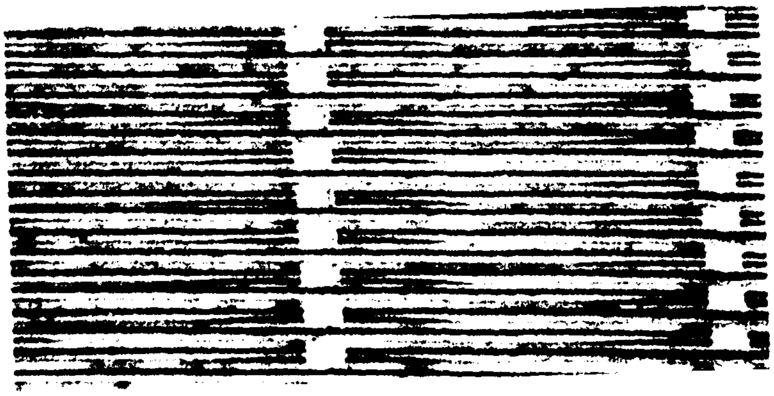

Figure 2 . Tissu SM1240 / TA6V

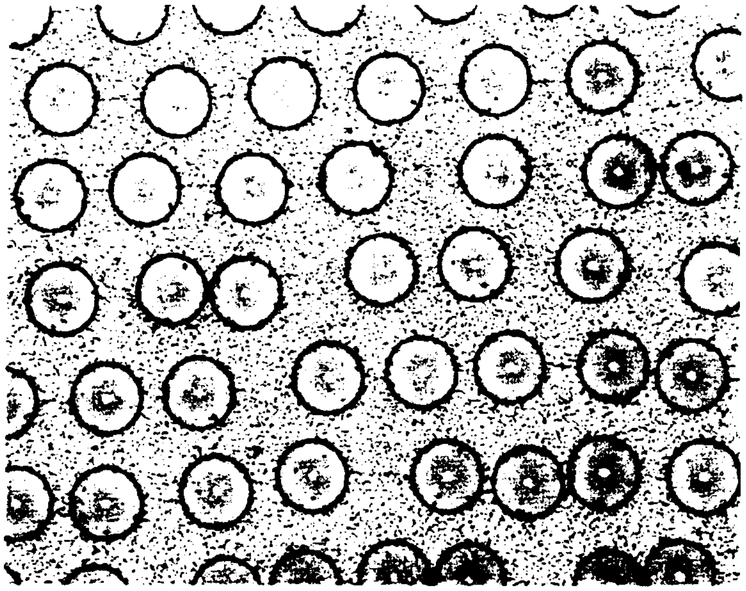

Figure 3 : Coupe transversale SM1240 / TA6V.

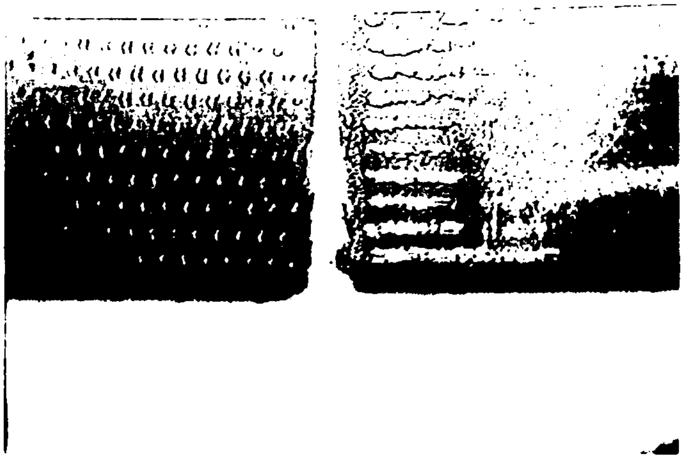

Figure 4 : Rupture dans les mors d' une éprouvette parallélépipédique.

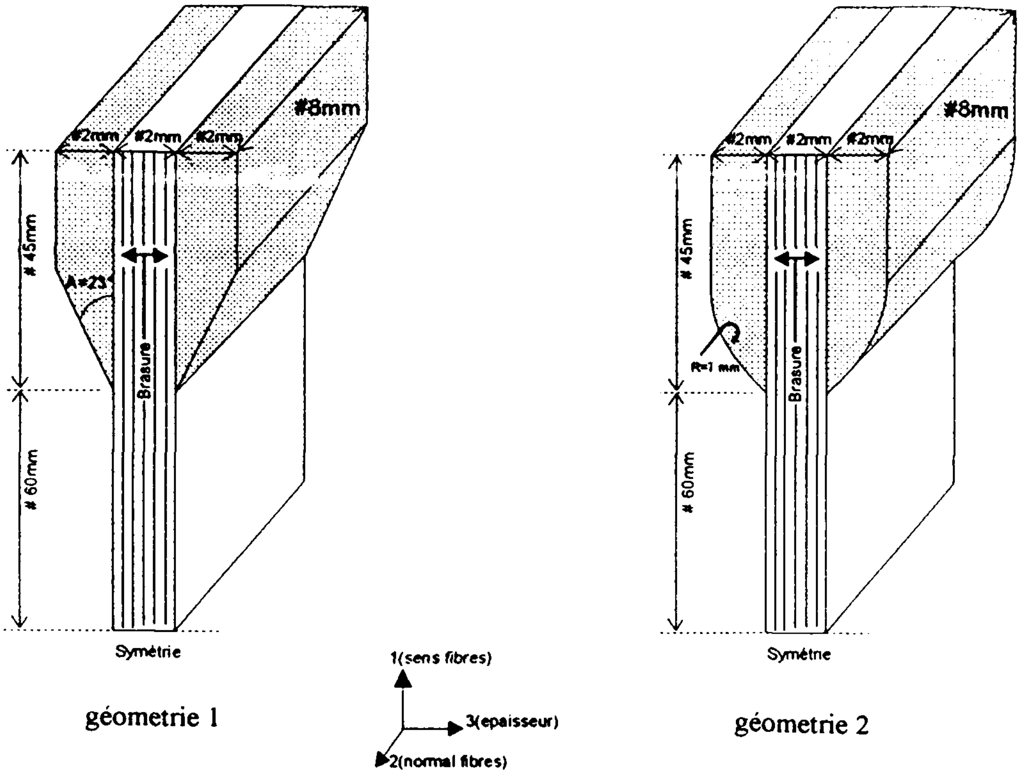
#8mm
#2mm
#2mm
#2mm
# 45mm
# 60mm
A=23°
Brasure
Symétrie
1(sens fibres)
3(epaisseur)
2(normal fibres)
#8mm
#2mm
#2mm
#2mm
# 45mm
# 60mm
R=1 mm
Brasure
Symétrie

géometrie 1

géometrie 2

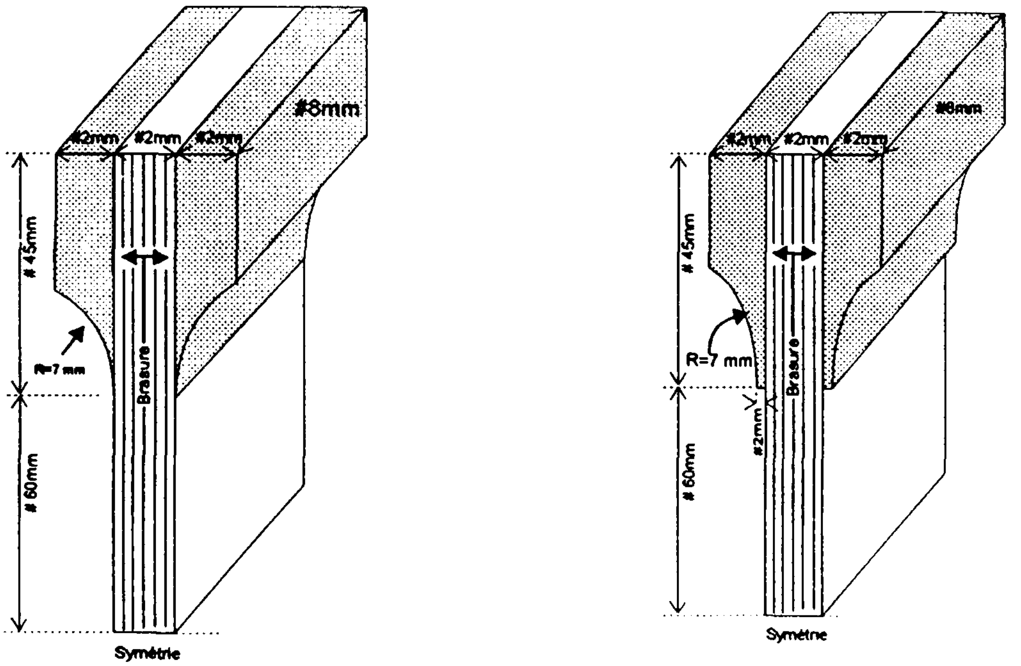
#8mm
#2mm
#2mm
#2mm
# 45mm
# 60mm
R=7 mm
Brasure
Symétrie
#8mm
#2mm
#2mm
#2mm
# 45mm
# 60mm
R=7 mm
#2mm
Brasure
Symétrie

géometrie 3

géometrie 4

Figure 5 : Géometries des éprouvettes étudiées par le calcul.

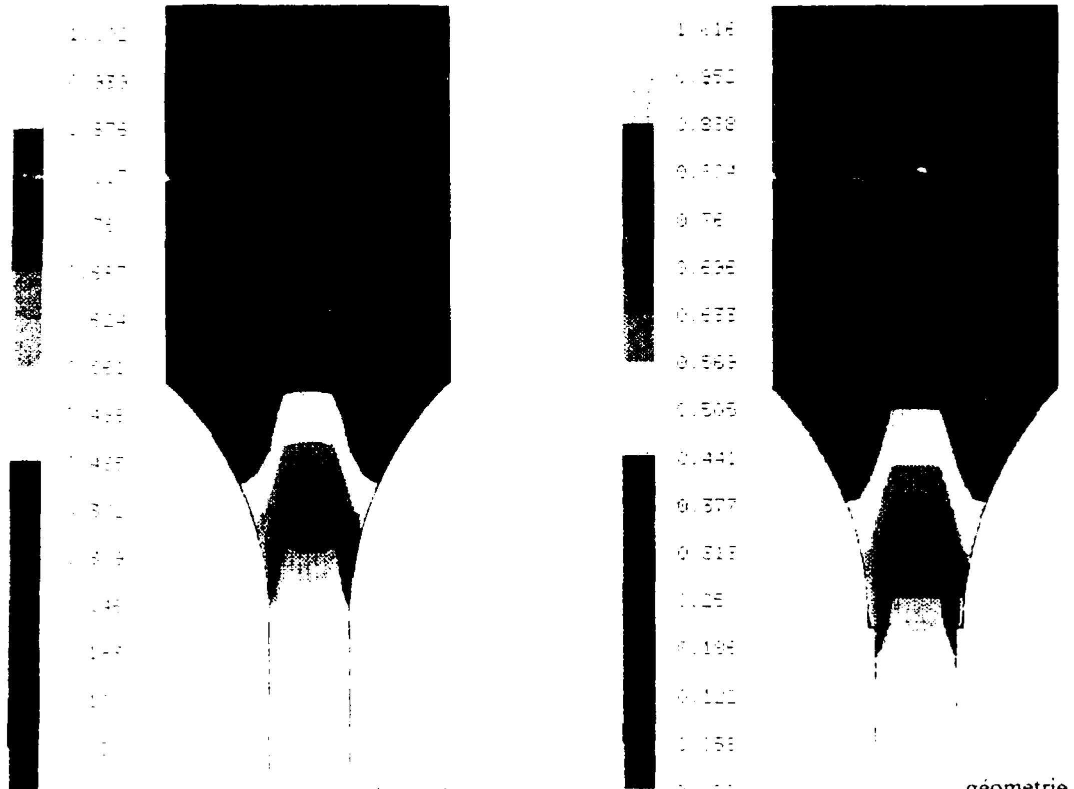

géometrie 3

géometrie 4

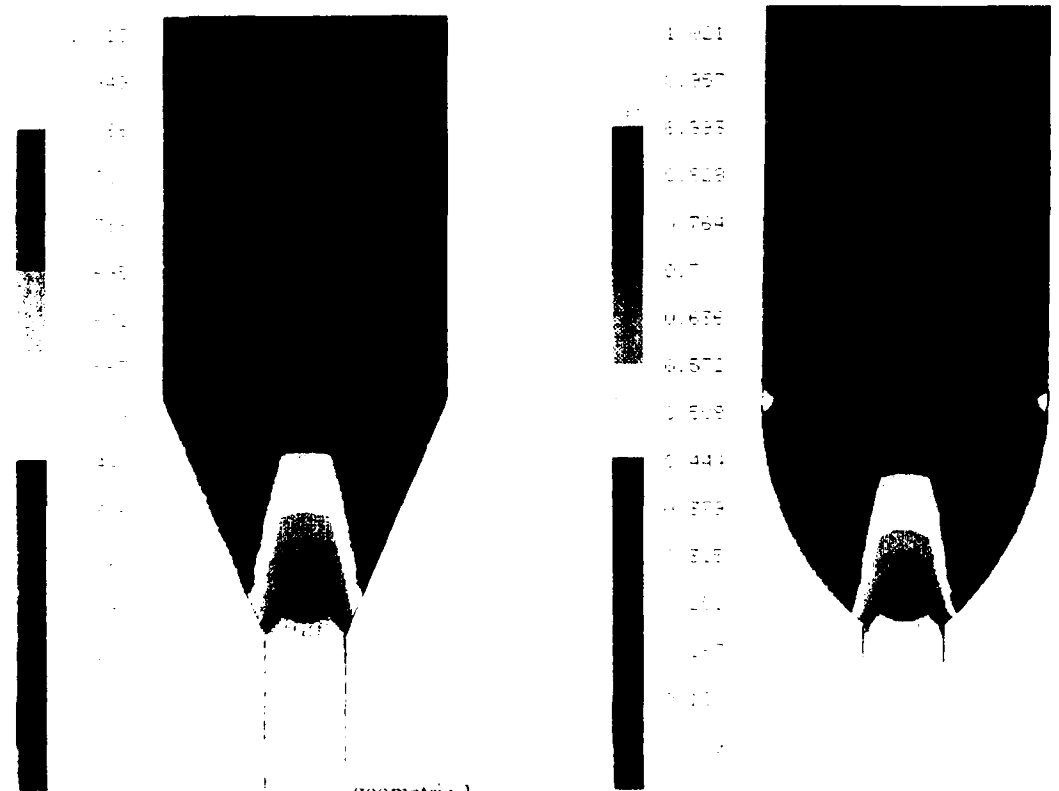

geometrie 1

geometrie 2

Figure 6 Repartiton des contraintes σ_{11} calculees
(Valeurs normees par rapport a σ_{11} nominal)

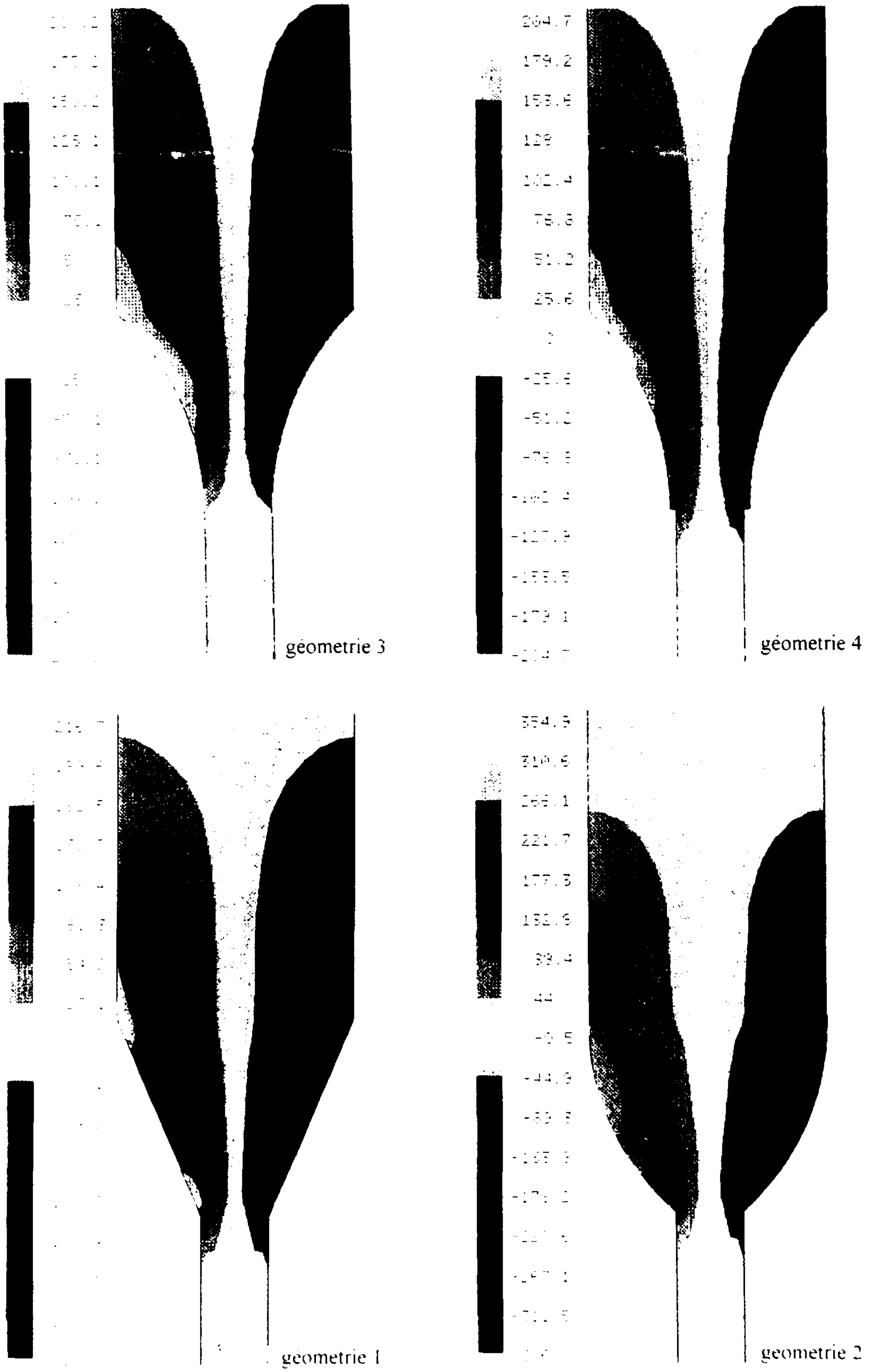

géometrie 3

géometrie 4

géometrie 1

geometrie 2

Figure 7 Repartition des contraintes τ_{12} calculees
(Valeurs normees par rapport a σ_{11} nominal * 10^{-3})

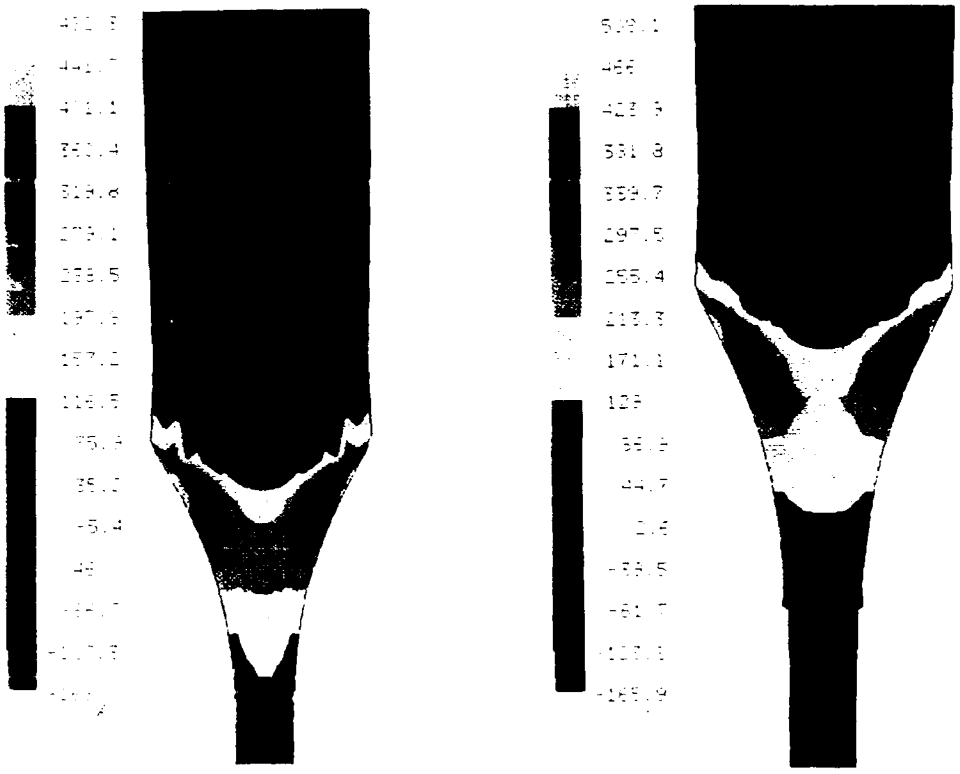

géometrie 3

géometrie 4

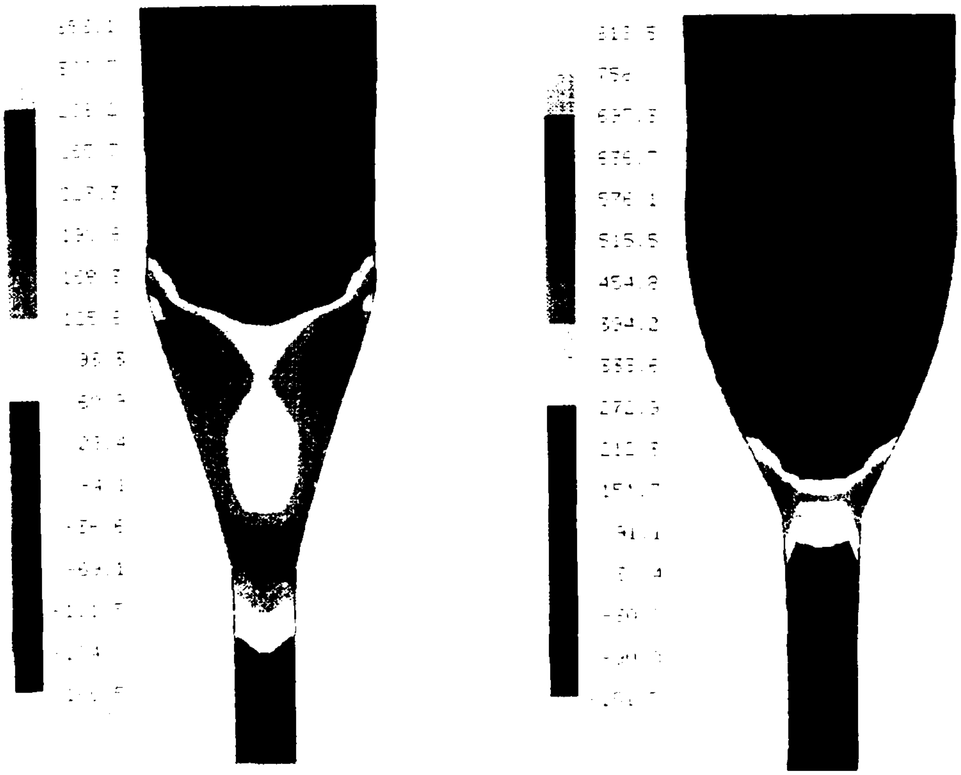

géometrie 1

geometrie 2

Figure 8 Repartition des contraintes σ_{22} calculees
(Valeurs normees par rapport à σ_{11} nominal * 10^{-3})

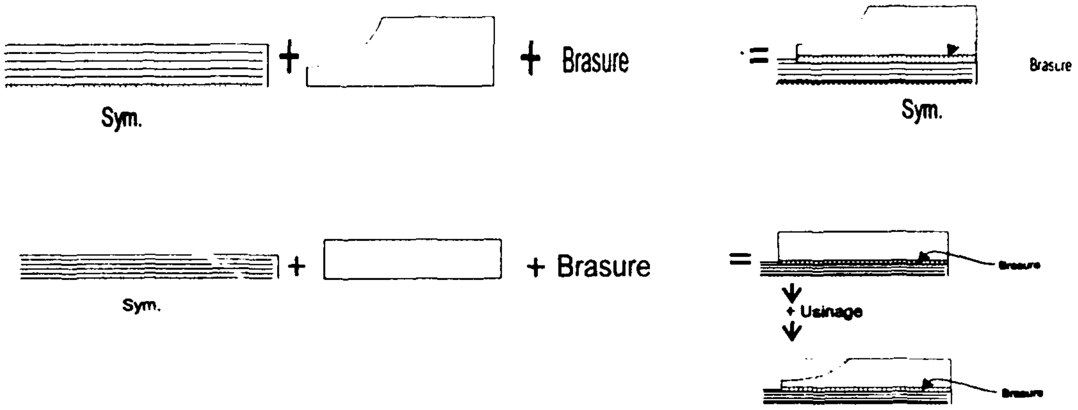
Sym.
+
+ Brasure
=
Brasure
Sym.
Sym.
+
+ Brasure
=
Brasure
+ Usinage
Brasure

Figure 9 : Schéma de fabrication des éprouvettes à talons.

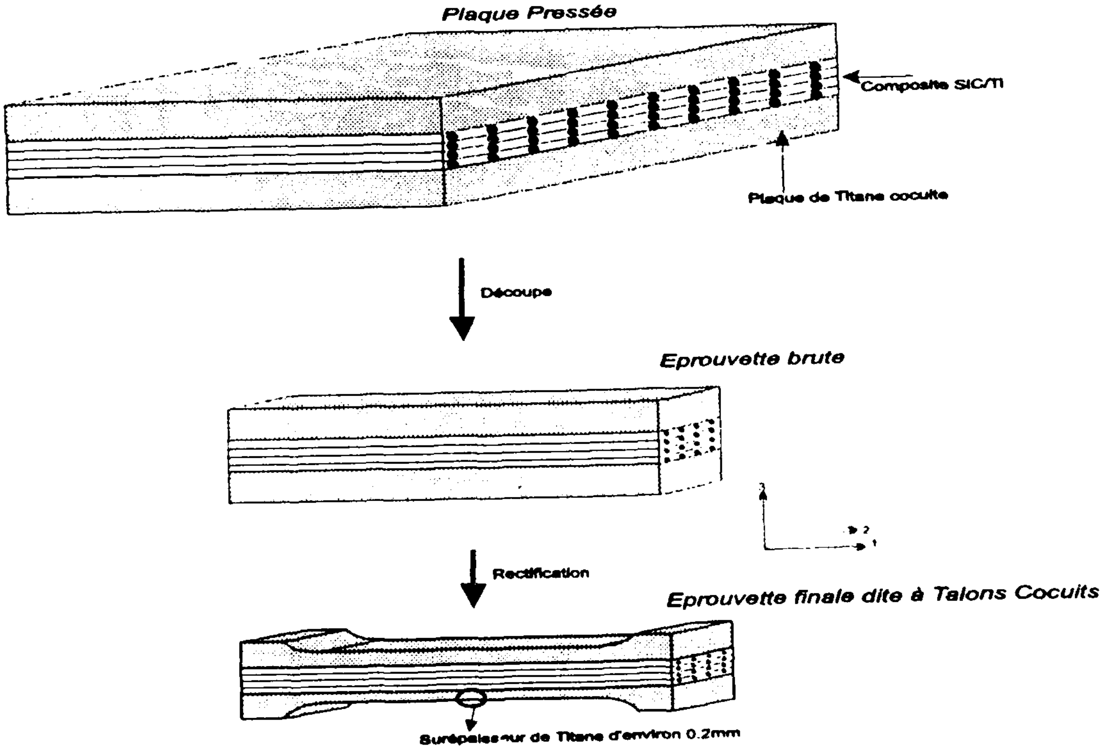
Plaque Pressée
Composite SiC/Ti
Plaque de Titane cocuite
Découpe
Eprouvette brute
3
2
1
Rectification
Eprouvette finale dite à Talons Cocuits
Surépaisseur de Titane d'environ 0.2mm

Figure 10 : Schéma de fabrication des éprouvettes à talons cocuits.

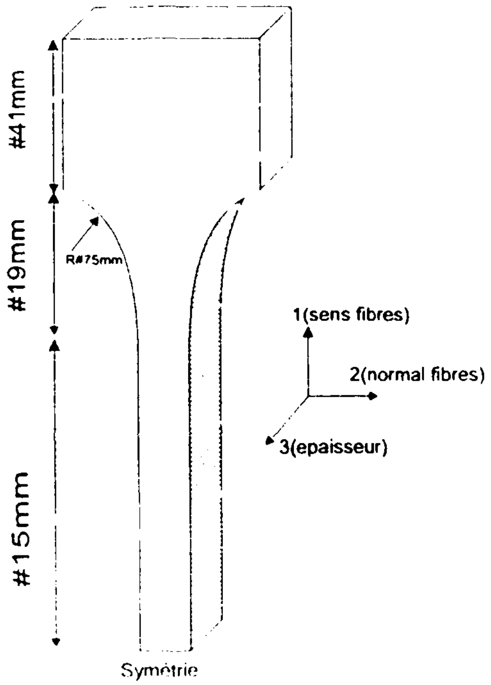
#41mm
#19mm
#15mm
R#75mm
1(sens fibres)
2(normal fibres)
3(epaisseur)
Symétrie

Figure 11 : Géométrie de l' éprouvette rayonnée.

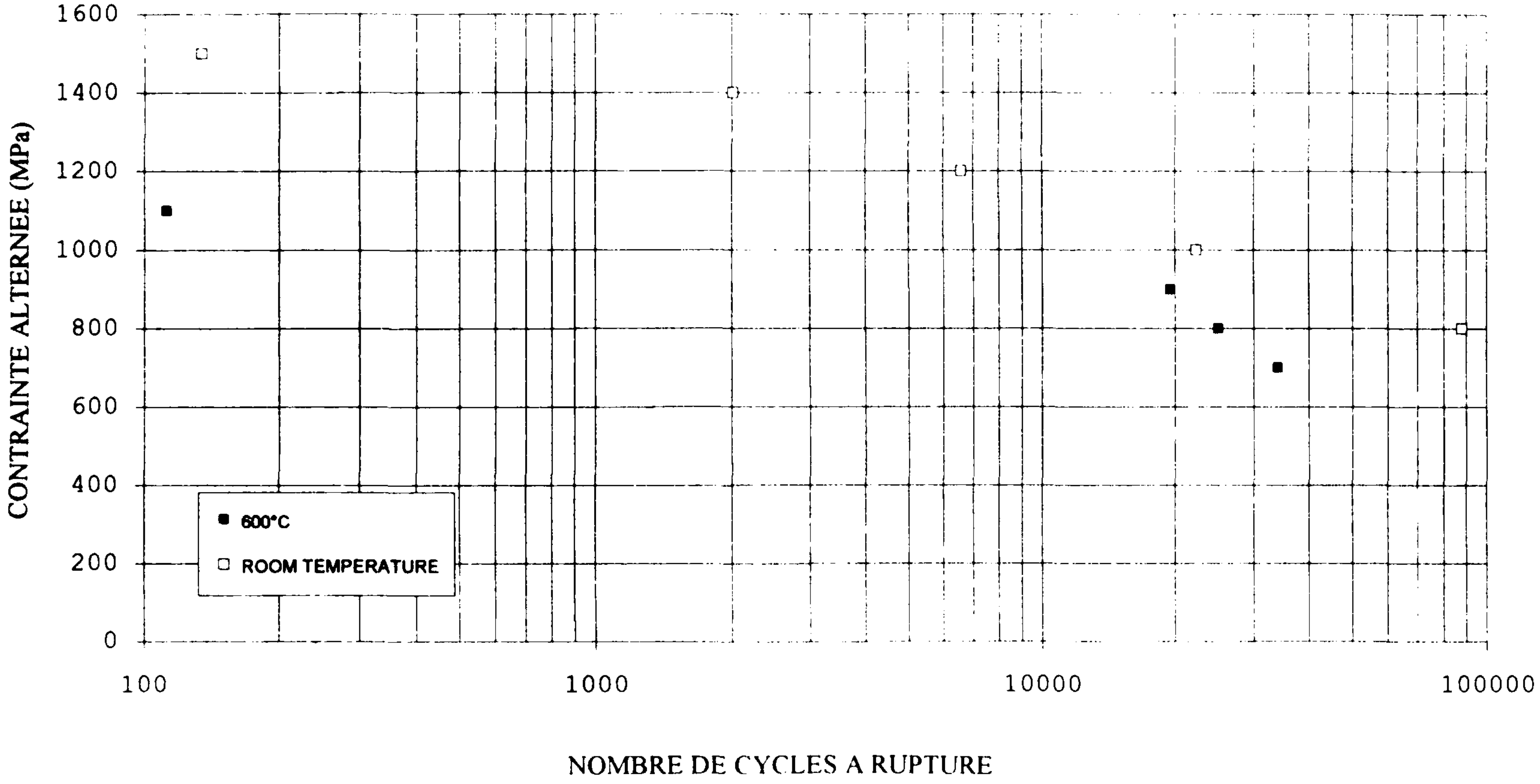

Figure 12 : comportement en fatigue oligocyclique SCS6/TA6V

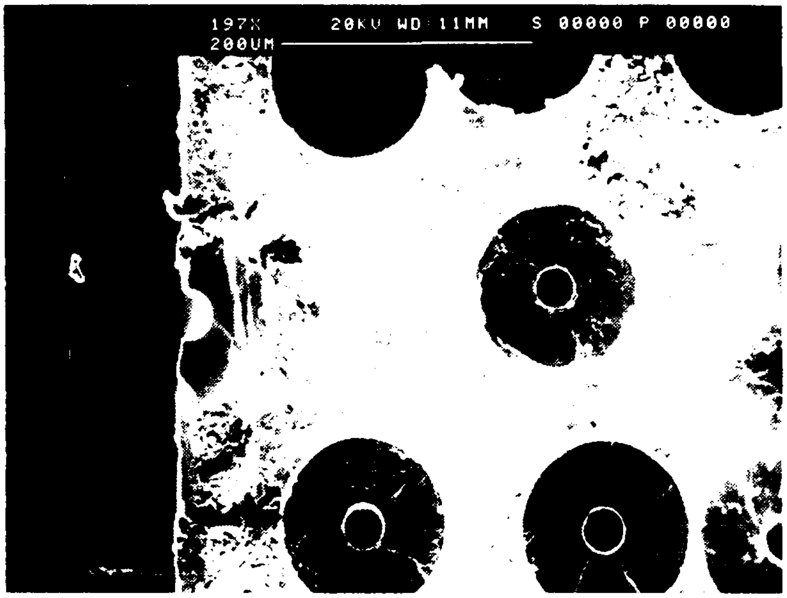
197X 20KV WD 11MM S 00000 P 00000
200UM

Figure 13 Facies de rupture en fatigue oligocyclique a temperature ambiante

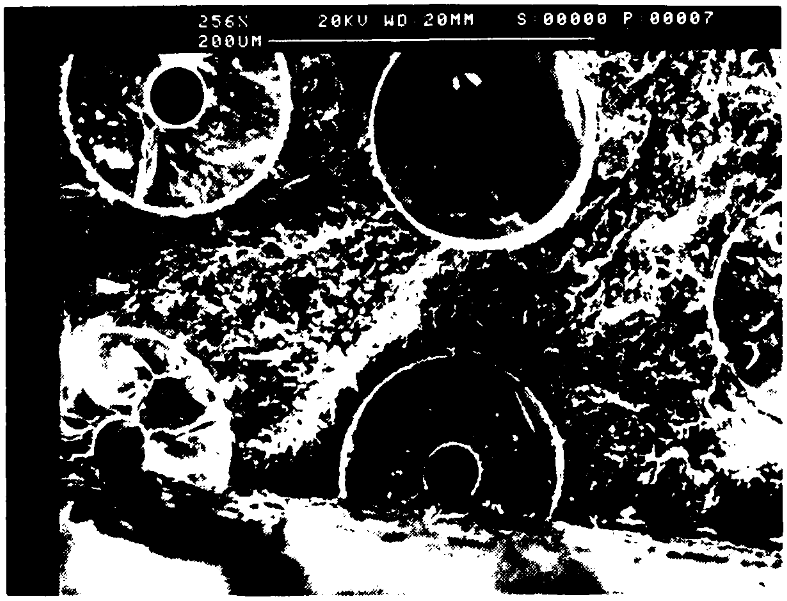
256X 20KV WD 20MM S 00000 P 00007
200UM

Figure 14 Facies de rupture en fatigue oligocyclique a 600 C

MODELLING AND TESTING FIBRE REINFORCED TITANIUM FOR DESIGN PURPOSES

L N McCartney
Division of Materials Metrology
National Physical Laboratory
Teddington, Middx. UK, TW11 0LW

SUMMARY

A review is given on some aspects of designing with continuous fibre reinforced titanium alloys. Issues that are addressed are as follows:

- Need for multiaxial constitutive relations describing behaviour of fibre reinforced titanium for:- monotonic loading at different temperatures, unloading at different temperatures, cyclic changes in load and temperature both in and out of phase, and general thermo-mechanical loading. Linear, yielding, incremental plasticity and time dependent deformations are considered.
- Need for reliable failure criteria that take account of the micromechanisms that contribute to the failure event.
- Role that micromechanical modelling can play in the development of reliable constitutive relations, and design methods.
- Need for validated test methods to measure the parameters that appear in the constitutive relations that are used for design purposes.

1. INTRODUCTION

One aspect of the design process involves predicting the performance of an engineering detail given its geometry and mode of loading, together with the mechanical and thermal properties of the materials used in the design. While geometry and loading mode are often at the discretion of the designer, the materials properties used in the design calculation must be measured experimentally. The objective of this paper is to discuss the relationship of materials properties and their measurement to design, and to show how modelling can help to identify materials parameters that need to be measured, and to develop new design procedures.

It is useful to set the scene by asking the following basic **three** questions:

1) How does one decide *which properties* characterise a given type of material?

2) Who wants to know values of materials properties, and how are such data used in design procedures?

3) How can materials properties be measured reliably?

To answer the **first** question, materials properties are defined by *constitutive equations* that relate basic quantities, such as stress, strain and temperature. Linear relationships involve materials parameters, such as Young's moduli, Poisson's ratios and thermal expansion coefficients, whose values for a given material need to be measured experimentally. For advanced materials, such as fibre reinforced metals, various constitutive equations have been used to characterise their non-linear behaviour, and these are often generalisations of isotropic equations for homogeneous metals to anisotropic situations. Such an approach is likely to be unreliable for composites as they

Presented at an AGARD Meeting on 'Characterisation of Fibre Reinforced Titanium Matrix Composites', September 1993.

are unlikely to behave as homogeneous materials. The combination of elastic fibres with thermo-viscoplastic matrices will lead to constraints of materials behaviour, and lead to effects caused by residual stresses arising from the thermal expansion mismatch between fibres and matrix. A more reliable approach is to use modelling techniques to determine the characteristics of the fibre reinforced metal, and to verify this behaviour by experiment.

To answer the **second** question, it is clear that the users of materials properties fall into the following categories:

a) Materials developers who need property measurements to assess the quality of their materials,

b) Component designers who need to select materials, and component geometries, that satisfy prescribed design requirements, including acceptable cost,

c) The engineers taking responsibility for the operation of engineering components in service.

Materials properties are used in design as input parameters for stress analysis calculations such as finite element and boundary element methods. For linear elastic materials the properties can frequently be used in hand calculations. The objective is to predict the performance (e.g. the deflection, maximum principal stress) as a function of geometry and loading mode. A design methodology can then be established based on failure criteria that limit deflections or loads to prescribed safe values. Predictions can be made of the response of a component to some externally applied stimuli, e.g. applied stresses and temperature, including cyclic profiles where stress and temperature can be either in or out of phase. Such responses are compared to design requirements. If predictions indicate that the component will not meet requirements at reasonable cost then it must be redesigned. When considering the performance of components in service other factors become important such as fracture toughness, fatigue and creep. In addition, the thermal degradation of composites (through chemical changes of fibres, matrix and interfaces) due to exposure to elevated temperatures can be an important factor. A discussion of fracture toughness, fatigue, creep and thermal degradation effects are, however, beyond the scope of this paper.

To answer the **third** question, there is a great need to measure properties with a minimum of scatter when testing is carried out in one or more laboratories, and a need to ensure that properties measured do not depend on the test method. If either of these requirements is violated then the data collected are of limited use in the activities (a-c) described above. It is well recognised that reliable design data can be obtained only if standardised test methods are available that have been properly validated by round robin testing and appropriate analysis of results. For fibre reinforced metals some properties will be needed to characterise properties for which no test methods currently exist. This emphasises the urgent needs to develop realistic constitutive relations characterising material behaviour, to identify materials parameters that need to be measured, and to develop validated methods of measurement.

As composite components often exhibit properties that differ from those measured in test coupons, it is also reasonable to ask whether materials property data obtained from coupons have any value in design procedures. A response to this point is that without reliable mechanical property information it will not be possible to select materials for a particular application, nor will it be possible to design a new component. The most reliable method of collecting these data is to use test coupons. If there is a difference between component and coupon data then it is necessary to identify why. The difference will probably because of the fact that manufacturing variables are having an effect on properties. For example, uneven cooling can lead to residual stresses which in turn lead to differing apparent properties. If the quantitative relations characterising the material took account of residual stresses then differences between the properties of coupons and components might be less. This approach points to the need in some cases for modelling the manufacturing processes used when making both coupons and components. Of particular relevance to fibre reinforced metals are the residual stresses induced during cooling from the manufacturing temperature to room temperature. Uneven fibre distribution in components, resulting from the manufacturing process, can also lead to apparent properties that differ from those measured using coupons.

2. SOME DESIGN CONSIDERATIONS

Fibre reinforced metals are currently being assessed for use in engineering components exploiting their light weight, increased stiffness and strength, and their high temperature performance. The task of designing components made of continuous fibre reinforced MMC is particularly difficult for a variety of reasons. The principal difficulty arises because of the yield of the metal matrix which can occur at relatively low strains at room temperature leading to non-linear stress-strain behaviour, and to a differing stress-strain response in compression. This means that non-linear behaviour and residual stresses must be taken into account during design. The relatively low proportional limit for these materials can mean that components will slightly change shape as soon as they are put into service. The anisotropy of the material has an effect on both the yield stress and on the work hardening characteristics, and needs to be taken into account in design.

The simplest designs for unidirectional (UD) fibre reinforced titanium components, such as hoop wound ring structures, try to exploit the improved properties obtained in the fibre direction. The behaviour of UD material in the axial direction is dominated by the linear elastic behaviour of the fibres. In contrast, UD material is weakest in the transverse direction, and exhibits highly non-linear behaviour when stressed in this direction, and also when subject to axial shear deformation. Designs can thus sometimes be based on material behaviour that is assumed to deform linear elastically. Such an approach is likely to be successful if transverse and axial shear stresses in a component are much lower than those in the fibre direction. Alternatively, design allowables for strengths in transverse tension and shear must be small with the consequence that inefficient conservative designs may result.

For fibre reinforced metals it is clear that there is a need to develop the quantitative relationships that will adequately model thermo-elastic-plastic behaviour taking account of material anisotropy. Having established the relationships, and having verified by experiment that they really do describe the actual behaviour of the material, it is then necessary to develop the test methods that can be used to measure the various parameters that appear in these relationships and thus characterise a particular material. For fibre reinforced metals the quantitative characterisation of materials behaviour is clearly where much research is needed. This must be completed before the design of MMC components using FEA can be reliably carried out.

In this paper an attempt will be made to indicate areas where there is currently uncertainty regarding design methodology, and how modelling can help to increase confidence in existing procedures or to develop new methods of design. The views expressed have been influenced by work of a generic nature (rather than specific) that is being undertaken by a UK MMC Structural Analysis Group involving participants from UK industry, Universities and Government Research Laboratories.

3. PRINCIPLES OF CONTINUUM MECHANICS USED IN DESIGN

Design procedures, whether using analytical methods or numerical techniques such as the finite element or boundary element methods, are based on the principles of continuum mechanics where the following conservation laws are imposed:

mass, linear momentum,
energy, angular momentum.

When considering energy balance, a thermodynamic framework needs to be employed if materials behaviour during temperature changes is to be considered. This then leads to the concept of entropy balance equations and irreversible thermodynamic (or dissipative) processes such as heat conduction and plasticity. Readers are referred to texts by Truesdell (Ref.1) and Eringen (Ref.2) for further details of the basic principles of continuum mechanics set in a thermodynamic framework. It is emphasised that design methods based on finite element analysis or boundary element techniques obey these axioms either exactly or approximately.

4. ROLE OF CONSTITUTIVE EQUATIONS

None of the principles of continuum mechanics outlined in section 3 say anything about the nature of the properties of a material. Additional relationships need to be specified, known as constitutive equations, which are at the heart of the design process characterising the mechanical, thermal, and electrical properties of materials. These relationships identify most of the materials properties that need to be measured. Furthermore they are also the relationships that are used in design procedures such as finite element and boundary element stress analyses.

In solid mechanics the most well known constitutive equations are the stress-strain relations of linear elasticity theory which introduce elastic constants such as Young's modulus and Poisson's ratio that need to be measured experimentally. For metals, plasticity is an important phenomenon that is modelled by constitutive equations of a more complex nature (see for example Ref.3). When metals deform at high temperatures creep or viscoplastic behaviour is observed (i.e. time dependent deformation).

Fibre reinforced metal matrix composites, such as silicon carbide reinforced titanium alloys, combine the properties of two materials having very different properties. The silicon carbide fibres behave essentially as linear thermo-elastic solids over a wide range of temperatures, while the titanium alloy matrix behaves as a thermo-viscoplastic solid. The constitutive relations that characterise the deformation properties are reasonably well known for fibres and matrix alone, but for composites made of these fibres embedded in a metal matrix there are no easy ways of deriving the constitutive relations that characterise their deformation behaviour (see Ref.4 for review of plasticity theories for fibrous composites). The constitutive equations once developed for fibre reinforced metals will identify new materials parameters that need to be measured, point to new requirements for standard test methods, and lead to new design methods.

Before stress analysis can be carried out using FEA it is necessary to have constitutive relations which adequately describe the thermo-elastic-plastic response of the material. Many FEA systems enable users to input their own descriptions of materials behaviour through the use of user-defined routines. Thus new types of constitutive equations can easily be put into engineering practice. The effects need to be understood of residual stress arising from the thermal expansion mismatch between fibre and matrix, and the effects of load and temperature variations on both the yield function and the work hardening. Especially for titanium composites, which will operate at elevated temperatures, the influence of temperature on the elastic-plastic response is an essential requirement. Specific areas, of relevance to design where quantitative relationships are required, are now discussed in the following sections.

5. LINEAR ELASTIC BEHAVIOUR

For the linear regions of the stress-strain curves of fibre reinforced metals the relevant constitutive equations are the linear stress-strain-temperature relations. For unidirectional fibre reinforced metals in the linear elastic regime, the material can be assumed to behave as a transverse isotropic solid, for which five elastic constants and two thermal expansion coefficients need to be measured. These are the longitudinal and transverse Young's moduli, Poisson's ratios and axial shear modulus, and the longitudinal and transverse thermal expansion coefficients. If the linear thermoelastic properties are known of fibres and matrix in the composite then the values of the thermoelastic constants of the composite are easily calculated using analytical formulae. The thermoelastic constants can also be measured and compared to predicted values. Models can be regarded as validated only if there is good agreement between prediction and experiment. Models validated in this manner can be used as the basis of quantitative design procedures.

Linear behaviour is observed in fibre reinforced metals to strains at which matrix yielding occurs inducing non-linear behaviour. The proportional limit in tension is usually lower than that in compression because of the thermal residual stresses that arise from thermal expansion mismatch between fibre and matrix. It is thus very important that the effects of the residual stresses are taken into account when carrying out stress analyses in the linear regime. One way of achieving this is to predict the size of the residual stresses by assuming that the stress-free temperature is known, and that the material behaves as a linear thermoelastic solid during cooling to lower ambient temperatures. For UD titanium composites the stress free temperature is thought to be around 500°C. For calculations of residual stress build-up during cooling it is important that the temperature dependence of modulus is taken into account (Ref.5). Corresponding calculations for laminates can be made.

For UD and laminated fibre reinforced metals, the important materials parameters that need to be measured are the thermoelastic constants. One measurement problem that has been encountered, especially for fibre reinforced aluminium, is the method used to measure elastic moduli. While Poisson's ratio can be calculated by taking the ratios of strains measured in orthogonal directions, the elastic moduli must be calculated by determining the gradient of the stress-strain curves. Such calculations lead to significant scatter in modulus values if the stress-strain data are subject to scatter and the stress-strain curve exhibits a very low proportional limit. As the proportional limit of titanium composites is higher than that for aluminium composites, the moduli for fibre reinforced titanium are capable of reasonably accurate measurement.

6. YIELD CRITERIA

Plasticity is regarded as a phenomenon of irreversible non-linear deformation that occurs instantaneously if the stress state satisfies some yield criterion, e.g. a critical yield stress is reached for uniaxial stress states. At elevated temperatures the uniaxial yield stress will reduce to much lower levels as the metals melting point is approached, and at the same time the material will exhibit time dependent behaviour (discussed in section 8 below).

For time-independent plasticity a yield function is needed which specifies when the composite begins to yield in a given stress state which might be triaxial, and at a given temperature. For homogeneous isotropic materials it is usual to assume that yield is governed by either the Tresca or the von Mises criterion. Continuum mechanics indicates (Ref.3) that for anisotropic materials other yield criteria are more appropriate but there is no guarantee that a fibre reinforced MMC will obey such yield criteria. For example, the von Mises yield criterion for anisotropic materials has the form (Ref.3) involving the stress components σ_{ij}

$$F(\sigma_{22}-\sigma_{33})^2+G(\sigma_{33}-\sigma_{11})^2+H(\sigma_{11}-\sigma_{22})^2$$
$$+ 2L\tau_{23}^2 + 2M\tau_{13}^2 + 2N\tau_{12}^2 = 1 \ .$$

The parameters F, G, H, L, M and N are materials parameters associated with the materials anisotropy that have to be measured experimentally, including their temperature dependence. It is thought highly unlikely that a yield criterion of this type will be appropriate for unidirectional fibre reinforced metals as the properties in the fibre direction are dominated by the elastic properties of the fibres.

7. INCREMENTAL PLASTICITY

Assuming time independent plasticity, an incremental law of plasticity is required determining the increment of plastic strain which accumulates during an incremental change of the stress field. This is the law that represents quantitatively the work hardening characteristics of the material. One approach of representing the plastic part of the stress-strain curve by a straight line of gradient less than the initial modulus may be too simplistic. It will be necessary to model this part of the curve more accurately taking account of the work hardening effects. The ideal would be to model the experimental results "exactly". However the function describing the work hardening behaviour would need to take proper account of multi-axial stress states and the anisotropy of the material. A model based on stress invariants consistent with the anisotropy of the material is thought to be essential. The simplest incremental laws for the plastic strain components ε_{ij} of an anisotropic material have the form (Ref.3)

$$d\varepsilon_{11}= \left[H(\sigma_{11}-\sigma_{22}) +G(\sigma_{11}-\sigma_{33})\right]d\lambda$$

$$d\varepsilon_{22}= \left[F(\sigma_{22}-\sigma_{33}) +H(\sigma_{22}-\sigma_{11})\right]d\lambda$$

$$d\varepsilon_{33}= \left[G(\sigma_{33}-\sigma_{11}) +F(\sigma_{33}-\sigma_{22})\right]d\lambda$$

$$d\gamma_{23} = L\tau_{23}d\lambda$$

$$d\gamma_{13} = M\tau_{13}d\lambda$$

$$d\gamma_{12} = N\tau_{12}d\lambda \ ,$$

where it should be noted that the materials parameters appearing in the incremental laws are identical to those used in the yield criterion. Again it is thought highly unlikely that incremental laws of this type will be appropriate for unidirectional fibre reinforced metals as the properties in the fibre direction are dominated by the elastic properties of the fibres.

When modelling the non-linear deformation which can arise in fibre reinforced metals it is necessary to determine the yield surface by measurement, and to check whether or not conventional incremental plasticity theory for anisotropic materials is adequate. As is apparent from above, according to incremental theory the mathematical relations describing the yield surface are sufficient to predict the work hardening behaviour of the material. This may not, however, be true for a fibre reinforced metal. The response of the material to temperature changes with and without load, and to load and/or temperature increases and reductions including cycling will also need to be characterised quantitatively.

8. TIME DEPENDENT BEHAVIOUR

At elevated temperatures metals exhibit an additional time-dependent non-linear mode of deformation known as creep, in addition to time-independent plasticity. When carrying out finite element stress analysis calculations for materials that exhibit time dependent behaviour, there is often the temptation to provide the FEA system with user-defined constitutive relations that involve time. For example, uniaxial creep data can be input in the form of strain-time relations for a range of stress levels. By using multiaxial creep deformation laws based on invariants of the deviatoric stress tensor (Ref.6) it is possible to use uniaxial creep data in multiaxial stress situations. Thus user-defined routines of this type would appear to have some promise for application to finite element calculations. However, it has to be recognised that the constitutive relations supplied by the user in this case involve time explicitly and this will lead to errors if applied to a problem where stress redistribution takes place. Time should not appear explicitly in constitutive relations (see Ref.7), and the fact that it is sometimes used in this manner indicates clearly that suitable constitutive relations need to be developed. For example, in Ref.5 it is suggested that creep deformation, relevant when a composite cools down from its manufacturing temperature, can be modelled by an equation of the form

$$\varepsilon = A\sigma^{n}t^{m}\exp[-Q/kT] ,$$

where T is the absolute temperature, and where the parameter t (the elapsed time) appears explicitly. Relations of this type represent the results of constant stress tests and, as they do not characterise materials behaviour under time dependent loads, they are *not* suitable for use as constitutive equations in finite element analysis.

For metals constitutive relations have been developed that involve time implicitly through the explicit use of internal state variables (Ref.8). For continuous fibre composites subject to creep the concept of internal state variables has also been used for uniaxial deformations (Ref.9).

9. FAILURE CRITERIA

The design engineer requires failure criteria, valid for multiaxial loading, that can be incorporated into FEA systems. It is extremely unlikely that current criteria used for polymer composites will be adequate for MMC. The need is to predict the level of loading at which failure occurs, together the location and mode of failure. There are several failure criteria that have been proposed in the literature, and implemented in FEA packages, for example, the Tsai-Hill, Tsai-Wu, Hoffman, and maximum principal stress and strain criteria. Because of the engineers' lack of confidence in the failure criteria offered as options in FEA packages, the approach sometimes taken for polymer composites is to work out failure stresses and locations using all available criteria and then design the component on the basis of the most pessimistic prediction! This approach is not adequate and emphasises our lack of sound knowledge concerning the failure of composites.

These failure criteria are based on continuum mechanics principles and do not take into account the fact that there may be defects in the material which are responsible for the failure. Fibre failures almost certainly initiate at defects in the fibres, while interface failure will initiate from interfacial defects. This suggests that it may be very difficult for FEA methods to predict the failure mode and location, and hence strength, with any degree of reliability. Some of the non-linearity in the stress-strain curve may arise from the fracture of fibres as the load is increased to failure. One consequence of this is that the stiffness of the composite may be reduced by a measurable amount, particularly for composites made of large diameter fibres. To assess this effect it would be useful to carry out a limited number of small load reversals during loading so that an estimate of modulus can be made at various parts of the stress-strain curve. A reducing modulus could be indicating some form of damage accumulation which may not be associated directly with plastic deformation. There may be some scope for devising new 'failure criteria' based on an agreed loss of a property that takes account of the micromechanisms of damage that contribute to the failure of the composite. Such an approach is thought to be more predictable than strength, and could, therefore, be the basis of more reliable 'failure criteria'.

For unidirectional composites, subject to loading that induces maximum principal stresses oriented more or less parallel to the fibres, the maximum principal stress criterion can be used to predict failure. The critical value of the maximum principal stress determines the failure of the composite in such special conditions and FEA can predict the failure initiation site.

10. ROLE OF MICRO-MECHANICAL MODELS

In sections 5-9 some of the problems associated with the choice of constitutive equation to describe the properties of continuous fibre reinforced metals have been described. To summarise the situation, most approaches are attempts to generalise well known continuum mechanics methods for homogeneous materials to inhomogeneous composites without any attempt to consider the physics of composite deformation.

A significant amount of work has been carried out attempting to model the deformation of continuous fibre composites using micro-mechanical models. Representative volume elements at the fibre/matrix level of undamaged composites are defined and a stress analysis carried out that predicts the effective stress-strain behaviour of the composite. The literature is far too large to review here. There are analytical models that are capable of predicting the thermoelastic constants of unidirectional and laminated composites in terms of fibre, matrix or ply properties, assuming perfect interface bonding. For titanium composites such models are useful for characterising linear behaviour only. Non-linear behaviour arising from matrix yield requires FE methods that can be used to predict the stress-strain response of the composite to axial tension, compression and shear, and to transverse tension, compression and shear loading. Provided that thermal residual stresses are taken into account, these methods will provide invaluable information regarding the onset of yield in fibre reinforced metals for multiaxial stress states, and on the development of plastic flow in the metal matrix. The stress-strain response to combined complex loading can also be predicted by such methods. It is only by carrying out such calculations that one can devise new more realistic constitutive relations, and check whether they describe materials behaviour adequately.

For composites operating at elevated temperatures, the time dependent creep deformation of the matrix becomes important. Questions that need to be asked are as follows:

How does a composite respond for complex loading states when it has been loaded to a non-linear part of the stress-strain curve and

i) the temperature is changed?

ii) the temperature is cycled?

iii) the temperature and stress are cycled both in and out of phase?

A great deal of research will be needed to solve these problems the solution of which will need to involve contributions from continuum mechanics, micromechanical modelling and experiment. Some approaches, based on FEA of representative volume elements subject to the complex load/temperature profiles described above, will require extensive numerical analysis and will produce results that are difficult to interpret when attempting to formulate realistic constitutive relations valid for general conditions of loading and thermal history. Because of this, there should be some scope for the use of analytical models that can indicate some characteristics of composite materials behaviour at both room and elevated temperatures. As some design methods assume that the maximum principal stress is almost aligned with the fibres in a unidirectional composite there is scope for using simple engineering methods based on parallel bar models of a composite (Ref.10). Also, methods using laminate theory and the vanishing fibre diameter model to represent single ply behaviour have much scope for development (Ref.11).

11. ASPECTS OF MEASUREMENT OF PROPERTIES

When new more realistic constitutive equations become available, the types of materials test that need to be carried out in order to measure parameters used in the constitutive relations, and thus fully characterise the fibre reinforced metal, will have been identified. Reliable testing techniques will be required to measure those properties needed for design calculations. As experience of testing accumulates and the new design methods become established, the need will develop for standard test methods to measure relevant parameters.

It is useful to specify the various stages involved in the development of testing standards. Once a test method has been developed it is necessary to establish first of all that it is capable of acceptable repeatability, i.e. acceptable levels of scatter are found when tests are repeated in one laboratory using identical test conditions. If this can be demonstrated for a range of similar types of material then it is necessary to establish that the test is capable of achieving acceptable reproducibility, i.e. acceptable levels of scatter result when a series of repeat tests are carried out in a series of laboratories under identical testing conditions. Such tests are carried out in round robin testing programmes. If the round robin testing of a particular test method has been shown, using recognised quantitative assessment methods, to be both repeatable and reproducible then it can then be considered for standardisation at national and/or international levels.

12. SUMMARY OF REQUIREMENTS NEEDED TO DEVELOP A DESIGN METHODOLOGY

There is a need to develop and validate experimentally the stress analysis techniques required to design engineering components made of fibre reinforced metals. In particular the needs are to:

* develop constitutive equations for carrying out the finite element stress analysis of fibre reinforced metal components. This activity should include an examination of the onset of yield, the anisotropy of yield and work hardening, the effects of temperature variations, the failure stress and strain, and the location of the failure.

* validate constitutive relations by critically assessing their ability to predict the behaviour of the material by comparison of prediction with experimental behaviour.

* identify mechanical property values needed for use by stress analyses, and prioritise their importance to the design of fibre reinforced titanium components.

* agree the best techniques for mechanical property measurement, including the carrying out of round robin testing needed to validate standardised test methods.

* carry out stress analyses of selected components and to compare predicted behaviour with experimental results.

- develop new failure criteria for design purposes that are based on relevant micromechanisms of damage initiation and growth in fibre reinforced metals.

Acknowledgements

The author would like to thank Dr Clive Allen, Rolls Royce plc, for discussions concerning design issues for fibre reinforced titanium alloys, and members of the UK MMC Structural Analysis Group with whom the author has collaborated for about four years, and who have shaped many of the ideas presented in this paper. Some of the background information presented in this paper arose from the 'Materials Measurement Programme', a programme of underpinning research financed by the UK Department of Trade and Industry.

Published with the permission of the Controller of Her Britannic Majesty's Stationery Office - British Crown Copyright 1993/DTI .

References

1. C Truesdell, 'Rational thermodynamics', McGraw-Hill Book Co. New York - London, 1969.

2. A C Eringen, 'Mechanics of continua', John Wiley & Sons Ltd. New York - London, 1967.

3. R Hill, 'The mathematical theory of plasticity', Clarendon Press, Oxford, 1950.

4. A Yehia, Bahei-El-Din & G J Dvorak, ASTM STP 1032, (1989), 103-129.

5. R P Nimmer, R J Bankert, E S Russell, G A Smith and P K Wright, J Comp. Tech. & Res. **13**, (1991), 3-13.

6. A F Johnson, in Proc. Euromechanics Colloquium 115 at Villard-de-Lans, Ed. J P Boehler, Martinus Nijhoff Publishers, The Hague - Boston - London, 1982.

7. L N McCartney, Phil. Mag. **33**, (1976), 689-695.

8. A M Othman, D R Hayhurst and B F Dyson, Proc. Roy. Soc. Lond. **A441**, (1993), 343-358.

9. S Goto and M McLean, Acta Met. & Mater. **39**, (1991), 153-164.

10. L N McCartney & T A E Gorley, Proc. 9th Riso International Symposium on Metallurgy and Materials Science, 1988, 439-446.

11. W S Johnson, M Mirdamadi & J G Bakuckas Jr. 'Fatigue of continuous fiber reinforced metallic materials' NASA Technical Memorandum 107700, Feb. 1993.

REPORT DOCUMENTATION PAGE

1. Recipient's Reference	2. Originator's Reference	3. Further Reference	4. Security Classification of Document
	AGARD-R-796	ISBN 92-835-0735-5	UNCLASSIFIED/ UNLIMITED

5. Originator
Advisory Group for Aerospace Research and Development
North Atlantic Treaty Organization
7 Rue Ancelle, 92200 Neuilly sur Seine, France

6. Title
CHARACTERISATION OF FIBRE REINFORCED TITANIUM MATRIX COMPOSITES

7. Presented at the 77th Meeting of the AGARD Structures and Materials Panel, held in Bordeaux, France, 27th—28th September 1993.

8. Author(s)/Editor(s)	9. Date
Various	February 1994

10. Author's/Editor's Address	11. Pages
Various	268

12. Distribution Statement There are no restrictions on the distribution of this document. Information about the availability of this and other AGARD unclassified publications is given on the back cover.

13. Keywords/Descriptors

Metal matrix composites
Titanium
Fiber composites
Aircraft engines
Airframes
Nondestructive tests
Stiffness
Tensile strength
Thermal resistance
Mechanical tests

14. Abstract

The combination of stiffness, strength and high temperature resistance provided by fibre reinforced titanium matrix composites offers major benefits for aircraft engine and airframe applications, where these materials could be used to reduce weight or improve performance.

This workshop on the subject of characterisation of titanium composites was intended to provide a forum for the exchange of information in this important area. Characterisation in this case refers to the understanding of the behaviour of the composites as it relates to the ability to predict their performance in real-life applications. It covers various topics that include mechanical test techniques, NDE methods, life prediction models and other factors that will affect the level of confidence with which these relatively new materials will be accepted for application.

With titanium composites, we are presently at a stage where matrix alloys, reinforcing fibres and composite consolidation processes are available for the fabrication of structural components.

AGARD Report 796
Advisory Group for Aerospace Research and Development, NATO
CHARACTERISATION OF FIBRE REINFORCED TITANIUM MATRIX COMPOSITES
Published February 1994
268 pages

The combination of stiffness, strength and high temperature resistance provided by fibre reinforced titanium matrix composites offers major benefits for aircraft engine and airframe applications, where these materials could be used to reduce weight or improve performance.

This workshop on the subject of characterisation of titanium composites was intended to provide a forum for

P.T.O.

AGARD-R-796

Metal matrix composites
Titanium
Fiber composites
Aircraft engines
Airframes
Nondestructive tests
Stiffness
Tensile strength
Thermal resistance
Mechanical tests

AGARD Report 796
Advisory Group for Aerospace Research and Development, NATO
CHARACTERISATION OF FIBRE REINFORCED TITANIUM MATRIX COMPOSITES
Published February 1994
268 pages

The combination of stiffness, strength and high temperature resistance provided by fibre reinforced titanium matrix composites offers major benefits for aircraft engine and airframe applications, where these materials could be used to reduce weight or improve performance.

This workshop on the subject of characterisation of titanium composites was intended to provide a forum for

P.T.O.

AGARD-R-796

Metal matrix composites
Titanium
Fiber composites
Aircraft engines
Airframes
Nondestructive tests
Stiffness
Tensile strength
Thermal resistance
Mechanical tests

AGARD Report 796
Advisory Group for Aerospace Research and Development, NATO
CHARACTERISATION OF FIBRE REINFORCED TITANIUM MATRIX COMPOSITES
Published February 1994
268 pages

The combination of stiffness, strength and high temperature resistance provided by fibre reinforced titanium matrix composites offers major benefits for aircraft engine and airframe applications, where these materials could be used to reduce weight or improve performance.

This workshop on the subject of characterisation of titanium composites was intended to provide a forum for

P.T.O.

AGARD-R-796

Metal matrix composites
Titanium
Fiber composites
Aircraft engines
Airframes
Nondestructive tests
Stiffness
Tensile strength
Thermal resistance
Mechanical tests

AGARD Report 796
Advisory Group for Aerospace Research and Development, NATO
CHARACTERISATION OF FIBRE REINFORCED TITANIUM MATRIX COMPOSITES
Published February 1994
268 pages

The combination of stiffness, strength and high temperature resistance provided by fibre reinforced titanium matrix composites offers major benefits for aircraft engine and airframe applications, where these materials could be used to reduce weight or improve performance.

This workshop on the subject of characterisation of titanium composites was intended to provide a forum for

P.T.O.

AGARD-R-796

Metal matrix composites
Titanium
Fiber composites
Aircraft engines
Airframes
Nondestructive tests
Stiffness
Tensile strength
Thermal resistance
Mechanical tests

the exchange of information in this important area. Characterisation in this case refers to the understanding of the behaviour of the composites as it relates to the ability to predict their performance in real-life applications. It covers various topics that include mechanical test techniques, NDE methods, life prediction models and other factors that will affect the level of confidence with which these relatively new materials will be accepted for application.

With titanium composites, we are presently at a stage where matrix alloys, reinforcing fibres and composite consolidation processes are available for the fabrication of structural components.

Papers presented at the 77th Meeting of the AGARD Structures and Materials Panel, held in Bordeaux, France 27th—28th September 1993.

ISBN 92-835-0735-5

the exchange of information in this important area. Characterisation in this case refers to the understanding of the behaviour of the composites as it relates to the ability to predict their performance in real-life applications. It covers various topics that include mechanical test techniques, NDE methods, life prediction models and other factors that will affect the level of confidence with which these relatively new materials will be accepted for application.

With titanium composites, we are presently at a stage where matrix alloys, reinforcing fibres and composite consolidation processes are available for the fabrication of structural components.

Papers presented at the 77th Meeting of the AGARD Structures and Materials Panel, held in Bordeaux, France 27th—28th September 1993.

ISBN 92-835-0735-5

the exchange of information in this important area. Characterisation in this case refers to the understanding of the behaviour of the composites as it relates to the ability to predict their performance in real-life applications. It covers various topics that include mechanical test techniques, NDE methods, life prediction models and other factors that will affect the level of confidence with which these relatively new materials will be accepted for application.

With titanium composites, we are presently at a stage where matrix alloys, reinforcing fibres and composite consolidation processes are available for the fabrication of structural components.

Papers presented at the 77th Meeting of the AGARD Structures and Materials Panel, held in Bordeaux, France 27th—28th September 1993.

ISBN 92-835-0735-5

the exchange of information in this important area. Characterisation in this case refers to the understanding of the behaviour of the composites as it relates to the ability to predict their performance in real-life applications. It covers various topics that include mechanical test techniques, NDE methods, life prediction models and other factors that will affect the level of confidence with which these relatively new materials will be accepted for application.

With titanium composites, we are presently at a stage where matrix alloys, reinforcing fibres and composite consolidation processes are available for the fabrication of structural components.

Papers presented at the 77th Meeting of the AGARD Structures and Materials Panel, held in Bordeaux, France 27th—28th September 1993.

ISBN 92-835-0735-5